03

ISSN 0386-5878
Technical Memorandum
of PWRI No.3035

RECENT SELECTED PUBLICATIONS AT EARTHQUAKE ENGINEERING DIVISION, PUBLIC WORKS RESEARCH INSTITUTE

October, 1991

Earthquake Engineering Division
Public Works Research Institute
Ministry of Construction
Tsukuba Science City, Ibaraki-ken, 305, Japan

「Copyright © (1991) by P.W.R.I.

All rights reserved. No part of this book may be reproduced by any means, nor transmitted, nor translated into a machine language without the written permission of the Director General of P.W.R.I.

この報告書は，土木研究所長の承認を得て刊行したものである。したがって，本報告書の全部又は一部の転載，複製は，土木研究所長の文書による承認を得ずしてこれを行ってはならない。」

Technical Memorandum
of PWRI No.3035

RECENT SELECTED PUBLICATIONS AT EARTHQUAKE ENGINEERING DIVISION, PUBLIC WORKS RESEARCH INSTITUTE

by

Kazuhiko Kawashima, Head
Earthquake Engineering Division

Synopsis:

At the Earthquake Engineering Division of the Public Works Research Institute, various researches for aiming to develop rational seismic design methods, seismic inspection and strengthening methods, seismic damage information systems and evaluation methods of loss estimation caused by an earthquake are being made.

This reports presents some of the selected publications on the research on seismic design, seismic inspection and strengthening of highway bridges, dynamic strength and ductility of structural components such as steel bridge piers and shield tunnel segments, structural response of menshin bridges (base isolated bridges), seismic response of embedded pipes, soil amplification, damping characteristics of cable stayed bridges, seismic damage information systems, and evaluation of indirect economical loss caused by an earthquake. They were presented at international conferences and workshops held in the last one years.

Key Word: SEISMIC DESIGN, SEISMIC INSPECTION, SEISMIC STRENGTHENING, SEISMIC RETROFIT, BASE ISOLATION, MENSHIN DESIGN, DUCTILITY, DYNAMIC STRENGTHENING, SHIELD TUNNEL, EMBEDDED PIPE, SOIL AMPLIFICATION, BRIDGE, BRIDGE PIER, ECONOMICAL EFFECTS, INDIRECT EFFECTS.

TABLE OF CONTENTS

1. Seismic Behavior of Buried Pipelines through Field Observation (3rd U.S. National Conference on Lifeline Earthquake Engineering, Los Angeles, CA, U.S.A., August 1991) ---------- 1

2. Amplification of Ground Acceleration Based on Measured Records (4th International Conference on Seismic Zonation, San Francisco, CA, U.S.A., August 1991) ---------- 13

3. New Seismic Design Specifications of Highway Bridges in Japan (22nd Joint Meeting, U.S.-Japan Panel on Wind and Seismic Effects, UJNR., Gathersburg, MA, U.S.A., May 1990) ---------- 23

4. Current Research Effects in Japan for Passive and Active Control of Highway Bridges against Earthquake (23nd Joint Meeting U.S.-Japan Panel on Wind and Seismic Effects, UJNR., Tsukuba, Japan, 1991) ---------- 41

5. Evaluation of Lateral Inertia Force of Bridges for Seismic Design (7th U.S.-Japan Bridge Workshop, Tsukuba, Japan 1991) ---------- 67

6. Behavior of Stiffened Box-Section Steel Bridge Piers in Seismic Regions from Model Test (7th U.S.-Japan Bridge Workshop, Tsukuba, Japan, 1991) ---------- 85

7. Estimation of Damping Characteristics of Cable Stayed Bride for Seismic Design (7th U.S.-Japan Bridge Workshop, Tsukuba, Japan, 1991---------- 101

8. Seismic Design, Seismic Strengthening and Repair of Highway Bridges in Japan (U.S.-Japan Workshop on Seismic Retrofit of Bridges, Tsukuba, Japan, 1990)---------- 119

9. Seismic Inspection and Seismic Strengthening of Reinforced Concrete Brides Piers with Termination of Main Reinforcement at Mid-height (U.S.-Japan Workshop on Seismic Retrofit of Brides, Tsukuba, Japan, 1990) ---------- 181

10. Repair and Retrofit of Steel Piers (U.S.-Japan Workshop on Seismic Retrofit of Bridges, Tsukuba, Japan, 1990) ---------- 213

11. Ductility of Steel Bridge Piers from Dynamic Loading Test (U.S.-Japan Seminar on Cyclic Buckling of Steel Structures and Structural Elements under Dynamic Loading Conditions, Osaka, Japan, 1991 ---------- 233

12. Estimation of the Defomation Capacity of Steel Bridge Piers (U.S.-Japan Seminar on Cyclic Buckling of Steel Structures and Structural Elements under Dynamic Loading Conditions, Osaka, Japan, 1991 ---------- 249

13. Damage Inspection Systems immediately after a Major Earthquake (4th U.S.-Japan Workshop on Earthquake Disaster Prevention for Lifeline Systems, Los Angeles, CA, U.S.A., 1991) ---------- 265

14. Seismic Inspection and Seismic Strengthening of Highway Bridges in Japan (4th U.S.-Japan Workshop on Earthquake Disaster Prevention for Lifeline Systems, Los Angeles, CA, U.S.A., 1991) ---------- 283

15. A Perspective of Menshin Design for Highway Bridges in Japan (1st U.S.-Japan Workshop on Bridges, Buffalo, NY, U.S.A., 1991) ---------- 319

16. Experiment and Analysis on Seismic Response of Menshin Bridges (1st U.S.-Japan Workshop on Earthquake Protective Systems for Bridges, Buffalo, NY, U.S.A., 1991) ---------- 345

17. Loading Test of Shield Tunnel Specimens Subjected to Alternative Ayial Loading (4th U.S. National Conference on Earthquake Engineering, Palm Springs, CA, U.S.A., 1990) ---------- 373

18. Evaluation of Indirect Economic Effects caused by the 1983 Nihonkai-Chubu, Japan, Earthquake (Earthquake Spectra, Vol.4, No.4, 1990) ---------- 385

19. Seismic Behavior of Cable Stayed Bridges (International Seminar on Cable-Supported Bridges with Emphasis on Steel Cable-Stayed Bridges, Yokohama, japan, 1991) ---------- 405

SEISMIC BEHAVIOR OF BURIED PIPELINES THROUGH FIELD OBSERVATION

by
Kazuhiko KAWASHIMA
Kinji HASEGAWA
and
Hiroyuki NAGASHIMA
Earthquake Engineering Division,
Public Works Research Institute

THIRD U.S. NATIONAL CONFERENCE ON
LIFELINE EARTHQUAKE ENGINEERING
Los Angeles, CA, U.S.A.
August 1991

Seismic Behavior of Buried Pipelines through Field Observation

Kazuhiko Kawashima[1], Kinji Hasegawa[2] and Hiroyuki Nagashima[3]

Abstract

This paper presents seismic response characteristics of embedded pipes based on field measurements. Strains induced in steel pipe and ductile pipes with expansion joints are studied. Special attention is placed for effect of bends on pipe response. Soil springs which are important in seismic design by means of the seismic deformation method is also studied based on the measured data.

Introduction

Seismic design of embedded pipes is generally made by the seismic deformation method[4] in which embedded pipes are assumed to respond in accordance with strain induced in ground during earthquakes. Pipes are considered to be beams elastically supported by soils when the stiffness of the soil is modelled by springs. Although the seismic deformation method has been adopted for seismic design of embedded lifeline facilities, measured data available for evaluating pipe response during earthquakes is very limited. Strong motion observation was initiated for measuring pipe response, because precise evaluation of pipe response in ground is essential for improving seismic design method. Special attention was paid to obtain response data for pipe with bends and expansion joints.

This paper presents an analysis of the measured data of pipe response, and soil spring stiffness to be used in the seismic deformation method is also presented.

---

[1]Head, Earthquake Engineering Division, Public Works Research Institute, Ministry of Construction, Tsukuba Science City, Ibaraki-ken, Japan 305
[2]Senior Research Engineer, ditto
[3]Assistant Research Engineer, ditto

Observation Systems

Fig.1 shows observation systems placed at Sodegaura city, about 50 km east of Tokyo, for measuring seismic behavior of embedded pipes. Continuous steel pipe with a diameter of 15 cm and ductile pipes with diameters of 15 cm and 30 cm are embedded 1 m below the ground surface. The length of the continuous steel pipe is 120 m and there is a bend at 20 m from the right end. The length of one element of the ductile pipe is 5 m in the 15 cm diameter pipe and 6 m in the 30 cm diameter pipe. They were jointed together by expansion joints which are capable of absorbing a relative deformation of ±10 % of pipe length in the axial direction and a rotation of ± 6 degrees. Stoppers for preventing excessive pulling-out are provided at the expansion joints.

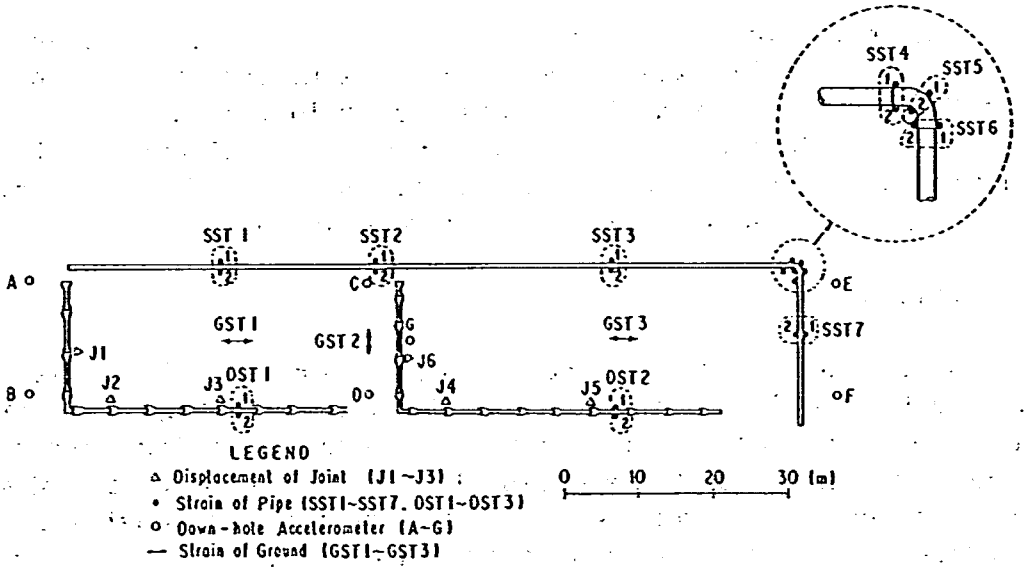


Figure 1. Observation Systems

Dense instrumentation is made to measure the pipe response. The strain induced in the steel and ductile pipes as well as relative displacements developed between two adjacent ductile pipe sections were measured. Strain gauges with coating against water are placed on the both sides of the pipes so that the flexural strain as well as the axial strain could be detected.

The ground acceleration and ground strain were measured. Three-components down-hole accelerometers were installed at six points to measure ground acceleration. The measured data was used to compute the averaged ground strain induced at the site. Special devices were installed 1 m below th ground surface to directly measure ground strain. The devices consist of two 80 cm diameter circular plates and a 6 cm diameter double tubed steel rod. The circular plates were connected to the double tubed steel rod.

Movement of the circular steel plates in accordance with soils vibration during earthquakes would develop small relative displacements between the two circular plates. Ground strain may be evaluated by dividing the relative displacement by the length of the double tubed steel rod. This device has been successfully used for measuring ground strain at several observation sites[1)3)].

All the measured signals are digitized with an interval of 1/100 second and recorded with a digital acquisition systems. Pre-event memory of about 10 seconds are provided to get full records from their start.

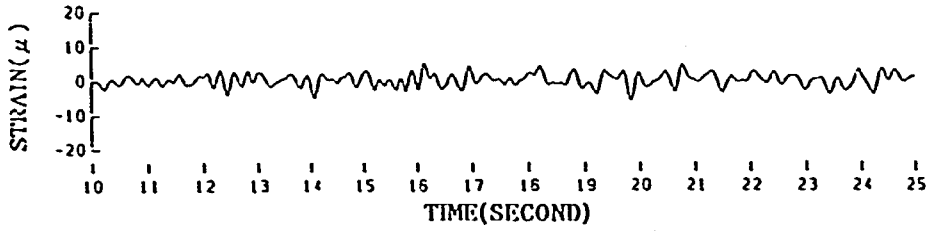
Measured Data

Observation was initiated in January 1989, and many records have been already obtained. Record which are large enough for analysis were measured by eight earthquakes as shown in Table 1.

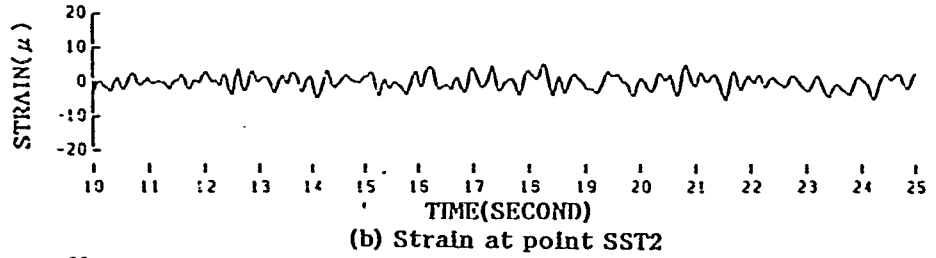
Table 1. Major Earthquakes Triggered

NO.OF EQ.	DATE	EPICENTER			MAGNITUDE (M)	FOCAL DEPTH (Km)
		EPICENTRAL REGION	LONGITUDE	LATITUDE		
EQ-1	1989.2.19	SOUTH-WEST OF IBARAKI-KEN	139°55'	36°00'	5.6	54
EQ-2	1989.2.28	NORTH OF CHIBA-KEN	140°12'	35°46'	4.6	74
EQ-3	1989.3. 6	NORTH OF CHIBA-KEN	140°44'	35°42'	5.9	61
EQ-4	1989.3.11	SOUTH OF IBARAKI-KEN	140°35	35°55'	4.9	42
EQ-5	1989.3.14	EAST OFF CHIBA-KEN	140°25'	35°28'	3.8	59
EQ-6	1989.3.18	NORTH OF CHIBA-KEN	140°43'	35°43'	5.2	58
EQ-7	1989.3.26	NORTH OF CHIBA-KEN	140°06'	35°45'	4.3	80
EQ-8	1989.4.26	NORTH OF CHIBA-KEN	140°29'	35°54'	5.3	65

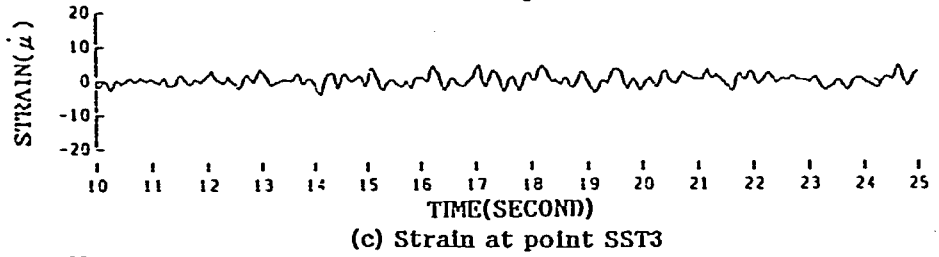
Fig. 2 shows the measured axial strain induced in the steel pipe and ground accelerations developed by an earthquake with epicentral distance of 61 km and an earthquake magnitude of 5.9. This earthquake is designated hereinafter as EQ 3 earthquake. The peak ground acceleration was about 14 to 22 cm/sec^2 and the peak pipe strain was about 4.8 to 6.5μ. It is interesting to note in Fig. 2 that although there are many similarities of the pipe strains between the three locations, the pipe strain are considerably different each other. This clearly shows that the pipe response in axial direction depends considerably on the response of nearby soil.



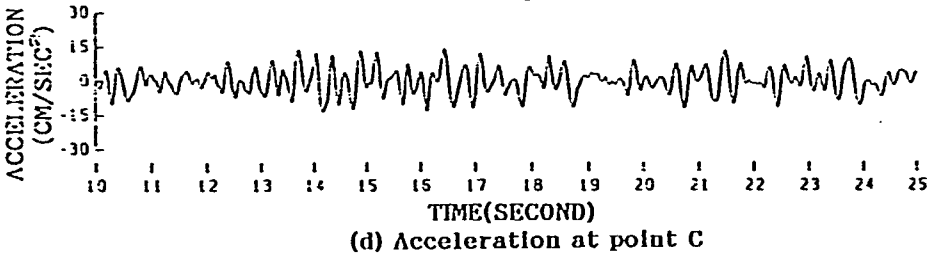
(a) Strain at point SST1



(b) Strain at point SST2

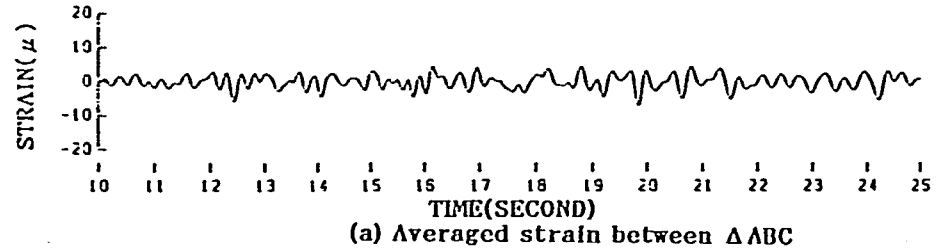


(c) Strain at point SST3

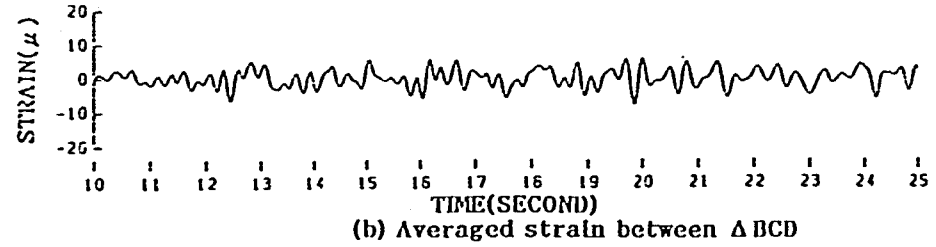


(d) Acceleration at point C

Figure 2. Measured Axial Strain of Steel pipe and Ground Acceleration at C Point during EQ 3



(a) Averaged strain between Δ ABC



(b) Averaged strain between Δ BCD

Figure 3. Ground Strain Computed for EQ 3 from Measured Ground Acceleration

Because the ground motion was small, the devices for measuring ground strain did not directly detect ground strain. Fig. 3 shows ground strains computed for the EQ 3 earthquake from measured ground accelerations. The measured ground accelerations were double integrated to obtain the ground displacements[7]. Assuming triangular elements such as Δ ABC and Δ BCD, the ground strain along pipe axis was computed with use of the standard finite element method[5]. Linear interpolation function for displacements was assumed in each finite element. If the ground strain computed for Δ ABC, which is the averaged ground strain between points A and C, is compared with the axial pipe strain at point SST1, in Fig. 2, it is found that the strains obtained are quite similar.

Fig. 4 shows axial strain induced during the EQ 3 earthquake in the ductile pipes. Almost no relative displacement was developed at the joints. It is interesting to note that the strain of the ductile pipe at the point DST-1 is quite similar with the strain of the steel pipe at the point SST-1. The strain of the ductile pipe is not necessarily smaller than the strain of the steel pipe. This implies that reduction of axial force induced in the ductile pipe due to the expansion joints was quite small during the EQ 3. The forces developed at the expansion joints during the EQ 3 were so small that friction at the expansion joints prevented slippage to occur between the adjacent pipe sections.

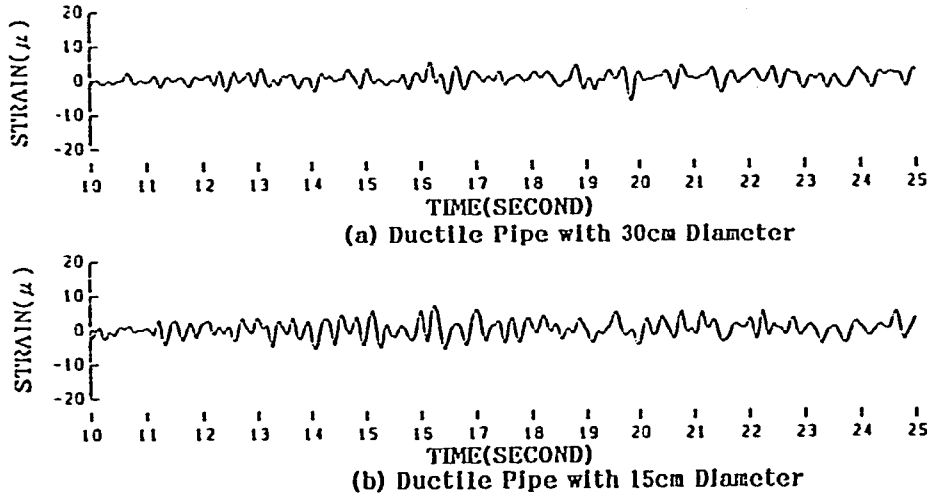


Figure 4. Measured Axial Strain of Ductile Pipe during EQ 3

Fig. 5 shows a distribution of peak strain along the steel pipe for the EQ 3 earthquake. Both axial and flexural strains are presented. It should be noted that although axial strain is predominant in the straight section, flexural strain becomes larger than the axial strain at the bends. Flexural strain has to be therefore taken into account in seismic design of pipes at bend

sections.

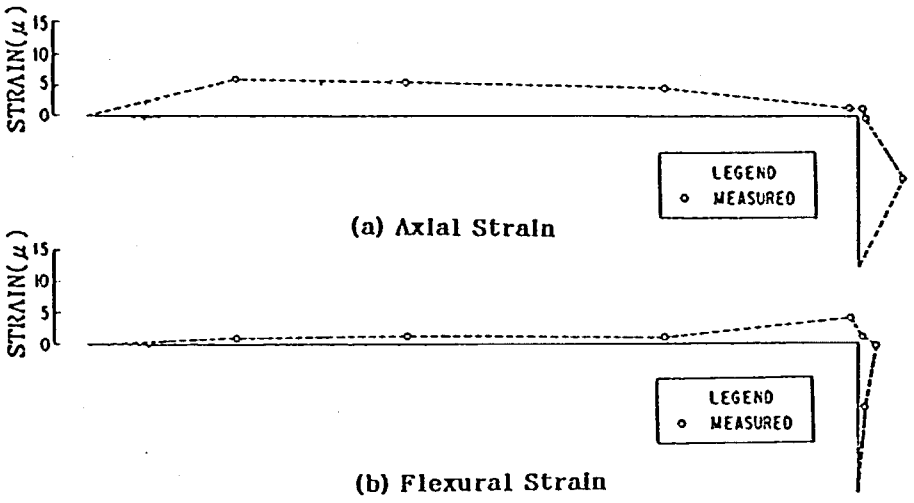


Figure 5. Peak Strain of Steel Pipe during EQ 3

Fig. 6 shows the axial strain of steel pipe vs. peak ground acceleration relation for the data obtained by the eight earthquakes presented in Table 1. Although number of the data obtained is still small, clear correlation between the pipe strain and the peak ground acceleration is observed. By increasing the number of data, this is expected to provide a practical estimation for the pipe strain induced during earthquakes.

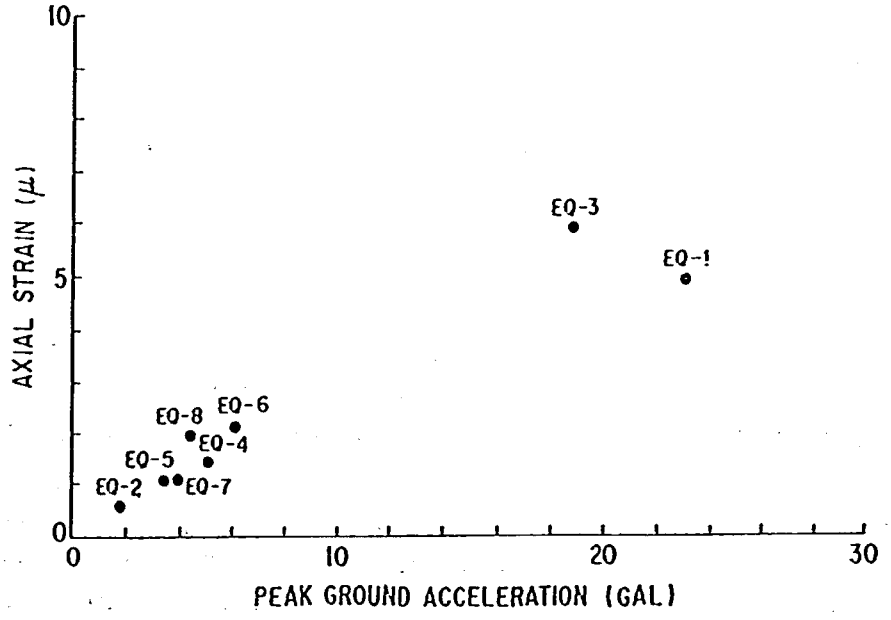


Figure 6. Axial Strain of Steel Pipe vs. Peak Ground Acceleration Relation

Evaluation of Soil Spring Stiffness

An analytical model presented in Fig. 7 is often adopted to estimate dynamic response analysis of embedded pipes[6]. The pipe is idealized by a beam elastically supported by springs which represent pipe -soil interaction. Soil response is computed by prescribing the input ground motion at the base rock.

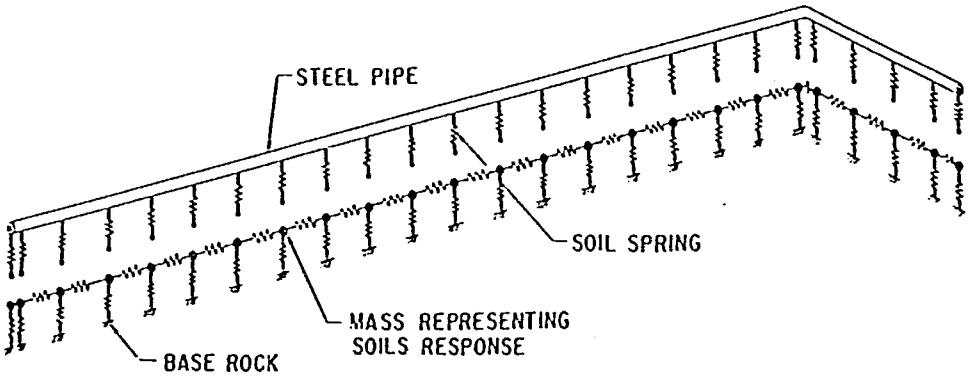


Figure 7. Analytical Model for Dynamic Response Analysis of Embedded Pipes

In the analytical model presented in Fig. 7, it is essential to determine the stiffness of the soil springs which elastically support correctly the pipe. Various methods have been proposed from analytical and experimental studies to estimate the soil springs. However due to limitation of measured data available for estimating soil springs based on measured seismic response data of pipes, few studies have been made for soil springs. Therefore, with use of the analytical model presented in Fig. 7, the soil springs stiffness were studied.

The response displacements of soils which were estimated from the measured accelerations were used for computing the pipe responses. The steel pipe was idealized by a discrete analytical model with 24 beam elements as shown in Fig. 8. Because the displacements which were computed from the measured accelerations were available at only six points, the displacements at each nodal point of the analytical model were computed from either linear interpolation or extrapolation of the displacements from the six points.

In the Design Specifications of Petroleum Pipelines[2], the soil spring stiffness is stipulated to be estimated as

$$K = c \cdot G_s \qquad (1)$$

where K : stiffness of soil spring per unit length, c : a coefficient, and G_s : shear moduli of soils. The shear moduli of soils are estimated

as

$$G_s = \gamma_t V_s^2 / g \qquad (2)$$

where γ_t : unit weight of soils, V_s : shear wave velocity of soils, and g : acceleration of gravity. In the specifications the coefficient c is stipulated to be determined by appropriate tests, and a value of 3.0 is recommended when such test data is not available.

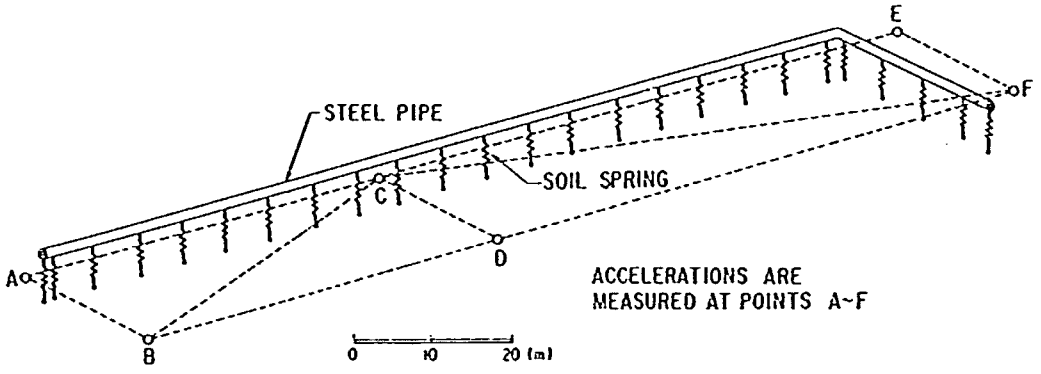


Figure 8. Analytical Model Used for Pipe Response

Therefore, as a first estimation, the stiffness K of soil spring was evaluated by Eq. (1). Shear wave velocity which was measured at three points in the observation site was about 150 m/sec at the depth between the ground surface and 15 meters below the ground surface. Because there was some scatter of the measured shear wave velocity depending on the site and depth, shear wave velocities of 100 m/sec, 200 m/sec and 300 m/sec were assumed in the analysis. Analyses were also made assuming that the shear wave velocity was infinitively large. According to this assumption, the pipe deforms in exactly the same manner as the ground strain.

Fig. 9 shows axial and flexural strain of the steel pipe computed for the EQ 3 earthquake. It is seen in Fig. 9 that the pipe strains computed are considerably larger than the measured pipe strain. The computed strains assuming shear wave velocities of 100 m/sec ~ 300 m/sec are almost the same, and they are also close with the computed pipe strain assuming the infinitively large shear wave velocity. This implies that Eq.(1) assuming the shear wave velocities from 100 m/sec to 300 m/sec gives an excessively large estimation of the soil spring. This was also seen from the fact that the increasing rate of the computed pipe strain from the ends is larger than that of the measured pipe strain.

The soil spring which gives realistic estimation for the measured pipe strain was therefore studied. Fig. 10 shows the approximation of the computed pipe strain assuming a soil spring stiffness of 2.94×10^6 N/m. The computed axial and flexural strain approximates quite well the measured pipe strain. The soil spring

stiffness of 2.94×10^5 N/m is predicted by assuming a coefficient "c" of about 3/40 when the averaged shear wave velocity of 150 m/sec is assumed in Eq.(1). From such evidence it may be said that the recommended value of 3 for the coefficient "c" in Eq.(1) is excessively conservative. It is important to precisely study the coefficient "c" which gives a realistic soil spring stiffness.

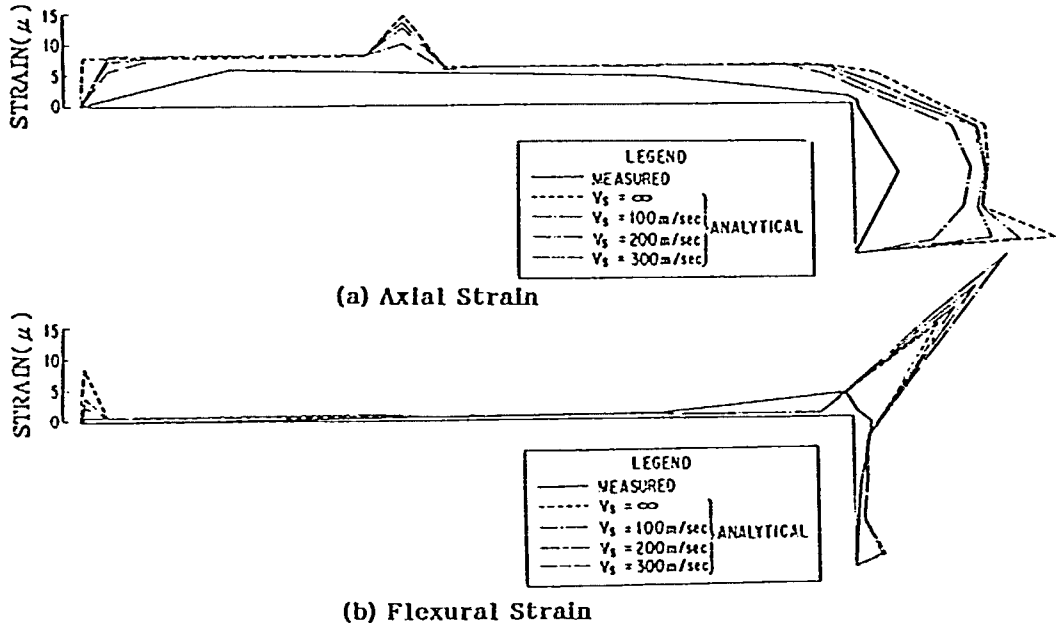


Figure 9. Computed Strain of Steel Pipe for EQ 3

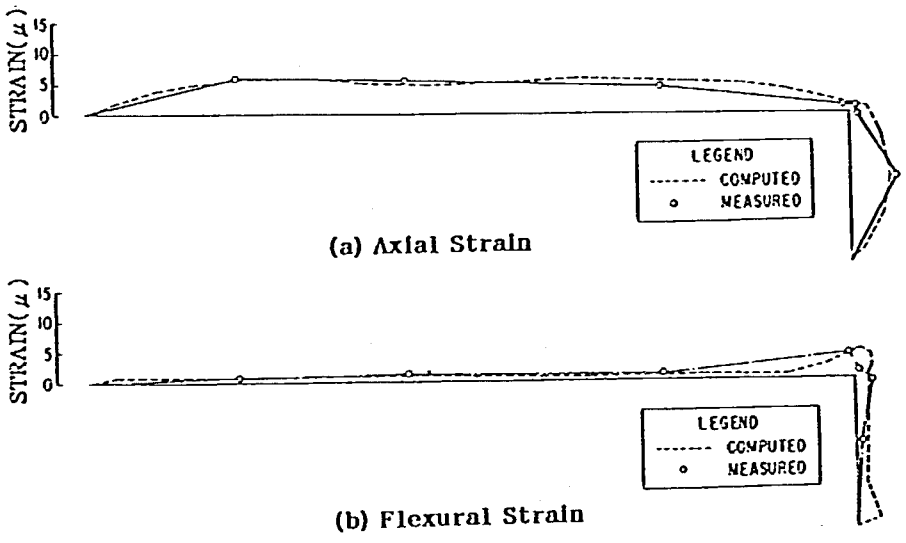


Figure 10. Best Correlation of Pipe Strain for EQ 3

Conclusions

For accumulating actual seismic behavior of embedded pipes during earthquakes, seismic observation of two types of pipes was initiated. Based on the analyses of the measured data on the strain of embedded pipes, the following conclusions may be deduced :

1) Although axial strain was predominant in the straight section, flexural strain is more predominant than axial strain at the bend section of the pipe. Flexural strain should be considered in seismic design at bend sections.

2) Considerably good correlation was observed between the measured axial strain of the pipe and the peak ground acceleration. Accumulation of measured data is expected to provide a realistic estimation method for the pipe strain based on the peak ground acceleration.

3) The computed pipe strain assuming Eqs.(1) and (2) was excessively larger than the measured pipe strain. It is thought that the spring stiffness predicted by Eq.(1) assuming the coefficient "c" of 3.0 is too conservative. Coefficient "c" has to be precisely studied by analyzing more measured data.

References

1)Iawamoto, T.et.al.: Observation of Dynamic Behavior of Buried Pipelines during Earthquakes, Eighth World Conference on Earthquake Engineering, San Francisco, U.S.A., 1984

2)Japan Road Association : Design Specifications of Petroleum Pipelines, 1974

3)Katayama, T. and Sato, N. : Ground Strain Measurement by a Very Densely Located Seismometer Array, Proc. 6th Japan Earthquake Engineering Symposium, Tokyo, 1982

4)Ministry of Construction : New Seismic Design Methods,Technical Note of PWRI, No. 1185, Public Works Research Institute, 1977

5)Okubo, T., Arakawa, T. and Kawashima, K. : Dense Instrument Array Program of the Public Works Research Institute and Preliminary Analysis of the Records, Eighth World Conference on Earthquake Engineering, San Francisco, U.S.A., 1984

6)Tamura, C., Okamoto, S. and Hamada, M. : Dynamic Behavior of a Submerged Tunnel during Earthquakes, Report of the Institute of Industrial Science, University of Tokyo, Vol.24, No.5, 1975

7)Tamura, K., Kawashima, K., Aizawa, K. and Takahashi, K. : Recording Accuracy of Digital Strong Motion Accelerographs with Independent Triggering and Recording Systems for Analysis of Finite Ground Strains Induced during Earthquakes, Proc. Japan Society of Civil Engineering, Vol. 392/I-9, 1988

AMPLIFICATION OF GROUND ACCELERATION BASED ON MEASURED RECORDS

by
Kazuhiko KAWASHIMA
and
Keiichi TAMURA

4th International Conference on Seismic
Zonation, Stanford, CA, U.S.A.
August 1991

AMPLIFICATION OF GROUND ACCELERATION BASED ON MEASURED RECORDS

KAWASHIMA Kazuhiko[1)*] and TAMURA Keiichi[2)]

ABSTRACT

Presented are underground acceleration records measured at three sites around the Tokyo Bay. Measurements were made at as deep as 127 m below the ground surface. Decreasing rate of peak accelerations and acceleration response spectra with depth is presented based on the measured data.

UNDERGROUND STRONG MOTION OBSERVATION

Strong motion observation at underground has been made at three sites around the Tokyo Bay since 1970. Three-components feed-back servo-type down-hole accelerometers were placed at surface, 27 m, 67 m and 127 m below the surface at Ukishima Park site, at surface, 70 m and 110 m below the surface at Futtu Cape site, and at surface, 80 m and 120 m below the surface at Kannozaki site.

Figure 1 shows the soil boring data at the three sites. The ground condition is significantly different between the sites. There are extremely soft alluvial clayey deposits at Ukishima Park site from the surface to 45 m below the surface. Shear wave velocity measured is only from 120 m/sec to 170 m/sec at the deposits. Alternation of sand and silty sand exists at Futtu Cape site from the surface to 42 m below the surface. Shear wave velocity at the deposits is from 240 m/sec to 300 m/sec. Kannonzaki site is of silty and sandy rocks. Although shear wave velocity was not measured, it may be 600 m/sec to 1000 m/sec. Because the rock is weathered near the surface, the accelerations recorded at the surface should not be considered as outcrop rock motions.

AMPLIFICATION OF PEAK ACCELERATION

Distribution of Peak Acceleration with Depth

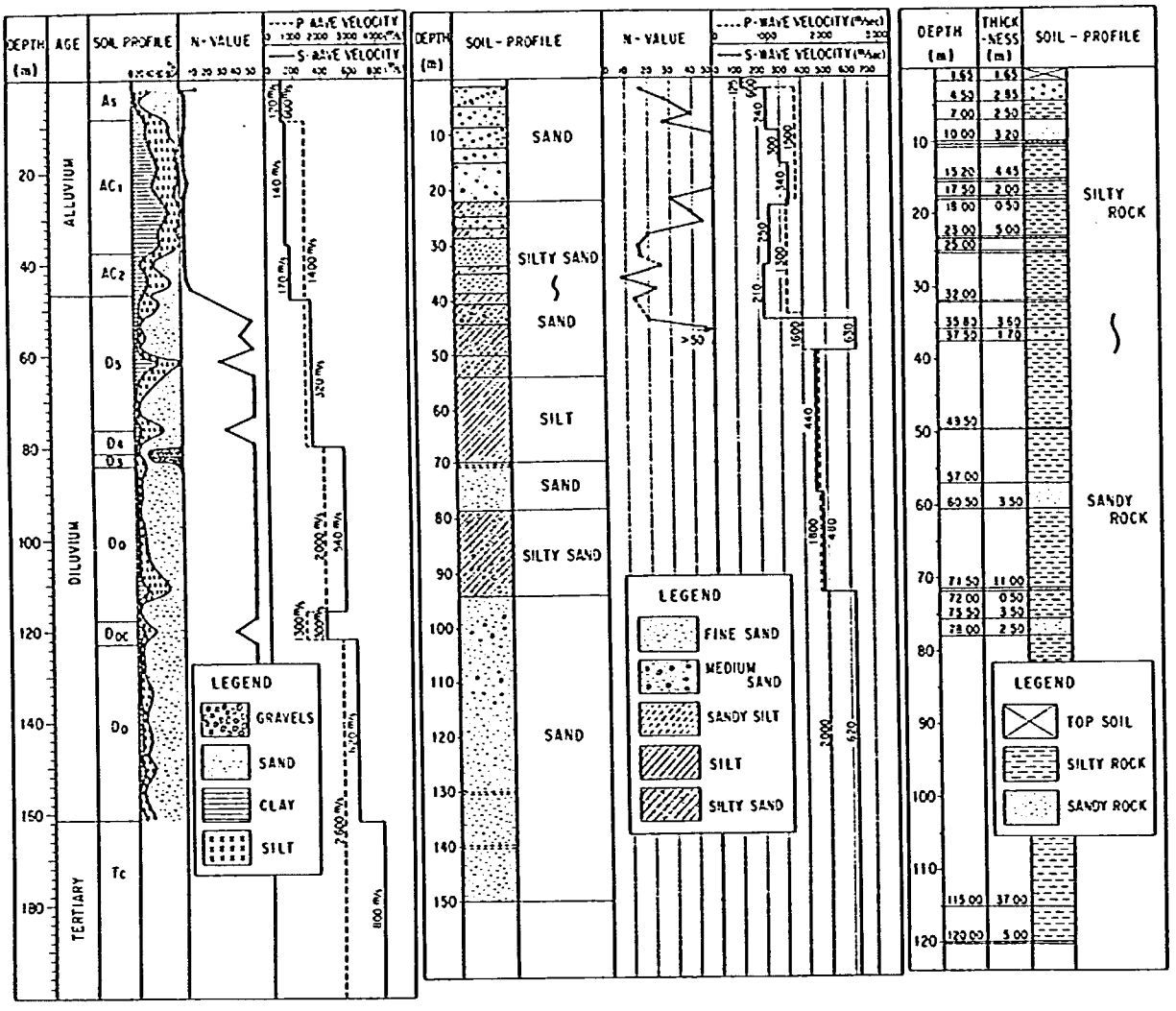
Figure 2 shows an example of underground accelerations measured at Ukishima site. It was recorded by an earthquake which occurred on August 4, 1974 with magnitude 5.8 at the epicentral distance of 50 Km. Figure 3 shows distribution of

---

1)Head, Earthquake Engineering Division, Earthquake Disaster Prevention Department, Public Works Research Institute, Ministry of Construction, Tsukuba Science City, Japan, 304

2) Seniou Research Engineer, Ground Vibration Division, ditto

*Presenting Author Underlined



(a) Ukishima Park (b) Futtsu Cape (c) Kannonzaki

FIGURE 1 Soil conditions

peak ground acceleration with depth. Although peak accelerations generally increase as the depth becomes small, it is noteworthy that decrease of accelerations with decreasing the depth also occurred.

Because the amplification of peak ground acceleration depends on earthquakes, a ratio defined as the peak ground acceleration at underground divided by that at the surface was computed. Average and standard deviation of the ratio over the measured data (28, 54, 124 records at Ukishima Park site, Futtsu Cape site and Knnonzaki site, respectively) were computed as shown in Figure 4. It is interesting to note that the deviation from the average is smaller at the soft soil site. To show the decreasing rate of peak acceleration with depth, decreasing rate γ defined as

$$\gamma_i = (r_i - r_{i+1}) / L_i \times 100 \qquad (1)$$

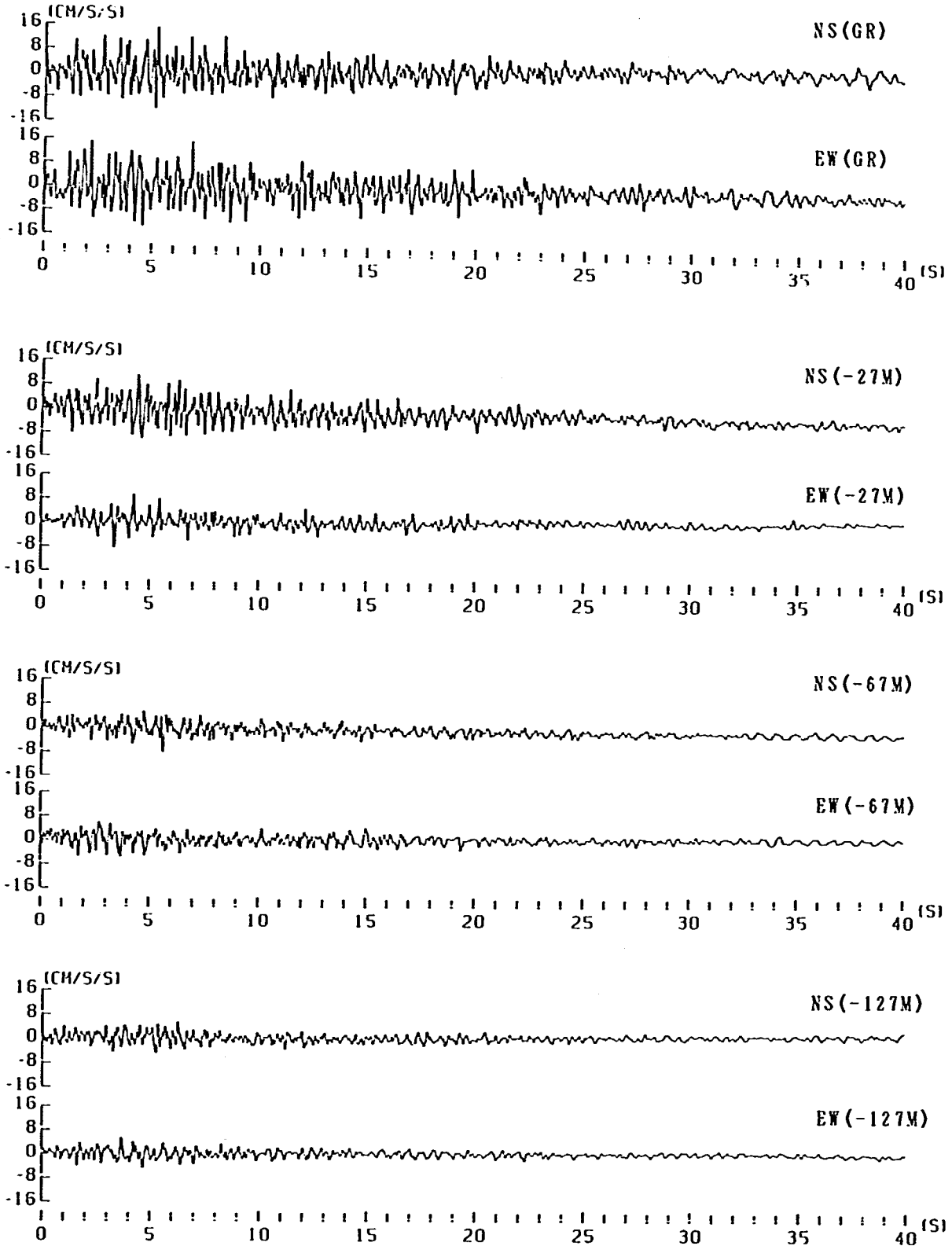
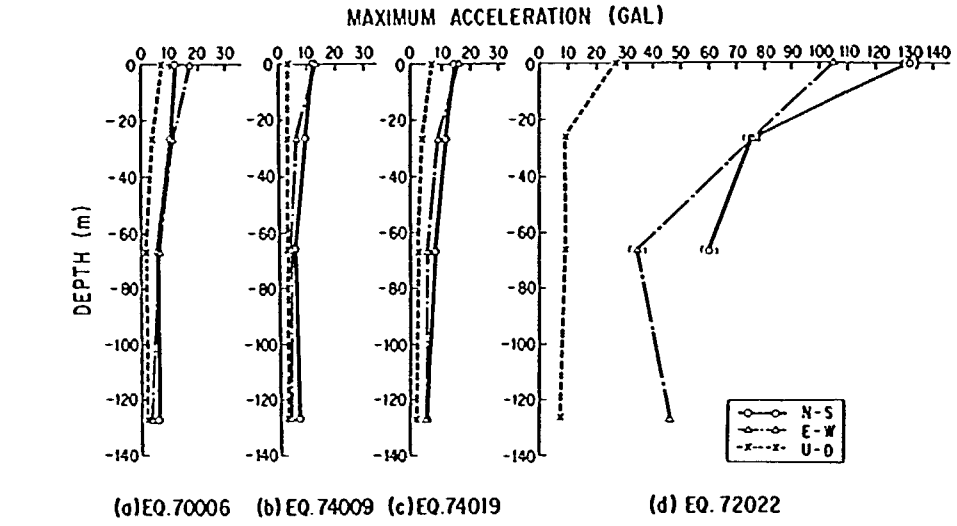
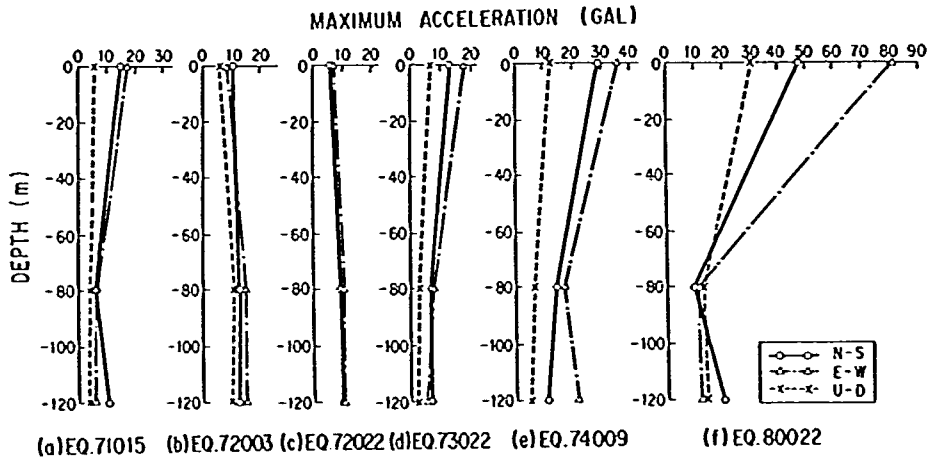


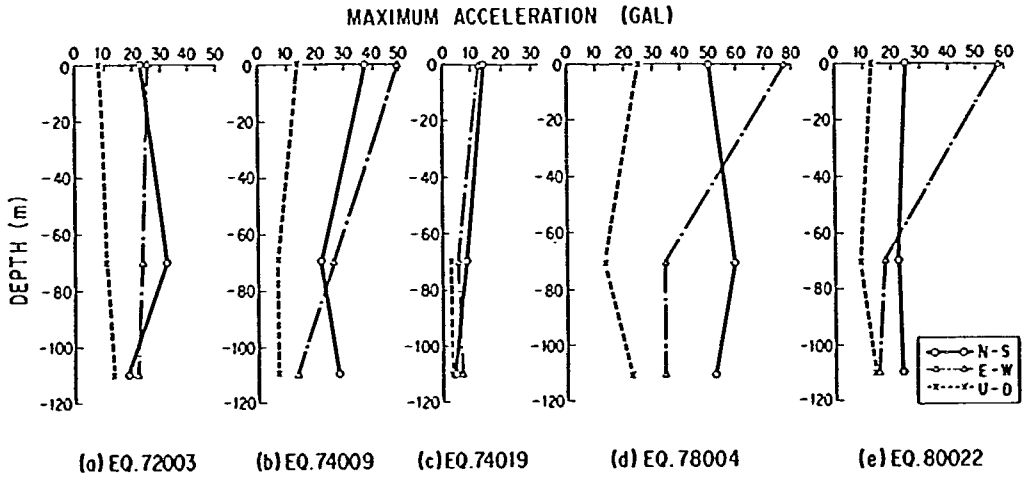
FIGURE 2 Measured acceleration at Ukishima Park



(1) Ukishima Park

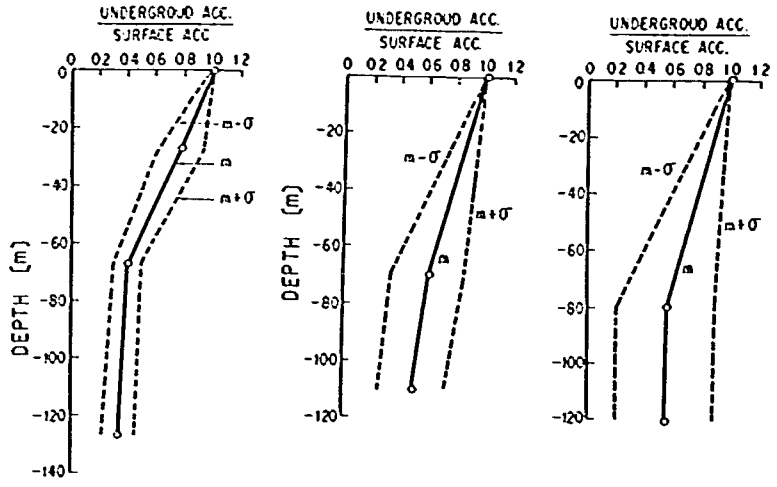


(2) Futtsu Cape



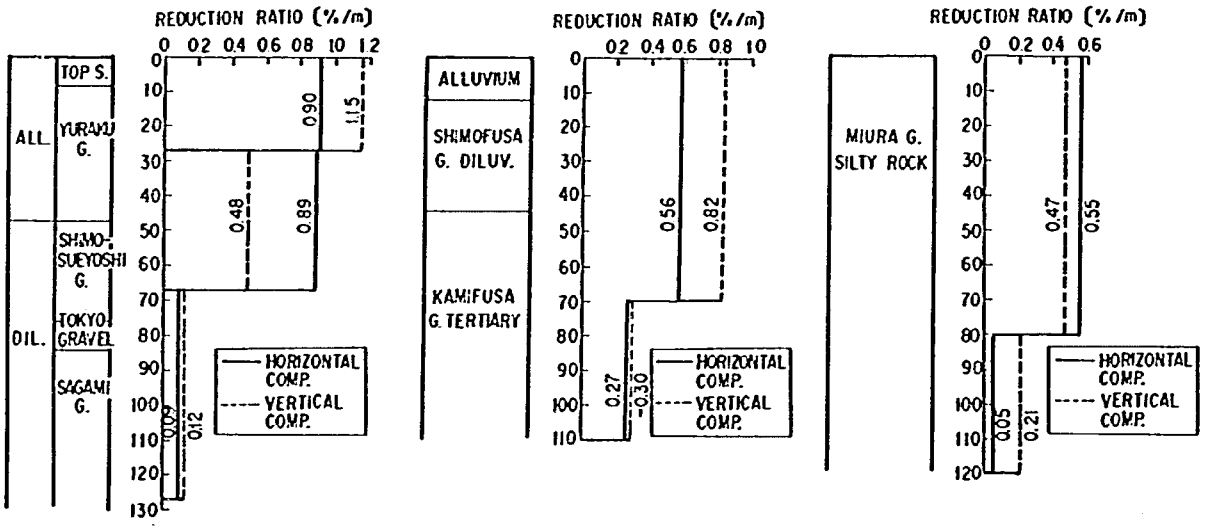
(3) Kannonzaki

FIGURE 3 Distribution of peak accelerations with depth



(a) Ukishima Park (b) Futtsu Cape (c) Kannonzaki
FIGURE 4 Averaged distribution of peak acceleration

was introduced, in which r_i = the averaged ratio of acceleration at i-th measuring point (acceleration at underground / acceleration at surface) and L_i = depth between i-th and (i+1)th measuring points. Figure 5 shows the averaged decreasing rate for the three sites. It is obvious that the averaged decreasing rate depends on the soil condition and the depth. For example, at Ukishima Park site, it is 0.9 %/m between the surface and 27 m below the surface, 0.89 %/m between 27 m and 0.09 %/m between 67 m and 127 m below the surface. At Kannonzaki site, it is 0.05 %/m between 80 m and 110 m below the surface, while it is 0.55 %/m between the surface and 80 m below the surface. The decreasing rate between the surface and 80 m below the surface is unexpectedly large, and it may be attributed to the amplification of the accelerations near the surface.



(a) Ukishima Park (b) Futtsu Cape (c) Kannonzaki
FIGURE 5 Averaged decreasing rate γ_i with depth

Attenuation of Peak Acceleration

Empirical attenuation of peak acceleration was estimated at each measuring point assuming the following equation

$$a_{max} = a \times 10^{bM} \times \Delta^{c} \qquad (2)$$

in which a_{max} = peak acceleration in gal (cm/sec^2), M = earthquake magnitude, Δ = epicentral distance in km, and a, b and c = coefficients to be determined by multiple regression analysis.

Assuming Equation (1), the attenuation between the three sites was compared as shown in Figure 6, in which comparison is given between the surface and the deepest measuring points (127 m at Ukishima Park, 110 m at Futtsu Cape site and 120 m at Kannonzaki site). Scatter of the predicted peak acceleration for given earthquake magnitudes and epicentral distances seems to be smaller at the deepest measuring point than that at the ground surface. It gives the explanation to assume base rock to compute soil response using the acceleration records measured at different points. However, it should be noted that the scatter between the three sites is still very large even at 110 ~ 127 m below the surface.

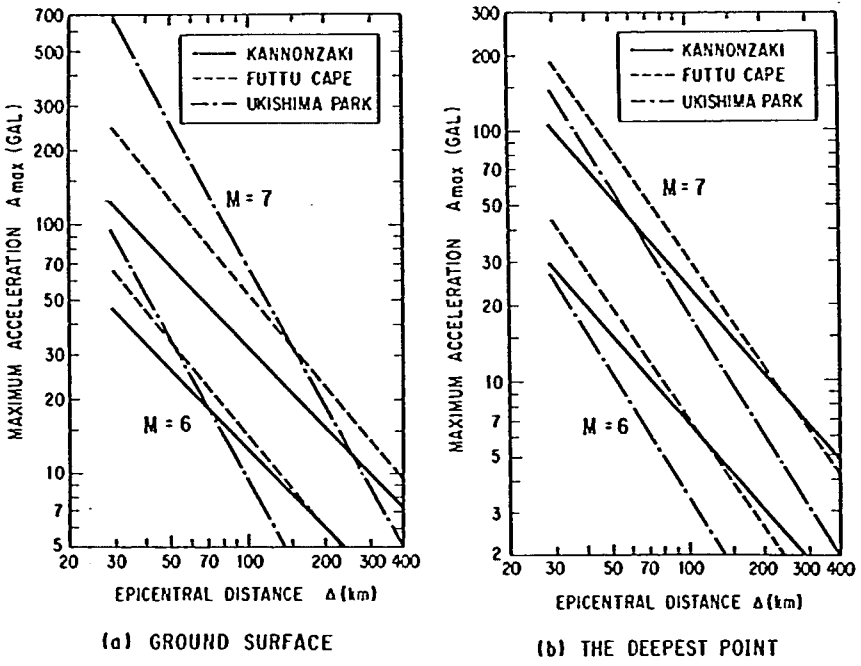


FIGURE 6 Comparison of attenuation of peak accelerations

AMPLIFICATION OF RESPONSE ACCELERATION

Soil amplification was also studied in terms of acceleration response spectra. Because direct average of the response acceleration spectra does not give

meaningful results, coefficient of response spectra R(T) was defined as

$$R(T) = S_A(T) / a_{max} \qquad (3)$$

in which $S_A(T)$ = response acceleration for natural period T (sec) and damping ratio of 0.05, and a_{max} = peak ground acceleration. Figure 7 shows the average and standard deviation of the coefficient R(T) at Ukishima Park site.

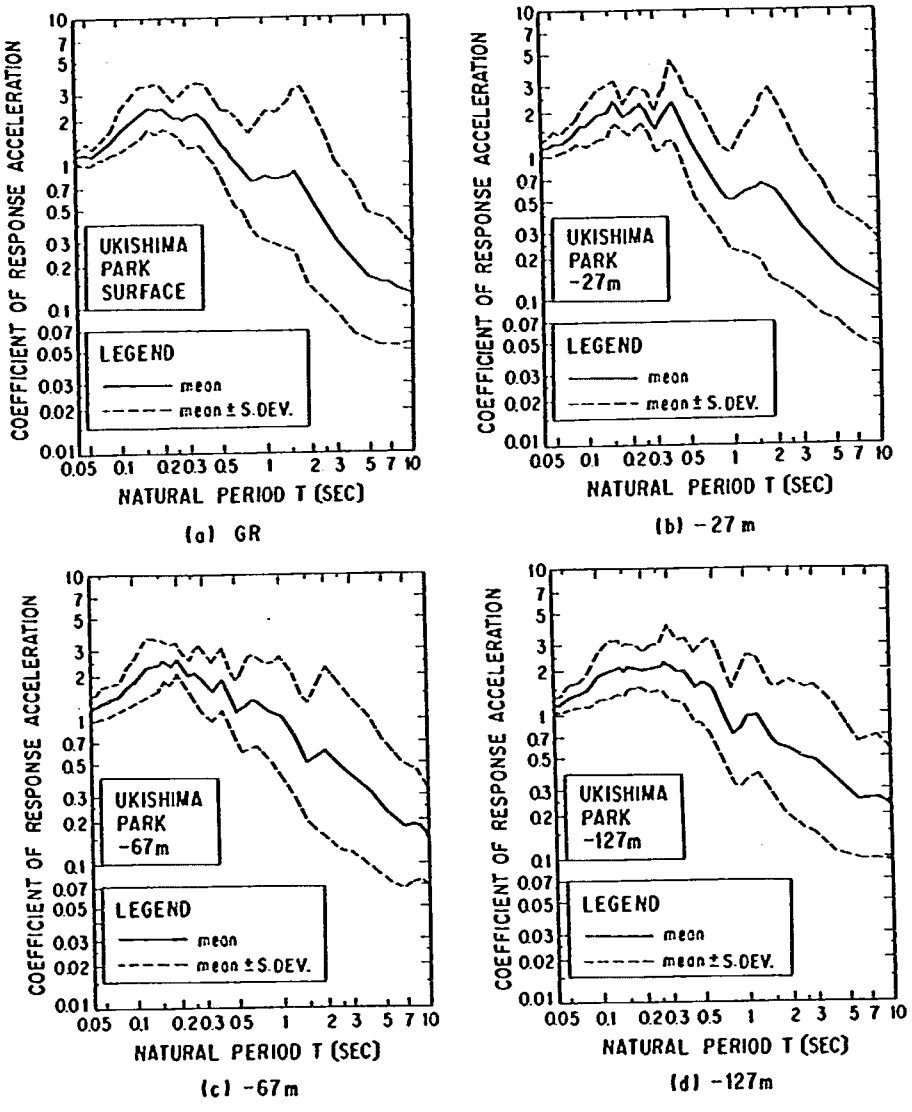


FIGURE 7 Averaged coefficient R(T) at Ukishima Park

To show the soil amplification, a ratio of the coefficient R(T) was defined as

$$\beta(T)^{i/j} = R(T)^i / R(T)^j \qquad (4)$$

in which $R(T)^i$ represents the coefficient R(T) at the i-th measuring point. Figure 8 shown the average and standard deviation of the ratio $\beta(T)^{i,j}$ at Ukishima Park site.

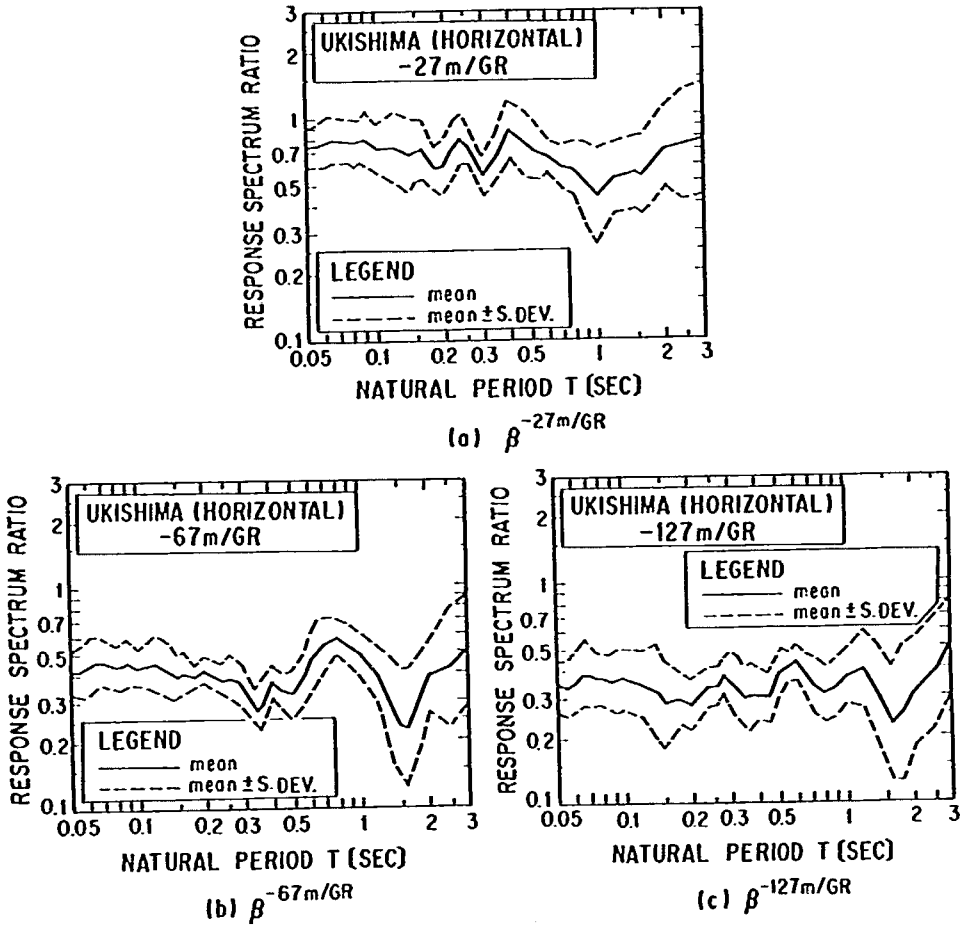


FIGURE 8 Average of $\beta(T)$ at Ukishima Park

CONCLUDING REMARKS

Because measured records were from small to moderate earthquakes, further observation is inevitable for studying soil amplification developed during large earthquakes.

REFERENCES

1. K. Kawashima, K. Aizawa and K. Takahashi : Attenuation of Peak Ground Acceleration, Velocity and Displacement Based on Multiple Regression Analysis of Japanese Strong Motion Records, Earthquake Engineering and Structural Dynamics 14:199-215(1986)

NEW SEISMIC DESIGN SPECIFICATIONS OF HIGHWAY BRIDGES IN JAPAN

by
Toshio IWASAKI
Kazuhiko KAWASHIMA
and
Kinji HASEGAWA
Public Works Research Institute
Ministry of Construction

22nd Joint Meeting
U.S. — Japan Panel on Wind and Seismic Effects, U.J.N.R.
Gaithersburg, Maryland, U.S.A.
May, 1990

NEW SEISMIC DESIGN SPECIFICATIONS OF HIGHWAY BRIDGES IN JAPAN

Toshio IWASAKI[1], Kazuhiko KAWASHIMA[2] and Kinji HASEGAWA[3]

ABSTRACT

Introduced are the new Seismic Design Specifications of Highway Bridges in Japan issued on February 1990. Main items of the revision including the seismic lateral force, evaluation of inertia force considering structural response, check of bearing capacity for lateral load for reinforced concrete pier and dynamic response analysis are presented.

KEY WORDS

Seismic Design, Design Method, Highway Bridge

1. INTRODUCTION

First requirement on lateral force for design of road bridge in Japan was included in "Draft Details of Road Structure" issued in 1926 with considerations of the damage caused by the Kanto Earthquake in 1923. It was stipulated in the draft details that the maximum lateral force expected to develop at the site shall be considered in seismic design. After experiencing significant damages during strong earthquakes seismic regulations were reviewed and amended several times as shown in Table 1. "Design Specifications of Steel Road Bridges (Draft)" were issued in 1914, and "Design Specifications of Steel Road Bridges" and their revised version were issued in 1934 and 1939, respectively. Although a requirement for lateral force was stipulated in these specifications, first comprehensive seismic design stipulations were issued in 1971 in a separate volume exclusively for seismic design as "Seismic Design Specifications of Road Bridges". It was described in the specifications that lateral force shall be determined depending on zone, importance and ground condition in seismic coefficient method and structural response shall be further considered in the modified seismic coefficient method. Evaluation on soil liquefaction was firstly incorporated in view of the damages caused by the Niigata Earthquake in 1964. The 1971 specifications were revised in a form of "Part V Seismic Design" of "Design Specifications of Road Bridges" in 1980. A rational evaluation method for soil liquefaction as well as practical countermeasures against the liquefaction was included in the specifications.

Since 1985 extensive efforts have been undertaken to establish more rational seismic design criteria for road bridges, with consideration of recent advantages of earthquake engineering and lessons gained from recent earthquakes. New specifications were were completed in 1990.

This paper outlines the new specifications (JRA, 1990) for seismic design of road bridges with emphasis on the stipulations revised.

2. BASIC PRINCIPLES FOR DEVELOPING NEW SPECIFICATIONS

Road bridge is a vital component of road, and it has to be safe enough against an earthquake so that function of road be maintained. It can be used without loosing any structural functions against small to moderate earthquakes with high to moderate possibility to occur at the site. Critical failure causing total collapse of the bridge has to be avoided even during a significant earthquake such as the Kanto Earthquake in 1923. Seismic design method has been gradually improved with consideration on damage experiences and advantage of earthquake engineering. Based on such improvement of seismic design method as well as various countermeasures against an earthquake, it is considered that seismic damages of road bridge have been decreasing as a total in recent years as shown in Table 2. However it is also important to note that new damages which have not been identified in the past earthquakes have been seen in recent earthquakes, due to improvement of seismic design method. This obviously shows that the countermeasures aiming only to minimize the damages developed in the past earthquake do not give a credit to avoid new type of damage in the future earthquake. In revising the design specifications, it is required to take account of such new type of

---

1) Director General, Public Works Research Institute
2) Head, Earthquake Engineering Divison of Earthquake Disaster Prevention Department, Public works Research Institute
3) Research Engineer,ditto

damage patterns.

In view of the understanding on the damage patterns of road bridges in recent earthquakes and advances of earthquake engineering, the following revisions were included in the New Seismic Design Specifications.

1) modification on classification of ground condition
2) unification of seismic coefficient method and modified seismic coefficient method including the revision of the seismic coefficient
3) evaluation method of inertia force for continuous bridges
4) improvement on strength of sandy soils against liquefaction
5) evaluation of bearing capacity of reinforced concrete piers for lateral force (ductility check)
6) design ground motion for dynamic response analysis as well as an analytical model

Table of content of the new specifications is the following :

Chapter 1 General
Chapter 2 Basic Principle of Seismic Design
Chapter 3 Load and Design Condition in Seismic Design
Chapter 4 Seismic Coefficient
Chapter 5 Bearing Capacity for Lateral Force of Reinforced Concrete Piers
Chapter 6 Dynamic Response Analysis
Chapter 7 Structural Details in Seismic Design
Chapter 8 Device to Expect Reduction of Lateral Force

(Appendix)
I. References on Liquefaction
II. Examples of Classification of Ground Condition
III. References on Design Ground Motion
IV. Example of Calculation of Natural Period and Inertia Force
V. Reference on Bearing Capacity of Reinforced concrete Piers for Lateral Force
VI. Practices of Structural Details

Table 3 shows the revised part or newly introduced parts in the new specifications, and Fig. 1 shows the flow-chart of seismic design.

3. CLASSIFICATION OF GROUND CONDITION

Classification of ground condition was changed from four groups to three groups as shown in Table 4 by combining the group 2 and group 3 into same group. The classification of the ground condition is made base on the characteristics value at the site specified as

$$T_G = 4 \sum_{i=1}^{I} \frac{H_i}{V_{si}} \qquad (1)$$

where
T_G : characteristic value (sec)
H_i : thickness of i-th subsoil layer (m)
V_{si} : shear wave velocity of i-th sublayer (m/sec)
I : sublayer's number counted from ground surface

The change was made because most of the seismic damage of road bridge in the past earthquake was likely to be developed on the group 4 with the difference between the ground group 2 and 3 being practically very small, and because difference of ground motion characteristics in terms of response acceleration spectra is few between the ground group 2 and 3. It was also taken into account that the classification of the ground condition based on the difference of characteristic value of only 0.2 second is practically quite hard in view of the fact that shear wave velocity is generally estimated from an empirical formulae based on N-value of standard penetration test.

4. SEISMIC COEFFICIENT

In the previous specifications, the seismic coefficient method was used for the bridges with pier height less or equal to 15 m and the modified seismic coefficient method was used for the bridges with pier height larger than 15 m. The modified seismic coefficient method was originally intended to apply to bridges with the natural period longer than 0.5 second. However, as various foundations becomes to be adopted on wide range of soil conditions, even bridges with pier height less than 15 m is likely to have the natural period longer than 0.5 second. This always caused confusion in selecting the seismic design method.

Therefore, the seismic coefficient method

and the modified seismic coefficient method was unified, and this is referred to as seismic coefficient method.

In the seismic coefficient method, the design seismic coefficient shall be determined by Eq.(2), but no less than 0.1.

$$k_h = c_z \cdot c_G \cdot c_I \cdot c_T \cdot k_{h0} \qquad (2)$$

where

k_h : design horizontal seismic coefficient,

k_{h0} : standard design horizontal seismic coefficient (=0.2),

c_z : modification factor for zone (refer to Fig. 2),

c_G : modification factor for ground condition (refer to Table 5),

c_I : modification factor for importance (refer to Table 6), and

c_T : modification factor for structural response (refer to Table 7). For computing inertia force associated with the weight of soils and dynamic earth pressure, c_T has to be 1.0.

In Eq.(2) the modification factors c_z and c_I are the same with the value specified in the previous specifications. The modification factor c_G was changed associated with the change of ground condition classification. The modification factor c_T, which represents the difference of lateral force due to structural response, corresponds to the modification factor β in the previous specifications. The modification factor β was formulated based on an analysis of 44 components of strong motion records obtained in Japan. The new modification factor c_T was determined from an analysis of earthquake response spectra base on 394 components of strong motion records obtained in Japan. Considerations that the seismic damage was likely to occur in bridges with short natural period were also included.

Fig. 3 shows an comparison of the seismic coefficient between the previous and new specifications assuming that $c_Z = c_T = 1.0$.

5. EVALUATION METHOD OF INERTIA FORCE

In the previous specification, for computing an inertia force associated with dead weight of superstructure, which is to be used in seismic design of substructure, the bridge is divided into several structural segments consisting of a substructure and the part of superstructure which is vertically supported by the substructure considered. Then, the inertia force (lateral force) used for the seismic design of substructure of the i-th structural segment is assumed to be determined as

$$F_{di} = k_{hi} R_i \qquad (3)$$

where

F_{di} : inertia force associated with dead weight of superstructure for design of i-th substructure

k_{hi} : seismic coefficient considered for i-th structural segment

R_i : reaction force developed at i-th substructure due to dead weight of the part of superstructure supported by the i-th substructure.

However as various type of bridge structures become to be constructed, it became apparent that the inertia force determined by Eq.(3) assuming that the bridge can be divided into several structural segments is inadequate, because the inertia force at each substructure significantly depends on flexibility and height of the substructure and type of the superstructure. Therefore, more rational method to evaluate the inertia force induced in the superstructure for the purpose of seismic design of substructure was required. The same demand also arises in the bridge where the superstructure and the substructure are not separated by means of bearing supports.

Therefore, in stead of the structural segment, a definition of seismic design structural unit, defined as the structural unit which can be considered to develop the same response during an earthquake, was newly introduced in the new specifications. Table 8 shows examples how the seismic design structural unit be selected for typical combinations of structural type and direction for evaluating the inertia force.

Natural period and the inertia force shall be determined as:

1)Seismic design structural unit consisting of a substructure and a part of superstructure supported by the substructure

In this case, there is essentially no difference with the previous specifications. Inertia force shall be determined by Eq.(4), and the natural period shall be computed as

$$T = 2.01 \sqrt{\delta} \qquad (4)$$

where

T : natural period, in second, of the seismic design structural unit

δ : lateral displacement, in meter, of

the substructure subjected to a lateral force equivalent with 80 % of the dead weight of a substructure above the ground surface assumed in seismic design and the dead weight of a part of the superstructure supported by the substructure.

It should be noted here that only the substructure on the ground surface assumed in seismic design shall be subjected to inertia force because the seismic force below the ground surface assumed in seismic design is disregarded in seismic design. The ground surface assumed in seismic design is generally taken as the bottom plane level of the footing in case of pile foundation. However, when the soil layers whose soil constant is assumed as zero due to possible soil failure such as liquefaction, the bottom of these layers is regarded as the ground surface assumed in seismic design.

2)Seismic design structural unit consisting of substructures and a part of superstructure supported by these substructures.

This is the case newly introduced in the new specifications. Natural period and the inertia force shall be evaluated in accordance with Fig. 4, i.e.,

i)Idealize a seismic design structural unit by a linear elastic frame model

ii)apply a lateral force equivalent with the dead weight of superstructure and substructure above the ground surface assumed in seismic design, and compute the natural period as

$$T = 2.01\sqrt{\delta} \qquad (5)$$

$$\delta = \frac{\int w(s)u(s)^2 ds}{\int w(s)u(s)ds} \qquad (6)$$

where

w(s) : dead weight of the seismic design structural unit (superstructure and substructure above the ground surface assumed in seismic design) at point s (tf/m)

u(s) : lateral displacement developed in the seismic design structural unit at point s (m) when subjected to w(s) in a direction considered in design.

iii)determine the seismic coefficient k_h depending on the natural period T.

iv)compute inertia force as

$$F_d = k_h \times F \qquad (7)$$

where

F_d : shear force (tf) / bending moment (tfm) due to inertia force

k_h : seismic coefficient

F : force developed in the seismic design structural unit when subjected to a lateral force equivalent with dead weight of seismic design structural unit above the ground surface assumed in seismic design (tf/tfm)

For substructure supporting girder bridges, shearing force developed at the center of gravity of superstructure shall be regarded as the lateral force for seismic design. However, when the inertia force computed by Eq.(7) is smaller than the inertia force computed by Eq.(3), the latter shall be adopted for design. This needs some explanations. The inertia force computed by Eq.(7) is approximately proportional to the stiffness of each substructure. This implies that the inertia force concentrates to the substructures with high stiffness, while reverse is true for the substructure with low stiffness. Inertia force takes even negative value when the stiffness of the substructure is extremely small as compared with other substrctures. However, when failure of the structure such as bearing supports occurs, the contribution of each substructure for supporting the inertia force of superstructure could be changed from the distribution computed by Eq.(7). Base on such considerations, lower limit for the inertia force evaluated by Eq.(7) was included.

6. STRENGTH OF SANDY SOIL LAYER FOR LIQUEFACTION

For saturated alluvial sandy layers within 20 m from the ground surface which have the water table within 10 m from the ground surface, and have D_{50}-value on the grain size accumulation curve between 0.02 and 2.0 mm, the liquefaction potential during an earthquake has to be checked. For those soil layers required for the check of liquefaction, liquefaction potential shall be evaluated in terms of liquefaction resistance factor F_L as

$$F_L = R/L \qquad (8)$$

where

F_L : liquefaction resistance factor

R : resistance of soil elements against dynamic load

L : dynamic load induced in soil ele-

ments during an earthquake

In the previous specifications the resistance R of soil elements against dynamic load was evaluated from N-value of standard penetration test and D_{50}-value. Because fine sand content is found an important factor, it was included for evaluating R.

7. CHECK OF BEARING CAPACITY OF REINFORCED CONCRETE PIERS FOR LATERAL FORCE

Even for a significant earthquake, the bridge has to avoid critical failure. Reinforced concrete pier which is the most important member for preventing critical failure of bridge has to have the required ductility as well as the strength. The check of bearing capacity for lateral load was introduced to avoid brittle failure of reinforced concrete piers in inelastic range. Check of bearing capacity for lateral load is advised for the reinforced concrete piers with small concrete section.

Fig. 5 shows a flow-chart of the check of bearing capacity of reinforced concrete piers for lateral force. Main steps of this check are the following :

1) Judgement of bearing capacity for lateral force

Bearing capacity for lateral force shall be checked as

$$P_a > k_{he} W \qquad (9)$$

where

P_a : bearing capacity of reinforced concrete pier for lateral force (tf)

k_{he} : equivalent horizontal seismic coefficient for check of bearing capacity for lateral load

W : equivalent dead weight (tf), and shall be determined as

$$W = W_u + c_P W_p \qquad (10)$$

$$c_P = \begin{cases} 0.5 & P_u \leqq P_a \\ 1.0 & P_u > P_a \end{cases} \qquad (11)$$

W_u : dead weight of a part of superstructure supported by the rein forced concrete pier (tf)

W_p : dead weight of the reinforced concrete pier (tf)

P_u : bearing capacity of reinforced concrete pier for flexural failure (tf)

P_a : bearing capacity of reinforced concrete pier for shear failure (tf)

When the check for the bearing capacity for lateral force by Eq.(9) cannot be satisfied, modification of the design has to be made so that the modified section, which is designed in accordance with the seismic coefficient method, satisfies Eq.(9). It is generally advised to increase the concrete section with decreasing the amount of reinforcement.

2)Equivalent horizontal seismic coefficient for check of bearing capacity for lateral force

Equivalent horizontal seismic coefficient for check of bearing capacity for lateral force shall be determined as

$$k_{he} = \frac{k_{ho}}{\sqrt{2\mu - 1}} \qquad (12)$$

$$k_{ho} = c_Z \cdot c_I \cdot c_R \cdot k_{hcD} \qquad (13)$$

where

k_{he} : equivalent horizontal seismic coefficient for check of bearing capacity for lateral force

k_{hc} : seismic horizontal coefficient for check of bearing capacity for lateral force

μ : allowable ductility factor

c_Z : modification factor for zone (refer to Fig. 2)

c_I : modification factor for importance (refer to Table 6)

c_R : modification factor for structural response (refer to Table 9)

K_{hcD} : standard horizontal seismic coefficient for check of bearing capacity for lateral force

The standard horizontal seismic coefficient k_{hcD} was determined so that it can represent a realistic ground motion developed during a significant earthquake with magnitude as large as 8.

3)Bearing capacity for lateral force and allowable ductility factor

Bearing capacity for lateral force P_a and the allowable ductility factor μ shall be determined based on the failure mode as :

a)Flexural failure

$$P_a = P_y + \frac{P_u - P_y}{\alpha} \qquad (14)$$

$$\mu = 1 + \frac{\delta_u - \delta_y}{\alpha \delta_y} \qquad (15)$$

where

P_u, δ_u : bearing capacity (tf) and ultimate displacement (m) for flexural failure

P_y, δ_y : yielding force (tf) an yielding

displament (m) for flexural failure

α : safety factor (=1.5)

b)Shear failure

$$P_a = P_s \quad (16)$$

$$\mu = 1 \quad (17)$$

where

P_s : bearing capacity (tf) for shear failure

8. DYNAMIC RESPONSE ANALYSIS

As number of bridges with complex dynamic response characteristic increases, unified stipulations for dynamic response analysis become required. Although only general consideration for selecting the input ground motion was described in the previous specifications, a simplified but practical input ground motion as well as an analytical model and evaluation of the results of the dynamic response analysis was introduced in the new specifications.

In principle, dynamic response analysis shall be made by means of response spectral analysis with use of an analytical model which simulates dynamic characteristics of the bridge. Acceleration response spectrum for the response spectrum analysis shall be determined as

$$S = c_Z \cdot c_I \cdot c_D \cdot S_0 \quad (18)$$

where

S : response spectrum for response spectrum analysis (gal)

c_Z : modification factor for zone (refer to Fig. 2)

c_I : modification factor for importance (refer to Table 6)

c_D : modification factor for damping, and shall be determined based on modal damping ratio h_i as

$$c_D = \frac{1.5}{40h_i + 1} + 0.5 \quad (19)$$

S_0 : standard response spectrum for response analysis method (gal) (refer to Table 10)

When the time history analysis is required, strong motion records which have the similar characteristics with S by Eq.(18) shall be used with the consideration on site condition and structural response of the bridge. Three ground acceleration records which were modified so that their response characteristics match with S_0 in Eq.(18) are provided in Appendix III. They can be used as the standard ground motions for the time history analysis.

Because the results of the dynamic response analysis highly depend on the analytical model and the properties assumed in the analysis, indiscriminate evaluation of the results is quite difficult. Therefore it is required to use the overall result of the analysis considering accuracy of the properties and the analytical model used in the analysis. It is stipulated in the new specifications that the results obtained by the dynamic response analysis shall be used for the check of seismic safety of the bridge based on the allowable stress and displacement which are referred in the seismic coefficient method.

9. CONCLUDING REMARKS

The proceeding pages presented the outline of the main points of the new Seismic Design Specifications for Highway Bridges issued in February 1990. In the new specifications, seismic coefficient method by combining the previous seismic coefficient method and the modified seismic coefficient method is adopted, and based on the allowable design approach this method is regarded as the basic seismic design method. Besides the design by means of the seismic coefficient method, for those bridges which require the check of ductility, the check of bearing capacity of reinforced concrete piers for lateral force is made. Dynamic response analysis can be made for the bridges which require precise analysis considering structural response.

REFERENCES

1) Kawakami,K., Kuribayashi,E., Iwasaki,T. and Iida,Y.: On Specifications for Earthquake Resistant Design of Highway Bridges, 7th Joint Meeting, Panel on Wind and Seismic Effects, UJNR, Tokyo, Japan, 1975

2) Kuribayashi,E., Iwasaki,T., and Ueda,O.: New Specifications for Earthquake Resistant Design of Highway Bridges in Japan, 12th Joint Meeting, Panel on Wind and Seismic Effects, UJNR, Washington, D.C., U.S.A., 1980

Table 1 History of Design Loads for Highway Bridges in Japan

Year	Name of Regulations	Design Live Loads				Impact Loads	Seismic Loads k: Horizontal Seissmic Coefficient	Major Earthquake
		Class	Truck Roller Loads Streetcar	Uniform Loads	Line Loads			
1) 1886	Order No. 13 Ministry of Home Affairs (MHA)			U-454 kg/m	–	not considered	not considered	
2)	Order MHA		R-13.6 t S-12.7	U-400 600 kg/m (carriage way) U-270 400 kg/m (footway)		not considered	not considered	
3) 1919	Road Laws MHA		R-13.6 t T-11.2 t S-30 t	Same as 2)	–	not considered	not considered	
4) 1926	Specifications for Design of Roads, Road Laws, MHA	1st 2nd 3rd	T-12 t T-8 T T-6 t	U-600 kg/m U-500 kg/m U-500 kg/m	–	considered	Seismic Coefficient Method K=0.15~0.4 depending on location and ground condition ($k_h \geq 0.3$ advised in Toyo, Yokohama)	
5) 1939	Specifications for Design of Steel Road Bridges, MHA	1st 2nd	T-13 t T-9 T	U-500 kg/m U-400 kg/m		considered	Seismic Coefficient Method k_h=0.2, k_v=0.1	1946, Nankai (M=8.1) 1948, Fukui (M=7.3) 1952, Tokachi-oki (M=8.2) 1964 Niigata (M=7.5)
6) 1956 (and 1964)	Revision of Specifications for Design of Steel Road Bridges, JRA	1st 2nd	T-20 t T-14 t	– –	L-20 (5t.m) L-14 (3.5 t/m)	considered	Seismic Coefficient Method k=0.1~0.35 depending on location and ground conditions	
7) 1964 to 1971	Specifications for Design of Substructure of Road Bridges, JRA	Same as 6)					Same k as (6) Detailed calculation methods	
8) 1971	Specifications for Earthquake-Resistant Design of Highway Bridges, JRA	Same as 6)					Seismic Coef. method k=0.1~0.24 (Rigid) Modified SCM. K=0.05~0.3 (Flexible)	1978 Miyagiken-oki (M=7.4)
9) 1980 Modified SCM	Part V Seismic Design Specifications for Highway Bridges JRA	Same as 6)					Seismic Coef. Method k=0.1~0.24 (Rigid) k=0.05~0.3 (Flexible) Earthquake Response Analysis (Very Flexible Bridges)	
10) 1990	Same as 9)	Same as 6)					Seismic Coefficient Method k=0.1~0.3 Bearing Capacity of RC Piers for Lateral Load Dynamic Response	1982 Urakawa-oki (M=7.1) 1982 Nihon-kai-chubu (M=7.7)

Table 2 Seismic Damage in Recent Earthquakes

Year	Major Earthquake	Change of Major Seismic Damage	Seismic Design Method	Seismic Inspection and Retrofitting
1920	1923 Kanto Earthquake (M7.9)	Failure of Superstructure due to Tilting/Movement of Foundation		
1930			1926 Initiation of Seismic Design (Stipulations for Road Construction)	
1940		Failure of Concrete around Fixed Bearing	1939 Introduction of Standard Seismic Coefficient (Specifications for Steel Bridge)	
1950	1946 Nankai Earthquake (M8.1) 1948 Fukui Earthquake (M7.3) 1952 Tokachi-oki Earthquake (M8.1)	Damage due to Liquefaction		
1960	1964 Niigata Earthquake (M7.5)	Failure of RC Piers, and Bearing	1956 Seismic Coefficient depending on Zone and Ground Condition (Specifications for Steel Bridge)	
1970			1971 • Seismic Coefficient depending on Zone, Ground Conditions, Importance and Structural Response • Introduction of Evaluation Method for Liquefaction (Specifications for Seismic Design)	1971 Seismic Inspection 1976 Seismic Inspection
1980	1978 Miyagi-ken-oki Earthquake (M7.4) 1982 Urakawa-oki Earthquake (M7.1) 1983 Nihon-kai-chubu Earthquake (M7.7)		1980 • Part V Seismic Design, Specifications for Design of Highway Bridge • Introduction of New Evaluation Method for Liquefactions	1979 Seismic Inspection 1986 Seismic Inspection
1990			1990 Part V Seismic Design, Specificatins for Design of Road Bridge	

Table 3 Table of Contents of 1990 Seismic Design Specifications of Highway Bridges

Contents		Same as 1980 Specs.	Modified		Newly Introduced
			Slightly	Completely	
Chapter 1	General 1.1 Scope	○			
	1.2 Definition of Term		○		
Chapter 2	Basic Principle for Seismic Design		○		
Chapter 3	Design Load and Design Condition in Seismic Design 3.1 Design Load and Load Combination in Seismic Design		○		
	3.2 Effect of Earthquake	○			
	3.3 Inertia Force 3.3.1 General			○	
	3.3.2 Calculation of Natural Period			○	○
	3.3.3 Calculation of Inertia Force			○	○
	3.4 Earth Pressure during Earthquake	○			
	3.5 Hydrodynamic Pressure during Earthquake		○		
	3.6 Classification of Ground Condition in Seismic Design		○		
	3.7 Soil Layers Whose Bearing Capacities are Reduced in Seismic Design 3.7.1 General				○
	3.7.2 Sandy Layer Vulnerable for Liquefaction		○		
	3.7.3 Very Soft Clayey and Silty Layer	○			
	3.7.4 Treatment of Soil Layers Whose Bearing Capacities are Reduced in Seismic Design	○			
	3.8 Ground Surface Assumed in Seismic Design	○			
Chapter 4	Design Seismic Coefficient 4.1 General	○			
	4.2 Design Horizontal Seismic Coefficient			○	
	4.3 Factors for Modifying Standard Design Horizontal Seismic Coefficient			○	
Chapter 5	Check of Bearing Capacity of Reinforced Concrete Pier for Lateral Load 5.1 General				○
	5.2 Check of Safety				○
	5.3 Horizontal Seismic Coefficient for Check of Bearing Capacity for Lateral Load 5.3.1 Equivalent Horizontal Seismic Coefficient for Check of Bearing Capacity for Lateral Load				○

Contents		Same as 1980 Specs	Modified		Newly Introduced
			Slightly	Completely	
Chapter 5 (cont't)	5.3.2 Design Horizontal Seismic Coefficient for Check of Bearing Capacity for Lateral Load				○
	5.4 Bearing Capacity for Lateral Load 5.4.1 Bearing Capacity for Lateral Load Allowable Ductility and Equivalent Natural Period				○
	5.4.2 Displacement and Lateral Load at Yielding and Ultimate Stage				○
	5.4.3 Bearing Capacity for Shear Failure				○
Chapter 6	Dynamic Response Analysis 6.1 General				○
	6.2 Analytical Method and Analytical Model 6.2.1 Analytical Method				○
	6.2.2 Analytical Model				○
	6.3 Input Motion for Dynamic Response Analysis 6.3.1 Acceleration Response Spectral Value for Response Spectral Analysis				○
	6.3.2 Grond Motion for Time History Analysis				○
	6.4 Check of Safety				○
Chapter 7	General Provisions for Structural Details in Seismic Design 7.1 General		○		
	7.2 Devices for Preventing Superstructures from Falling 7.2.1 General		○		
	7.2.2 Stoppers at Movable Bearing		○		
	7.2.3 Length between End of Girder and Edge of Substructure		○		
	7.2.4 Devices for Preventing Superstructure from Falling		○		
	7.3 Structural Details at Bearing		○		
Chapter 8	Devices Expecting to Reduce Seismic Effects			(○)	
Appendices	I. References on Liquefaction		○		
	II. Examples of Classification of Ground Condition		○		
	III. Reference on Design Ground Motion			○	
	IV. Example of Calculation of Natural Period and Inertia Force			○	
	V. Reference on Bearing Capacity of Reinforced Concrete Pier for Lateral Load and Example of Calculation				○
	VI. Practices of Structural Details		○		

Table 4 Classification of Ground Conditions

1980 Specifications			1990 Specifications	
1	$T_G < 0.2$	(Rock)	I	$T_G < 0.2$
2	$0.2 \leqq T_G < 0.4$	(Diluvium)	II	$0.2 \leqq T_G < 0.6$
3	$0.4 \leqq T_G < 0.6$	(Alluvium)		
4	$0.6 \leqq T_G$	(Soft Alluvium)	III	$0.6 \leqq T_G$

Table 5 Ground Condition Factor c_G

Ground Group	I	II	III
c_G	0.8	1.0	1.2

Table 6 Importance Factor c_I

Group	c_I	Definition
1st class	1.0	Bridges on expressway (limited access highways), general national road and principal prefectural road. Important bridges on general prefectural road and municipal road.
2nd class	0.8	Other than the above

Table 7 Structual Response Factor c_T

Ground Group	Structural Response Coefficient c_T		
Group I	$T < 0.1$ $c_T = 2.69T^{1/3} \geqq 1.00$	$0.1 \leqq T \leqq 1.1$ $c_T = 1.25$	$1.1 < T$ $c_T = 1.33T^{-2/3}$
Group II	$T < 0.2$ $c_T = 2.15T^{1/3} \geqq 1.00$	$0.2 \leqq T \leqq 1.3$ $c_T = 1.25$	$1.3 < T$ $c_T = 1.49T^{-2/3}$
Group III	$T < 0.34$ $c_T = 1.80T^{1/3} \geqq 1.00$	$0.34 \leqq T \leqq 1.5$ $c_T = 1.25$	$1.5 < T$ $c_T = 1.64T^{-2/3}$

Table 8 Seismic Design Structual Unit

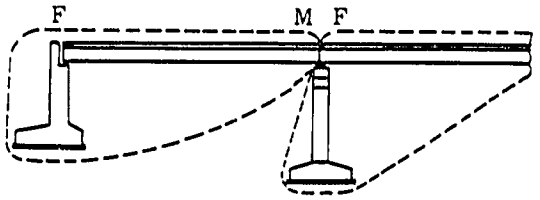
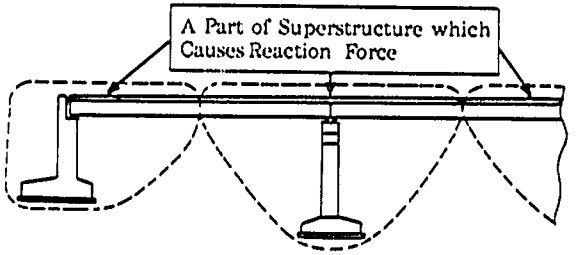
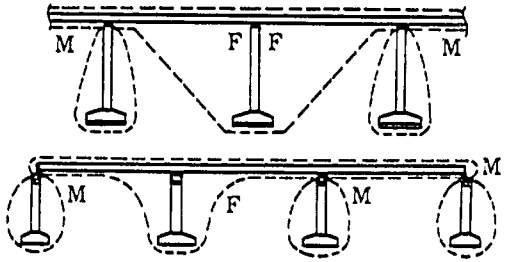
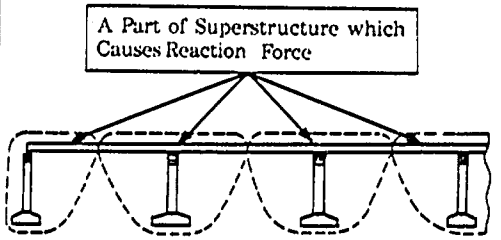
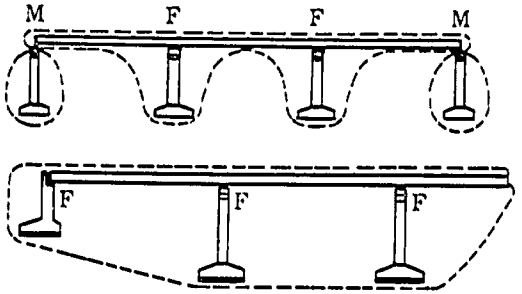
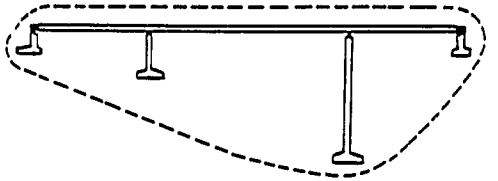
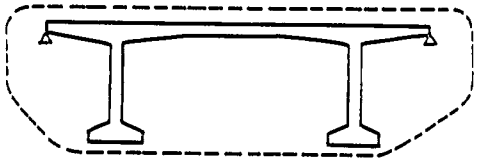
	Longitudinal			Transverse			Seismic Design Unit
Simple Girder							Regarded as A Unit Consisting of A Substructure and A Part of Superstructure Supported by the Substructure
Continuous Girder	Support Condition in Longitudinal Direction	Fixed at One Support		Difference of Natural Period between Piers	Small		
		Fixed at Multiple Supports			Large		Regarded as A Unit Consisting of Substructures and the Superstructure Supported by the Substructures
Arch, Frame and Others							

Table 9 Structual Response Factor c_R

Ground Group	Structural Response Coefficient c_R		
Group I	$T_{EQ} \leqq 1.4$ $c_R = 0.7$		$1.4 < T_{EQ}$ $c_R = 0.876T_{EQ}^{-2/3}$
Group II	$T_{EQ} < 0.18$ $c_R = 1.51\ T_{EQ}^{1/3} \geqq 0.7$	$0.18 \leqq T_{EQ} \leqq 1.6$ $c_R = 0.85$	$1.6 < T_{EQ}$ $c_R = 1.16T_{EQ}^{-2/3}$
Group III	$T_{EQ} < 0.29$ $c_R = 1.51T_{EQ}^{1/3} \geqq 0.7$	$0.29 \leqq T_{EQ} \leqq 2.0$ $c_R = 1.0$	$2.0 < T_{EQ}$ $c_R = 1.59T_{EQ}^{-2/3}$

Table 10 Structual Response Spectral Value S_o

Ground Condition	S_o (gal)		
Group I	$T_i < 0.1$ $S_o = 431T_i^{1/3} \geqq 160$	$0.1 \leqq T_i \leqq 1.1$ $S_o = 200$	$1.1 < T_i$ $S_o = 220/T$
Group II	$T_i < 0.2$ $S_o = 427T_i^{1/3} \geqq 200$	$0.2 \leqq T_i \leqq 1.3$ $S_o = 250$	$1.3 < T_i$ $S_o = 325/T_i$
Group III	$T_i < 0.34$ $S_o = 430T_i^{1/3} \geqq 240$	$0.34 \leqq T_i \leqq 1.5$ $S_o = 300$	$1.5 < T_i$ $S_o = 450/T_i$

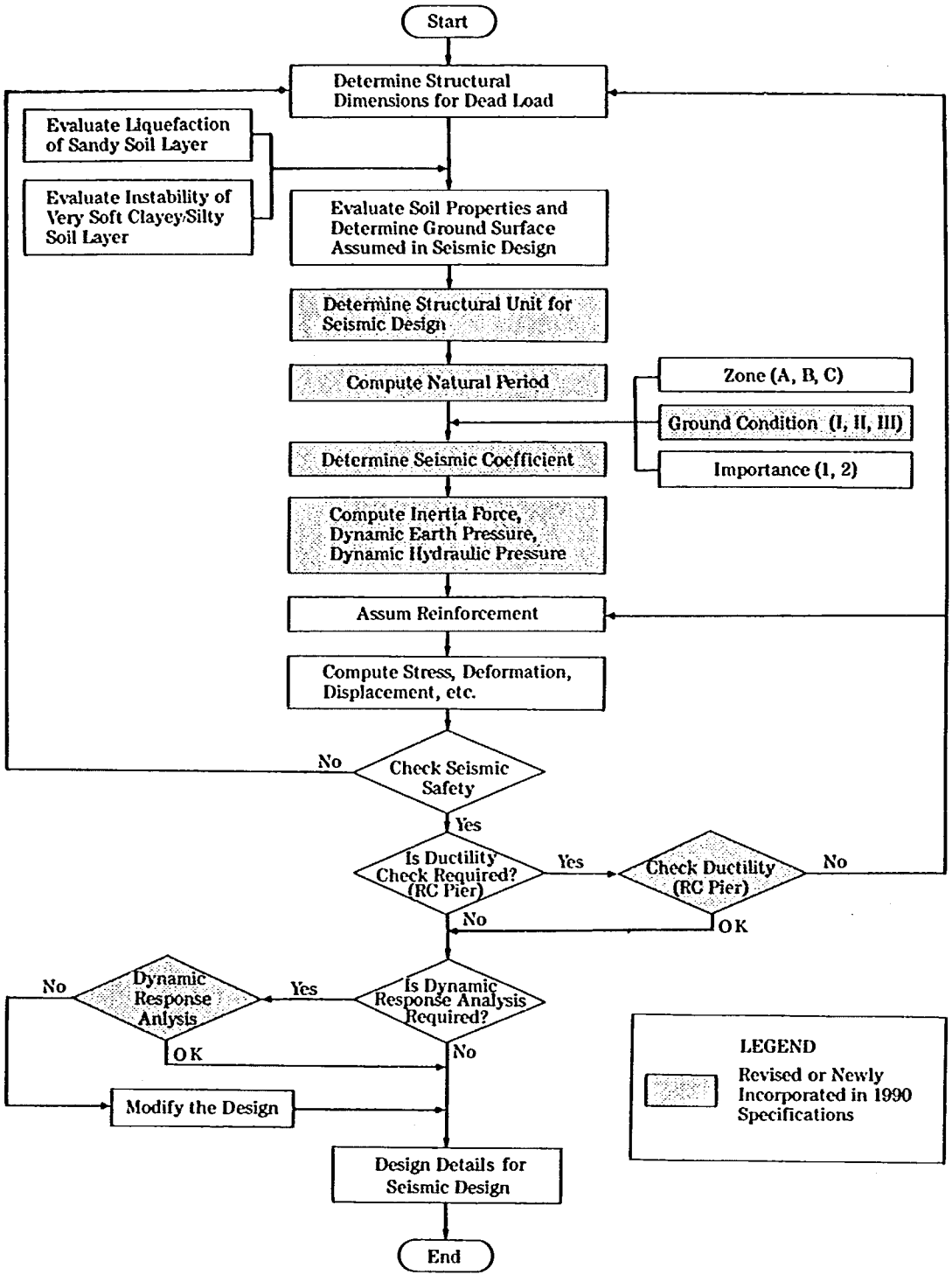


Fig.1 Flow of Seismic Design of Highway Bridge

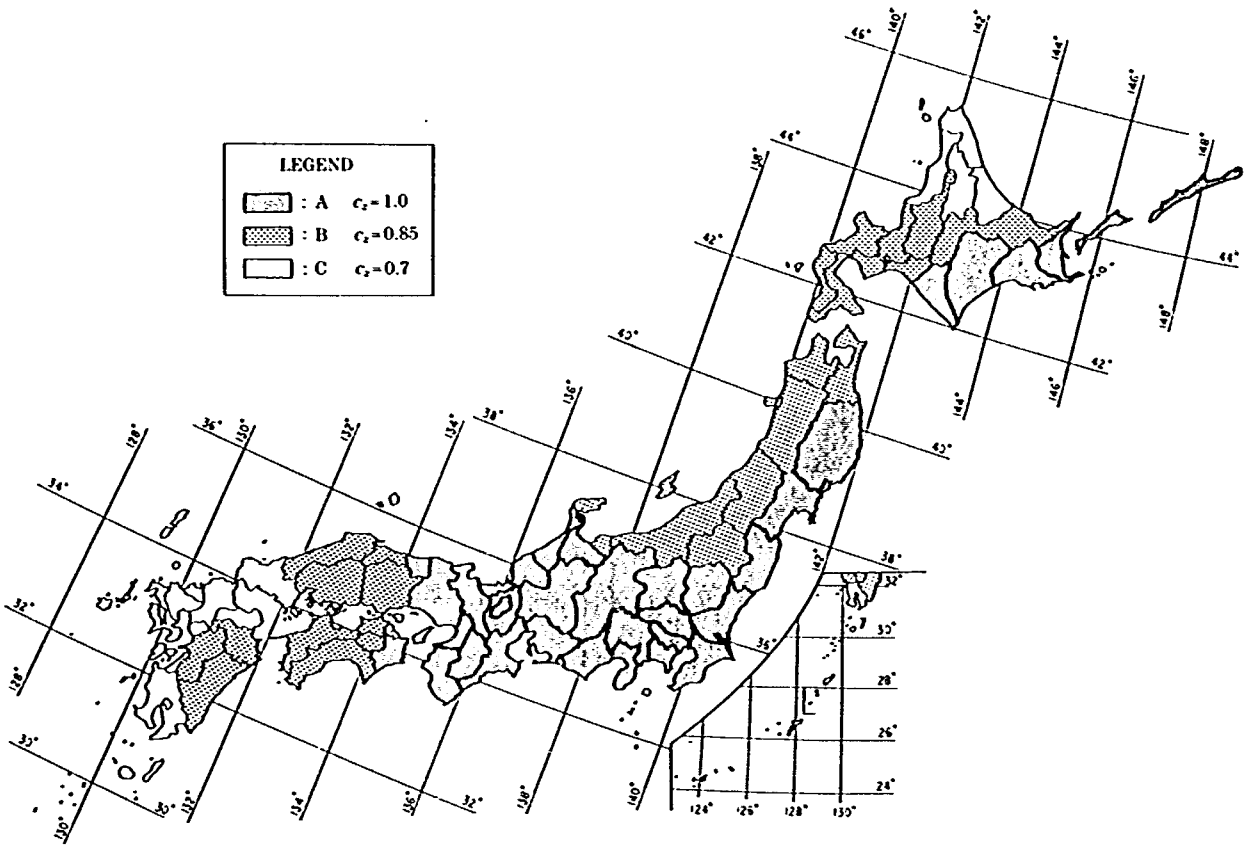
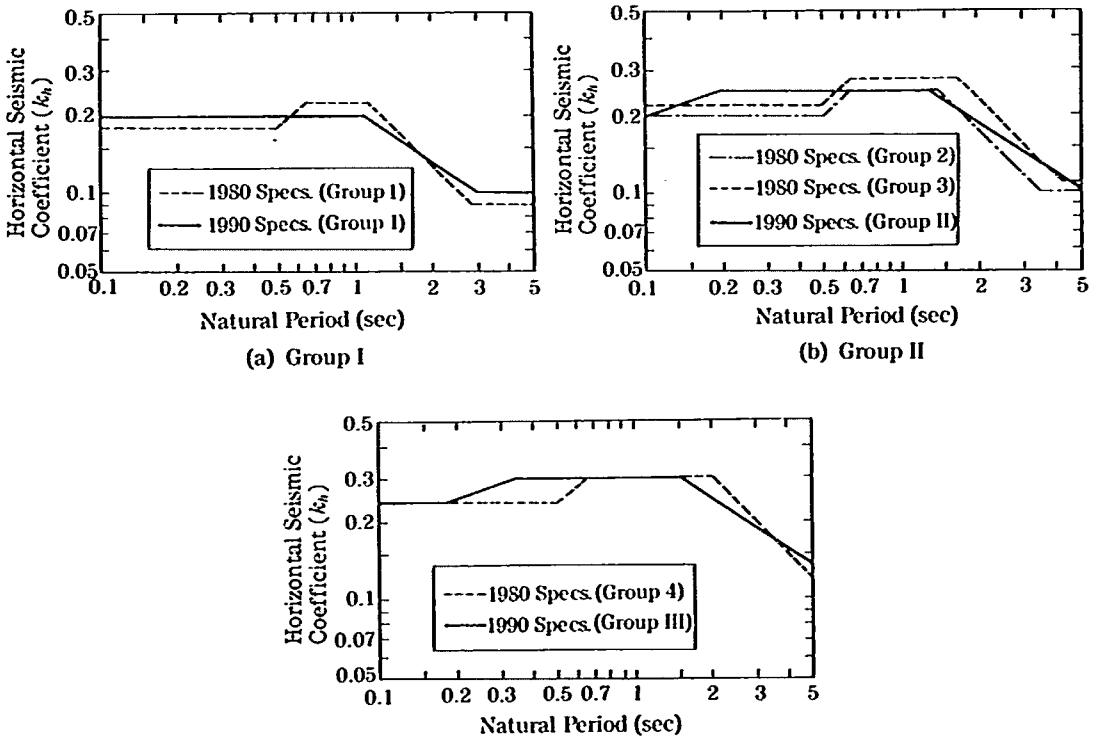


Fig.2 Seismic Zoning Map and Modification Coefficient c_z



(a) Group I

(b) Group II

(c) Group III

Fig.3 Comparison of Seismic Coefficient between 1980 and 1990 Specifications

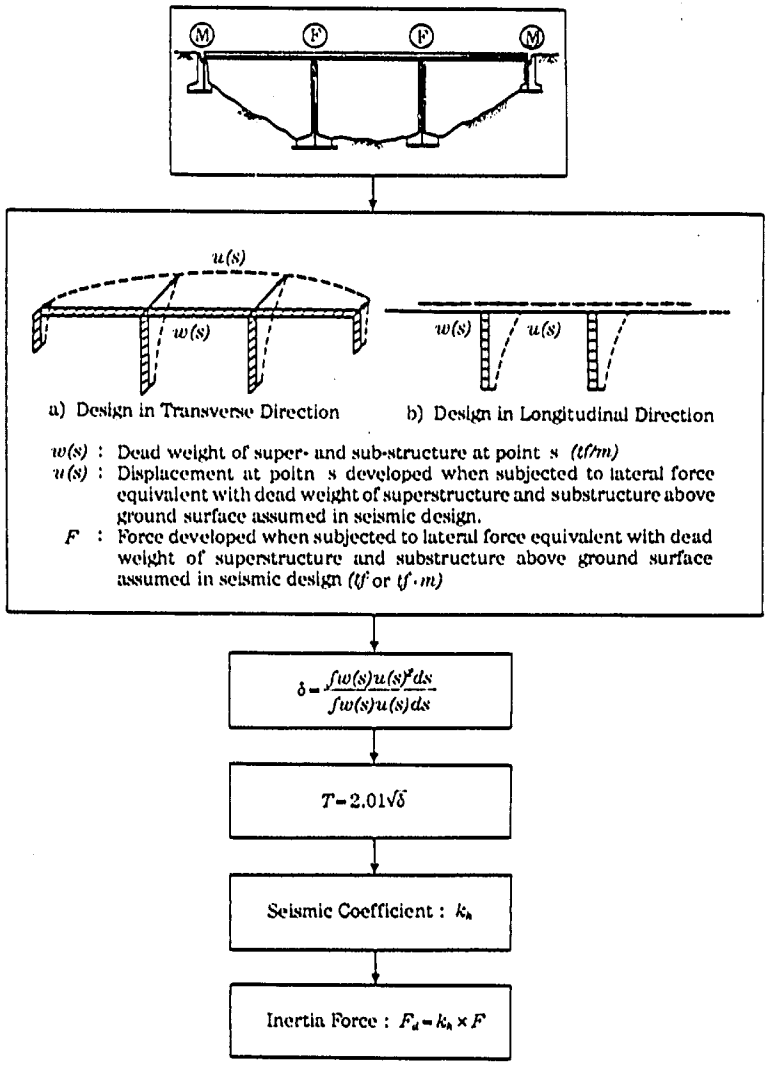


Fig.4 Determination of Inertia Force

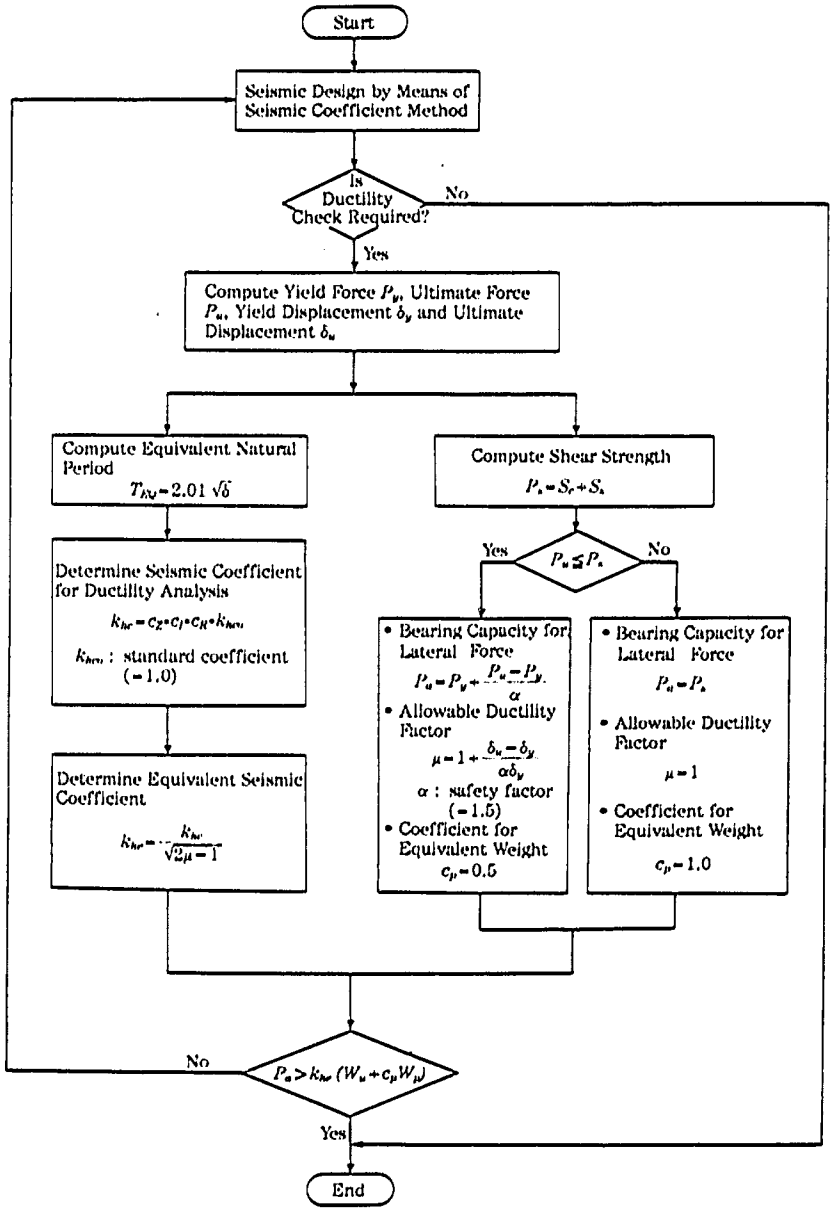


Fig.5 Check of Bearing Capacity of Reinforced Concrete Pier for Lateral Force

CURRENT RESEARCH EFFORTS IN JAPAN FOR PASSIVE AND ACTIVE CONTROL OF HIGHWAY BRIDGES AGAINST EARTHQUAKE

by
Kazuhiko KAWASHIMA
Kinji HASEGAWA
Shigeki UNJOH
Hiroyuki NAGASHIMA
and
Hideyuki SHIMIZU
Public Works Research Institute
Ministry of Construction

23rd Joint Meeting
U.S. — Japan Panel on Wind and Seismic Effects, U.J.N.R.
Tsukuba Science City, Japan
May 1991

CURRENT RESEARCH EFFORTS IN JAPAN FOR PASSIVE AND ACTIVE CONTROL OF HIGHWAY BRIDGES AGAINST EARTHQUAKE

Kazuhiko KAWASHIMA[1], Kinji HASEGAWA[2], Shigeki UNJOH[3], Hiroyuki NAGASHIMA[3], and Hideyuki SHIMIZU[4]

ABSTRACT

This paper presents current research activities on passive, active and hybrid control for application to bridge structures conducted at the Public Works Research Institute.

KEY WORDS : Highway Bridges, Menshin Systems, Active Control, Hybrid Control

1. INTRODUCTION

Menshin systems (Base-isolation), which is being introduced for application to highway bridges in Japan[1,2], is to reduce earthquake response of highway bridges by "Passive Means". On the other hand, active control is to control it by "Active Means." Since external energy supply required to reduce the bridge response to satisfactory level is significant during a significant earthquake in the active control, it is still in a laboratory. Therefore, "Hybrid" control, which is a combination of advantages of passive and active control, is promising for reducing the earthquake response of structures with small amount of external energy. The development of hybrid control for improving the seismic safety of highway bridges, which can not be achieved by extending current seismic design method, is expected[1].

A series of researches, and developments on passive, active and hybrid control for highway bridges have been made at the Public Works Research Institute since 1987. This paper briefly presents current research activities on passive, active and hybrid control for application to bridge structures conducted at the Public Works Research Institute.

2. DEVELOPMENT OF MENSHIN SYSTEMS

2-1 Joint Research Program on Menshin Systems for Highway Bridges

For studying the application of the menshin systems (passive control) to the seismic design of highway bridges, a committee chaired by Professor Tsuneo Katayama, University of Tokyo, was formulated through 1986 to 1989 at the Technology Research Center for National Land Development. Three programs were studied in the committee, i.e., 1) a survey of menshin devices which can be used for highway bridges, 2) a study on the key points of the design of menshin highway bridges, and 3) designs of menshin highway bridges. As the final accomplishment of the study, "Guidelines for Design of Menshin Bridges (draft)" was published in 1989[3].

Based on the study above, the three-year joint research program on the menshin systems for highway bridges is now underway between Public Works Research Institute and twenty eight private firms since the year of 1989. The goal of the program is to develop the menshin design method and the new menshin devices for highway bridges in order to improve the seismic performance of new and existing bridges with less cost by the menshin systems. Fig.1 shows the research items of the program, which are outlined in the follows[4].

2-2 Development of New Menshin Devices

A lot of base isolation devices which are similar to the menshin device have been ever developed for building structures. However, the menshin devices for highway bridges have to be more compact and more weather-proof than the devices for building structures since the menshin devices would be installed at narrow and exposed crests of bridge columns. The new menshin devices should be developed exclusively for menshin highway bridges to be effectively constructed in Japan.

The following ten new devices in the six types are now being developed under the research program.

1) High Damping Rubber Bearing----- 4 devices
2) Sliding Friction Damper---------- 2 devices
3) Steel Damper ---------- 1 device
4) Roller Menshin Bearing ---------- 1 device
5) Link Bearing ---------- 1 device
6) Viscous Damper ---------- 1 device

All developed menshin devices but the link bearing were tested by the loading experiment system of PWRI under the same loading conditions to verify their performance. In the tests, the cyclic lateral force was given to the devices by the actuator under the constant axial force, which is equivalent to the dead load of the superstructure, as shown in Photo 1. Since the performance of some devices could be affected by the temperature, the tests were conducted in the room shown in Photo 2, where the temperature was kept at 20 ℃.

---

1) Head of Earthquake Engineering Division, Earthquake Disaster Prevention Department, Public Works Research Institute, Ministry of Construction, Tsukuba Science City, 305 Japan
2) Senior Research Engineer, ditto
3) Research Engineer, ditto
4) Assistant Research Engineer, ditto

Fig.2 shows the lateral force vs. displacement hysteresis loops of a high damping rubber bearing and a sliding friction damper. It is said that the damping effect of every tested devices is satisfactory for highway bridges and the dynamic character is also stable with the smooth hysteresis loop.

The standard of the test procedure for menshin devices are being specified under the research program in order to certify the other devices which would be developed for highway bridges in future. There are two main items in the procedure, one of which is related to the performance as a support such as the check of the vertical stiffness, and the other is related to the dynamic horizontal performance as a menshin device such as the check of the stability under the repeated cyclic lateral loading, the check of the dependency on the loading velocity or frequency, the check of the dependency on the axial force, the check of the dependency on the lateral loading direction and the check of the dependency on the temperature. The test condition for each item and the evaluation of the test result have been formulated. The size and shape of the specimens, the loading test apparatus and the loading process will be standardized.

2-3 Development of Expansion Joints and Restrainers for Menshin Bridges

The knock-off mechanism and the finger expansion joint which is distinguished from the regular finger joints by the transverse movement, are being developed under the research program. The restrainer which consists of the steel bar installed in the crest of the substructure and the steel casing with the high damping rubber inside installed under the superstructure, is also being developed.

The knock-off mechanism is illustrated in Fig.3[5]. If the excessive displacement of the girder toward the abutment were brought by earthquakes, the apron of the slab would collide with the top portion of the abutment. Since the portion is not actually fixed to the abutment itself, it would be squeezed into the backfill behind the abutment to ease the impact induced by the collision.

The mechanism was tested as shown in Fig.4, in which the top portion was pressed back into the backfill by the actuator, in order to observe the situation of the squeeze and the damage of the backfill, and measure the resistant force of the backfill[6]. Photos 3 and 4 show the specimen and the situation after the test, respectively. Fig.5 shows the lateral force vs. displacement curve of the mechanism. It is seen that the impact force could be mitigated and the extensive displacement of the girder would be controlled by the mechanism.

2-4 Development of Menshin Design Method

Fig.6 illustrates the flow of the menshin design method, in which the two levels of the design earthquake loading are considered as limited states. The lower level, Level 1, is equivalent to the design seismic force of the seismic coefficient method regulated in the Design Specifications of Highway Bridges - Part V Seismic Design. This represents the seismic force for moderate earthquakes which are supposed to take place with higher probability. The higher level, Level 2, is equivalent to the design seismic force of the check of the bearing capacity of the reinforced concrete columns for the lateral force regulated in the specification, for larger earthquakes, such as Kanto earthquake in 1923, which are supposed to take place rarely[7][8]. The design procedure will be formulated, being based on the flow.

2-5 Application of Menshin Design

Since expansion joints make annoying noise and are vulnerable to the traffic load, continuous bridges tend to be constructed recently with the demand of lowering the number of joints. Therefore, one target of the menshin systems is to construct continuous bridges. The multi-span continuous bridge with the girder length more than 1 km, which is called in the research program as a super multi-span continuous bridge, is highlighted as a crucial research item. It was concluded that the super multi-span continuous bridge with 26 spans as shown in Fig.7 could be constructed with the menshin system.

Existing simple girders would be connected one another in order to also decrease expansion joints between adjacent simple girders. Since the inertia force of the girder transmitted to each substructure might be varied by the connecting, the strengthening of some substructures would be required due to the lack of the bearing capacity. It was deduced that the distribution of the inertia force could be intentionally adjusted with proportion to the capacity of each substructure, by the replacement of the existing ordinary fixed or movable bearings with the menshin devices. The construction method and the structural detail of the connecting and the replacement will be examined under the research program.

2-6 Draft Manual for Menshin Design of Highway Bridges

The program will be accomplished in March, 1992. The draft manual of the menshin design method, the contents of which are shown in the follows, is to be composed as the fruits of the research program.

Chapter 1 INTRODUCTION

1.1 Purpose of Manual

1.2 Application of Manual
1.3 Definitions of Terms

Chapter 2 BASIC CONCEPTS
2.1 Purpose of Menshin Design
2.2 Earthquake Levels and Limited States
2.3 Seismic Design Force of Menshin Design
2.4 Design Method and Criterion of Safety Check
2.5 Basic Flow Charts of Menshin Design
2.6 Application of Menshin Design

Chapter 3 DESIGN AND CHECK OF SUPERSTRUCTURE

Chapter 4 DESIGN AND CHECK OF SUBSTRUCTURE
4.1 General
4.2 Design Acceleration for Substructure

Chapter 5 DESIGN METHOD OF MENSHIN DEVICES
5.1 Basic Concept of Design
5.2 Design Acceleration for Menshin Devices
5.3 Rubber Bearing
5.4 Lead Rubber Bearing
5.5 High Damping Rubber Bearing
5.6 Steel Damper
5.7 Friction Damper
5.8 Viscous Damper

Chapter 6 CHECK OF MENSHIN BRIDGES BY DYNAMIC ANALYSIS
6.1 General
6.2 Input Motion of Dynamic Analysis
6.3 Dynamic Analysis Method
6.4 Safety Check by Dynamic Analysis

Chapter 7 STRUCTURAL DETAILS OF MENSHIN BRIDGES
7.1 General
7.2 Restrainers
7.3 Structural Details of Menshin Devices
7.4 Structural Details of Expansion Joints

Chapter 8 CERTIFICATION TESTS OF MENSHIN DEVICES
8.1 General
8.2 Dynamic Loading Test
8.3 Static Loading Test
8.4 Ultimate State Test

Chapter 9 RETROFITTING BY MENSHIN DESIGN
9.1 General
9.2 Application of Menshin Design for Retrofitting
9.3 Design Method of Menshin Devices for Retrofitting
9.4 Construction of Menshin Devices for Retrofitting
9.5 Structural Details of Retrofitting

Appendix I References for Design
Appendix II Design Examples

3. CONSTRUCTION OF MENSHIN HIGHWAY BRIDGES

3-1 Pilot Construction of Menshin Highway Bridges

Five pilot menshin highway bridges as shown in Table 1 are under construction with the supervision of Ministry of Construction, in order to verify the performance of the menshin system. One of them, Miyagawa Bridge in Shizuoka-ken, was completed and opened for the public traffic in March 15, 1991 as the first menshin highway bridge in Japan.

3-2 Miyagawa Bridge
- First Menshin Highway Bridge -

1)Outline of Miyagawa Bridge

The Miyagawa bridge located at Haruno-machi, Shu-ti-gun, Shizuoka-ken, is a three-span continuous steel plate girder bridge with the total length of 105.8 m and the width of 10.5 m as shown in Fig.8, which spans over the Ketagawa river as a bridge of the national highway No. 362[9]. The rubber bearings with the lead plug inserted at the center shown in Photo 5, which were developed in New Zealand and are usually designated as lead rubber bearings [10][11], were used as the menshin devices. Although the lead rubber bearing is originally movable to any lateral direction, the restrainers were installed to prevent the bearing from the transverse movement so that the menshin system works only in longitudinal direction.

2)Menshin Design

The bridge was designed in accordance with the Design Specifications of Highway Bridges. Table 2 summarizes the natural period, the design horizontal acceleration and the design relative displacement of the bearing for both the seismic coefficient method and the check of the bearing capacity of the reinforced concrete columns for the lateral force. The design acceleration is 0.2 g with the natural period of 0.76 sec in the seismic coefficient method. It is 0.54 g with the natural period of 1.01 sec in the check of the bearing capacity, when energy dissipation effect of the base-isolated devices is taken into account. However, since the bridge is one of the first menshin bridges in Japan, the damping effect of the devices was not taken into account in the check of the bearing capacity. Therefore, the design acceleration of 0.7 g which was obtained by assuming that the energy dissipation of the devices is zero, was used in the check of the bearing capacity.

Since the menshin system triggers off the larger displacement of the superstructure relative to the substructure than the ordinary bridges, the sufficient gap should be kept between the abutment and the girder, and at the expansion joint. On the other hand, the larger gap at the expansion joint would bring the vulnerability to the traffic load. Therefore, the following concept was adopted that the gap between the abutment and the girder should be decided as the girder would not collide to the abutment when it is subject to earthquakes for the check of the bearing capacity, and the gap at the expansion joint should be made equivalent to the relative displacement developed at the expansion joint by earthquakes of the seismic coefficient method. It was followed that the gaps between the abutment and the girder were 150 mm and the gaps at the expansion joints were 50 mm.

3) Field Vibration Test

The free vibration tests were conducted under the joint research program between the Earthquake Engineering Division of PWRI and the Shizuoka-ken government prior the opening in order to verify the effect of the menshin system. The three hydraulic static jacks owned by the Research Institute of Japan Highway Public Corporation were placed between the temporary steel frames assembled under the girder and the A2 abutment as shown in Photo 6. The force capacity of each jack is 150 tf and the maximum stroke is 150 mm. The force created by the jack can be released more rapidly than the regular static jack to develop the free vibration. The girder was forced by the jack to move against the abutment in the longitudinal direction to a certain displacement. The maximum displacement was decided as 8 cm so that the total force of the jacks should not exceed the capacity of the abutment.

The accelerations on the girder at each substructure (8 points), the accelerations on the crests of the substructures (8 points) and the displacement of the girder relative to each substructure (8 points) were recorded during the free vibration tests.

Fig.9 shows the relative displacement of the girder on the A2 abutment when the force of the jack was released at 8 cm. It is observed in the figure that the free vibration of the girder was developed in 0.75 sec after the release and the girder came nearly to a stop at 4 sec, remaining the residual displacement of 5.4 cm by the plastic resistant force of the lead plug.

Fig.10(a) shows the general model for the lateral load vs. displacement relation of the lead rubber bearing. Since the load consists of the linear restoring force of the rubber and the plastic restoring force of the lead plug, the relation can be expressed as a combination of the linear spring model and the friction model shown in Figs.10(b) and (c), respectively. The natural period and the damping effect was analyzed with a simple single degree of freedom oscillation system as shown in Fig.11, which is a model for the girder and the lead rubber bearings.

The spring constant and the friction force necessary for the analysis were obtained from the result of the loading tests, which had measured the lateral load vs. displacement relation of the lead rubber bearing prior to the construction, as 2,351 tf/m and 173.8 tf, respectively. The result of the analysis is also shown with a dotted line in the Fig.9.

The analysis evaluates the test very well in the first 0.75 sec after the release. It can be derived that the dynamic performance of the menshin bridge could be assessed with the parameters obtained from the loading test of the bearing itself. The gradual decrease of the relative displacement after 0.75 sec observed in the test, could have to do with the creep of the lead plug.

The traffic vibration tests were also conducted by running the trucks under the joint research program between the Structure Division of PWRI and the Shizuoka-ken government. No unusual vibration due to the menshin system was monitored around the bearing.

The long-term measurement of the residual relative displacement after the release at 8 cm will be done since the end of a series of tests. The displacement was recovered to 0.9 cm at about one month later. It is said that the residual displacement of the bearing cause no practical problem.

At the Miyagawa bridge, the strong motion observation is now being made by the Shizuoka-ken government and Ground Vibration Division of PWRI.

4. ACTIVE CONTROL FOR SEISMIC RESPONSE OF HIGHWAY BRIDGES

4-1 Introduction

Applicability of an Active Mass Damper (refers as AMD in the following) for controlling earthquake response of highway bridges was investigated by using a single-degree-of freedom model and reported in the last joint meeting. The results showed that a great deal of external energy is required in order to control earthquake response in appropriate level by means of AMD. The mass and/or stroke required are excessively large, and it seems not practical to control seismic response of bridge structures against a significant earthquake [12][13]. Hence, it is of great importance to develop hybrid control by combination of passive and active means.[13]

Development of hybrid control technology

was initiated at the Public Works Research Institute since 1989. Preliminary study on control of seismic response of highway bridges using multiple AMDs, which is basis for hybrid control is presented here.

The cooperative research program is being executed as a U.S.-Japan cooperative research program through the the Panel on Wind and Seismic Effects, UJNR. The program is being conducted at the Public Works Research Institute in Japan side, and at the National Institute for Standards and Technology, and at National Center for Earthquake Engineering Research[14] with supports of National Science Foundation in U.S. side. Major subjects of the program in Japan side includes investigations on ① passive control method and ② active control method for application to hybrid control as well as ③ optimum hybrid control which combines them appropriately.

4-2 Highway Bridge Analyzed and Analytical Conditions

For studying where is the best point for control and effect of multiple control by means of AMD, the transverse response of three-span continuous girder bridge with length of 150m as shown in Fig.12 is analyzed. The bridge is modeled as a two-dimensional spring-mass model. Fundamental natural frequency is 1.67Hz, and this is a first flexural mode of the deck. The first mode is most predominant in the transverse response of the bridge.

For controlling the deck response by means of one AMD, the weight of a driving mass is assumed as 180tf, which corresponds to about 1/10 of the deck weight (1,950tf). Control by means of two AMDs was also studied, in which two AMDs were assumed to be installed on the girder at the P_1 and P_2 piers, respectively. Three cases are analyzed, that is, their weights are assumed to be 180tf each, 90tf each, and 120tf and 60tf (180tf in total). The spring coefficients, which supports driving masses, are assumed so that fundamental natural frequency of the mass of AMD be 1/4 of fundamental natural frequency of the bridge analyzed. Structural damping ratio of the bridge is assumed as 5%. A standard ground acceleration, which is specified in "Part V Seismic Design[7][8]" of the "Design Specifications for Highway Bridges", is used as an input motion.

Control algorithm of AMD follows the classical optimum feedback control method. The control force driving the mass of AMD is assumed as a linear combination of the values proportional to displacement and velocity of the structure and AMD. Proportional coefficients are called as control gain, and the optimum gain obtained by solving Riccatti's Algebraic Equation[15][16] is used.

4-3 Effect of Controlling Point by AMD

In order to investigate an optimum control point, the earthquake response analyses are conducted. AMD is assumed to be placed at the some points on the girder. Fig.13 shows peak response displacement and peak response acceleration of the girder. It is more effective in reducing seismic response of the girder when the AMD is installed near the center of the girder. Comparing with uncontrolled one, peak displacement of the girder decreases to 1/4 and peak acceleration decreases to about half. On the other hand, effectiveness is smaller when AMD is placed near the abutments. For example, when AMD is placed on Abutment A_2, although the response displacement becomes smaller by 15% than uncontrolled one, displacement response near the ends of girder becomes larger by about 13 times the uncontrolled displacement.

Therefore, it is more effective to install AMD at the point where the mode value of predominant mode shape is largest.

4-4 Effect of Multiple Control

In order to investigate effectiveness of multiple control, the earthquake response is analyzed, in which AMDs are assumed to be installed on the P_1 and P_2 piers. Fig.14 shows peak displacement and peak acceleration of the girder controlled at the two points. Results controlled by only one AMD is also shown in Fig.14 for comparison. Two-point control makes possible to decrease the seismic response of girder more significantly than the control by only one AMD. Effectiveness of control of the response and control force required by AMDs with the weight of masses of 180tf is almost same as those of 90tf both. Effect of the weight of driving masses appears only in stroke lengths of driving masses. The strokes of driving mass when the weight of driving masses is 90tf both is twice those when the weight is 180tf. Therefore, the weight of driving masses affects the stroke lengths of driving masses, but does not affect the effectiveness of control. The similar results can be obtained when the weight of driving masses are 60tf and 120tf each.

4-5 Concluding Remarks up to the Present

1) It is most effective that the AMD is installed at the point where the mode shape value of a predominant mode is largest for controlling the seismic response of continuous girder bridges.
2) Two-point control using AMDs is more effective than one-point control in reducing the displacement response and acceleration response of the girder. Since multiple control makes it possible to control the deck response against any mode shapes, it is required to further investigate the effect of the multiple-point control in detail.

5.DEVELOPMENT OF A VARIABLE DAMPER

5.1 Basic Concept of A Variable Damper for Highway Bridges

The variable damper is basically a viscous damper and the viscous damping force is variable depending on the response of structures (highway bridges) as shown in Fig.15. For instance, the damping coefficient of the damper is larger during the vibration within a small amplitude and the damper has the same function as a fixed bearing support against braking load of vehicles. It is, however, movable against the load with low velocity, such as elongation of girder by temperature change. Once an earthquake occurs and amplitude of vibration of girder becomes larger up to a certain level, the damping coefficient of damper decreases so that energy dissipation be optimum and inertia force to the substructure be adjusted appropriately. Furthermore, when the vibrational amplitude becomes excessive, the damping coefficient increases gradually in order to suppress the amplitude and so that the damper have a function as a stopper. Therefore, the variable damper has the advantages of an usual viscous damper-stopper, a passive energy dissipator and a stopper with a shock absorber. The required external energy by the variable damper for altering the damping coefficient is greatly smaller than usual active control devices because the width of the orifice of the damper can be changeable with a small amount of energy.

5.2 Earthquake Response Analysis of Multi-Degree-of-Freedom System with Variable Dampers

The equations of motion for a linear multi-degree-of-freedom model with the variable dampers may be written as

$$\underline{M}\,\ddot{\underline{x}} + (\underline{C} + \underline{C_v})\,\dot{\underline{x}} + \underline{K}\,\underline{x} = -\underline{M}\,\ddot{x}_D \qquad (1)$$

in which $\underline{M}$, $\underline{C}$ and $\underline{K}$ represent mass, damping and stiffness matrices of the structure, respectively. $\underline{x}$ and x_D denote displacement vector and ground displacement, respectively. $\underline{C_v}$ denotes a damping matrix of the variable dampers and is given by a function of relative displacement and relative velocity between the nodes where the variable dampers are installed. Since $\underline{C_v}$ is time-varying, Eq.(1) has to be solved by a direct integration method. According to the Newmark β method, velocity and displacement are assumed as

$$\dot{x}_i = \dot{x}_{i-1} + (1-\alpha)\Delta t\cdot\ddot{x}_{i-1} + \alpha\cdot\Delta t\cdot\ddot{x}_i \qquad (2)$$

$$x_i = x_{i-1} + \Delta t\cdot\dot{x}_{i-1} + (1/2-\beta)(\Delta t)^2\cdot\ddot{x}_{i-1} + \beta(\Delta t)^2\cdot\ddot{x}_{i-1} \qquad (3)$$

in which α and β are parameters of the Newmark β method and if a constant acceleration method is assumed α and β have to be taken 0.5 and 0.25, respectively.

Using the above analytical method, a computer program, named as "VDAM", which can analyse earthquake response of multi-degree-of-freedom system with the variable dampers was developed.

5-3 Highway Bridge Analyzed and Analytical Conditions

In order to investigate effectiveness of the variable damper, a simple span girder bridge, as shown in Fig.16, with a span length of 30m is analysed in the longitudinal direction. The model bridge has elastic isolator and the variable dampers are assumed to be installed between the superstructure and the top of substructure. The spring constant of elastic isolator is defined so that a fundamental natural period of the bridge be 1 second.

Fourteen cases in total are analysed as shown in Figs.17 and 18. In Case 1 the variable damper is not installed, in Cases 2 and 3 the damping coefficient of the damper is in dependent of displacement and/or velocity. The damping coefficients of Cases 2 and 3 are given so that damping ratio of critical be 5% (Case 2) and 100% (Case 3). In Cases 4 and 5, the damping coefficient is dependent on relative displacement as shown in Fig.17. Peak relative displacement d_u is defined as a peak relative displacement computed in Case 2 and it was assumed as 19.4cm. In Cases 6 and 7, the damping coefficient is dependent on relative velocity as shown in Fig.17. Peak velocity v_u is defined as a peak value (113 cm/s) computed in Case 2. Case 8 is a combination of Cases 4 and 6 and the damping coefficient of the damper is dependent on relative displacement and relative velocity.

A ground motion acceleration which was modified so that the response spectra matches with the target spectra is used as an input ground acceleration. The acceleration response spectrum, which is specified in "Part V Seismic Design" of the "Design Specifications for Highway Bridges", for the check of bearing capacity of reinforced concrete piers, is assumed as the target spectra.

Damping ratio of critical of a model bridge is assumed 2% as a modal damping.

5-4 Effectiveness of Variable Dampers on Earthquake Response of Highway Bridges

Table 3 shows the peak response of girder and the variable damper, where the peak values of displacement, velocity and acceleration of the girder and damping force, relative displacement and relative velocity of the damper are presented. Figs.19 and 20 compare time histories of displacement and acceleration

of the girder and damping force of the variable damper between Case 1 (without the variable damper), Case 5 (displacement dependent) and Case 7 (velocity dependent).

According to these results, the following remarks may be pointed out:

1) If the damping coefficient is dependent on relative displacement of the damper, it is effective to set larger damping coefficient around zero displacement (Case 5). The peak damping force in Case 5 becomes 58.2×2tf which corresponds to 48.2% of the weight of the deck (241.5tf). The damping force of 96.4tf makes reduction of acceleration of girder to 566gal/1300gal = 43.5%, and relative displacement of the girder to 13.25cm/33.04cm = 40.1% comparing with Case 1 in which the variable damper is not installed.

2) The damping force required to control the response up to the same level is smaller in displacement dependent dampers (cases 4 and 5) than in velocity dependent dampers (cases 6 and 7). This is because pulse-type large damping forces are required in the velocity dependent dampers. Large damping coefficient at the time when large velocity is developed causes large damping force. On the other hand, since the damping force is dispersed as time large damping forces are not required in the displacement dependent dampers.

3) The time history displacement shows that the variable dampers operate satisfactorily as a stopper which also has a function as a shock absorber without an impact response.

5-5 Development of A Pilot Model of the Variable Damper

Photos 7 - 9 show a pilot model of the variable damper developed. The model is designed so that the damping force be variable within 20kgf to 200kgf, maximum relative displacement of damper piston be ±5cm, and the weight be about 40kgf. The variable damper consists of an usual viscous damper and a control system. Damping characteristics of the variable damper is now being studied. Model experiments are planed.

5-6 Concluding Remarks up to the Present

1) In the displacement dependent dampers, it is effective to set larger damping coefficient around zero displacement.

2) The damping force required to control the response up to the same level is smaller in the displacement dependent dampers than in the velocity dependent dampers.

3) The time history response shows that the variable dampers operate satisfactorily as a stopper which also has a function as a shock absorber without an impact response.

4) The pilot model of the variable damper was developed. Experimental study on the characteristics and control method of the variable damper is being studied.

5) The variable damper seems to be near a practical use.

6.CONCLUSIONS

This paper briefly presents current research and development activities on passive, active and hybrid control for application to bridges structures conducted at Public Works Research Institute. It is thought that these technologies may become very important in future for constructing super-multiple continuous girder bridges, long-span bridges, bridges with high-rise piers, and bridges in urban area with strict land use restrictions.

REFERENCES

1) Kawashima, K. : Development and Future Scope of Seismic Isolation of Structures, - A Review -, Proc. of Japan Society of Civil Engineers, Structural Eng./Earthquake Eng., Vol.398/ I -10, 1988

2) Buckle, I. : Development and Application of Base Isolation and Passive Energy Dissipation - A World Review -, Proc. of A Seminar and Workshop on Base Isolation and Passive Energy Dissipation, pp.153～174, San Francisco, U.S.A., March 1986.

3) Guidelines for Design of Base-Isolated Highway Bridges, Final Report of A Committee for Study of Application of Base Isolation to Seismic Design of Highway Bridges (Chairman : Professor T. Katayama), Technology Research for National Land Development, March 1989

4) Public Works Research Institute : Report of Joint Research between PWRI and 28 Private Firms on Development of Menshin Systems for Highway Bridges, Technical Report of Cooperative Research, No.44 and No.60, March 1990 and March 1991, Public Works Research Institute

5) Chapman, H. E. and Kirkcaldie, D. K. : Seismic Design of Base Isolated Bridges Incorporating Mechanical Energy Dissipators, Transit New Zealand's 1990 Bridge Design and Research Seminar, Christchurch, New Zealand, November 1990

6) Goto, Y., Kikuchi, Y. and M. Kuroiwa : Investigation on a Knock-off Device as an Expansion Joint for Menshin Bridges, Proceedings of the 46th Annual Meeting of Japan Society of Civil Engineers, October 1991

7) Japan Road Association : Part V Seismic Design of the Design Specifications for Highway Bridges, February 1990

8) Iwasaki, T., Kawashima, K. and Hasegawa, K. : New Seismic Design Specifications for Road Bridge in Japan, 22nd Joint Meeting

U.S.-Japan Panel on Wind and Seismic Effects, U.J.N.R., NIST, Gaithersburg, May 1990
9) Matsuo, Y., O-ishi, A., Hara, K. and Yamashita, M. : Design and Construction of Miyagawa Bridge, - First Menshin Bridge in Japan -, Bridge and Foundation, Vol.91, No.2, pp15-21, February 1991
10) Taylor, R. G., and Robison, W. H. : High-strain Test on Lead Rubber Bearings for Earthquake Loadings, Bull. of the New Zealand National Society for Earthquake Engineer, Vol.17, No.2, pp90-105, June 1984
11) Bulling, I. J. and Kirkcaldie, D. K. : Base Isolation of Bridges in New Zealand, Proc. of New Zealand-Japan Workshop on Base Isolation of Highway Bridges, Wellington, New Zealand, November 1987
12) Kawashima, K., Hasegawa, K. and Yoshida, T. : Active Control of Seismic Response of Structure by Means of Mass Damper, Civil Engineering Journal, Vol.31-5, May 1989
13) Taguchi, J., Iwasaki, T., Adachi, Y., Sasaki, Y. and Kawashima, K. : U.S.-Japan Cooperative Research Program on Hybrid Control of Seismic Response of Bridge Structures, 22nd Joint Meeting, U.S.-Japan Panel on Wind and Seismic Effects, U.J.N.R., NIST, Gaithersburg, May 1990
14) Feng, Q. and Shinozuka, M. : Use of A Variable Damper for Hybrid Control of Bridge Response Under Earthquake, U.S. National Workshop on Structural Control Research, University of Southern California, CA., U.S.A., October 1990
15) Ito, M. : Automatic Control, Shokodo Publishing Co., February 1983
16) Kalman, R. E. : Contributions to the Theory of Optimal Control, Proc. 1959 Mexico City Conference on Differential Equations, Mexico City, 1960, pp102-199

Table 1 Pilot Program for Construction of Menshin Highway Bridges

Owner	Name of Bridge	Type of Superstructure	Total Length
Hokkaido developing Bureau	On-netoh Bridge	Steel Girder	456 m
Tohoku Regional Construction Bureau, MOC	Nagakigawa Bridge	Steel Girder	97 m
Iwate-ken	Maruki Bridge	Prestressed Concrete	92 m
Tochigi-ken	Daiichi Karasuyama Bridge	Prestressed Concrete	260 m
Shizuoka-ken	Miyagawa Bridge	Steel Girder	110 m

Table 2 Natural Period, Design Acceleration and Design Relative Displacement

Design Method	Item	A1	P1	P2	A2
Seismic Coefficient Method	Natural Period (sec)	0.764			
	Design Acceleration (g)	0.20			
	Design Relative Displacement (mm)	28.2	21.8	20.2	28.0
Check of Bearing Capacity	Natural Period (sec)	1.01			
	Design Acceleration (g)	0.54			
	Design Relative Displacement (mm)	133	109	105	130

Table 3 Peak Response of Deck and Variable Damper

(a) Full Control

Analytical Cases		Deck			Variable Damper			
		Displacement (cm)	Velocity (cm/sec)	Acceleration (cm/sec²)	Damping Force (tf)	Relative Displacement (cm)	Relative Velocity (cm/sec)	Total Energy Absorption (tf·m)
1	No Control	33.04	189.0	1300	—	—	—	—
2	Constant Damping ($h_1 = 0.05$)	25.63	148.7	1012	8.8	19.41	113.1	65.41
3	Constant Damping ($h_2 = 1.0$)	7.97	45.1	481	47.1	5.73	30.4	81.51
4	Displacement Dependent Damping	23.33	140.7	1043	39.2	17.32	142.2	70.70
5	Displacement Dependent Damping	13.25	84.8	566	58.8	10.18	123.6	93.62
6	Velocity Dependent Damping	21.10	131.3	1117	140.3	16.05	169.4	78.41
7	Velocity Dependent Damping	20.35	126.7	1029	109.8	15.44	147.4	76.38
8	Displacement and Velocity Dependent Damping	20.96	122.7	1136	129.3	15.72	168.1	80.52

(b) Partial Control

Analytical Cases		Deck			Variable Damper			
		Displacement (cm)	Velocity (cm/sec)	Acceleration (cm/sec²)	Damping Force (tf)	Relative Displacement (cm)	Relative Velocity (cm/sec)	Total Energy Absorption (tf·m)
5	Displacement Dependent Damping	13.25	84.8	566	58.8	10.18	123.6	93.62
9	Control When $v > 0$	19.05	113.7	765	70.2	14.72	177.4	94.30
10	Control When $v < 0$	19.22	115.5	776	71.8	14.94	181.8	96.21
11	Control When $d \cdot v > 0$	20.53	127.9	909	67.6	15.40	167.9	92.20
12	Control When $d \cdot v < 0$	20.34	114.9	826	65.2	15.95	230.4	82.58
13	Control When $d > 0$	18.87	114.7	953	104.6	16.29	231.3	80.25
14	Control When $d < 0$	20.28	117.8	886	73.1	17.11	226.7	77.49

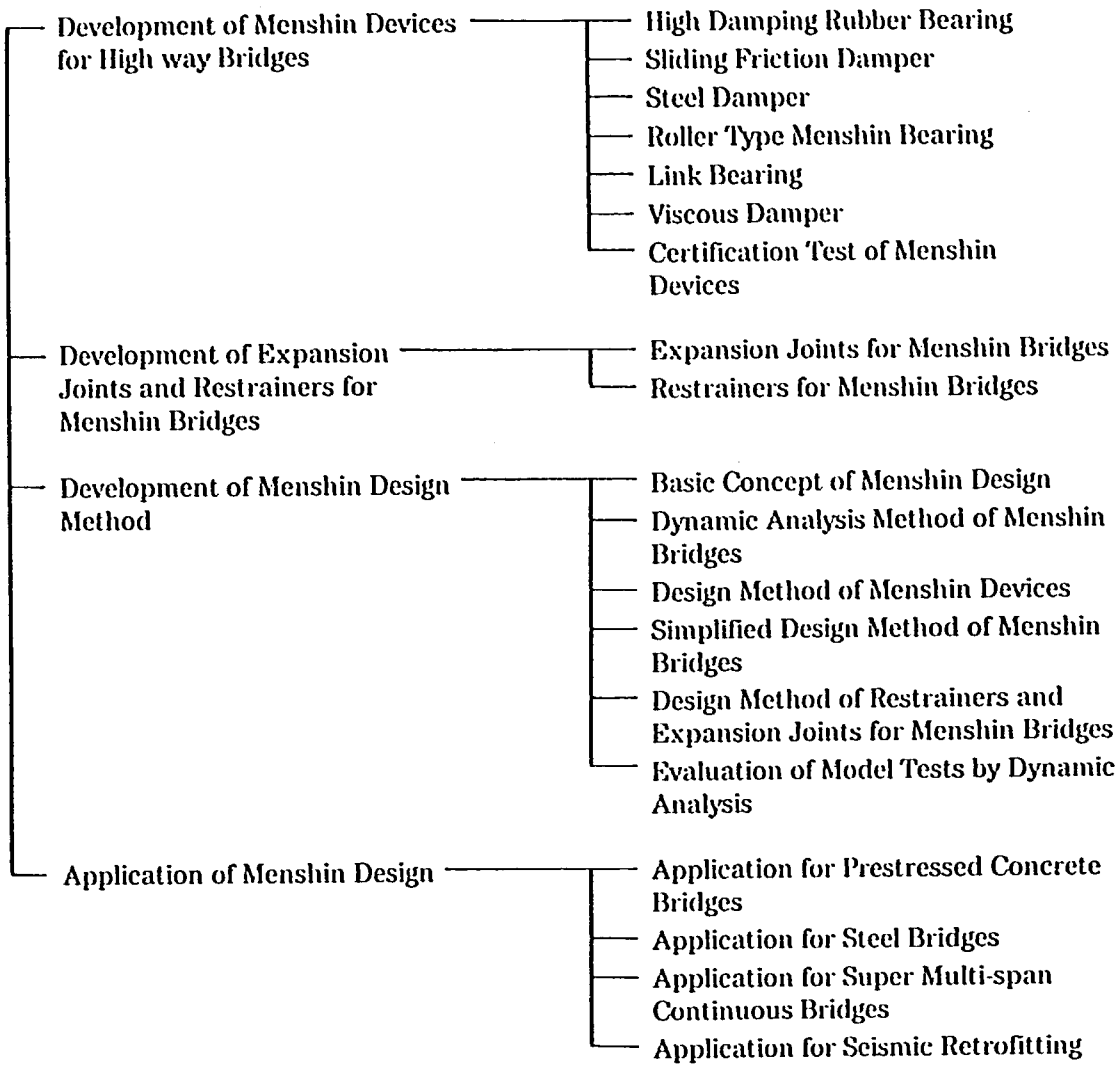
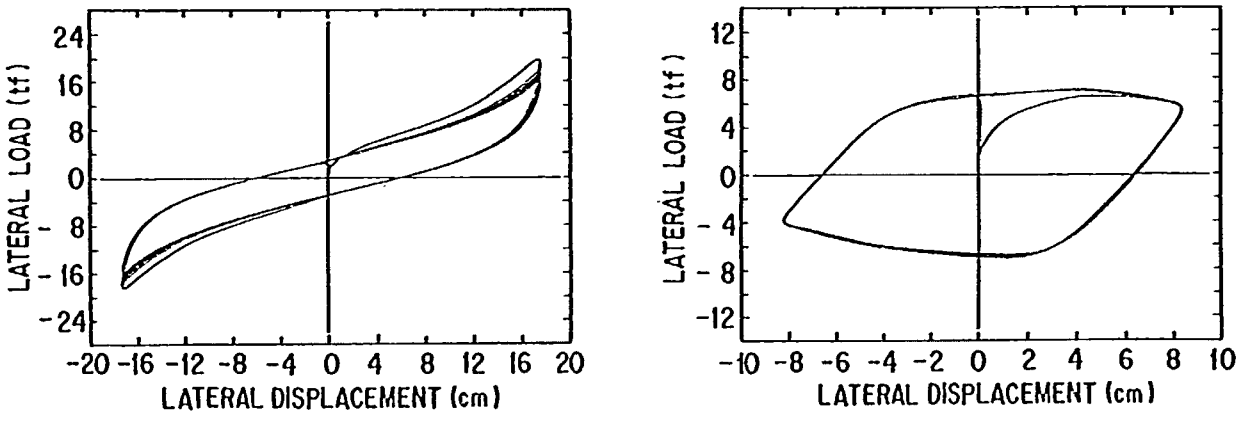


Fig.1 Research Items of Joint Research Program



(a) High Damping Rubber Bearing (b) Sliding Friction Damper

Fig.2 Lateral Load vs. Displacement Hysteresis Loop

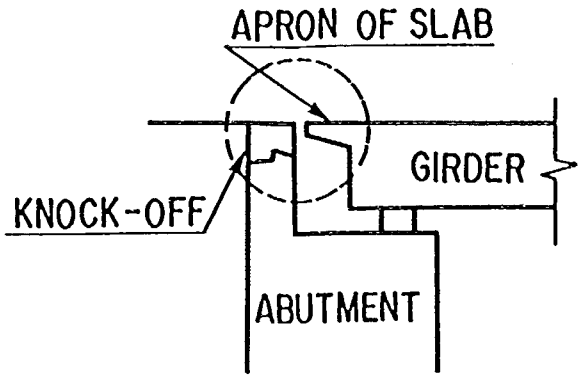


Fig.3 Knock-off Mechanism

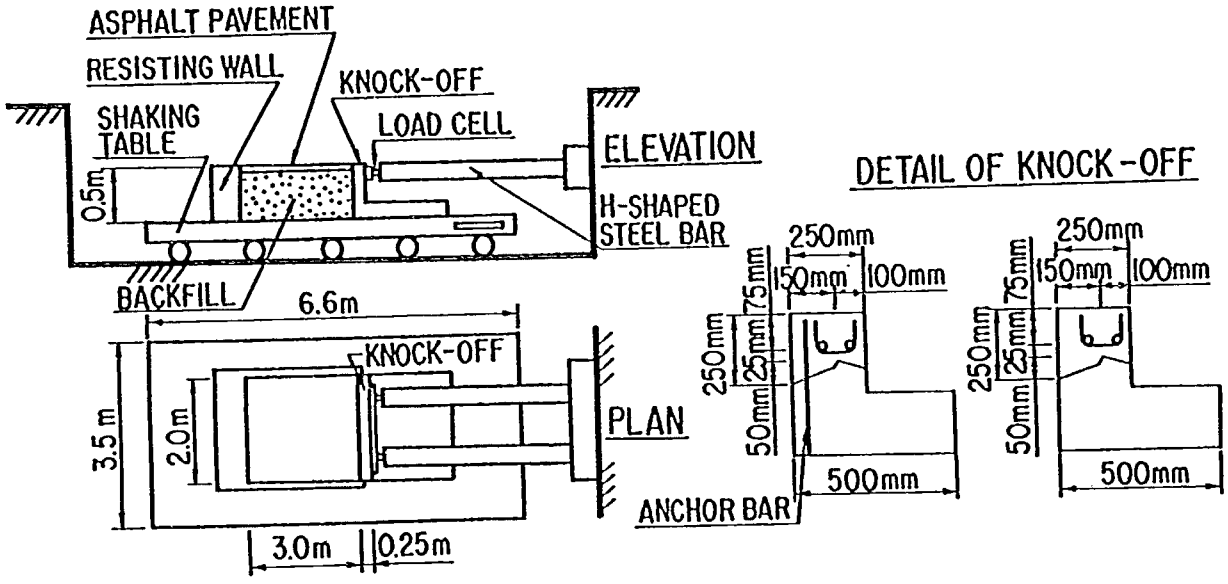


Fig.4 Experiment of Knock-off Mechanism[5]

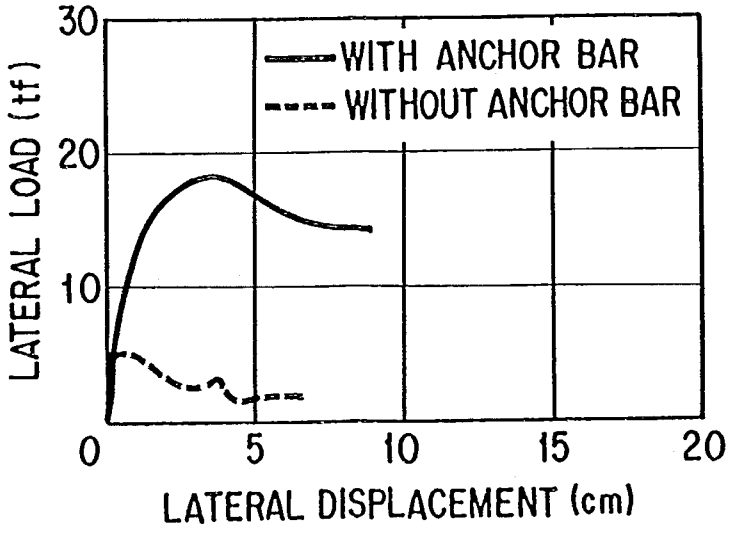


Fig.5 Lateral Load vs. Displacement Relation of Knock-off Mechanism[6]

[Item]	[Object]	[Analysis Method]	[Design Force Level]
Assumption of Initial Dimension	Substructure	Static Analysis	Level 1
Design	Menshin Device	Static Analysis	Level 2
	Substructure		Level 1
Check	Menshin Device Substrcture	Static Analysis	Level 2
		Dynamic Analysis	Level 1
			Level 2
Structural Detail	Expansion Joint		(Level 2)
	Restrainer		(Level 3)

Fig.6 Basic Flow Chart of Menshin Design

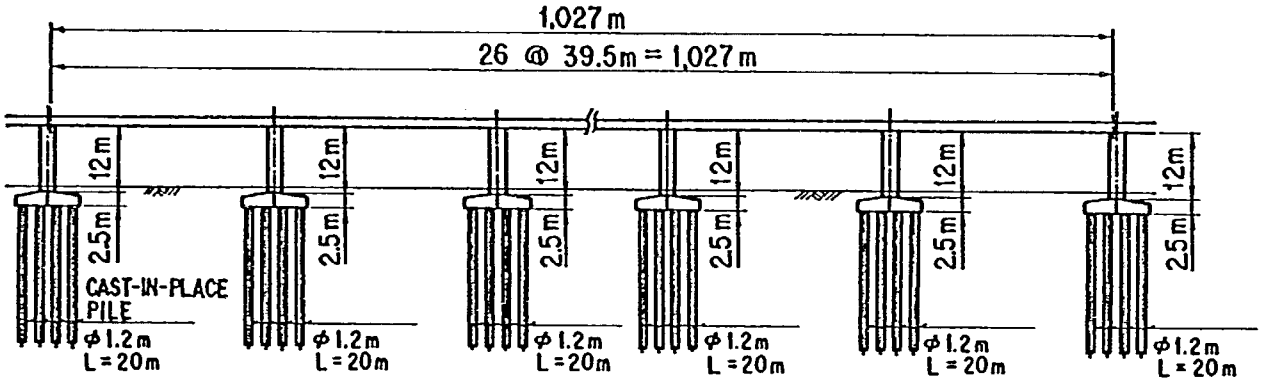


Fig.7 Super Multi-span Continuous Bridge

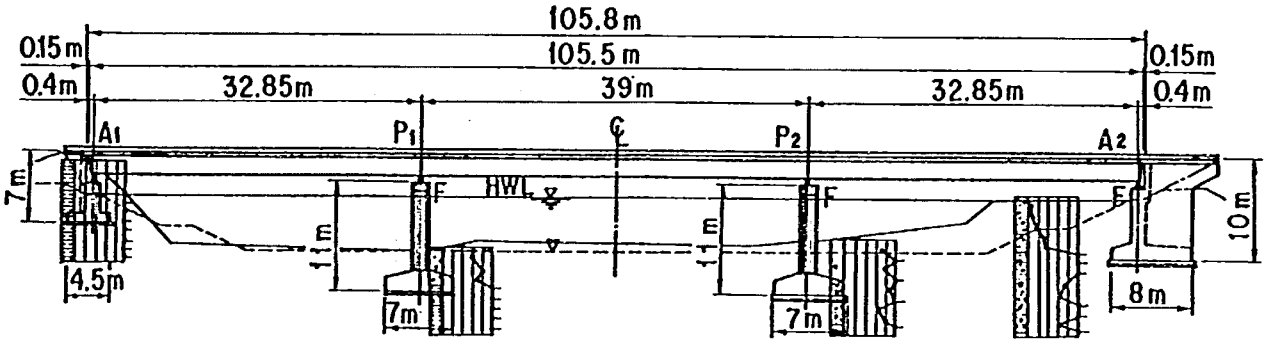


Fig.8 Miyagawa Bridge

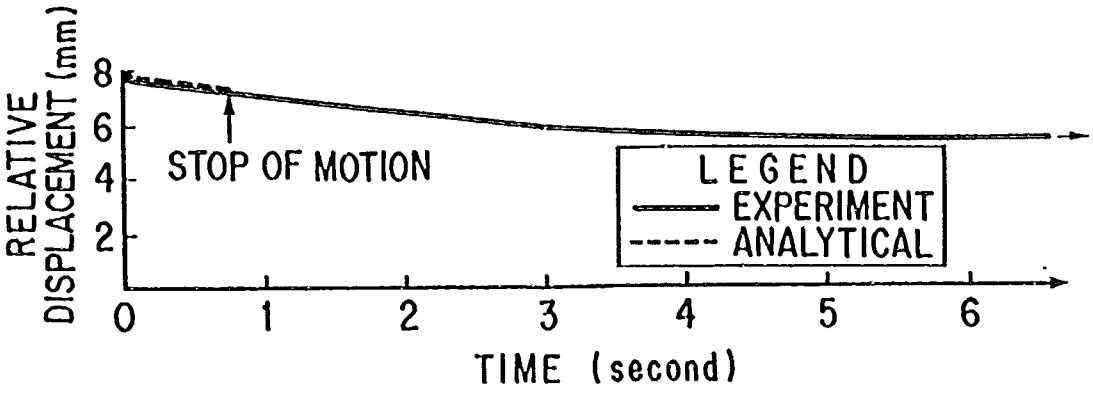
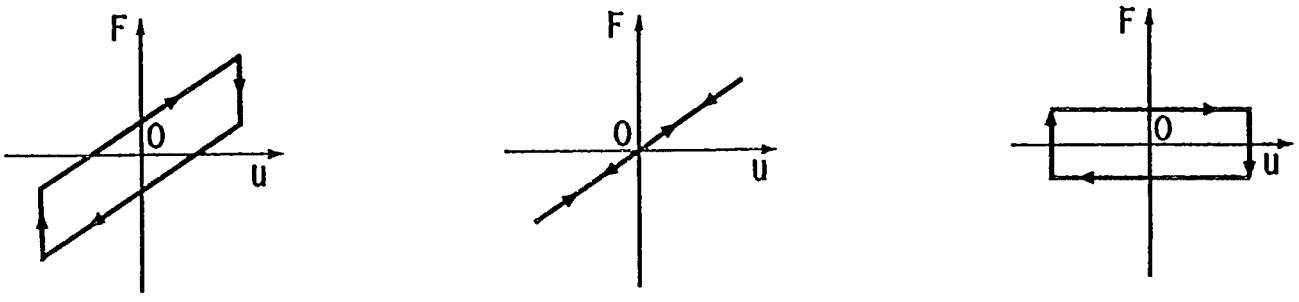


Fig.9 Relative Displacement after Release



(a) Lateral Load vs Lateral Displacement Relation of LRB

(b) Elastic Spring

(c) Friction Force

Fig.10 Load vs. Displacement Relation of LRB

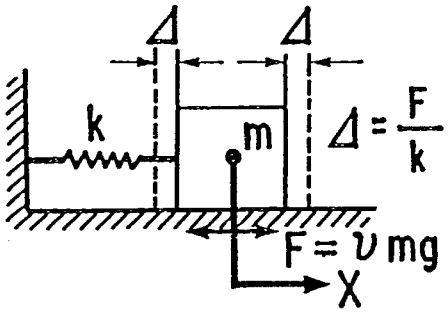
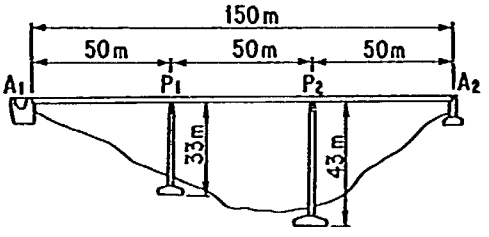
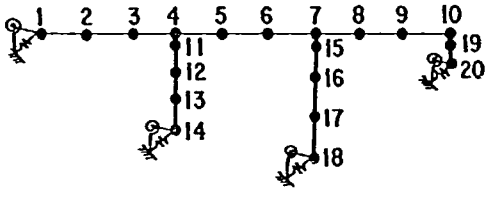


Fig.11 Single Degree of Freedom



(a) Highway Bridge Analyzed

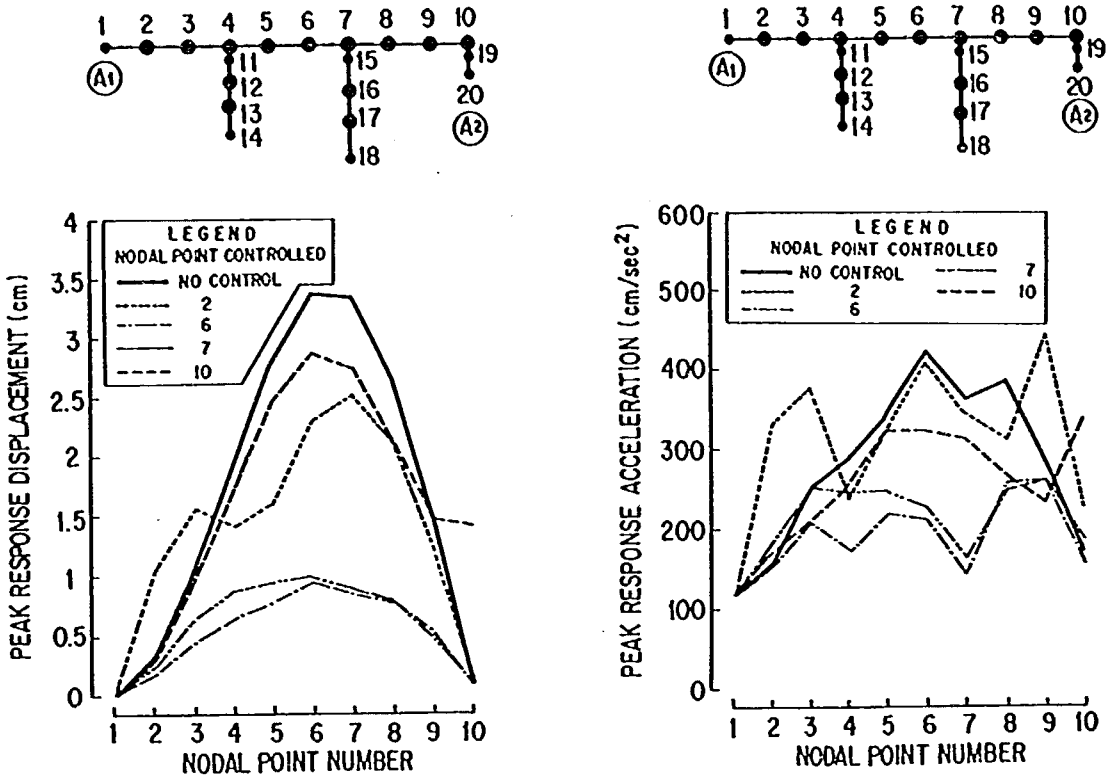


(b) Analytical Idealization



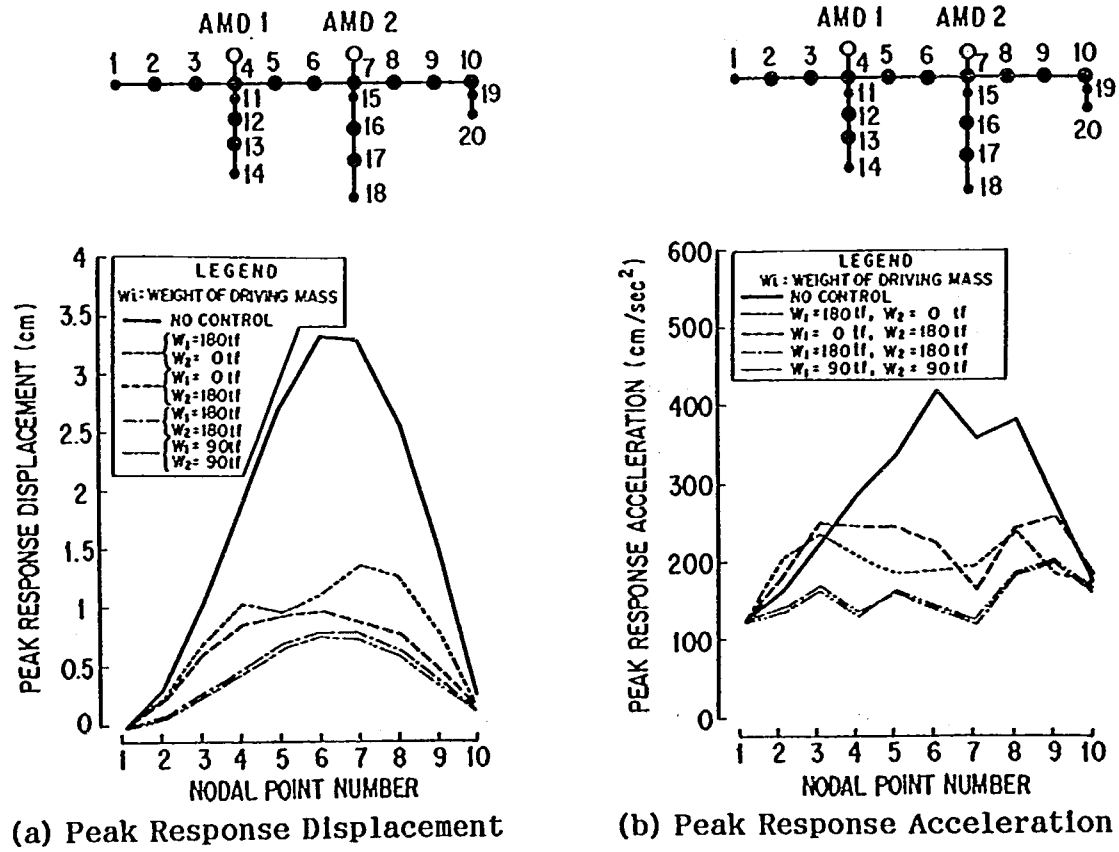
(c) Fundamental Natural Mode of Vibration (f_1=1.67Hz)

Fig.12 Highway Bridge Analyzed and Analytical Idealization



(a) Peak Response Displacement (b) Peak Response Acceleration

Fig.13 Effect of Controlling Point by AMD



(a) Peak Response Displacement (b) Peak Response Acceleration

Fig.14 Effect of Multiple Control by AMDs

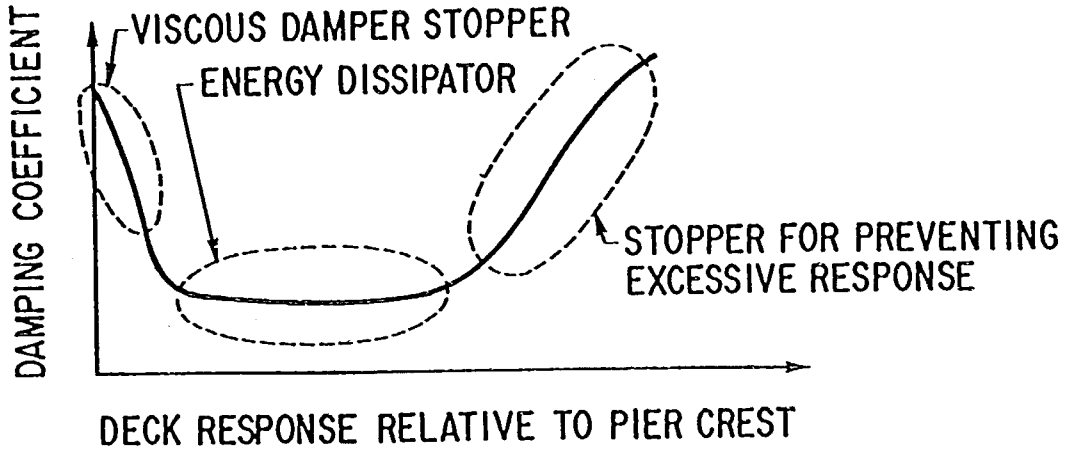


Fig.15 Basic Concept of Variable Dampers

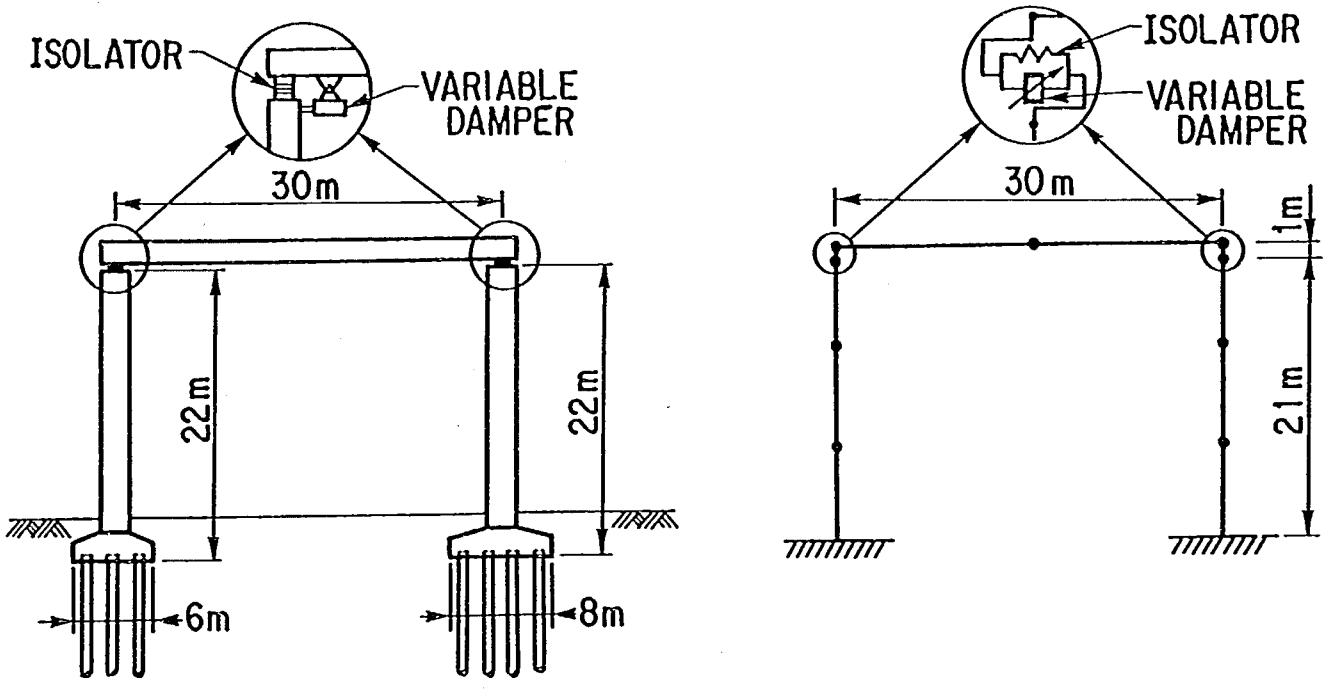
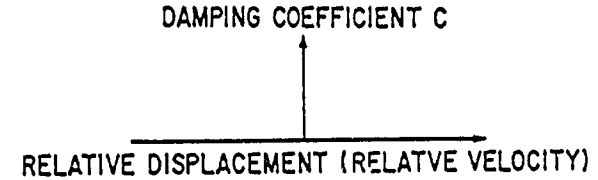
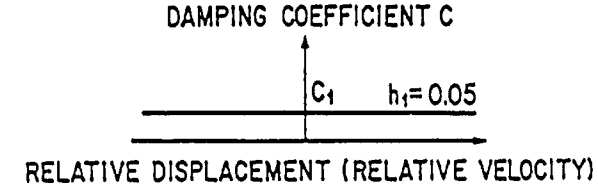


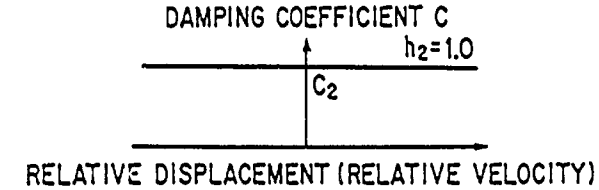
Fig.16 Highway Bridge Analyzed and Analytical Idealization



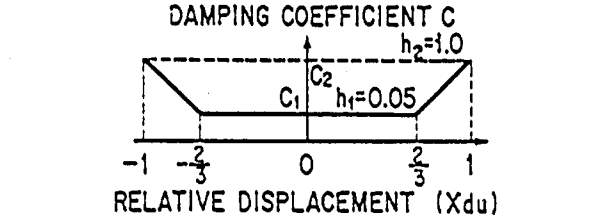
(a) Case 1: No Control



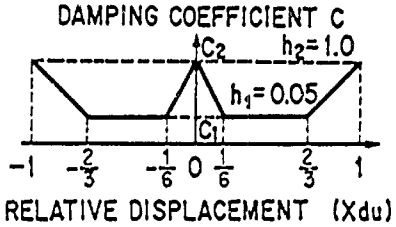
(b) Case 2: Constant Damping ($h_1 = 0.05$)



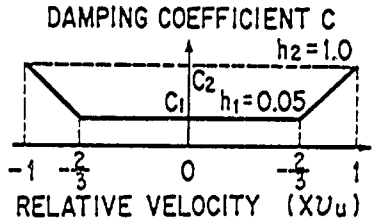
(c) Case 3: Constant Damping ($h_2 = 1.0$)



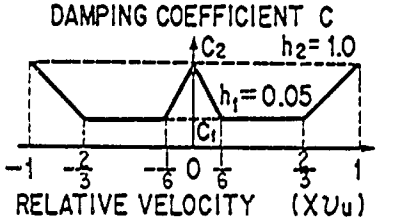
(d) Case 4: Displacement Dependent Damping (du = 19.41 cm)



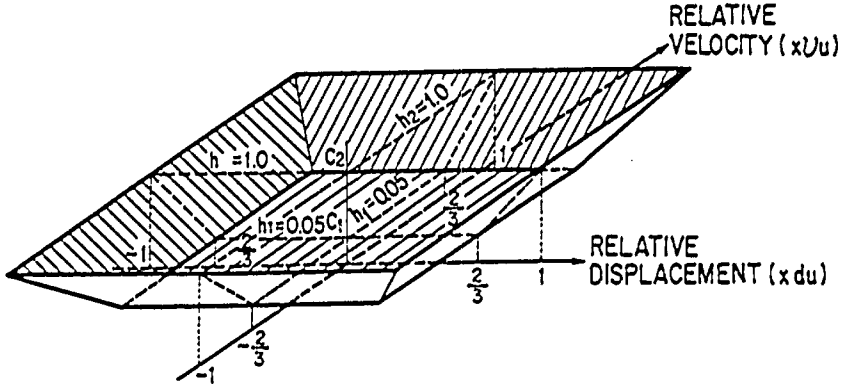
(e) Case 5: Displacement Dependent Damping (du = 19.41 cm)



(f) Case 6: Velocity Dependent Damping (Vu = 113.1 cm/sec)

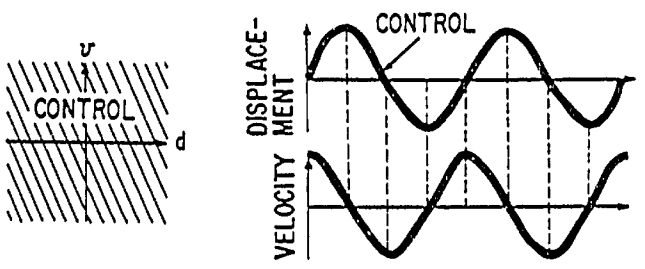


(g) Case 7: Velocity Dependent Damping Constant Damping (Vu = 113.1 cm/sec)

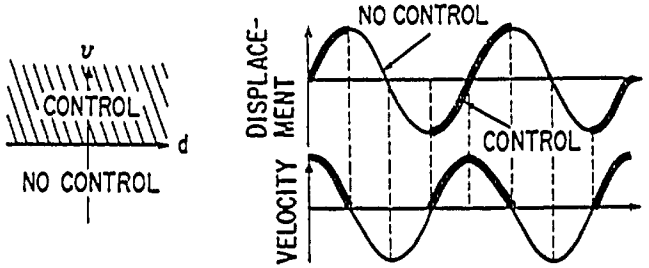


(h) Case 8: Displacement and Velocity Dependent Damping (du =19.41 cm, Vu = 113.1 cm/sec)

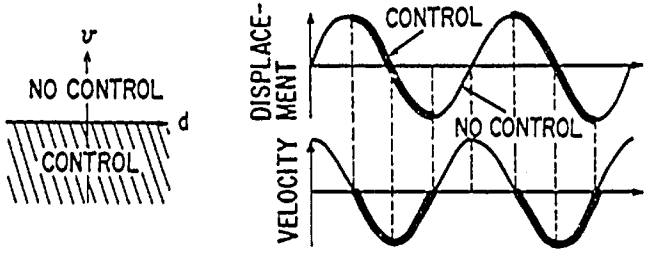
Fig.17 Analytical Cases for Full Control



(a) Case 5

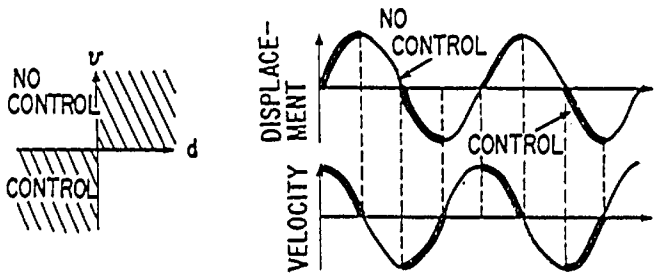


(b) Case 9 (Control when $v > 0$)

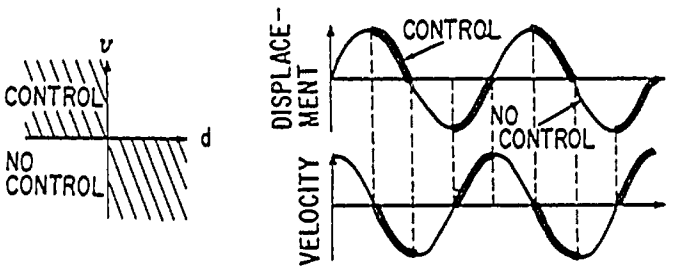


(c) Case 10 (Control when $v < 0$)

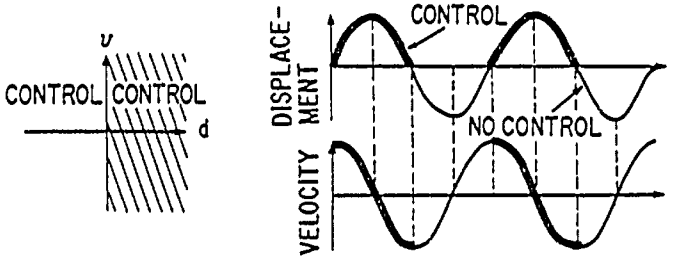
Fig.18 Analytical Cases for Partial Control



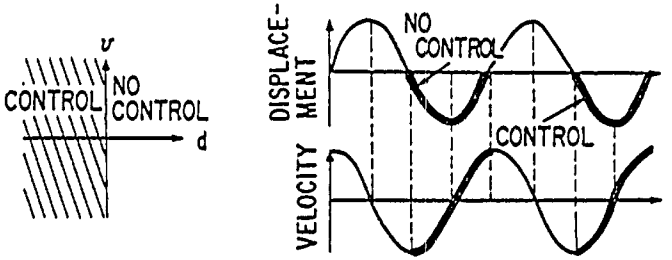
(d) Case 11 (Control when $dv > 0$)



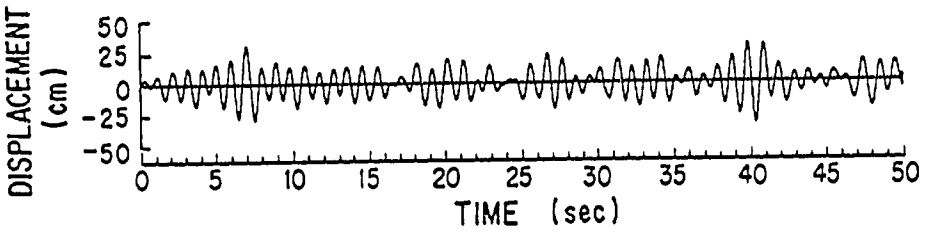
(e) Case 12 (Control when $dv < 0$)



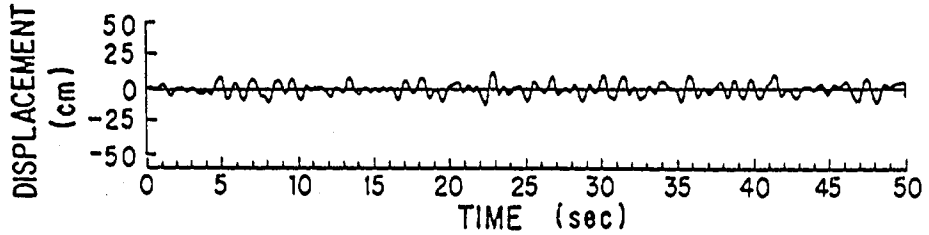
(f) Case 13 (Control when $d < 0$)



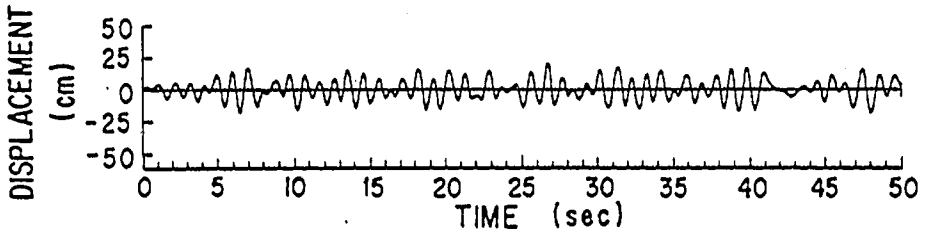
(g) Case 14 (Control when $d < 0$)



(a) Case 1: No Control

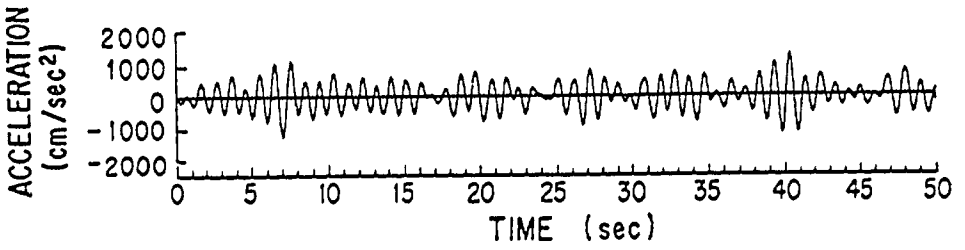


(b) Case 5: Displacement Dependent Damping

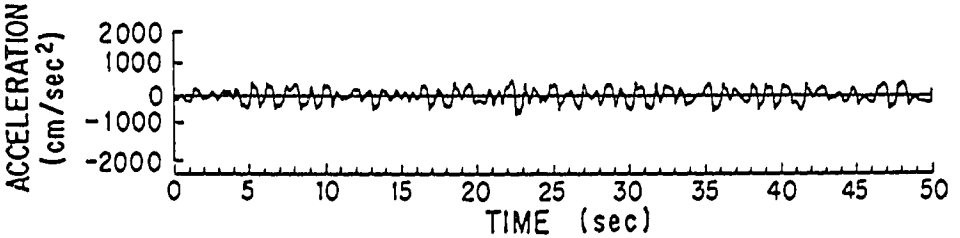


(c) Case 7: Velocity Dependent Damping

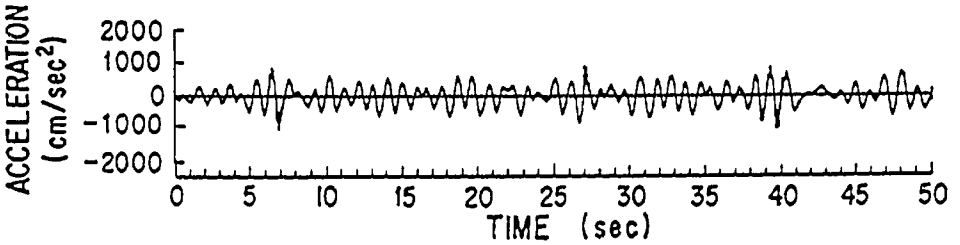
(a) Displacement



(a) Case 1: No Control



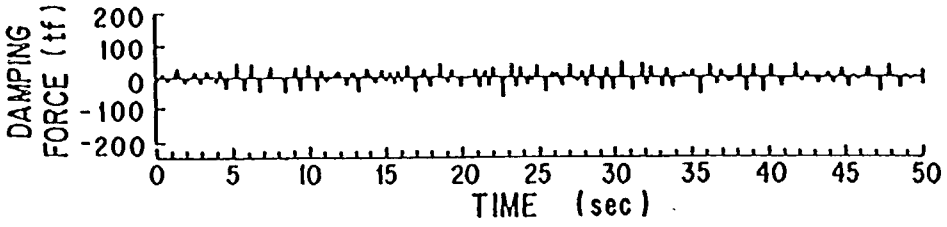
(b) Case 5: Displacement Dependent Damping



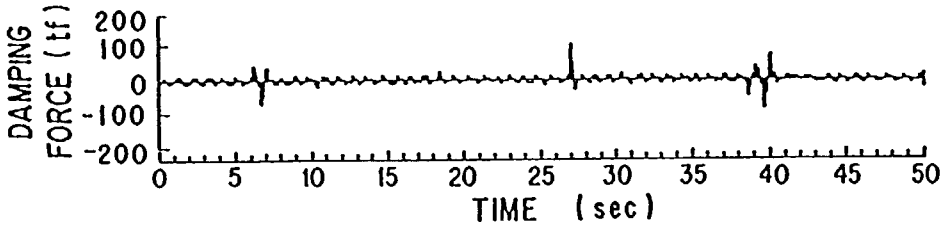
(c) Case 7: Velocity Dependent Damping

(b) Acceleration

Fig.19 Computed Response of Deck

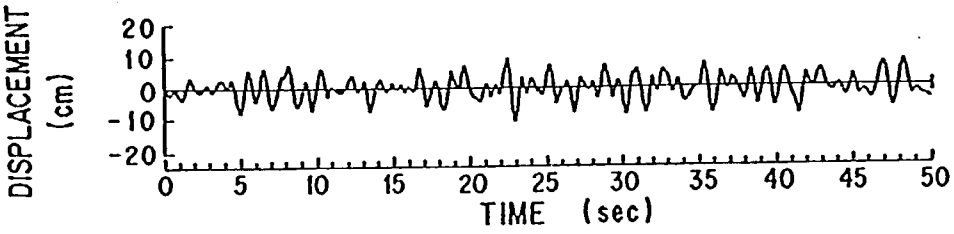


(a) Case 5: Displacement Dependent Damping

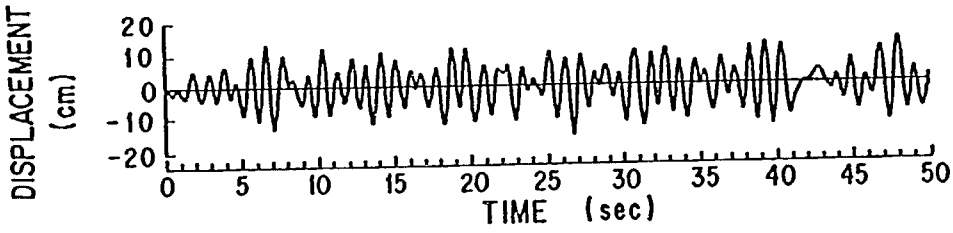


(b) Case 7: Velocity Dependent Damping

(1) Damping Force

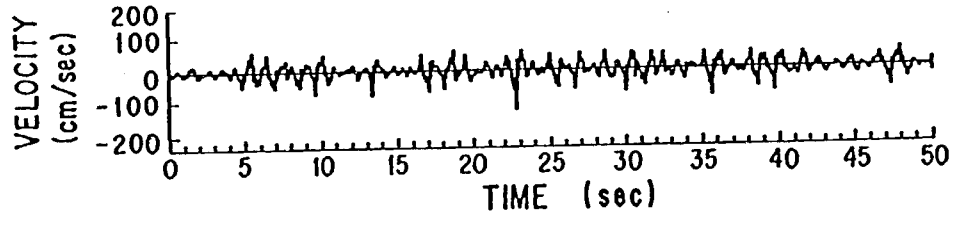


(a) Case 5: Displacement Dependent Damping

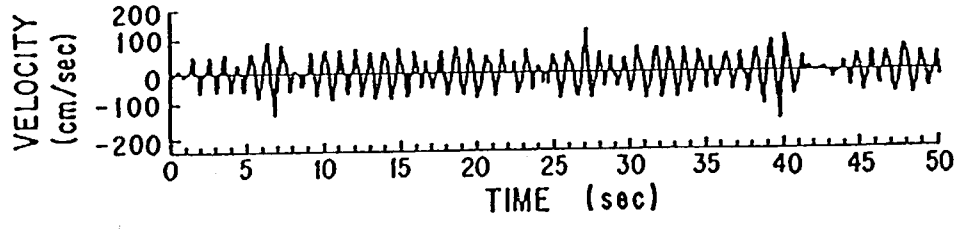


(b) Case 7: Velocity Dependent Damping

(2) Displacement



(a) Case 5: Displacement Dependent Damping



(b) Case 7: Velocity Dependent Damping

(3) Velocity

Fig.20 Computed Response of Variable Dampers

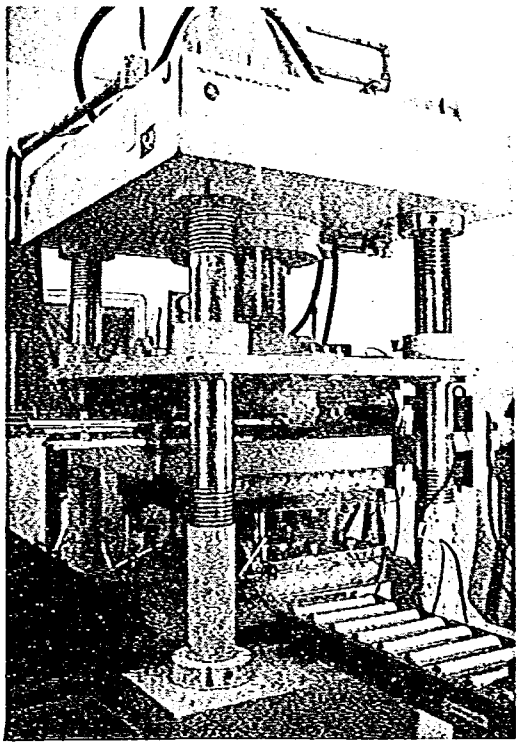


Photo 1 Loading Experiment System for Menshin Devices

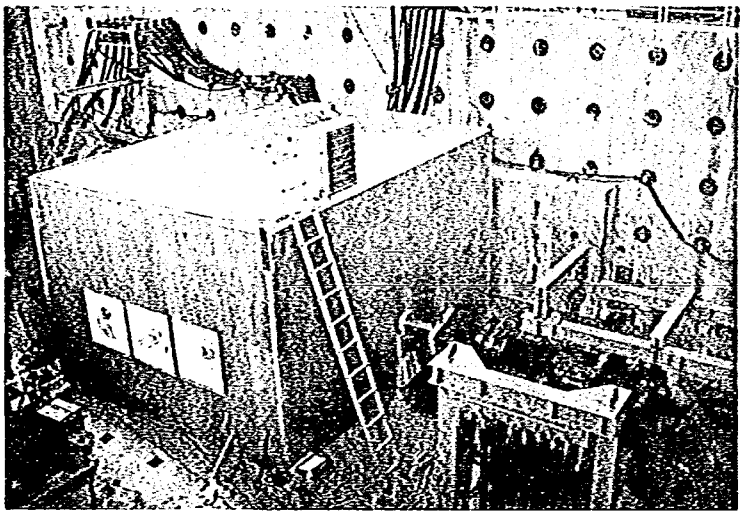


Photo 2 Constant Temperature Room for Test of Menshin Devices

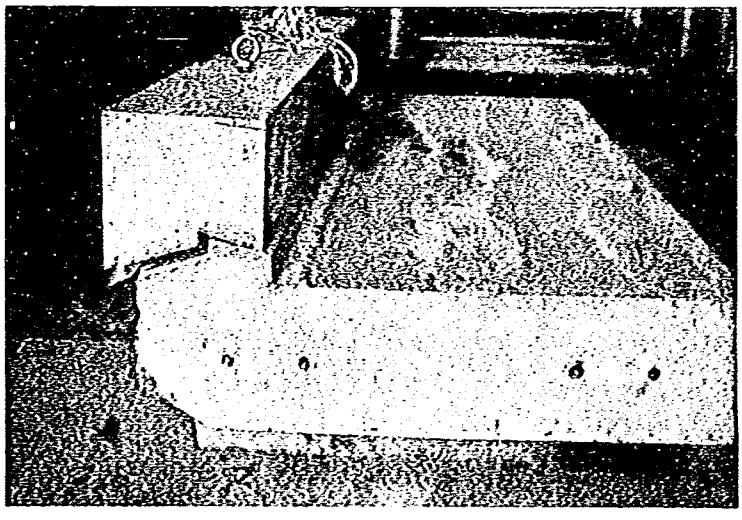


Photo 3 Model of Knock-off Mechanism[5]

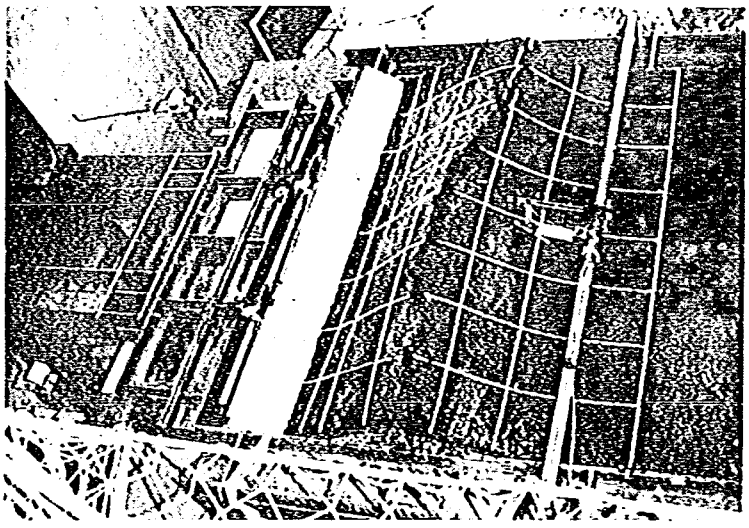


Photo 4 Situation after Test[6)]

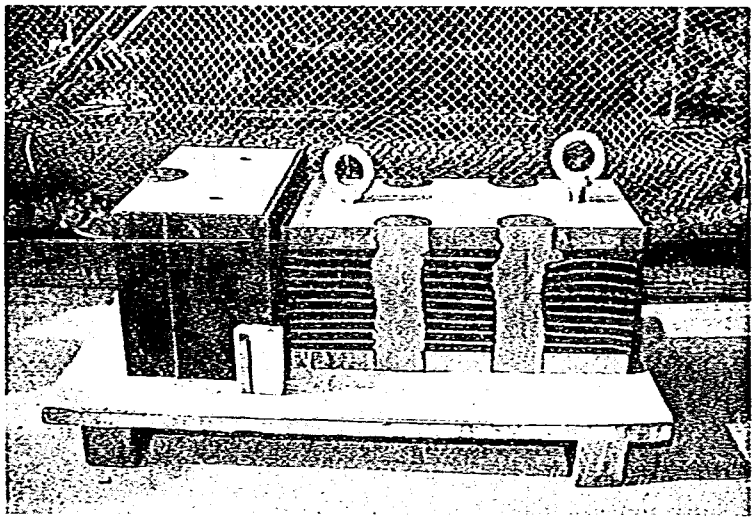


Photo 5 Lead Rubber Bearing

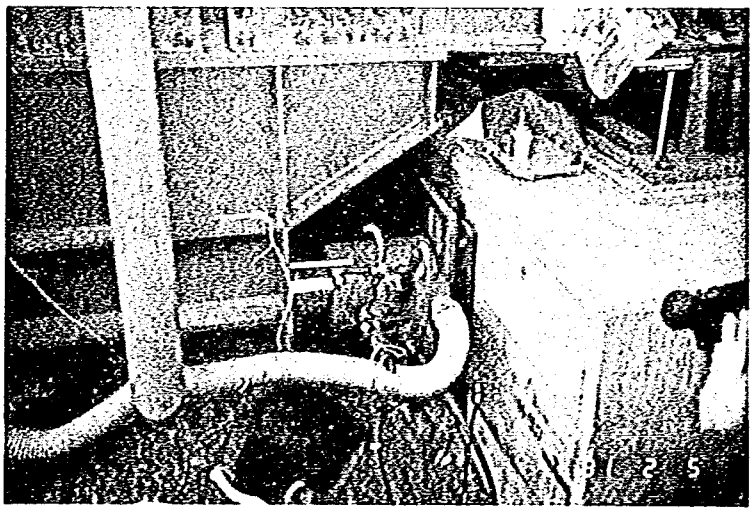


Photo 6 Hydraulic Static Jack

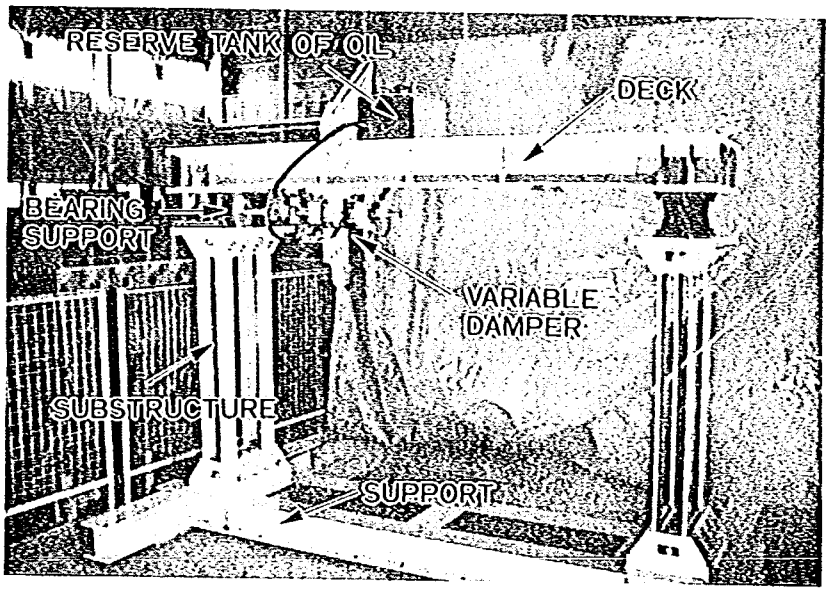


Photo 7 Bridge Model with Variable Damper

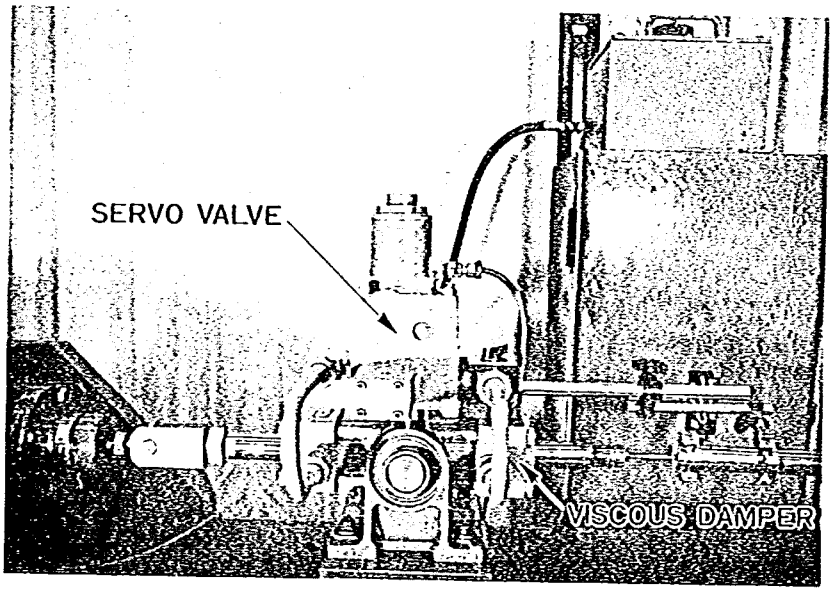


Photo 8 Variable Damper

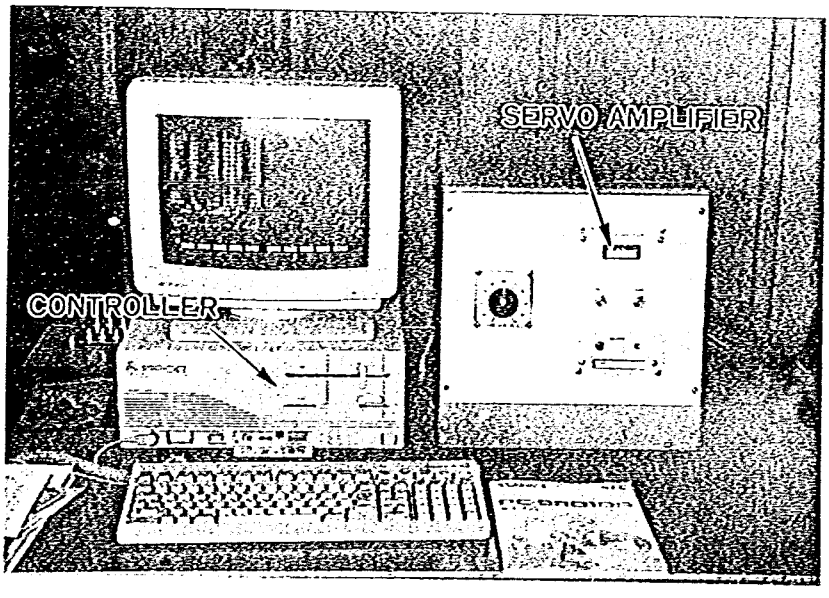


Photo 9 Control System for Variable Damper

EVALUATION OF LATERAL INERTIA FORCE OF BRIDGES FOR SEISMIC DESIGN

by
Kazuhiko KAWASHIMA
and
Kinji HASEGAWA
Public Works Research Institute
Ministry of Construction

THE 7TH U.S. — JAPAN BRIDGE WORKSHOP
Tsukuba Science City, Japan
May 8 and 9, 1991

EVALUATION OF LATERAL INERTIA FORCE OF BRIDGES FOR SEISMIC DESIGN

By Kazuhiko KAWASHIMA[1] and Kinji HASEGAWA[2]

1: Head, Earthquake Engineering Division,
Public Works Research Institute,
Ministry of Construction, Japan
2: Senior Research Engineer, ditto

In the current design practice, for determining a lateral force due to an inertia force developed in a superstructure, which is used for seismic design of substructures, a bridge is generally divided into sub-structures consisting of a substructure and a part of superstructure supported by the substructure. The lateral force considered in seismic design of a substructure in transverse direction is generally computed by multiplying a seismic coefficient with a reaction force developed at the relevant substructure. However as various types of bridge become to be constructed, it became apparent that the lateral force computed by the traditional method is not always adequate. The lateral force at each substructure significantly depends on flexibility of the substructures. This paper proposes a method to evaluate a lateral force of a superstructure for seismic design of substructures based on a static and simple calculations. Validity of the proposed method is also presented through numerical calculations. Application of the method in combination with the traditional method in view of consistency and continuity of the design method is proposed.

1 INTRODUCTION

Because dimensions of bridge substructures are determined in most cases from a requirement of seismic effects, evaluation of a lateral force which is used for seismic design of substructures is of great importance. Seismic design method of highway bridges was firstly introduced in a form of clear stipulations in "Design Specifications of Steel Highway Bridges" issued in 1956 by the Japan Road Association. It was stipulated in the specifications that the lateral force considered in seismic design of a substructure in transverse direction shall be computed by multiplying a seismic coefficient with a reaction force developed at the relevant substructure. This method has been widely adopted for seismic design of highway bridges in Japan.

However as various types of bridge structures become to be constructed, it became apparent that the lateral force computed by the method specified in the specifications is not always adequate[1)]. The lateral force at each substructure significantly depends on flexibility and height of the substructures. Therefore, more rational and comprehensive method which can be used to evaluate an inertia force induced in a superstructure for the purpose of seismic design of substructures is required. The same demand also arises in those bridges where a superstructure and substructures are not separated by means of bearing supports. In such bridges, direct application of the stipulations are quite difficult.

This paper proposes a method to evaluate a lateral force of a superstructure for seismic design of substructures based on a static and simple calculation, and also shows its validity through numerical calculations. Application of the method in combination with the traditional

method in view of consistency of the design method is also presented.

2 COMPUTATION OF LATERAL FORCE

For determining a lateral force due to an inertia force developed in a superstructure, which is used for seismic design of substructures, a bridge is generally idealized as shown in Fig. 1. In longitudinal direction, a bridge is generally supported by fixed bearings at least at one support with the others being supported by movable bearings. This is simply to avoid an excessive stress induced in a deck due to variation of temperature.

A lateral force in longitudinal direction at fixed supports is given as[2)]

$$F_d = k_h \times W \qquad (1)$$

in which, F_d : lateral force associated with an inertia force of a superstructure for seismic design of substructures in longitudinal direction, k_h : seismic coefficient, and W : dead weight of a superstructure. An effect of friction force developed due to relative movement of a deck at movable bearings is generally disregarded for evaluating Eq.(1). The friction force is applied to relevant substructures as an external force transferred from the superstructure to the substructures as shown in Fig. 1(a).

A lateral force in transverse direction is more complicated. Because both fixed and movable bearings do not allow relative movement between a deck and substructures in transverse direction, the bridge has to be analyzed as a whole structure to compute lateral forces for use of seismic design of individual substructures. However because this makes the calculation complicated, a bridge is generally divided into several structural segments as shown in Fig. 1(b), which consist of a substructure and a part of superstructure supported by the substructure. Then, a lateral force used for seismic design of a substructure in an i-th structural segment is assumed as

$$F_{di} = k_{hi} \times R_i \qquad (2)$$

in which F_{di} : lateral force associated with an inertia force induced in a superstructure in transverse direction for seismic design of i-th substructure, k_{hi} : seismic coefficient for i-th substructure, and R_i : reaction force developed at i-th substructure due to dead weight of a part of substructure supported by the i-th substructure.

This traditional method, which is referred hereinafter as a reaction force method, assumes that stiffness of a deck is zero. If this assumption is valid, a structural segment can then be taken out for analysis from the bridge without any interaction with remaining parts. Such assumption may only be applied to those bridges which are supported by extremely stiff substructures as compared with the stiffness of the superstructure. Lateral forces are not generally proportional with reaction forces. They vary depending on stiffness of a superstructure and substructures depending on support conditions.

As various types of bridges become to be adopted, more comprehensive and accurate method became required. This requirement is significant for computing a lateral force in transverse direction for a bridge supported with piers with various height. Furthermore, the requirement also arises in bridges which are rigidly or elastically supported by several substructures. In such bridges, the lateral forces in longitudinal direction depend on stiffness of the substructures. For those bridges where a

superstructure is not separated from substructures with use of bearings, lateral force has to be carefully calculated considering whole response of the bridge.

On the other hand from a view point of structural analysis, an effort required for analysis in recent years becomes much less with use of mini- and personal-computers as well as wide spread of software for structural analysis, and it became possible to analyze a whole bridge with various structural and boundary conditions. Therefore, taking the advance of structural analysis into account, it is require to develop a new method which can be used for analyzing bridges for seismic design purpose. This method should be simple and accurate enough to be adopted widely for practical design. Considering that dynamic response analysis is regarded by design engineers as " a special analysis " which is far from the practical design, the method is expected to be based on static calculations avoiding an eigen value analysis.

Based on such requirements, a simple static analysis method, which is referred hereinafter as a static frame method, is proposed for practical and engineering estimation of lateral force for seismic design of bridges.

3 STATIC FRAME METHOD

Because mass distribution of a bridge concentrates at its deck, bridges response in a way of an inverted pendulum. Because first mode is generally predominant in total response, a peak response displacement of the bridge can be approximated as

$$u^{max} \fallingdotseq u_1^{max} = \beta_1 \cdot S_D(T_1, h_1) \cdot \phi_1 \qquad (3)$$

in which, u^{max}: peak response displacement when all modes are considered, u_1^{max} : peak response displacement of first mode, β_1 : mode participation factor for first mode, $S_D(T_1, h_1)$: displacement response spectrum for a natural period T_1 and a damping ratio h_1, and ϕ_1 : first natural mode.

Natural period of bridges can be approximately computed by the Rayleigh method[3]. A first mode shape is generally approximated with a static deformation shape when it is subjected to a static distributed load equivalent with a dead weight. Denoting a displacement of a bridge subjected to a dead weight as $u_d(s)$ at point s, response displacement of the bridge $u(s)$ may be approximated with use of the static displacement $u_d(s)$ as

$$u(s) = u_d(s)\sin(\omega_d t) \qquad (4)$$

in which ω_d represents an angular frequency of the bridge when the static displacement $u_d(s)$ is assumed. It is assumed hereinafter that $u_d(s)$ is non-dimensional.

Assuming the bridge as a one degree of freedom system, the maximum kinetic energy K_{max} of the bridge may be written as

$$K_{max} = (1/2)\omega_d^2 \int_s M(s)\, u_d(s)^2 ds \qquad (5)$$

in which M(s) represents mass at the point s.

On the other hand, the maximum strain energy U_{max} may be written as

$$U_{max} = (1/2) \int_s M(s)\, u_d(s)\, g\, ds \qquad (6)$$

in which g represents an acceleration of gravity.

Because K_{max} and U_{max} should be equal, one obtains from Eqs.(5) and (6)

$$\omega_d^2 \int_s M(s) u_d(s)^2 ds = \int_s M(s) u_d(s) g ds \qquad (7)$$

From Eq.(7), natural period can be obtained as

$$T_d = 2\pi / \omega_d = 2\pi \sqrt{\frac{\int_s M(s)\, u_d(s)^2 ds}{\int_s M(s)\, u_d(s)\, g\, ds}} \qquad (8)$$

Defining a coefficient δ as

$$\delta = \frac{\int_s M(s)\, u_d(s)^2 ds}{\int_s M(s)\, u_d(s) ds} \qquad (9)$$

, the natural period can be approximated as

$$T_d = 2.01 \sqrt{\delta} \qquad (10)$$

Eq.(10) may be much better than Eq.(8) because it is the same type of equation which has been used in practical design since the Part V Seismic Design of the Design Specifications of Highway Bridges[2] issued in 1980. Because in design calculation, weight is much more frequently referred to than mass, substituting the weight in stead of the mass, Eq.(9) can be rewritten as

$$\delta = \frac{\int_s W(s)\, u_d(s)^2 ds}{\int_s W(s)\, u_d(s) ds} \qquad (11)$$

in which W (s) represents distributed dead weight at point s.

Once first natural period of the bridge can be determined, a seismic coefficient k_h may be assigned. Then, it is required to determine the lateral force transferred from the superstructure to the substructures. When computing the static displacement u_d (s) of the bridge subjected to the dead weight in lateral direction, one can simultaneously compute force F (s) induced at point (section) s in the bridge. Because F (s) represents the force induced in the bridge when it is subjected to the lateral force equivalent with the gravity force in lateral direction, the force induced in the bridge when subjected to the lateral force equivalent with the seismic coefficient k_h can be computed as

$$F_d(s) = F(s) \times k_h \qquad (12)$$

It should be noted here that F_d (s) can be treated as either an internal force or an external force. When F_d (s) is considered as an internal force, it represents a sectional force developed at point (section) s as a result of the inertia force. On the other hand, when F_d (s) is considered as an external force, it represents an inertia force to be applied at a section s. Therefore considering consistency with the current design practice, it is appropriate to regard F_d (s) as :

1) For girder bridges, a horizontal force F_d (s) at a gravity center of a superstructure shall be regarded as a lateral force H which represents an inertia force of the superstructure transmitted to the substructure. The lateral force H shall be applied to the substructure as an external force at the gravity center of the superstructure.
2) For those bridges for which a superstructure and substructures are not separated such as an arch bridge, the force F_d (s) given by Eq.(12) shall be used as a sectional force induced in the bridge as a result of the inertia force.

In the static frame method, a bridge can be analyzed as a whole

structure instead of dividing it into several sub-structures consisting of a substructure and a part of superstructure supported by the substructure. However, structural units considered in the analysis should be as simple as possible for seismic design purpose because it makes the calculation simple and easy to check the result. For such purpose, a design structural unit is defined here to identify a structural unit which has to be analyzed as a whole structure.

The design structural unit is proposed to be selected as shown in Table 1. For those bridges in which a superstructure and substructures are not separated by bearing supports, both the superstructure and the substructures shall be considered as the same design structural unit. In girder bridges, the design structural unit has to be changed depending on the direction considered in design.

In longitudinal direction, when a superstructure is supported with fixed bearings by substructure(s) in the direction considered in design, both the superstructure and the substructure(s) shall be included in the same design structural unit. Substructure(s) supporting a superstructure with movable bearings in the direction considered in design may be considered as independent design structural unit(s), because an inertia force exceeding a friction force is not transmitted from the superstructure to the substructures. The friction force developed due to movement of the superstructure relative to the substructures at the movable bearings shall be considered as an external force in that direction for the substructures. It should be noted that even if a superstructure is supported with movable bearings by substructures, the superstructure and the substructures shall be included in the same design structural unit in the direction for which relative movement is not developed at the movable bearings.

In transverse direction, a superstructure and substructures shall be included in the same structural unit. However, because the reaction force method gives a reasonable approximation when the superstructure is supported by the substructures with almost equal stiffness, the substructure and a part of the superstructure supported by the substructure may be considered as the design structural unit.

As a summary, in the static frame method, natural period and the lateral force/sectional force is proposed to evaluate as (refer to Fig. 2)

i) idealize a design structural unit by a linear elastic frame model
ii) apply a distributed lateral force equivalent with dead weight of the superstructure and the substructure in a horizontal direction considered in seismic design, and compute a static displacement $u_d(s)$ and a sectional force $F(s)$.
iii) compute natural period T by Eq.(10).
iv) determine a seismic coefficient k_h depending on the natural period T.
v) compute either an inertia force or sectional force by Eq.(12)

The static frame method assumes that it considers only first mode; it uses a static deformation of a bridge subjected to a dead weight instead of first mode shape; it computes first natural period by the Rayleigh method. Although the static frame method gives more realistic results than the reaction force method, it gives an only approximate result. When the above-described assumptions can not be adopted, structural response has to be computed by a dynamic response analysis.

Finally it should be noted that although the computation process is

different, the static frame method gives the same inertia force/sectional force with a method in which a bridge is directly subjected to a lateral force equivalent with the dead weight multiplied with a seismic coefficient. Even by now when a bridge is complicated, this method has been often used. From such point of view, the static frame method is not necessarily a new method but only one of traditional methods which includes a sub-process to compute a natural period.

4 ACCURACY OF STATIC FRAME METHOD IN COMPARISON WITH DYNAMIC RESPONSE ANALYSIS

For evaluating validity of the static frame method, a comparative study of the static frame method with dynamic response analysis was made for the same highway bridges against the same input ground motions. Analyzed were 36 bridges with varying various conditions as

i) topographical condition
bridges crossing a valley, bridges crossing a river, and overcrossings in urban area

ii) type of superstructure
material(steel and prestressed concrete), shape of cross section (girder bridge and box), number of span, and span length

iii) pier type
wall type piers, single columns, frame piers, steel piers, and flexible piers

iv) pier height

v) type of foundation
spread foundations, caisson foundations and pile foundations

vi) soil condition
ground group I, II and III specified in the Part V Seismic Design of the Design Specifications of Highway Bridges[4)]

Analysis was made for bridge responses in transverse direction, because this is a major concern for evaluating an application of the static frame method. Strong motion records measured on ground surface near the Kaihoku Bridge during the 1978 Miyagi-ken-oki Earthquake with an earthquake magnitude of 7.4 and on ground surface near the Tsugaru Bridge during the 1983 Nihon-kai-chubu Earthquake with an earthquake magnitude of 7.7 were used for time history analysis. In the static frame method, a seismic coefficient determined as

$$k_h = S_A(T_1, h_1) / g \qquad (13)$$

was used so that the same input ground motion with the dynamic response analysis be assumed, in which T_1 : first natural period computed by Eq.(10), $S_A(T_1, h_1)$: response acceleration of the input record with the natural period T_1 and damping ratio h_1. Damping ratio was assumed as 5 % for both the dynamic response analysis and the static frame method.

Although the analysis was made for the 36 bridges, results are presented with emphasis on analysis for two bridges as shown in Fig. 3. A-Bridge represents a 3 span continuous steel girder bridge with an equal span length of 30 m over a river. Both ends are supported by abutments. B-Bridge has the same superstructure, but is an overcrossing in urban area. The superstructure is supported by four piers with almost the same stiffness.

Fig. 4 compares the static displacement $u_d(s)$ with exact first mode $\phi_1(s)$. Although $\phi_1(s)$ shows larger deformation of the deck between the

two abutments than $u_d(s)$ in the A-Bridge, overall mode shape $\phi_1(s)$ is well approximated by $u_d(s)$. The eigen value analysis predicts first natural period of 0.41 second for the A-Bridge and 0.3 second for the B-Bridge while the static frame method predicts 0.40 second for the A-Bridge and 0.29 second for the B-Bridge. It is said that the predicted natural period by the static frame method gives a fairly good approximation to the exact natural period. For reference, when the natural period is computed in the reaction force method, it takes a value of 0.21 second for the substructure including the P1 abutment, 0.49 second for the substructure including the P1 pier and for the substructure including the P2 pier, and 0.28 second for the substructure including the A2 abutment. It is apparent that the natural period is considerably underestimated for the two abutments and overestimated for the two piers.

Fig. 5 shows a distribution of the maximum bending moment and shear force when the bridges are subjected to the Kaihoku Record. As well as the results by the static frame method and the dynamic response analysis, results by the reaction force method are also presented in Fig. 5 for comparison. The static frame method gives a realistic approximation for both bridges. This clearly means that the assumptions of the static frame method presented in the preceding chapter are reasonably adopted for engineering analysis of the two bridges.

It is interesting to note here that how the forces predicted by the reaction force method differs with the results predicted by the dynamic response analysis. In the A-Bridge, the reaction force method gives a fairly close result with the dynamic response analysis. However in the B-Bridge, the reaction force method gives considerable underestimation for the sectional force at A1, A2 and P1. This is due to the fact that stiffness of A1, A2 and P1 is significantly larger than the stiffness of P2.

Fig. 6 shows a comparison of natural periods predicted by the static frame method and the eigen value analysis for the 36 bridges. Natural periods predicted by the reaction force method are also presented for comparison. The natural periods predicted by the static frame method give reasonably good approximation to the natural period predicted by the eigen value analysis.

Fig. 7 shows comparisons of the maximum bending moment developed at bottom of the P1 and P2 piers between the static frame method and the dynamic response analysis for the 36 bridges. Results predicted by the reaction force method are also presented for comparison. The static frame method gives a reasonably close agreement for engineering design purpose with the dynamic response analysis. On the other hand, scatter of the bending moment predicted by the reaction force method is considerable.

5 APPLICATION OF STATIC FRAME METHOD FOR EVALUATION OF LATERAL FORCE OF BRIDGES

Although it is apparent that the static frame method gives more rational lateral force for design of substructures, application of the method has to be carefully examined because direct application of the method would result in considerable difference with the current practice in design. To examine the difference in design of substructures by introducing the static frame method, distribution of lateral forces for each substructure was studied for 3 bridges as shown in Fig. 8. The three bridges have the same superstructures consisting of steel girders with a span length of 30 m.

Difference between the three bridges is only substructure condition, i.e., No.1-Bridge is an overcrossing in urban area with almost the same pier height. No.2-Bridge is a typical 3 span continuous bridge crossing a river. No.3-Bridge is a typical bridge crossing a valley, and has piers with different height. The No.2 and the No.3 Bridges have abutments at both ends.

To compare the three bridges on the same basis, transverse responses of the bridges were computed assuming a seismic coefficient of 0.2 with regardless of natural periods. Dependence of seismic coefficient on the natural periods was disregarded here because the natural period of the three bridges are in the range where the design seismic coefficient takes the same value based on the Part V Seismic Design of the Design Specifications of Highway Bridges[4].

Table 2 shows a comparison of lateral forces (shear forces) which are to be used as inertia forces from the superstructure to the substructures. Because the reaction force method has been widely used by now for seismic design, a special attention was paid how an adoption of the static frame method gives different distributions of lateral forces in design as compared with the reaction force method. Based on Table 2, characteristics of the static frame method in comparison with the reaction force method may be summarized as

1) In the No.1-Bridge, the lateral force predicted by the static framemethod is almost the same with that predicted by the reaction forcemethod. Based on classical elastic theory, reaction force of 3 span continuous beam with an equal span length subjected to uniformly distributed load is 1.0 at both end supports and 2.75 at the two intermediate supports. The lateral force predicted by the reaction force method is, of course, proportional to such reaction force. Because the stiffness of the four piers is almost the same, the static frame method gives a close distribution of the lateral force with the reaction force method.
2) In the No.2-Bridge, the reaction force method predicts the same lateral force distribution with the No.1-Bridge because the superstructure is of the same. On the other hand, the static frame method gives a larger lateral force than the reaction force method by a factor of 2 at the both abutments, and gives almost 40 % lateral force at the two piers. This is simply due to the fact that the stiffness of the abutments are considerably higher than that of the piers.
3) Because in the No.3-Bridge there is a difference in the stiffness between the two piers in addition to the difference of the stiffness between the abutments and the piers, lateral forces predicted by the static frame method are much different with those of the reaction force method. Particular interest is a very small lateral force developed at P2, where the lateral force predicted by the static frame method is only 13 % of the value computed by the reaction force method.

It is apparent from such comparisons that by adopting the static frame method, lateral forces developed at stiff substructure are likely to increase as compared with the current design method, and vice versa for substructures with low stiffness.

Although it is no doubt that the static frame method gives more rational and realistic lateral force than the reaction force method,

considerable changes of the lateral force distribution have to be carefully examined from view point of consistency and continuity of design. When a design of the substructures is made based on the lateral force predicted by the static frame method for the No.2 and No.3-Bridges, sectional dimensions of the piers in transverse direction may be considerably reduced as compared with the current design. Because dimensions of the abutment are selected so that they support an earth pressure of back soils, abutments have generally much redundancy for their bearing capacity in transverse direction. Therefore it is not required to increase the size of the abutments.

Therefore, major change associated with the adoption of the static frame method into the current design practice is that smaller dimensions can be adopted for piers in transverse direction, although an increase of dimensions is required for some piers which have higher stiffness than others. If this is adopted, piers become more flexible, as a whole, than the current design practice. Before adopting the static frame method, the following items have to be considered:

1) Because bridge design is made based on the allowable stress design approach, careful attention has to be paid on what would happen on bridge behavior as a total after parts of the bridge, such as bearing supports and foundations, suffer damage when subjected to larger ground motion than considered as a form of a seismic coefficient. It should be noted that damage of bearing supports occurred as a matter of fact in the past large earthquakes. It is still very difficult to predict bridge response during destructive earthquakes even with sophisticated nonlinear dynamic response analyses.
2) Associated deeply with the reaction force method, it has been the Japanese practice to construct stiff piers, which, in turn, makes seismic force induced in a superstructure limited. Therefore it is very special that the sectional dimensions of the superstructure be determined due to seismic effects. Intention has been paid to construct strong substructures against destructive earthquakes. It should be emphasized that seismic experiences gained in the past are for such bridges. Therefore, sudden decrease of the lateral force for seismic design of piers should be avoided, because it would cause different type of seismic damages never experienced in the past.
3) As is the case of the No.3-Bridge, the lateral force at the flexible pier becomes considerably small. Depending on stiffness of the substructures, the lateral force developed at the flexible pier may take even negative value, which means that the pier can not support even its inertia force but transmits its inertia force to other substructures through the deck.

Based on such considerations, a highly engineering judgement for the minimum lateral force in seismic design seems inevitably important. Therefore it is proposed to use the static frame method as

1) For those bridges with small difference of stiffness between piers, such as the No.1 and No.2-Bridges in Fig. 9, lateral forces shall be computed by the reaction force method.
2) For those bridges with considerable difference of stiffness between piers, such as the No.3-Bridge in Fig. 9, lateral forces shall be computed by the static frame method. However, in girder bridges the lateral forces shall not be smaller that the values computed by the

reaction force method.

It should be noted here that the minimum lateral force was included based on an engineering judgement considering experiences on bridge seismic design and on seismic damages in the past, and consistency and continuity with the current design practice.

6 CONCLUDING REMARKS

The preceding pages presented a new seismic design method referred herein as a static frame method for computing lateral forces, and applications of the method. Because the static frame method considers stiffness of deck, it gives more realistic distribution of lateral force than the reaction force method. Because in the reaction force method, reaction forces are only requirements for design of substructures, it was likely that the design of substructures was made without considering total safety of bridge structures. By adopting the static frame method, it is hoped that attention is given to how bridges behave during destructive earthquakes.

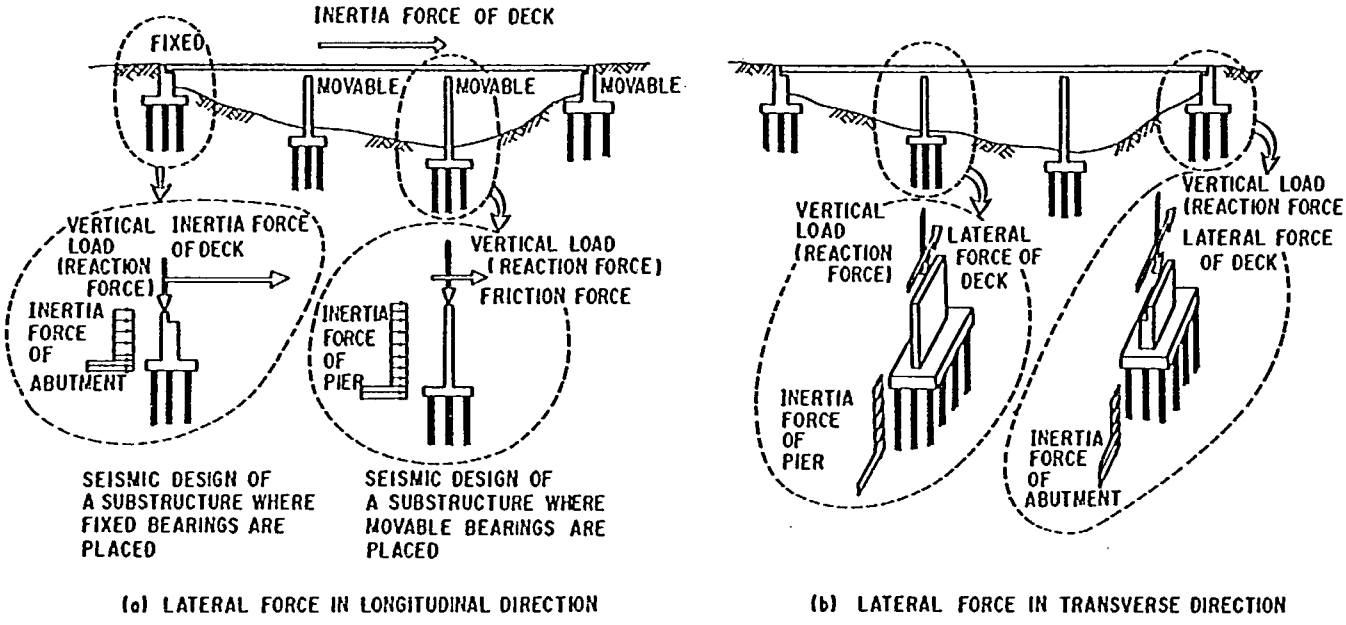
The static frame method was adopted in the Part V Seismic Design of the Design Specifications of Highway Bridges[4] issued from the Japan Road Association in February 1990.

ACKNOWLEDGEMENT

For developing the static frame method presented in this paper, various suggestions were made in the Bridge Committee of the Japan Road Association. Special thanks are to Mrs. Yasuo Tada, Tatuo Asama, Syouichi Saeki, Kaname Yahagi, and Yoshiyuki Enami. The authors would like to express their sincere thanks for valuable guidance and discussions for the committee members.

REFERENCES

1) Asanuma, H. : Damage Report on the Shizunai Bridge, Civil Engineering Journal, Vol. 25-11, 1983
2) Part V Seismic Design of Design Specifications of Highway Bridges (previous version), Japan Road Association, 1980
3) Clough, R.W. and Penzien, J. : Dynamics of Structures, MacGraw-Hill, 1975
4) Part V Seismic Design of the Design Specifications of Highway Bridges (new version), Japan Road Association, 1990



(a) LATERAL FORCE IN LONGITUDINAL DIRECTION

(b) LATERAL FORCE IN TRANSVERSE DIRECTION

Fig.1 Evaluation of Lateral Force by Reaction Force Method

Table 1 Design Structural Units

	Longitudinal			Transverse			Design Structural Unit
Simple Girder Bridges	F M F			A Part of Superstructure which Develops a Reaction Force at the Relevant Substructure			Regarded as A Design Structural Unit Consisting of A Substructure and A Part of Superstructure Supported by the Substructure
Continuous Girder Bridges	Support Condition in Longitudinal Direction: Fixed at One Supp't	M F F M M F M M		Difference of Natural Period between Piers: Small	A Part of Superstructure which Develops a Reaction Force at the Relevant Substructure		
	Fixed at Multiple Supp't	M F F M F F F		Large			Regarded as A Design Structural Unit Consisting of Substructures and the Superstructure Supported by the Substructures
Arch, Frame and Other Types of Bridges							

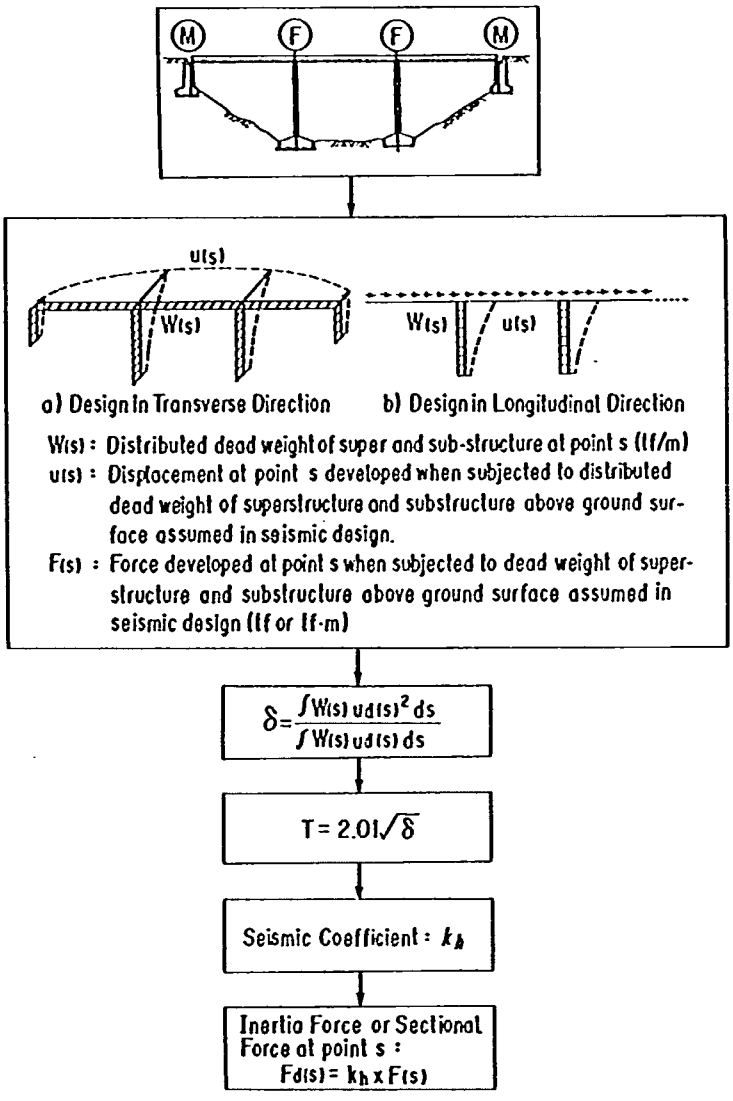
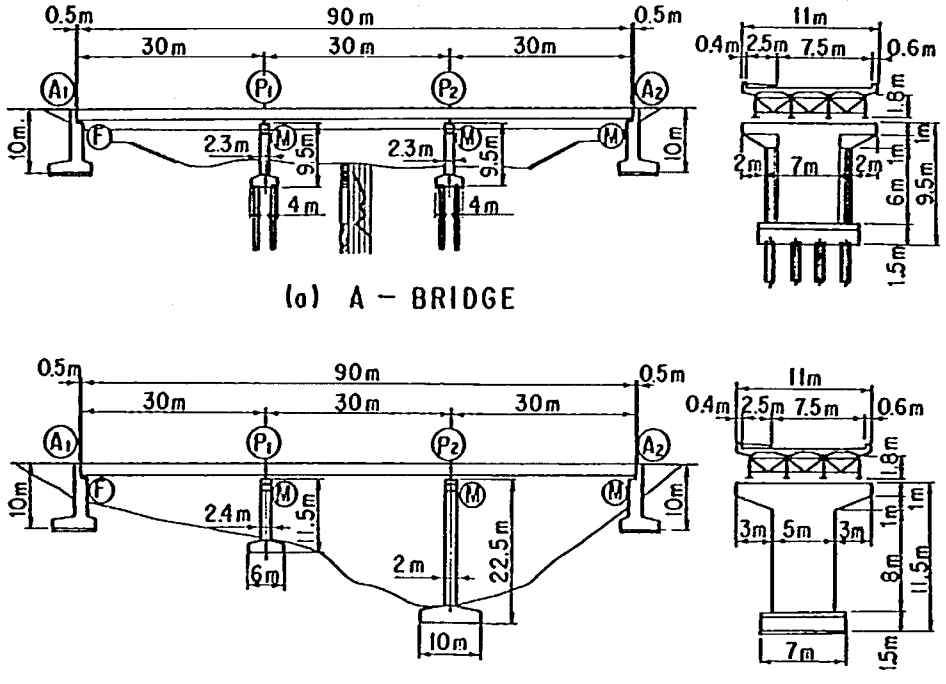


Fig.2 Flow of Static Frame Method



(a) A – BRIDGE

(b) B – BRIDGE

Fig.3 A- and B-bridges Analyzed

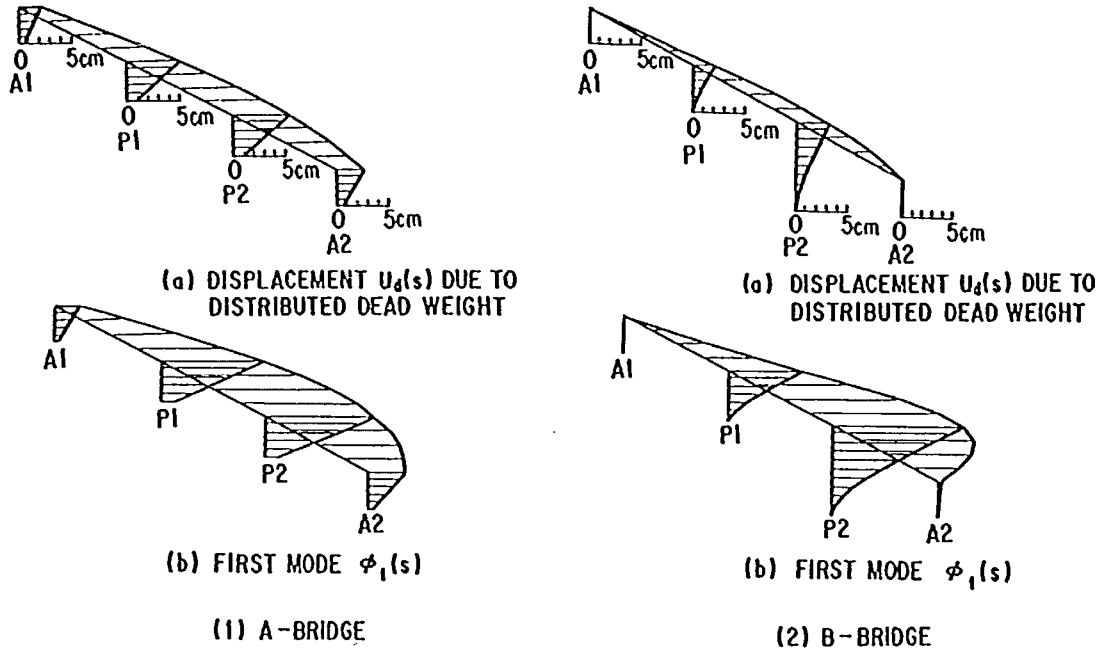


Fig.4 Comparison of Static Deformation and First Mode Shape

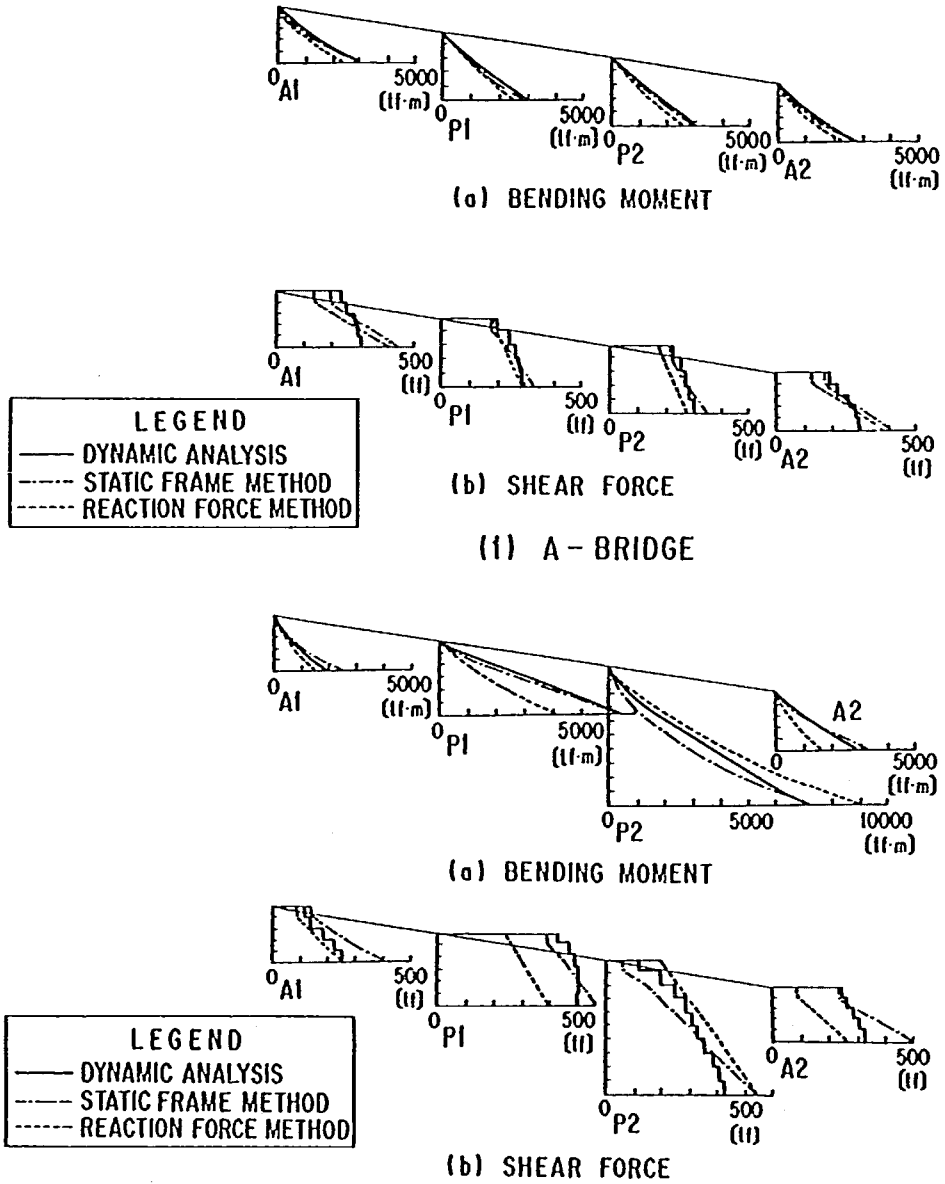
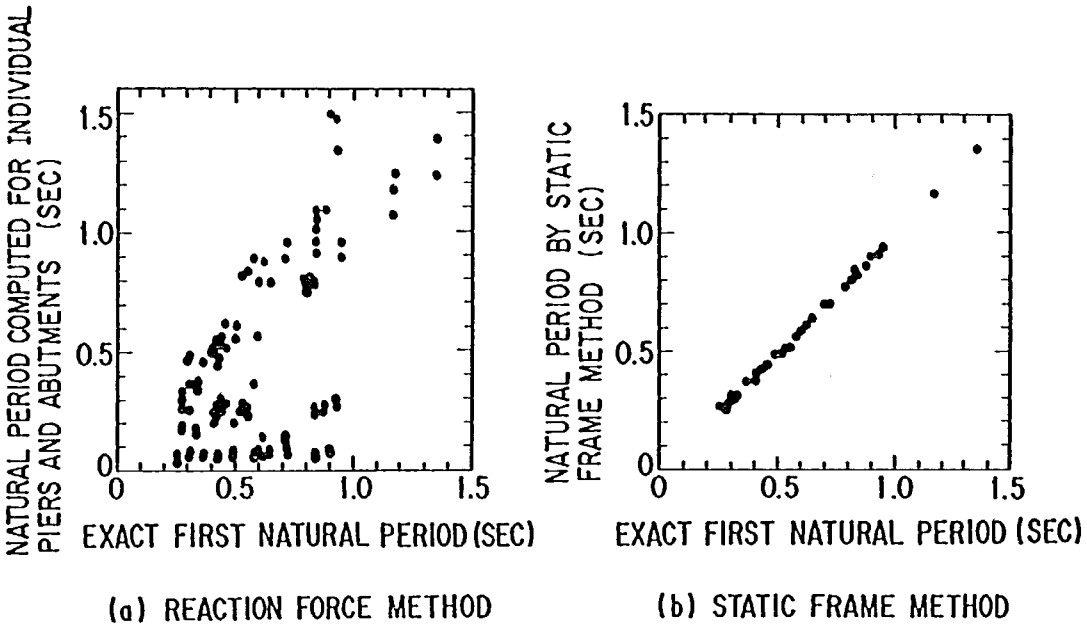
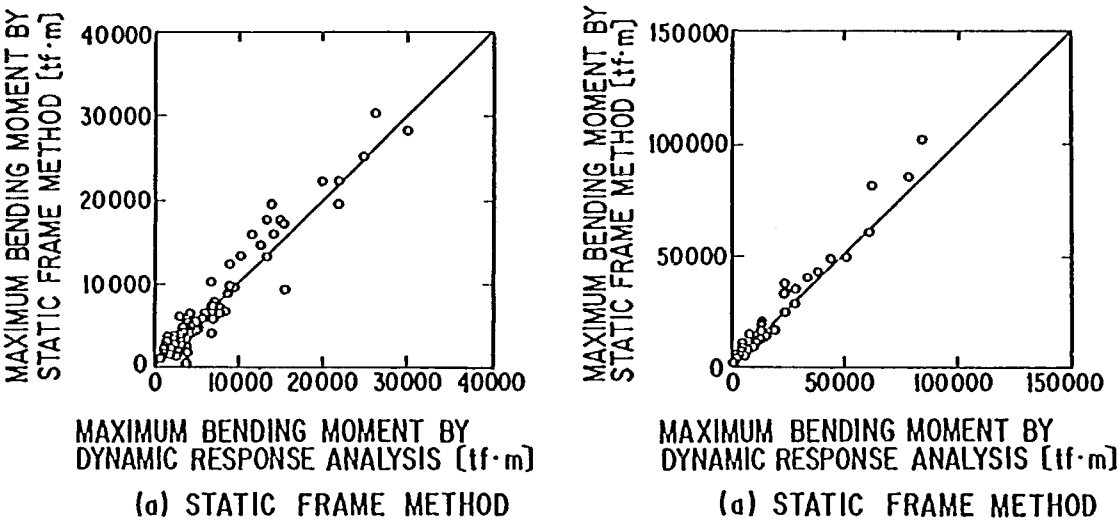


Fig.5 Maximum Bending Moment and Shear Force

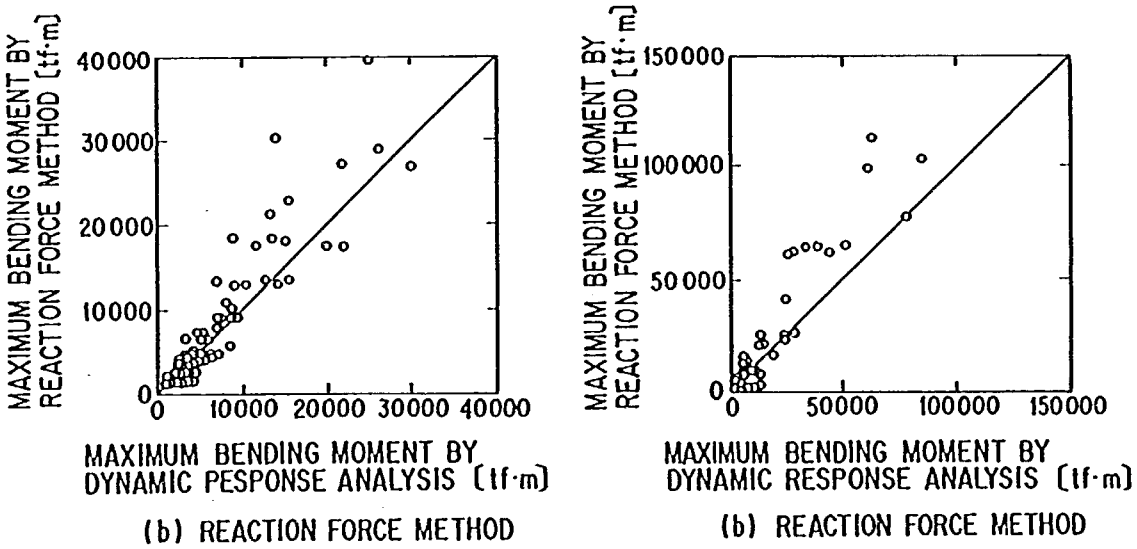


(a) REACTION FORCE METHOD (b) STATIC FRAME METHOD

Fig.6 Comparison of Natural Period



(a) STATIC FRAME METHOD (a) STATIC FRAME METHOD



(b) REACTION FORCE METHOD (b) REACTION FORCE METHOD

(1) KAIHOKU RECORD (2) TSUGARU RECORD

Fig.7 Comparison of Maximum Bending Moment

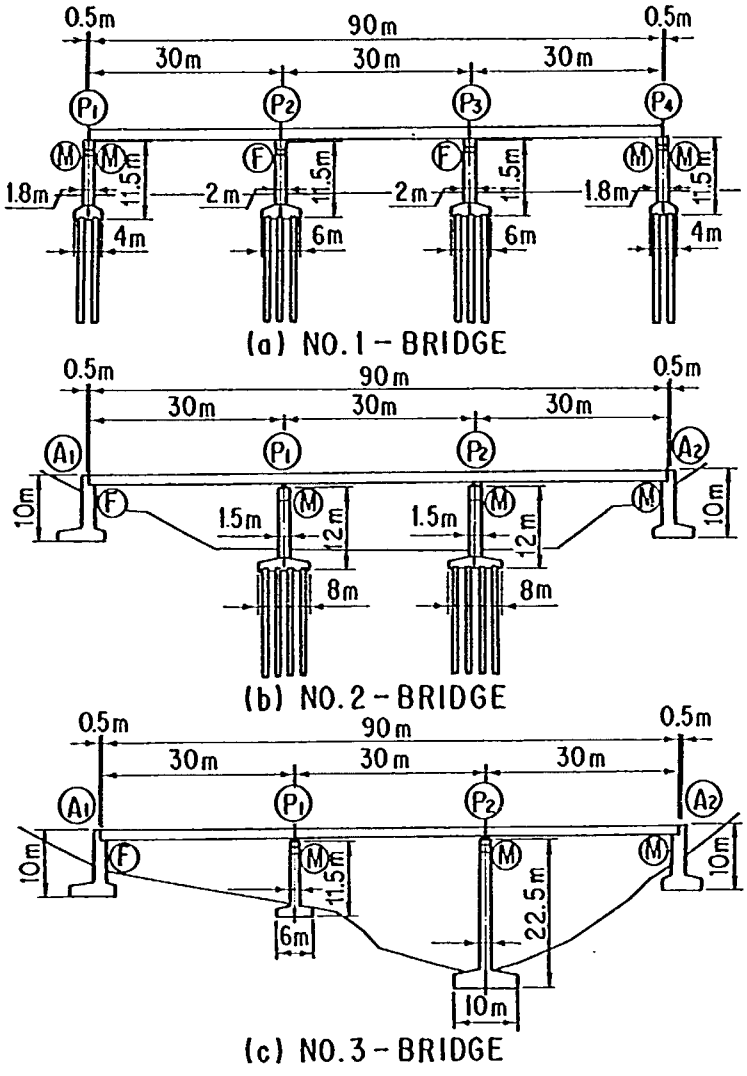


Fig.8 Three Bridges Analyzed by Static Method

Table 2 Distribution of Lateral Force

BRIDGES	ANALYTICAL METHODS	A1 (P1)	P1 (P2)	P2 (P3)	A2 (P4)
NO.1-BRIDGE	REACTION FORCE METHOD	27.6	75.9	75.9	27.6
	STATIC FRAME METHOD	25.4	78.1	78.1	25.4
NO.2-BRIDGE	REACTION FORCE METHOD	27.6	75.9	75.9	27.6
	STATIC FRAME METHOD	54.7	48.0	50.5	53.9
NO.3-BRIDGE	REACTION FORCE METHOD	27.6	75.9	75.9	27.6
	STATIC FRAME METHOD	32.5	101.4	9.8	63.1

BEHAVIOUR OF STIFFENED BOX-SECTION STEEL BRIDGE PIERS IN SEISMIC REGIONS FROM MODEL TESTS

by
Gregory A. MACRAE
Kazuhiko KAWASHIMA
K. HASEGAWA
T. IKEUCHI
and
K. OSHIMA
Public Works Research Institute
Ministry of Construction

THE 7TH U.S. — JAPAN BRIDGE WORKSHOP
Tsukuba Science City, Japan
May 8 and 9, 1991

Behaviour of Stiffened Box-Section Steel Bridge Piers in Seismic Regions from Model Tests

by Gregory A. MacRae[1]

Kazuhiko Kawashima[2]

K. Hasegawa[3]

T. Ikeuchi[4]

and K. Oshima[5]

ABSTRACT

Twenty-two model stiffened box-shape steel bridge pier specimens of the type commonly used in Japan were tested in order to obtain their strength and ductility capacity and to understand their behaviour. Hollow specimens and specimens partially filled with concrete were tested both under applied lateral loading and shaking table testing. It was found that the specimens failed by overall buckling of one side as well as local panel buckling and fracture. The strength of specimens with concrete infill was increased however their deformation capacity was decreased. Specimens tested on the shaking table sustained yielding predominantly in one direction with little absorption of energy. This was different from that assummed by the applied lateral loading regimes. Specimens with greater section slendernesses generally had lower ductility capacities. A method for estimating the strength of these specimens which was independent of the effect of the section slenderness was found to be satisfactory.

INTRODUCTION

Steel bridge piers, which are constructed by welding thin plate together, have been used over the past 30 years for the construction of bridges in Japan. The construction cost of these piers is generally more than that of reinforced concrete piers but their section size is significantly less making them ideal for use in city locations where land prices are high and where there are restrictions on construction space. In some cases concrete is placed inside these piers to provide extra protection if a vehicle collides into them. Damage has not been observed in these sort of piers to date and few tests have been carried out to investigate their likely behaviour during an earthquake.

Twenty-two steel pier specimens were tested in order to assess their strength and ductility capacity because it is realized that accelerations greater than the design level may be developed in bridges during a major earthquake. Applied loading tests and shaking table tests were performed on hollow pier specimens with different configurations of internal stiffeners and on specimens which were partially filled with concrete. In this paper some of the more important aspects of the behaviour of these specimens are summarized.

SPECIMEN CONSTRUCTION, DESIGN REQUIREMENTS AND TESTING METHODS

The test specimen sizes were selected to be scaled down versions of real piers. The box-shaped sections consisted of 4 major plates to which ribs and diaphrams were welded for stiffening and strengthening. Real piers are generally large enough that a person may enter and weld from the inside but this construction technique was unable to be used on the smaller pier specimens. The specimen was therefore constructed in stages as shown in Figure 1. Weld was applied to the inside of the specimen before the final web-plate was welded into place from the outside. The diaphrams extended outside the section on one side to facilitate the welding of the final web plate to the specimen. The longitudinal stiffeners on the inside of the final web plate were discontinuous at the diaphram positions and at the base.

---

[1] Overseas Researcher, Earthquake Engineering Division, Public Works Research Institute, Tsukuba
[2] Head, Earthquake Engineering Division, Public Works Research Institute, Tsukuba, Japan
[3] Senior Researcher, Earthquake Engineering Division, Public Works Research Institute, Tsukuba
[4] Chief Design Engineer, Metropolitan Expressway Public Corporation, Tokyo, Japan
[5] Construction Division Manager, Hanshin Expressway Public Corporation, Kobe Construction Bureau, Osaka, Japan

Design was carried out according to the Japanese bridge design code [1] which is based on elastic design considerations. The background to the buckling design criteria for these piers is published in design guidelines [2]. There are two important section slenderness ratios which are required to be greater than certain values in order that premature buckling does not reduce their strength. They are:

1) The panel slenderness ratio, b/(nft), which must be less than 28 or 24 for Grades SS41 or SM50 steel respectively. This check ensures that local panel buckling will not occur before the yield strength of the section is reached. Local panel buckling refers to buckling panels between the vertical stiffeners. In this ratio b is the width of the section (cm), t is the plate thickness (cm), n is the number of panels divided by vertical stiffeners, as shown in Figure 2, and f is given as $f = 0.65(\phi/n)^2 + 0.13(\phi/n) + 1.0$, ϕ is the stress gradient given as $\phi = (\sigma_2 - \sigma_1)/\sigma_1$, and σ_2 and σ_1 are the stresses at each edge of the plate, where $\sigma_1 > \sigma_2$, and compressive stress is defined as positive. It was conservatively assumed that f = 1.0 in the panels which yielded.

2) The gamma ratio, $\gamma_1/\gamma_{1,req}$, which must be greater than unity. This check ensures that overall buckling of one side of the pier will not occur before the yield strength of the section is reached. The stiffness of each panel and longitudinal stiffener was used to obtain an equivalent stiffness for the side as a whole and the effect of the lateral stiffeners was also considered. The value of γ_l, which is the relative stiffness of the longitudinal stiffeners, was able to be calculated as $\gamma_l = I_l/(bt^3/11)$ where the value of I_l is given below. The value of $\gamma_{1,req}$ was able to be calculated using the appropriate value from Equations 1 or 3 as described below.

i) Equation 1 should be used to calculate $\gamma_{1,req}$ when α is not greater than α_0 and the moment of inertia I_t (cm^4) of a transverse stiffener satisfies Equation 2.

$$\gamma_{1,req} = 4\alpha^2 n\left(\frac{t_o}{t}\right)^2(1 + n d_l) - \frac{(\alpha^2+1)^2}{n} \quad (t \geq t_o)$$

$$\gamma_{1,req} = 4\alpha^2 n(1 + n d_l) - \frac{(\alpha^2+1)^2}{n} \quad (t < t_o) \qquad (1)$$

$$I_t \geq \frac{bt^3}{11} \cdot \frac{1 + n\gamma_{1,req}}{4\alpha^3} \qquad (2)$$

ii) Equation 3 should be used in all other cases such as when the effect of the transverse stiffeners in the computation of $\gamma_{1,req}$ is insignificant and their effect is ignored.

$$\gamma_{1,req} = \frac{1}{n}\left[\left\{2n^2\left(\frac{t_o}{t}\right)^2(1 + n d_l) - 1\right\}^2 - 1\right] \quad (t \geq t_o)$$

$$= \frac{1}{n}\left[\{2n^2(1 + n d_l) - 1\}^2 - 1\right] \quad (t < t_o) \qquad (3)$$

where

α is the aspect ratio of stiffened plate, $\alpha = a/b$,

α_0 is the critical aspect ratio, $\alpha_o = \sqrt[4]{1 + n\gamma_l}$

a is the spacing of transverse stiffeners (cm)

b is the width of stiffened plate (cm)

d_l is the ratio of the longitudinal stiffener cross sectional area to that of the main plate, $d_l = A_l/(bt)$, (cm)

A_l is the area of each longitudinal stiffener, $A_l = b_s t_s$

I_l is the second moment of area of each longitudinal stiffener. The code requires that the moment of inertia of stiffeners such as those used in steel piers be calculated about the surface of the stiffened plate on the stiffener side. The value of I_l is therefore given as $I_l = b_s^3 t_s/3$.

t_o is the minimum thickness of plate which is given as b/(28fn) for SS41 and b/(24fn) for SM50 plate. A more general expression for the allowable buckling ratio of compact sections using the allowable yield stress is given in Equation 4.

$$\frac{b}{t_o.n.f} \cdot \frac{\sqrt{F_y}}{1047.7} = 1.0 \qquad (4)$$

t_s is the thickness of each longitudinal stiffener

A further ratio, the gamma* ratio [2], γ_1/γ_1^*, is able to be used to predict whether local panel buckling or overall buckling of one side will occur first as shown in Figure 3. If $\gamma_1/\gamma_1^* > 1$ then local buckling of the panels between the longitudinal stiffeners is the expected initial buckling mode but if $\gamma_1/\gamma_1^* < 1$ then overall buckling of one side is expected. The value of γ_l^* is given in Equation 5.

$$\gamma_1^* = 4\alpha^2 n(1+n d_l) - \frac{(\alpha^2+1)^2}{n} \quad (\alpha \le \alpha_o)$$

$$= \frac{1}{n}\left[\{2n^2(1+n d_l)-1\}^2 - 1\right] \quad (\alpha > \alpha_o) \qquad (5)$$

Typical test setups are given for the applied lateral loading and shaking table testing at the laboratory facilities of the Public Works Research Institute in Figures 4 and 5. The levels of axial load, N, used were in all cases less than 11% of the yield axial load, N_y. The applied loading tests were carried out by controlling the displacement of the lateral loading ram. This displacement was later corrected to take account of the rotation at the base. Cyclic loading tests of larger specimens was performed at a frequency of 0.013 Hz while for the smaller specimens a frequency of about 0.33 Hz was used. In the shaking table testing, the shaking table was initially excited with sine-waves of different frequencies and low amplitudes to determine the elastic response period of the specimen on the table. Scaled versions of the acceleration record obtained at Hachiro-gata during the Nihon-kai-chubu earthquake of 26 May 1983 were used as the basic input ground motions. The time-axis was reduced to one-half of the actual time to adjust the predominant frequency of the records so that the relationship between the period and the response spectrum shape would be more like that expected for a real bridge pier.

The yield displacement, d_y, was defined as the displacement at which yielding first occurred in an extreme fibre of the section. The yield load, H_y, and yield displacement, d_y, were able to be calculated before the test started from the measured section properties and from the results of the material tests. The same loading regime, yield load, H_y, and yield displacement, d_y, were used in the concrete infilled specimens as in the hollow specimens in order to investigate the effect of the concrete infill. The ultimate displacement, d_u, was calculated as the point at which the backbone curve of the hysteresis diagram became less than the yield load, H_y. The backbone curve was constructed by connecting the points of maximum displacement in the cycle with the highest load for each displacement ductility. The ductility capacity, μ, was defined as the ultimate displacement, d_u, divided by the yield displacement, d_y.

SPECIMENS TESTED

The differences between the twenty two tests on steel specimens which were conducted at the Public Works Research Institute are described in summary form in Tables 1 and 2 where the section size, main plate thickness, size of longitudinal stiffeners, number of longitudinal stiffeners, lateral stiffener spacing and size, gamma ratio ($\gamma_1/\gamma_{1,req}$), panel slenderness ratio (b/nft), gamma* ratio (γ_1/γ_1^*), distance from the base of the specimen to the point of application of the load and to the level of concrete infill, the grade of the steel, the properties of the steel obtained from material tests, the specimen axial load ratio (N/N_y), the number of cycles of loading applied to each specimen as well as the calculated and actual periods of the specimens on the shaking table are given. The calculated yield strength and yield displacement are given in Table 3. The section properties for all of the specimens tested satisfied the current recommendations of the present Japanese code "Specifications for Highway Bridges" [1].

Specimens S1 to S12 had sections of the same size. Specimen S1 is shown in Figure 6. Specimen S2 was the same as Specimen S1 except that the weld size was 4.5mm rather than 3mm and Specimens S3 to S12 all had 3 to 4mm weld sizes. Specimens S1 and S3 to S9 had the same internal construction but were subject to different loading regimes. Specimens S3, S4, and S5 were tested on the shaking table with 2x, 3x and 4x the earthquake record magnitude while all other specimens of this size were subjected to applied lateral loading. Specimen S7 was the same as Specimen S6 except that the loading regime applied to Specimen S7 was of decreasing magnitude (1 cycle to μ = 5, 4, 3, 2 and 1). All other specimens in applied load tests were subjected to increasing displacement ductilities. Specimens S1, S6, S8, and S9 were subjected to 10, 1, 3 and 5 cycles to each displacement ductility respectively. Specimens S13 to S18 were larger specimens which were tested by applied lateral loading. Specimens S16 and S17 were partially filled with concrete and Specimen S17 was the same as Specimen S16 except that it had a "T"-shaped internal longitudinal stiffener. Specimens S19 to S22 were smaller specimens with the same internal steel construction. Specimens S20 and S22 were partially filled with concrete. Specimens S19 and S20 were tested by applied lateral loading and Specimens S21 and S22 were tested on the shaking table. Specimens S13 to S18 were larger specimens constructed from SM50 steel with a specified allowable yield stress of 1900kgf/cm^2 [1]. All other specimens were constructed from SS41 steel with a specified allowable yield stress of 1400kgf/cm^2 [1].

TEST RESULTS

Hysteretic Behaviour

Test results for all specimens showing the yield and maximum loads, specimen overstrength factor ($\phi_S = P_{max}/P_y$), yield and ultimate displacements, ductility ($\mu = d_u/d_y$) and mode of failure are given in Table 3. The hysteretic behaviour, strength, mode of failure and deformation capacity are described below.

The hysteretic behaviour of all hollow specimens subjected to applied lateral loading was similar. From the hysteresis loops of Specimen S1, shown in Figure 7, it may be seen that little energy was absorbed before the cycles to a displacement ductility, μ, of 2. At $\mu = 3$ the loop size increased and was fat showing that a large amount of energy was absorbed. Buckling was first observed during these cycles. A large amount of strength degradation was developed during the cycles to $\mu = 4$ as the buckling deformation of the plate increased. The strength continued to decrease after the defined failure point.

The concrete-filled specimens generally had stable hysteresis loops with a post-elastic stiffnesses of about 14% of the initial stiffness before fracture occurred. At this point there was a sudden loss of load carrying capacity as shown for Specimen S16 in Figure 8.

The behaviour of Specimen S5, which was subjected to shaking table testing with four times the Hachiro-gata record, is shown in Figure 9. This behaviour was typical of all of the specimens tested on the shaking table. The loop followed the shape of the backbone curve of the specimens tested by applied lateral loading. Yielding occurred almost entirely in one direction resulting in the energy absorbed being similar to that in a monotonic test. The maximum displacements observed were larger than those estimated by the equal energy assumption and there were large residual displacements at the top of these specimens at the end of the tests.

Effect of Loading Type

The curve shape and ductility capacity of Specimens S1, S8 and S9, which were obtained using regimes with 10, 3 and 5 cycles of loading to each displacement ductility respectively, had similar results as shown in Figure 10. The deformation capacity of Specimen S6, which was subjected to only 1 cycle of loading to each displacement ductility, had a greater ductility capacity. Dependence of ductility on the number of load cycles was smaller in these steel pier tests than in reinforced concrete piers [3]. The strength of the specimens on the shaking table dropped off more slowly than those tested by applied lateral loading because they were subjected to only a small amount of yield reversal. Specimen S7, which was subjected to decreasing displacement ductilities, did not fail but had a backbone curve similar to that of monotonically loaded specimens because the first cycle of loading determined this curve.

It would normally be expected that the number of cycles of loading would strongly influence the deformation capacity of members subjected to both axial load and cyclic loading because axial shortening occurs and increases the damage [4]. This axial shortening is proportional to the cumulative inelastic rotation within the region of yielding before buckling becomes severe [5]. The fact that there was little difference in the behaviour of the pier specimens which were subjected to between 3 and 10 load cycles to each ductility is thought to be because low levels of axial load were applied in these tests.

The behaviour of Specimens S1 and S2 were almost identical. The 3.0mm welds of Specimen S2 were strong enough to develop the full section strength but were insufficient to form a truly composite section. However, the welds remained together long enough to achieve the same ductility as that attained by Specimen S1 which had a 4.5mm weld.

There was a large difference between the monotonic type of hysteresis loop observed in the shaking table testing and the hysteresis loop from the applied loading tests. A research program is presently underway at the Public Works Research Institute to understand why very little reversal of yielding occurred in the shaking table tests by running dynamic analyses of piers with different bilinear stiffness factors.

Mode of Failure

1) Overall Buckling of One Side

Specimens with a gamma* ratio up to about 2.0 had a failure mechanism of overall buckling of one side after several load reversals. While the specimens with gamma* ratios less than 1.0 failed by pure overall buckling of one side, the specimens with gamma* ratios between 1.0 and 2.0 sustained buckling of the panels between the longitudinal stiffeners before the longitudinal stiffeners carried the load and overall buckling of one side caused strength loss. The maximum amplitude of buckling generally occurred mid-distance between the base of the specimen and the first lateral stiffener and the wavelength of the buckle was spread over the whole base panel. The web of the section also started to buckle as the longitudinal stiffeners twisted. Strength was rapidly lost during the later stages of buckling and finally the weld connecting the flange and

web together fractured. This mode of "overall buckling of one side" is shown for Specimen S1 in Figure 11 where Face 1 and Face 3 are the flanges. In the shaking table tests, in which yielding occurred predominantly in one direction, it was found that buckling generally became severe on only one side of the specimen.

While buckling was generally concentrated in the base section of most of the specimens there were cases where some buckling was also observed in the adjoining section. In Specimen S13 it was found that buckling was concentrated in the second section up from the base on one flange and on the opposite flange deformation in the two bottom sections caused twisting of the first lateral stiffener from the base. Buckling was observed in the adjoining section as well as the base section of Specimen S14 and also slightly in Specimens S1 and S19. Deformation in more than one section would be expected to increase the overall deformation capacity of these specimens.

2) Panel Buckling and Fracture

Limited panel buckling occurred in specimens with large gamma* ratios and fracture of the steel near the base of the specimens caused final failure. When the gamma* ratio is large the gamma ratio is also required to be high in order that the panel buckling limits are not violated. Therefore, local panel buckling will not generally occur until a large amount of inelastic strain has been sustained. The buckle wavelength was much smaller than when overall buckling of one side occurred. Fracture occurred in Specimen S11 at the centre of the buckle where the strain was concentrated and fracture near or in the weld at the base of both Specimens S11 and S12 was also observed. These types of fracture are very dependent on the strength of the weld, on the amount of welding residual stresses in the plate, the fracture strengths of the steel and the weld, and on any material discontinuities which may initiate fracture.

The concrete-filled specimens suffered little buckling and failed by fracture of the weld or of the steel beside the weld at the base. It seems as though the concrete cracked at the base of the specimen causing concentrated localised deformation in the steel plate beside the concrete crack which eventually resulted in fracture. This mode of behaviour is especially likely to occur if the uncracked section strength is considerably greater than the overstrength of the cracked section because only one crack will occur giving the behaviour shown in Figure 12. The use of the "T"-shaped longitudinal stiffener in Specimen S17 was of no benefit as the mode of failure of concrete-filled specimens was fracture near the base rather than buckling. It seems as though filling the specimens with concrete to 1/3 of their height was satisfactory to ensure that the major amount of the deformation occurred at the base rather than above the level of concrete infill.

Strength

The specimen overstrength, ϕ_S, which was calculated as the ultimate specimen strength, P_{max}, divided by the initially calculated strength, P_y, ranged from 1.27 to 2.14 times as shown in Table 3. The increase in the strength of the hollow specimens above the yield strength was thought to occur for the following reasons: the section stresses may be more like that assumed by plastic behaviour in which all the fibres in the section are at yield, strain hardening increases the strength, and the axial load on the section will allow even larger overstrength values to be obtained [5]. The strength of concrete-filled specimens were 1.26 and 1.34 times greater than that of the identical hollow specimens because the concrete also resisted load. The average overstrength values were 43% and 84% for hollow and concrete-filled specimens respectively.

Lay [6] has proposed an empirical method, based on the results of experiments on steel beams, to estimate the maximum strength of a steel member, P_{max}, as a function of the material overstrength, $\phi_{om} = \sigma_{max}/\sigma_y$, and plastic load, P_p, as $P_{max} = (\phi_m + 1)/2.P_p$ where $P_p = S/Z.P_y$ and S and Z are the plastic and elastic section modulii respectively. When this method was used on Specimen S13 it was found that the ratio of the plastic strength to the yield strength, P_p/P_y, considering the effect of axial load was 1.155 and the maximum stress, σ_{max}, divided by the yield stress, σ_y, of the steel material used in this specimen was 1.43. The predicted strength was therefore $(1.43 + 1)/2 \times 1.155P_y = 1.40P_y$ which was close to the actual strength of $1.38P_y$. It may be seen in Figure 13 that this method estimated the strengths of the specimens to ±10%. The strengths of Specimens S1 to S5 were not included in this figure because it was considered that there were some gross errors in the material tests for these specimens. The maximum strengths of Specimens S1 to S5 were even greater than $\phi_{om}P_p$. The slenderness of the sections did not seem to effect the maximum strengths because these members were compact.

Deformation Capacity

The ductility capacity was generally greater in the more compact sections than in those with more slender characteristics as may be seen from the results of Specimens S13, S14, S15 and S18, in which the ductilities were 4.21, 3.05, 3.99 and 3.13, as well as Specimens S10, S11 and S12, in which the ductilities were 3.34, 4.11 and 4.31. However, the ductility of Specimen S1, which was 4.33, was higher than for Specimens S10, S11, and S12. This is possibly because some buckling occurred in the section above the base as well as in the base section in this specimen.

The specimens tested on the shaking table had large maximum displacement and ductility capacities because they were subjected to little reversal of loading and their behaviour was almost monotonic. Similarly, the ductility capacity of Specimen S6 of 5.04 was larger than that of Specimens S1 of 4.33, S2 of 4.02, S8 of 3.67 and S9 of 3.81 as a result of it only being subjected to one cycle of loading at each ductility step.

Placing concrete inside these specimens did not increase the ductility capacity due to the difference in the mode of failure. The ductility capacity of the Specimen S16, which was filled with concrete was 10% less that of Specimen S15 which was identical but hollow. Similarly the ductility capacity of Specimen S20, which was filled with concrete was 23% less that of Specimen S19.

The backbone curves of specimens tested with 10 cycles of applied loading to each ductility are given in Figure 14. It may be seen that the ductility capacities of these specimens, calculated from the point when the backbone curve became less than the yield strength, ranged between 3 and 5. A method for predicting the deformation capacity of steel specimens has also been produced from the testing described herein which considers the maximum strain in an equivalent plastic hinge length and the resistance against buckling [7].

SUMMARY

The results of 22 tests on hollow and concrete-filled steel specimens with different configurations of internal steel using applied lateral loading and shaking table testing were described in this paper. The major findings are given below:

1) The ductilities of the specimens tested with between 3 and 10 cycles of loading to each displacement step ranged from 3.67 to 4.33. These ductilities increased with the number of cycles of loading. However the specimen subjected to one cycle of loading to each displacement step and the specimen tested on the shaking table had increased ductilities of 5.09 and 12.9 respectively.
2) The specimens tested on a shaking table sustained little reversal of yielding. Their load history was therefore different from the assumed lateral loading regime in the applied lateral load tests.
3) The final mode of buckling of specimens with a gamma* ratio less than about 2.0 was overall buckling of one side. The major buckling deformation in these specimens generally occurred midway between the base and the first lateral stiffener.
4) Severe local panel buckling and fracture were observed in specimens with a gamma* ratio greater than 2.0.
5) Concrete infill increased the strength and decreased the deformation capacity of specimens in these tests.
6) The maximum strengths of the compact hollow sections could be estimated satisfactorily without considering the effects of section slenderness.
7) The ductility capacities of specimens tested by applied lateral loading ranged from about 3 to 5.
8) The displacement ductility capacity generally decreased for members with greater section slendernesses.

REFERENCES

1. Japan Road Association, "Specifications for Highway Bridges", Part II : Steel Bridges, English Edition, 1987.
2. Subcommittee on Stability Design, "Guidelines for the Stability of Steel Structures", edited by Fukumoto Y, Committee on Steel Structures, Japan Society of Civil Engineers, 1987.
3. Kawashima K. and Koyama T., "Effect of Number of Cycles of Loading Cycles on Dynamic Characteristics of Reinforced Concrete Bridge Piers", Proc. JSCE, Structural Eng., Earthquake Eng., Vol. 15, No. 1, 1988.
4. Popov E. P., Bertero V. V. and Chandramoulli S., "Hysteretic Behaviour of Steel Columns", UCB/EERC 75-11, September 1975.
5. MacRae G. A., Carr A. J., and Walpole W. R., "The Seismic Response of Steel Frames", Research Report 90-06, Department of Civil Engineering, University of Canterbury, 1990.
6. Lay M. G., "Flange Local Buckling in Wide-Flange Shapes", *Journal of the Structural Division*, ASCE, ST6, December 1965, p95-116.
7. MacRae G. A. and Kawashima K., "Estimation of the Deformation Capacity of Steel Bridge Piers", US-Japan Workshop on Cyclic Buckling of Steel Structures and Structural Elements under Dynamic Loading Conditions, Osaka, 1-3 July 1991.

Table 1. Pier Characteristics (a)

Pier	Section Size (mm) b + 2t	b	Plate Thick. t(mm)	Longitudinal Stiffeners Size (mm^2)	No. n-1	Lateral Stiffener Spacing (mm)	Size (mm^2)	Gamma Ratio >1.0	bIE_Y tfn <1047	Gamma' Ratio
S1	409 x 400		4.5	35x3.2	3	350	55x3.2	1.559	831	0.950
S2	409 x 400		4.5	35x3.2	3	350	55x3.2	1.559	831	0.950
S3	409 x 400		4.5	35x3.2	3	350	55x3.2	1.559	831	0.950
S4	409 x 400		4.5	35x3.2	3	350	55x3.2	1.559	831	0.950
S5	409 x 400		4.5	35x3.2	3	350	55x3.2	1.559	831	0.950
S6	409 x 400		4.5	35x3.2	3	350	55x3.2	1.559	831	0.950
S7	409 x 400		4.5	35x3.2	3	350	55x3.2	1.559	831	0.950
S8	409 x 400		4.5	35x3.2	3	350	55x3.2	1.559	831	0.950
S9	409 x 400		4.5	35x3.2	3	350	55x3.2	1.559	831	0.950
S10	409 x 400		4.5	40x3.2	3	350	55x3.2	2.259	831	1.38
S11	409 x 400		4.5	50x3.2	3	350	55x3.2	4.158	831	2.54
S12	409 x 400		4.5	50x10.	3	350	55x3.2	8.110	831	5.01
S13	800 x 820		10.	64x6.0	5	300	112x4.5	6.409	580	1.746
S14	800 x 820		10.	64x6.0	5	680	112x4.5	1.127	580	0.294
S15	800 x 820		10.	64x6.0	5	390	112x4.5	3.583	580	1.017
S16	800 x 820		10.	64x6.0	5	390	112x4.5	>3.583	580	1.017
S17	800 x 820		10.	64x6.0	5T	390	112x4.5	>3.583	580	1.017
S18	800 x 820		10.	64x6.0	4	390	112x4.5	3.117	599	1.290
S19	329 x 320		4.5	30x3.2	3	260	50x32	2.299	666	0.854
S20	329 x 320		4.5	30x3.2	3	260	50x32	>2.299	666	
S21	329 x 320		4.5	30x3.2	3	260	50x32	2.299	666	0.854
S22	329 x 320		4.5	30x3.2	3	260	50x32	>2.299	666	

Table 2. Pier Characteristics (b)

Pier	Height to Load (m)	Height of Concrete (m)	Steel Strength Grade	Youngs Modulus ($x10^5$ kgf/cm^2)	Yield Stress (kgf/cm^2)	Material Over-strength ϕ_{om}	Axial Load (tf)	Axial Load Ratio	Load Cycles	Calculated Period (sec)	Actual Period (secs)
S1	2.40	-	SS41	1.321	2133	1.045	20	0.110	10	-	-
S2	2.40	-	SS41	1.321	2133	1.045	20	0.110	10	-	-
S3	2.40	-	SS41	1.321	2133	1.045	20	0.110	x2H	.422	.490
S4	2.40	-	SS41	1.321	2133	1.045	20	0.110	x3H	.422	.481
S5	2.40	-	SS41	1.321	2133	1.045	20	0.110	x4H	.422	.476
S6	2.40	-	SS41	1.736	2089	1.349	20	0.083	1	-	-
S7	2.40	-	SS41	1.736	2089	1.349	20	0.083	1 (decr)	-	-
S8	2.40	-	SS41	1.848	2977	1.318	20	0.079	3	-	-
S9	2.40	-	SS41	1.848	2977	1.318	20	0.079	5	-	-
S10	2.40	-	SS41	1.736	2089	1.349	20	0.082	10	-	-
S11	2.40	-	SS41	1.736	2089	1.349	20	0.078	10	-	-
S12	2.40	-	SS41	1.736	2089	1.349	20	0.054	10	-	-
S13	6.00	-	SM50	1.729	3845	1.432	105	0.092	10	-	-
S14	6.00	-	SM50	1.729	3845	1.432	105	0.092	10	-	-
S15	6.00	-	SM50	1.729	3845	1.432	105	0.092	10	-	-
S16	6.00	2.00	SM50	1.729	3845	1.432	105	0.092	10	-	-
S17	6.00	2.00	SM50	1.729	3845	1.432	105	0.092	10	-	-
S18	6.00	-	SM50	1.729	3845	1.432	105	0.092	10	-	-
S19	2.40	-	SS41	1.591	2418	1.54	20	0.078	10	-	-
S20	2.40	0.78	SS41	1.591	2418	1.54	20	0.078	10	-	-
S21	2.40	-	SS41	1.591	2418	1.54	20	0.078	3&3.5H	0.46	0.500
S22	2.40	0.78	SS41	1.591	2418	1.54	20	0.078	3&3.5H	0.46	0.454

Table 3. Calculated and Experimental Loads and Displacements

Pier	Calculated Yield Load P_y (tf)	Maximum Load P_{max} (tf)	Specimen Overstrength ϕ_s	Calculated Yield Displ. d_y (mm)	Maximum Displ. d_u (mm)	Ductility d_u / d_y μ	Mode of Failure
S1	8.6	13.8	1.60	13.5	58.5	4.33	Buckling
S2	8.6	14.2	1.65	13.5	54.3	4.02	Buckling
S3	8.6	-	-	13.5	-	-	No failure
S4	8.6	-	-	13.5	-	-	No failure
S5	8.6	15.9	1.85	13.5	173.5	12.9	Buckling
S6	11.7	16.5	1.41	13.9	70.0	5.04	Buckling
S7	11.7	16.9	1.44	13.9	-	-	Buckling
S8	12.4	17.3	1.40	13.9	51.0	3.67	Buckling
S9	12.4	17.1	1.38	13.9	53.0	3.81	Buckling
S10	12.4	15.0	1.27	13.9	46.7	3.34	Buckling
S11	12.4	17.2	1.41	13.9	57.5	4.11	Buckling-Base Weld Failure
S12	12.4	23.7	1.43	13.9	62.1	4.31	Base Weld Failure
S13	59.4	81.7	1.38	62.1	261.3	4.21	Buckling
S14	59.4	79.1	1.33	62.1	189.2	3.05	Buckling
S15	59.4	80.0	1.35	62.1	247.7	3.99	Buckling
S16	59.4	100.0	1.69	62.1	221.9	3.57	Base Weld Failure
S17	59.4	101.0	1.70	62.1	222.1	3.57	Base Weld Failure
S18	59.4	76.1	1.33	62.0	194.2	3.13	Buckling
S19	6.5	10.4	1.60	16.3	85.1	5.19	Buckling
S20	6.5	13.9	2.14	16.3	65.3	3.98	Base Weld Failure
S21	6.5	12.4	-	16.3	116.	-	Buckling
S22	6.5	14.5	-	16.3	88.	-	Base and Side Weld Failure

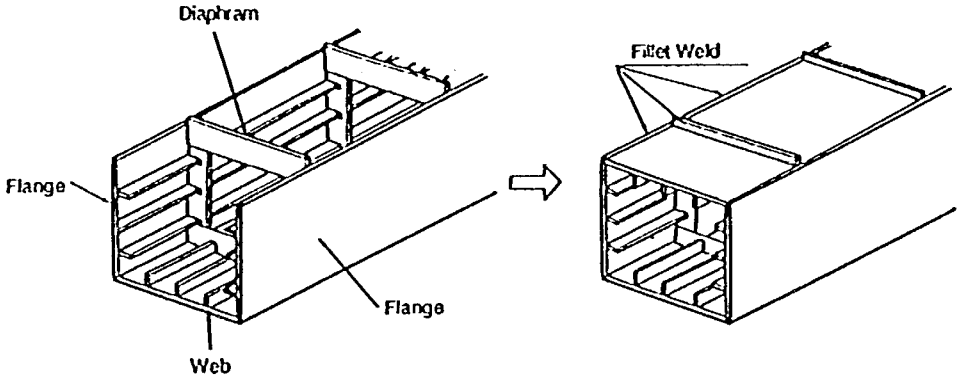


Figure 1 - Pier Construction

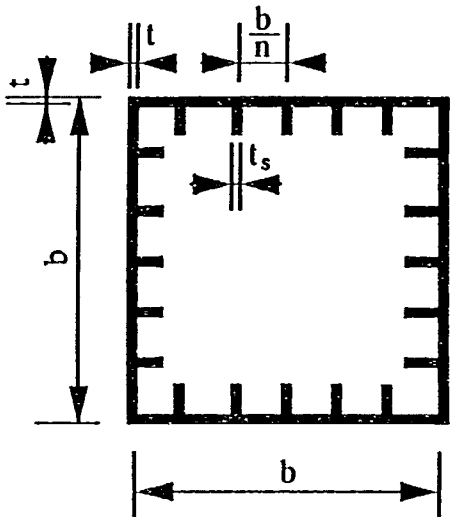
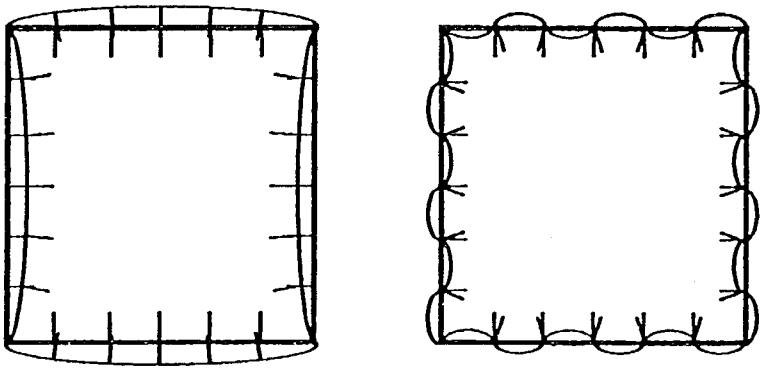


Figure 2 - Section Dimensions



(a) Overall buckling of One Side

(b) Local Panel Buckling

Figure 3 - Modes of Deformation

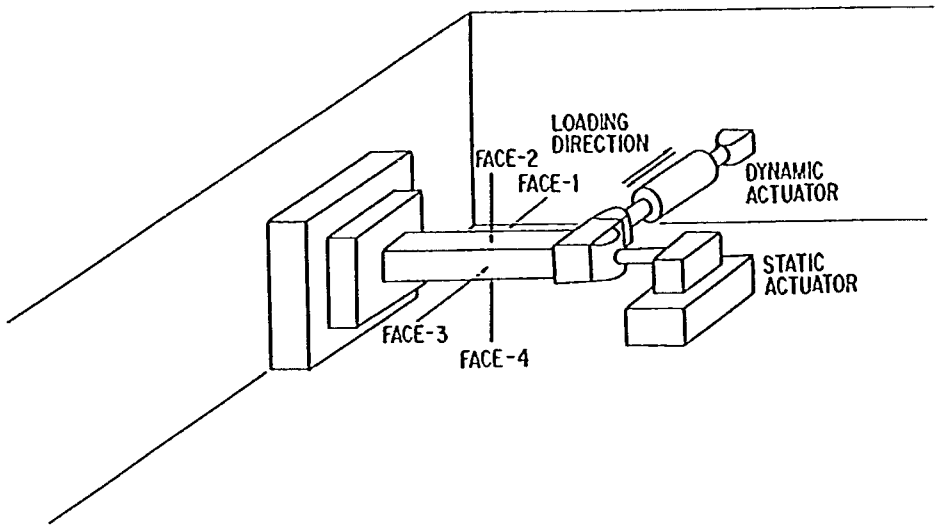


Figure 4 - Applied Load Setup

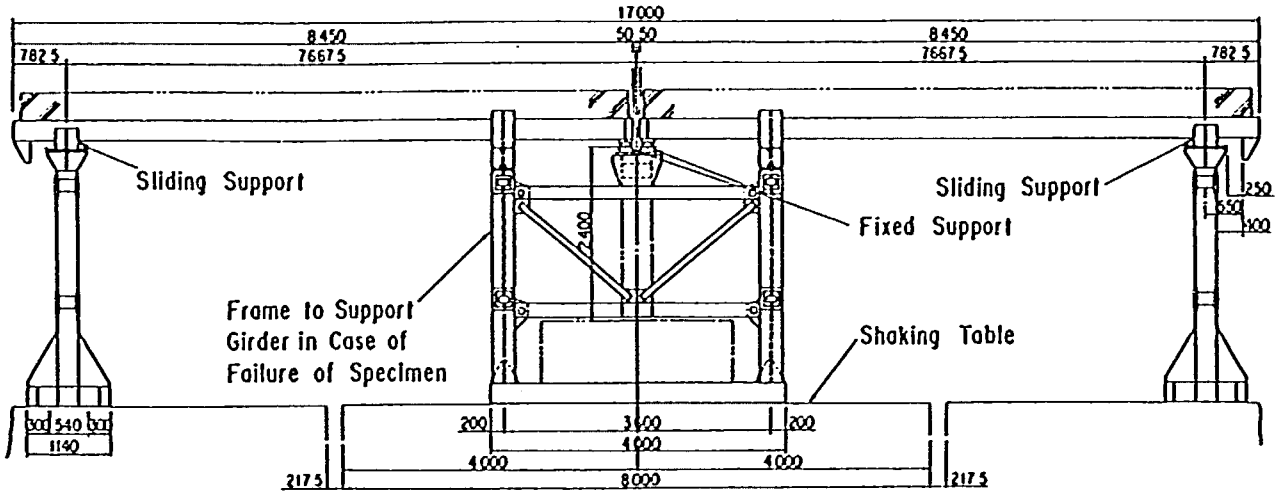


Figure 5 - Shaking Table Setup

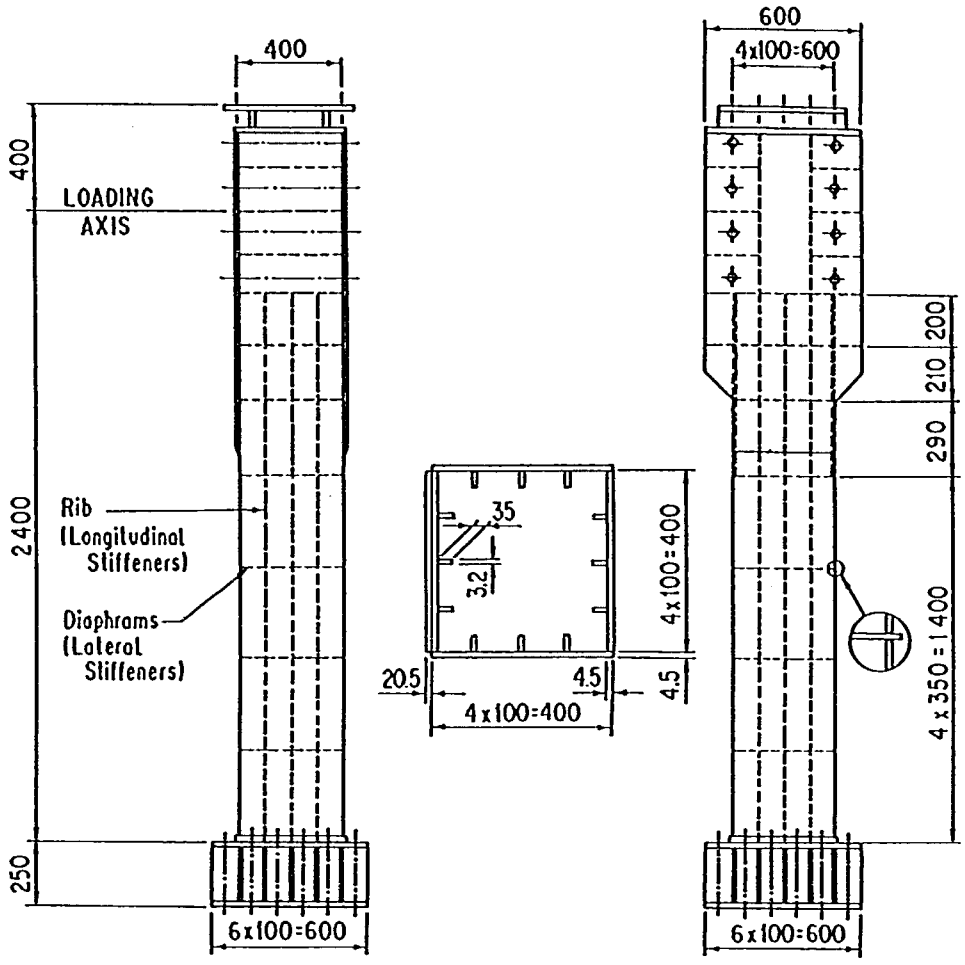


Figure 6 - Specimen S1

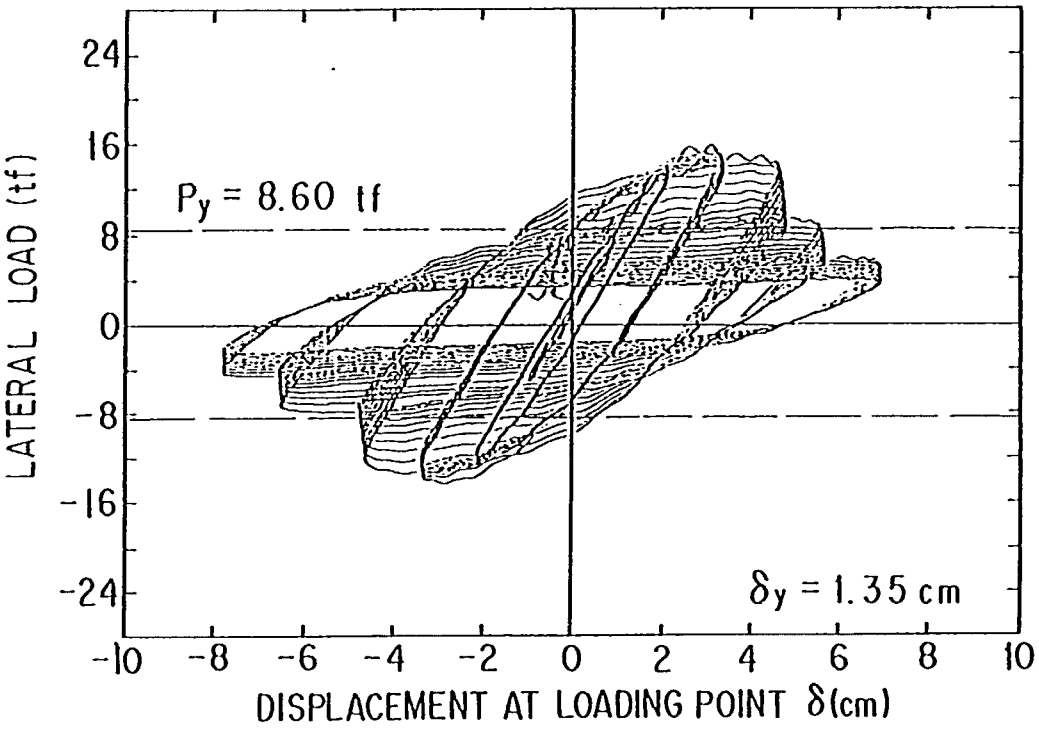


Figure 7 - Hollow Specimen Hysteresis Curve - Specimen S1

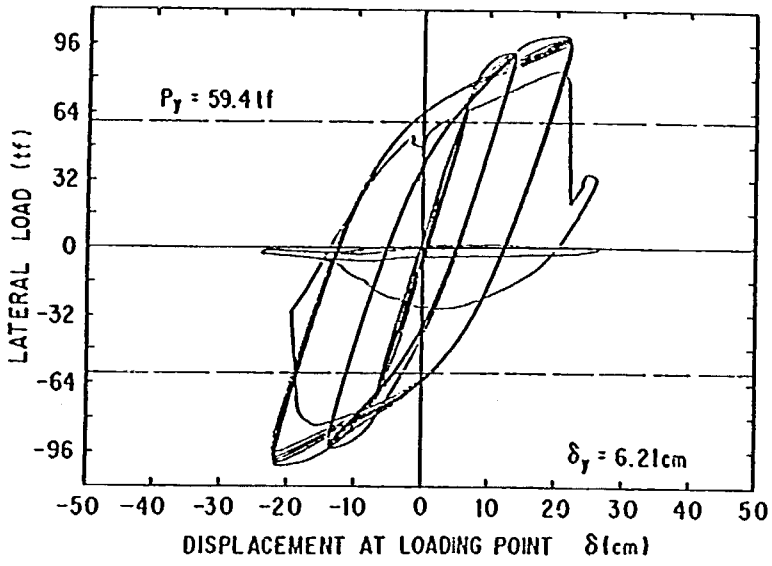


Figure 8 - Concrete-Filled Specimen Hysteresis Curve - Specimen S16

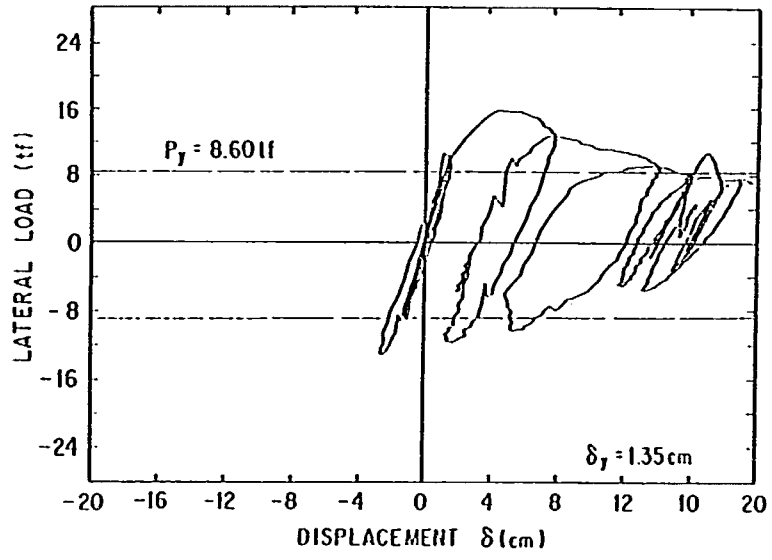


Figure 9 - Hysteresis Loop of Specimen on the Shaking Table - Specimen S5

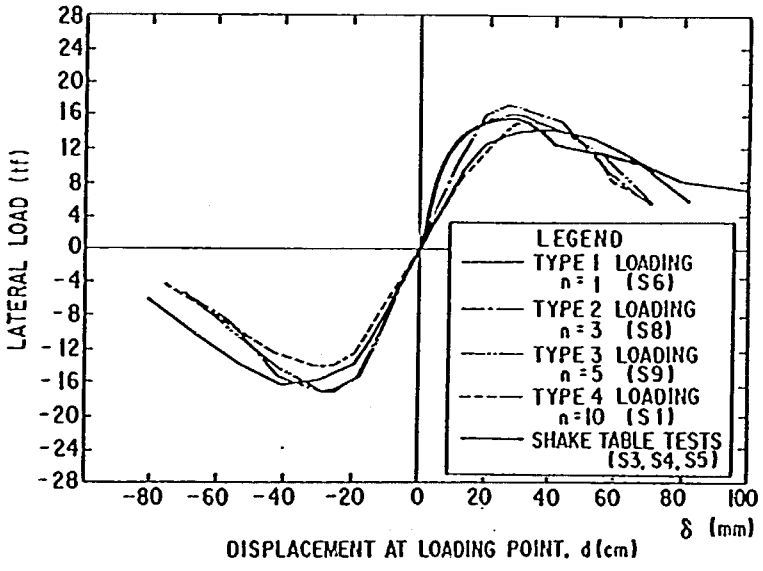


Figure 10 - Backbone Curve of Specimens S1, S6, S8, S9 and Shaking Table Tests

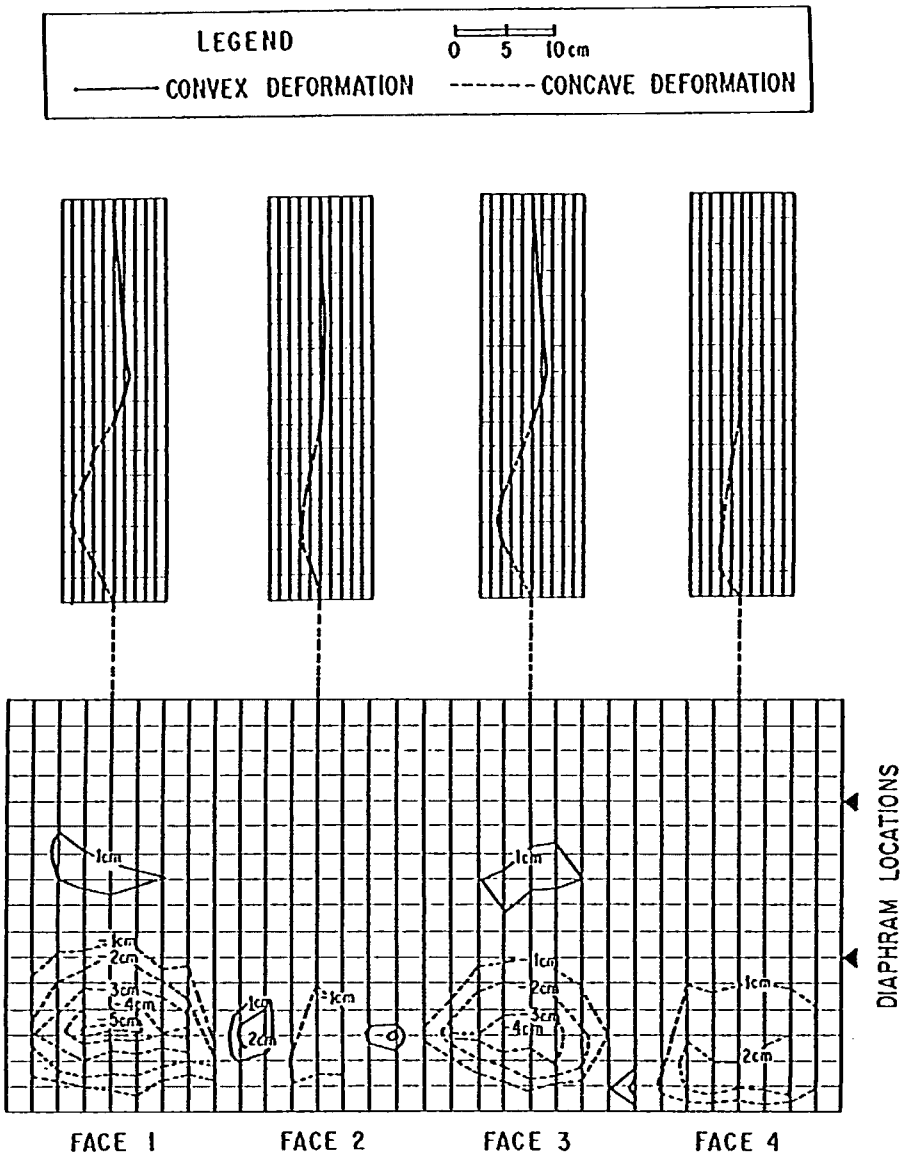


Figure 11 - Buckling of Specimen S1 at the End of the Test

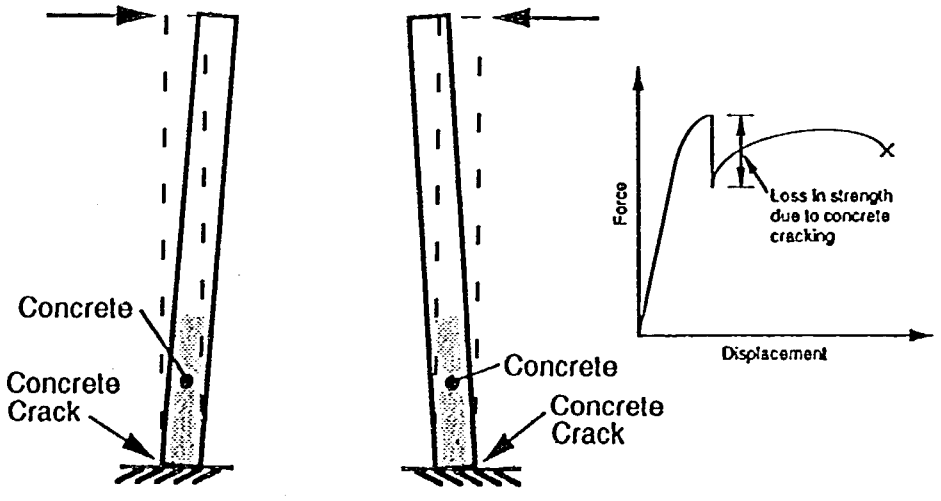


Figure 12 - Deformation of Concrete-Filled Piers

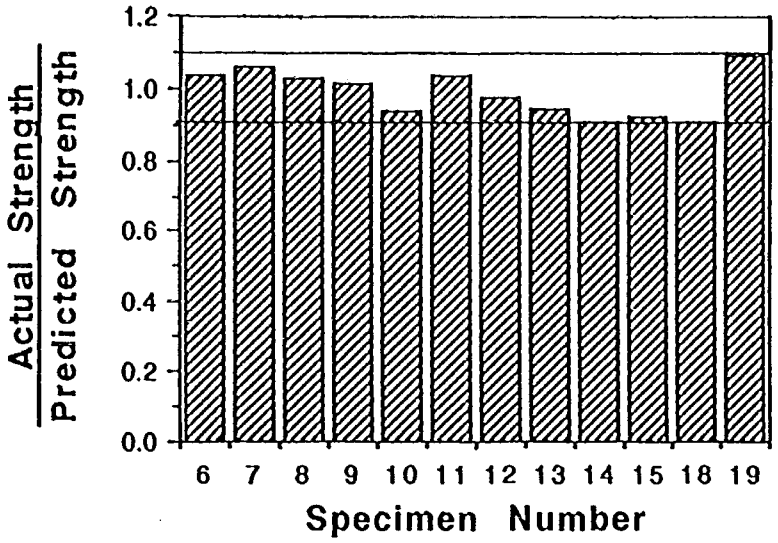


Figure 13 - Comparison of Overstrengths

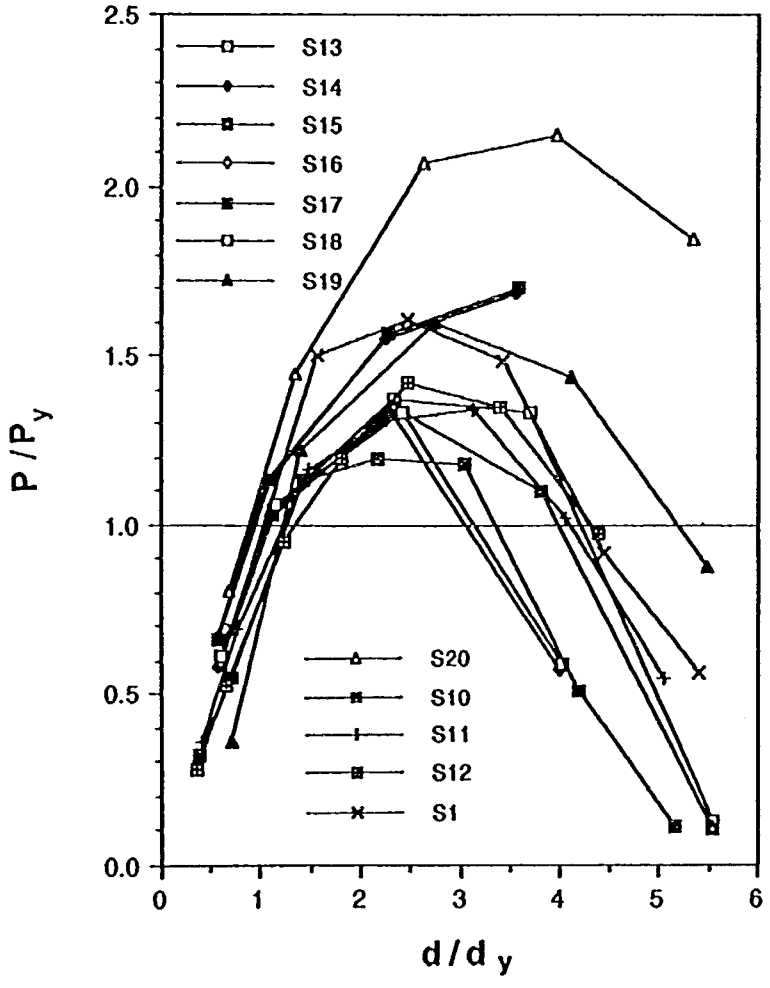


Figure 14 - Comparison of Specimen Backbone Curves

ESTIMATION OF DAMPING CHARACTERISTICS OF CABLE STAYED BRIDGE FOR SEISMIC DESIGN

by
Kazuhiko KAWASHIMA
Shigeki UNJOH
and
Meguru TSUNOMOTO
Earthquake Engineering Division
Public Works Research Institute

7TH U.S. — JAPAN BRIDGE WORKSHOP
Tsukuba Science City, Japan
May 8 and 9, 1991

ESTIMATION OF DAMPING CHARACTERISTICS OF CABLE STAYED BRIDGE FOR SEISMIC DESIGN

Kazuhiko KAWASHIMA[1], Shigeki UNJOH[2] and Meguru TSUNOMOTO[3]

1)Head of Earthquake Engineering Division, Earthquake Disaster Prevention Department, Public Works Research Institute, Ministry of Construction, Tsukuba Science City, Japan
2)Research Engineer, ditto
3)Design Office, Oriental Construction, Co. Ltd., formerly Visiting Research Engineer of Earthquake Engineering Division, Public Works Research Institute

SUMMARY

Although damping characteristics are very important for seismic design of cable stayed bridges, few investigations have been so far made. It is well known from field forced vibration tests conducted for a number of cable stayed bridges that damping ratio estimated from the tests gives much smaller values than the value generally assumed in seismic design. This paper presents a method to evaluate a damping ratio of cable stayed bridges based on energy dissipation. Defining an energy dissipation function for each sub-structure, an evaluation of energy dissipation of cable stayed bridges is examined. Validity of the method is studied through a comparison with model free oscillation test results. With use of the method, oscillation amplitude and cable shape type dependence of the damping ratio of the model bridge was clearly predicted.

INTRODUCTION

According to a number of forced vibration tests conducted for cable stayed bridges at site, it is well known that natural mode as well as natural frequency can be predicted with fairly good accuracy by means of linear analyses which assume appropriate mass and stiffness distribution. However, for a damping ratio which is essential for structural analysis, quite smaller values than the values assumed in seismic design have likely been obtained from such forced excitation tests. Because response of cable stayed bridges varies significantly depending on a damping ratio, it is of great importance to evaluate damping characteristics of cable stayed bridges for seismic design.[1)2)3)]

For developing an estimation method of a damping ratio of cable stayed bridges, correlations of measured damping ratio with several parameters representing structural characteristics of cable stayed bridges, such as natural frequency, span length and pier height, have been attempted. However, because factors contributing to damping ratio of cable stayed bridges vary complicatedly from bridge to bridge, analytical approaches capable of evaluating the damping characteristics of cable stayed bridges for seismic design purpose have not yet proposed.

This paper describes a method of estimating a damping ratio of cable stayed bridges based on energy dissipation, and clarifies its validity through a comparison with free oscillation tests of a scaled model.

EVALUATION METHOD OF DAMPING RATIO

There are various factors causing energy dissipation in cable stayed bridges. Energy dissipation are generally developed by material nonlinearity, structural damping such as friction at movable bearings, radiation of energy from foundations to subground, and friction with air. Predominant factors contributing to damping characteristics of cable stayed bridges varies with structural types. However, an important point to estimate a damping ratio of cable stayed bridges is to evaluate total energy dissipation. Because the energy dissipation capability may not be the same in whole bridge system, it is required to evaluate the energy dissipation in each structural segment depending on type of energy dissipation. Once the energy dissipation in individual structural segments can be determined, the total energy dissipation in a whole structural system can be evaluated by summing up the energy dissipation developed in each structural segment.

Based on such considerations, it is assumed to evaluate energy dissipation in whole bridge as;

1) Divide a cable stayed bridge into several structural segments in which energy dissipation capability can be considered practically the constant. Such a structural segment is referred hereinafter as "a sub-structure". For instance, a cable stayed bridge may be divided into deck(s), tower(s) and cables. Energy dissipation due to material nonlinearity is considered prevailing in such sub-structures. Bearing supports may also be considered as a sub-structure because energy dissipation due to friction occurs at the bearings.[4]

2) When the i-th sub-structure is idealized by a n-degree of freedom discrete system, the strain energy E_j^i of the i-th sub-structure for j-th mode may be represented as

$$E_j^i = \frac{1}{2} \sum_k (u_j^{ik})^T \cdot k^i \cdot u_j^{ik} \qquad (1)$$

where

u_j^{ik} : amplitude at node k of i-th sub-structure for j-th mode, i.e.,

$$u_j^{ik} = \{ u_j^{i1}, u_j^{i2}, \cdots, u_j^{ik}, \cdots, u_j^{in} \}^T \qquad (2)$$

k^i : stiffness matrix of the i-th sub-structure

Strain energy of the whole structural system for j-th mode can, then, be evaluated as

$$E_j = \sum_i E_j^i \qquad (3)$$

3) For the i-th sub-structure where energy dissipation due to material nonlinearity is predominant, the energy dissipation associated with j-th mode may be represented as

$$\delta E_j^i = f_j^i(E_j^i) \qquad (4)$$

where

δE_j^i : energy dissipation in i-th sub-structure for j-th mode

E_j^i : strain energy in i-th sub-structure for j-th mode
f_j^i : function relating δE_j^i with E_j^i

The function f_j^i represents how the energy dissipation in i-th substructure δE_j^i be developed in a function of the strain energy in i-th sub-structure E_j^i, and it would vary depending on type of the structure and material. Therefore, this is referred hereinafter as "an energy dissipation function". Because it is quite difficult in most cases to directly evaluate the energy dissipation function f_j^i from analytical studies, it should be determined based on appropriate experiments.

4) For i-th sub-structure where the energy dissipation function f_j^i is such a form that it can be represented in terms of a displacement at a specific point u_j^{ik} within the i-th sub-structure, the energy dissipation function may be represented as

$$\delta E_j^i = f_j^i(u_j^{ik}) \tag{5}$$

where
δE_j^i: energy dissipation in i-th sub-structure for j-th mode
u_j^{ik} : displacement at point k in i-th sub-structure for j-th mode
f_j^i : energy dissipation function relating δE_j^i with u_j^{ik}

5) Energy dissipation in the whole structural system can be obtained by summing up the energy dissipation developed in individual sub-structures determined by Eqs.(4) and/or (5) as

$$\delta E_j = \sum_i \delta E_j^i \tag{6}$$

where
δE_j : total energy dissipation in whole structure for j-th mode
δE_j^i : energy dissipation in i-th sub-structure for j-th mode

6) Damping ratio of the whole structure for j-th mode may then be obtained from Eq.(4) and Eq.(6) as

$$h_i = \frac{\delta E_j}{4\pi E_i} \tag{7}$$

EVALUATION OF ENERGY DISSIPATION FUNCTION

Cable Stayed Bridge Model Analyzed To show an evaluation of the energy dissipation function, it is appropriate to refer a specific bridge for which actual damping characteristics have been accurately estimated. For such purpose, a model oscillation test with use of a model shown in Fig.1 and Photo 1 was made.[5] The bridge model was made for simulating the Meiko-nishi Bridge[6] with a scale factor of 1/150. Because detailed study on this model bridge was already reported, only outline of the model which is required to understand the analysis presented in this paper will be described here.

Main objectives of the experiments were to study how damping ratio varies in accordance with cable shape type and number of cables. For such purpose, cable shape and number of cables were varied as shown in Fig.2 as parameters to

be studied with main parts of the tower, the deck and the cables being the same. The bridge model was statically displaced either in lateral (longitudinal) direction or in vertical direction, and by smoothly releasing the deck, free oscillation was developed. As will be presented later in Fig.3, the initial deformation is of antisymmetric mode in the free oscillation in longitudinal direction, and is of symmetric mode in the free oscillation in vertical direction. From decay of the free oscillation of the deck, damping ratio of the bridge model was estimated. Although the test was conducted for the connection between the deck and the tower being either free or fixed, only the condition that the deck is free to move from the tower (in this case, the deck is supported only by the cables) is analyzed in this paper for making the experiments to determine the energy dissipation function of sub-structures simple.

Fig.3 shows mode shapes and natural frequencies computed by an elastic analytical model which considers geometrical stiffness to take a compression force induced in the deck and the tower into account. As shown in Table 1 the computed natural frequencies agree well with the experiments.

Figs.4 and 5 show how the damping ratio of the bridge model varies in accordance with the oscillation amplitude and the type of cable shape. It should be noted here that the predicted damping ratio which will be described later is also presented in Figs.4 and 5 for comparison. From Figs.4 and 5, the following characteristics were found on the damping ratio of the bridge model.[5)]

1) The damping ratio of the cable stayed bridge model in longitudinal oscillation increases as the cable shape changes from fan type (type 3A and 2A) to harp type (type 3E and 2C). This tendency is more significant in the model with 3 cables than in the model with 2 cables.

2) On the contrary to 1), the damping ratio of the cable stayed bridge model in vertical flexure oscillation decreases as the cable type changes from the fan type (3A and 2A) to the harp type (3E and 2C). Similar with 1), this tendency is more significant in the model with 3 cables than the model with 2 cables.

3) Based on 1) and 2), when comparing the damping ratio of the cable stayed bridge model in longitudinal oscillation with that in vertical flexural oscillation, the damping ratio in longitudinal oscillation is larger in the harp shape than the damping ratio in vertical flexure oscillation. However, the damping ratio in the longitudinal oscillation and the damping ratio in the vertical flexural oscillation becomes closer to each other as the cable type changes from the harp type to the fan type; and the relation between them is even reversed in the type 3A.

4) The damping ratio increases as the oscillation amplitude increases. Such characteristics are significant in longitudinal oscillation, and, on the contrary, are insignificant in vertical flexure oscillation.

It is the objective of this study to clarify the validity of the evaluation method presented in previous chapter for evaluating the damping ratio through comparisons with the model test results. It is of great interest to know how realistically the above-described damping characteristics of the model bridge can be predicted by the analysis.

For analyzing the damping ratio of the model bridge, the tower, the girder and the anchoring portion of the cables to the tower are considered here as the sub-structure, because these parts contribute to the energy dissipation of the model.

Energy Dissipation Function of Tower For estimating the energy dissipation function of the tower, a simple free oscillation test of the tower was made as shown in Fig.6. Only the tower was taken out from the whole bridge model, and it was supported as a cantilever beam with one of the ends being fixed and the other being free. To avoid energy dissipation at the bottom of the cantilever tower, a special attention was paid to fix it rigidly to a rigid steel member. A weight was placed on the free end of the tower to study the effect of axial force induced in the tower. The weight placed on the free end of the tower was varied from 0.85 kgf to 5.1 kgf. Because the axial force induced at the bottom of the tower due to dead weight of the deck is 6.87 kgf and 6.81 kgf for the model with number of cables of 3 and 2, respectively, the weight of the mass corresponds to 12 % to 74 % of the axial force of the tower. By smoothly releasing the tower top from a displaced position, a free oscillation simulating a first mode was developed. Amplitude of the tower was measured at 33 cm from the bottom by means of an uncontact displacement sensor. From decay of the free oscillation, damping ratio of the tower was estimated.

It should be noted here that the deformation of the isolated tower developed during the free oscillation may not be the same with the deformation of the tower when it is excited as a part of the whole bridge. Although it is the most desirable to evaluate the energy dissipation function for a deformation mode which is actually induced in the tower as a part of the whole bridge, it is quite difficult to displace the isolated tower in such a form. Therefore the difference of the deformed shape of the tower between the actual deformation of the tower as a part of the whole bridge and the cantilever first mode was disregarded here. However, because the relation between $\delta E_j'$ and E_j' given by Eq.(1) may be regarded free from mode shape as will be described later, an energy dissipation function determined for a mode shape would be used for an energy dissipation function for other mode shapes. The validity of this assumption may be verified by comparing the damping ratio estimated by Eq.(7) with the damping ratio obtained experimentally for the whole bridge model.

Fig.7 shows how the damping ratio of the tower varies with the amplitude of the oscillation and the mass of the weight. Predicted damping ratio which will be described later is also presented for comparison. Although there is some scatters at oscillation amplitude smaller than 0.5 mm, this is due to low accuracy of the measurements in such small oscillation amplitude. According to Fig.6, the damping ratio of the tower increases as a whole as the oscillation amplitude as well as the mass of the weight increases.

Why the damping ratio increases as the axial force of the tower increases may require an explanation. The total energy E_j of the structural system oscillating in j-th mode shape comes from two contributions, i.e., energy E_{ej} associated with geometrical stiffness[7] due to compression force induced in the tower and the deck, and strain energy E_{sj} associated with the deformation of the structure as

$$E_j = E_{sj} + E_{ej} \tag{8}$$

Because the energy dissipation during oscillation is developed only by the strain energy E_{sj} and free from the energy E_{ej}, the energy dissipating function f_j may be represented as

$$\delta E_j = f_j (E_{sj}) \tag{9}$$

in which δE_j represents the energy dissipation during the oscillation. Therefore, damping ratio of the tower may be obtained by substituting Eqs.(8) and (9) into Eq.(7) as

$$h_j = \frac{\delta E_j}{4\pi E_j} = \frac{f_j(E_{sj})}{4\pi (E_{sj} + E_{gj})} \tag{10}$$

Because the energy dissipation E_{gj} associated with the geometrical stiffness takes a negative value if the axial force of the tower is positive (compressive), the damping ratio presented by Eq.(10) increases as the axial force becomes larger.

Because the damping ratio h_j of the tower can be determined through the decay of the free oscillation and the total energy E_j can be computed from Eq.(8), one can determine the energy dissipation δE_j by substituting h_j and E_j into Eq.(10).

Fig.8 shows the relation between δE_1 and E_{s1}. Because the oscillation test was made only for the first mode, Fig.8 represents δE_j vs. E_{sj} relation for j = 1. The relation seems almost independent of the weight of the mass placed on the tower top. Then, it is approximated here as

$$\delta E_{s1} = \Sigma \alpha_i \cdot E_{s1} \cdot \beta_i \tag{11}$$

After determining the coefficients α_i and β_i based on a least square fit, it was obtained as

$$\delta E_{s1} = 0.016 E_{s1} + 0.0021 E_{s1}^{3/2} \tag{12}$$

Based on Eq.(12), the damping ratio vs. the oscillation amplitude of the tower is obtained as shown in Fig.7. It is seen that the predicted damping ratio agrees reasonably well with the experimental result.

Energy Dissipation Function of Deck As was the tower, a part of the deck was taken out from the whole bridge model and was supported as a cantilever beam with a weight being placed as shown in Fig.9. Length of the cantilever deck was varied as 40 cm and 60 cm so that an effect of the deck length on the damping ratio be studied. Because the deck length varies the mode shape, this would show how the energy dissipation function depends on the mode shape.

Fig.10 shows a relation between the damping ratio estimated from the decay of free oscillations and the oscillation amplitude measured at 30 cm from the bottom. Predicted damping ratio which will be described later is also presented for comparison. As is the case for the tower, the damping ratio of the cantilever deck increases as the oscillation amplitude and the weight of the mass increase. It is interesting to note that the damping ratio of the deck is appreciably larger than the damping ratio of the tower. The tower consists of only steel frame, while the deck is fabricated by assembling the main beam, transverse beam and lead weight. The larger damping ratio of the deck may be attributed to an energy dissipation associated with the transverse beam and lead weight attached to the main beam.

Fig.11 shows an relation between δE_{s1} and E_{s1} of the catilever deck. It is interesting to note that the effect of the deck length on δE_{s1} vs. E_{s1} relation is quite small. Therefore, neglecting the effect of the catilever deck length,

the relation between δE_{s1} and E_{s1} may be approximated as

$$\delta E_{s1} = 0.016E_{s1} + 0.083E_{s1}^{1.37} \quad (13)$$

Predicted damping ratio by Eq.(13) agrees fairly well with the experimental result as shown in Fig.10.

Energy Dissipation Function of Anchoring Portion of Cables To simulate an energy dissipation at the cable anchoring portion, where an energy dissipation is developed due to friction between the cables and the anchoring devices as well as deformation of the plate spring (refer to Fig.1), the cable anchoring portion was taken out from the whole bridge model, and a free oscillation test of this sub-structure was made as shown in Fig.11. To isolate the energy dissipation at the cable anchoring portion, both ends of the tower were fixed so that the energy dissipation associated with the tower deformation be as small as possible. Furthermore, the deck was supported by two cables so that flexure deformation of the deck in vertical direction during the free oscillation test be small. To study an effect of the tension force developed in the cables, two masses were placed on the deck. The oscillation amplitude in bridge axis direction was measured at one of the two ends of the deck.

Fig.12 shows a relation between the damping ratio and the oscillation amplitude of the model idealizing the anchoring portion. Being different from the tower and deck, the amplitude dependence of the damping ratio varies in a complicated manner depending on the oscillation amplitude. This seems to be developed probably because the friction between the cables and the anchoring devices delicately changes depending on the oscillation amplitude. Modeling of a cable anchoring portion of the prototype cable stayed bridge is quite complicated and difficult in the scaled model. However, it is considered less important to study such complexity of the amplitude dependence of the damping ratio of the anchoring portion, because the purpose of this study is to clarify the validity for evaluating the total energy dissipation.

Fig.13 shows a relation between the energy dissipation, angular frequency of the free oscillation and the oscillation amplitude at the cable anchoring portion, in which θ and ω represent an angle between the tower and the cable (refer to Fig.11) and angular frequency of the free oscillation. It is interesting to note that the energy dissipation in the sub-structure depends on the angular frequency of the free oscillation. The effect of the tension force induced in the cables by means of two masses placed on the deck seems less significant.

By approximating the relation between δE, θ and ω presented in Fig. 13, the energy dissipation at the cable anchoring portion may be written as

$$\delta E = 0.018\omega^{2.15} \cdot \theta^{2} \quad (14)$$

EVALUATION OF CABLE-STAYED BRIDGE MODEL BASED ON ENERGY DISSIPATION FUNCTIONS OF SUB-STRUCTURES

Damping ratio of the cable stayed bridge model was evaluated based on the energy dissipation functions of the sub-structures determined in the preceding chapter. Predicted damping ratio by Eq.(7) assuming the energy dissipation functions of the sub-structures by Eqs.(12), (13) and (14) is presented in

Figs.4 and 5 in comparison with the experimental results. The predicted damping ratio may be characterized as

1) The predicted damping ratio of the cable stayed bridge model in longitudinal oscillation increases as the cable type changes from the fan type (type 3A and 2A) to the harp type (type 3E and 2C). The dependence of the predicted damping ratio on the oscillation amplitude increases in the same order with the experiments. Such characteristics agree fairly well with the experiments, although the predicted damping ratio is underestimated as the cable type approaches to the harp type.

2) The predicted damping ratio of the cable stayed bridge model in vertical flexure oscillation is almost independent of the cable type. Although the damping ratio estimated from the experiments slightly decreases as the cable type changes from the fan shape to the harp shape when the number of cable is 3, the overall characteristics of the predicted damping ratio seem fairly close with the experimental results.

Through the comparison stated above, it can be said that the estimation method of the damping ratio by Eq.(7) using the energy dissipation functions determined for individual sub-structures is apparently able to realistically simulate the damping characteristics of the bridge model evaluated from the experiments. As a whole, the predicted damping ratio is somewhat smaller than the experimental results probably because of the energy dissipation which are not considered in this analysis would contributed to the total energy dissipation. Therefore, if the energy dissipation at each portion is further evaluated in detail, it may be possible to further enhance the accuracy of the above estimation.

CONCLUSIONS

An evaluation method of the damping ratio of cable stayed bridges by determining an energy dissipation functions for individual sub-structures was presented, and the validity of the method was examined through a comparison with the results of model free oscillation tests.

Through the analysis presented herein, the following conclusions may be deduced:

1) To clarify complicated damping characteristics of cable-stayed bridges, it is important to accurately study energy dissipations in individual sub-structures with a special attention to in what mechanism the energy dissipation is made.

2) Dependence of damping ratio on the cable shape type and oscillation amplitude, which was evaluated through the model free oscillation test of the cable stayed bridge model, can be realistically predicted for longitudinal oscillation and vertical flexural oscillations by the method presented in this paper.

3) It is recommended to clarify the complicated damping characteristics of cable stayed bridges, which have so far been measured based on a number of field forced vibration tests, paying fully attention to the fact that the damping ratio of cable stayed bridges greatly varies depending on the energy dissipation in individual sub-structures. It would be quite important to note that which sub-structure contributed in the field forced vibration tests to the total energy dissipation for mode shapes studied. It is also recommended to conduct careful forced vibration tests for cable stayed bridges using the method

presented in this paper. Tests to determine the energy dissipation functions for sub-structures have to be well implemented for such purpose.

REFERENCES

1) Ito, M. and Katayama, T. : Damping Characteristics of Bridges, Proc. Japan Society of Civil Engineering, Vol.117, 1965 (in Japanese)
2) Kawashima, K., Unjoh, S. and Tsunomoto, M : Damping Characteristics of Cable Stayed Bridges for Seismic Design, Report of the Public Works Research Institute, Ministry of Construction, 1991
3) Kawashima, K., Unjoh, S. and Azuta, Y. : Analysis of Damping Characteristics of A Cable Stayed Bridge Based on Strong Motion Records, Structural Eng./Earthquake Eng., Vol.7, No.1, pp.181-190, 1990
4) Kawashima, K. and Unjoh, S. : Damping Characteristics of Cable Stayed Bridges Associated with Energy Dissipation at Movable Supports, Structural Eng./Earthquake Eng., Vol.6, No.1, pp.145-152, 1989
5) Kato, N., Iioka, Y. and Kawahito, T. : Design of Meiko-nishi Bridge, Bridges and Foundations, 1983(in Japanese)
6) For example, Nishioka, T.: Analysis on Structural Vibration, Bai-hu-kan, 1987 (in Japanese).

Table 1 Comparison of Natural Frequencies between Predicted and Experiments

CABLE TYPE		LONGITUDINAL MODE		VERTICAL MODE	
		EXPERIMENTAL	PREDICTED	EXPERIMENTAL	PREDICTED
THREE CABLES	TYPE 3A	0.54	0.54	0.66	0.68
	TYPE 3B	0.61	0.61	0.65	0.67
	TYPE 3C	0.76	0.76	0.65	0.66
	TYPE 3D	0.96	0.97	0.64	0.65
	TYPE 3E	1.38	1.41	0.65	0.65
TWO CABLES	TYPE 2A	0.48	0.49	0.62	0.63
	TYPE 2B	0.67	0.68	0.61	0.62
	TYPE 2C	0.92	0.95	0.60	0.59

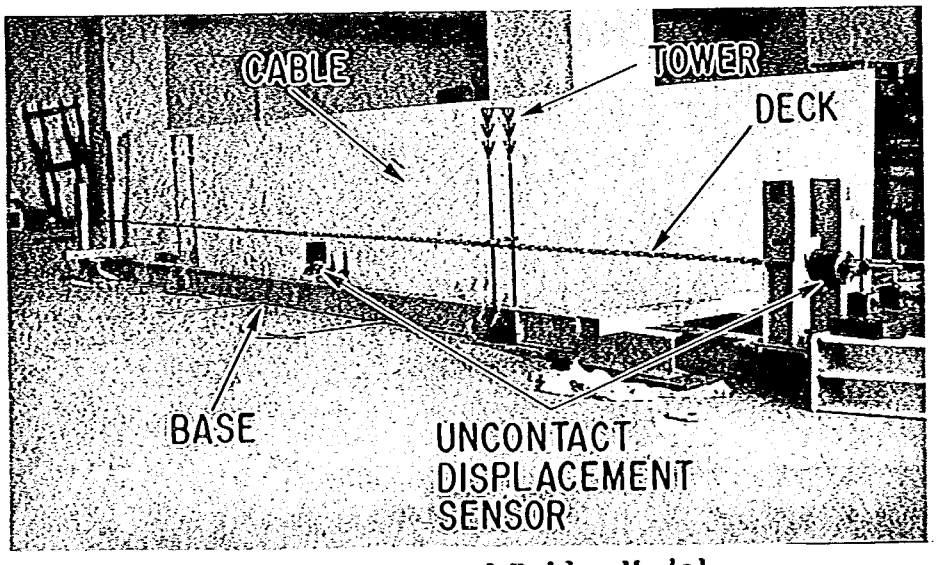


Photo 1 Cable Stayed Bridge Model

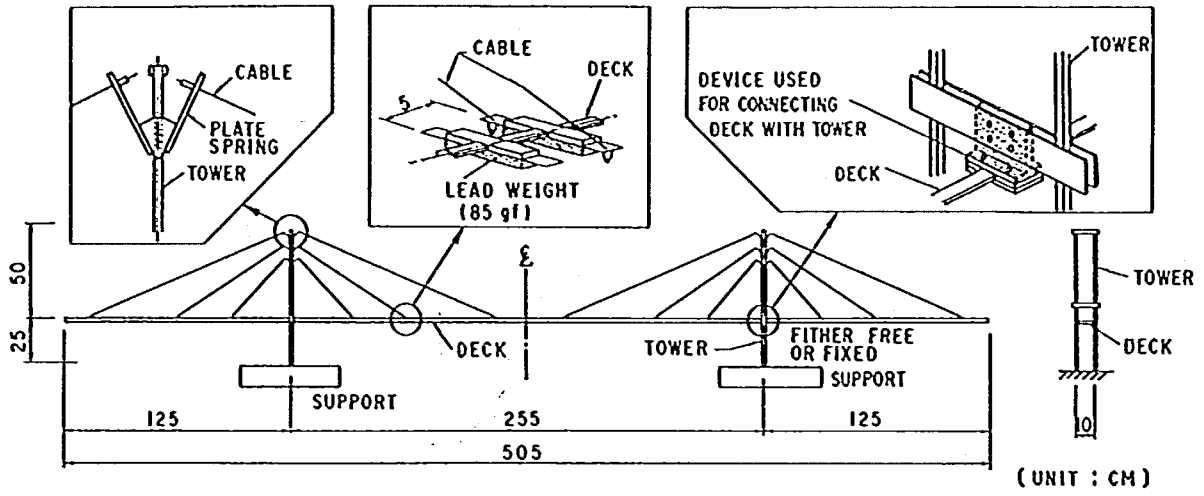
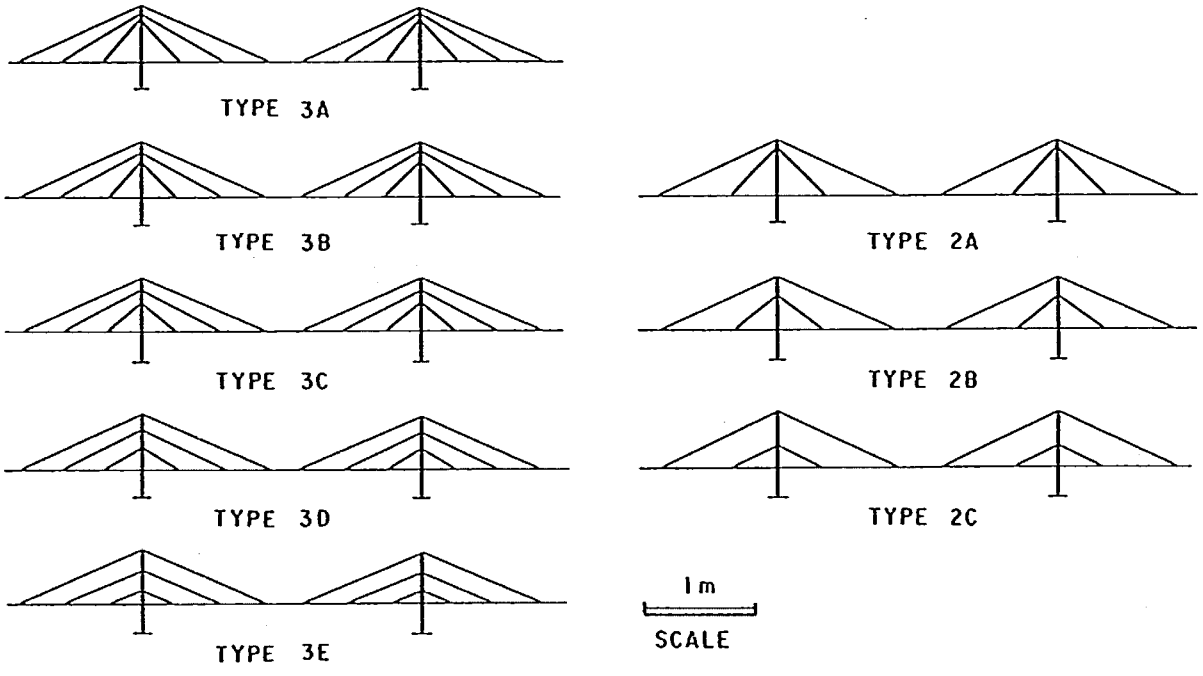
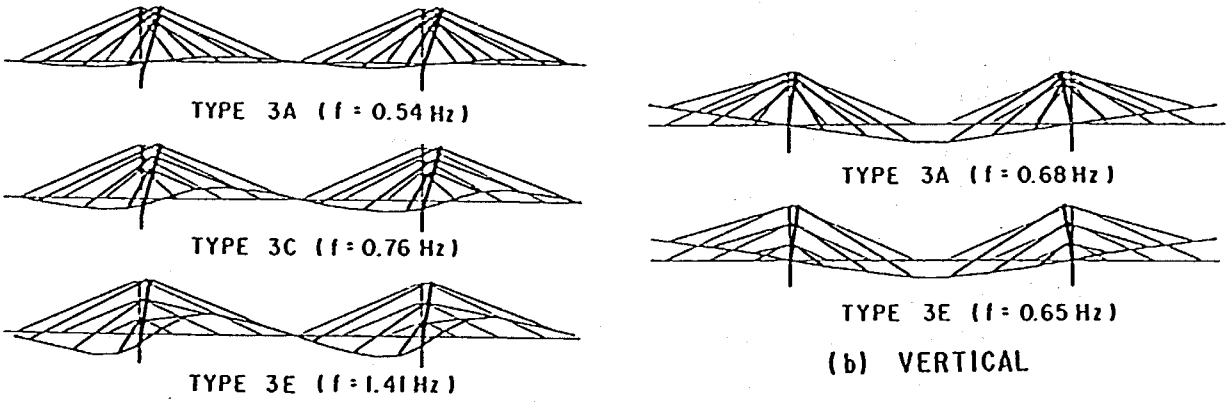


Fig. 1 Cable Stayed Bridge Model



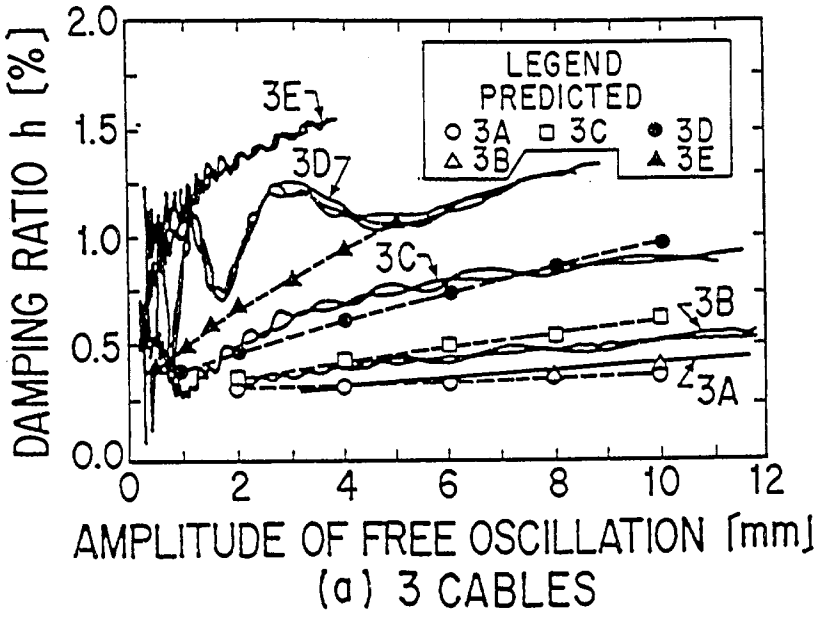
(a) THREE CABLES (b) TWO CABLES

Fig. 2 Cable Configulations



(a) LONGITUDINAL (b) VERTICAL

Fig. 3 Predicted Natural Frequency and Natural Mode Shape



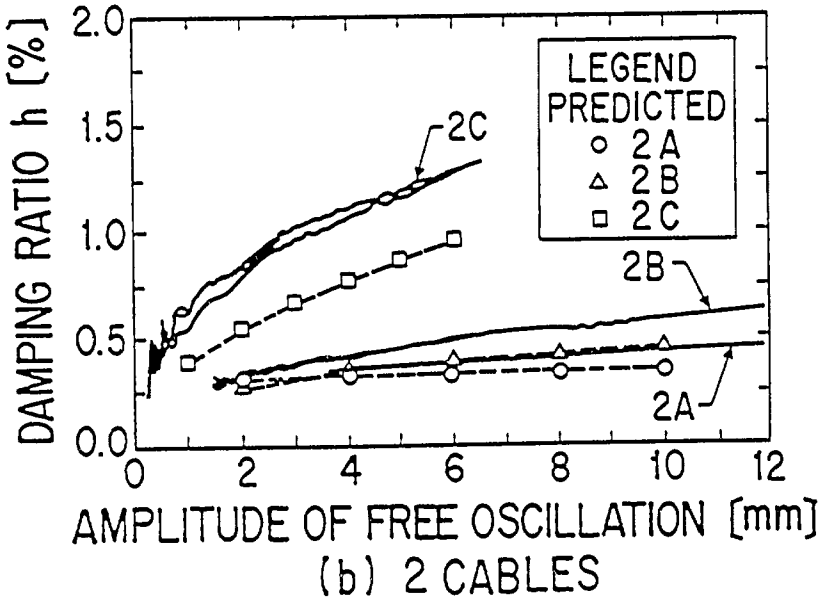
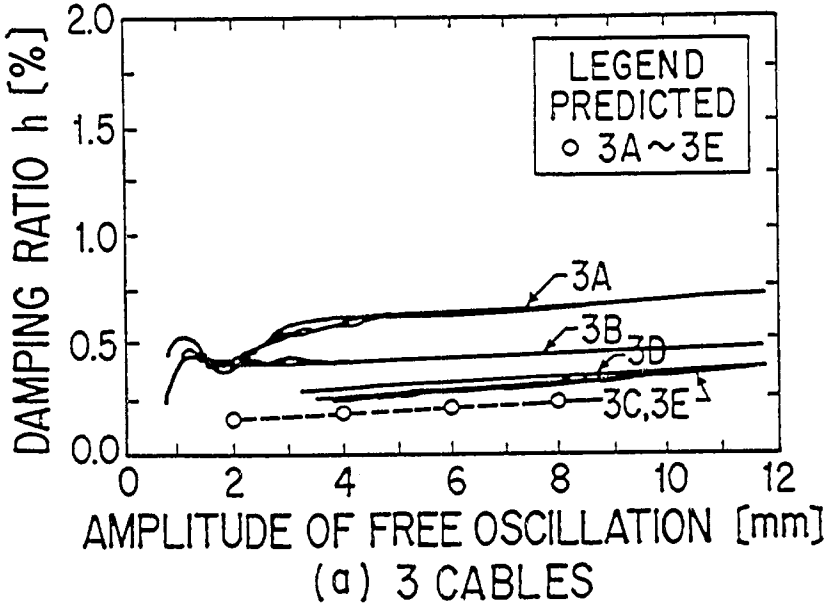


Fig. 4 Damping Ratio for Oscillation in Longitudinal Direction



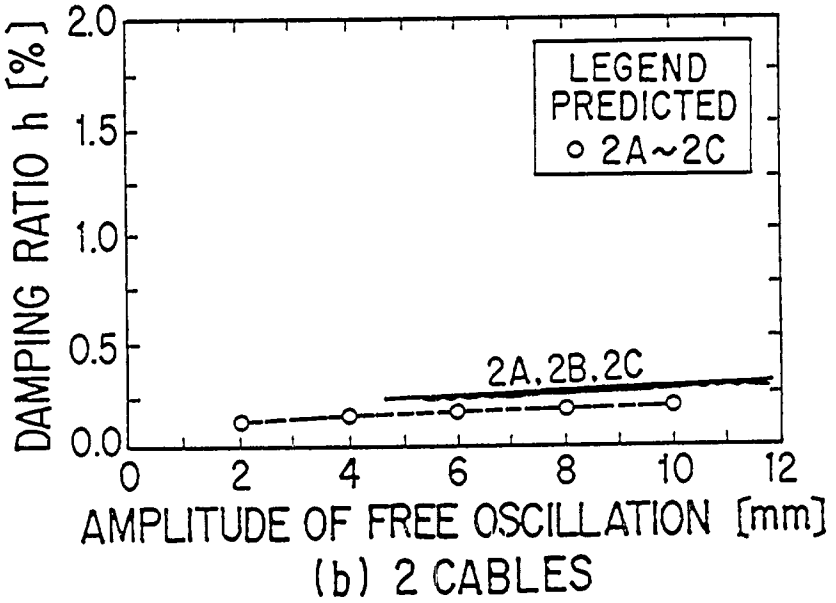


Fig. 5 Damping Ratio for Oscillation in Vertical Direction

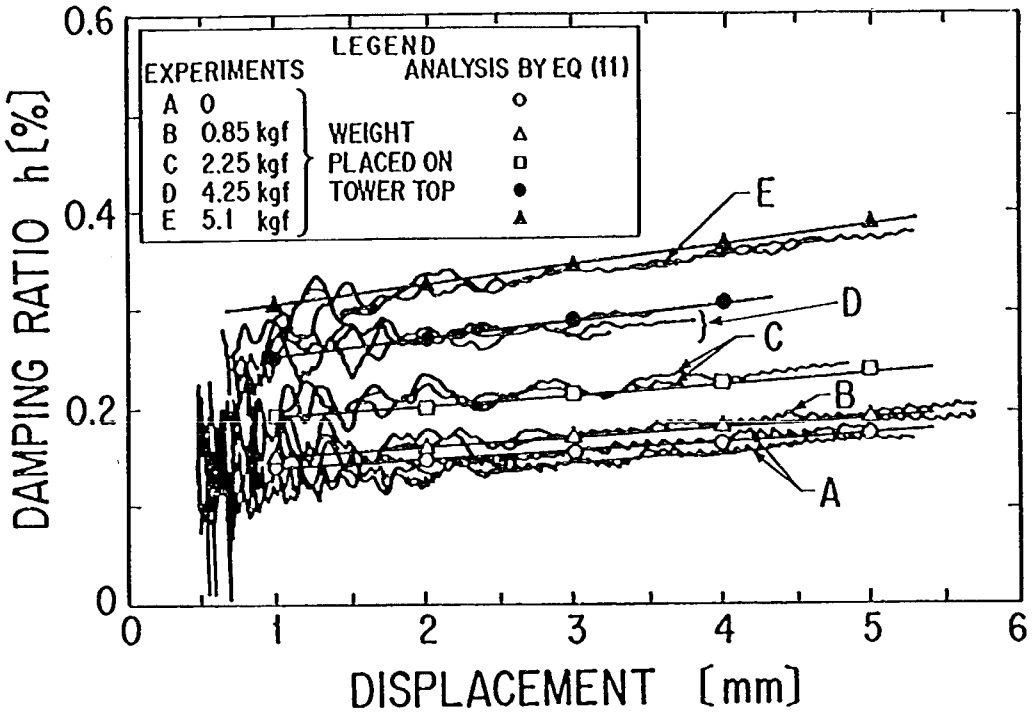


Fig. 7 Damping Ratio vs. Displacement Relation for Tower

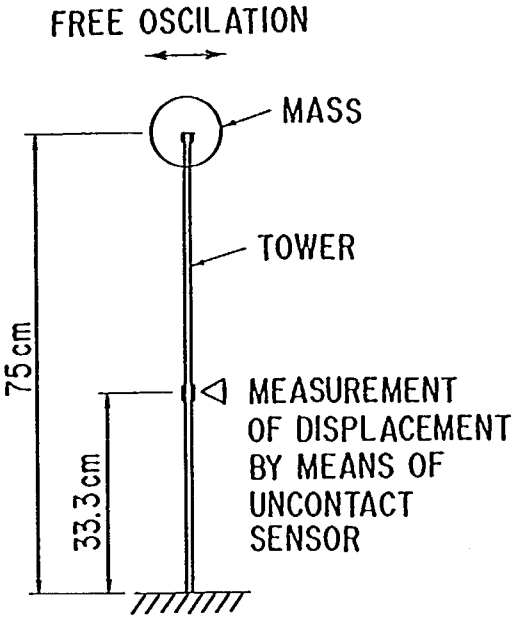


Fig. 6 Tower Model for Free Oscillation

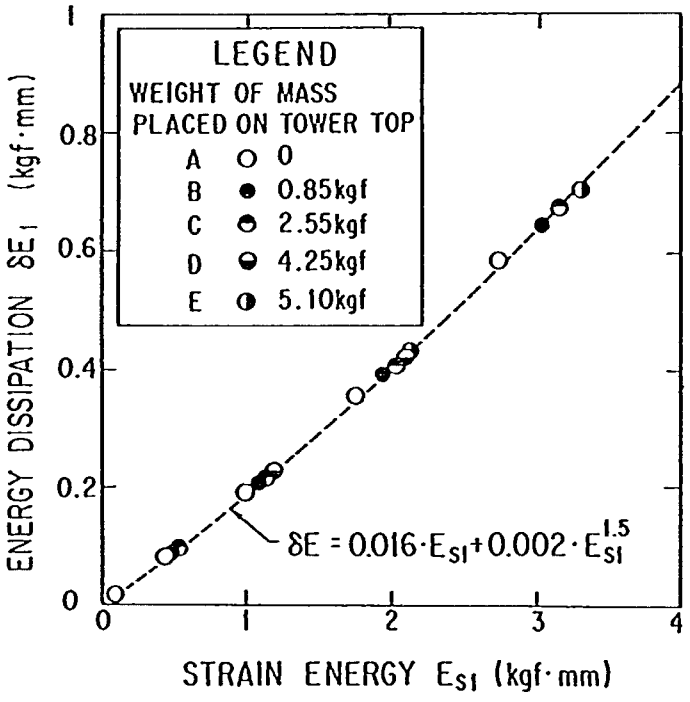


Fig. 8 Energy Dissipation δE_1 vs. Strain Energy E_{s1} Relation for Tower

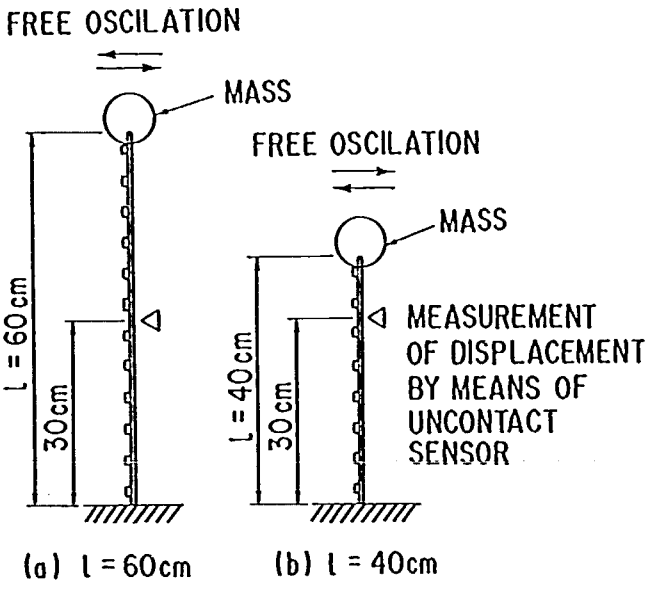
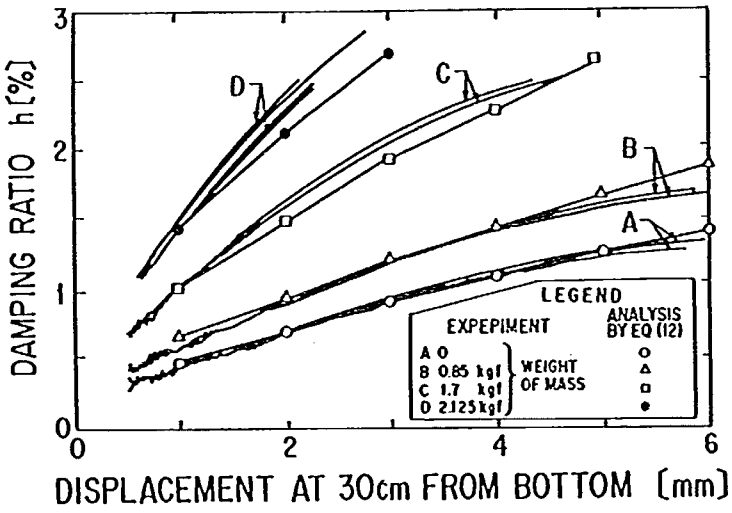
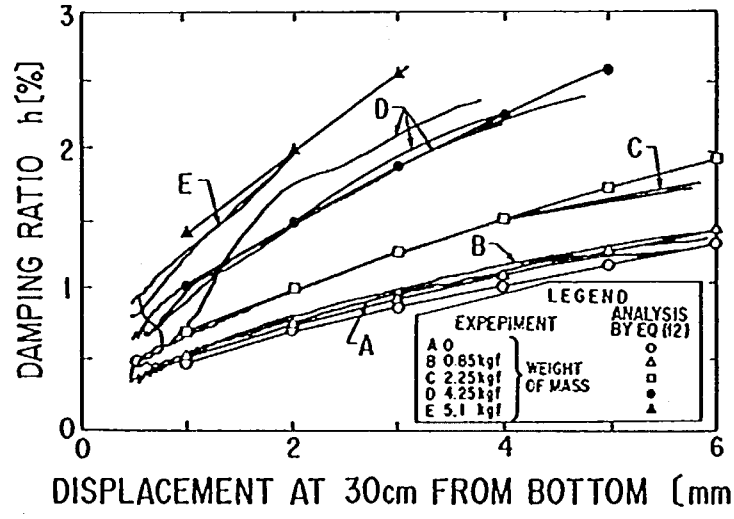


Fig. 9 Deck Model for Free Oscillation



(a) l = 40 cm



(b) l = 60 cm

Fig. 10 Damping Ratio vs. Displacement Relation for Deck

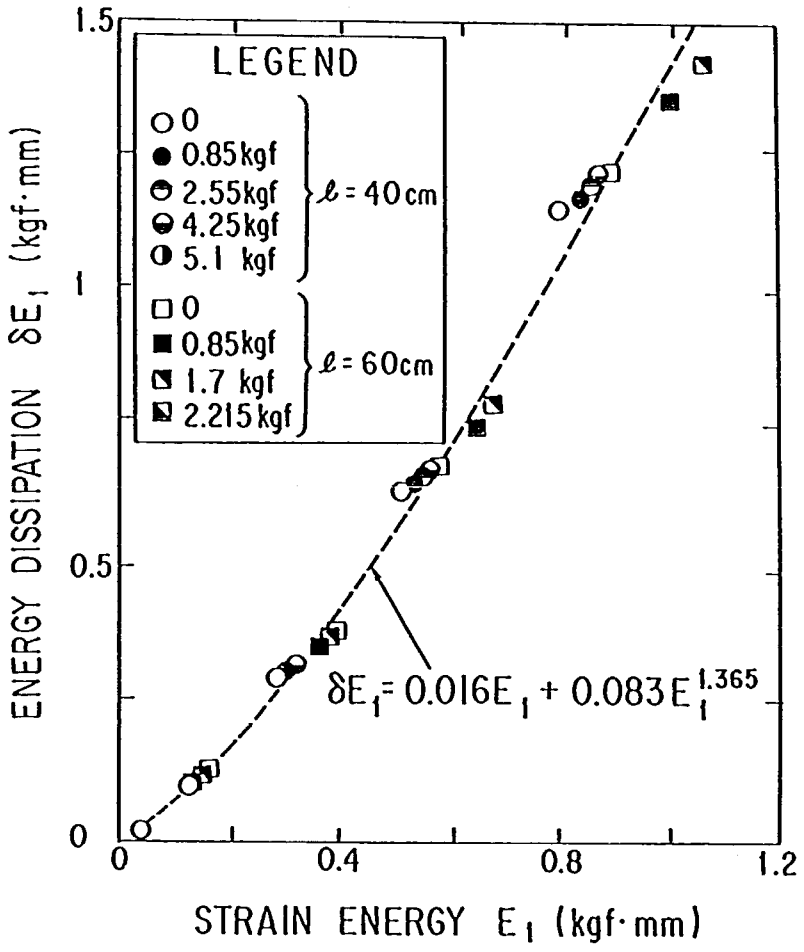


Fig. 11 Energy Dissipation δ E_1 vs. Strain Energy E_1 Relation for Deck

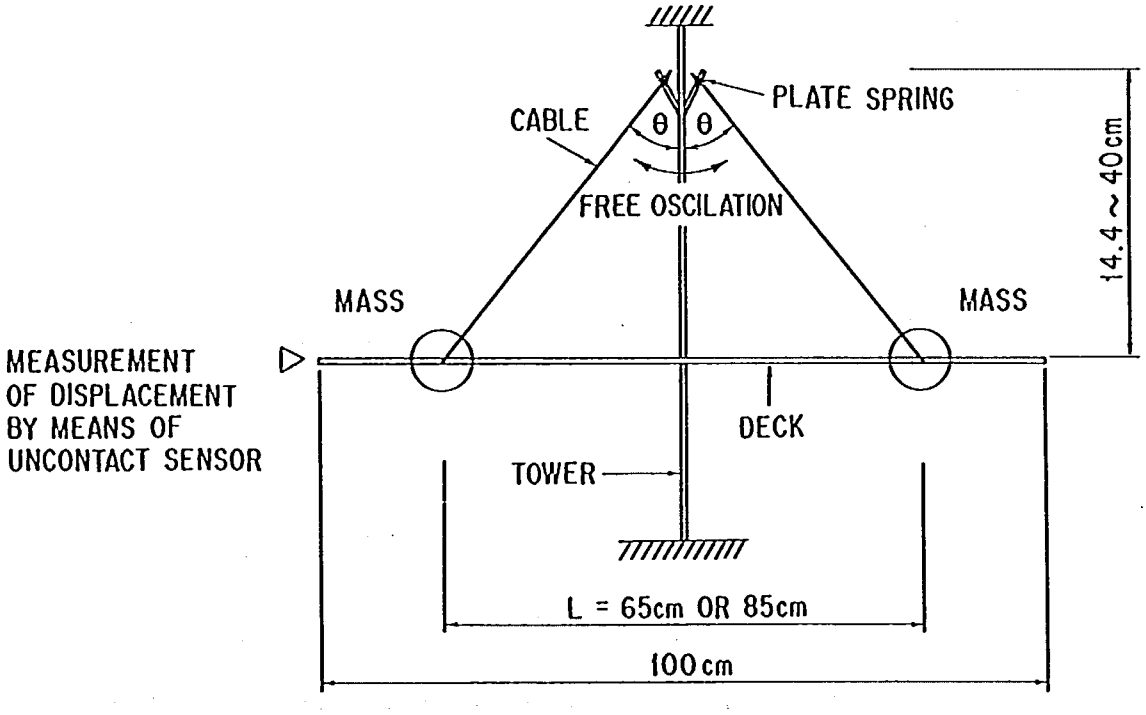


Fig. 12 Anchoring Portion Model for Free Oscillation

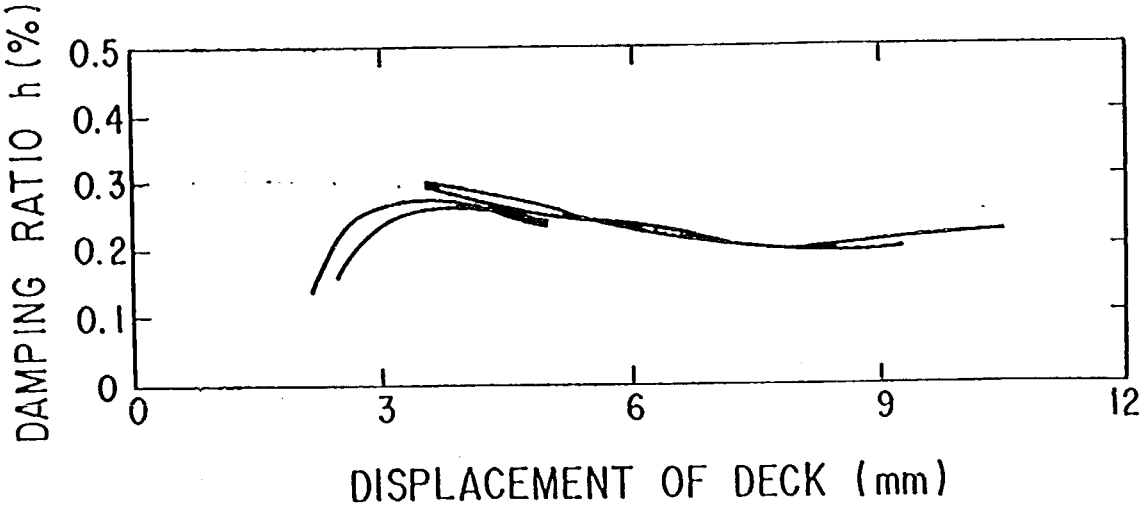


Fig. 13 Damping Ratio vs. Displacement Relation for Anchoring Portion

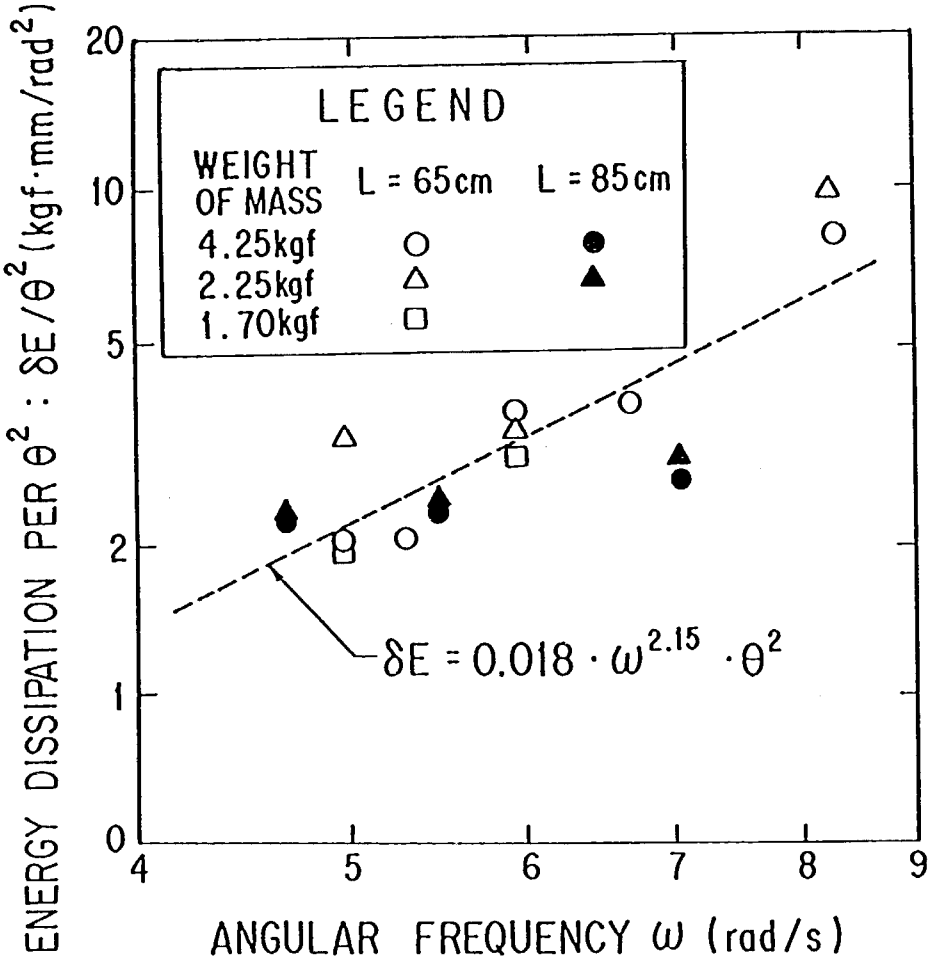


Fig. 14 Energy Dissipation, Angular Frequency and Oscillation Amplitude Relation for Anchoring Portion

SEISMIC DESIGN, SEISMIC STRENGTHENING AND REPAIR OF HIGHWAY BRIDGES IN JAPAN

by
Kazuhiko KAWASHIMA
Earthguake Engineering Division
Public Works Research Institute

U.S. — JAPAN WORKSHOP ON SEISMIC
RETROFIT OF BRIDGES
Tsukuba Science City, Japan
December 1990

PRESENT EARTHQUAKE ENGINEERING EFFORTS TO MITIGATE EARTHQUAKE HAZARDS OF ROAD TRANSPORTATION FACILITIES IN JAPAN

Kazuhiko KAWASHIMA

Head, Earthquake Engineering Division, Public Works Research Institute, Ministry of Construction, Tsukuba Science City, Ibaraki-ken, Japan

SUMMARY

This paper presents earthquake hazard mitigation efforts for road transportation facilities in Japan. Emphasis is placed on seismic disaster prevention measures for highway bridges. Description is firstly given to seismic damage developed in the past earthquakes and the history of the development of the seismic design method. Current seismic practice is then presented based on the latest version of Seismic Design Specifications of Highway Bridges issued by the Ministry of Construction in 1990. Description is also given to new technical developments for passive and hybrid control of highway bridges, and for disaster information gathering and processing systems. Seismic inspection and strengthening methods based on the past experiences are presented. Finally, an assessment and repair method for seismically damaged highway bridges is presented.

INTRODUCTION

Located along the Pacific Seismic Belt, Japan is one of the most seismically disastrous countries in the world and has often suffered significant damage from large earthquakes. Considerable efforts have been paid to earthquake hazard mitigation for transportation facilities. In particular, seismic safety of highway bridges has been a major concern because damage of highway bridges causes extensive interruption of road transportation and restoration often requires long time.

This paper presents pre-earthquake and post-earthquake measures for mitigating earthquake hazards on road transportation facilities in Japan, with emphasis on countermeasures for highway bridges. Development of new technology for reducing structural response by means of passive and hybrid control, and for disaster information gathering and processing systems is also presented.

DAMAGES OF HIGHWAY BRIDGES IN THE PAST EARTHQUAKES

Highways in Japan consist of the Expressways (3,721 km), National Highways (46,661 km), Prefectural Roads (128,202 km), and Municipal Roads (925,138 km). Along the highways and roads, excluding the Municipal Roads, there are about 50,000 bridges with the length of 15 m or longer.

Table 1 shows the highway bridges which suffered damages in the past earthquakes since the Kanto Earthquake of 1923. It should be noted that although there were many bridges which suffered damages due to earthquakes, number of bridges which fell down is only 15.

Based on the survey of the damaged bridges, it is pointed out that there were three major factors which contributed to the damages of the bridges as[1] :

a) weakness of substructure,
b) weakness of bearing supports, and
c) weakness of surrounding subsoils.

From such factors, the following types of damages were most often developed in the past :

a) substructure : tilting, settlement, sliding, cracks, and overturning
b) superstructure : movement, buckling and cracks near the supports, and falling of girder
c) bearing supports : failure of supports, and pull-out or rupture of anchor bolts

Table 1 Damage of Highway Bridges in the Past since Kanto Earthquake of 1923

DATE	EARTHQUAKE	MAGNITUDE	NUMBER OF BRIDGES DAMAGED	NUMBER OF BRIDGES WHICH FELL DOWN
1923. 9. 1	KANTO	7.9	1,785	6
1946.12.21	NANKAI	8.1	346	1
1948. 6.28	FUKUI	7.3	243	4
1949.12.26	IMAICHI	6.4	1	0
1952. 3. 4	TOKACHI-OKI	8.1	128	0
1962. 4.30	MIYAGI-KEN-HOKUBU	6.5	187	0
1964. 6.16	NIIGATA	7.5	98	3
1968. 2.21	EBINO	6.1	10	0
1968. 5.16	TOKACHI-OKI	7.9	101	0
1978. 1.14	IZU-OHSHIMA	7.0	7	0
1978. 6.12	MIYAGI-KEN-OKI	7.4	95	1
1982. 3.21	URAKAWA-OKI	7.1	5	0
1983. 5.26	NIHON-KAI-CHUBU	7.7	176	0
1984. 9.14	NAGANO-KEN-SEIBU	6.8	14	0
TOTAL			3,191	15

Although these sorts of damage are the ones commonly observed in the past earthquakes, the damage types have been changing in accordance with the progress of the seismic design method and improvement of construction practice. Seismic damage since the 1923 Kanto Earthquake may be classified into three stages from their significance [2] (refer to Table 2).

Stage 1 - Damage due to Inadequate Strength of Foundations

After experiencing the destructive damage of the 1923 Kanto Earthquake the first requirements for seismic design of highway bridges were included in the "Details of Road Structures (Draft)" issued by the Ministry of Internal Affairs in 1926. No seismic effects were considered for design of highway bridges prior to the Kanto Earthquake. Even after the first stipulations issued in 1926, seismic design was not adequate because the stipulations only described design force levels without providing a detailed design method or design details. Therefore, seismic safety of bridge substructures was inadequate until the 1950's when seismic design for foundations and substructures came to be widely adopted.

In those days, when seismic effects were either disregarded or inadequately considered, seismic damage was characterized by failure of foundations and substructures as shown in Photos 1 and 2. In most cases, foundations tilted, moved or even overturned due to inadequate strength of the foundations and the surrounding subsoils. This led to falling-off of the superstructures.

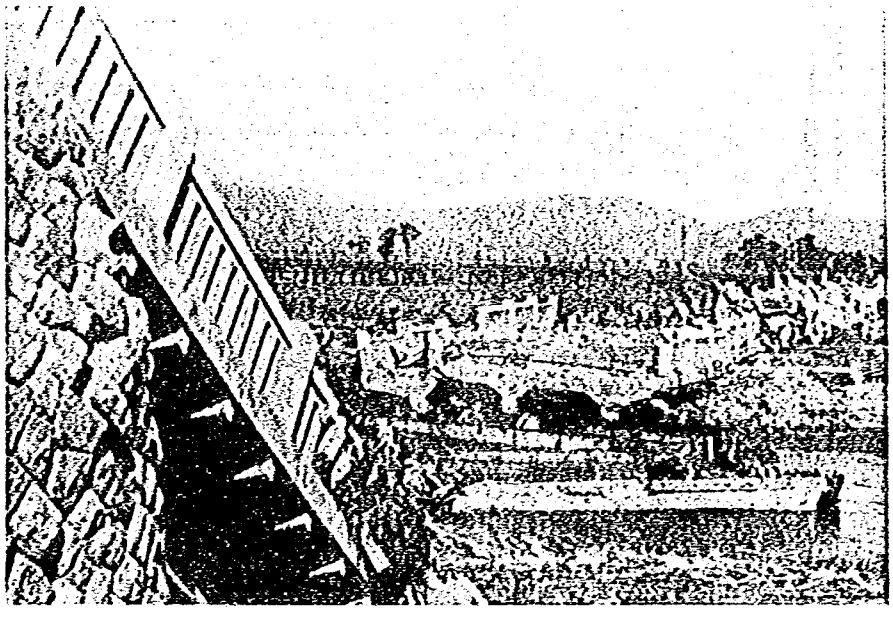


Photo 1 Damage of Sakawa-gawa Bridge on National Highway No. 1 by the Kanto Earthquake of 1923

Table 2 Change of Damage Types

Year	Major Earthquakes	Change of Major Seismic Damage	Seismic Design Method	Seismic Inspection and Strengthening
1920	1923 Kanto Earthquake (M7.9)	Failure of Superstructure due to Tilting/Movement of Foundation	1926 Initiation of Seismic Design (Details of Road Structures)	
1930				
1940		Failure of Concrete around Fixed Bearing	1939 Introduction of Standard Seismic Coefficient (Design Specifications of Steel Highway Bridges)	
	1946 Nankai Earthquake (M8.1)	Damage due to Liquefaction		
	1948 Fukui Earthquake (M7.3)			
1950	1952 Tokachi-oki Earthquake (M8.1)			
		Failure of RC Piers, and Bearing	1956 Seismic Coefficient depending on Zone and Ground Condition (Design Specifications of Steel Highway Bridges)	
1960	1964 Niigata Earthquake (M7.5)			
1970			1971 • Seismic Coefficient depending on Zone, Ground Conditions, Importance and Structural Response • Introduction of Evaluation Method for Liquefaction (Specifications for Seismic Design)	1971 Seismic Inspection
	1978 Miyagi-ken-oki Earthquake (M7.4)			1976 Seismic Inspection
1980	1982 Urakawa-oki Earthquake (M7.1)		1980 • Part V Seismic Design, Specifications for Design of Highway Bridges • Introduction of New Evaluation Method for Liquefactions	1979 Seismic Inspection
	1983 Nihon-kai-chubu Earthquake (M7.7)			1986 Seismic Inspection
1990			1990 Part V Seismic Design, Specifications for Design of Highway Bridges	

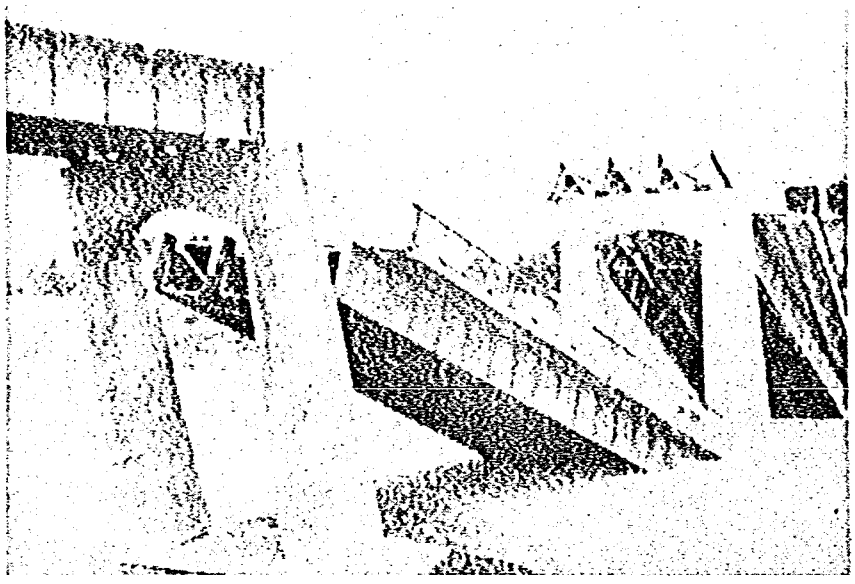


Photo 2 Damage of Nakazuno Bridge by the Fukui Earthquake of 1948

Stage 2 - Damage due to Soil Liquefaction

Although the damage due to inadequate strength of foundations became less frequent in accordance with the improvement of seismic design and construction methods, the next stage of damage encountered was soil failure during the 1964 Niigata Earthquake. Soil liquefaction, which took place extensively around sites, caused destructive damage to bridges. Photos 3 and 4 shows the falling-off of the decks of the Showa Bridge. Extensive soil movement associated liquefaction caused large lateral movements of bent pile foundations, which caused the dropping off of the deck.

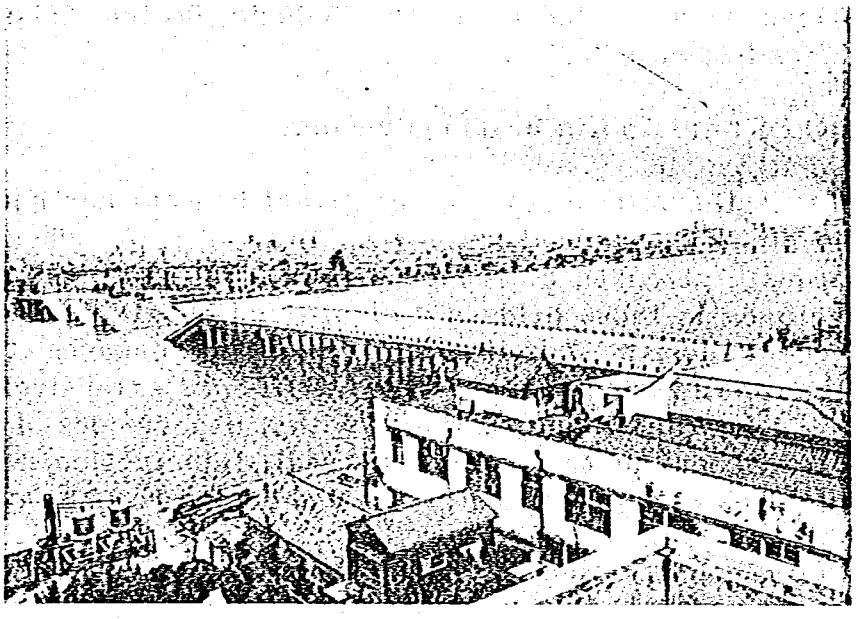


Photo 3 Damage of Showa Bridge by the Niigata Earthquake of 1964

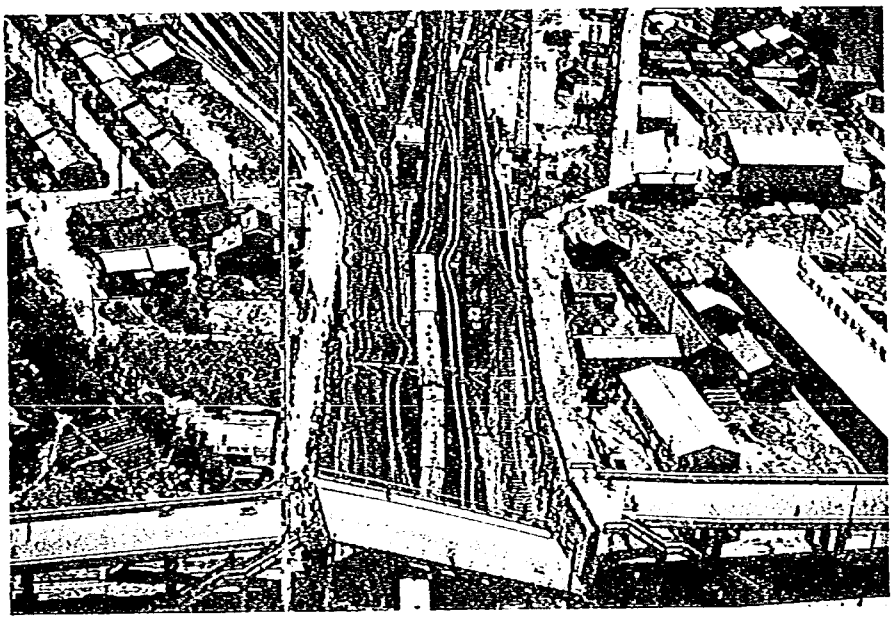


Photo 4 Damage of Higashi-Kosen Bridge by the Niigata Earthquake of 1964

Through the damage, it was learned that it is important to take account of liquefaction in design of bridges, and various studies for assessing and evaluating the effects of liquefaction were initiated. Through such studies, the first stipulations for assessment of liqvefaction were introduced in the "Seismic Design Specifications of Highway Bridges" in 1971.

One more important lesson gained from the Niigata Earthquake was that devices for preventing falling-off of superstructures from the crest of substructures are required. It was considered that even if large relative movements between the deck and substructures occurred due to either failure of substructures or failures of soils such as soil liquefaction, critical failure causing falling-off of deck could be prevented if such devices were provided. Various devices were then developed, and design recommendations were included in the Seismic Design Specifications of Highway Bridges issued in 1971.

Stage 3 - Damage to Piers and Bearing Supports

In recent earthquakes including the Miyagi-ken-oki Earthquake (M7.4) of 1978 and the Nihon-kai-chubu Earthquake (M7.7) of 1983, substantial damage due to inadequate strength of foundations and effects of soil liquefaction was not developed in those bridges designed and constructed in accordance with the recent design specifications. However, damages to reinforced concrete piers and bearing supports were developed extensively as shown in Photos 5, 6 and 7. This is due to the fact that other modes of failures such as tilting or movement of the foundations, soil liquefaction, and falling-off of superstructures were prevented by the new design recommendations.

The new strengthening and earthquake resistant countermeasures brought damage at the next weak points such as the reinforced concrete piers and

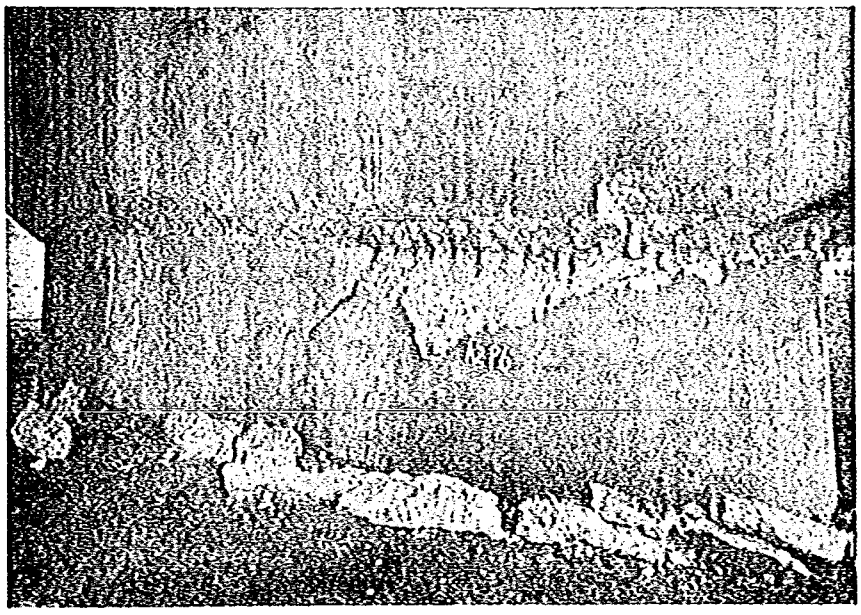


Photo 5 Damage to Reinforced Concrete Piers of Sendai Bridge by the Miyagi-ken-oki Earthquake of 1978

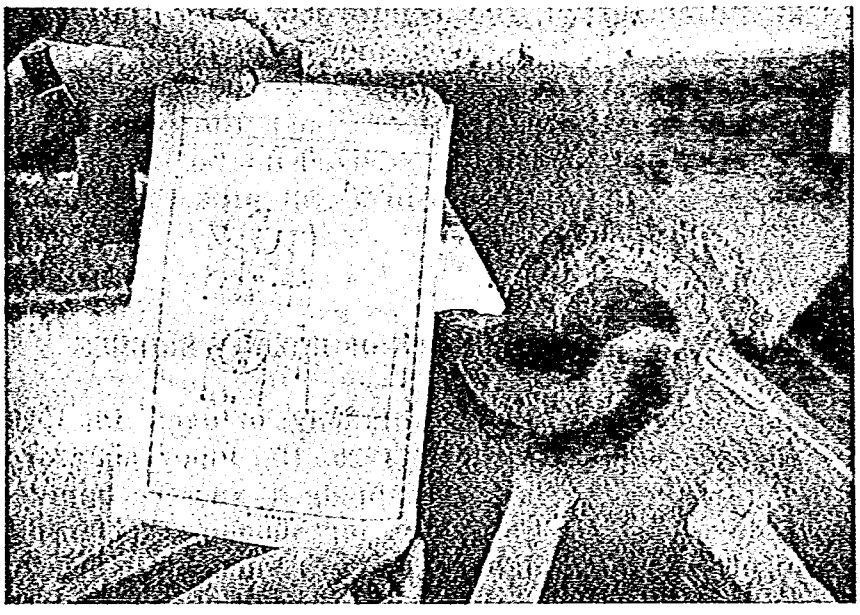


Photo 6 Damage to Bearing Supports of Da-te Bridge by the Miyagi-ken-oki Earthquake of 1978

the bearing supports. This obviously shows that countermeasures aiming only to minimize the damage observed in the past earthquakes do not necessarily contribute to avoid new types of damage in the future earthquakes. It is now required to take account of total seismic safety of highway bridges, and this was the main scope of the latest revision of the seismic design specifications in 1990.

It should be noted here that the damage shown in Photo 7 was developed

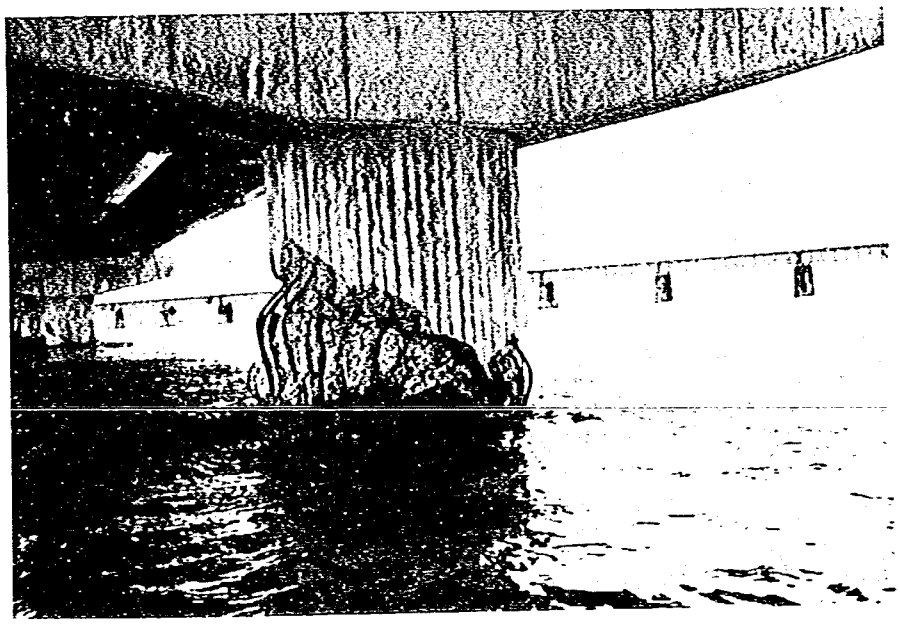


Photo 7 Damage to Reinforced Concrete Piers of Shizunai Bridge by the Urakawa-oki Earthquake of 1982

by shear at the mid-height of the reinforced concrete piers where main reinforcement was terminated. In the design specifications issued prior to 1980, the main reinforcement was terminated with the bond length of 12 times the diameter of the main reinforcement. Through the damage, such as that shown in Photo 7, the bond length was revised in the 1980 specifications to 12 times the diameter of the main reinforcement plus the effective width of the pier.

HISTORY OF SEISMIC DESIGN OF HIGHWAY BRIDGES

Seismic design was initiated for highway bridges in 1926 after the experience of the Kanto Earthquake in 1923. The importance of considering seismic effects in design of highway bridges was recognized from the extensive damage developed by the Kanto Earthquake. The first stipulations requiring seismic effects for highway bridges were included in "Details of Road Structures (Draft)" issued by the Ministry of Internal Affairs in 1926. It was stipulated in the draft details that the maximum lateral force expected to develop at the site shall be considered in seismic design. It was also recommended in the draft details that 30 % of gravity force shall be adopted for the reconstruction of the bridges damaged by the Kanto Earthquake at Tokyo and Yokohama.

After experiencing significant damage during strong earthquakes seismic regulations were reviewed and amended several times as shown in Table 3. "Design Specifications of Steel Highway Bridges (Draft)" were issued in 1939, and "Design Specifications of Steel Highway Bridges" and their revised version were issued in 1956 and 1964, respectively. A seismic lateral force of 20 % of the gravity force was stipulated in these specifications. The 20 %

Table 3 History of Design Seismic Loads for Highway Bridges in Japan

Year	Name of Regulations	Seismic Design Methods	Other Stipulations for Seismic Effects	Major Earthquakes
1886	Order No. 13, Ministry of Internal Affairs	Not Considered	Not Considered	1881 Nohbi (M8.4) 1923 Kanto (M7.9)
1926	Details of Road Structures (Draft), Road Law, MIA	Seismic Coefficient Method k_H=0.15~0.4 ($k_H \geqq 0.3$ advised in Tokyo and Yokohama)	Not Considered	
1939	Design Specifications of Steel Highway Bridges (Draft), MIA	Seismic Coefficient Method (k_H=0.2, k_V=0.1)	Not Considered	1946 Nankai (M8.1) 1948 Fukui (M7.3)
1956 (and 1964)	Design Specifications of Steel Highway Bridges, Ministry of Construction	Seismic Coefficient Method (k_H=0.1~0.35)	Not Considered	1952 Tokachi-oki (M8.2) 1964 Niigata (M7.5)
1971	Specifications for Seismic Design of Highway Bridges, MOC	• Seismic Coefficient Method (k_H=0.1~0.24) • Modified Seismic Coefficient Method (k_H=0.05~0.3)	• Evaluation of Sandy Layers Vulnerable to Liquefaction • Device for Preventing Falling-off of Superstructure	1978 Miyagi-ken-oki (M7.4)
1980	Part V Seismic Design of Design Specifications of Highway Bridges, MOC	• Seismic Coefficient Method (k_H=0.1~0.24) • Modified Seismic Coefficient Method (k_H=0.05~0.3) • Check of Deformation Capability of RC Piers • Dynamic Response Analysis	• F_L-Method for Evaluation of Liquefaction • Device for Preventing Falling-off of Superstructure	1982 Urakawa-oki (M7.1) 1983 Nihon-kai-chubu (M7.7)
1990	Part V Seismic Design of Design Specifications of Highway Bridges, MOC	• Seismic Coefficient Method (k_H=0.1~0.3) • Check of Bearing Capacity of RC Piers for Lateral Force • Dynamic Response Analysis	• F_L-Method for Evaluation of Liquefaction • Device for Preventing Falling-off of Superstructure	

gravity force was considered for long time as a basic design force for highway bridges.

The first comprehensive seismic design stipulations were issued by the Ministry of Construction in 1971 in a separate volume exclusively for seismic design as "Specifications for Seismic Design of Highway Bridges"[3]. It was described in the specifications that lateral force shall be determined depending on zone, importance and ground condition in the static lateral force method (seismic coefficient method) and structural response shall be further considered in the modified static lateral force method (modified seismic coefficient method). Evaluation of soil liquefaction was firstly incorporated in view of the damage caused in the 1964 Niigata Earthquake. Design details to increase the seismic safety such as devices for preventing falling-off of superstructure from substructures were newly introduced. Design methods for substructures were also issued between 1964 and 1971 in the form of "Design Specifications of Substructures". Therefore, it is considered that considerable increase of seismic safety was made for those

bridges designed and constructed in accordance with the 1971 Specifications.

The 1971 specifications were revised by the Ministry of Construction in the form of "Part V Seismic Design" of the "Design Specifications of Highway Bridges" in 1980. The Design Specifications of Highway Bridges consist of "Part I Common Part", "Part II Steel Bridges", "Part III Concrete Bridges", "Part IV Foundations", and "Part V Seismic Design". Although the Part V was essentially the same as the 1971 Specifications, a rational evaluation method for predicting soil liquefaction as well as practical design methods at the time when liquefaction is judged to occur[4] was included in the Part V Seismic Design.

The latest specifications were issued by the Ministry of Construction in February 1990 in the form of "Part V Seismic Design " for the " Design Specifications of Highway Bridges"[5][6]. Major revisions introduced in the 1990 Specifications were unification of static lateral force method (seismic coefficient method) and the modified static lateral force method (modified seismic coefficient method) including the revision of the seismic design force, a new method for computing inertia force for multi-span continuous bridges, a new ductility check for reinforced concrete piers, and detailed stipulations for dynamic response analysis. These revisions were incorporated based on the recent studies for predicting earthquake ground motions and strength of reinforced concrete piers[7]～[12].

SEISMIC DESIGN OF HIGHWAY BRIDGES

Outline

Highway bridges are vital components of highways, and they have to be safe enough against earthquakes so that the function of highways be maintained. They have to be used without loosing any structural functions against small to moderate earthquakes which have high to moderate possibility of occurring at the site. Critical failures causing total collapse of a bridge have to be avoided even during significant earthquakes such as the Kanto Earthquake of 1923.

The "Part V Seismic Design" of the "Design Specifications of Highway Bridges" is applied for the seismic design of highway bridges with span lengths not longer than 200 meters. The specifications stipulate the adoption of the static lateral force method (seismic coefficient method) based on the allowable stress design approach. A check of the ductility for reinforced concrete piers (Check of Bearing Capacity of Reinforced Concrete Piers for Lateral Force) and dynamic response analysis are recommended in accordance with flow chart presented in Fig. 1. Emphasis is placed on the need to install devices for preventing falling-off of the superstructures from the substructures.

The "Part V Seismic Design" of the "Design Specifications of Highway

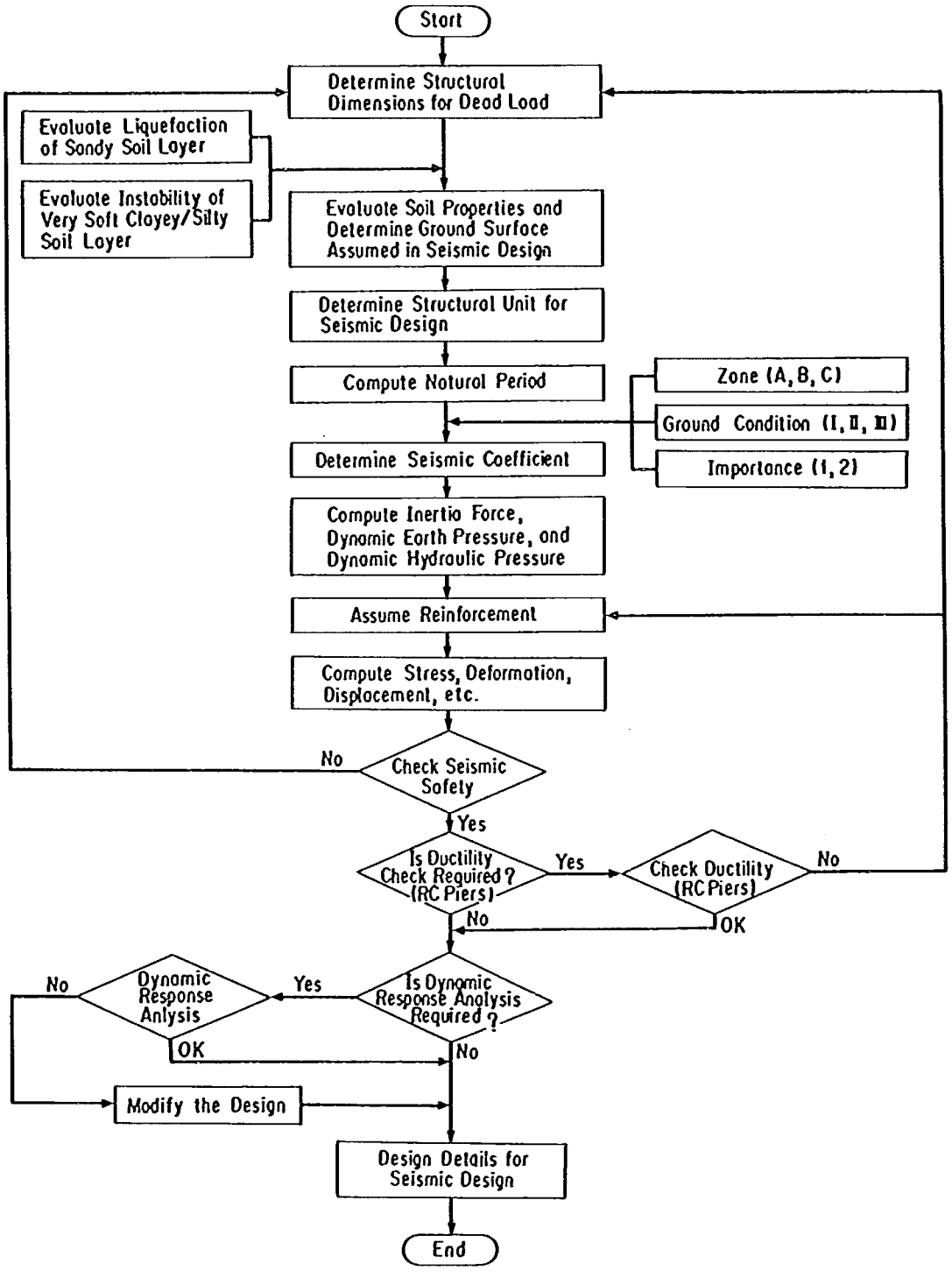


Fig.1 Flow of Seismic Design of Highway Bridge

Bridges" have the contents as[5] :

Chapter 1 General
1.1 Scope and Application
1.2 Definition of Terms
Chapter 2 Basic Principles of Seismic Design
Chapter 3 Loads and Design Conditions in Seismic Design
3.1 Loads and Combinations for Seismic Design
3.2 Effects of Earthquakes
3.3 Inertia Force
3.3.1 General
3.3.2 Computation Method of Natural Period
3.3.3 Computation Method of Inertia Force
3.4 Dynamic Earth Pressure
3.5 Hydrodynamic Pressure
3.6 Ground Conditions for Seismic Design
3.7 Soil Layers of Which Bearing Capacity Shall be Decreased in Seismic Design
3.7.1 General
3.7.2 Sandy Layers Vulnerable to Liquefaction
3.7.3 Very Loose Clayey and Silty Soil Layers
3.7.4 Soil Layers of Which Bearing Capacity Shall be Decreased and Treatment of the Layers
3.8 Ground Surface Assumed in Seismic Design
Chapter 4 Seismic Coefficient
4.1 General
4.2 Standard Horizontal Seismic Coefficient
4.3 Modification Factors for Standard Horizontal Seismic Coefficient
Chapter 5 Check of Bearing Capacity of Reinforced Concrete Piers for Lateral Force
5.1 General
5.2 Check of Safety
5.3 Horizontal Seismic Coefficient for Check of Bearing Capacity of Reinforced Concrete Piers for Lateral Force
5.3.1 Equivalent Horizontal Seismic Coefficient for Check of Bearing Capacity of Reinforced Concrete Piers for Lateral Force
5.3.2 Horizontal Seismic Coefficient for Check of Bearing Capacity of Reinforced Concrete Piers for Lateral Force
5.4 Bearing Capacity of Reinforced Concrete Piers for Lateral Force
5.4.1 Bearing Capacity of Reinforced Concrete Piers for Lateral Force, Allowable Ductility Factor, and Equivalent Natural Period
5.4.2 Bearing Capacity, Yielding Force, Ultimate Displacement and Yielding Displacement
5.4.3 Bearing Capacity of Reinforced Concrete Piers for Shear
Chapter 6 Dynamic Response Analysis
6.1 General
6.2 Dynamic Response Analysis Method and Analytical Models
6.2.1 Method of Dynamic Response Analysis

6.2.2 Analytical Models
6.3 Input Ground Motions for Dynamic Response Analysis
6.3.1 Acceleration Response Spectra for Modal Response Spectral Analysis
6.3.2 Accelerations for Time History Analysis
6.4 Check of Seismic Safety
Chapter 7 Structural Details in Seismic Design
7.1 General
7.2 Device for Preventing Falling-off of Superstructure from Substructures
7.2.1 General
7.2.2 Devices for Preventing Falling-off of Superstructure
7.2.3 Distance between Edge of Crest of Substructure and Edge of Deck
7.2.4 Devices for Fall of Deck
7.3 Design Details for Seismic Design at Bearing Supports
Chapter 8 Devices for Reducing Lateral Force

〈Appendix〉
I. References on Liquefaction
II. Examples of Classification of Ground Condition
III. References on Design Ground Motion
IV. Example of Computation of Natural Period and Inertia Force
V. Reference on Bearing Capacity of Reinforced Concrete Piers for Lateral Force
VI. Practices of Design Details for Seismic Design

Seismic Lateral Force for Static Lateral Force Method

(1) In the static lateral force method (seismic coefficient method), the horizontal design seismic coefficient shall be determined by Eq.(1), but no less than 0.1.

$$k_h = c_z \cdot c_G \cdot c_I \cdot c_T \cdot k_{h0} \qquad (1)$$

where

k_h : design horizontal seismic coefficient,
k_{h0} : standard design horizontal seismic coefficient (=0.2),
c_z : modification factor for zone (refer to Fig. 2),
c_G : modification factor for ground condition (refer to Table 4),
c_I : modification factor for importance (refer to Table 5), and
c_T : modification factor for structural response (refer to Table 6). For computing inertia force associated with the weight of soils and dynamic earth pressure, c_T shall be 1.0.

Fig. 3 shows the horizontal seismic coefficient assuming $c_z = c_I = 1.0$.

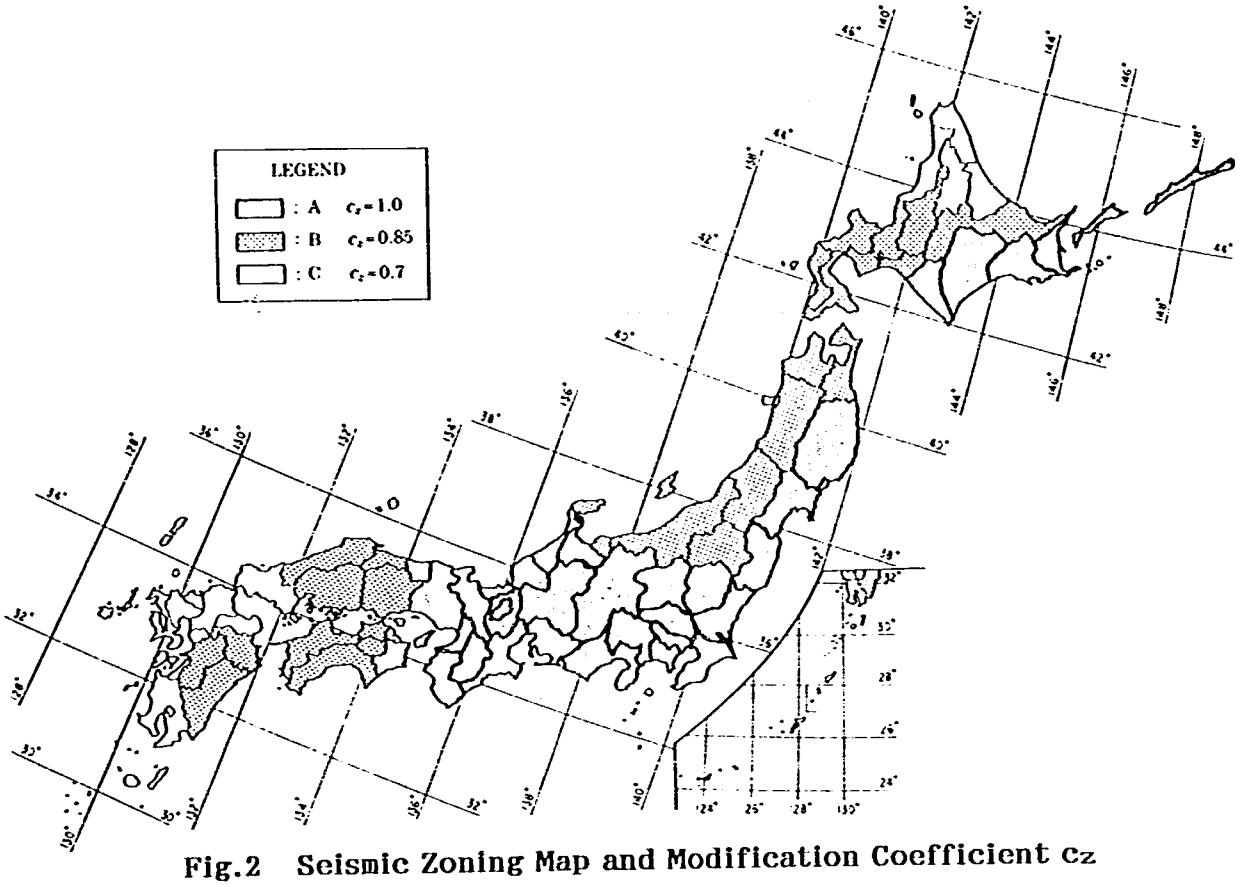


Fig.2 Seismic Zoning Map and Modification Coefficient c_Z

Table 4 Ground Condition Factor c_G

Ground Group	I	II	III
c_G	0.8	1.0	1.2

Table 5 Importance Factor c_I

Group	c_I	Definition
1st class	1.0	Bridges on expressway (limited access highways), general national road and principal prefectural road. Important bridges on general prefectural road and municipal road.
2nd class	0.8	Other than the above

Table 6 Structural Response Factor c_T

Ground Group	Structural Response Coefficient c_T		
Group I	$T < 0.1$ $c_T = 2.69T^{1/3} \geqq 1.00$	$0.1 \leqq T \leqq 1.1$ $c_T = 1.25$	$1.1 < T$ $c_T = 1.33T^{-2/3}$
Group II	$T < 0.2$ $c_T = 2.15T^{1/3} \geqq 1.00$	$0.2 \leqq T \leqq 1.3$ $c_T = 1.25$	$1.3 < T$ $c_T = 1.49T^{-2/3}$
Group III	$T < 0.34$ $c_T = 1.80T^{1/3} \geqq 1.00$	$0.34 \leqq T \leqq 1.5$ $c_T = 1.25$	$1.5 < T$ $c_T = 1.64T^{-2/3}$

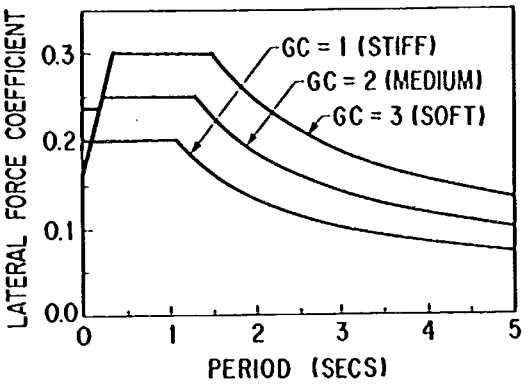


Fig.3 Horizontal Seismic Coefficient k_h for Static Lateral Force Method ($c_Z = c_I = 1.0$)

(2) The vertical design seismic coefficient may be generally considered as zero, except for bearing supports.

(3) The seismic lateral force for structural members, soils and water below the "ground surface assumed in seismic design" shall be considered as zero. The ground surface assumed in seismic design depends on soil condition at the site, and is generally assumed as the base level of footing for pile foundations.

(4) Hydrodynamic pressure and earth pressure during earthquakes are stipulated in the specifications.

(5) Increase of allowable stresses of materials may be considered in seismic design. The magnitude of the increase for specific materials is specified in the respective parts. For seismic design of substructures, the allowable stress is increased 1.5 times for a load combination of primary load and seismic effects.

Classification of Ground Condition

Ground conditions are classified into three groups according to Table 7, in which characteristic value T_G shall be evaluated by Eq.(2).

Table 7 Classification of Ground Condition

GROUND CONDITION	DEFINITION	APPROXIMATE ESTIMATION
GROUP I	$T_G < 0.2$ SEC	TERTIALY OR OLDER
GROUP II	$0.2 \leqq T_G < 0.6$ SEC	ALLUVIUM AND DILUVIUM
GROUP III	$0.6 \leqq T_G$	SOFT ALLUVIUM

$$T_G = \sum_i \frac{4h_i}{V_{Gi}} \qquad (2)$$

where

T_G : characteristic value (sec)
H_i : thickness of i-th subsoil layer (m)
V_{si} : shear wave velocity of i-th sublayer (m/sec)
i : sublayer's number counted from ground surface

Evaluation Method of Inertia Force

Inertia forces in the static lateral force method shall be applied to bridges in two ways depending on the seismic design structural unit. The seismic design structural unit shall be selected in accordance with Table 8.

Natural period and the inertia force shall be determined as:

1) Seismic design structural unit consisting of a substructure and the part of superstructure supported vertically by the substructure

Natural period and inertia force shall be determined by Eqs.(3) and (4)

$$F_{ai} = k_{hi} R_i \quad (3)$$

$$T = 2.01 \sqrt{\delta} \quad (4)$$

where
F_{ai} : inertia force associated with dead weight of superstructure for design of i-th substructure
k_{hi} : seismic coefficient considered for i-th structural segment
R_i : reaction force developed at i-th substructure due to dead weight of the part of superstructure supported by the i-th substructure.
T : natural period, in second, of the seismic design structural unit
δ : lateral displacement, in meter, of the substructure subjected to a lateral force equivalent with 80 % of the dead weight of a substructure above the ground surface assumed in seismic design and the dead weight of a part of the superstructure supported by the substructure.

2) Seismic design structural unit consisting of several substructures and the part of superstructure supported vertically by the substructures.

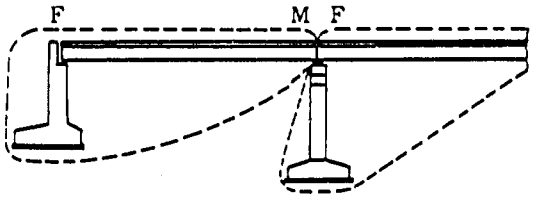
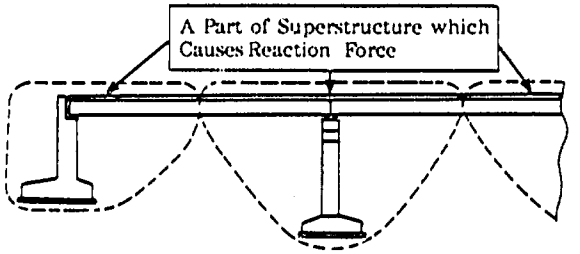
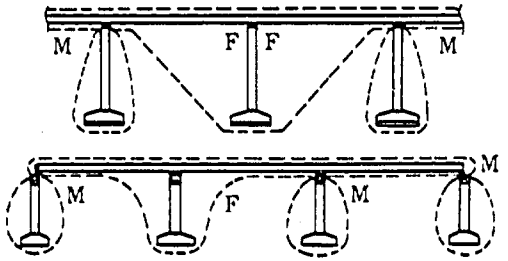
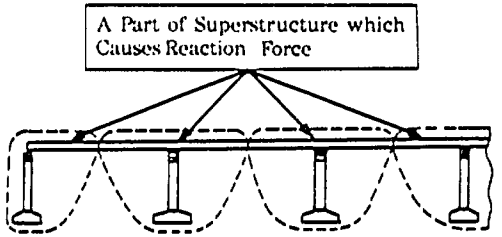
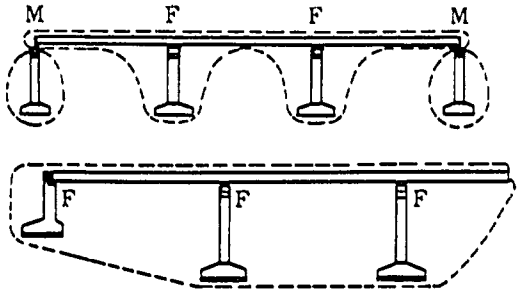
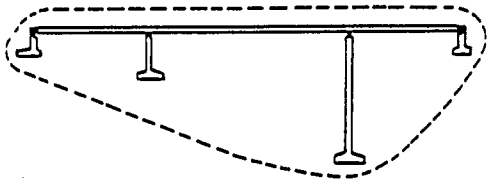
Inertia force shall be evaluated in accordance with Fig. 4, i.e.,

i) idealize the bridge by a linear elastic frame model
ii) apply a lateral force equivalent with the dead weight of superstructure and substructures above the ground surface assumed in seismic design, and compute the natural period as

$$T = 2.01 \sqrt{\delta} \quad (5)$$

$$\delta = \frac{\int w(s)u(s)^2 ds}{\int w(s)u(s) ds}$$

Table 8 Seismic Design Structural Unit

<table>
<tr><th></th><th colspan="4">Longitudinal</th><th colspan="2">Transverse</th><th>Seismic Design Unit</th></tr>
<tr><td>Simple Girder</td><td colspan="4"> 
</td><td colspan="2"> 
</td><td rowspan="2">Regarded as A Unit Consisting of A Substructure and A Part of Superstructure Supported by the Substructure</td></tr>
<tr><td rowspan="2">Continuous Girder</td><td rowspan="2">Support Condition in Longitudinal Direction</td><td>Fixed at One Support</td><td> 
</td><td rowspan="2">Difference of Natural Period between Piers</td><td>Small</td><td> 
</td></tr>
<tr><td>Fixed at Multiple Supports</td><td> 
</td><td>Large</td><td>  </td><td>Regarded as A Unit Consisting of Substructures and the Superstructure Supported by the Substructures</td></tr>
<tr><td>Arch, Frame and Others</td><td colspan="4">  </td><td colspan="2">  </td></tr>
</table>

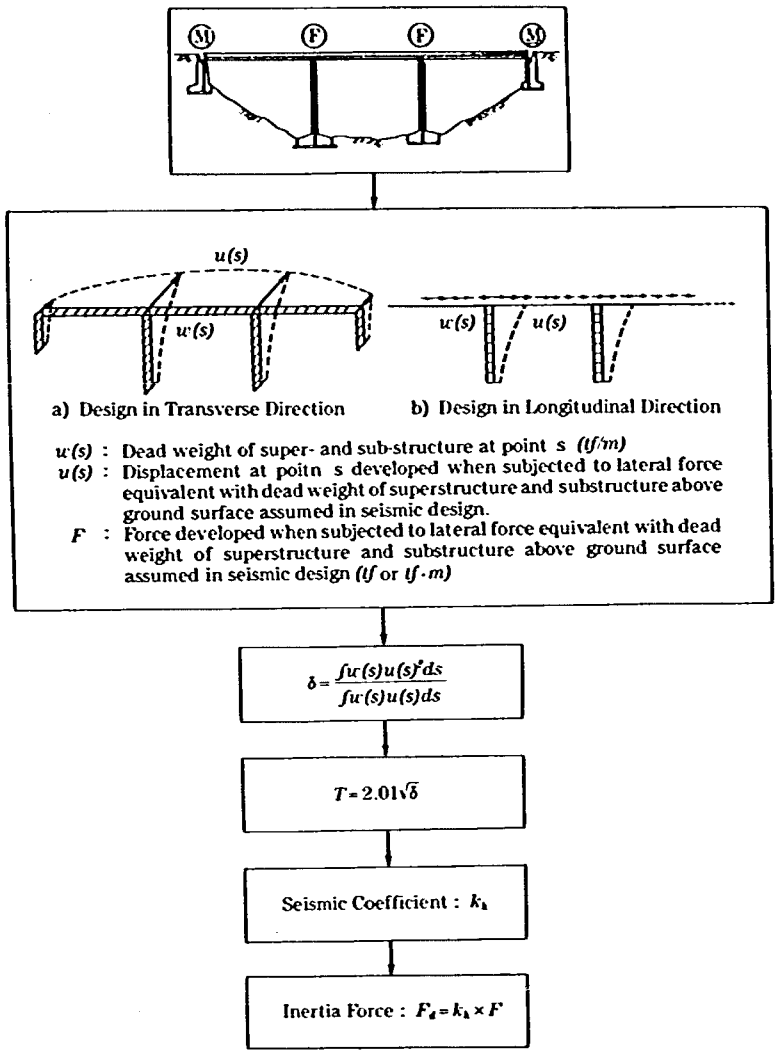


Fig.4 Determination of Inertia Force

where

w(s) : dead weight of the seismic design structural unit (superstructure and substructure above the ground surface assumed in seismic design) at point "s" (tf/m)

u(s) : lateral displacement developed in the seismic design structural unit at point "s" (m) when subjected to w(s) in the direction considered in design.

iii) determine the seismic coefficient k_h depending on the natural period T.

iv) compute inertia force as

$$F_d = k_h \times F \tag{7}$$

where

F_d : shear force (tf) or bending moment (tfm) due to inertia force

k_h : seismic coefficient

F : force developed in the seismic design structural unit when subjected to a lateral force equivalent to the dead weight of the

seismic design structural unit above the ground surface assumed in seismic design (tf/tfm)

For substructures supporting girder bridges, the shear force developed at the center of gravity of the superstructure shall be regarded as the lateral force for seismic design of substructures. However, when the inertia force computed by Eq.(7) is smaller than the inertia force computed by Eq.(3), the latter shall be adopted for design. This needs some explanation. The inertia force computed by Eq.(7) is approximately proportional to the stiffness of each substructure. This implies that the majority of the inertia force tends to be carried by the substructures with higher stiffness. Depending on the stiffness distribution of substructures, the inertia force carried by piers with lower stiffness takes even negative values. However, if failure of the structure, such as at a bearing support, occurs, the contribution of load carried by each substructure will be changed from the distribution computed by Eq.(7). Based on such considerations, a lower limit for the inertia force evaluated by Eq.(7) is included.

Strength of Sandy Soil Layer for Liquefaction

(1) Sandy Soil Layer Needed to be Checked for Liquefaction

Saturated alluvial sandy layers which have the water table within 10 m from the ground surface and have D_{50}-values on the grain size accumulation curve between 0.02 and 20. mm are vulnerable to liquefaction up to a depth of 20 m below the ground surface, and liquefaction potential of these layers shall be estimated according to item (2).

(2) Estimation of Liquefaction

For those soil layers which are judged to be vulnerable to liquefaction, liquefaction potential shall be checked based on the liquefaction resistance factor F_L defined as

$$F_L = R / L \tag{8}$$

where

F_L : liquefaction resistance factor

R : resistance of soil elements against dynamic load defined as

$$R = R_1 + R_2 + R_3$$

$$R_1 = 0.0882\sqrt{\frac{N}{\sigma_v' + 0.7}}$$

$$R_2 = \begin{cases} 0.19 & (0.02\ \text{mm} \leqq D_{50} \leqq 0.05\ \text{mm}) \\ 0.225\log_{10}(0.35/D_{50}) & (0.05\ \text{mm} < D_{50} \leqq 0.6\ \text{mm}) \\ -0.05 & (0.6\ \text{mm} < D_{50} \leqq 2.0\ \text{mm}) \end{cases}$$

$$R_3 = \begin{cases} 0.0 & (0\ \% \leqq F_C \leqq 40\ \%) \\ 0.004F_C - 0.16 & (40\ \% < F_C \leqq 100\ \%) \end{cases}$$

N : N-value of standard penetration test

D_{50} : averaged grain size on grain size accumulation curve

F_C : fine sand (grain size less than 74 μm) content

L : dynamic load induced in soil elements during an earthquake

defined as

$$L = r_d \cdot k_s \frac{\sigma_v}{\sigma_v'}$$

$r_d = 1.0 - 0.015x$

x : depth from the ground surface (m)

k_s : seismic coefficient for evaluating liquefaction, and shall be determined as

$k_s = c_z \cdot c_G \cdot c_I \cdot k_{s0}$

c_z, c_G and c_I : modification factors for zone, ground condition, and importance(refer to Fig. 2, Table 4 and Table 5)

k_{s0} : standard design horizontal seismic coefficient for check of liquefaction (= 0.15)

σ_v: total overburden pressure (kgf/cm^2), and

$\sigma_v = \{\gamma_{t1} h_w + \gamma_{t2} (x - h_w)\} /10$

σ_v': effective overburden pressure (kgf/cm^2), and

$\sigma_v' = \{\gamma_{t1} h_w + \gamma'_{t2} (x - h_w)\} /10$

Soil layers having liquefaction resistance factors, F_L, smaller than 1.0 shall be judged to liquefy during earthquakes.

(3) Treatment of Soil Layers Which Were Judged to Liquefy

For those soil layers which were judged to liquefy in the above estimation and which are within 20 m from the ground surface, the spring stiffness and other soil constants shall be either neglected or reduced in seismic design as shown in Fig. 5, by multiplying the original spring stiffness and other soil constants by the reduction factor D_E which is determined in accordance with F_L-value and tabulated in Table 9.

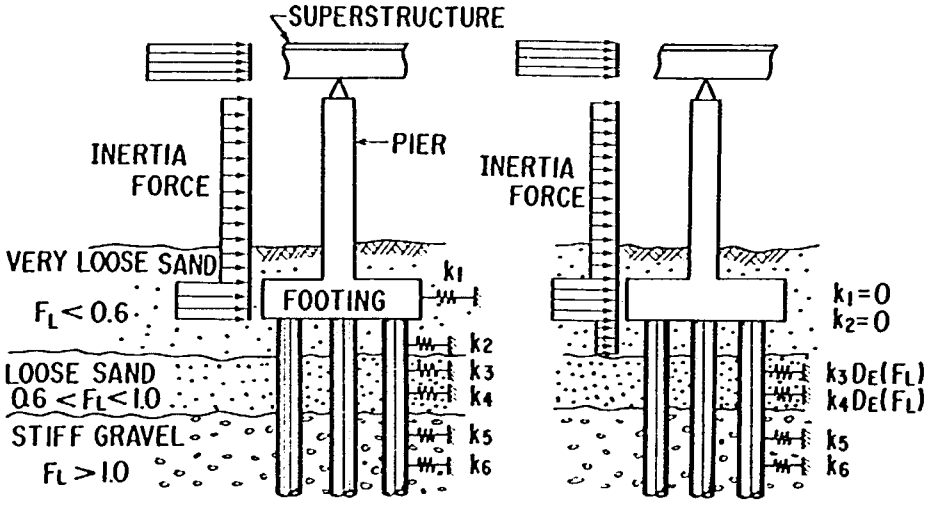


Fig.5 Treatment of Soil Layers Vulnerable to Liquefaction

Check of Bearing Capacity of Reinforced Concrete Piers for Lateral Force

To prevent reinforced concrete piers from failing in a brittle manner, it is recommended that the bearing capacity of the reinforced concrete piers be checked in accordance with the flow-chart presented in Fig. 6.

Table 9 Decreasing Rate D_E of Soil Constants Depending on F_L Value

F_L-VALUE	DEPTH FROM GROUND SURFACE	D_E
$F_L \leqq 0.6$	$0m \leqq x \leqq 10m$	0
	$10m < x \leqq 20m$	1/3
$0.6 < F_L \leqq 0.8$	$0m \leqq x \leqq 10m$	1/3
	$10m < x \leqq 20m$	2/3
$0.8 < F_L \leqq 1.0$	$0m \leqq x \leqq 10m$	2/3
	$10m < x \leqq 20m$	1

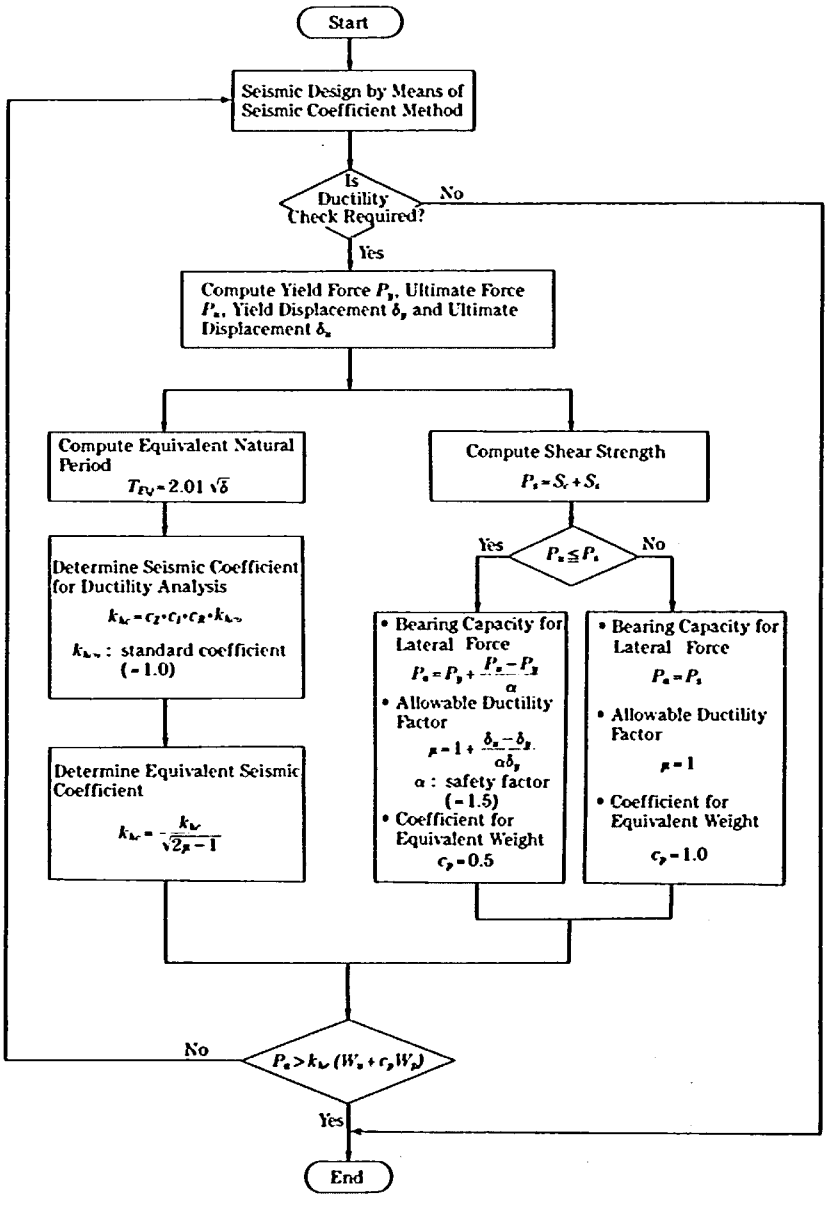


Fig.6 Check of Bearing Capacity of Reinforced Concrete Pier For Lateral Force

1) Judgement of bearing capacity of reinforced concrete piers for lateral force

Bearing capacity of reinforced concrete piers for lateral force shall be checked as

$$P_a > k_{he}W \tag{9}$$

where

P_a : bearing capacity of the reinforced concrete piers for lateral force (tf)

k_{he} : equivalent horizontal seismic coefficient for check of bearing capacity of the reinforced concrete piers for lateral load

W : equivalent dead weight (tf), and shall be determined as

$$W = W_u + c_P W_p \tag{10}$$

$$c_P = \begin{cases} 0.5 & P_u \leqq P_s \\ 1.0 & P_u > P_s \end{cases} \tag{11}$$

W_u : dead weight of a part of superstructure supported by the reinforced concrete piers (tf)

W_p: dead weight of the reinforced concrete piers (tf)

P_u: bearing capacity of reinforced concrete piers for flexural failure (tf)

P_s: bearing capacity of reinforced concrete piers for shear failure (tf)

2) Equivalent horizontal seismic coefficient for check of bearing capacity of reinforced concrete piers for lateral force

Equivalent horizontal seismic coefficient for check of bearing capacity of reinforced concrete piers for lateral force shall be determined according to the equal energy assumption as

$$k_{he} = \frac{k_{hc}}{\sqrt{2\mu - 1}} \tag{12}$$

$$k_{hc} = c_Z \cdot c_I \cdot c_R \cdot k_{hco} \tag{13}$$

where

k_{he} : equivalent horizontal seismic coefficient for check of bearing capacity of reinforced concrete piers for lateral force

k_{hc} : horizontal seismic coefficient for check of bearing capacity of reinforced concrete piers for lateral force

μ : allowable ductility factor

c_Z : modification factor for zone (refer to Fig. 2)

c_I : modification factor for importance (refer to Table 5)

c_R : modification factor for structural response (refer to Table 10)

k_{hco}: standard horizontal seismic coefficient for check of bearing capacity of reinforced concrete piers for lateral force

The standard horizontal seismic coefficient k_{hco} was determined to

Table 10 Structual Response Factor c_R

Ground Group	Structural Response Coefficient c_R		
Group I	$T_{EQ} \leqq 1.4$ $c_R = 0.7$		$1.4 < T_{EQ}$ $c_R = 0.876T_{EQ}^{-2/3}$
Group II	$T_{EQ} < 0.18$ $c_R = 1.51\ T_{EQ}^{1/3} \geqq 0.7$	$0.18 \leqq T_{EQ} \leqq 1.6$ $c_R = 0.85$	$1.6 < T_{EQ}$ $c_R = 1.16T_{EQ}^{-2/3}$
Group III	$T_{EQ} < 0.29$ $c_R = 1.51T_{EQ}^{1/3} \geqq 0.7$	$0.29 \leqq T_{EQ} \leqq 2.0$ $c_R = 1.0$	$2.0 < T_{EQ}$ $c_R = 1.59T_{EQ}^{-2/3}$

represent a realistic ground motion developed during a significant earthquake with magnitude as large as 8. Fig.7 shows the horizontal seismic coefficient k_{hO} for the check of bearing capacity of reinforced concrete piers for lateral force when $c_Z = c_I = 1.0$.

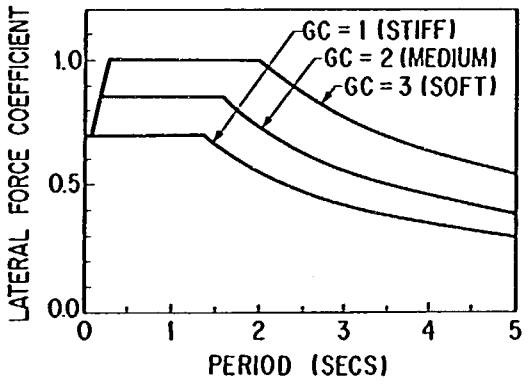


Fig. 7 Horizontal Seismic Coefficient k_{hO} for Check of Bearing Capacity of Reinforced Concrete Piers for Lateral Force ($C_Z = c_I = 1.0$)

3) Bearing capacity of reinforced concrete piers for lateral force and allowable ductility factor

Bearing capacity of reinforced concrete piers for lateral force P_a and the allowable ductility factor μ shall be determined based on the failure mode as :

a)Flexural failure

$$P_a = P_y + \frac{P_u - P_y}{\alpha} \tag{14}$$

$$\mu = 1 + \frac{\delta_u - \delta_y}{\alpha\ \delta_y} \tag{15}$$

where

P_u, δ_u : bearing capacity (tf) and ultimate displacement (m) for

flexural failure

P_y, δ_y : yielding force (tf) and yielding displacement (m) for flexural failure

α : safety factor (= 1.5)

b)Shear failure

$$P_A = P_s \quad (16)$$

$$\mu = 1 \quad (17)$$

where

P_s : bearing capacity (tf) for shear failure

Photos 8 and 9 show dynamic loading tests and shaking table tests conducted to study inelastic behavior of reinforced concrete piers[11][12].

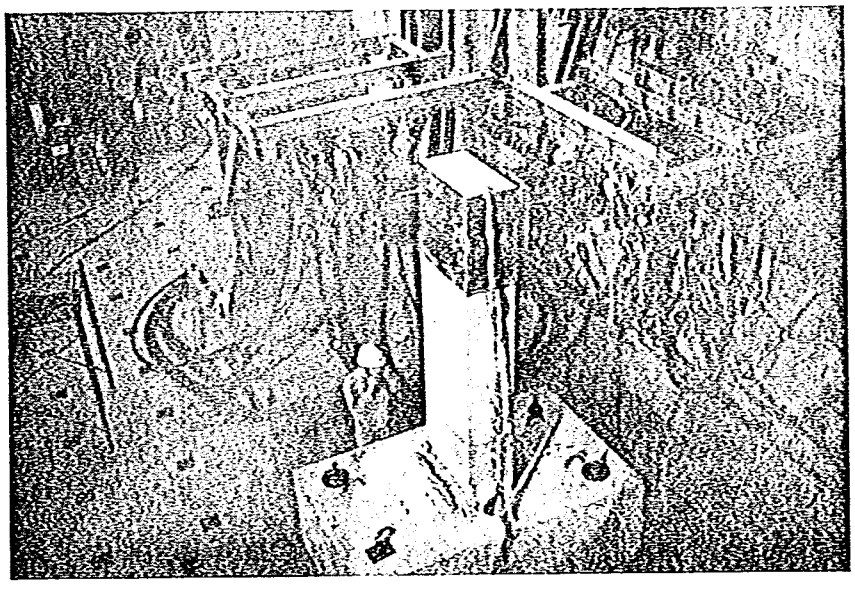


Photo 8 Dynamic Loading Tests of Reinforced Concrete Pier Models

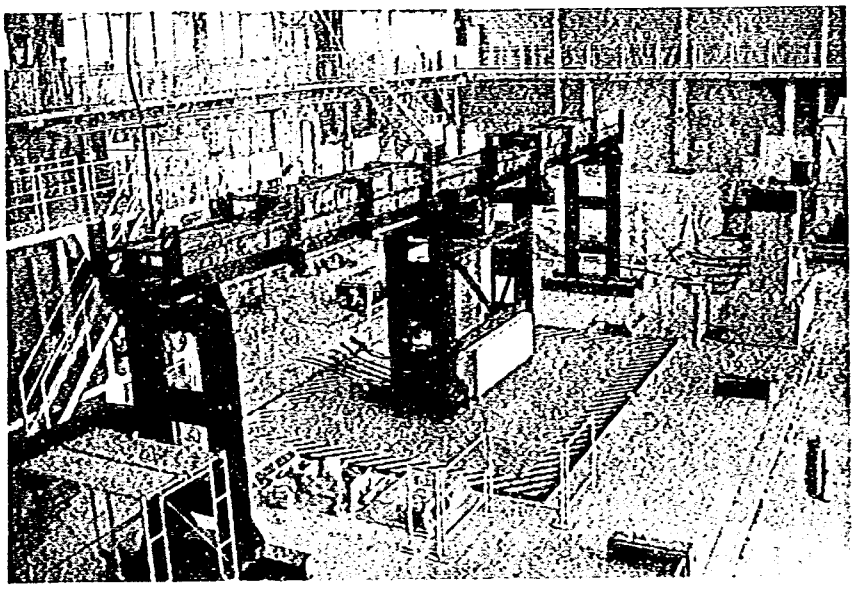


Photo 9 Shaking Table Tests of Reinforced Concrete Pier Supporting Two Span Simply Supported Girders (Weight = 40 tf)

Dynamic Response Analysis

For bridges with complicated dynamic response and for new types of bridges, dynamic response analysis is recommended to be made to check seismic safety of the design made by means of the static lateral force method.

In principle, dynamic response analysis shall be made by means of modal response spectral analysis with use of an analytical model which simulates dynamic characteristics of the bridge. Acceleration response spectrum for the modal response spectrum analysis shall be determined as

$$S = c_Z \cdot c_I \cdot c_D \cdot S_0 \tag{18}$$

where

S : response spectrum for modal response spectrum analysis (gal (=cm/sec^2))

c_Z : modification factor for zone (refer to Fig. 2)

c_I : modification factor for importance (refer to Table 5)

c_D : modification factor for damping, and shall be determined based on modal damping ratio h_i as

$$c_D = \frac{1.5}{40h_i + 1} \tag{19}$$

S_0 : standard response spectrum for modal response analysis method (gal) (refer to Table 11)

Table 11 Standard Response Spectral Value S_0 for Modal Dynamic Response Analysis

Ground Condition	S_0 (gal)		
Group I	$T_i < 0.1$ $S_0 = 431T_i^{1/3} \geqq 160$	$0.1 \leqq T_i \leqq 1.1$ $S_0 = 200$	$1.1 < T_i$ $S_0 = 220/T$
Group II	$T_i < 0.2$ $S_0 = 427T_i^{1/3} \geqq 200$	$0.2 \leqq T_i \leqq 1.3$ $S_0 = 250$	$1.3 < T_i$ $S_0 = 325/T_i$
Group III	$T_i < 0.34$ $S_0 = 430T_i^{1/3} \geqq 240$	$0.34 \leqq T_i \leqq 1.5$ $S_0 = 300$	$1.5 < T_i$ $S_0 = 450/T_i$

Fig. 8 shows the design response spectra assuming $c_Z = c_I = 1.0$ and $c_D = 1.0$ ($h_i = 5$ %). Fig. 9 shows the modification factor c_D.

When a time history analysis is required, strong motion records which have the similar characteristics with S by Eq.(18) shall be used with the consideration on site condition and structural response of the bridge. Three

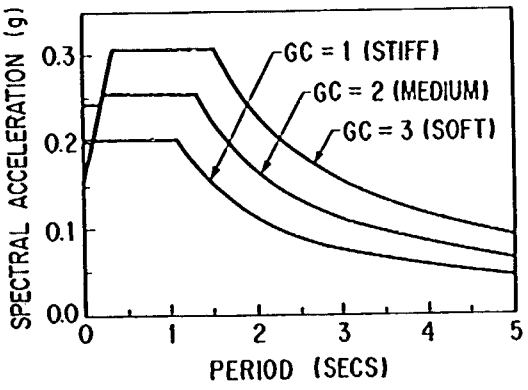


Fig. 8 Design Acceleration Response Spectra S_D for Dynamic Response Analysis ($c_Z = c_I = 1.0$ and $c_D = 1.0$ ($h_i = 0.05$))

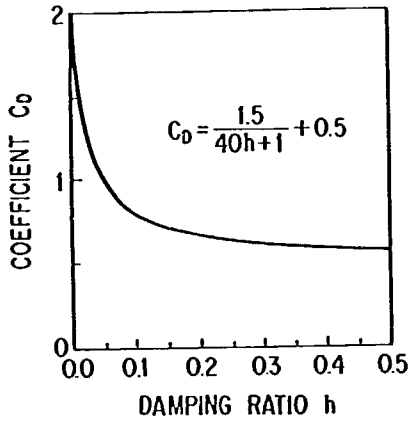


Fig. 9 Modification Factor c_D

ground acceleration records which were modified in frequency domain so that their response characteristics match with S_D in Eq.(18) are provided in the Specifications.

Device for Preventing Superstructure from Falling

Because connections between superstructure and substructure or between two adjacent superstructures are quite susceptible to earthquake damage, special structural considerations are required to prevent falling-off of the superstructure from the substructures due to damage of those sections. For such a purpose, the following measures are applied as shown in Fig. 10 :

(1) At movable bearings, devices to prevent dislodgement of upper-bearings from the lower-bearings (stopper) are provided

(2) At the both ends of superstructure, either of the following measures are used to prevent the superstructure from dislodging from the crest of the substructures :

a) The distance from the edge of superstructure to the edge of sub-

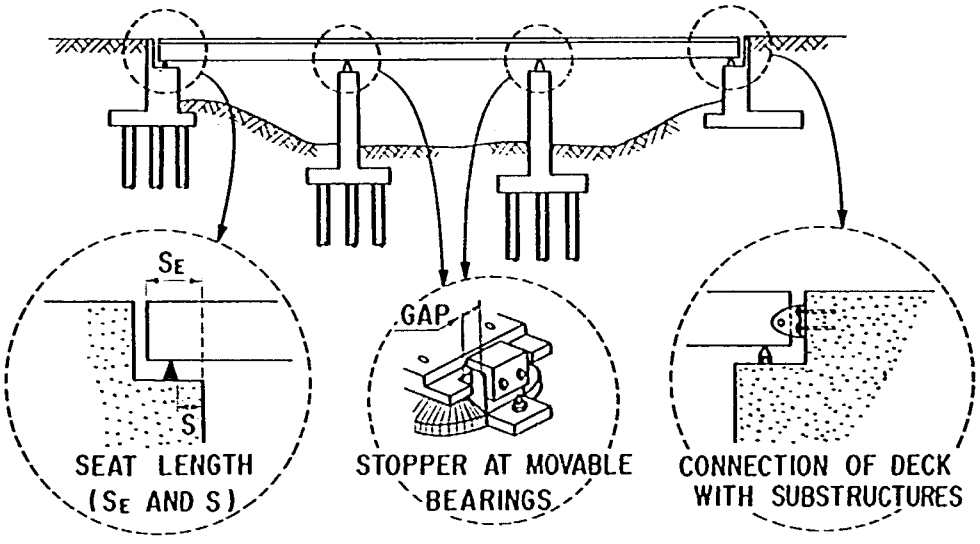


Fig. 10 Devices for Preventing Superstructure from Falling

structure (Seat Length) S_E shall be longer than the value as

$$S_E = \begin{cases} 70 + 0.5 \times l & l \leqq 100 \text{ m} \\ 80 + 0.4 \times l & l > 100 \text{ m} \end{cases} \quad (20)$$

in which S_E and l represent the seat length in cm and the span length in m, respectively.

b) Installation of devices for preventing falling-off of superstructure from substructures

(3) In addition to the items (1) and (2), the distance from the edge of the bearing supports to the edge of substructure (Bearing Seat Length) S shall be longer than the value as

$$S = \begin{cases} 20 + 0.5 \times l \\ 30 + 0.4 \times l \end{cases} \quad (21)$$

in which S and l represent the bearing seat length in cm and the span length in m, respectively

DEVELOPMENT OF PASSIVE AND HYBRID CONTROL OF HIGHWAY BRIDGES

Development of Guidelines for Design of Base-Isolated Highway Bridges

For studying the application of base isolation technology to seismic design of highway bridges, a committee chaired by Professor Tsuneo Katayama, University of Tokyo, was formulated through 1986 to 1989 at the Technology Research Center for National Land Development. Three programs were studied in the committee, i.e., 1) a survey of isolators and energy dissipators which can be used for highway bridges, 2) a study on the key points of the design of base-isolated highway bridges, and 3) design of base-isolated highway bridges. As the final accomplishment of the study,

"Guidelines for Design of Base-Isolated Highway Bridges (draft) " was published in 1989[14].

The draft guidelines includes the following contents:

Chapter 1 General
1.1 Related Regulations
1.2 Definition of Terms
Chapter 2 Fundamental Strategy of Base Isolation Design
Chapter 3 Design of Isolators and Energy Dissipators
3.1 General
3.2 Design Displacement of Base Isolation Device
3.3 Equivalent Natural Frequency and Damping Ratio of Base Isolator
3.4 Dynamic Characteristics of Base Isolation Device
3.5 Static Characteristics of Base Isolation Device
Chapter 4 Design of Base-Isolated Highway Bridge
4.1 General
4.2 Static Lateral Force Method
4.2.1 General
4.2.2 Horizontal Design Seismic Coefficient
4.2.3 Evaluation of Natural Period of Base-Isolated Bridge
4.2.4 Evaluation of Sectional Force and Displacement due to Inertia Force
4.3 Check of Bearing Capacity for Lateral Force
4.3.1 General
4.3.2 Seismic Coefficient used to Check Bearing Capacity for Lateral Force
4.3.3 Evaluation of Natural Period
4.3.4 Evaluation of Damping Ratio
4.3.5 Evaluation of Sectional Force and Displacement due to Inertia Force
4.3.6 Equivalent Seismic Coefficient Used to Check Bearing Capacity for Lateral Force
4.3.7 Bearing Capacity for Lateral Force
Chapter 5 Dynamic Response Analysis
5.1 Method of Dynamic Response Analysis
5.2 Modelling of Base-Isolated Bridges by Dynamic Response Analysis
5.3 Input Motion for Dynamic Response Analysis
5.3.1 Input Motion to Check Design by Means of Static Lateral Force Method
5.3.2 Input Motion to Check Bearing Capacity for Lateral Force
5.4 Investigation of Safety
Chapter 6 General Provisions for Design of Structural Details
6.1 General
6.2 Distance between Structures
6.3 Design Gap of Expansion Joint
6.4 Devices for Preventing Falling-off of Superstructure from Sub structure
6.5 General Provisions for Design Details of Base Isolation Devices

Appendix

I Design of Base-Isolated Highway Bridges
II Design Method of Base Isolation Devices
III Example of Design Calculation of a Base-Isolated Highway Bridge Constructed on Group I Ground Condition Site
IV Example of Design Calculation of a Base-Isolated Highway Bridge Constructed on Group II Ground Condition Site
V Example of Structural Details
VI Example of Various Base-Isolation Devices

Joint Research between PWRI and 28 Private Firms for Developing Base Isolation Systems for Highway Bridges

Based on the study presented above, a joint research program between PWRI and 28 private firms on "Development of Base-Isolation Systems for Highway Bridges" was initiated in 1989 for aiming to develop further practical design methods for base-isolated highway bridges which are both safe and cost efficient[17]. The research is scheduled to be completed in 1992.

Scopes of the joint research contain the following research and development programs :

1) Development of isolators and energy dissipators suitable for highway bridges by using new materials and technology
2) Development of expansion joints and falling-off prevention devices suitable for base-isolated bridges
3) Development of design methods for base-isolated bridges
4) Application of base-isolation for highway bridges

In the project 1), it is aimed to develop less expensive isolators and energy dissipators which have better characteristics and are superior for long-term use. In the project 4), application of the base isolation for super-long multiple-continuous highway bridges with a total length over 1 km and for the seismic retrofitting of vulnerable existing highway bridges are being investigated.

The 28 private firms consist of material makers such as rubber and automobile tire makers, bearing supports fabricators, consulting engineering firms, steel superstructure fabricating companies, and general constructors.

Table-12 shows the research subjects and contributions. Photos 10 and 11 show dynamic loading tests of isolators and shaking table tests of a base-isolated highway bridges model conducted at the Public Works Research Institute for studying effectiveness of the base isolation.

Table 12 Research Theme and Organizations of Joint Research between the Public Works Research Institute and 28 Private Firms for Developing Base Isolation Systems of Highway Bridges

Research Theme	P	Ka	Si	Ob	Ku	Tn	H	Ni	Su	M	G	OR	Ti	I	Nk	Ko	Ns	Ol	Y	To	Bs	Bb	Se	Sh	Pc	J	N	Chief	Sub-Chief
1. Development of Device for Isolation																													
1.1 High Energy Absorbing Rubber Bearing								○					○						○	○	○	○	○	○			Ol	Bs
1.2 Friction Damper															○													
1.3 Steel Damper								○									○											
1.4 Link Bearing Develop of																		○										
1.5 Viscous Damper																												
1.6 Test Method	○							○							○		○	◎	○	○	○	○	○	○				
2. Development of Expansion Joint and Falling-off Prevention Device for Isolated Bridge																												
2.1 Expansion Joint				○									○														Tc	—
2.2 Falling-off Prevention Device	○												○					○										
3. Development of Design Method for Isolated Bridge																												
3.1 Design Philosophy	○	○	○	○		○						○	◎					○							○	○	○	
3.2 Dynamic Responce Analysis Method	○		○		○	◎		○			○			○													Ka	Pc
3.3 Design Method of Device for Isolation	○						○	○				◎	○		○		○	○	○	○	○	○	○	○				
3.4 Simplified Design Method	○	○	◎		○	○					○	○													◎			
3.5 Design Method of Expansion Joint and Falling-off Prevention Device	○			○			○								○			○										
4. Application of Base Isolation to Bridge																												
4.1 Application to Prestressed Concrete Bridge	○	◎							○	○			○															
4.2 Application to Steel Bridge	○													○	○	○											Ob	J
4.3 Application to Multiple Super-long Bridge	○			◎					○							○												
4.4 Application to Seismic Retrofit	○									○				○				○										

P: Public Works Research Institute, Ka: Kajima, Si: Shimizu, Ob: Ohbayashi, Ku: Kumagai, Tn: Takenaka Doboku + Takenaka, H: Hazama, Ni: Nishimatsu, Su: Sumitomo, M: Mitsui, G: Goyoh, Ok: Okumura, Ti: Taisei + Tokyo Fablic + Nippon Chuzo, I: Ishikawajima Harima, Nk: NKK + Nippon Chuzo, Ko: Kobe Steel, Ns: Nippon Seiko, Oe: Oiles, Y: Yokohama Rubber, To: Toyo Rubber, Bs: Bridgestone, Bb: BBM, Se: Seibu Polymer, Sh: Showa Densen, Pc: Pacific Consultants, J: Japan Engineering Consultant, N: New Structural Engineering Consultants.

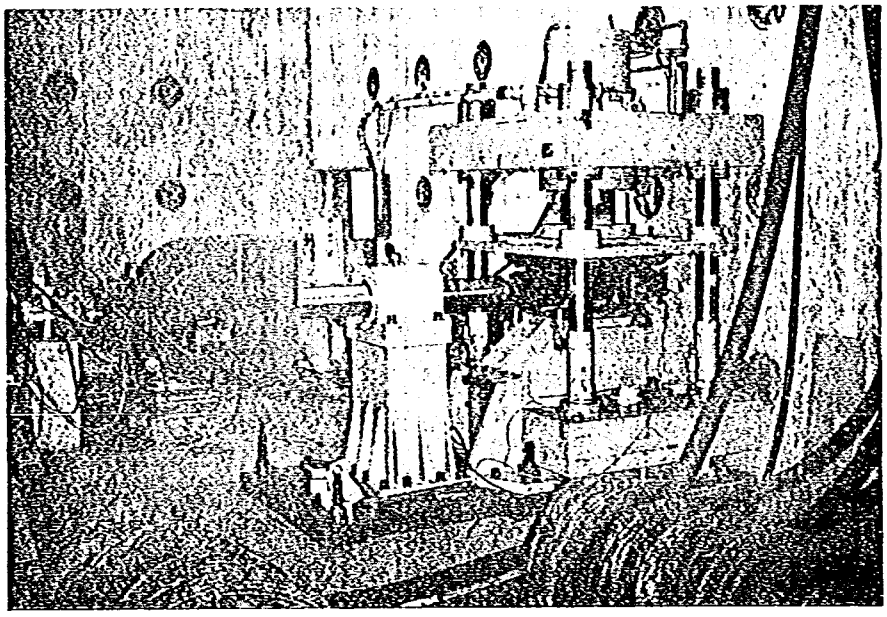


Photo 10 Dynamic Loading Tests of Isolators and Energy Dissipators

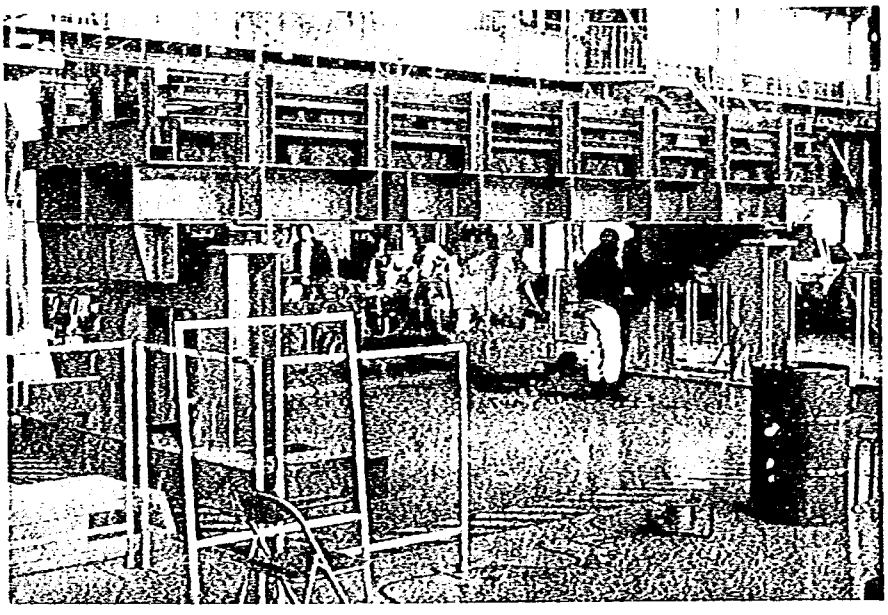


Photo 11 Shaking Table Tests of a Base Isolated Bridge Model

Construction of Base-Isolated Highway Bridges

Seven base-isolated highway bridges as shown in Table-13 are currently being constructed by or with the support of the Ministry of Construction for the purpose of incorporating base isolation in practical use. After completion of the construction, a series of experiments including push-pull tests, forced excitation tests with use of eccentric-mass shakers and strong motion observations are scheduled for studying the dynamic characteristics of the bridges.

Fig.11 shows the Nagaki-gawa Bridge[18] which is now under construction by the Ministry of Construction.

Table 13 Construction Project of Base-Isolated Highway Bridges

Owner	Bridge Name	Type of Super-structure	Length (m)
Hokkaido Developing Bureau	Onnetoh Bridge	Steel Girder	456
Tohoku-Regional Bureau, MOC	Nagaki-gawa Bridge	〃	97
Kantoh-Regional Bureau, MOC	Not Yet Selected	Not Yet Decided	Not yet Determined
Chubu-Regional Bureau, MOC	〃	〃	〃
Iwate-ken	Maruki Bridge	Prestressed Concrete	92
Tochigi-ken	Karasuyama Bridge	〃	250
Shizuoka-ken	Miyagawa Bridge	Steel Girder	110

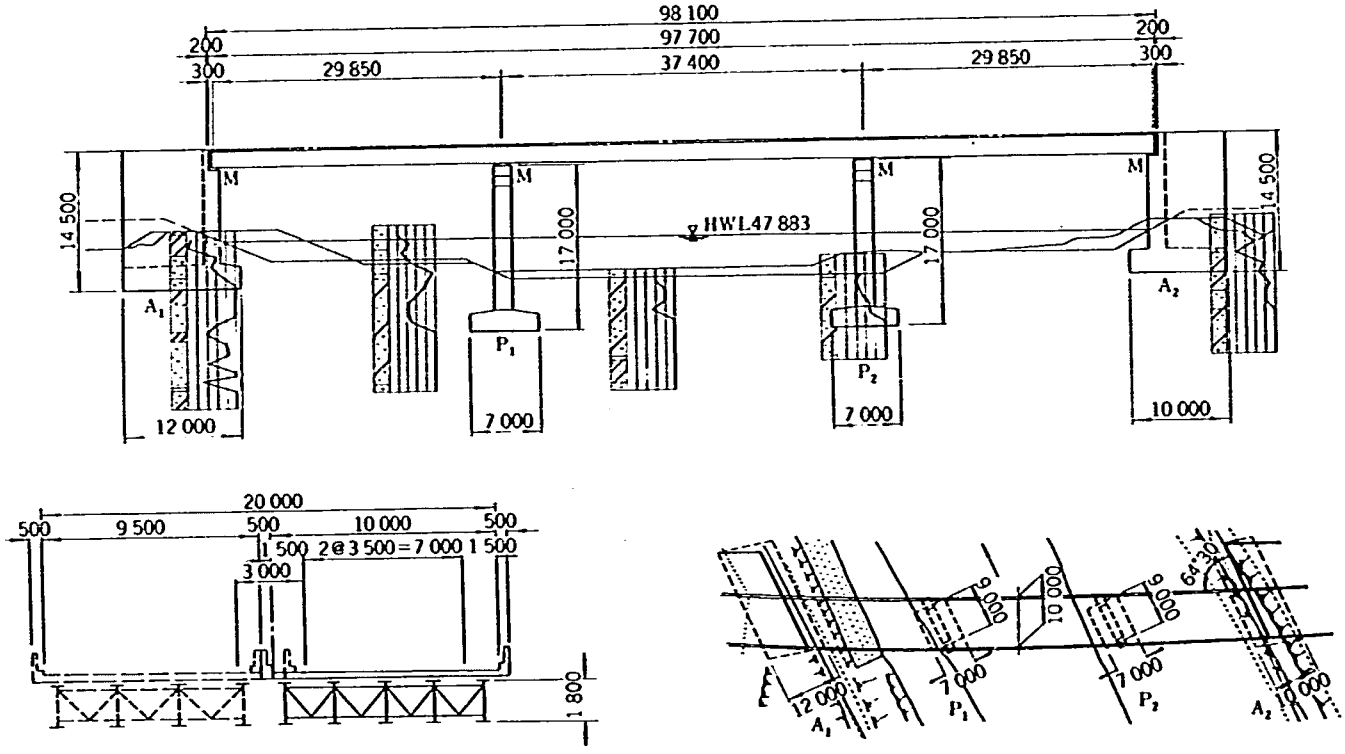


Fig. 11 General View of Nagaki-gawa Bridge

Hybrid Control of Structural Response

A combination of active and passive control, which is designated here as hybrid control, seems attractive for reducing energy supply for active control. Decrease of structural response by means of passive control will make the energy supply requirement for active control small enough to achieve the control of structural response within a satisfactory level during significant earthquakes. Increase of lateral displacement of decks induced by the passive control may be improved by the active control.

A 5-year research program on hybrid control of seismic response was initiated in1990 at the Public Works Research Institute[17]. The objectives of this research program are to study applications of hybrid control for

bridge structures such as

1) Control of super long-span continuous bridges
2) Control of bridges on relatively soft ground
3) Improvement of seismic performance of bridges on the important urban routes

As part of this research, the following items are considered for study :

1) Development of passive control elements suitable for hybrid control systems
   - Development of variable dampers
   - Development of damper with fail-safe functions
2) Development of active control systems suitable for hybrid control
3) Development of optimal hybrid control systems by combining 1) and 2)

Among these developments, the variable damper is quite a unique device in which the viscous coefficient is varied depending on structural response displacement and velocity so that the best energy dissipation can be made. The viscous coefficient is also controlled to increase smoothly after the structural response displacement becomes excessively large so that the variable damper acts as a stopper.

This research program is to be executed as a U.S.-Japan cooperative research program through the Panel on Wind and Seismic Effects of UJNR.

SEISMIC INSPECTION AND SEISMIC STRENGTHENING

Outline

The nationwide seismic inspection and seismic strengthening of highway bridges were made in 1971, 1976, 1979, 1986 by the Ministry of Construction. The first and second seismic inspection of 1971 and 1976 were to inspect deteriorated highway bridges susceptible to falling-off of superstructure during earthquakes. The third and fourth seismic inspection of 1979 and 1986 was to classify structural resistance of highway bridges against falling-off of superstructures during destructive earthquakes. For those bridges which were judged vulnerable to severe damages during earthquakes, seismic strengthening works have been made. In the 1986 inspection, about 40,000 bridges were inspected and 11,700 bridges were found to require seismic strengthening. Most of them require installation of the device for preventing superstructure falling-off from the substructures.

Seismic Inspection of Vulnerability of Highway Bridges

Seismic inspection methods to detect highway bridges vulnerable to earthquakes have been developed and amended several times to reflect progress of bridge earthquake engineering and lessons gained from the past seismic damage. The most important requirement for the inspection method was

to be able to assess the vulnerability of a number of highway bridges at the site without complex calculations. The latest seismic inspection method[19] which was referenced in the 1986 seismic inspection was formulated on the statistical analyses of 105 bridges damaged in the past earthquakes[20].

In the statistical analyses, factors which are likely to affect the seismic vulnerability of highway bridges were firstly studied with use of the Type II quantification analysis. The rank of damage degree was classified into high vulnerability (Rank A), moderate vulnerability (Rank B) and low vulnerability (Rank C) as shown in Table 14. From the analysis of the past seismic damage, 15 items, as shown in Table 15, were selected as the factors likely to affect seismic vulnerability. The 15 items consists of four principal factors, i.e., intensity of earthquake ground motions, properties of superstructure and substructures, devices for preventing falling-off of superstructure from substructures, and ground condition. Each item was further divided into several categories.

Table 14 Definition of Seismic Vulnerability

Rank	Vulnerability of Seismic Damage	Rank of Damage Degree in Table-1
Rank A—High Vulnerability	Possibility for suffering damage or damage degree is high	5 Falling-off of Superstructure or 4 Extensive Damage
Rank B—Moderate Vulnerability	Possibility for suffering damage or damage degree is moderate	3 Moderate Damage
Rank C—Low Vulnerability	Possibility for suffering damage or damage degree is low	2 Slight Damage or 1 Minor Damage or 0 No Damage

Predicted damage rank y_i was assumed to have a form of

$$y_i = \sum_j \sum_k \delta_{ijk} \cdot x_{jk} \qquad (22)$$

in which x_{jk} represents a weighting factor for the k-th category of the j-th item, and δ_{ijk} represents a variable corresponding to the category k in the item j of the i-th bridge. The variable δ_{ijk} was so defined that it takes a value of 1 if the characteristics of the i-th bridge correspond to the category k in the item j, and is 0 otherwise. The weighting factor x_{jk} was determined so as to minimize the sum of square of the difference between the predicted damage rank and the actual damage rank.

From the weighting factors presented in Table 15, the effects of each item were found as shown in Table 16. The following considerations were subsequently included in the statistical analysis to formulate an inspection method.

a) Because the objectives of the inspection method are to assess the seismic vulnerability of highway bridges subjected to ground shaking of JMA Intensity V or larger (peak ground acceleration larger than 0.25 g), the Intensity of Peak Ground Acceleration a_{max} is dropped from the evaluation item assuming that a_{max} is larger than 0.25 g.

Table 15 Items and Categories Which Affect Seismic Vulnerability of Highway Bridges

Item	Category	Seismic Damage Rank						Results of Statistical Analysis		
		0 No Damage	1 Minor Damage	2 Slight Damage	3 Moderate Damage	4 Extensive Damage	5 Falling-off of Superstructure	Normalized Score	Range	Partial Correlation Coefficient
① Intensity of Peak Ground Acceleration a_{max} [cm/sec²]	$a_{max} < 200$	1 (5%)			1 (5%)			0.169	1.219	0.343
	$200 \leqq a_{max} < 300$	13 (68%)	5 (42%)	36 (65%)	8 (40%)	1 (13%)		−0.283		
	$300 \leqq a_{max} < 400$	5 (26%)	5 (42%)	18 (33%)	10 (50%)	6 (75%)	4 (40%)	0.176		
	$400 \leqq a_{max} < 500$		2 (17%)	1 (2%)	1 (5%)	1 (13%)	2 (20%)	0.936		
	$500 \leqq a_{max}$						4 (40%)	0.616		
② Design Specifications	1926 or 1939	1 (5%)		6 (11%)	6 (30%)	5 (63%)	7 (70%)	0.517	0.740	0.319
	1956 or 1964	17 (89%)	6 (50%)	41 (75%)	11 (55%)	3 (38%)	3 (30%)	−0.223		
	1971 or 1980	1 (5%)	6 (50%)	8 (15%)	3 (15%)			0.284		
③ Type of Superstructure	Gerber or Simply Supported Girder (2 or More Spans)	12 (63%)	7 (58%)	40 (73%)	17 (85%)	8 (100%)	10 (100%)	0.031	0.390	0.161
	One-span Simply Supported Girder, or Countinuous Girder with 2-spans or More	5 (26%)	3 (23%)	11 (20%)	2 (10%)			−0.232		
	Arch, Frame, One-span Continuous Girder, Cable stayed Bridge, Suspension Bridge	2 (11%)	2 (17%)	4 (7%)	1 (5%)			−0.308		
④ Shape of Superstructure	Skewed or Curved	3 (16%)	1 (8%)	4 (7%)				−0.396	0.424	0.122
	Straight	16 (84%)	11 (92%)	51 (93%)	20 (100%)	8 (100%)	10 (100%)	0.027		
⑤ Materials of Superstructure	RC or PC	7 (37%)	5 (42%)	22 (40%)	7 (35%)	1 (13%)	6 (60%)	−0.141	0.233	0.131
	Steel	12 (63%)	7 (58%)	33 (60%)	13 (65%)	7 (88%)	4 (40%)	0.092		
⑥ Slope in Bridge Axis	6% or Steeper			1 (2%)		1 (13%)	1 (10%)	0.919	0.941	0.161
	Less than 6%	19 (100%)	12 (100%)	54 (98%)	20 (100%)	7 (88%)	9 (90%)	−0.023		
⑦ Device to Prevent Falling-off of Superstructure	None	1 (5%)	1 (8%)	20 (36%)	8 (40%)	6 (75%)	10 (100%)	0.459	1.106	0.358
	One Device	16 (83%)	6 (50%)	28 (51%)	11 (55%)	2 (25%)		−0.181		
	Two Devices or More	2 (11%)	5 (42%)	7 (13%)	1 (5%)			−0.647		
⑧ Type of Substructure	Single-line Bent Pile	1 (5%)		5 (9%)	2 (10%)		3 (30%)	0.292	0.411	0.178
	Reinforced Concrete Frame	1 (5%)	1 (8%)	9 (16%)	8 (40%)	4 (50%)	4 (40%)	0.259		
	Others	17 (89%)	11 (92%)	41 (75%)	10 (50%)	4 (50%)	3 (30%)	−0.119		
⑨ Height of Pier H	$10m \leqq H$	4 (21%)	5 (42%)	12 (22%)	8 (40%)	2 (25%)	3 (30%)	0.172	0.284	0.125
	$5m \leqq H < 10m$	7 (37%)	3 (25%)	29 (53%)	7 (35%)	6 (75%)	5 (50%)	−0.038		
	$H < 5m$	8 (42%)	4 (33%)	14 (25%)	5 (25%)		2 (20%)	−0.112		
⑩ Ground Condition	Extremely Soft in Group 4	1 (5%)			1 (5%)	2 (25%)		0.523	0.983	0.273
	Group 4	5 (26%)		2 (4%)	11 (35%)	4 (50%)	7 (70%)	0.224		
	Group 3	3 (16%)	8 (67%)	33 (60%)	6 (30%)	1 (13%)	3 (30%)	0.040		
	Group 2	1 (5%)	1 (8%)	8 (15%)	1 (5%)			0.112		
	Group 1	9 (47%)	3 (23%)	12 (22%)	1 (5%)	1 (13%)		−0.451		
⑪ Irregularity of Supporting Ground	Irregular		1 (8%)	1 (2%)	4 (20%)	1 (13%)		0.307	0.420	0.104
	Almost Uniform	19 (100%)	11 (92%)	54 (98%)	16 (80%)	7 (88%)	10 (100%)	−0.024		
⑫ Effect of Soil Liquefaction	Liquefiable			4 (7%)	2 (10%)	2 (25%)	6 (60%)	0.724	0.816	0.255
	Non liquefiable	19 (100%)	12 (100%)	51 (93%)	18 (90%)	6 (75%)	4 (40%)	−0.092		
⑬ Effect of Scouring	Recognized				1 (5%)			0.312	0.315	0.033
	None	19 (100%)	12 (100%)	55 (100%)	19 (95%)	8 (100%)	10 (100%)	−0.003		
⑭ Materials of Substructure	Plane Concrete in Accordance with 1926 Specs or 1939 specs.				1 (5%)		2 (20%)	0.995	1.020	0.167
	RC, PC, Steel or Unreinforced Concrete in Accordance with Specs in 1956 or Later	19 (100%)	12 (100%)	55 (100%)	19 (95%)	8 (100%)	8 (80%)	−0.025		
⑮ Type of Substructure	Timber, Brick, Masonry, Other Old Unknown Materials		1 (8%)	1 (2%)	1 (5%)	1 (13%)	4 (40%)	0.383	0.697	0.171
	RC Piles, Pedestal Piles or Pier Supported by Two Independent Caissons	2 (11%)	1 (8%)	9 (16%)	4 (20%)	2 (25%)	2 (20%)	−0.314		
	Foundations Designed by Specs. in 1971 or Later	17 (89%)	10 (83%)	45 (82%)	15 (75%)	5 (63%)	4 (40%)	0.034		

Table 16 Factors Which Affect Seismic Vulnerability of Highway Bridges

Items	Seismic Vulnerability
① Design Specifications	Those designed in accordance with 1926 or 1939 Specifications have higher vulnerability
② Type of Superstructure	• Gerber or simply supported girders with 2 or more spans have higher vulnerability • Arch, frame, continuous girders, cable-stayed bridges or suspension bridges have lower vulnerability
③ Shape of Superstructure	Skewed or curved bridges do not necessarily have higher vulnerability than straight bridges
④ Materials of Superstructure	Reinforced concrete bridges or prestressed concrete bridges have lower vulnerability than steel bridges although the difference is small
⑤ Slope in Bridge Axis	Bridges with slope in bridge axis have higher vulnerability
⑥ Device for Preventing Falling-off of Superstructure	Bridges with devices for preventing falling-off of superstructure have lower vulnerability
⑦ Type of Substructure	Bridges supported by single-line bent piles or by reinforced concrete frame placed on two separate caisson foundations have higher vulnerability
⑧ Height of Piers	Bridges supported by higher piers have higher vulnerability
⑨ Ground Condition	Bridges constructed on soft soil have higher vulnerability
⑩ Effect of Soil Liquefaction	Bridges constructed on sandy soil layers susceptible to liquefaction have higher vulnerability
⑪ Irregularity of Supporting Soil Condition	Bridges constructed on soils with irregularity of supporting conditions have higher vulnerability
⑫ Effect of Scouring	Bridges where the surface soils are scoured have higher vulnerability
⑬ Materials of Substructures	Bridges supported by plane-concrete substructures designed in accordance with 1926 or 1939 specifications have higher vulnerability
⑭ Type of Foundation	Bridges supported by timber, brick, masonry or other old unknown type substructures have higher vulnerability
⑮ Intensity of Ground Motion	Bridges subjected to higher intensity of ground acceleration have higher vulnerability. In particular, vulnerability becomes quite high when the bridges are subjected to peak ground acceleration larger than 400 gal (0.4g)

b) Evaluation of the strength of reinforced concrete piers at the mid-height where main reinforcement is terminated was introduced.

c) Because collapse, such as falling-off of superstructure, generally occurred because of excessive relative movements between the superstructure and the substructures, and failure of substructures due to inadequate strength, the evaluation of the seismic vulnerability for both the relative movement and for the strength of substructures should be made.

d) Even if there are some unsatisfactory conditions in the evaluation, final evaluation may not consider them to be critical if the remaining factors are in good evaluation. Consequently, it was decided that those bridges with at least one "critical" or "safe" condition are to be considered

to have either high or low seismic vulnerability. Below are some examples of evaluation of such specific types of structure :

- Those designed in accordance with the 1980 Specifications shall be classified into Rank C (safe) unless appreciable deterioration is detected
- Those constructed by timber, brick, masonry, or old unknown materials shall be classified into Rank A (vulnerable).
- Those supported by single-line bent piles foundation which are constructed on loose alluvial sandy layer vulnerable to liquefaction or very loose clayey deposits shall be classified into Rank A (vulnerable).
- Single-span simply supported girder bridges with the span length less than 15 m shall be classified into Rank C (safe).

The procedure of seismic inspection and an inspection sheet are shown in Fig. 12 and Table 17, respectively[19)20)]. The evaluation of the seismic vulnerability is made in accordance with the points which reflect the vulnerability to excessive relative movement between superstructure and substructures (point X), and the strength of substructures (point Y) as shown in Table 18.

Table 18 Evaluation of Seismic Vulnerability

Rank of Seismic Vulnerbility	Evaluation Points		
	X	Y	
		$Pc = 1.0$	$Pc \neq 1.0$
A—Vulnerable	$X \geqq 60$	$Y \geqq 10$	$Y \geqq 100$
B—Moderate	$20 \leqq X < 60$	$5 \leqq Y < 10$	$50 \leqq Y < 100$
C—Safe	$X < 20$	$Y < 5$	$Y < 50$

Note) Out of two ranks obtained from X-point and Y-point, higher rank (A is the highest) shou'd be taken as the final ranking of the bridge inspected. For obtaining eva'uation points X and Y, refer to Tab'e-2.

Seismic Strengthening of Highway Bridges Vulnerable to Earthquakes

Table 19 shows the feasibility of seismic strengthening against the 16 factors which would affect the seismic vulnerability of highway bridges (refer to Table 16). Among the 16 factors, ⑥ Devices for Preventing Falling-off of the Superstructure, ⑦Type of Substructure, ⑩Effect of Soil Liquefaction, ⑫Effect of Scouring, ⑬Materials of Substructures, ⑭Types of Foundation, and ⑯Effect of Termination of Main Reinforcement at Mid-height are the factors for which countermeasures for strengthening the bridge are feasible. Countermeasures against for the remaining 9 factors can not be made unless the whole bridge be replaced.

Fig. 13 shows how the countermeasures can be made for the above described 7 factors. Installation of devices for preventing falling-off of superstructure, strengthening of foundations, and strengthening of piers and abutments are the main measures of seismic strengthening.

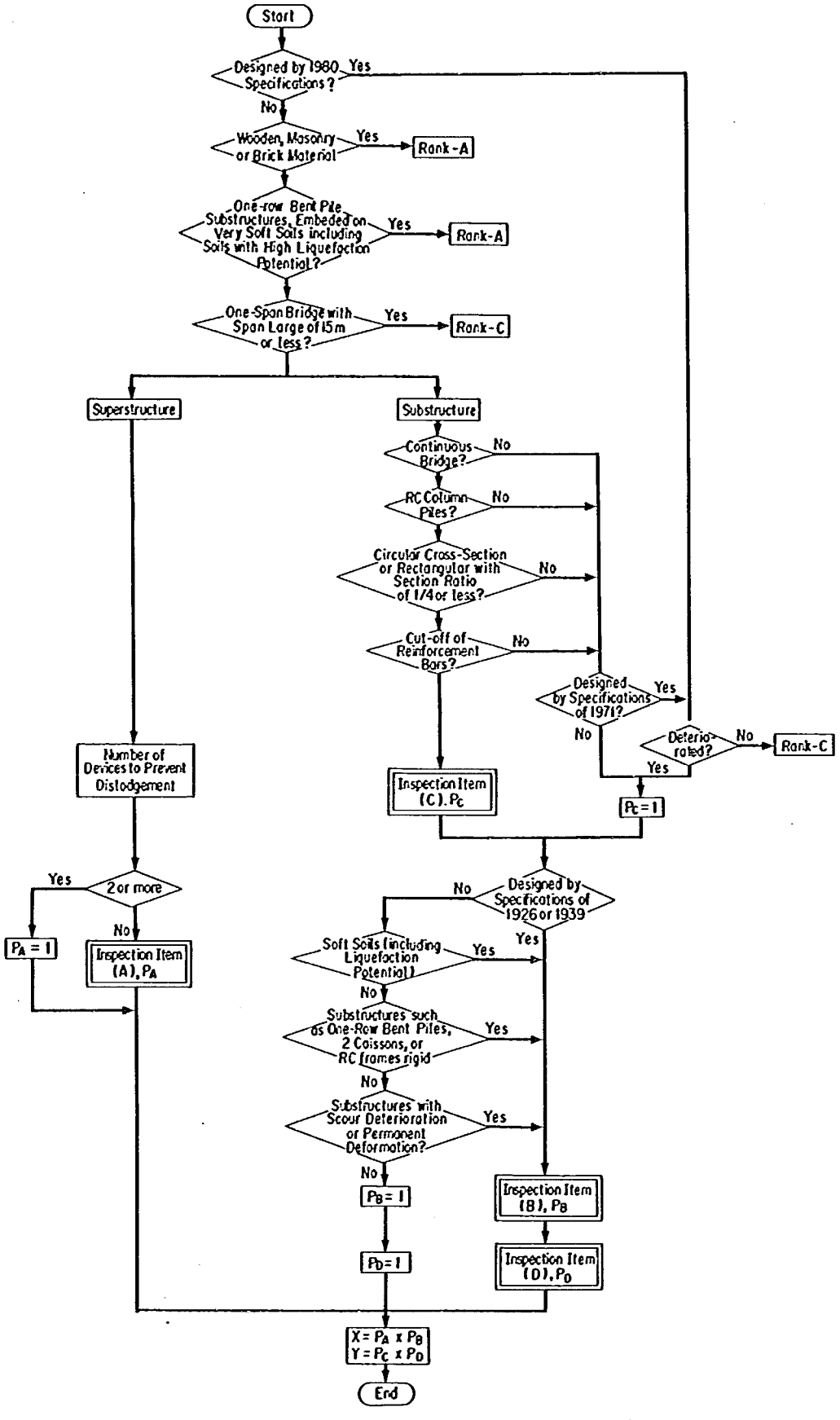


Fig. 12 Procedure of Seismic Inspection for Highway Bridges

Table 17 Inspection Sheet for Seismic Vulnerability of Highway Bridges

Point of Inspection		Factors of Inspection	Evaluation
Inspection for Vulnerability to Develop Excessive Deformation	Inspection Format (A)	① Design Specifications	4.0: 1926 Specs. or 1939 Specs / 2.0: 1956 Specs. or 1964 Specs / 1.0: 1971 Specs. or 1980 Specs.
		② Superstructure Type	3.0: Gerber Girder or Simply-supported Girders with Two Spans or More / 1.5: Simply-supported Girder or Continuous Girders Consisting of Two Spans or More / 1.0: Arch, Flame, Continuous Girder (One Span), Cable-stayed Bridge, Suspension Bridge
	Inspection for Deformation of Superstructure	③ Shape of Superstructure	1.2: Skewed or Curved Bridge / 1.0: Straight Bridge
		④ Material's of Superstructure	1.2: Rc or PC / 1.0: Steel
		⑤ Gradient	1.2: 6% or Steeper / 1.0: Less Than 6%
		⑥ Falling-off Prevention Device	2.0: None / 1.0: One Device
		$P_A = ① \times ② \times ③ \times ④ \times ⑤ \times ⑥$	$P_A =$
	Inspection Format (B)	⑦ Type of Substructure	2.0: Single-line Bent Pile Foundation / 1.0: Others
		⑧ Height of Pier H	2.0: $H \geqq 10m$ / 1.5: $5 \leqq H < 10m$ / 1.0: $H < 5m$
		⑨ Ground Condition	5.0: Extremely Soft in Group 4 / 2.5: Group 4 / 2.0: Group 3 / 1.2: Group 2 / 1.0: Group 1
	Inspection for Deformation of Substructure	⑬ Effects of Liquefaction	2.0: Liquefiable / 1.0: Non-liquefiable
		⑪ Supporting Ground Condition	1.2: Irregular / 1.0: Almost Uniform
		⑫ Scouring	1.5: Recognized / 1.0: None
		$P_B = ⑦ \times ⑧ \times ⑨ \times ⑬ \times ⑪ \times ⑫$	$P_B =$
Inspection for Vulnerability to Develop Failure Due to Inadequate Strength of Substructure	Inspection Format (C)	⑬ Shear Span Ratio (h/D)	2.0: $1 < h/D < 4$ / 1.0: $h/D \geqq 4$ / 0.5: $h/D \leqq 1$
		⑭ Tension Cracks in Flexure at Terminated Point of Main Reinforcement	2.0: Cracks Will Occur / 1.0: Cracks Will Possibly Occur / 0.3: Cracks will Not Occur
	Inspection for Strength of RC Pier at Termination of Reinforcement	⑮ Safety Factor for Yield Strength at Terminated Section of Main Reinforcement ⑮-1 S_{my}	3.0: $S_{my} \leqq 1.1$ / 2.0: $1.1 < S_{my} < 1.5$ / 0.5: $S_{my} \geqq 1.5$
		⑮-2 S_{mu}	3.0: $S_{mu} \leqq 1.1$ / 2.0: $1.1 < S_{mu} \leqq 1.3$ / 1.0: $1.3 < S_{mu} < 1.5$ / 0.5: $S_{mu} \geqq 1.5$
		⑯ Shear Stress σ (tf/m²)	3.0: $\sigma \geqq 45$ / 2.0: $30 \leqq \sigma < 45$ / 1.0: $15 \leqq \sigma < 30$ / 0.5: $\sigma < 15$
		$P_C = ⑬ \times ⑭ \times ⑮\text{-}1 \times ⑮\text{-}2 \times ⑯$	$P_C =$
	Inspection Format (D)	⑰ Failure of Fixed Supports and Proximity	5.0: Extensive Failure / 2.0: Small Failure / 1.0: None
		⑱ Extraordinary Damage of Pier	5.0: Extensive Damage / 2.0: Small Damage / 1.0: None
		⑲ Materials of Substructure	2.0: Plane Concrete Older Than 1926 Excluding Gravity-type Abutment / 1.0: Others
	Inspection for Strength of Substructure	⑳ Construction method of Foundation	2.0: Timer Pile, Masonry, Brick, Other Old Construction Methods / 1.5: RC Piles, Pedestal Piles, Pier Supported by Two Independent Caissons / 1.0: Foundation Designed by 1971 Specs. and Other Later Specs.
		㉑ Foundation Type	1.5: RC Flame Supported by Two Independent Caisson Foundations / 1.0: Others
		㉒ Extraordinary Failure of Foundation	2.0: Recognized / 1.0: None
		$P_D = ⑰ \times ⑱ \times ⑲ \times ⑳ \times ㉑ \times ㉒$	$P_D =$
Evaluation of Deformation and Strength			$X = P_A \times P_B =$ and $Y = P_C \times P_D =$

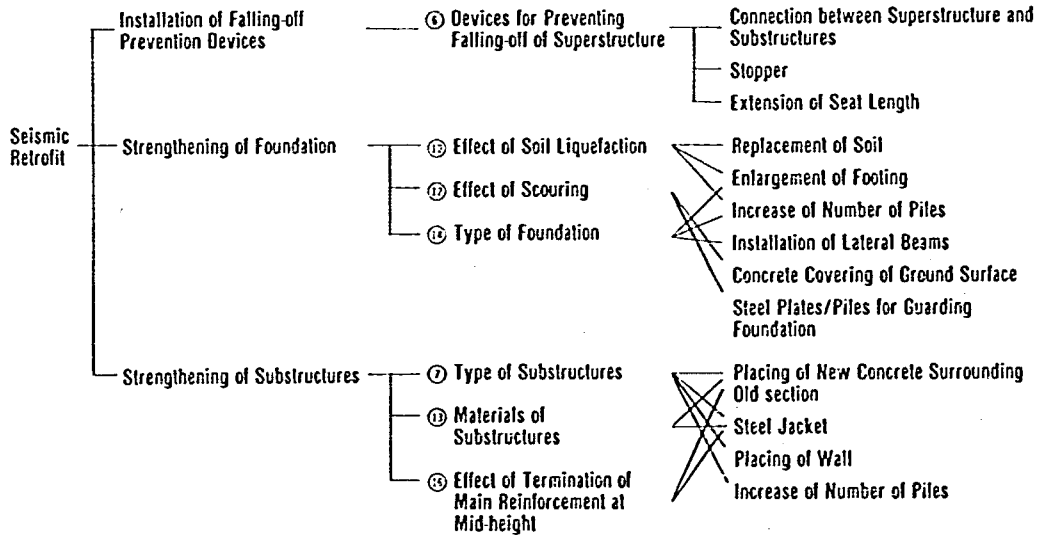


Fig. 13 Selection of Seismic Strengthening Measures for Highway Bridges

Table 19 Feasibility of Seismic Strengthening for 16 Factors Which Affect Seismic Vulnerability of Highway Bridges

Items	Feasibility of Seismic Strengthening	Principles of Countermeasures
① Design Specifications	×	———
② Type of Superstructure	×	———
③ Shape of Superstructure	×	———
④ Materials of Superstructure	×	———
⑤ Slope in Bridge Axis	×	———
⑥ Device for Preventing Falling-off of Superstructure	O	Installation of Devices
⑦ Type of Substructure	O	Strengthening of Substructures
⑧ Height of Piers	×	———
⑨ Ground Condition	×	———
⑩ Effect of Soil Liquefaction	O	Strengthening of Fundations or Strengthening of Surrounding Soils
⑪ Irregularity of Supporting Soil Condition	×	———
⑫ Effect of Scouring	O	Treatment for Prevention of Scouring, or Strengthening of Foundations
⑬ Materials of Substructures	O	Strengthening of Substructures
⑭ Type of Foundation	O	Strengthening of Foundations
⑮ Intensity of Ground Motion	×	———
⑯ Effect of Termination of Main Reinforcement at Mid-height	O	Strengthening of Substructures

Note O Items for which seismic strengthening is feasible
× Items for which seismic strengthening is not feasible

Figs. 14, 15 and 16 show the methods for selecting the installation of the stoppers at movable supports, falling-off prevention devices, and elongation of seat length S_E and bearing seat length S as measures of seismic strengthening for existing bridges. The methods are based on a number of practices in the past[19),20)].

Figs. 17 and 18 show measures for strengthening foundations and strengthening substructures for existing bridges, respectively.

Photos 12 and 13 show dynamic loading tests of reinforced concrete piers which have the termination of main reinforcement at mid-height. Effectiveness of steel jacket is studied.

The seismic inspection and strengthening methods of transpotion facilities including highway bridges were compiled and published from the Japan Road Association in the form of the "Guide Specifications for Earthquake Hazard Mitigation for Transportation Facilities - Pre-Earthquake Countermeasures -" in 1987[21)].

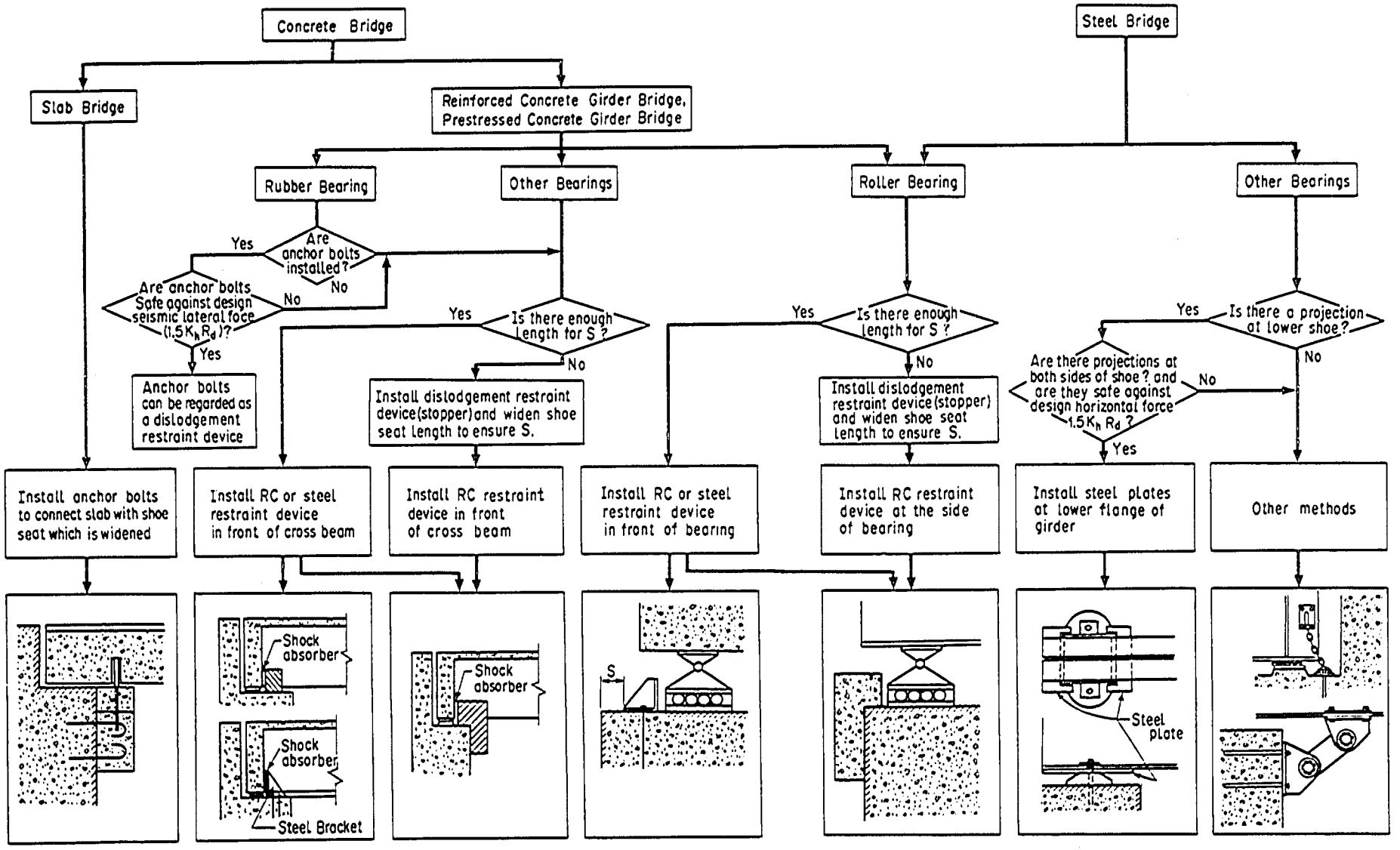


Fig. 14 Installation of Stopper at Movable Bearings for Existing Bridges

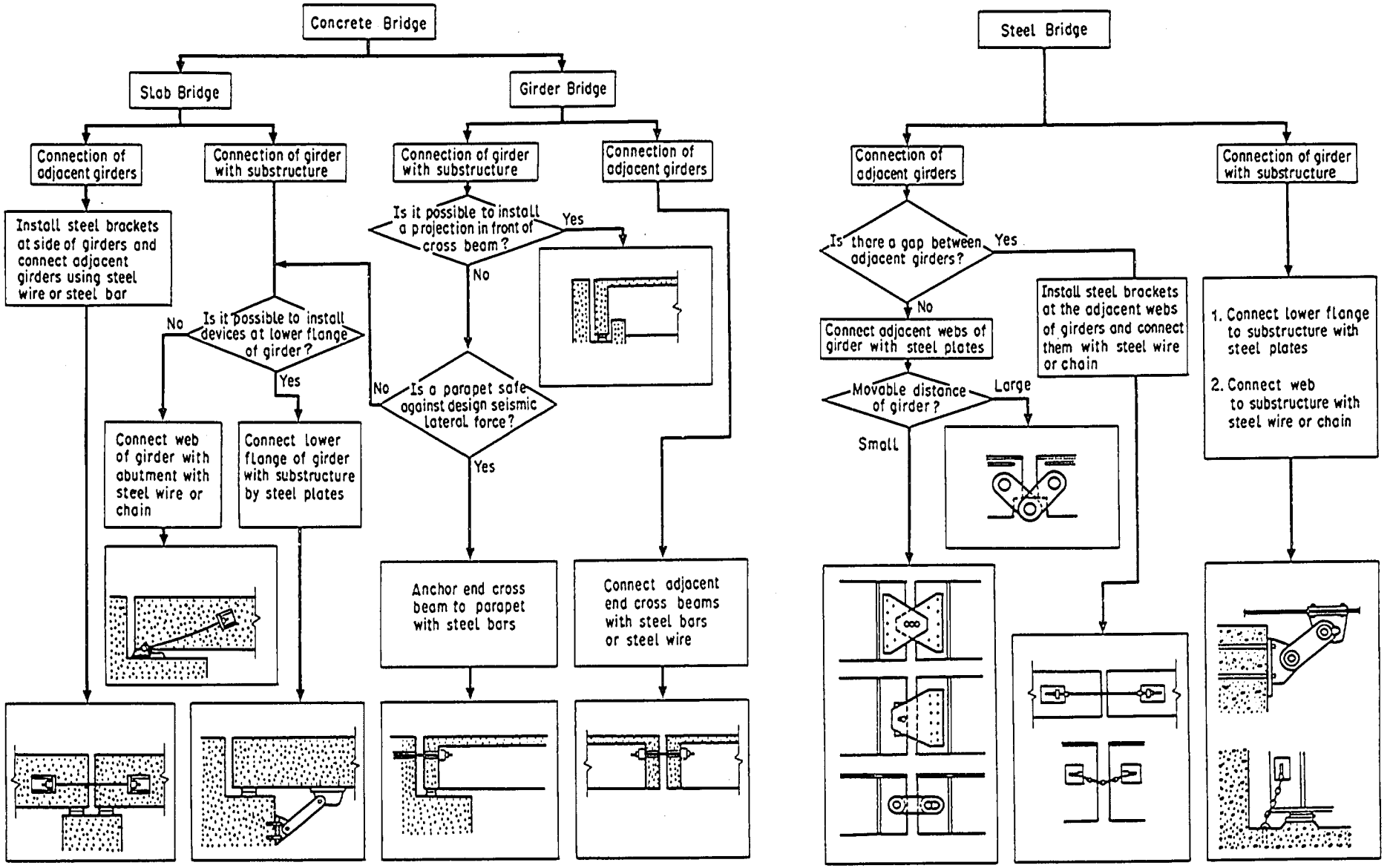


Fig. 15 Installation of Devices Connecting Deck and Substructure, and Device Connecting Two Adjacent Decks for Existing Highway Bridges

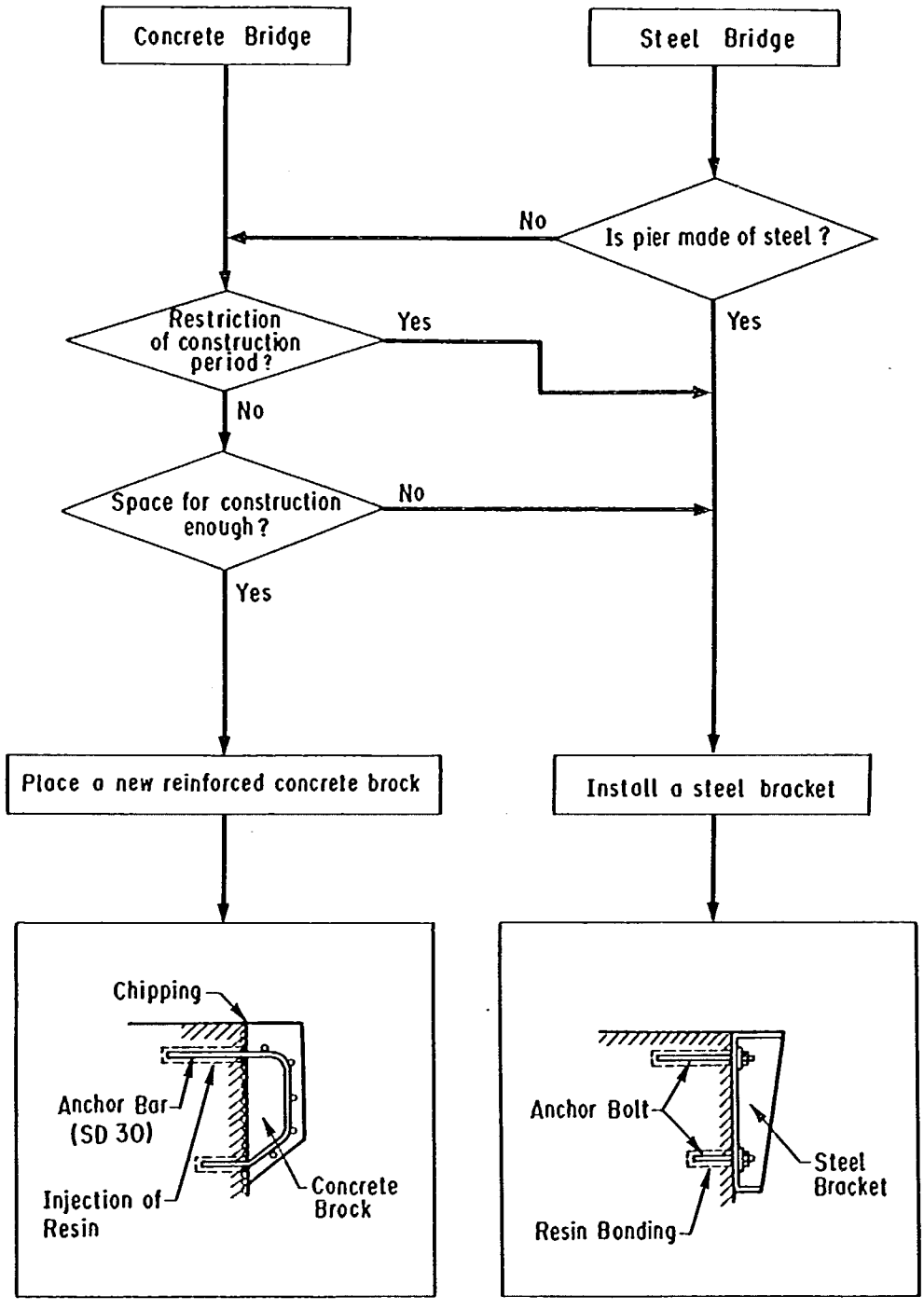
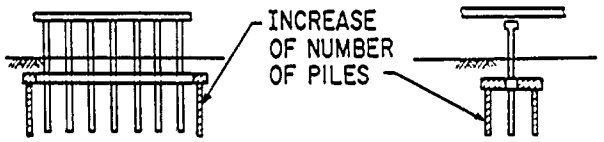
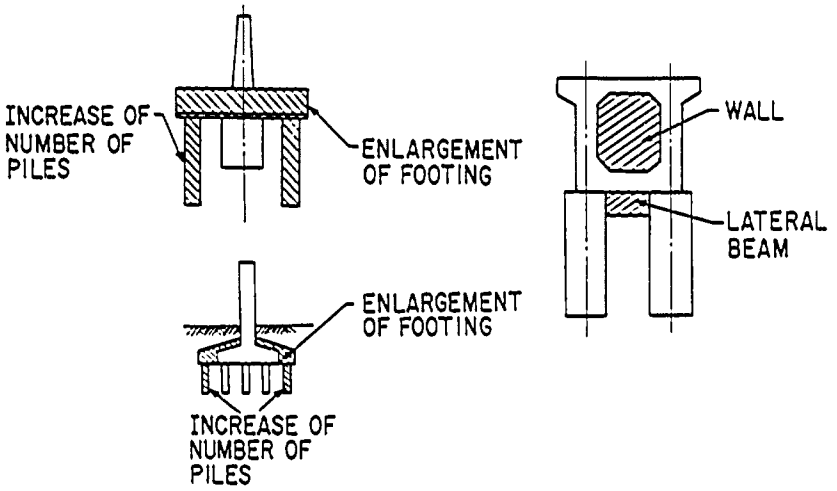


Fig. 16 Elongation of Seat Length S_E and Bearing Seat Length S for Existing Highway Bridges



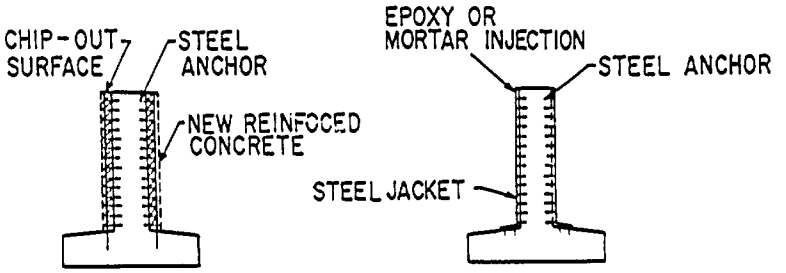
(1) STRENGTHENING OF
BENT PILE



(2) STRENGTHENING
OF FOUNDATION
WITH INADEQUATE
BEARING CAPACITY

(3) STRENGTHENING
OF RC FRAME
ON TWO INDEPENDENT
CAISSON FOUNDATIONS

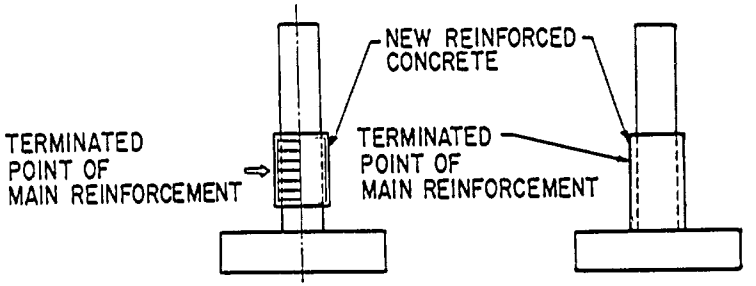
Fig. 17 Strengthening of Foundations



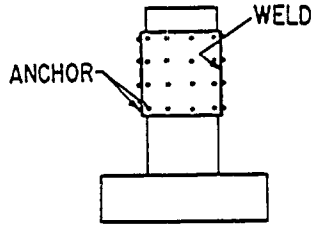
(A) NEW RC SECTION

(B) STEEL JACKET

(1) STRENGTHENING OF WEAK PIERS



(A) NEW RC SECTION



(B) STEEL JACKET

(2) STRENGTHENING OF RC PIERS WITH TERMINATION
OF MAIN REINFORCEMENT AT MID-HEIGHT

Fig. 18 Strengthening of Piers

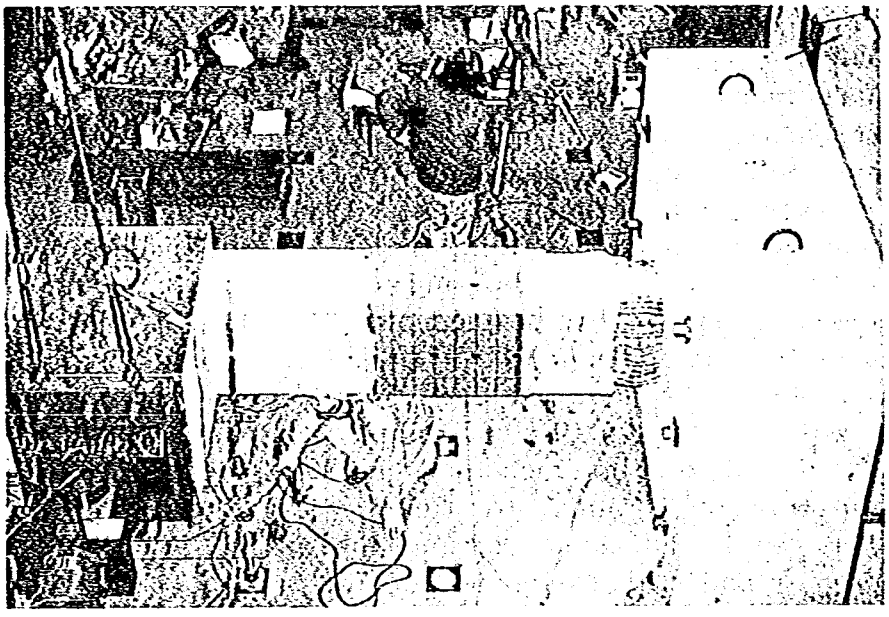


Photo 12 Loading Tests of Reinforced Concrete Pier with Termination of Main Reinforcement at Mid-height (Square Section)

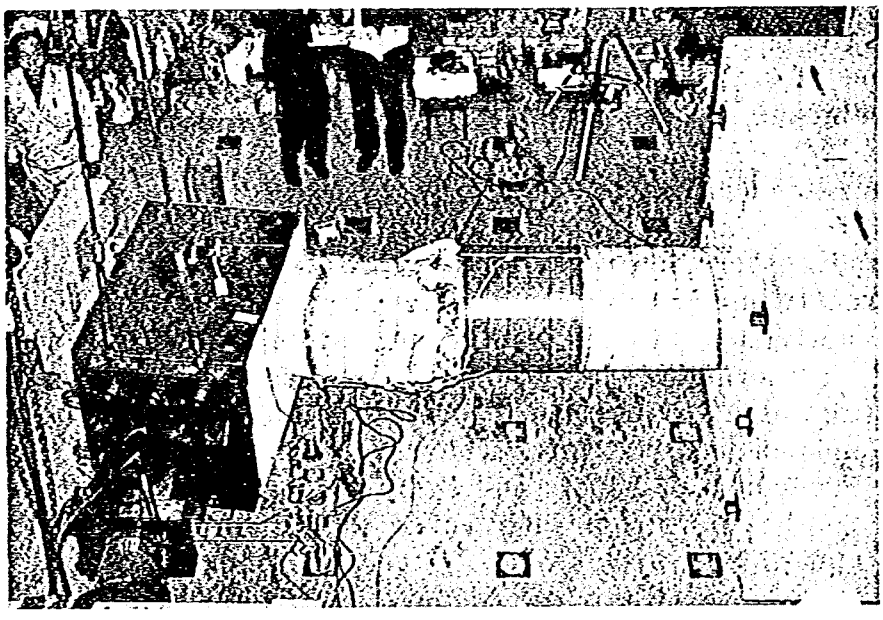


Photo 13 Loading Tests of Reinforced Concrete Pier with Termination of Main Reinforcement at Mid-height (Circular Section)

REPAIR OF TRANSPORTATION FACILITIES DAMAGED BY EARTHQUAKES

Outline

The recent advancement in earthquake engineering has enabled transportation facilities and structures to be safely designed and constructed. Catastrophic disasters due to the entire collapse of structures have decreased, and accordingly the number of human fatalities has become appreciably smaller during recent large earthquakes. It is

considered, however, that partial failures may still take place in future large earthquakes, as observed in recent ones. In view of such facts, post-earthquake measures are still of significant concern.

A comprehensive 5 year research project entitled "Development of Repair Methods for Structures Damaged by Earthquakes," was made by the Ministry of Construction between 1981 and 1986. The project is to develop post earthquake measures by providing procedures of inspection, assessment of damage extent, repair methods, and overall evaluation for reparing seismically damaged structures. In executing the project, the Technological Research Center for National Land Development established the Committee for Development of Repair Methods for Civil Engineering Structures Damaged by Earthquakes, which was chaired by Dr. Shunzo Okamoto, Professor Emeritus of the University of Tokyo. Final accomplishment of the project was compiled in 1986 in the form of " Manual for Repair Methods for Civil Engineering Structures Damaged by Earthquakes"[23]. The essence of the Manual in the area of the repair and restoration method for transportation facilities was later reorganized and published from the Japan Road Association in the form of "Guide Specifications for Earthquake Hazard Mitigation for Transportation Facilities - Pre-Earthquake Countermeasures -" [24].

This chapter outlines the Manual for the assessment of damage extent and repair method of seismically damaged transportation facilities with placing emphasis on highway bridges from the Manual.

Flow of Repair and Restoration

Repair and restoration of seismically damaged transportation facilities must be correctly and immediately conducted because it significantly affects restoration activities of the public and stabilization of national life. Repair and restoration is made in accordance with the disaster countermeasures plans by correctly understanding the whole damage, and by consulting and exchanging information with related organizations and authorities. Procedure of repair and restoration after the occurrence of an earthquake can be classified into three stages as shown in Fig. 19. The fundamental aims of the three stages are the following :

(1) First Stage of Repair and Restoration

To inspect an outline of damage with emphasis on damage of critical and important facilities as early as possible, and to decide the strategy for repair and restoration. When large secondary disasters are likely to happen, it is necessary to conduct appropriate urgent treatments.

(2) Second Stage of Repair and Restoration

To inspect the damage of all facilities and structures, and to judge the necessity of temporary repair and restoration with consideration of possible large secondary disasters, urgency for restoration, types and importance of the facilities, and the time required for initiation of permanent restoration. When temporary repair and restoration are required, it is necessary to promptly repair, by considering priority and restoration level.

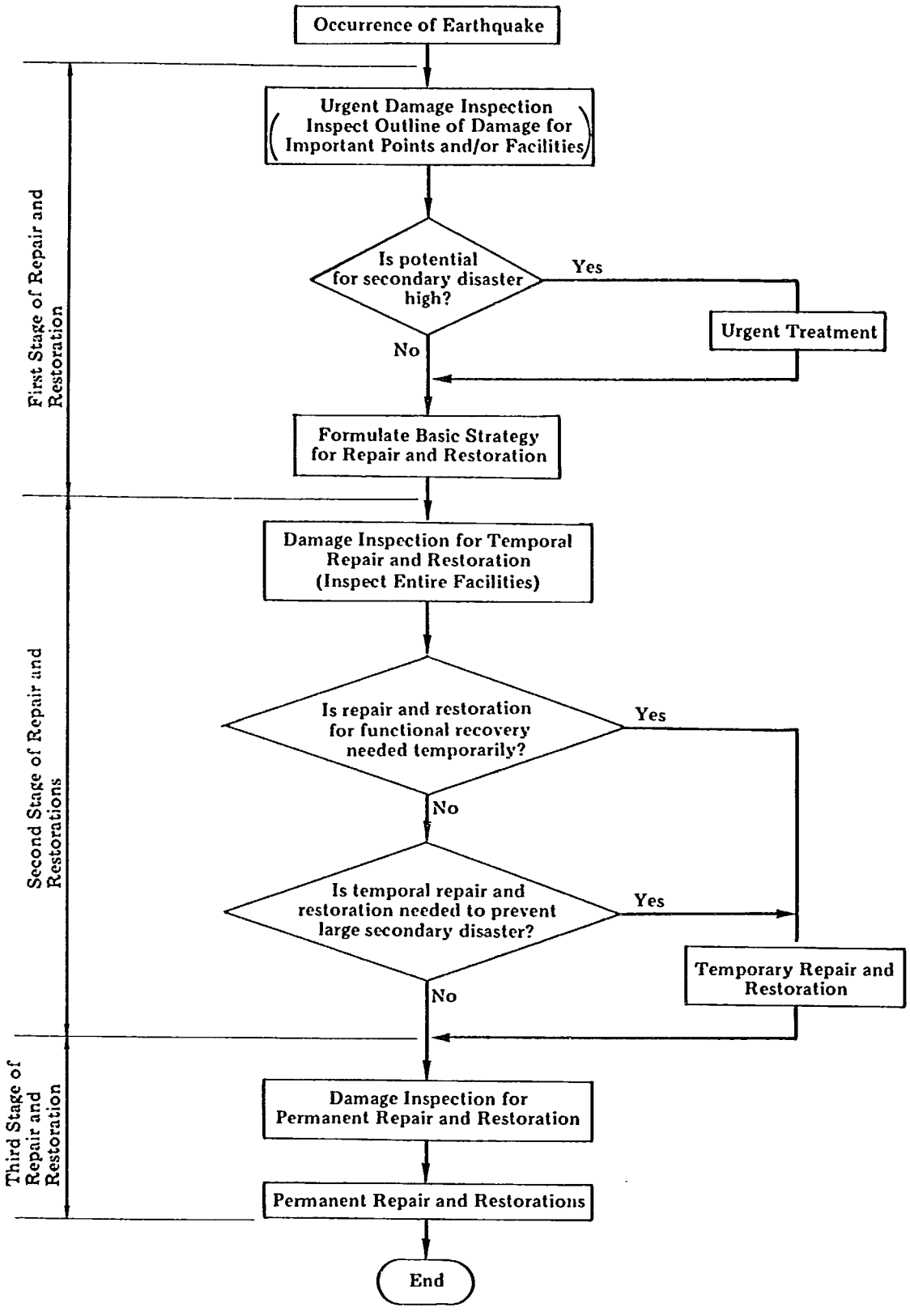


Fig. 19 Procedure of Repair and Restoration of Seismically Damaged Facilities

(3) Third Stage of Repair and Restoration

To determine the level required for permanent repair and restoration based on the considerations of importance, location of the damage, damage degree, difficulties of repair and restoration, and future construction plans, and to conduct permanent repair and restoration by taking future development plans and restoration plans into account.

Urgent Inspection and Urgent Treatment of Highway Bridges (1st Stage)

Fig. 20 shows a procedure of the urgent inspection and urgent treatment for transportation facilities. It should be noted that main purpose of the urgent inspection is to survey whether the road is passable. Detailed inspection and repair could not be made at this stage because it would require considerable time. Such a detailed inspection would also

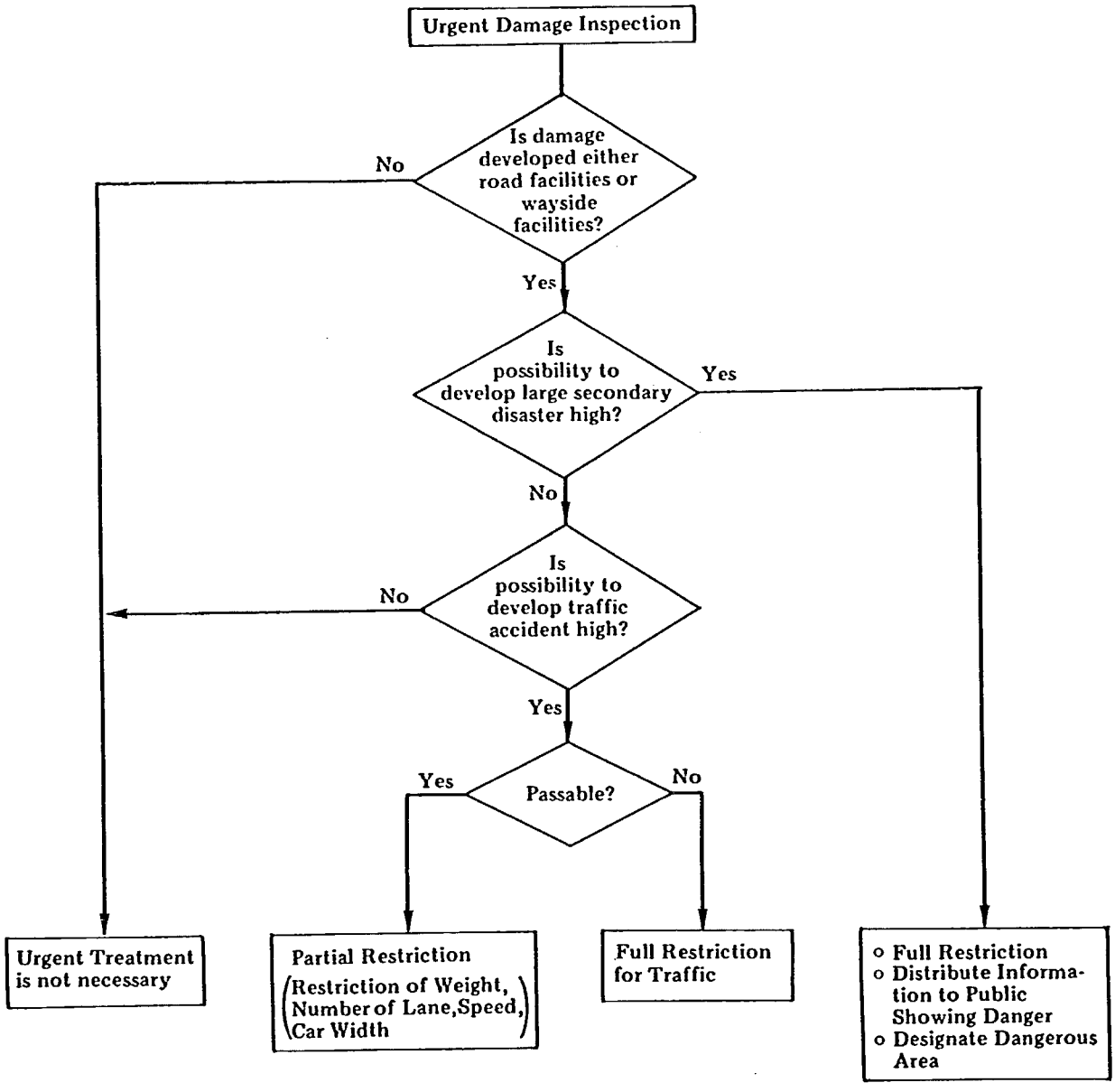


Fig. 20 Procedure of Urgent Inspection and Urgent Treatment

prevent the formulation of a repair plan at the head-quarters. Table 20 shows main check points for the urgent damage inspection.

Damage Inspection for Temporary Repair, and Temporary Repair Method for Highway Bridges (2nd Stage)

Table 21 shows types of damage developed in highway bridges. Among the various types of damage, failure of piers, failure of seat concrete (concrete supporting bearings) and rupture of main structural members of superstructure are regarded as critical damages which are liable to cause falling off of superstructure. Therefore, damage inspection at the urgent inspection stage is to be made for these three types of damage first.

The degree of damage at the 2nd stage is required to be decided based on bearing capacity (load capacity) of the bridge structure and road surface condition. Because suspension of traffic on highway bridges would critically affects essential post-earthquake transportation, it is required to judge whether damaged bridges can be used even for short period for emergency transportation.

i) Damage degree depending on bearing capacity

A : No Damage	- No special damage is detected
B : Slight Damage	- Damaged, but not considerable for short term service
C : Medium Damage	- Considerable damage, but may be used for short-term service unless progress of damage due to aftershocks and live load is not developed.
D : Critical Damage	- Possible falling-off of superstructure has to be taken in mind
E : Falling-off	- Falling-off of superstructure

Fig. 21 shows examples of how the damage degree is judged for reinforced concrete piers suffering cracks, spalling-off of concrete and rupture of main reinforcement in a form of flexure failure at the base. Fig. 22 shows the same example for the degree of damage at the bearing supports. It is suggested that inspectors should judge the damage degree by comparing the actual damage with Figs. 21 and 22. Similar tables are prepared for various types of damage including shear failure of reinforced concrete piers and for the failure of superstructures.

ii) Damage degree depending on road surface condition

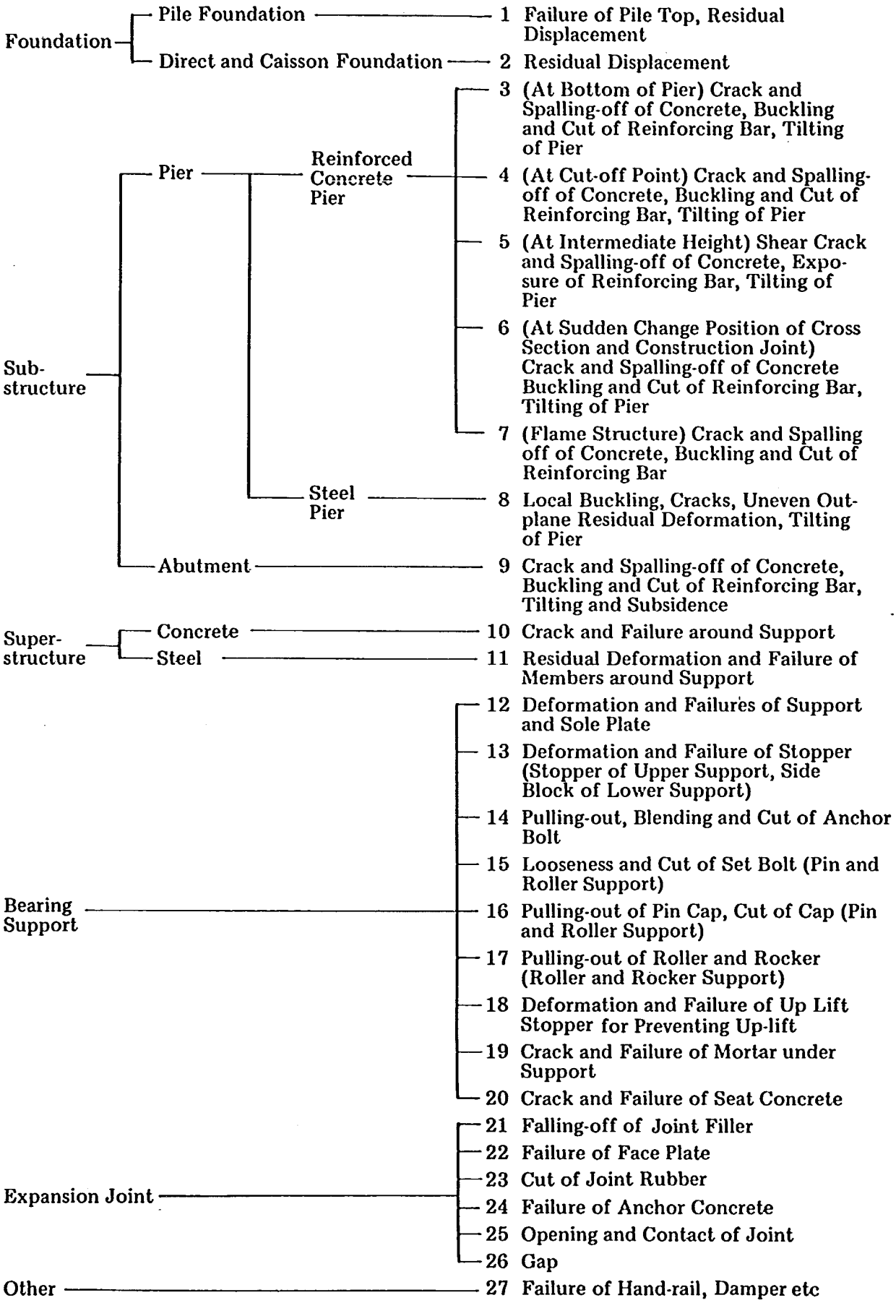
a : No Damage	- No special damage is detected
b : Passable with Care	- Damaged, but can be opened for short term traffic if sufficient care is paid
c : Unpassable	- Badly damaged, and has to be closed

Fig. 23 represents a procedure for deciding whether highway bridges be closed or opened with care.

Table 20 Check Points for Urgent Inspection

Facilities				Check Point
Road Itself	Road	Flat Road		Large Subsidence of Road Surface
		Low ~ High Embankment		Large Subsidence of Road Surface, Large Subsidence and Failure of Embankment
		Natural and Cut Slope		Huge Failure of Slope, Large Fallen Stone on Road, Large Failure of Road
	Bridge	General		Fall-off of Bridge
		From the Surface		Slipping off and Gap of Hand Rail Sudden Change of Leveling Large Opening, Upheaval and Gap at Expansion Joint
		Side View	Superstructure	Sudden Change of Deformation and Leveling
			Substructure	Large Subsidence, Tilting, Large Cracks and Spalling-off of Concrete
	Tunnel			Large Slope Failure near Tunnel, Large Spalling-off of Covering Concrete
	Common Duct			Uplift to Ground Surface, Critical Damage of Storing Facilities
	Culvert and Underground Pedestrian Pass			Large Subsidence on Road Surface
	Pedestrian Bridge			Falling-off, Critical Failure of Pier
Other	Way-side Facilities			Collapse of Building on Road Secondary Disaster caused by Damage of Road Facilities
	Exclusive Use Facilities			Influence of Damage of Exclusive Use Facilities on Road
	Others			Critical Innaduation, Tsunami, Fire, etc.

Table 21 Damage Types of Bridges



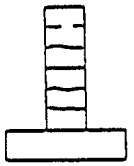
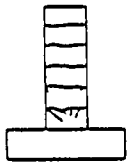
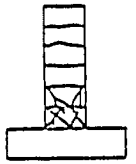
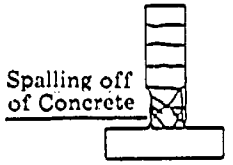
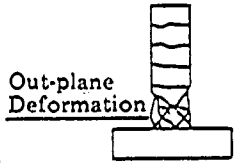
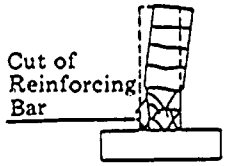
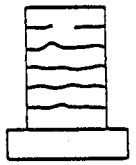
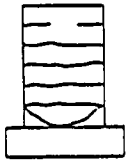
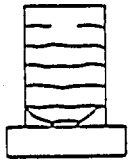
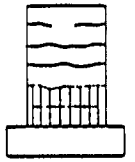
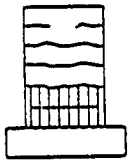
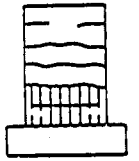
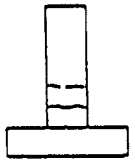
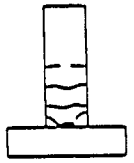
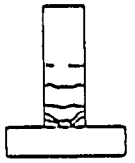
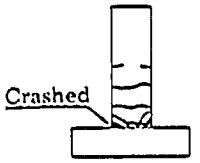
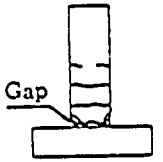
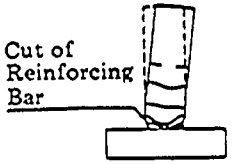
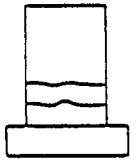
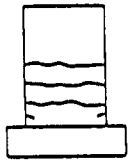
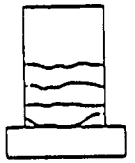
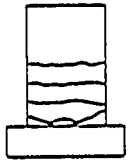
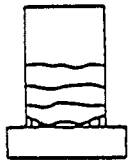
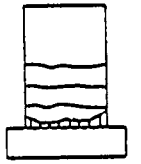
Observed Damage			1 Only Small Cracks	2 Diagonal Cracks (Not Penetrated)	3 Diagonal Cracks (Penetrated)	4 Spalling-off of Cover Concrete	5 Out-Plane Deformation of Reinforcing Bar	6 Cut of Reinforcing Bar and Tilting of Pier
Out-view of Damage		Side View						
		Front View						
		Side View						
		Front View						
Damage-Degree			B: Slight Damage	B: Slight Damage	B: Slight Damage	C: Medium Damage	C: Medium Damage	D: Critical Damage
Residual Strength			Pu (1.1 Py ~ 1.3 Py)	Pu (1.1 Py ~ 1.3 Py)	1.1 Py	1.0 Py	less than Py	less than Py
Residual Deformability			70%	50%	30%	10%	0%	0%

Fig. 21 Damage Degree of Reinforced Concrete Piers Subjected to Flexural Failure at Base

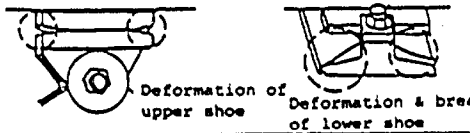
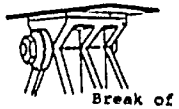
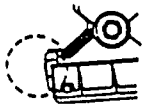
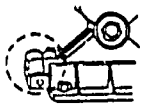
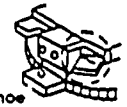
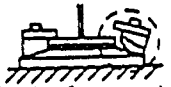
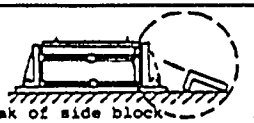
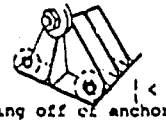
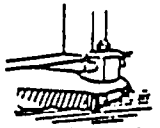
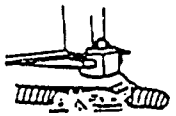
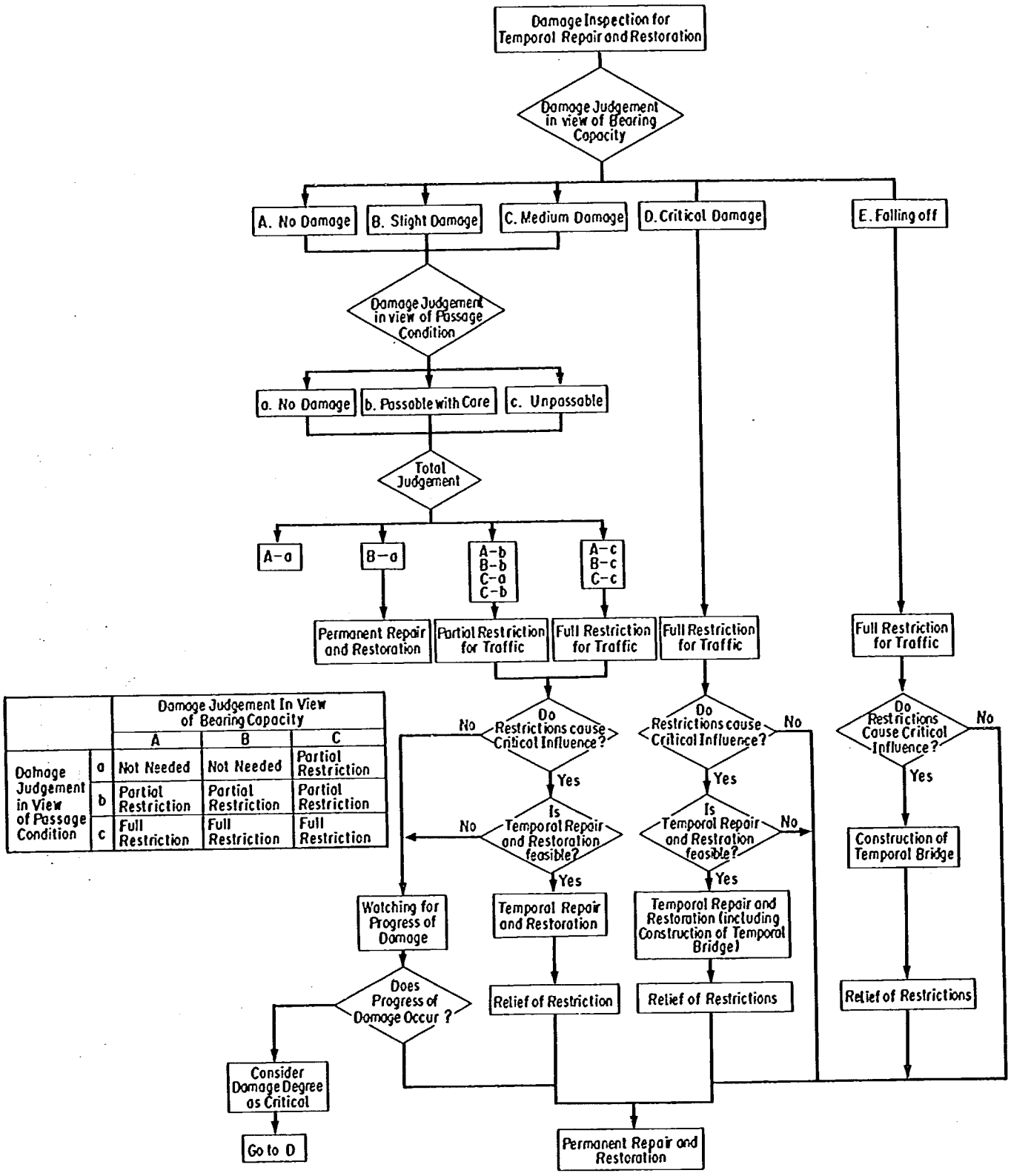
	B : Small damage	C : Medisum damage	D : Extensive damage
Cast section of upper & lower shoe	 Deformation of upper shoe; Deformation & break of lower shoe		
Set bolt	 Looseness of set bolt	 Break of set bolt	 Break of set bolt and damage of sole plate & hub
Roller	 Falling off of roller	 Falling off of roller	
Pin and pin cqp	 Falling off of pin cap	 Sheaing of pin	
Upper shoe stopper	 crack of upper shoe stopper	 Break of upper shoe stopper	
Side block	 Deformation of side block;  Crack of upper shoe stopper	 Break of side block stopper bolt;  Break of upper shoe stopper	
Anchor bolt	 < 1cm Falling off of anchor bolt(<1cm)	 > 1cm Falling off anchor bolt(> 1cm)	 Break of anchor bolt
Shoe pedestal mortar and concrete	 Crack of shoe pedestal mortar;  Crack of shoe pedestal concrete	 Rupture of shoe pedestal mortar;  Rupture of shoe pedestal concrete	 Rupture of shoe pedestal concrete

Fig. 22 Damage Degree of Bearing Supports



Damage Judgement in View of Passage Condition	Damage Judgement In View of Bearing Capacity A	B	C
a	Not Needed	Not Needed	Partial Restriction
b	Partial Restriction	Partial Restriction	Partial Restriction
c	Full Restriction	Full Restriction	Full Restriction

Fig. 23 Procedure of Judgement for Temporary Repair of Bridges

Damage Inspection for Permanent Repair, and Permanent Repair Method of Highway Bridges (3rd Stage)

For permanent repair, the degree of damage has to be decided from a different inspection than that used by the temporary repair. Inspection of repair needs is required for long term use in the 3rd stage. Upgrading may be required for those bridges which suffered critical damage. The damaged degree is determined as

A : No Damage	- No damage or minor damage which does not affect function for long-term service.
B : Slight Damage	- Damage which does not affect the bearing capacity
C : Medium Damage	- Damage which affects the bearing capacity
D : Critical Damage	- Damage which significantly affects the bearing capacity

Time required, cost, workability, availability of construction materials and visual appearance of repairing works have to be considered. Table 22 represents one of examples of a permanent repair method for reinforced concrete piers which suffered flexure failure at the base.

DEVELOPMENT OF INFORMATION GATHERING AND PROCESSING SYSTEMS FOR SEISMIC DAMAGE MITIGATION

After a destructive earthquake, it is of significant importance to immediately gather correct information on the extent of damage in the area affected by the earthquake. Road transportation is expected to be interrupted in a very large earthquake, particularly in urban areas such as Tokyo, as a result of damage of not only transportation facilities but of falling-off of building attachments along the road. Confusion of people and automobiles left on road would also cause considerable disruption to the transportation. It is required therefore to develop new information gathering and processing systems which will enable the extent of damage to be recognized immediately after the earthquake for formulating a repair and restoration strategy.

A comprehensive 5 year research program entitled " Development of Information Gathering and Processing Systems for Disaster Mitigation" was initiated in 1988 by the Ministry of Construction. The objectives of this research project were to develop new information correction and processing systems, using advanced new technology, for various disasters such as earthquakes, floods and debris flows. Key items of the research development are (refer to Fig. 24) ;

a) Bird's eye information correction systems from helicopters,
b) On-line information processing systems, and
c) Real-time digital mapping systems.

Table 22 Permanent Repair of Reinforced Concrete Bridge Piers with Flexural Failure at Bottom

Level of Damage		Repair and Restoration Method	Design for Normal Load	Design by Ductility Analysis	
	Damage Patter Presented in Fig. 4-2			Yield Stage	Ultimate Stage
Before Yield of Reinforcing Bar	Before Stage 1	Injection of Epoxy Regin	Normal	Normal	Normal
		Covering by Reinforced Concrete	Hybrid	Hybrid	Hybrid
		Covering by Steel Plate	Hybrid	Hybrid	Hybrid
After Yield but Before Ultimate	Stage 2 and 3	Injection of Epoxy Regin	2/3 Es for Reinforcing Bar	2/3 Es for Reinforcing Bar	Normal
		Covering by Reinforced Concrete	Ignore Original Section	1/3 Es for Original Reinforcing Bar	Hybrid
		Covering by Steel Plate	Ignore Original Section	1/3 Es for Original Reinforcing Bar	Hybrid
After Ultimate	Stage 4, 5 and 6	Covering by Reinforced Concrete	Ignore Original Section	Ignore Original Section	Hybrid

Note 1) Normal: Usual design procedure in accordance with Design Specifications of Highway Bridge.

2) Hybrid: Original damaged section can be treated to work for load with new section.

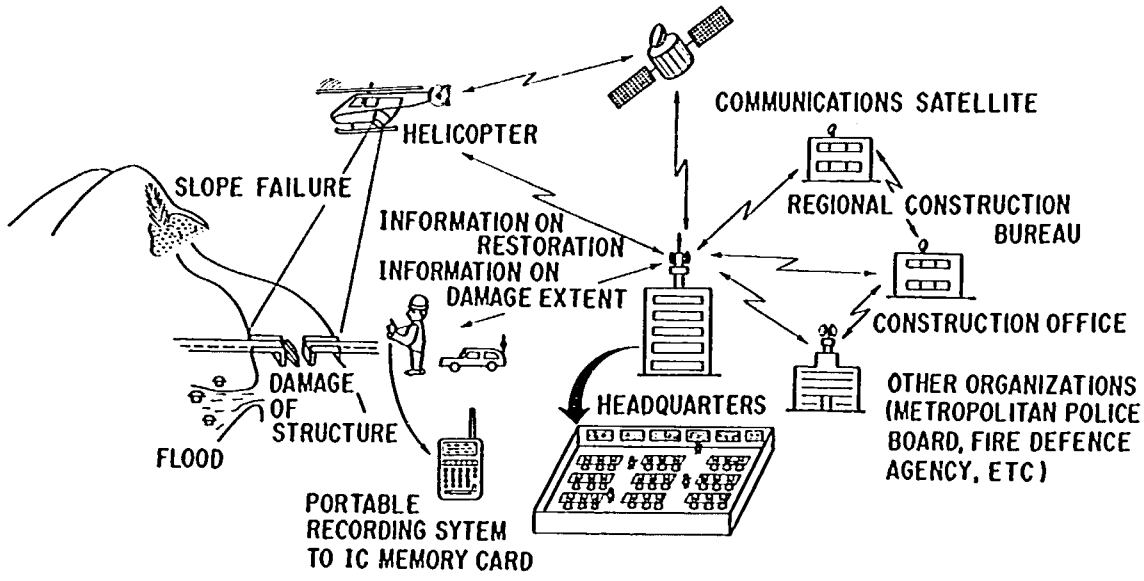


Fig. 24 Information Gathering and Processing Systems

For this purpose, measuring technology of the degree of seismic damage of structures, using helicopter picture information and new media high-grade disaster prediction methods as well as planning systems for repair and restoration in the damaged area are under development. To avoid distortion of information during transferring information from the regional office to headquarters, it is aimed to develop visual motion picture systems.

In executing the project, the Technological Research Center for National Land Development established the Committee for the Development of Disaster Information Systems, which is chaired by Dr. H. Umemura, Professor Emeritus of the University of Tokyo. Final accomplishments of the project are to be compiled in 1992 in the form of guidelines.

CONCLUDING REMARKS

The preceding pages presented the present earthquake engineering efforts to mitigate earthquake hazards of road transportation facilities in Japan. Japan has been experiencing many destructive earthquakes in the past and it is critically important that the functions for rescue, evacuation, repair and restoration be able to be carried out. Replacement and strengthening of existing highway bridges is extremely difficult in urban areas. Transportation facilities, in particular important ones such as highway bridges, have to be provided with a very high level of seismic safety.

The level of seismic safety required for transportation facilities has been increasing in recent years as a result of past experiences where confusion caused by the interruption was considerable in urban area. Indirect damage caused by the interruption of urban transportation was much larger than the direct damage. It is therefore required to develop new seismic design and countermeasure concepts which enable structures with higher and with various levels of seismic safety to be constructed.

ACKNOWLEDGEMENTS

The author would like to express his sincere thanks to Mr.Kanoh, T. and Iida, H., staff members of the Earthquake Engineering Division of the Public Works Research Institute, for their assistance in making the manuscript. Special thanks are extended to Dr.Gregory MacRae, visiting research engineer at the Public Works Research Institute from New Zealand, for his suggestions and corrections to the manuscript.

REFERENCES

1) Iwasaki, T., Penzien, J. and Clough, R.W.: Literature Survey - Seismic Effects on Highway Bridges, Report No. EERC 71-11, Earthquake Engineering Research Center, University of California, Berkeley, 1972
2) Kawashima, K. : Seismic Design and Seismic Damage Mitigation of Highway Bridges, Journal of Road, 1990
3) Japan Road Association : Seismic Design Specifications for Highway Bridges, 1976
4) Iwasaki, T., Tatsuoka, F., Tokida, K., and Yasuda, S. : A Practical Method for Assessing Soil Liquefaction Potential Based on Case Studies at Various Sites in Japan, Proc. 6th Japan Earthquake Engineering Symposium, 1978, Tokyo
5) Japan Road Association : "Part V Seismic Design" of the "Design Specifications for Highway Bridges", 1990
6) Iwasaki, T., Kawashima, K. and Hasegawa, K. : New Seismic Design Specifications of Highway Bridges in Japan, 22nd Joint Meeting, U.S.-Japan Panel on Wind and Seismic Effects, UJNR, Gaithersburg, U.S.A., May 1990
7) Kawashima, K, Aizawa, K. and Takahashi, K. : Attenuation of Peak Ground Motions and Absolute Acceleration Response Spectra, Report of the PWRI, Vol. 166, Public Works Research Institute, 1985
8) Katayama, T., Iwasaki, T. and Saeki, M. : Statistical Analysis of Earthquake Acceleration Response Spectra, Proc. Japan Society of Civil Engineers, Vol. 275, 1978
9) Kawashima, K. and Hasegawa, K. : New Seismic Design Method of Multi-span Continuous Bridges, Bridges and Foundations, Vol. 90-10, 1990
10) Ohta, M.: A Study on Earthquake Resistant Design for Reinforced Concrete Bridge Piers of Single-Column Type, Report of the Public Works Research Institute, Vol. 153, 1980
11) Kawashima, K. and Koyama, T. : Effects of Cyclic Loading Hysteresis on Dynamic Behavior of Reinforced Concrete Bridge Piers, Structural Eng./Earthquake Eng., Vol. 5, Vo.2, Proc. of Japan Society of Civil Engineers, 1988, and Kawashima, K. and Koyama, T. : Effects of Number of Loading Cycles on Dynamic Characteristics of Reinforced Concrete Bridge Piers, Structural Eng./Earthquake Eng., Vol.5, No.1, Proc. of the Japan Society of Civil Engineers, 1988
12) Kawashima, K. and Hasegawa, K. : Hysteretic Behavior of Reinforced Concrete Bridge Piers by Dynamic Loading Tests and Shaking Table Tests, 9th World Conference on Earthquake Engineering, Tokyo/Kyoto, Japan,

1988
13) Hamada, M., Yasuda, S., Isoyama, R. and Emoto, K. : Observation of Permanent Ground Displacements Induced by Soil Liquefaction, Proc. of Japan Society of Civil Engineers, Vol. 376, III-6, 1986, and, Hamada, M., Yasuda, S., Isoyama, R. and Emoto, K. : Study on Liquefaction-Induced Permanent Ground Displacements and Earthquake Damage, Proc. of Japan Society of Civil Engineers, Vol. 376, III-6, 1986
14) Guidelines for Design of Base-Isolated Highway Bridges, Final Report of A Committee for Study of Application of Base Isolation to Seismic Design of Highway Bridges (Chairman : Professor T. Katayama), Technology Research Center for National Land Development, March 1989
15) Kawashima, K. : Development and Future Scope of Seismic Isolation of Structures - A Review -, Proc. of Japan Society of Civil Engineering, Structural Eng./Earthquake Eng., Vol.398/I-10, Proc. of JSCE, 1988
16) New Zealand- Japan Workshop on Base Isolation of Highway Bridges, Head Office of Ministry of Works and Development, Wellington, New Zealand, 1987
17) Taguchi, J., Iwasaki, T., Adachi, Y. and Kawashima, K. : U.S.-Japan Cooperative Research Program on Hybrid Control of Seismic Response of Bridge Structures, 22nd Joint Meeting, U.S.-Japan Panel on Wind and Seismic Effects, UJNR, Gaithersburg, Maryland, U.S.A., 1990
18) Kakizaki, H. and Itoh, T.: Design of the Nagaki-gawa Bridge - A Based Isolated Bridge, Bridge and Foundation, Vol. 24, No.9, 1990
19) Japan Road Association:Countermeasures for Roads against Earthquakes, 1986
20) Kawashima, K. and Unjoh, S.: An Inspection Method of Seismically Vulnerable Existing Highway Bridges, Structural Eng./Earthquake Eng., Vol.7, No.1, Proc. Japan Society of Civil Engineers, April 1990
21) Japan Road Association : Guide Specifications for Earthquake Hazard Mitigation for Transportation Facilities - Pre-Earthquake Countermeasures -, 1987
22) Kawashima, K, Unjho, S. and Azuta, Y.: Examples of Seismic Strengthening of Highway Bridges, Technical Note of PWRI, No.2674, Public Works Research Institute, 1988
23) Public Works Research Institute : Manual for Repair Methods for Civil Engineering Structures Damaged by Earthquakes, Technical Note of the Public Works Research Institute, Vol.45, December 1986 (in Japanese). Translated version is published from the National Center for Earthquake Engineering Research, University of New York, Buffalo, U.S.A.
24) Japan Road Association : Guide Specifications for Earthquake Hazard Mitigation for Transportation Facilities - Post-Earthquake Countermeasures-, 1987 (in Japanese)

SEISMIC INSPECTION AND SEISMIC STRENGTHENING OF REINFORCE CONCRETE BRIDGE PIERS WITH TERMINATION OF MAIN REINFORCEMENT AT MID-HEIGHT

by
Kazuhiko KAWASHIMA
Shigeki UNJOH
and
Hiroyuki IIDA

U.S. — JAPAN WORKSHOP ON SEISMIC RETROFIT OF BRIDGES
Tsukuba Science City Japan
December 1990

SEISMIC INSPECTION AND SEISMIC STRENGTHENING OF REINFORCED CONCRETE BRIDGE PIERS WITH TERMINATION OF MAIN REINFORCEMENT AT MID-HEIGHT

K. Kawashima (I)
S. Unjoh(II)
H. Iida(III)
Presenting Author : S. Unjoh

SUMMARY

This paper presents an experimental study on seismic inspection and seismic strengthening methods for reinforced concrete bridge piers which have termination of the main reinforcement, without enough anchorage lengths, at mid-height. The effect of the anchorage length of the main reinforcement was studied through the tests of 15 reinforced concrete pier specimens. The effect of the length and thickness of a steel jacket, and the use of injected material between the existing concrete and the steel jacket was also studied for developing a strengthening method.

INTRODUCTION

During recent earthquakes including the Miyagi-ken-oki Earthquake of 1978 and the Urakawa-oki Earthquake of 1982,[1),2)] reinforced concrete piers of highway bridges which have termination of main reinforcement at mid-height and short anchorage lengths have suffered serious damage. Photos 1 and 2 show the damage to reinforced concrete piers at this zone. Because the bending moment developed in the pier subjected to a lateral force P decreases as the height from the base increases, the amount of main reinforcement is generally decreased by terminating a number of bars at mid-height as shown in Fig.1. For short piers constructed prior to 1980, half of the reinforcement was terminated at approximately mid-height of the pier because in the design specifications, it was stipulated that the reinforcement can be terminated at the point 20 times of a diameter of the reinforcement higher than the point where the stress of reinforcement decreases to 50% of the allowable stress, therefore, only this length was generally provided. Since the damage to reinforced concrete piers at the anchorage zone results in a brittle shear failure,[3)-6)] such damage should be prevented.

Through the past experiences of damage to piers, the design specifications for highway bridges were revised in 1980,[7)] in which, anchorage length was increased from 20 times the diameter of the reinforcement to effective width of the pier plus 20 times of the diameter of the reinforcement. The allowable stress of concrete for shear in the anchorage zone also reduced by 33%.

(I) Head, Earthquake Engineering Division, Earthquake Disaster Prevention Department, Public Works Research Institute, Ministry of Construction, Tsukuba Science City, 305, Japan
(II) Research Engineer, ditto
(III) Assistant Research Engineer, ditto

Because a large number of piers were designed according to the specifications issued prior to 1980, inspection and strengthening are required for piers with this short anchorage length.

The Ministry of Construction made seismic inspections of highway bridges throughout the country in 1971, 1976, 1979 and 1986. In the latest inspection, approximately 40 thousand bridges were inspected, and about 11 thousand bridges were found to require seismic strengthening. Although most of these bridges require installation of devices for preventing falling-off of the superstructure, some bridges detected require strengthening measures because of the short anchorage length of the main reinforcement in the pier.

There are several possible ways to strengthen such reinforced concrete piers. One method may be to place new reinforced concrete section around the existing section to support the lateral load. However, in this method, the increase of the mass of the pier tends to require an increase of the load resistance of the foundation. To avoid this situation, the pier may be strengthened by means of a steel jacket wrapped around the existing pier and construction will be simpler than adding new reinforced concrete.

In order to develop a seismic inspection method and seismic strengthening method for reinforced concrete bridge piers which have high vulnerability to develop serious damage at the mid-height where the main reinforcement is terminated during earthquakes, a series of dynamic loading tests were conducted at the Public Works Research Institute, partially in cooperation with the Metropolitan Expressway Public Corporation and the Hanshin Expressway Public Corporation.

This paper presents some of the preliminary results of the studies of effect of the anchorage length of the main reinforcement and length of the steel jacket required to prevent failure at the termination points.

TEST SPECIMENS AND EXPERIMENTAL SET-UP

Test Specimens

a) Test specimens for evaluating vulnerability

In order to evaluate the failure mode of the reinforced concrete piers with an inadequate anchorage length of the main reinforcement, 7 specimens with square sections of 50cm×50cm were constructed as shown in Table 1. The scale of the specimens is assumed to be about 1/5 of a prototype pier.

Among the 7 specimens, Specimens 1, 2, 3 and 4, which have a shear span ratio of 5.4, were constructed with different anchorage lengths of main reinforcement as shown in Fig.2. Other characteristics are the same among the four specimens. Forty deformed reinforcing bars (yield strength is 3,000 kgf/cm^2) with a diameter of 13mm were placed as main reinforcement so that main reinforcement ratio was 2.03% at the base. Round reinforcing bars (yield strength is 2,400 kgf/cm^2) with a diameter of 9mm were placed every 25cm as tie reinforcement. The tie reinforcement ratio was 0.1%.

In Specimen 1, all reinforcement is continuous from the base to the top without termination at mid-height. In Specimen 2, the main reinforcement is terminated at the point where the stress induced in the reinforcement becomes one half of the allowable stress. Therefore, no anchorage length was provided in specimen 2. On the other hand, Specimens 3 and 4 were constructed with anchorage lengths of D/2 and D, respectively, in which D represents the width (=50cm) of the pier.

Specimens 10, 11 and 12 had a shear span ratio of 9.9. Although reinforced concrete piers with such proportions are rarely adopted, the test was made to study the mode of failure under the condition that the bending moment will be more predominant than shear force in design. The layout of the main and tie reinforcement were the same as Specimens 1, 2, 3 and 4. Anchorage lengths were 0, D/2 and D for Specimens 10, 11 and 12, respectively, as shown in Fig.3.

b) Test specimens for verifying strengthening method

To study the effect of the steel jacket, 8 specimens were tested as shown in Table 2. Specimens from 13 to 17 had a square section of 50cm×50cm, and a shear span ratio of 5.6 as shown in Fig.4. Forty six deformed reinforcing bars (yield strength is 3,000 kgf/cm^2), each with a diameter of 10mm were placed as main reinforcement. The main reinforcement ratio was 1.31% at the base. Round reinforcing bars (yield strength is 2,400 kgf/cm^2) with a diameter of 6mm were placed every 25cm as tie reinforcement. The tie reinforcement ratio was 0.05%. The effectiveness of a 1mm thick steel jacket with the length of 1D was studied in Specimens 13 and 14. The steel jacket was placed centrally about the termination point so that it covered the region of D/2 above and below this point. Two types of material were injected between the steel jacket and the surface of existing concrete piers to investigate their behaviour. They were nonshrinking concrete mortar (Specimen 13) and epoxy resin (Specimen 14). Because the length of a steel jacket of 1D was not enough to prevent the failure at the termination point, it was elongated to 1.5D for Specimen 15 (concrete mortar) and Specimen 16 (epoxy resin) as will be described later. The steel jacket was placed over the region D above and D/2 below the termination point, respectively. To study effect of the thickness of steel jacketing, a 0.6mm thick steel jacket was used on Specimen 17, in which the epoxy resin was adopted for injection.

Specimens 18, 19 and 20 had wall type construction with section dimensions of 40cm×160cm as shown in Fig.5. Sixty four deformed reinforcing bars (yield strength is 3,000 kgf/cm^2) with a diameter of 10mm were placed as the main reinforcement. The main reinforcement ratio was 0.76% at the base. Round reinforcing bars (yield strength is 2,400 kgf/cm^2) with a diameter of 6mm were placed every 20cm. The tie reinforcement ratio is 0.08%. No strengthening was performed on Specimen 18 which had no anchorage length of the main reinforcement. Specimens 19 and 20 were strengthened by steel jackets with lengths of 1.5D and 2D, respectively, in which D represents the width of the shorter side of the section. Concrete mortar was injected into both specimens.

Loading Conditions

All specimens were laterally loaded at the top and were subjected to axial loading as shown in Fig.6. An electro-hydraulic dynamic actuator and static jack were used for the loading.

The specimens were subjected to a reversed cyclic lateral loading history under displacement control as shown in Fig.7.[11),12)] The load was incrementally increased in about 10 steps up to the yielding of the main reinforcement at the base. The displacement developed at the pier crest, where the main reinforcement yielded at the base is defined hereafter as the yield displacement δ_0, and it is used as a reference value to specify the

loading displacement applied to the specimens.

Extensive electric instrumentation was used to measure and record the basic deformation parameters such as the strain in the main and tie reinforcement as well as the displacement and acceleration at the loading point.

VULNERABILITY OF REINFORCED CONCRETE PIERS WITH INADEQUATE ANCHORAGE LENGTH

Effect of Anchoring Length

a) Specimen with shear span ratio of 5.4

Fig.8 shows the effect of the anchorage length in the tests of Specimens 1, 2, 3 and 4, which had square cross sections of 50cm× 50cm and a shear span ratio of 5.4.

Fig.8(a) shows the failure mode of the specimens. In Specimen 1, in which main reinforcement was continuous from the bottom to the top without termination, flexural cracks were firstly developed at the base. As the loading increased, the cracks progressed and spalling-off of the cover concrete developed. The specimen finally failed in flexure at the base.

In Specimen 2, which had zero anchorage length, flexural cracks were firstly developed at the termination point. The flexural cracks progressed and the specimen finally failed in shear at the termination point.

In Specimen 3, which had an anchorage length of D/2, flexural cracks were developed at both the termination point and at the base of the pier. As the loading increased, the cracks at the base progressed significantly, and the specimen finally failed in flexure at the base.

In Specimen 4, which had an anchorage length of D, the failure mode was almost same with that of Specimen 1. The anchorage length of D was considered to be sufficient to prevent failure at the termination point.

Based on the test results of Specimens 1, 2, 3 and 4, the position where the cracks occurred was seen to give a indication of the position where failure would eventually occur.

Fig.8(b) compares the strain induced in the main reinforcement of the specimens. It should be noted that the accuracy of strain measurement over about 3,000 μ was poor due to the limited capability and damage of strain gauges.

Larger strains were developed at the base in Specimens 1 and 4 while a strain as large as that at the base was developed at the termination point in Specimens 2 and 3 and the strain at the termination point was larger in Specimen 2 than in Specimen 3. This corresponds to the difference of the failure mode observed in these specimens.

Fig.8(c) shows the envelope of load-displacement hysteresis loops and equivalent hysteresis damping ratio. It is obvious that the lateral load resistance of Specimen 2, which failed at the termination point, is considerably smaller than that of other specimens. The equivalent damping ratio did not seem to be affected directly by the failure mode.

b) Specimens with shear span ratio of 9.9

Fig.9 shows the effect of the anchorage length on Specimens 10, 11 and 12, which had the same square cross section (50cm× 50cm) and a shear span ratio of 9.9.

Fig.9(a) shows the failure mode of the specimens. In Specimen 10, in which no anchorage length was provided, flexural cracks were firstly developed at the termination point. As the loading increased, the cracks progressed and spalling-off of the cover concrete developed. Although rupture of the main reinforcement did not occur, the load resistance of the pier suddenly decreased in the first cycle to $5\delta_0$ in plus direction, therefore testing was terminated to protect the loading equipment. The specimen finally failed in shear.

In Specimen 11, which had an anchorage length of D/2, flexural cracks were developed at the termination point as well as at the base as shown in Fig.10. Slightly greater shear cracks were also initiated at the termination point during the cycles to $2\delta_0$. However, significant flexural cracks and spalling-off of the cover concrete developed after the cycles to $3\delta_0$ and the specimen finally failed at the base. Tensile rupture of five reinforcing bars occurred at the base during the $6\delta_0$ loading.

In Specimen 12, which had an anchorage length of D, the flexural cracks were developed at the base and a few cracks were observed at the termination point. The specimen finally failed in flexural at the base.

Fig.9(b) compares the strain induced in the main reinforcement of these specimens. The strain at the termination point and at the base reached the yield strain ($1{,}800\,\mu$) during the $1\delta_0$ loading in all specimens. As the loading displacement increased, the strain substantially increased at these two points. In Specimen 12, which failed in flexure at the base, the strain at the termination point almost reached the yielding strain even during the $1\delta_0$ loading. Although the difference in the strain distributions of the specimens was small up to the $4\delta_0$ loading cycles it is thought that the difference in the strains of the specimens would increase after this value.

Fig.9(c) shows the envelope of the load-displacement hysteresis loops and the equivalent hysteresis damping ratio. Noticeable differences in the envelope are not observed up to the $4\delta_0$ loading where a sudden decrease of the load occurred in the specimen 10. This corresponded to the failure at the termination point as was described above. Because the failure occurred on the first loading to $+5\delta_0$, the effect of failure was not observed in the equivalent damping ratio.

SEISMIC STRENGTHENING BY MEANS OF A STEEL JACKET

Reinforced Concrete Pier with Square Section

Fig.11 shows the effect of the steel jacket strengthening method on Specimens 13, 14, 15, 16 and 17. The length of the steel jacket was the main interest in these tests.

Fig.11(a) shows the failure mode of the specimens. In Specimens 13 (mortar injection) and Specimen 14 (epoxy resin), which were strengthened with 1D long steel jackets, flexural cracks were developed at the base. As the loading increased, the cracks progressed, and the specimens finally failed in flexure at the base. Fig.11(b)(1) and (2) compare the strain induced in the main reinforcement in Specimens 13 and 14. Although the strain in the region covered by the steel jacket was small, the strain at the upper end of the steel jacket reached the yielding strain during the $1\delta_0$ loading cycles. It became greater than the yielding strain with increasing loading displacement. Fig.12 compares the deformation, in the vertical direction,

induced in the steel jacket. The strain was only about 100μ (Specimen 13) ~ 200μ (Specimen 14) even during 3δ_0 loading. As will be discussed later, the strain induced in Specimen 14 was slightly larger than that induced in Specimen 13. (This shows the difference of contact between the steel jacket and the concrete surface). After the 7δ_0 loading cycles, the steel jacket was taken out to inspect the damage at the termination point. Although a single moderate crack was developed as shown in Photo 3 and 4, progress of the failure at the termination point was prevented by the steel jacket. Only minor cracking occurred at the upper end of the jacket. Based on the test results, it was considered that the length of 1D was insufficient to prevent failure at the termination point.

Specimen 15 (mortar injection) and Specimen 16 (epoxy resin) were strengthened by a 1.5D long steel jacket and were then tested.

In Specimen 15, flexural cracks were developed at the base. However, as the loading increased, shear cracks were developed at the lower end of the steel jacket and the specimen finally failed in shear at this zone as shown in Fig.11(a)(3). The concrete mortar between the concrete surface and the steel jacket was crushed and the steel jacket deformed as shown in Photo 5. Fig.11(b)(3) shows the strain induced in main reinforcement. During the 3δ_0 loading cycles, it exceeded the yield strain. The strain was slightly larger at the lower end of the jacket. The tie reinforcement yielded during the 3δ_0 loading cycles and the concrete mortar was crushed and outward buckling of steel jacket occurred. Fig.13(1) shows the deformation, in the vertical direction, induced in the steel jacket. The strain takes the maximum value at the center of the jacket. The strain was about 1200μ, which is much larger than that induced in Specimen 13 which had a jacket length of 1D. It means that the steel jacket with length of 1.5D worked much effectively than the steel jacket with length of 1D. It should be noted that effect of the outward buckling of the steel jacket which was described above cannot be clearly seen in Fig.13 because it shows the strain of steel jacket in vertical direction.

On the other hand, in Specimen 16, flexural cracks were developed at the base, where the specimen finally failed in flexure as shown in Photo 6. This clearly showed the difference of the injection material between the concrete surface and the steel jacket. Epoxy resin was better than the concrete mortar in this test because separation of the steel jacket from the concrete surface did not occur developed in the epoxy injected specimen. However, the effectiveness of such injected materials has to be evaluated from other viewpoints such as durability for long-term use. As shown in Fig.11(b)(4), the strain induced in the main reinforcement was slightly smaller than that in Specimen 15. Deformation of the steel jacket in the vertical direction is almost the same as that of Specimen 15 as shown in Fig.13(2).

In Specimen 17, in which a thinner steel plate (t=0.6mm) was used. The failure mode was almost the same as that developed in Specimen 15 (t=1mm). The crushing of the steel occurred at the lower end of the jacket, and the bond effect of epoxy resin were cut off during 4δ_0 loading cycles. The deformation of the jacket were of the same order as that developed in Specimen 15. The strain induced in the main reinforcement and strain of the steel jacket in vertical direction were larger than those of Specimen 16 as shown in Fig.11(b)(5) and Fig.13(3). This clearly shows the effect of the different thicknesses of the steel jacket.

Reinforced Concrete Piers with Wall Type Section

Fig.14 shows the effect of the steel jacket strengthening method on Specimens 18, 19 and 20.

Fig.14(a) shows the failure mode of the specimens. In Specimen 18, which was not strengthened by the steel jacket, flexural cracks were developed both at the termination point and at the base. As the loading increased, the cracks significantly progressed at the termination point until the specimen finally failed at this zone.

In Specimen 19, which was strengthened by a 1.5D long steel jacket, cracks progressed at the base where the specimen finally failed in flexure. When the steel jacket was removed from the concrete pier after the $7\delta_0$ loading cycles, a horizontal crack was found at the termination point.

In Specimen 20 which was strengthened by a 2D long steel jacket, the failure mode was almost identical with that of Specimen 19. However, no crack was observed at the termination point when the jacket was removed after the $7\delta_0$ loading cycles.

Fig.14(b) compares the strain induced in the main reinforcement of Specimens 19 and 20. Although, the strain induced in the main reinforcement at the strengthened region was less than 100μ up to $3\delta_0$ loading in Specimen 19, the strain suddenly increased and exceeded the yielding strain at the termination point during the $4\delta_0$ loading cycles. On the other hand, the strain induced in the main reinforcement at the strengthened zone was small even during large displacements in Specimen 20. Therefore, 2D may be required as a length of the steel jacket in order for the termination point to have no effect. Fig.15 compares the strain induced in the steel jacket, in the vertical direction, it is very small, and takes a value of only 200μ even during the cycles to $3\delta_0$ and yielding of tie reinforcement was not developed in Specimens 19 and 20.

Fig.14(c) shows the envelope of the load-displacement hysteresis loops and the equivalent damping ratio. The load resistance of Specimen 18 suddenly decreased during the $5\delta_0$ loading cycles. The load resistance of Specimens 19 and 20 increased by about 10% than that of Specimen 18 when the steel jacket was used. The difference in the load resistance of Specimens 19 and 20 was insignificant. The equivalent damping ratio of Specimen 20 during the $5\delta_0$ and $6\delta_0$ loading cycles was smaller that of Specimen 21 because the number of main reinforcing bars ruptured at the base was greater than Specimen 20.

EVALUATION OF VULNERABILITY

Based on the tests described above, it may be important to estimate the strength of reinforced concrete piers at the termination point in relation to the strength at the base. If the strength at the termination point is smaller than that at the base, shear failure, which results in extensive damage in a brittle manner, is likely to occur.

To evaluate the strength of piers, the load resistance is defined as shown in Fig.16 in terms of the bending moment as

$$S = S^T/S^B \quad (1)$$

$$S^T = M_y{}^T/M^T \quad (2)$$

$$S^B = M_y{}^B/M^B \quad (3)$$

where

S : failure mode factor

S^T and S^B : a factor representing the strength at the termination point and at base, respectively

M^T and M^B : bending moment developed at the termination point and base, respectively when the pier is subjected to a lateral force at top

M_y^T and M_y^B : yielding bending moment at termination point and at base, respectively,

In Eqs.(2) and (3), the yielding bending moment is defined as the bending moment at which the reinforcement begins to yield. S^T and S^B defined in Eqs.(2) and (3) determine the likelihood of yielding at the termination point and base, respectively. If $M_\square^T$ is defined to be the bending moment developed at the termination point when M_y^B equals to M_y, Eq.(1) can be written as

$$S = M_y^T / M_\square^T \qquad (4)$$

Fig.17 shows how the failure mode factor varies along pier in the Specimens 1 and 3. Specimen 1 failed at the termination point while the specimen 3 failed at the base. The failure mode factor S at the termination point takes 0.92 and 1.1 in Specimen 1 and Specimen 3, respectively. Although the difference is not necessarily so large, it may be said that the failure mode factor may be used to identify the failure mode.

Fig.18 shows the failure mode factors at the termination point for all specimens which have termination of main reinforcement at mid-height. Failure is likely to be developed at the termination point when the failure mode factor is less than 1.1 although there are some scatters. On the other hand, flexural failure at the base tends to be developed when the failure mode factor is larger than or equal to 1.1.

Fig.19 shows the distribution of the failure mode factor for Specimen 13 which was strengthened by the steel jacket. For computing the failure mode factor by Eq.(1), it was assumed that no separation is developed between the concrete surface and the steel jacket, and that the steel jacket behaves as main reinforcement. The increase of concrete strength and ductility by increasing the confining pressure by means of the steel jacket was disregarded in the calculations.

Fig.20 shows the failure mode factor for all specimens strengthened. The minimum value of the failure mode factors at the upper end and lower end of the steel jacket as well as at the termination point is presented in Fig.20. All specimens strengthened failed at the base although two specimens (Specimens 15 and 17) suffered outward deformation of the steel jacket and shear failure occurred at the lower end of the jacketed zone. If such failure can be regarded as minor, it may be said failure at the termination zone was prevented when the failure mode factor was larger than 1.1. However, because the number of data is inadequate, this needs further study. Special attention should be paid to study the difference of injection material.

CONCLUDING REMARKS

For the evaluating seismic vulnerability of reinforced concrete bridge piers which have termination of main reinforcement and inadequate anchorage

length and for evaluating effectiveness of repair by using steel jackets, a series of dynamic loading tests were made on specimens with square and wall type sections. Based on the test results presented herein, the following conclusions are made:

1) For preventing shear failure at the termination point, the anchorage length should be longer than 1D, where D is the width of the cross section.

2) Whether shear failure at the termination point is developed or not may be evaluated by the failure mode factor S defined by Eq. (1). If the failure mode factor S is smaller than 1.1, shear failure is likely to be developed at the termination point. When the failure mode factor S is larger than or equal to 1.1, flexural failure at the base tends to be developed.

3) Steel jackets can be used to strengthen piers vulnerable to shear failure at the termination point. The minimum length of the steel jacket may be from 1.5 to 2.0 times the pier width D.

4) Epoxy resin seems better than concrete mortar as an injection material, because separation of steel jacket from concrete surface is more restricted. However effectiveness of the epoxy resin should be examined from other aspects including durability for long-term use. Use of steel bars to anchor the steel jacket as well as the concrete mortar may be an alternative approach to be studied.

5) For evaluating the effectiveness of steel jackets, the failure mode factor S by Eq.(1) may be used. Although further study is required, it may be tentatively said that failure at the termination point is prevented if the failure mode factor is larger than 1.1.

REFERENCES

1) Public Works Research Institute, "Report on the Disaster Caused by the Miyagi-ken-oki Earthquake of 1978," Vol.159, March 1983 (in Japanese)

2) Narita, N., Murakami, M. and Asanuma, H., "Report of the Investigation on Earthquake Damage to Sizunai Bridge," 15th Joint Meeting, U.S.-Japan Panel on Wind and Seismic Effects, U.J.N.R., Tsukuba, Japan, 1983

3) Yamamoto, T., Ishibashi, T., Ohtsubo, M. and Kobayashi, S., "Experimental Study on Seismic Capacity of Bridge Piers with Termination of Longitudinal Reinforcement," Proc. of JSCE, Vol.348/V-1, Aug., 1984

4) Iwasaki, T., Kawashima, K., Hagiwara, R., Hasegawa, K., Koyama, T. and Yoshida, T., "Experimental Investigation on Hysteretic Behaviour of Reinforced Concrete Bridge Pier Columns," 17th Joint Meeting, U.s.-Japan Panel on Wind and Seismic Effects, U.J.N.R., Tsukuba, Japan, May, 1985

5) Ozaka, Y., Suzuki, M. and Kobayashi, S., "Investigation on the Effect of Termination of Longitudinal Reinforcement on Shear Strength of RC Beam," Proc. of JSCE, Vol.366/V-4, Feb., 1986

6) Ozaka, Y., Suzuki, M., Miyamoto, M. and Kobayashi, S., "Evaluation of Shear Strength of RC Beam with Termination of Longitudinal Reinforcement," Proc. of JSCE, Vol.378/V-1, Feb., 1987

7) Japan Road Association, "Specifications for Highway Bridges in Japan", May, 1980

8) Kawashima, K. and Unjoh, S., "An Inspection Method of Seismic Vulnerability of Existing Highway Bridges," Proc. of JSCE, No.416/I-13, April 1990

9) Japan Road Association, "Manual for Seismic Countermeasure Methods for Roads against Earthquakes, " March 1988

10) Kawashima, K., Unjoh, S. and Iida, H, "Seismic Inspection and Strengthening Methods for Reinforced Concrete Piers with Termination of Main Reinforcement at Mid-height," Technical Note of PWRI, Public Works Research Institute, Nov. 1990
11) Kawashima, K. and Koyama, Y., "Effect of Number of Loading Cycles on Dynamic Characteristics of Reinforced Concrete Bridge Pier Column," Proc. of JSCE, No.392/I-9, Apr. 1988
12) Kawashima, K. and Koyama, T., "Effects of Cyclic Loading Hysteresis on Dynamic Behavior of Reinforced Concrete Bridge Piers," Proc. of JSCE, No.398/I-10, Oct. 1988

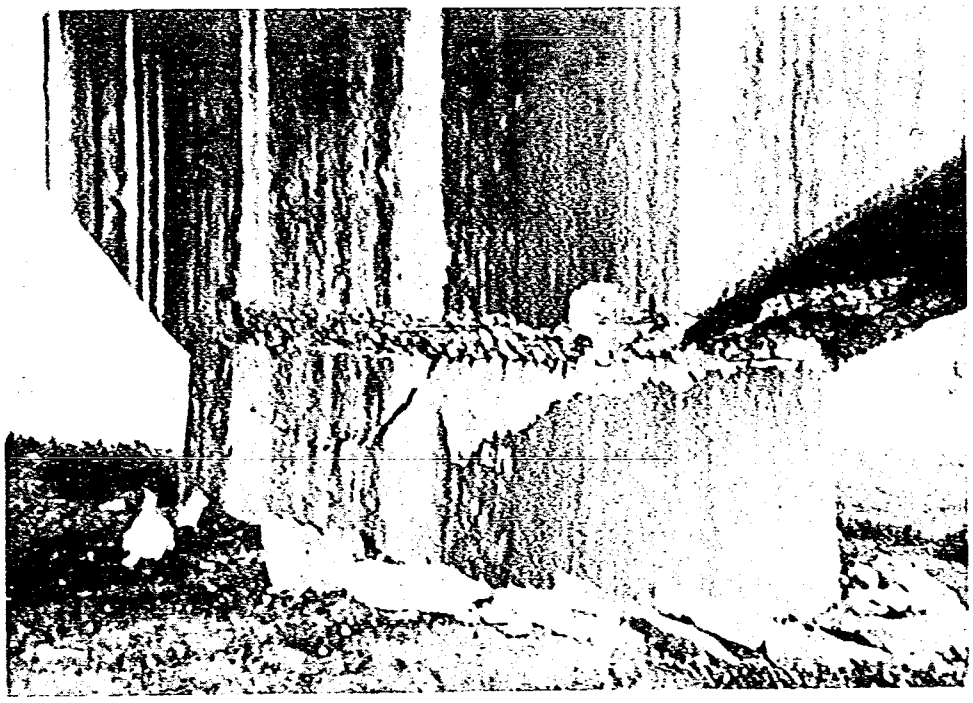


Photo 1 Pier Damage of the Sendai Bridge during the Miyagi-ken-oki Earthquake of 1978

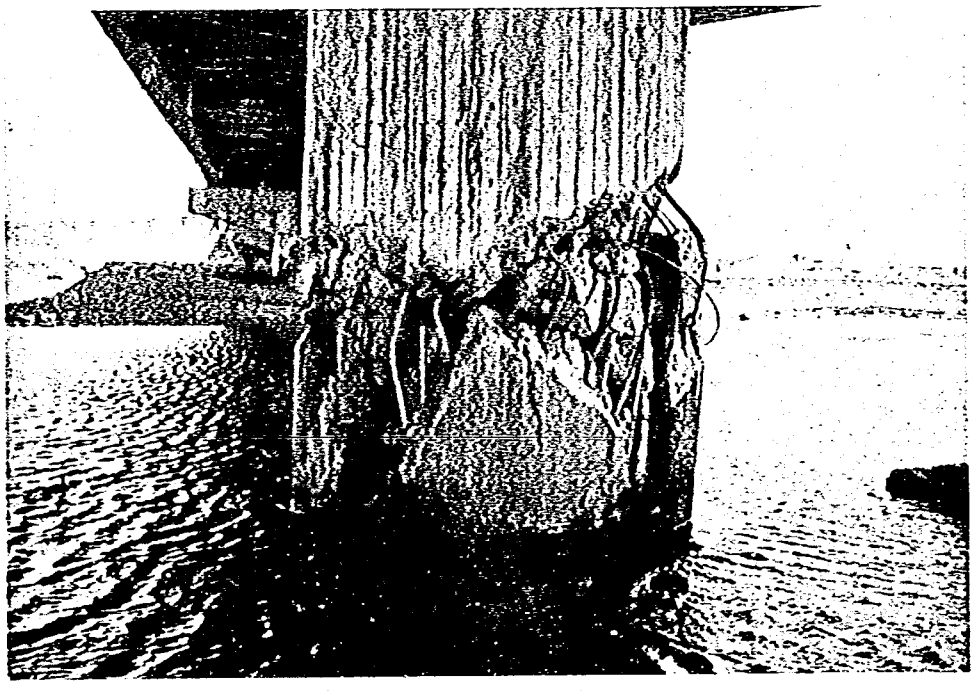


Photo 2 Pier Damage of the Sizunai Bridge during the Urakawa-oki Earthquake of 1982

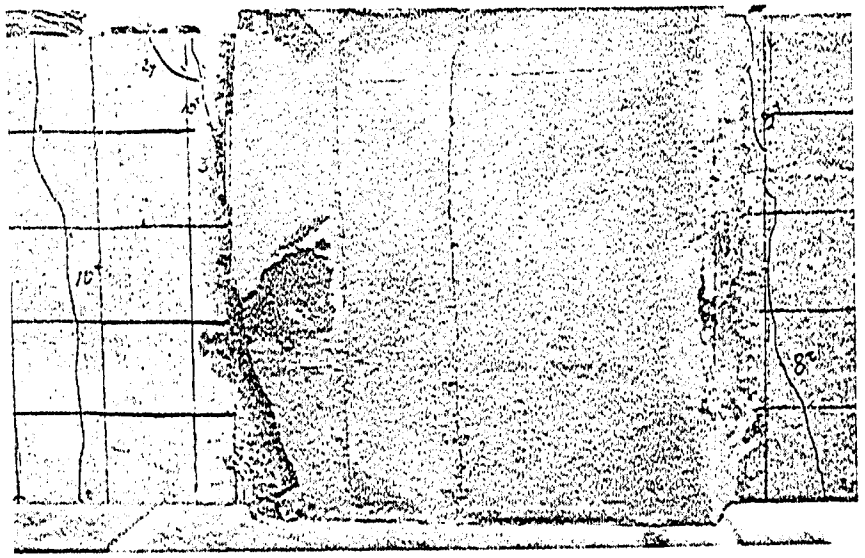


Photo 3 Crack along the Termination Point of Specimen 13 Strengthened by a 1D Long Steel Jacket with Concrete Mortar

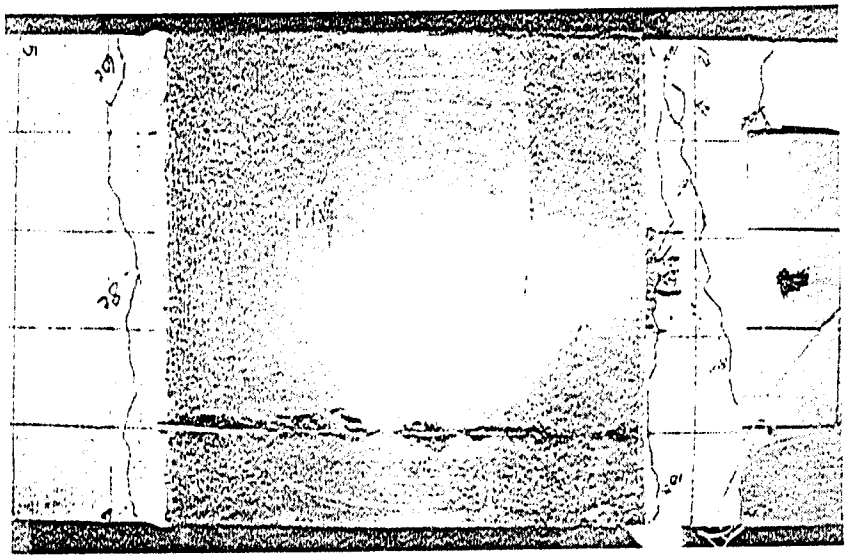


Photo 4 Crack along the Termination Point of Specimen 14 Strengthened by a 1D Long Steel Jacket with Epoxy Resin

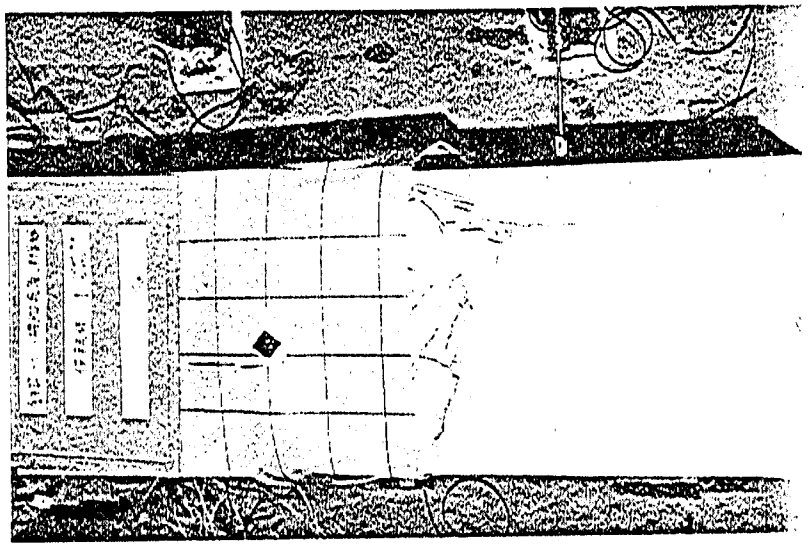


Photo 5 Deformed Steel Jacket and Crushing of the Injected Concrete Mortal in Specimen 15

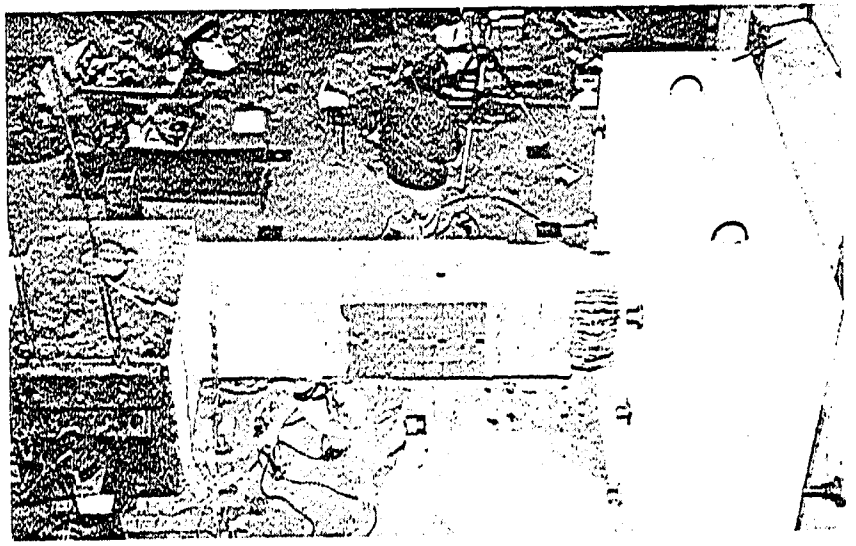


Photo 6 Effect of a Steel Jacket for Strengthening Reinforced Concrete Square Pier with Shear Span Ratio of 5.6 (Specimen 16)

Table 1 Test Specimens for Evaluating Vulnerability

Specimen No.		S－1	S－2	S－3	S－4	S－10	S－11	S－12
Cross Section [cm]		50 × 50						
Covering Depth of Concrete [cm]		3.5						
Effective Height [cm]		250				460		
Shear-Span Ratio		5.4				9.9		
Longitudinal Reinforcing Bar (Deformed Bar)	Material and Diameter [mm]	SD30, D13						
	Termination Point of Main Reinforcement from Base [cm]	Without Termination	110	135	160	180	205	230
	Ratio of Reinforcement [%] (after Termination [%])	2.03 (1.02)						
	Yield Strength [kgf/cm^2]	3,144				3,525		
Hoop Tie	Material and Diameter [mm]	SR24, ϕ 9						
	Ratio of Reinforcement [%]	0.10						
	Yield Strength [kgf/cm^2]	2,776				2,910		
Concrete	Material	Portland Cement						
	Max Grain Size of Aggregate [mm]	10						
	Uni-Axial Strength [kgf/cm^2]	327	332	325	429	429	409	390
Lateral Force	Direction of Loading	1-direction						
	Velocity of Loading [cm/sec]	5				10		
	Number of Loading for Each Specific Displacement	10						
	Loading Displacement [cm]	1.3				4.25		
Axial Force	Axial Force [tf]	4.11				25		
	Axial Stress [kgf/cm^2]	1.64				10		

Table 2 Test Specimens for Verifying Strengthening Method

Specimen No.		S－13	S－14	S－15	S－16	S－17	S－18	S－19	S－20
Cross Section [cm]		50×50					40×160		
Covering Depth of Concrete [cm]		3.5							
Effective Height [cm]		260							
Shear-Span Ratio		5.6					7.1		
Longitudinal Reinforcing Bar (Deformed Bar)	Material and Diameter [mm]	SD30, D10							
	Termination Point of Main Reinforcement from Base [cm]	90					80		
	Ratio of Reinforcement [%] (after Termination [%])	1.31 (0.63)					0.76 (0.38)		
	Yield Strength [kgf/cm²]	3,640		4,173	3,640	4,173	3,740		
Hoop Tie	Material and Diameter [mm]	SR24, φ6							
	Ratio of Reinforcement [%]	0.05					0.08		
	Yield Strength [kgf/cm²]	2,501		4,423	2,501	4,423	3,637		
Concrete	Material	Portland Cement							
	Max Grain Size of Aggregate [mm]	10							
	Uni-Axial Strength [kgf/cm²]	412	447	460	363	447	360	336	426
Lateral Force	Direction of Loading	1-direction							
	Velocity of Loading [cm/sec]	5							
	Number of Loading for Each Specific Displacement	10							
	Loading Displacement [cm]	1.5					1.7		
Axial Force	Axial Force [tf]	28.8					64		
	Axial Stress [kgf/cm²]	11.52					10		
Steel Jacket	Material (Width [cm], Thickness [mm])	SPCC (1D, 1)	SPCC (1D, 1)	SPCC (1.5D, 1)	SPCC (1.5D, 1)	SPCC (1.5D, 0.6)	－	SPCC (1.5D, 1)	SPCC (2D, 1)
	Injection Material and Thickness [mm]	Concrete Mortar 20	Epoxy Resin 3	Concrete Mortar 20	Epoxy Resin 3	Epoxy Resin 3	－	Concrete Mortar 20	Concrete Mortar 20

Note) SPCC represents "Cold Rolled Steel Sheet".

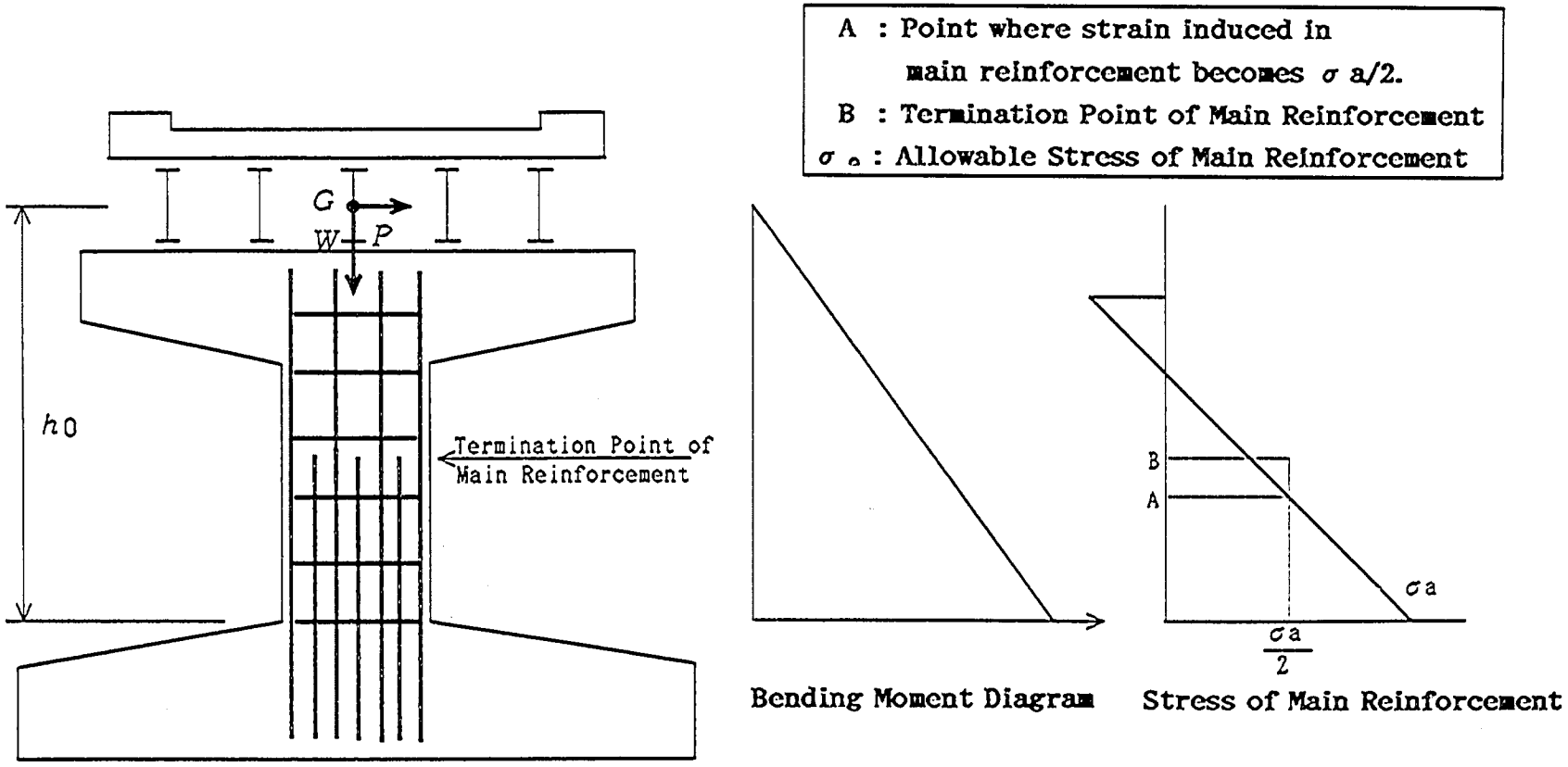


Fig.1 Termination of Main Reinforcement at Mid-Height

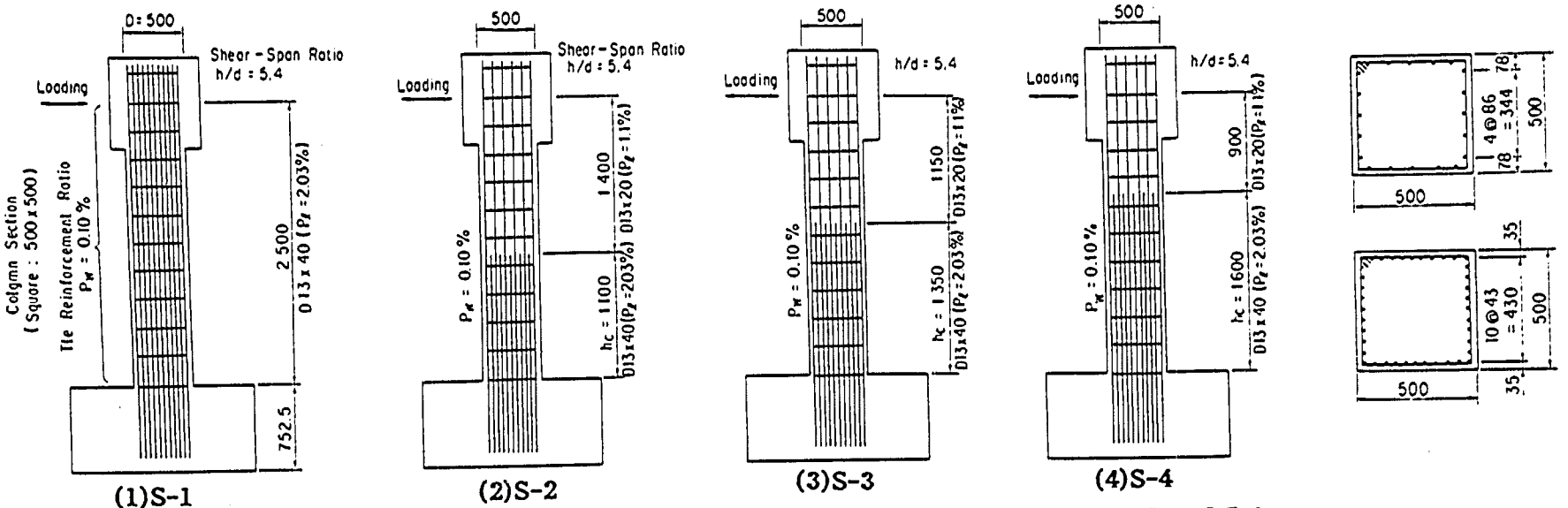


Fig.2 Reinforced Concrete Pier Specimens with Shear Span Ratio of 5.4 to study Effect of Anchorage Length of Main Reinforcement

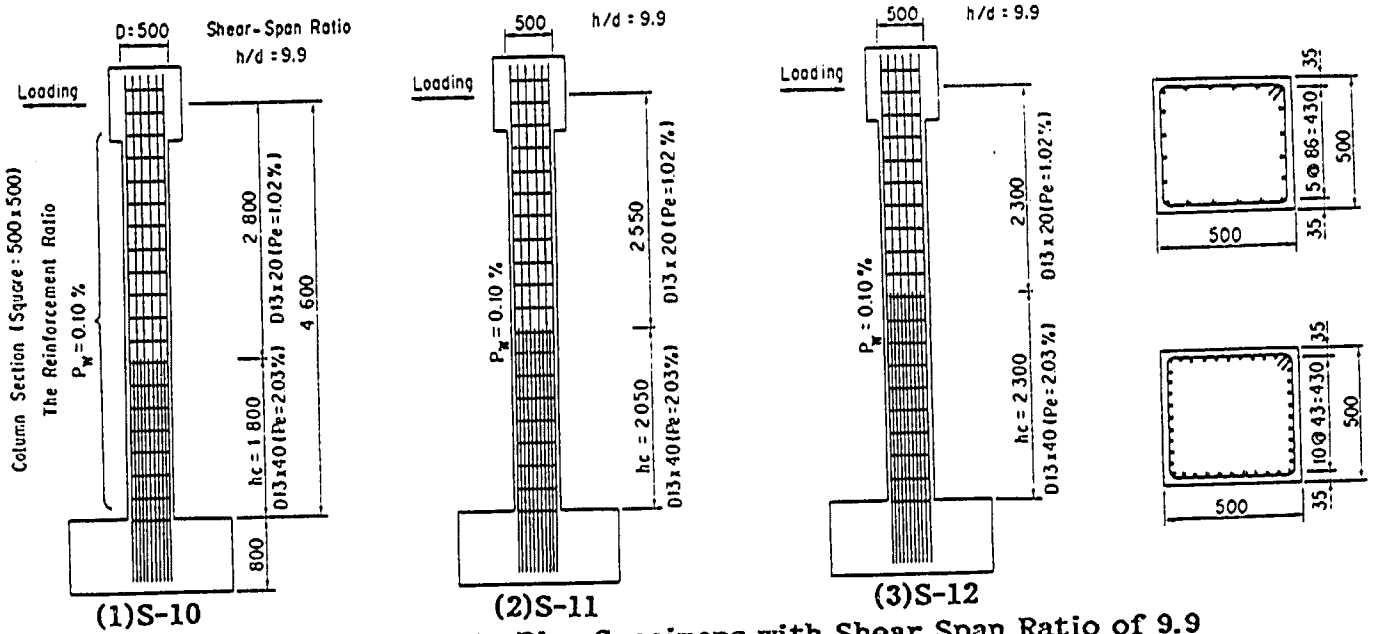


Fig.3 Reinforced Concrete Pier Specimens with Shear Span Ratio of 9.9 to study Effects of Anchorage Length of Main Reinforcement

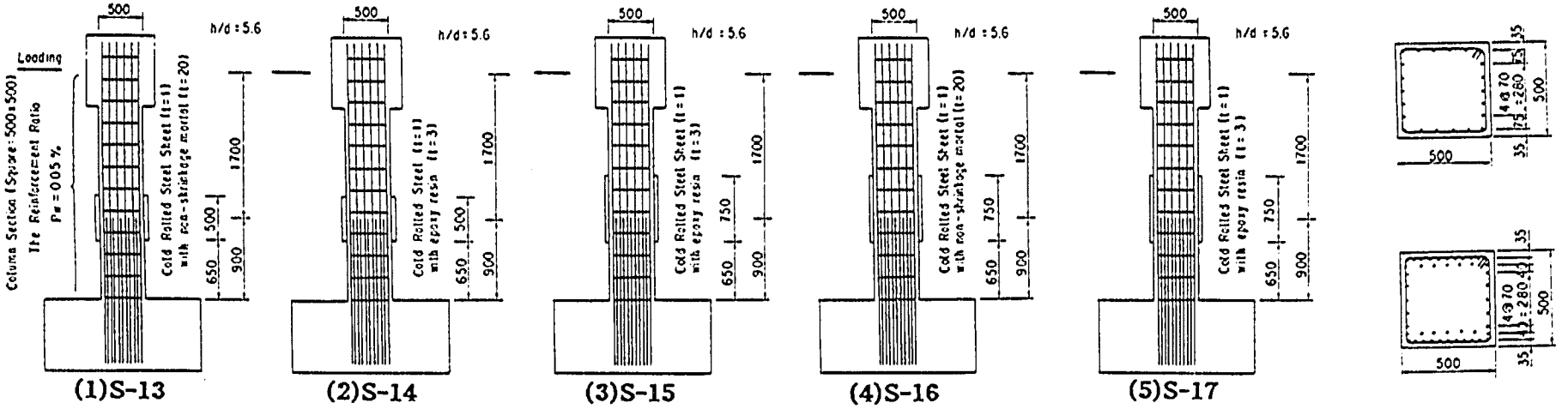


Fig.4 Reinforced Concrete Square Pier Specimens with Shear Span Ratio of 5.6 to study Strengthening Method by Means of A Steel Jacket

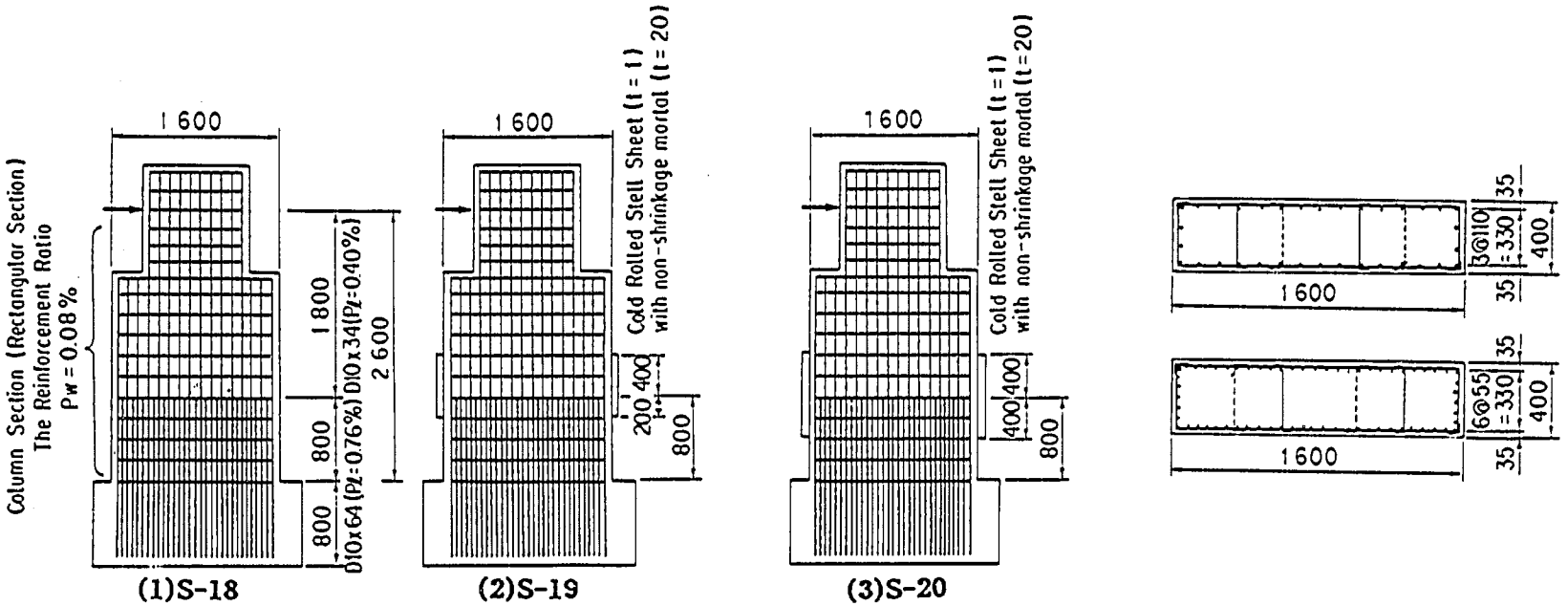


Fig.5 Reinforced Concrete Wall Type Pier Specimens with Shear Span Ratio of 7.1 to study Strengthening Method by Means of A Steel Jacket

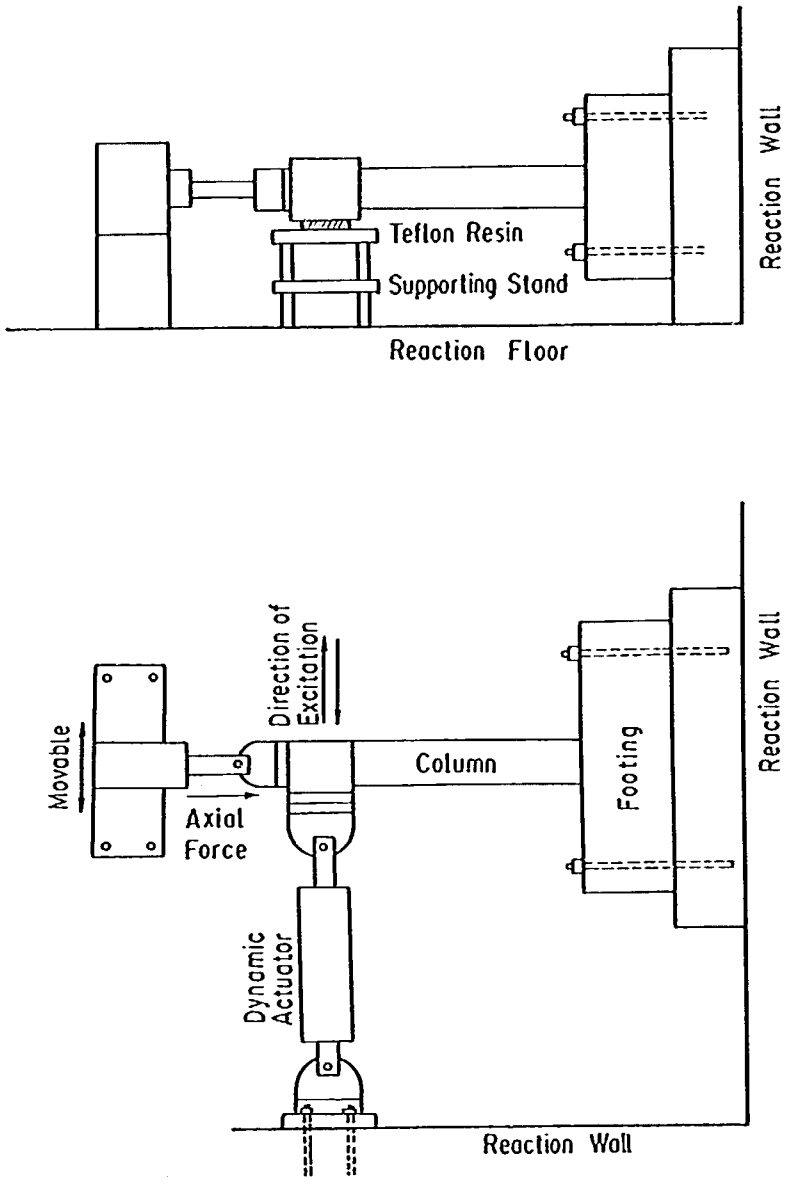


Fig.6 Experimental Set-up

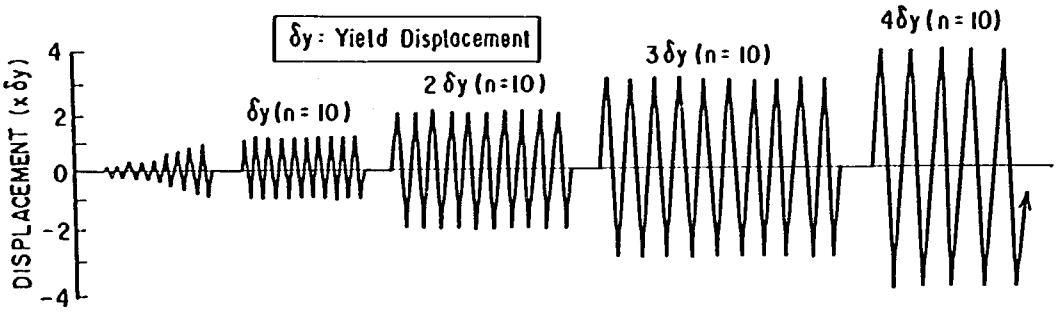
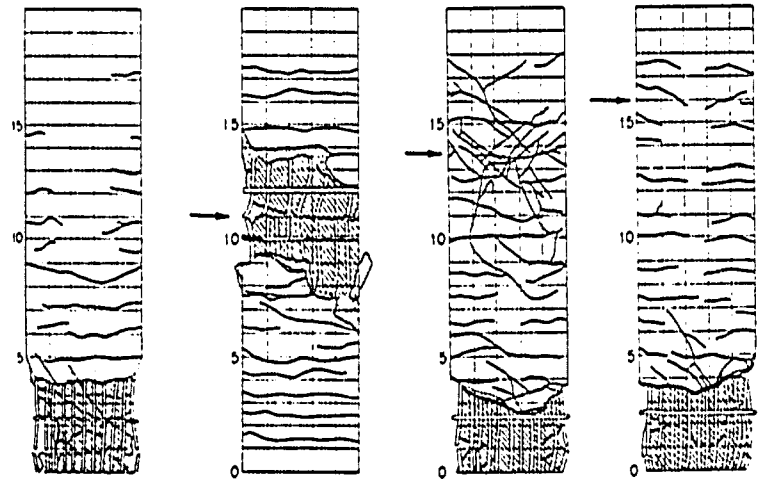
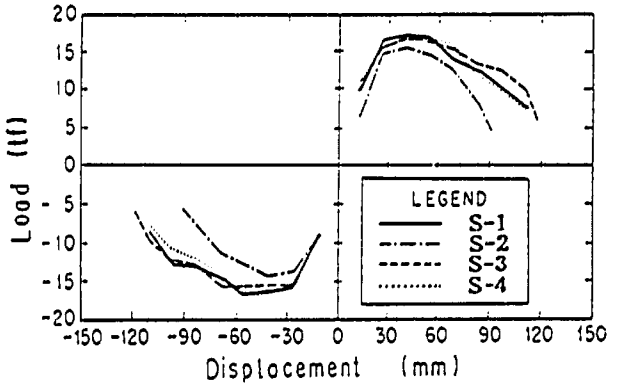
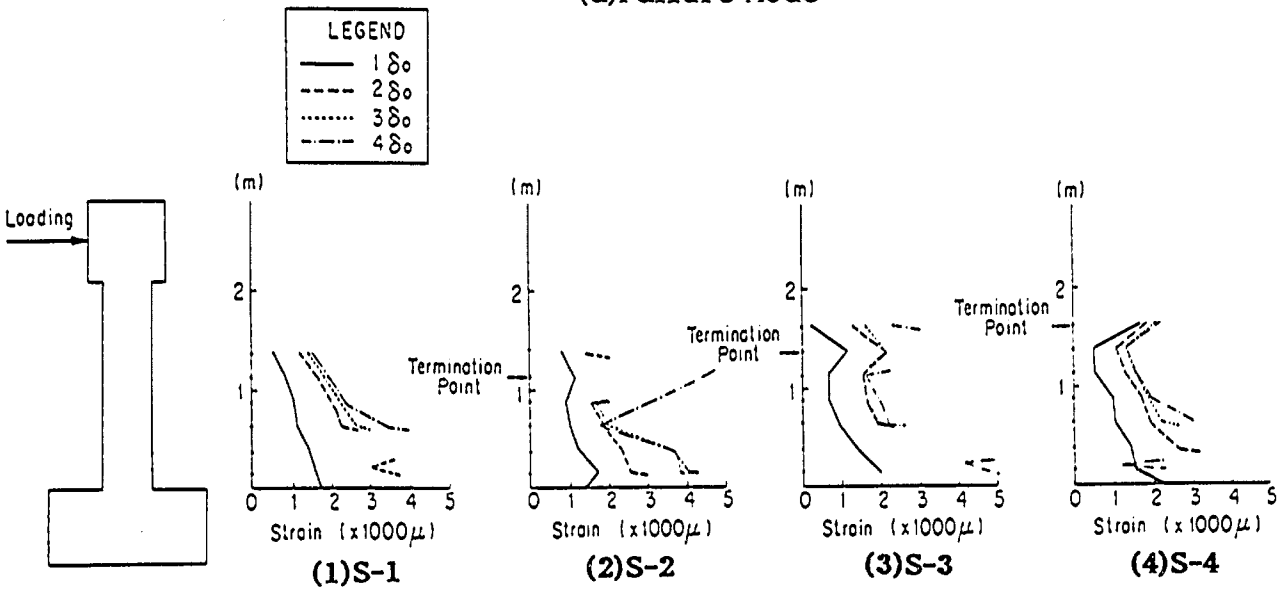


Fig.7 Step-wise Increasing Symmetric Loading Displacement

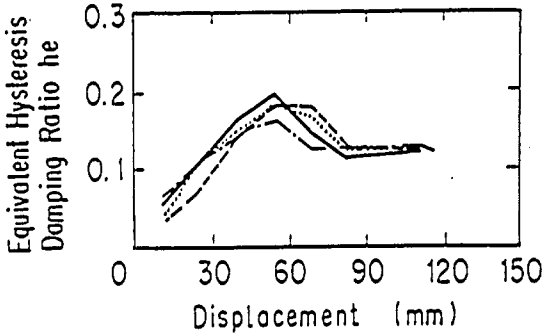


(a)Failure Mode



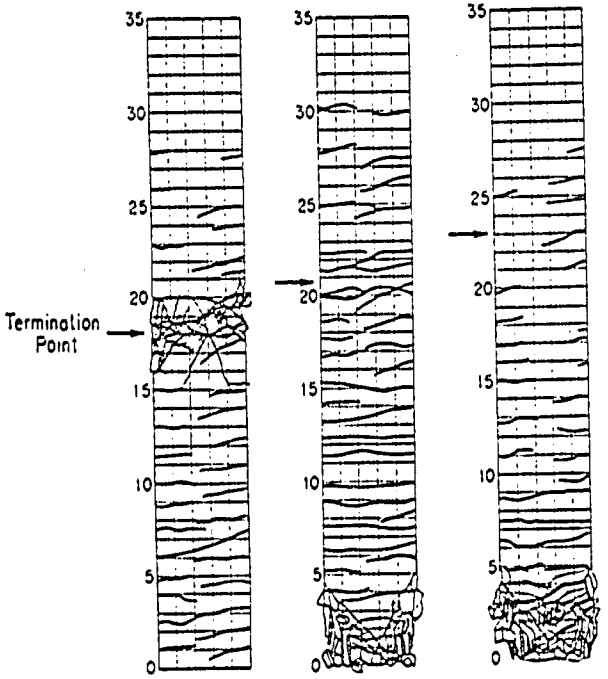


(b)Strain Developed in Main Reinforcement

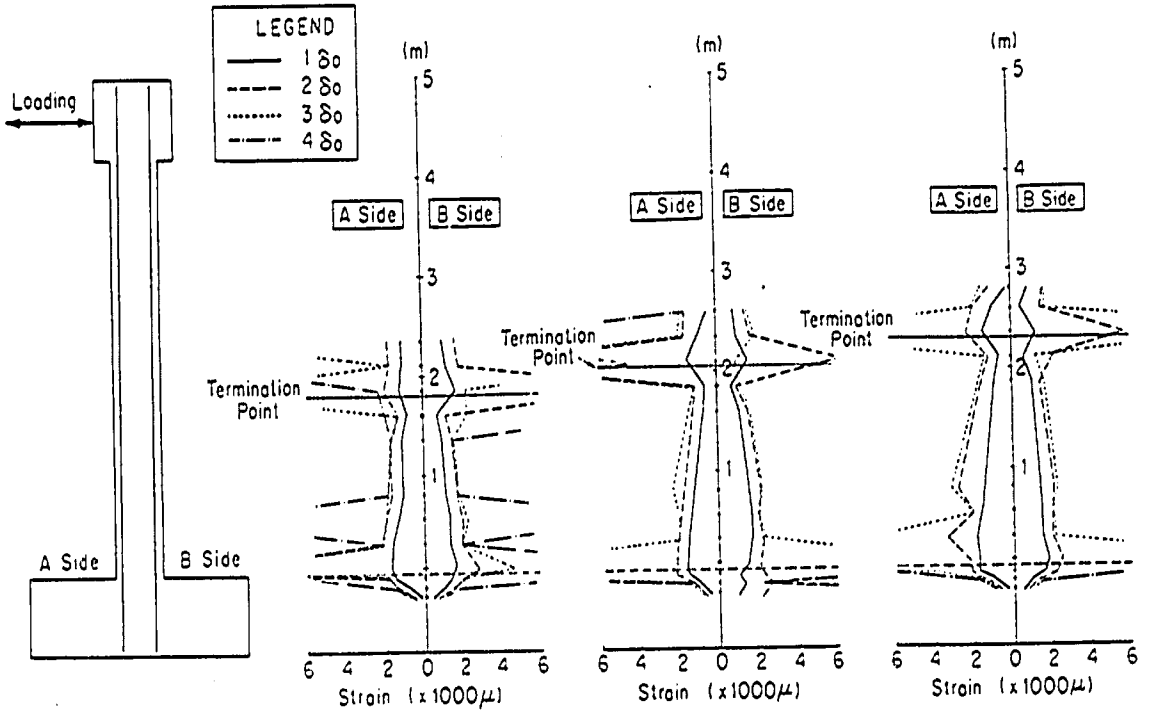


(c)Envelope of Load-Displacement Hysteresis Loops and Equivalent Hysteresis Damping Ratio

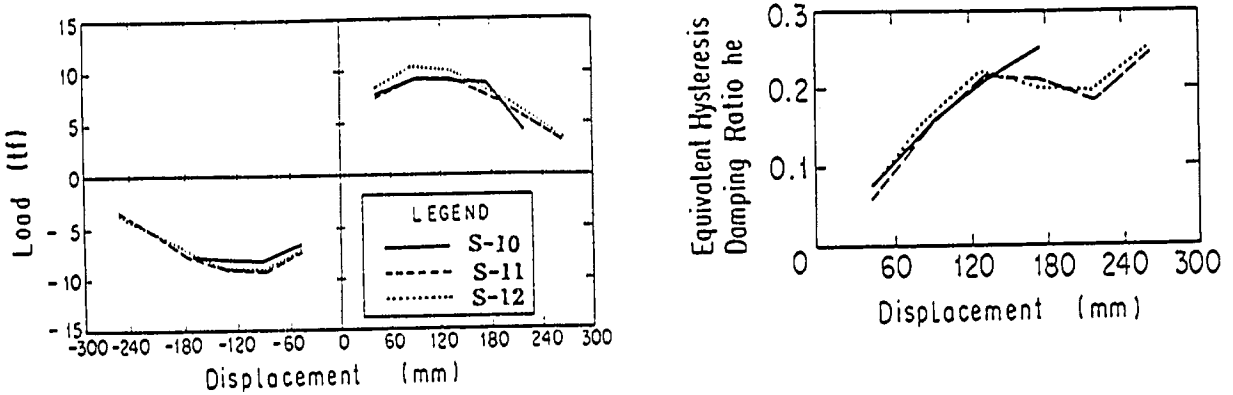
Fig.8 Effect of Anchorage Length for Specimens with Shear Span Ratio of 5.4 (Specimens 1 to 4)



(a)Failure Mode



(b)Strain Developed in Main Reinforcement



(c)Envelope of Load-Displacement Hysteresis Loops and Equivalent Hysteresis Damping Ratio

Fig.9 Effect of Anchorage Length for Square Specimens with Shear Span Ratio of 9.9 (Specimens 10, 11 and 12)

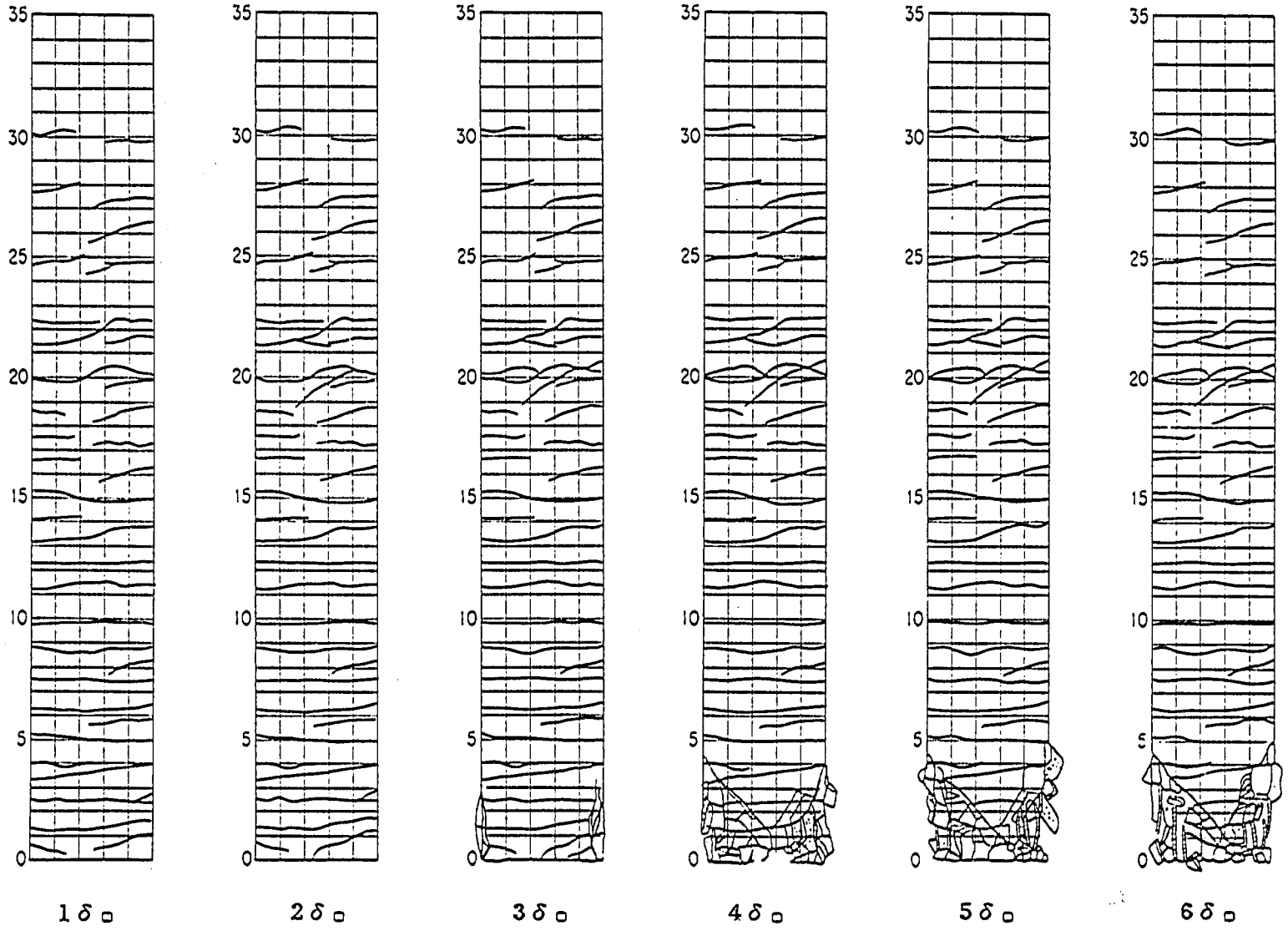
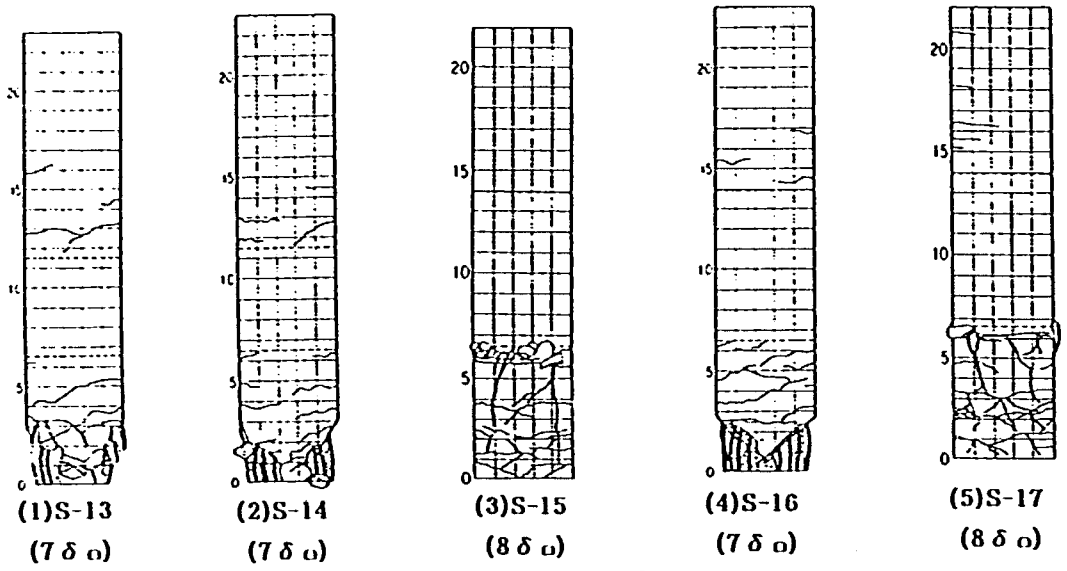
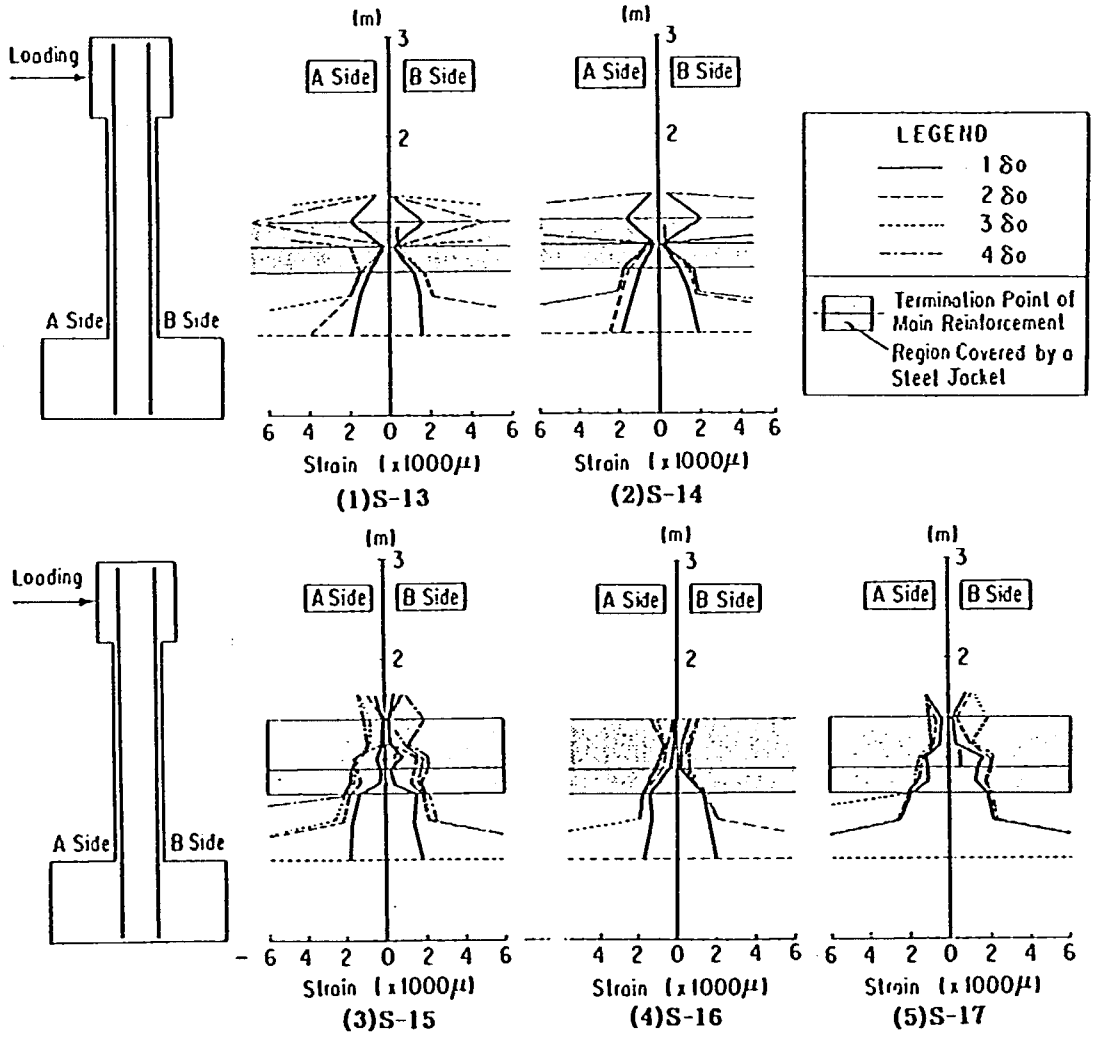


Fig.10 Effect of Anchorage Length of Main Reinforcement in Terms of Progress of Failure Mode for Specimens with Shear Span Ratio of 9.9 (Specimen 11)



(a)Failure Mode



(b)Strain Developed in Main Reinforcement

Fig.11 Effect of Strengthening Method by A Steel Jacket for Square Specimens with Shear Span Ratio of 5.6 (Specimens 13 to 17)

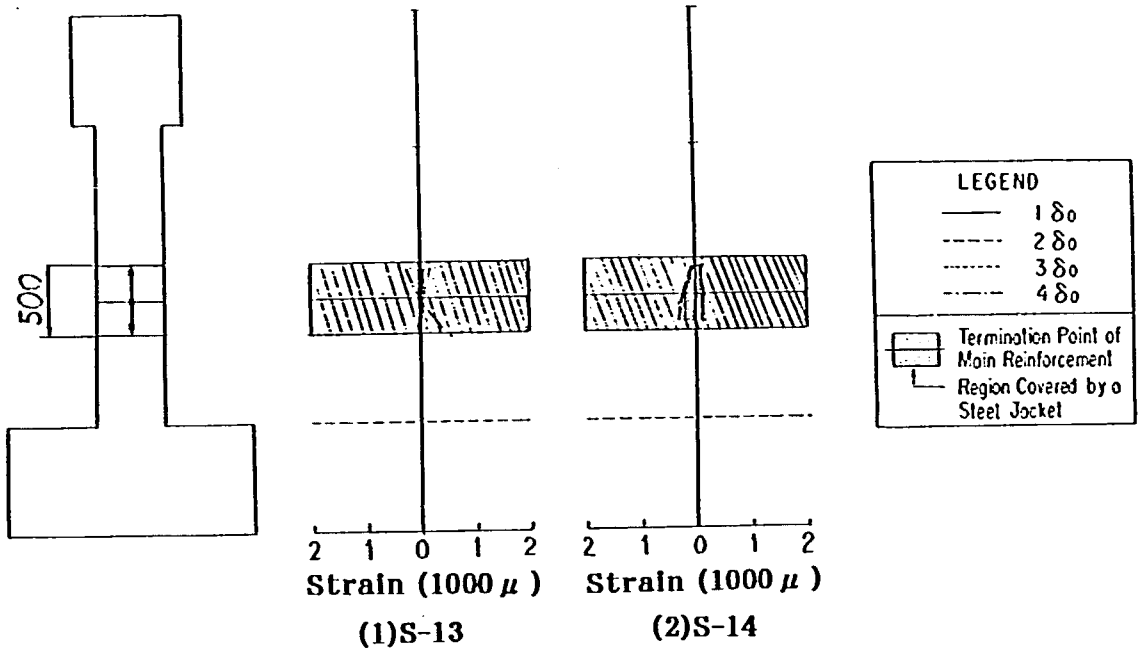


Fig.12 Strain induced in the 1D Long Steel Jacket, in Vertical Direction, in Specimen 13 (Mortar Injection) and Specimen 14 (Epoxy Injection)

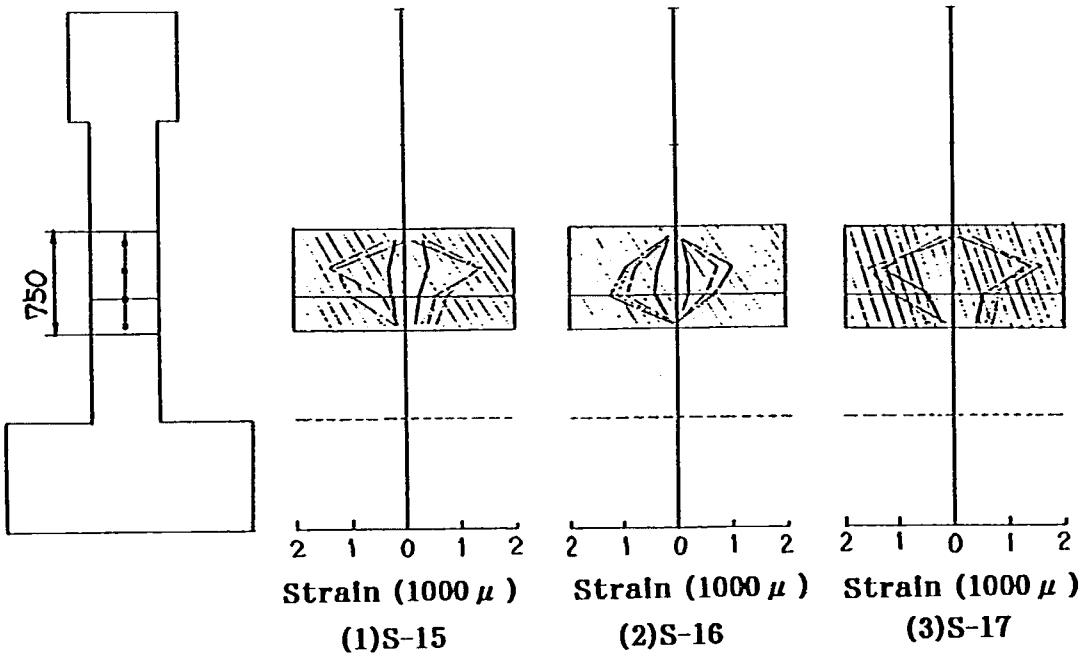
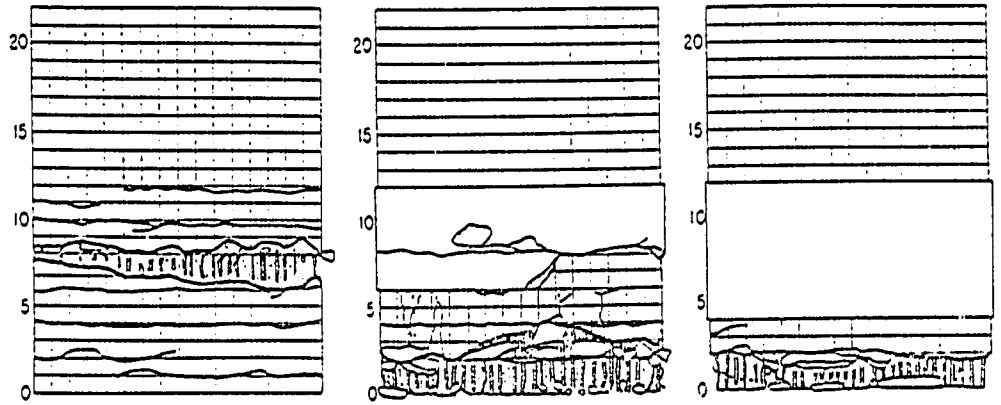
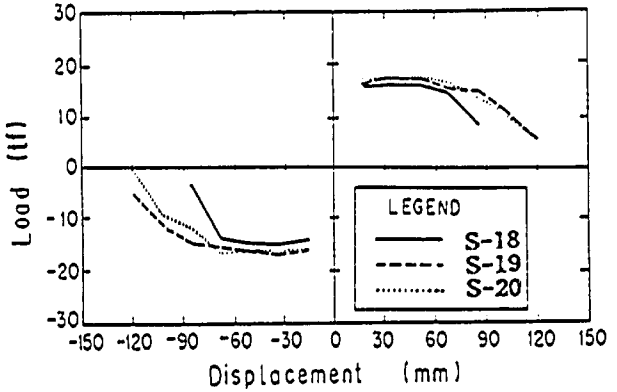


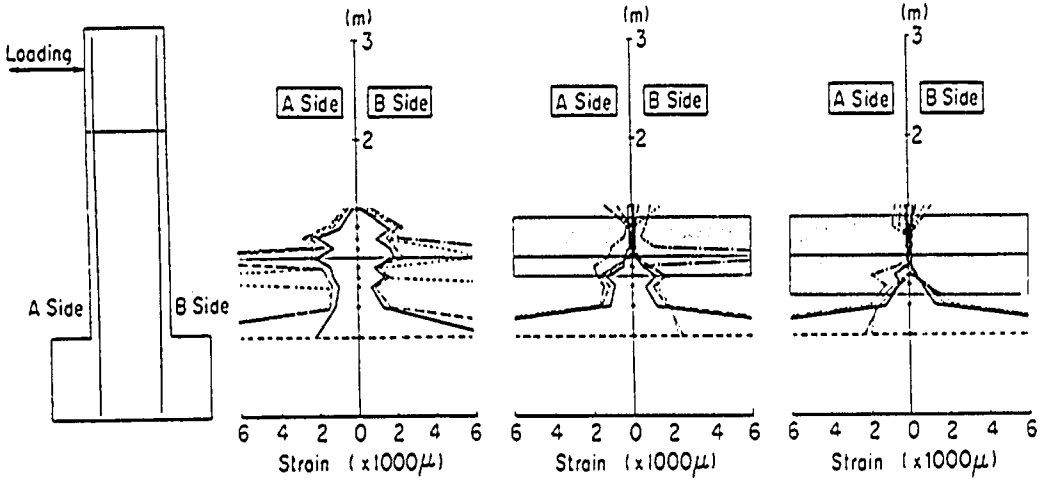
Fig.13 Strain induced in the 1.5D Long Steel Jacket, in Vertical Direction, in Specimen 15 (Mortar Injection), Specimen 16 (Epoxy Injection) and Specimen 17 (Epoxy Injection, t=0.6mm)



(1)S-18 ($5\delta_o$)　(2)S-19 ($7\delta_o$)　(3)S-20 ($7\delta_o$)

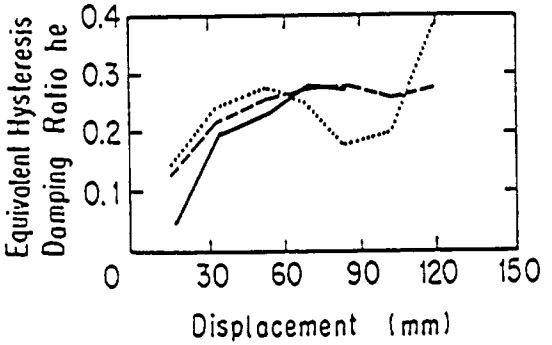
(a)Failure Mode





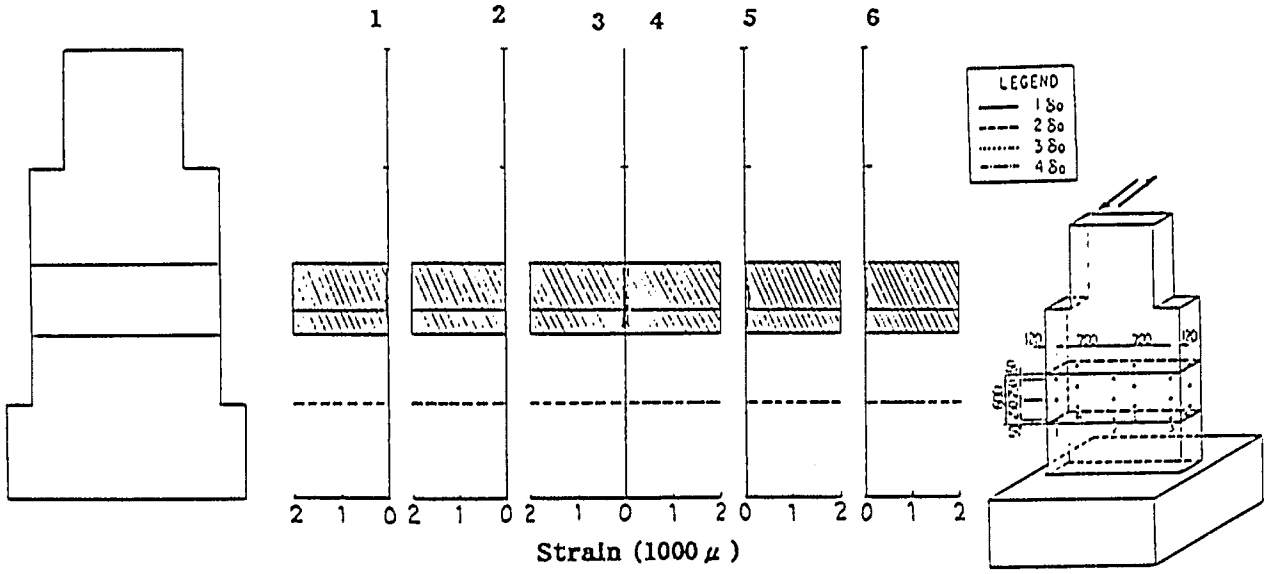
(1)S-18　(2)S-19　(3)S-20

(b)Strain Developed in Main Reinforcement

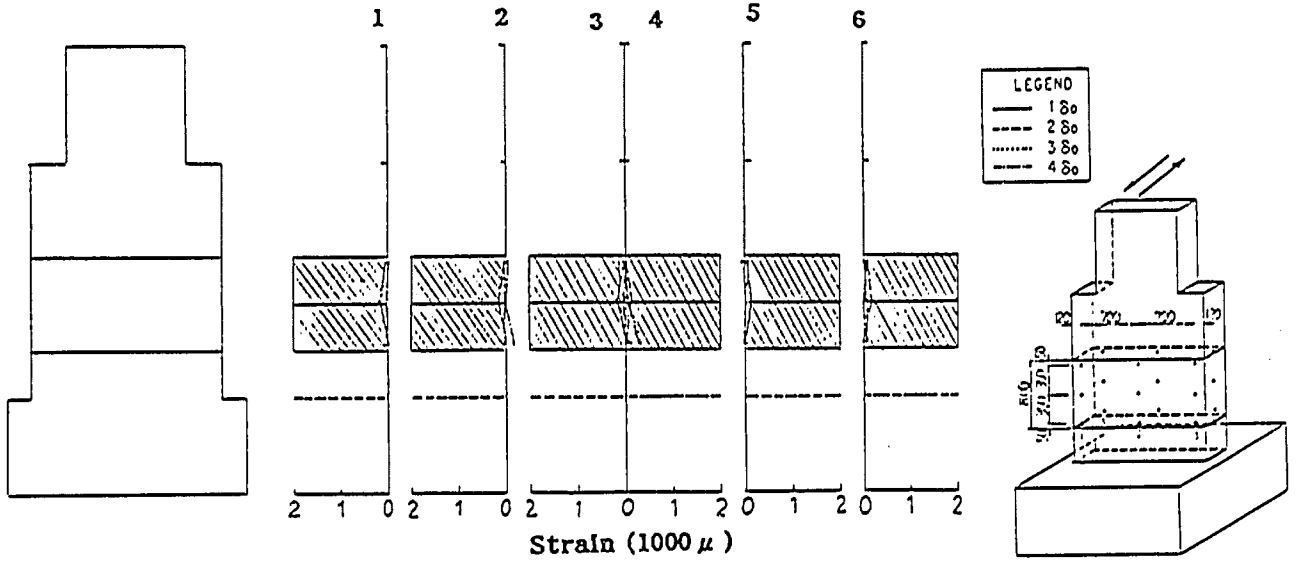


(c)Envelope of Load-Displacement Hysteresis Loops and Equivalent Hysteresis Damping Ratio

Fig.14 Effect of Strengthening Method by a Steel Jacket for Wall Type Specimens with Shear Span Ratio of 7.1 (Specimens 18, 19 and 20)



(1)Specimen 19 strengthened by 1.5D Long Steel Jacket and Mortar Injection



(2)Specimen 20 strengthened by 2D Long Steel Jacket and Mortar Injection

Fig.15 Strain induced in the Steel Jacket in Vertical Direction

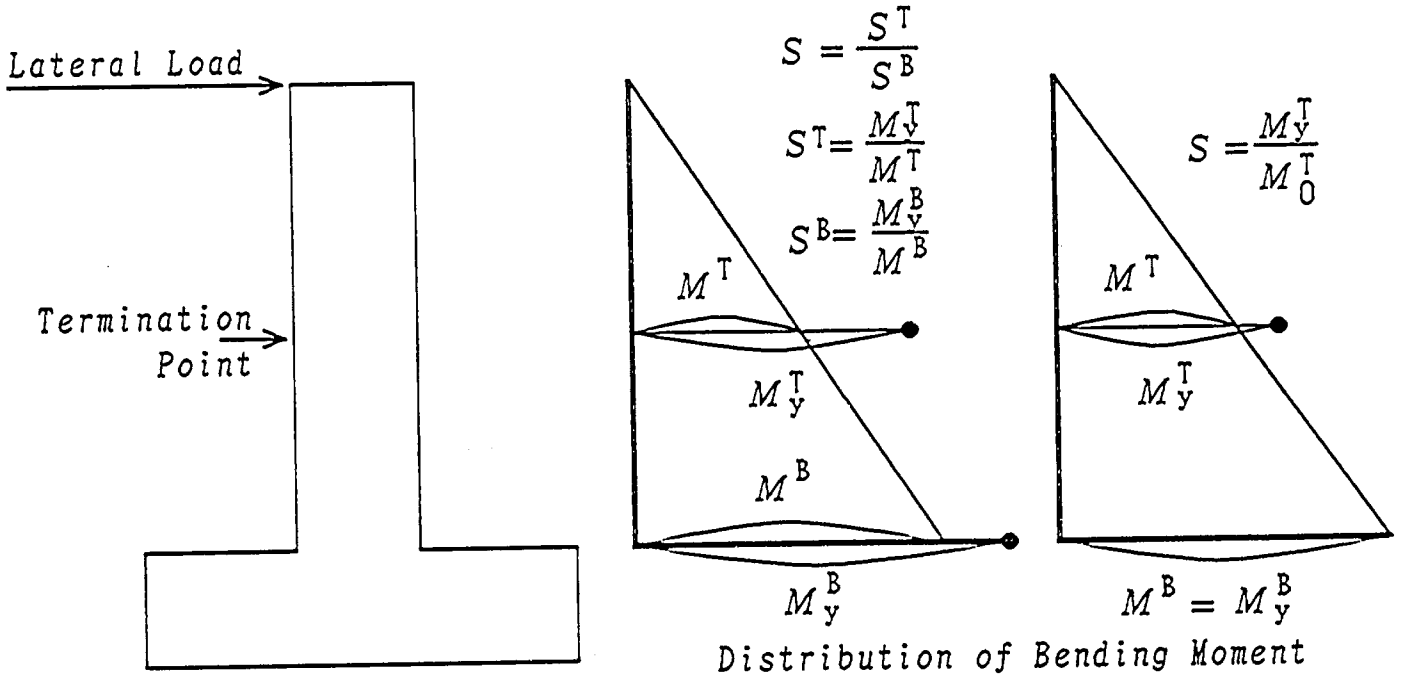
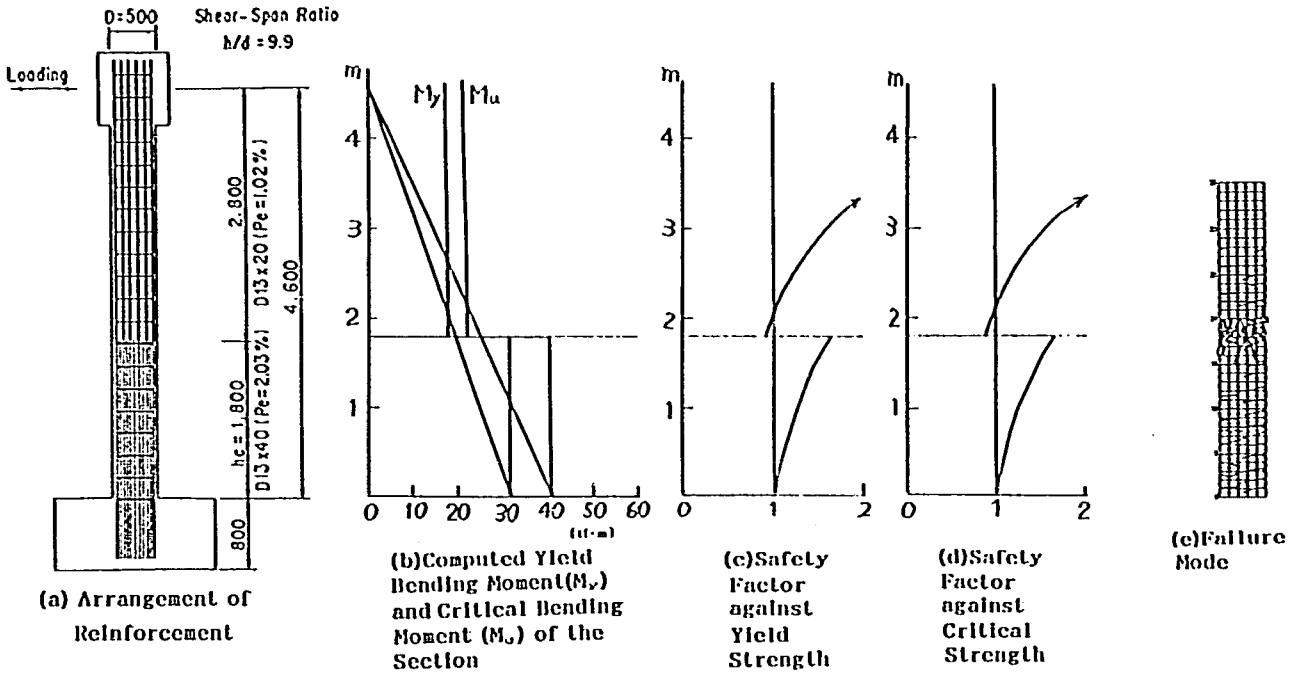


Fig.16 Definition of Failure Mode Factor to Evaluate Vulnerability of Reinforced Concrete Piers with Termination of Main Reinforcement



(a) Arrangement of Reinforcement

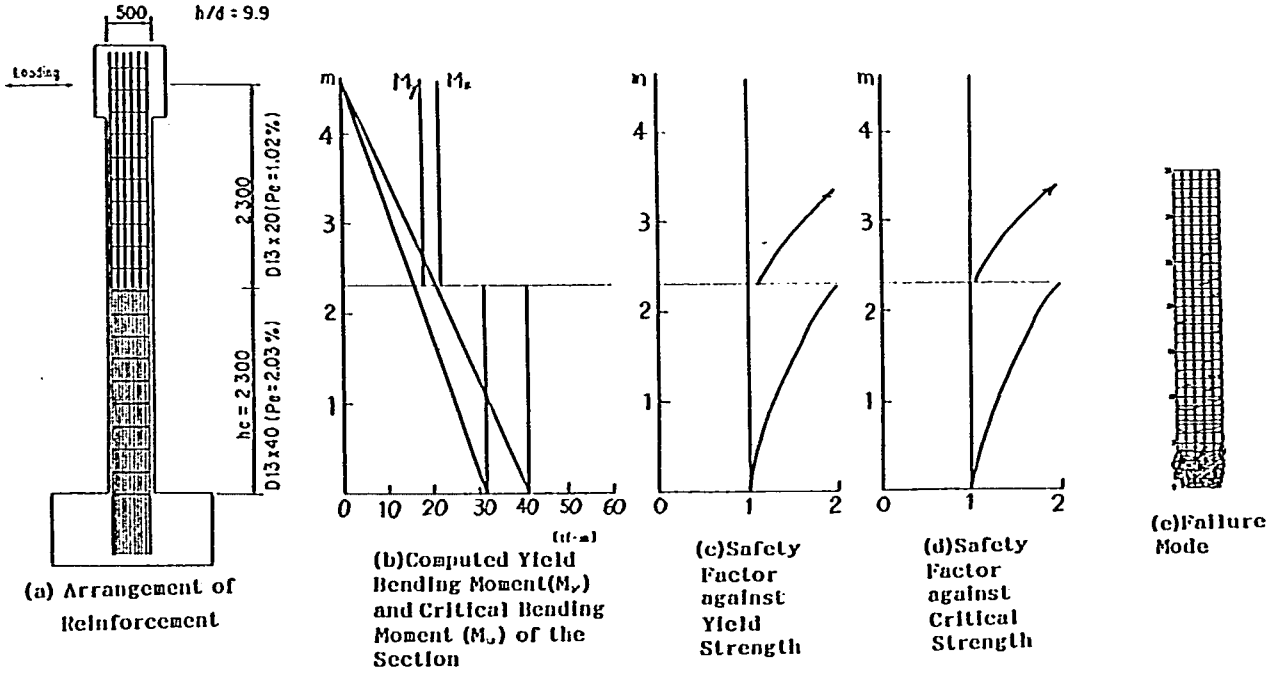
(b)Computed Yield Bending Moment(M_y) and Critical Bending Moment (M_u) of the Section

(c)Safety Factor against Yield Strength

(d)Safety Factor against Critical Strength

(e)Failure Mode

(1)Specimen 1



(a) Arrangement of Reinforcement

(b)Computed Yield Bending Moment(M_y) and Critical Bending Moment (M_u) of the Section

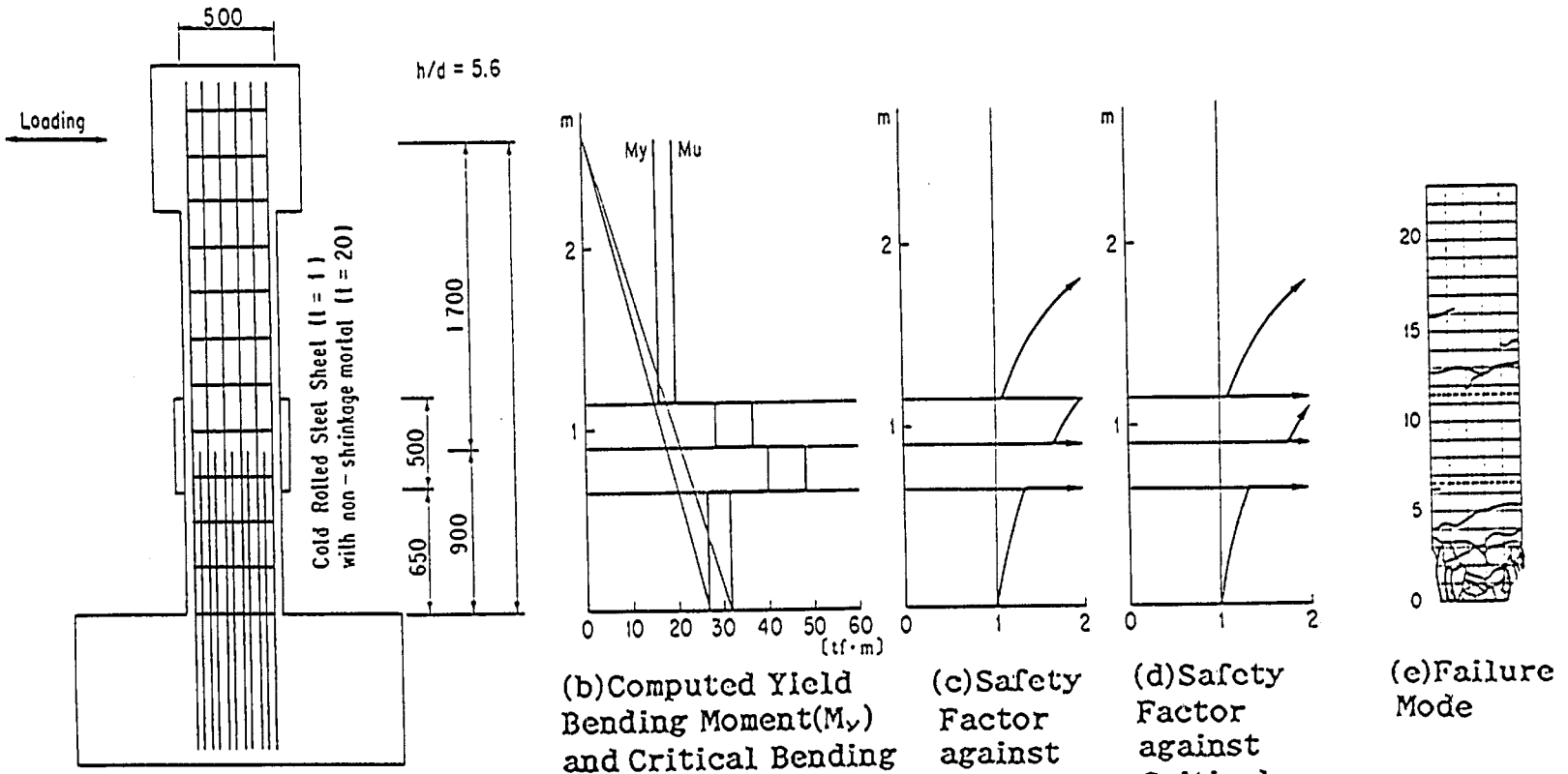
(c)Safety Factor against Yield Strength

(d)Safety Factor against Critical Strength

(e)Failure Mode

(2)Specimen 3

Fig.17 Evaluation of Failure Mode Factors for Specimens 1 and 3



(a) Arrangement of Reinforcement

(b)Computed Yield Bending Moment(M_y) and Critical Bending Moment (M_u) of the Section

(c)Safety Factor against Yield Strength

(d)Safety Factor against Critical Strength

(e)Failure Mode

Fig.19 Evaluation of Failure Mode Factors for Specimen 13

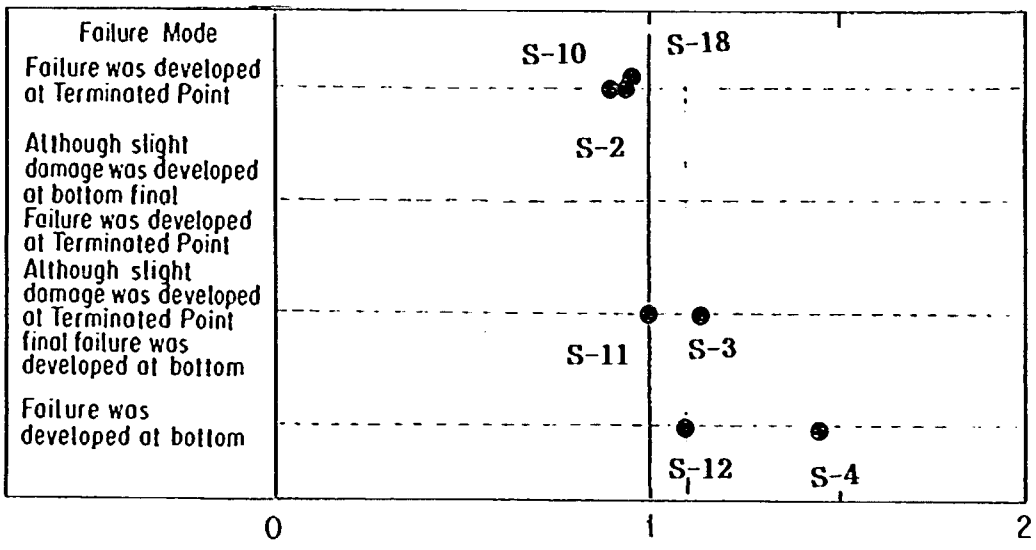


Fig.18 Evaluation of Failure Mode in Terms of Failure Mode Factor

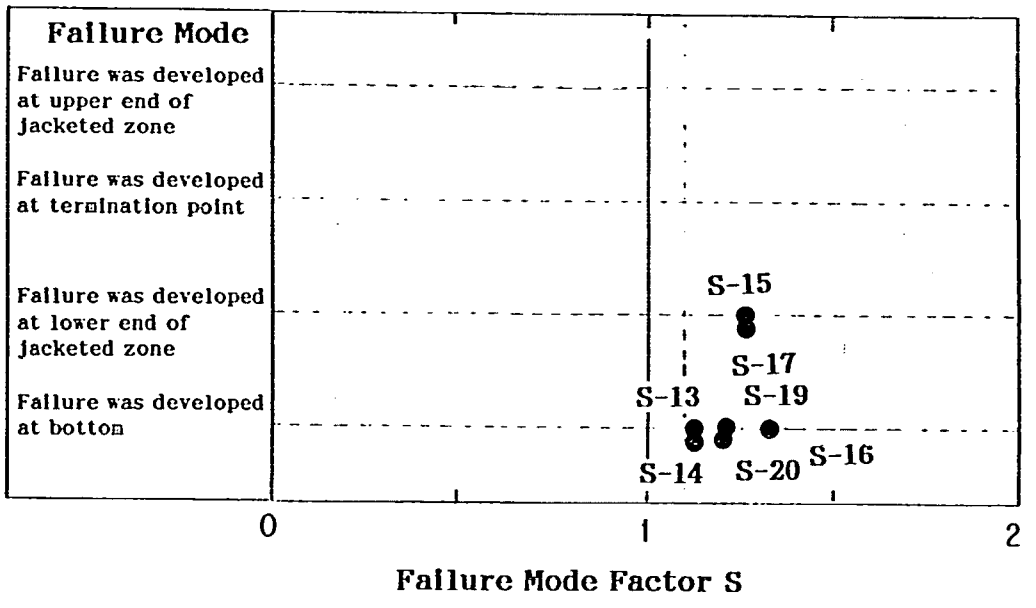


Fig.20 Evaluation of Failure Mode in Terms of Failure Mode Factor for Specimens Strengthened by a Steel Jacket

REPAIR AND RETROFIT OF STEEL PIERS

by
Gregory A. MACRAE
Kazuhiko KAWASHIMA
and
Kinji HASEGAWA

U.S. — JAPAN WORKSHOP ON SEISMIC RETROFIT OF BRIDGES
Tsukuba Science City, Japan
December 1990

REPAIR AND RETROFIT OF STEEL PIERS

Gregory A. MACRAE[1]
Kazuhiko KAWASHIMA[2]
Kinji HASEGAWA[3]

Presenting Author : Gregory A. MacRae

ABSTRACT

Two types of external steel plates were welded onto the outside of rectangular hollow steel bridge pier specimens in order to repair them after they had been subjected to moderate and large amounts of earthquake-type action. The strength and ductility capacity of the repaired specimens was found to be better than that of the original specimens when further deformation was imposed. Retrofit of piers by adding concrete increased the strength of the piers by up to 34% but brittle fracture sometimes decreased the ductility capacity. A method of increasing the deformation capacity without increasing the strength was proposed.

INTRODUCTION

Steel bridge piers have been used over the past 30 years for the construction of bridges on the national road transportation network in Japan. The construction cost of these piers is generally more than that of reinforced concrete piers but the section size is significantly smaller making them ideal for use in city locations where land prices are high and where there are restrictions on construction space. Damage has not been observed in this sort of pier to date during a real earthquake and tests to understand their strength, ductility capacity and repairability have only recently been performed.

It is anticipated that steel piers supporting existing bridges may yield in a major earthquake because inertia forces of more than three times the design load resistance level are expected to be developed. These piers are expected to behave in one of two ways:

1) Piers may successfully resist the earthquake by deforming inelastically. However, if there is a major loss of strength or a large amount of deformation then effective repair methods will be required so that the pier resistance will be sufficient during future major earthquakes, or
2) Piers may suffer severe damage and be unrepairable. Retrofit is therefore required before the earthquake occurs in order to ensure satisfactory behaviour.

The tests described here were carried out to find effective methods for repair and retrofit of steel piers [1] and the results were included in the Manual of Seismically Damaged Civil Engineering Structures [2].

A typical steel pier of the sort used in Japan is shown in Figure 1. It consists of four plates welded together into a box shape and other plates are welded internally to provide longitudinal and lateral stiffness. Design of this pier type is carried out according to the "Specifications for Highway Bridges" issued by the Ministry of Construction [3]. Two types of buckling which are checked during the design are:

a) overall buckling of one side, and
b) local buckling of the panel between the longitudinal stiffeners (local panel buckling).

These deformation modes are shown in Figure 2(a) and (b) respectively. An indication of which of these modes of buckling is likely to occur first is also available [4].

The method of retrofit which should be used on a pier depends on the type of buckling deformation and failure mechanism which is likely to occur. Tests on twenty two piers have been conducted at PWRI in order to understand their strength and deformation capacity [5]. Points of interest from these tests related to the mode of failure of piers and which may affect the retrofit or repair procedure are:

1) The height of the major buckle was midway between the base and the first lateral stiffener in the piers which failed by overall buckling of one side.

---

[1] Researcher, Earthquake Engineering Division, Public Works Research Institute, Tsukuba, Japan
[2] Head, Earthquake Engineering Division, Public Works Research Institute, Tsukuba, Japan
[3] Senior Research Engineer, Earthquake Engineering Division, PWRI, Tsukuba, Japan

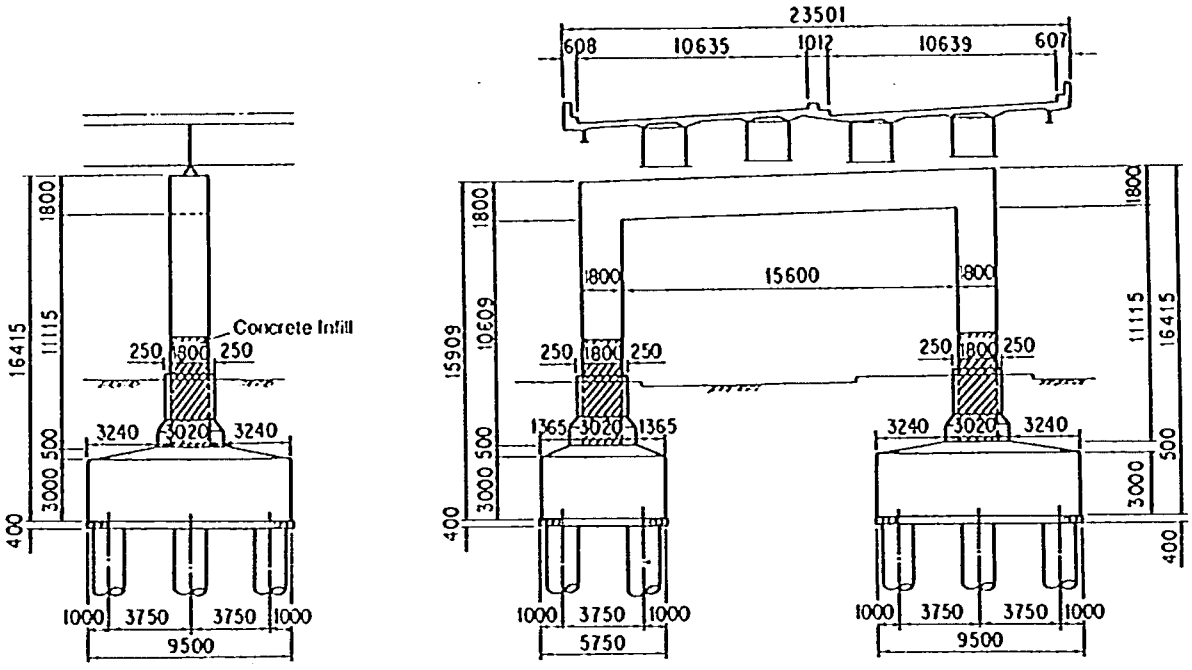


Figure 1. Elevation of a Typical Pier

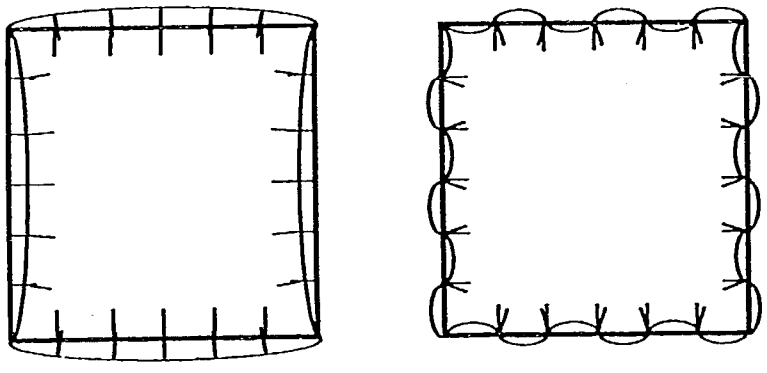


Figure 2. Modes of Buckling

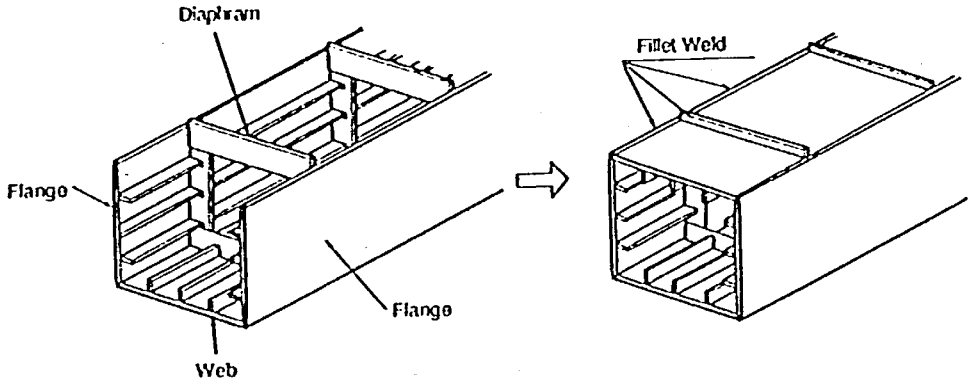


Figure 3. Construction Drawing

2) Piers which failed by local panel buckling sustained either a very localized buckle or no buckle at all and failed by fracture of the steel near or in the weld at the base.
3) Some piers with concrete infill over the bottom third of their height were also tested . The added concrete may be considered as a method of pier retrofit. The results of these tests are discussed later in this paper.
4) Piers tested on the shaking table underwent very little yield reversal and the displacement at the top increased only in one direction. Large residual displacements were observed at the top of the piers after the tests were completed which indicated that full repair may be difficult to perform.

REPAIR OF STEEL PIERS

Test Specimens

Real piers are generally large enough that a person may enter and weld from the inside but the pier specimens used in these tests were too small for this construction technique to be used. The pier was therefore constructed in stages as shown in Figure 3. Weld was applied to the inside of the specimen before the final web-plate was welded into place from the outside. The diaphrams extended outside the section on one side to facilitate the welding of the final web plate to the specimen. The longitudinal stiffeners on the inside of the final web plate were discontinuous at the diaphram positions and at the base.

Four piers of the type shown in Figure 4 were tested in the test configuration shown in Figure 5. The effectiveness of repair with "strengthening plates" or "contact plates" as shown in Figure 6 was investigated. These methods are discussed in detail later in the paper. The third panel from the top was constructed from a weaker steel (SM50Y steel) than the other panels (SM58 steel). This region was made weak so that the inelastic action would occur there and so that repair could be carried out easily. Damage in actual piers would be expected to occur in the base section and foundation concrete may need to be dug out in order to retrofit. The section sizes are given in Table 1 and the calculated yield strengths, yield displacements and plastic strength of each specimen are given in Table 2. Displacement-controlled cyclic applied lateral loading was applied to multiples of the yield displacement, d_y, where d_y was calculated as the displacement at the loading point when the compression flange at the base of the middle section (SM50Y steel) yielded.

Table 1: Specimen Sizes (mm)

Central Region (SM50Y Steel)	Flange Size b_f x t_f	600 x 7.1
	Web Size b_w x t_w	600 x 6.4
	Rib Size b_r x t_r	50 x 6.4
Base Region (SM58 Steel)	Flange Size b_f x t_f	600 x 8.2
	Web Size b_w x t_w	600 x 7.3
	Rib Size b_r x t_r	50 x 6.3

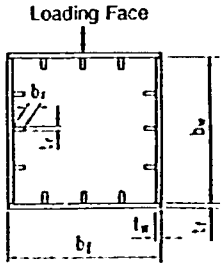


Table 2: Predicted Yield Force, P_y, Yield Displacement, d_y, and Plastic Force, P_p.

Specimen Number		Repair Method	P_y (tf)	d_y (mm)	P_p (tf)
Original Pier	1, 2, 3, 4	-	47	2.8	62
Repaired Pier	2R	Strengthening Plate	125	3.6	139
	3R	Strengthening Plate	125	3.4	140
	4R	Contact Plate	76	3.6	76

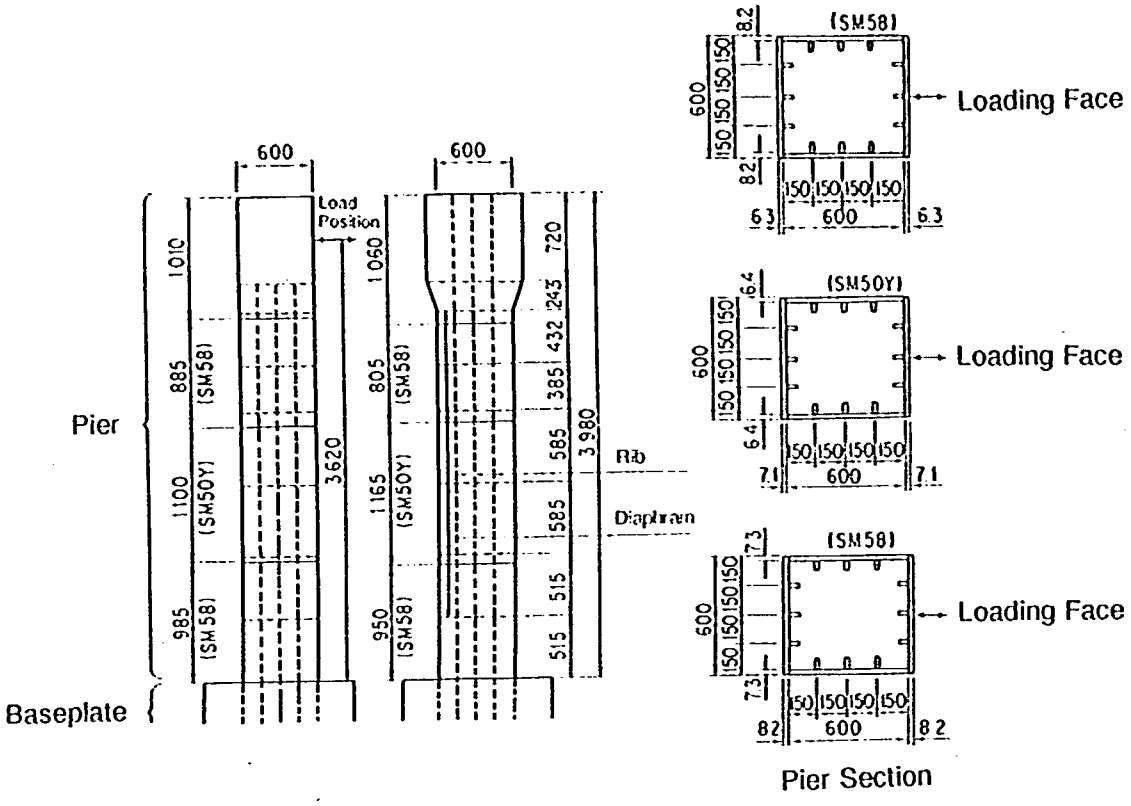


Figure 4. Piers Tested

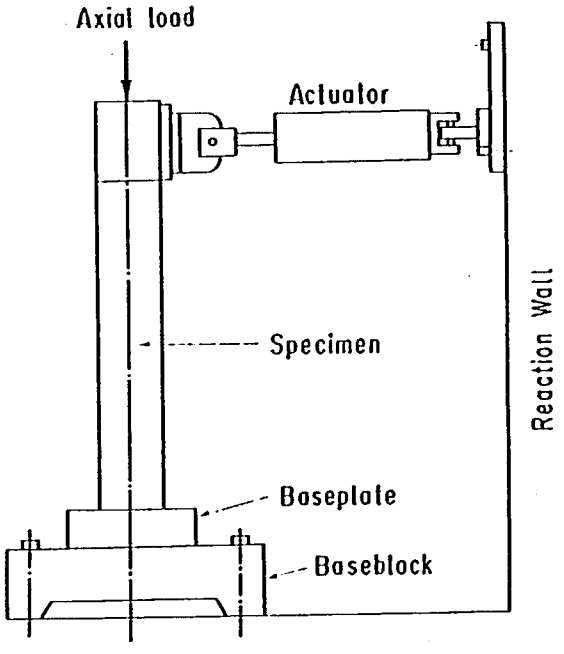


Figure 5. Test Set-up

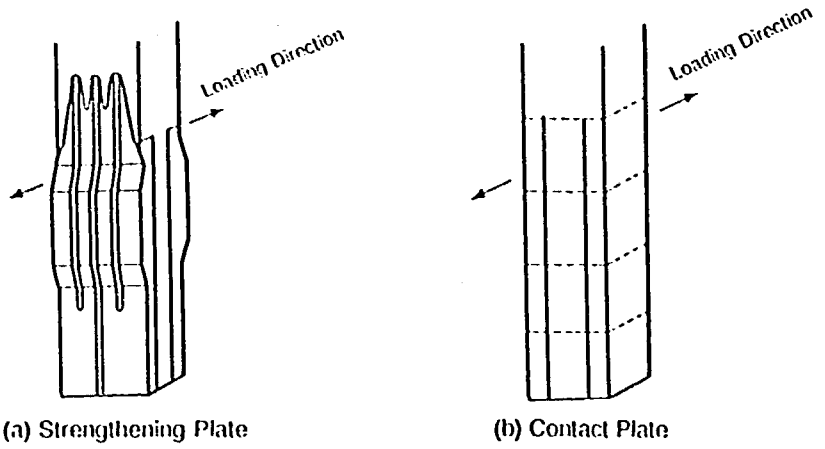


Figure 6. Repair Methods

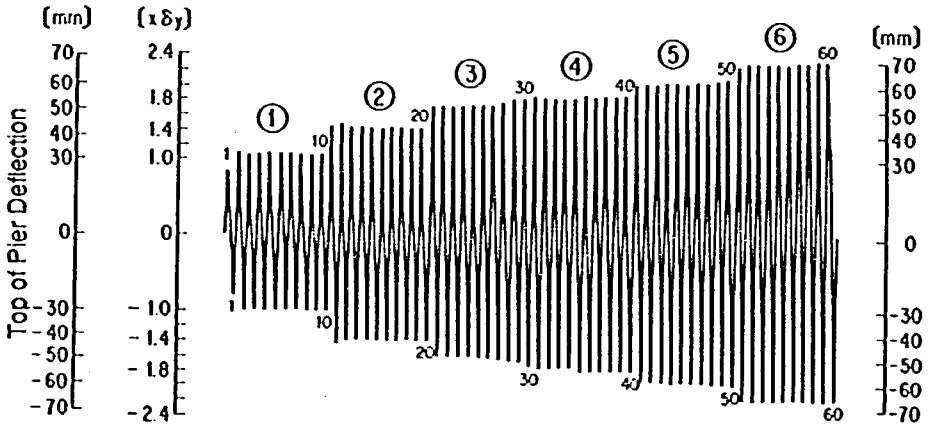


Figure 7. Loading Regime of Specimen 1

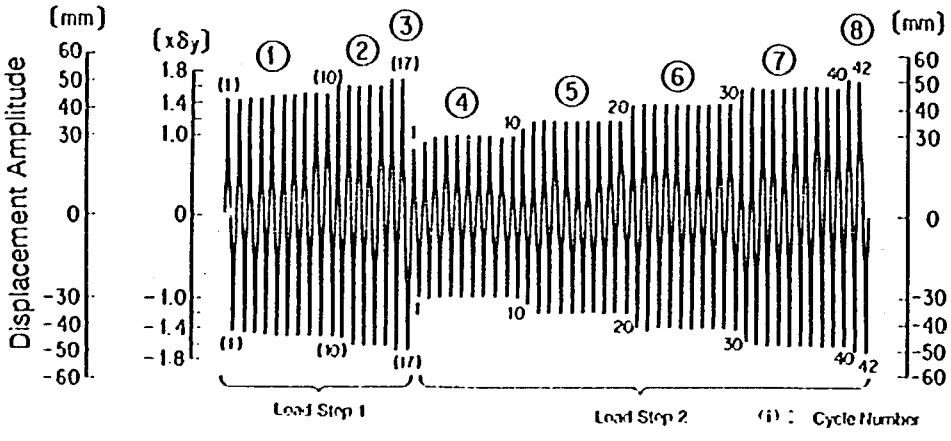


Figure 8. Loading Regime of Specimen 2

Purpose and Procedure for Each Test

Test 1 (Specimen 1)

Specimen 1 was tested in order to obtain the maximum load resistance, the load-displacement hysteresis relationship and the amount of buckling deformation of an unrepaired specimen at each displacement ductility step. This specimen was treated as a standard for the testing of the later specimens. It was tested quasi-statically (2.4mm/sec) with 10 cycles of repeated cyclic loading to the same displacement amplitude using displacement-controlled applied loading. The displacements used were $1.0d_y$, $1.4d_y$, $1.6d_y$, $1.8d_y$, etc. increasing in steps of $0.2d_y$ until the ultimate condition as shown in Figure 7.

Test 2 (Specimen 2)

This test was conducted in two stages as shown in the loading regime of Figure 8. The aim of the first stage was to damage the pier. The loading regime was then reapplied in the second stage so that the influence of the smaller, gradually increasing cyclic displacements could be observed. This was done to give an indication of the behaviour of a pier under reapplied load such as may occur during aftershocks.

Firstly, ten cycles of loading were carried out to the displacement at which 10mm buckling deformation was observed to occur in Specimen 1. As the buckling deformation was still smaller than 10mm after this applied loading, 10 more cycles were applied at each displacement step, which was increased by $0.1d_y$, until this deformation was attained as shown in load steps 1 to 3 of Figure 8. Thereafter, in order to investigate the behaviour when the load was reapplied, 10 cycles of repeated cyclic loading were carried out with amplitudes increasing from d_y with a step of $0.2d_y$ until the flange deformation increased to 15mm as shown in load steps 4 to 8 of Figure 8.

Test 3 (Specimen 2R)

The repairability of Specimen 2 with strengthening plates was checked with the applied lateral load method of Test 1 after it had been damaged in Test 2.

Test 4 (Specimen 3)

The specimen was to be damaged to the maximum predicted deformation for which repair with strengthening plates could be performed (20mm). Ten cycles of loading were carried out to the displacement at which 20mm buckling deformation was observed to occur in Specimen 1. As the buckling deformation was still smaller than this value after this applied loading, 10 more cycles were applied to each displacement step, which was increased by $0.1d_y$, until this deformation was attained.

Test 5 (Specimen 3R)

Specimen 3 was retested after it had been repaired with strengthening plates using the applied lateral load method of Test 1.

Test 6 (Specimen 4)

Specimen 4 was damaged to the maximum predicted deformation for which repair with contact plates could be carried out (5mm). Ten cycles of loading were applied to the displacement at which this buckling deformation was observed to occur in Specimen 1. As the buckling deformation was still smaller than 5mm after this applied loading, 10 more cycles were applied to each displacement step, which was increased by $0.1d_y$, until this deformation was attained.

Test 7 (Specimen 4R)

Specimen 4 was retested with the applied lateral load method of Test 1 after it had been repaired with contact plates.

Repair Method

i) Repair by Strengthening Plates

The strengthening plate method of repair was used when the buckling was large and the lateral resistance of the pier was negligible. This was carried out by attaching stiffening plates, with a strength equivalent to the strength of the original plates, to the pier. A set of stiffening plates were placed on the middle section of the piers (SM50Y steel) as shown in Figure 9. The non-bracketed values in this figure were the measured sizes from Specimen 2R and the bracketed values were from Specimen 3R. The stiffening plate was placed 20mm from the pier face so that repair could be made if buckling out from the face of the pier occurred. The repair process, as shown in Figure 10, was carried out in the following stages:

1) A plate was welded flush against the web,
2) A spacer was welded at the diaphram position, and
3) The strengthening plate was welded into position.

ii) Repair by Contact Plates

The contact plate method was used when the deformation sustained by the pier was small and when significant residual strength of the flange was expected. A contact plate of breadth 140mm (one-quarter of the pier breadth) and thickness 6mm was attached as shown in Figure 11. The contact plates were sized and the connected to the pier according to "Part II Steel Bridges" of the "Specifications for Highway Bridges" [3]. The limits for the thickness of the plate, t_1, to be attached on the outside are :

$$1.5\, t_2 \geq t_1 \geq b_2/24 \qquad (1)$$

where t_2 is the inside flange thickness and b_2 is the outside attached flange thickness. A plate thickness of 6mm was used which was satisfactory as t_2 was 7.3mm (over the SM50Y middle portion), b_2 was 140mm and Equation (1) became

$$11\text{mm} \geq t_1 \geq 5.8\text{mm} \qquad (2)$$

Results

Specimen 1

Approximately the same hysteresis loop shape was observed at each load-displacement cycle to the same displacement ductility and buckling was observed on at least two sides before the maximum load resistance of 60.9tf was attained as shown in Figure 12. This strength was greater than the theoretical yield load but less than the theoretical plastic load of 62tf given in Table 2 due to buckling. Panel buckling deformation increased and rapid stiffness and force deterioration was observed after the maximum force was reached. It may be seen that most of the inelastic deformation occurred over the weak panel as illustrated in Figure 13 as was desired. The mode of buckling was overall buckling of one side as shown in Figure 2a.

Specimens 2R, 3R and 4R

The maximum strength of Specimen 2 was 62tf and the flange deformation was 15mm after it had been loaded with the regime shown in Figure 8. This strength was close to that obtained from Specimen 1 of 60.9tf. No strength degradation occurred even during the second stage of loading where 42 cycles were applied. The maximum strength after repair was 129tf as illustrated in the load-displacement hysteresis diagram of Figure 14. This test was stopped prematurely because the lateral loading ram malfunctioned. It is probable that a higher strength and deformation could have been attained with further cycles of loading because no strength degradation occurred. The deformation of these panels at the end of Test 3 was very small as shown in Figure 15.

The maximum strength of Specimen 3 was 60tf and the flange deformation was 20mm. No strength degradation occurred during these cycles as shown in Figure 16 and this strength was close to that obtained from Specimen 1 of 60.9tf. The repaired specimen, like the other specimens, was tested to

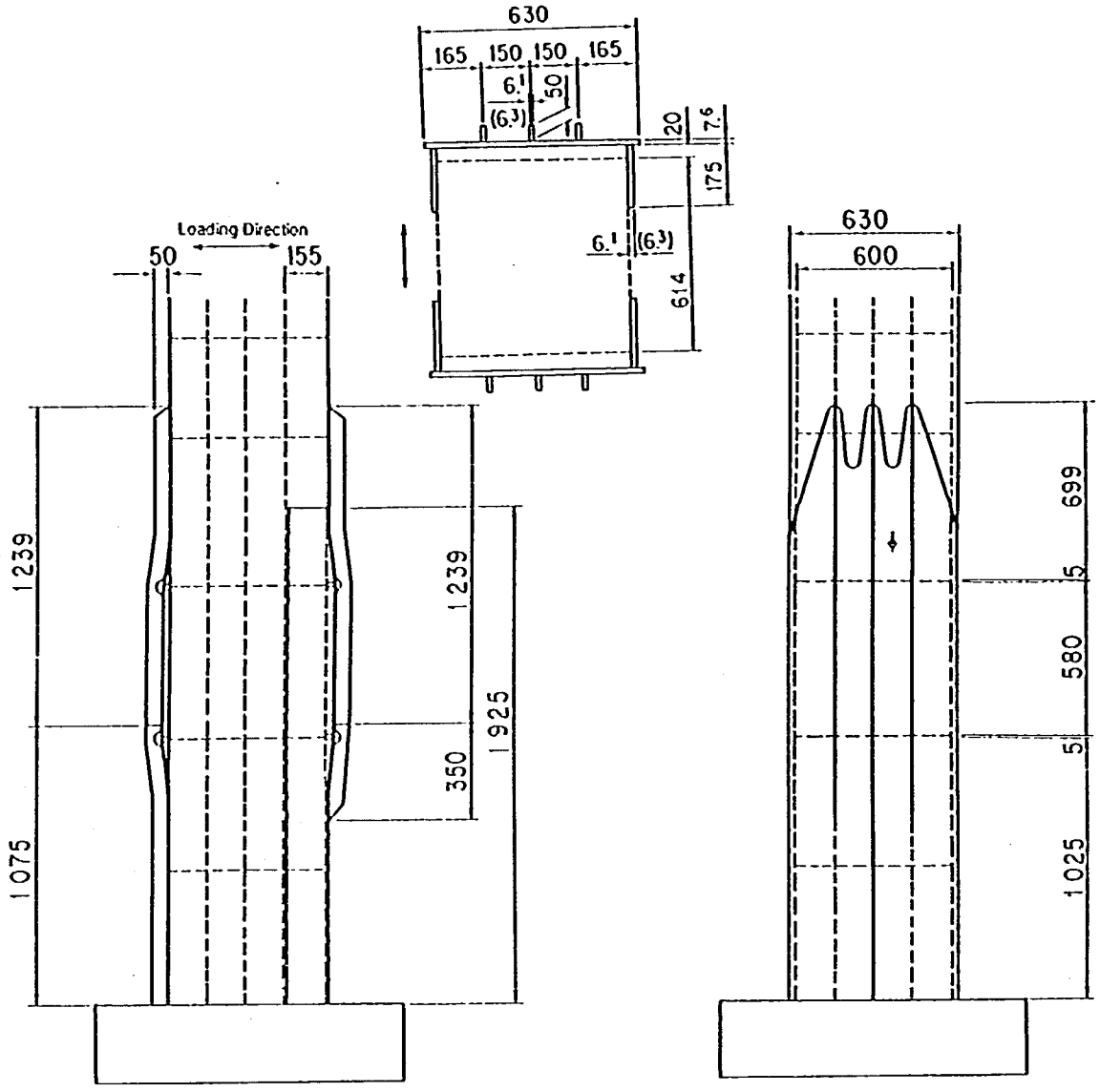


Figure 9. Strengthening Plate Repair Method

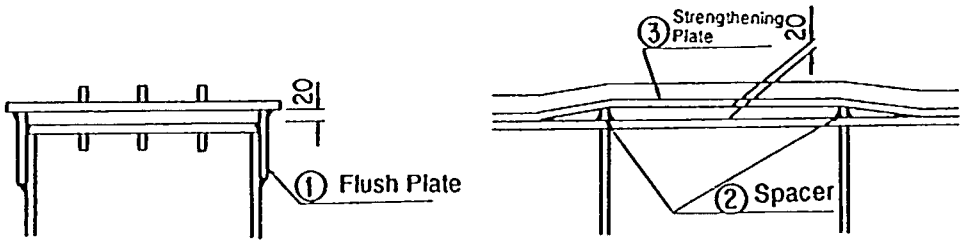


Figure 10. Order of Repair for the Strengthening Method

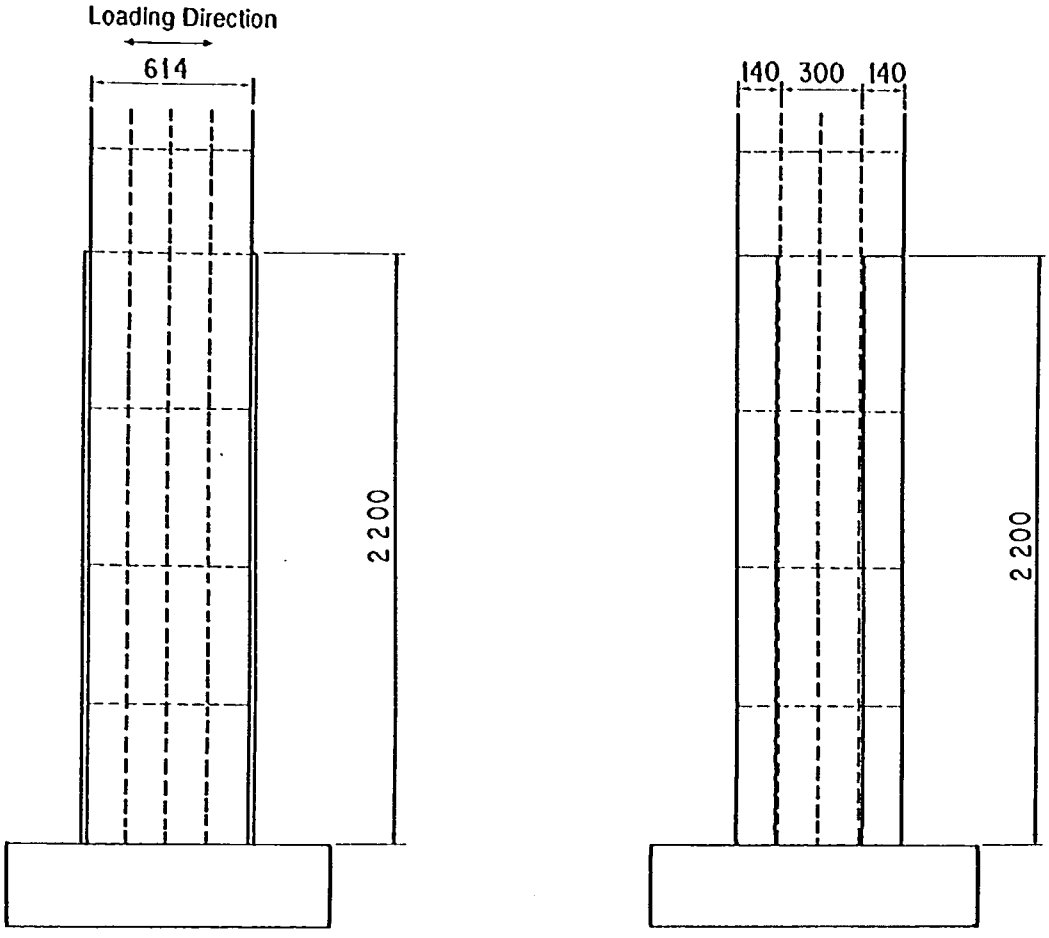


Figure 11. Contact Plate Repair Method

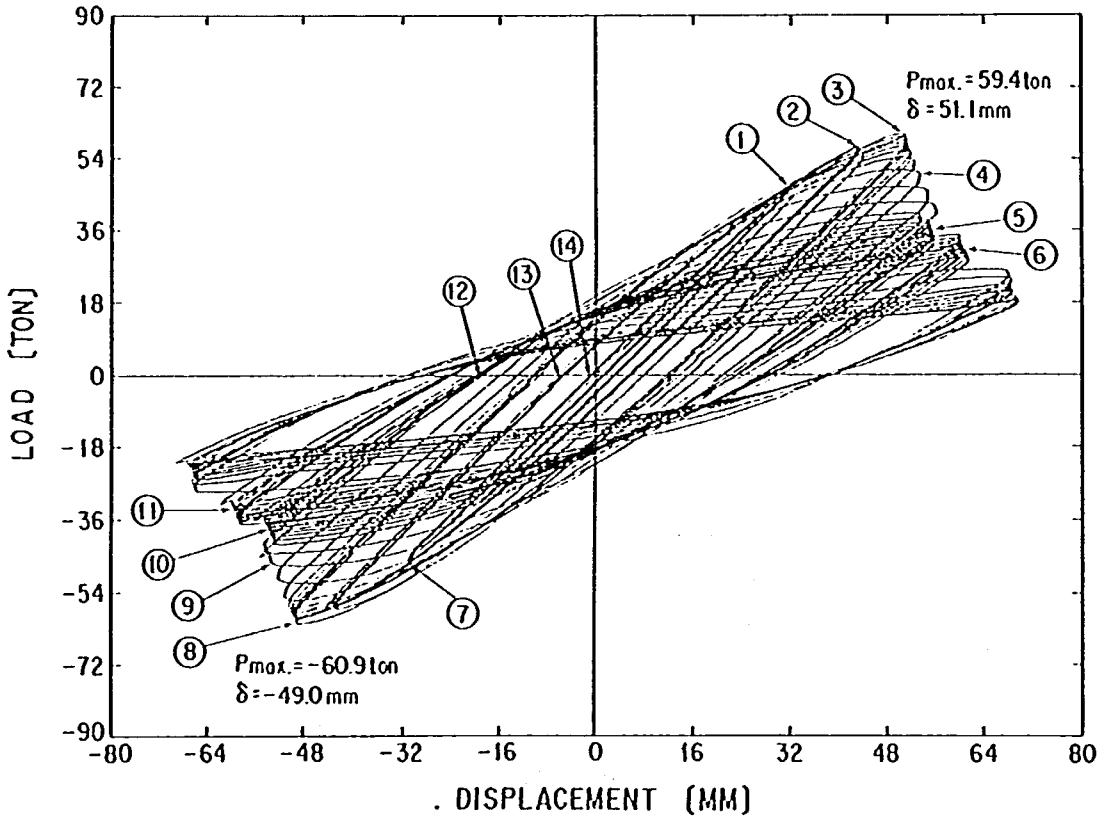


Figure 12. Hysteresis Loops of Specimen 1

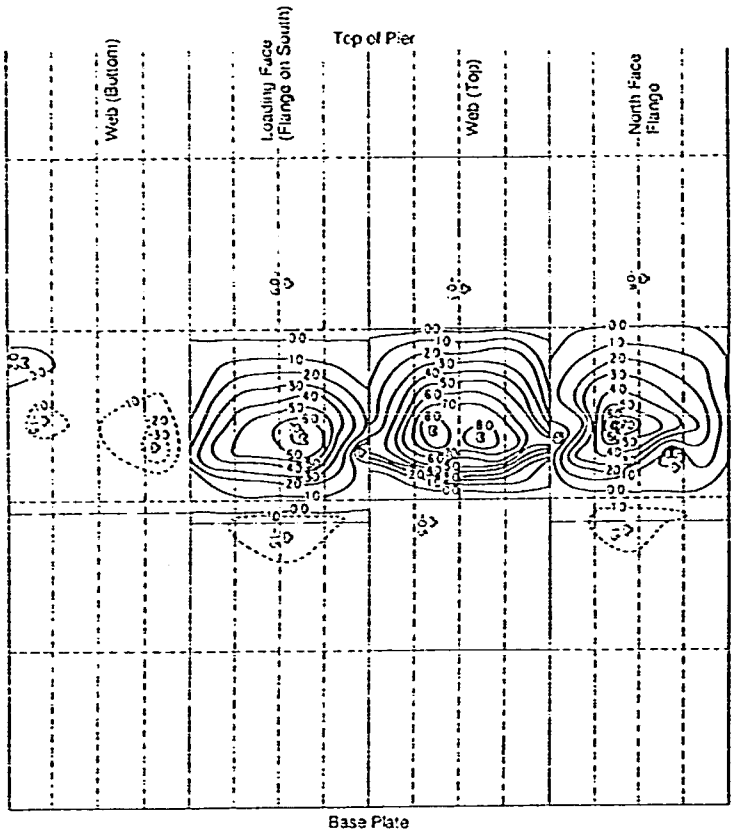


Figure 13. Deformation of Specimen 1

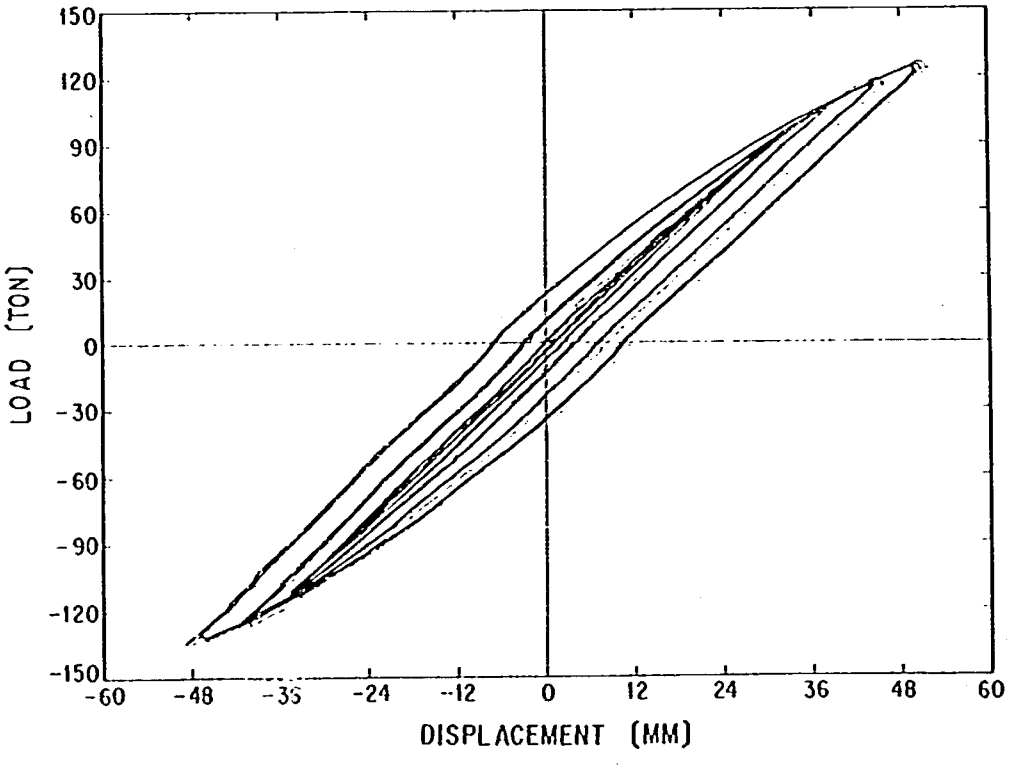


Figure 14. Hysteresis Loops of Specimen 2R

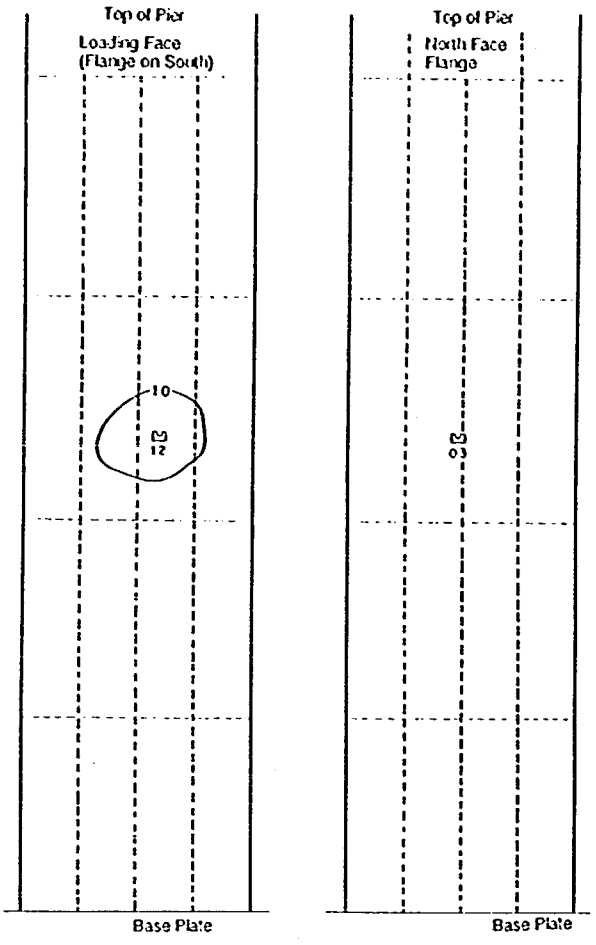


Figure 15. Specimen 2R Deformation

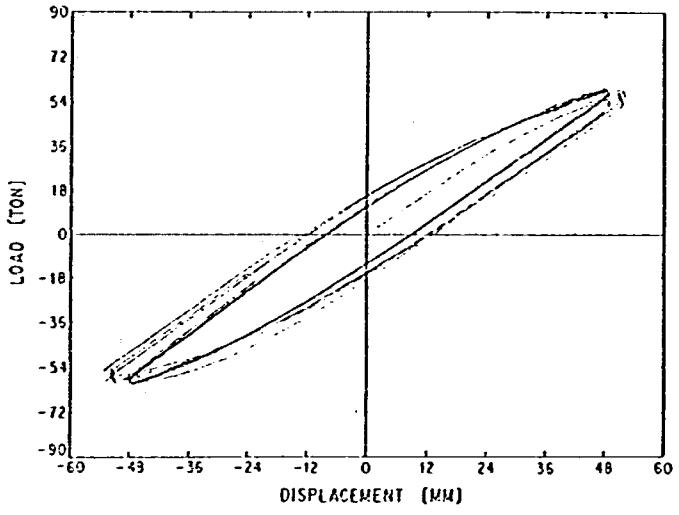


Figure 16. Specimen 3 Hysteresis Loops

the stage at which it could be shown that the behaviour, in terms of both strength and deformation capacity, was better than that of Specimen 1. Severe strength loss occurred after the maximum strength of 130tf was attained as shown in Figure 17 and buckling deformation of up to 6.5cm was observed as illustrated in Figure 18.

The remaining strength of Specimen 4 was 61tf and the flange deformation was 5mm. No strength degradation occurred during these cycles. The maximum strength after repair was 81tf, as shown in Figure 19, and buckling deformation of up to 50mm was observed as illustrated in Figure 20.

The fact that Specimen 2 sustained no strength degradation even during the second stage of loading in which 42 cycles were applied shows that the number of cycles of applied loading up to the displacement of $1.8d_y$ and panel deformation of 15mm was not an important parameter to assess the behaviour of this pier. However, at larger displacements a significant decrease in strength with each load cycle occurred as a result of the accumulation of buckling deformation as was seen in the behaviour of Specimen 1 during the cycles to a displacement ductility of 2.2. It is shown in Figure 21 that the responses of Specimens 2R and 3R, which were repaired by the same method, were almost identical and that all the repair methods were effective in increasing the lateral load resistance and the deformation capacity of the specimens above that of the unrepaired specimen.

RETROFIT OF PIERS WITH CONCRETE INFILL

Piers Tested

Four piers were filled with concrete over the bottom part of their height as part of the testing program of 22 piers at PWRI [5]. Filling real piers with concrete is commonly carried out to reduce the damage which may occur as a result of a vehicle collision with the pier. Before the testing it was thought that the addition of concrete to the piers would increase the deformation capacity because buckling of the plate toward the centre of the section was inhibited.

a) Large Pier Testing (800mm x 800mm)

Two specimens which were filled with concrete over the bottom one-third of their height were tested and one further test was carried out on a regular hollow pier. The first concrete-filled specimen had regular "I"-shaped longitudinal stiffeners while the second had "T"-shaped ones as shown in Figure 22. It was considered that the "T"-shaped stiffener would be beneficial to increase the pier deformation capacity by reducing the possibility of buckling of the panel away from the pier face. Ten load cycles were applied to displacement ductilities of 1, 2, 3, and 4 ... etc. The ultimate displacement for calculating the displacement ductility was taken as the point when the backbone curve of the hysteresis loop became less than the calculated yield strength. The effect of the concrete infill was neglected in all calculations.

Large Pier Test Results

The backbone curves for the concrete-filled piers and the hollow pier are compared in Figure 23. The calculated maximum strengths divided by the yield strength were 1.69, 1.69 and 1.35 and the ductilities were 3.57, 3.57 and 3.99 for the concrete-filled specimens and the hollow specimen respectively. It may be seen that the specimen with the "T"-shaped stiffeners behaved in an almost identical manner to the regular specimen with "I"-shaped stiffeners because the mode of failure of both concrete-filled specimens was brittle fracture of the steel above the base weld rather than buckling failure as was observed in the hollow specimen. The "T"-shaped stiffener had no beneficial effect in concrete-filled specimens. It is thought that cracking of the concrete at the base of the piers occurred causing all inelastic deformation to be concentrated in the steel beside the weld as shown in Figure 24 [5].

b) Small piers (320mm x 320mm)

Two other smaller specimens, each one-third filled with concrete, were also tested. The first was tested by applied lateral loading (10 cycles to displacement ductilities of 1, 2, 3.. etc. until failure) and the second was tested on the shaking table. Identically constructed hollow specimens were also tested in the same way. It was found in these tests that the fillet weld at the base of the concrete-filled specimens fractured and that the deformation capacity was the same as that of the hollow piers.

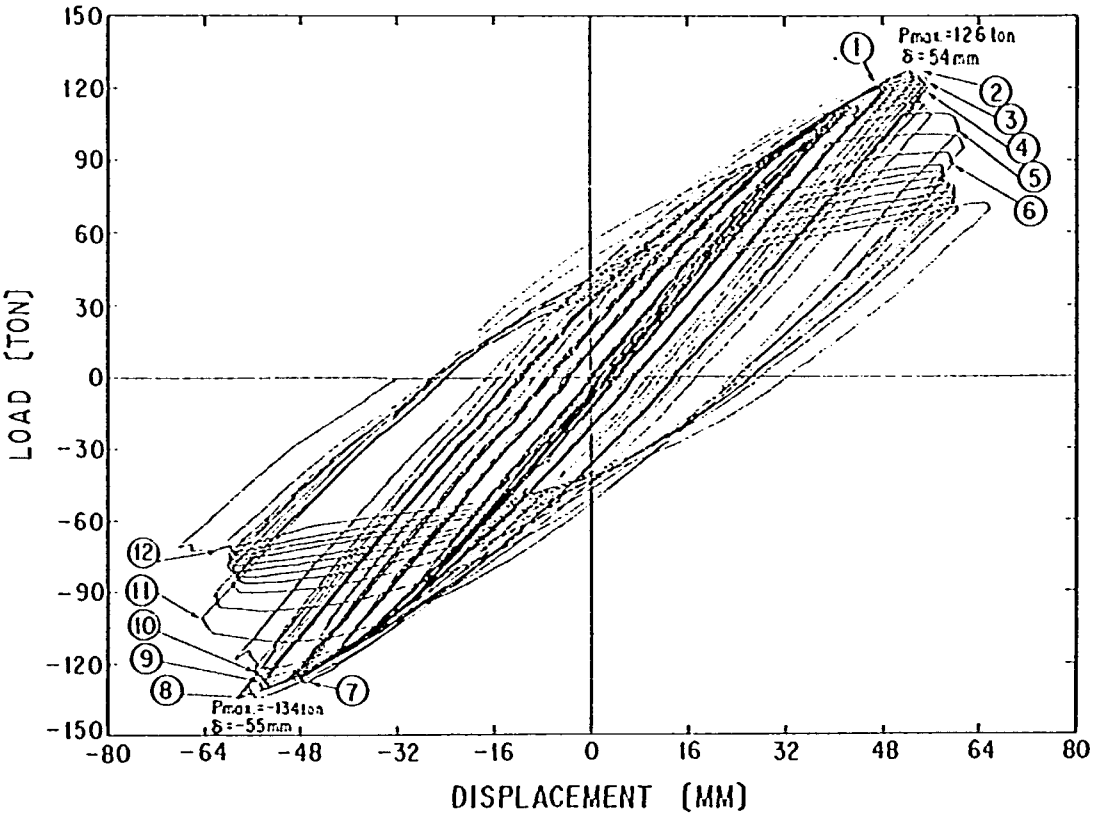


Figure 17. Specimen 3R Hysteresis Loops

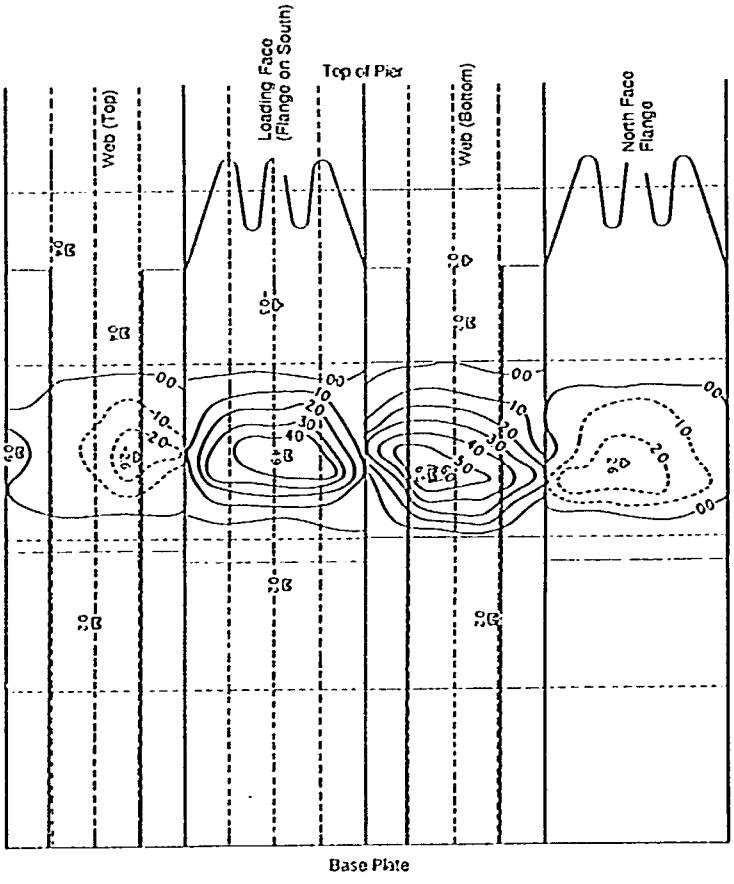


Figure 18. Specimen 3R Deformation

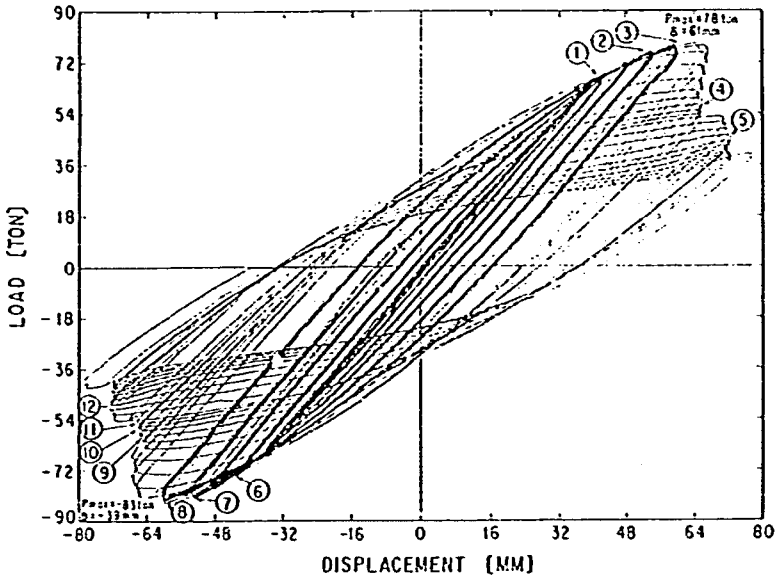


Figure 19. Hysteresis Loops of Specimen 4R

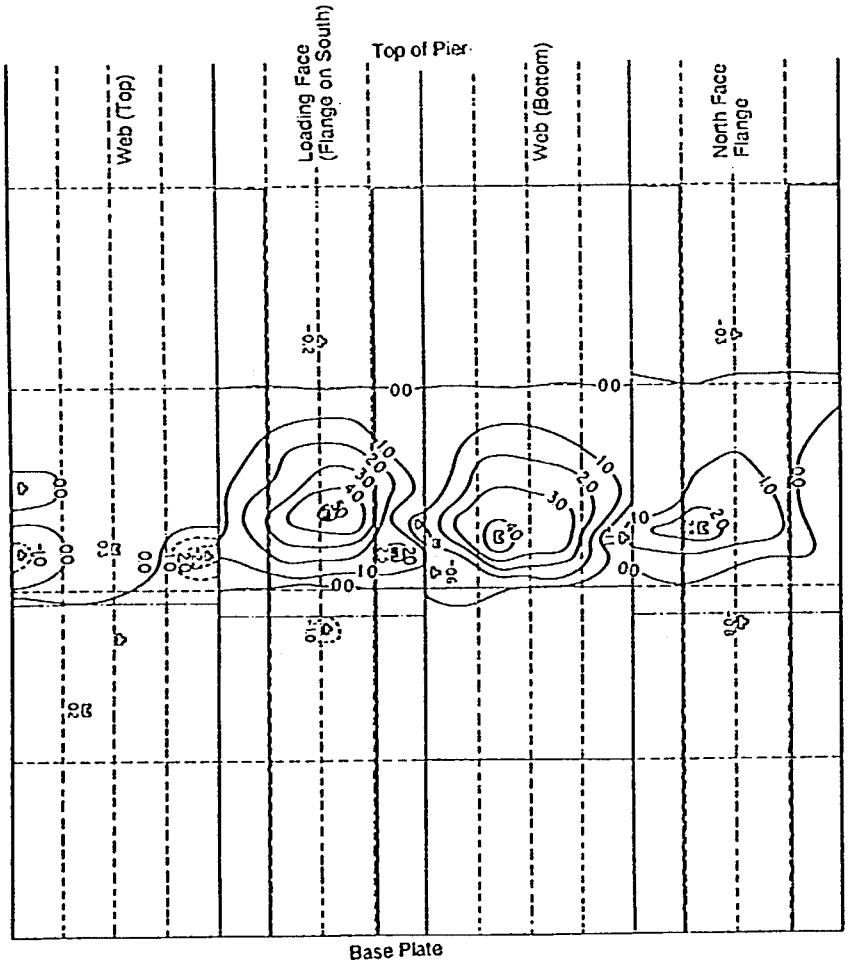


Figure 20. Deformation of Specimen 4R

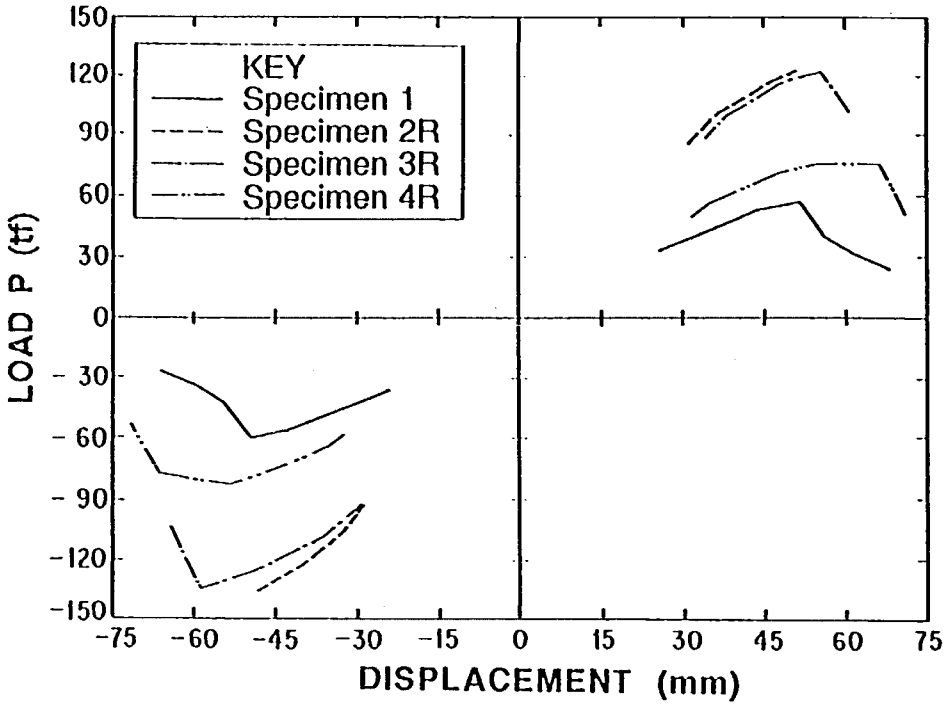


Figure 21. Retrofitted Specimens Backbone Curve Comparison

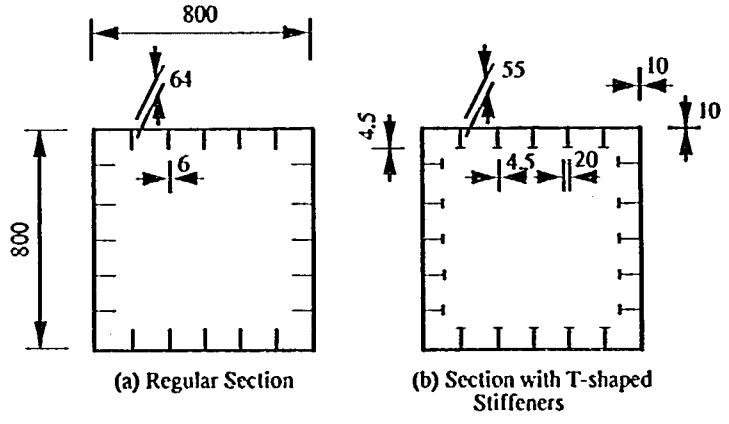


Figure 22. Concrete-filled Section Types

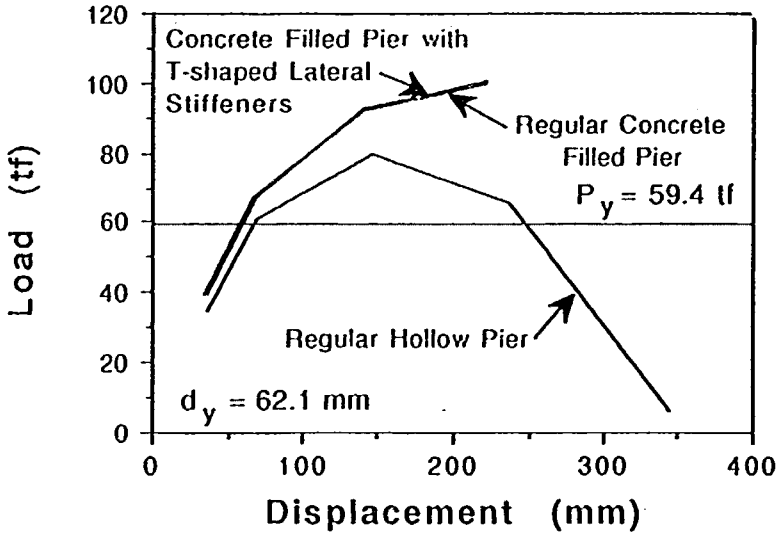


Figure 23. Backbone Curves of Empty and Concrete-Filled Piers

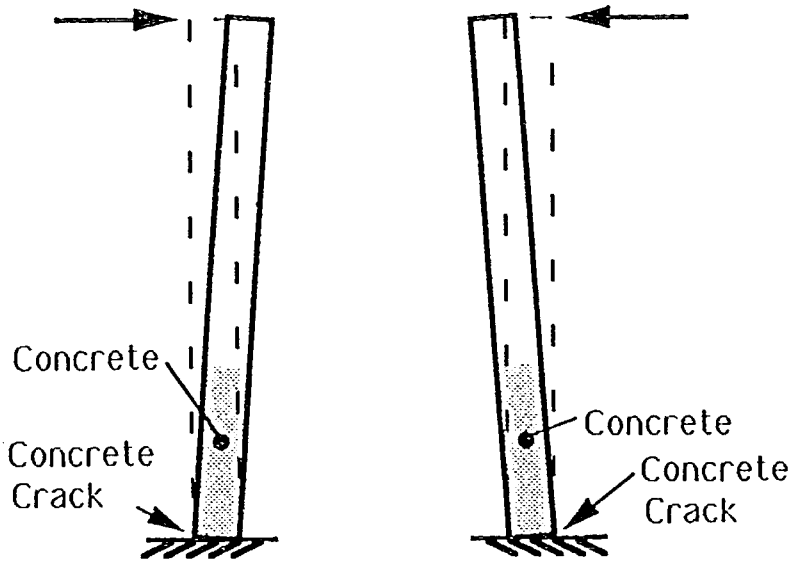


Figure 24. Concrete-Filled Pier Deformation

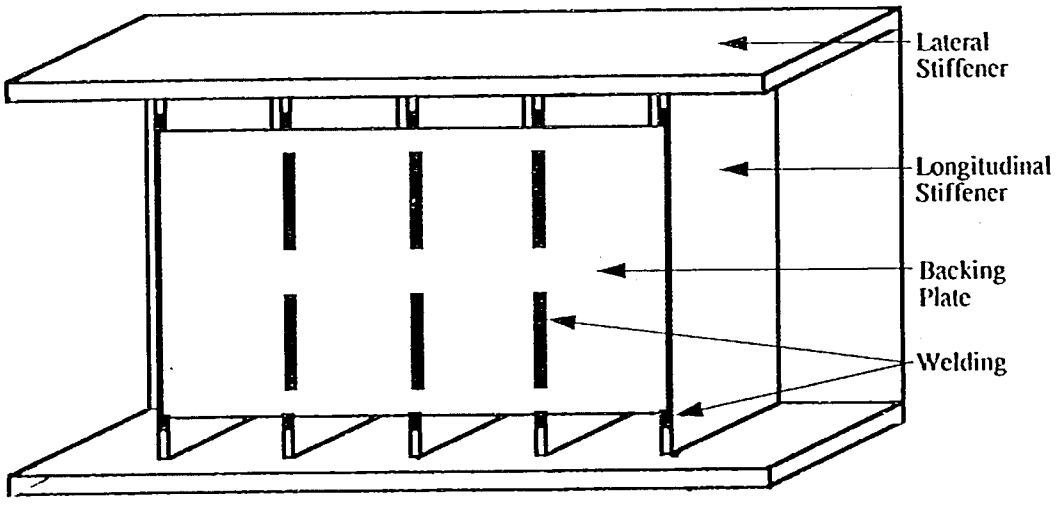


Figure 25. Retrofit by using an Internal Steel Plate

The strength of the specimens retrofitted by concrete infill was increased by between 17% and 34% and a sudden brittle failure occurred at the base of the specimens at the same or at a lower displacement than in the hollow piers. The overall seismic resistance of the specimens when evaluated by the equal energy methods was increased by the addition of concrete, however, the overall seismic resistance may decrease when the equal displacement methods are used.

ALTERING DEFORMATION CAPACITY WITHOUT INCREASING STRENGTH

While it may be generally desirable to increase the strength as well as the deformation capacity of piers in order to provide greater earthquake resistance, there may be instances where the ductility capacity alone is desired to be increased. If the load resistance of the foundation is similar to that of the pier, an increase in the pier strength will result in a movement of the area of damage from the pier into the foundation. A method to increase the deformation capacity of the pier without increasing the strength may be required if inelastic foundation deformation is undesirable. The method proposed is to use a steel plate on the back of the longitudinal stiffeners as illustrated in Figure 25 in order to reduce the twisting of these stiffeners and to provide the centre of the side with a greater flexural strength to resist buckling. If the steel plate is only placed in the middle region of the panel then the overall strength of the pier should not increase significantly. It is thought that care may be required in the attachment of the plate to the pier in order to avoid concentration of strain in the pier below the plate. This method is expected to be most effective in piers which fail by overall buckling of one side because the buckle of these piers is concentrated in the centre where the stiffeners will be of most effect. The method may be of little or no use in piers which fail by weld fracture.

CONCLUSIONS

The following conclusions may be made about the repair and retrofit methods of rectangular steel piers using steel plates and concrete infill which were investigated:

1) Repair using "strengthening plates" and "contact plates" increased the strength of the damaged piers and at least the same deformation capacity was obtained in the cases examined.
2) "T"-shaped longitudinal stiffeners were of no benefit because the mode of failure of concrete-filled piers was brittle fracture near the base weld rather than buckling.
3) Retrofit by filling piers with concrete may increase the strength but may even decrease the ductility capacity.
4) It may be possible to increase the deformation capacity without increasing the stiffness by using internal stiffening plates.

ACKNOWLEDGEMENTS

The authors wish to express their thanks to the Metropolitan Expressway Public Corporation and the Hanshin Expressway Public Corporation for their support in conducting the research described herein.

REFERENCES

1. Kawashima K., Hasegawa K., Koyama T. and Yoshida T., "Dynamic Loading Tests of Steel Bridge Piers for Developing Repair Methods", Technical Note of PWRI, Vol. 2498, Public Works Research Institute, 1988 (in Japanese).
2. Public Works Research Institute: Manual for Repair Methods for Civil Engineering Structures Damaged by Earthquakes, Technical Note of the Public Works Research Institute, Vol. 45, December 1986 (in Japanese). Translated version is published from the National Centre for Earthquake Engineering Research, University of New York, Buffalo, USA.
3. Japan Road Association, "Specifications for Highway Bridges", February 1990.
4. Subcommittee on Stability Design, "Guidelines for the Stability of Steel Structures", edited by Fukumoto Y., Committee on Steel Structures, Japan Society of Civil Engineers, 1987.
5. Kawashima K., MacRae G. A. and Hasegawa K., "The Strength and Ductility of Steel Piers", Technical Report of PWRI, Public Works Research Institute, Tsukuba, Japan (to be published).

DUCTILITY OF STEEL BRIDGE PIERS FROM DYNAMIC LOADING TESTS

by
Kazuhiko KAWASHIMA
Gregory A. MACRAE
Kinji HASEGAWA
Takefumi IKEUCHI
and
Kazuya OSHIMA

U.S. — JAPAN SEMINAR ON CYCLIC BUCKLING
OF STEEL STRUCTURES AND STRUCTURAL
ELEMENTS UNDER DYNAMIC LOADING CONDITIONS
Osaka, Japan
July 1991

Ductility of Steel Bridge Piers from Dynamic Loading Tests

by
Kazuhiko Kawashima, Head
Earthquake Engineering Division, Public Works Research Institute, Tsukuba, Japan
Gregory A. MacRae
Overseas Researcher, Earthquake Engineering Division, PWRI, Tsukuba
K. Hasegawa
Senior Researcher, Earthquake Engineering Division, PWRI, Tsukuba
T. Ikeuchi
Chief Design Engineer, Metropolitan Expressway Public Corporation, Tokyo
and K. Oshima
Construction Division Manager, Hanshin Expressway Public Corporation, Kobe
Construction Bureau

ABSTRACT

Twenty-two model stiffened box-shape steel bridge pier specimens of the type commonly used in Japan were tested in order to obtain their strength and ductility capacity and to understand their behaviour. Hollow specimens and specimens partially filled with concrete were tested both under applied lateral loading and shaking table testing. It was found that the specimens failed by overall wall buckling as well as local panel buckling and fracture. The strength of specimens with concrete infill was increased however their deformation capacity was decreased. Specimens tested on the shaking table sustained yielding predominantly in one direction with little absorption of energy. This was different from that assummed by the applied lateral loading regimes. Specimens with greater section slendernesses generally had lower ductility capacities. A method for estimating the strength of these specimens which was independent of the effect of the section slenderness was found to be satisfactory.

INTRODUCTION

Steel bridge piers, which are constructed by welding thin plate together, have been used over the past 30 years for the construction of bridges in Japan. The construction cost of these piers is generally more than that of reinforced concrete piers but their section size is significantly less making them ideal for use in city locations where land prices are high and where there are restrictions on construction space. In some cases concrete is placed inside these piers to provide extra protection if a vehicle collides into them. Damage has not been observed in these sort of piers to date and few tests have been carried out to investigate their likely behaviour during an earthquake.

Twenty-two steel pier specimens were tested in order to assess their strength and ductility capacity because it is realized that accelerations greater than the design level may be developed in bridges during a major earthquake. Applied loading tests and shaking table tests were performed on hollow pier specimens with different configurations of internal stiffeners and on specimens which were partially filled with concrete. In this paper some of the more important aspects of the behaviour of these specimens are summarized.

SPECIMEN CONSTRUCTION, DESIGN REQUIREMENTS AND TESTING METHODS

The test specimen sizes were selected to be scaled down versions of real piers. The box-shaped sections consisted of 4 major plates to which ribs and diaphrams were welded for stiffening and strengthening. Real piers are generally large enough that a person may

enter and weld from the inside but this construction technique was unable to be used on the smaller pier specimens. The specimen was therefore constructed in stages as shown in Figure 1. Weld was applied to the inside of the specimen before the final web-plate was welded into place from the outside. The diaphrams extended outside the section on one side to facilitate the welding of the final web plate to the specimen. The longitudinal stiffeners on the inside of the final web plate were discontinuous at the diaphram positions and at the base.

Design was carried out according to the Japanese bridge design code [1] which is based on elastic design considerations. The background to the buckling design criteria for these piers is published in design guidelines [2]. There are two important section slenderness ratios which are required to be greater than certain values in order that premature buckling does not reduce their strength. These two ratios, which are described more fully in the accompanying paper [3] are:

1) The **panel slenderness ratio, b/(nft)**, where b, n and t are given in Figure 2, must be less than 28 or 24 for Grades SS41 or SM50 steel respectively. The value of f was taken as 1 for the inelastic structures. This check ensures that local panel buckling will not occur before the yield strength of the section is reached. Local panel buckling refers to buckling in the panels between the vertical stiffeners.

2) The **gamma ratio, $\gamma_l/\gamma_{l,req}$**, which must be greater than unity. This check ensures that overall wall buckling of the pier will not occur before the yield strength of the section is reached. The stiffness of each panel and longitudinal stiffener was used to obtain an equivalent stiffness for the side as a whole and the effect of the lateral stiffeners was also considered.

A further ratio, the **gamma* ratio, γ_l/γ_l^***, [2] is able to be used to predict whether local panel buckling or overall wall buckling will occur first as shown in Figure 3. If $\gamma_l/\gamma_l^* > 1$ then local buckling of the panels between the longitudinal stiffeners is the expected initial buckling mode but if $\gamma_l/\gamma_l^* < 1$ then overall wall buckling is expected.

Typical test setups are given for the applied lateral loading and shaking table testing at the laboratory facilities of the Public Works Research Institute in Figures 4 and 5. The levels of axial load, N, used were in all cases less than 11% of the yield axial load, N_y. The applied loading tests were carried out by controlling the displacement of the lateral loading ram. Cyclic loading tests of larger specimens were performed at a frequency of 0.013 Hz while for the smaller specimens a frequency of about 0.33 Hz was used. In the shaking table testing, the shaking table was initially excited with sine-waves of different frequencies and low amplitudes to determine the elastic response period of the specimen on the table. Scaled versions of the acceleration record obtained at Hachiro-gata during the Nihon-kai-chubu earthquake of 26 May 1983 were used as the basic input ground motions. The time-axis was reduced to one-half of the actual time to adjust the predominant frequency of the records so that the relationship between the period and the response spectrum shape would be more like that expected for a real bridge pier.

The yield displacement, d_y, was defined as the displacement at which yielding first occurred in an extreme fibre of the section. The yield load, H_y, and yield displacement, d_y, were able to be calculated before the test started from the measured section properties and from the results of the material tests. The loading regime, yield load, H_y, and yield displacement, d_y, used in the concrete infilled specimens were the same as those used in the hollow specimens in order to investigate the effect of the concrete infill. The ultimate displacement, d_u, was calculated as the point at which the backbone curve of the hysteresis diagram became less than the yield load, H_y. The backbone curve was constructed by connecting the points of maximum displacement in the cycle with the

highest load for each displacement ductility. The ductility capacity, μ, was defined as the ultimate displacement, d_u, divided by the yield displacement, d_y.

SPECIMENS TESTED

The differences between the twenty two tests on steel specimens which were conducted at the Public Works Research Institute are described in summary form in Table 1 where the section size, main plate thickness, size of longitudinal stiffeners, number of longitudinal stiffeners, lateral stiffener spacing and size, gamma ratio ($\gamma_l/\gamma_{l,req}$), panel slenderness ratio (b/nft), gamma* ratio (γ_l/γ_l^*), distance from the base of the specimen to the point of application of the load and to the level of concrete infill, the grade of the steel, the properties of the steel obtained from material tests, the specimen axial load ratio (N/N_y), the number of cycles of loading applied to each specimen as well as the calculated and actual periods of the specimens on the shaking table are given. The calculated yield strength, P_y, and yield displacement, d_y, are given in Table 2. The section properties for all of the specimens tested satisfied the current recommendations of the present Japanese code "Specifications for Highway Bridges" [1].

Specimens S1 to S12 had sections of the same size. Specimen S1 is shown in Figure 6. Specimen S2 was the same as Specimen S1 except that the weld size was 4.5mm rather than 3mm and Specimens S3 to S12 all had 3 to 4mm weld sizes. Specimens S1 and S3 to S9 had the same internal construction but were subject to different loading regimes. Specimens S3, S4, and S5 were tested on the shaking table with 2x, 3x and 4x the earthquake record magnitude while all other specimens of this size were subjected to applied lateral loading. Specimen S7 was the same as Specimen S6 except that the loading regime applied to Specimen S7 was of decreasing magnitude (1 cycle to μ = 5, 4, 3, 2 and 1). All other specimens in applied load tests were subjected to increasing displacement ductilities. Specimens S1, S6, S8, and S9 were subjected to 10, 1, 3 and 5 cycles to each displacement ductility respectively. Specimens S13 to S18 were larger specimens which were tested by applied lateral loading. Specimens S16 and S17 were partially filled with concrete and Specimen S17 was the same as Specimen S16 except that it had a "T"-shaped internal longitudinal stiffener. Specimens S19 to S22 were smaller specimens with the same internal steel construction. Specimens S20 and S22 were partially filled with concrete. Specimens S19 and S20 were tested by applied lateral loading and Specimens S21 and S22 were tested on the shaking table. Specimens S13 to S18 were larger specimens constructed from SM50 steel with a specified allowable yield stress of 1900kgf/cm^2. All other specimens were constructed from SS41 steel with a specified allowable yield stress of 1400kgf/cm^2 [1].

TEST RESULTS

HYSTERETIC BEHAVIOUR:

Test results for all specimens showing the yield and maximum loads, specimen overstrength factor ($\phi_s = P_{max}/P_y$), yield and ultimate displacements, ductility ($\mu = d_u/d_y$) and mode of failure are given in Table 2. The hysteretic behaviour, strength, mode of failure and deformation capacity are described below.

The hysteretic behaviour of all hollow specimens subjected to applied lateral loading was similar. From the hysteresis loops of Specimen S1, shown in Figure 7, it may be seen that little energy was absorbed before the cycles to a displacement ductility, μ, of 2. At μ = 3 the loop size increased and was fat showing that a large amount of energy was absorbed. Buckling was first observed during these cycles. A large amount of strength

degradation was developed during the cycles to $\mu = 4$ as the buckling deformation of the plate increased. The strength continued to decrease after the defined failure point.

The concrete-filled specimens generally had stable hysteresis loops with a post-elastic stiffnesses of about 14% of the initial stiffness before fracture occurred. At this point there was a sudden loss of load carrying capacity as shown for Specimen S16 in Figure 8.

The behaviour of Specimen S5, which was subjected to shaking table testing with four times the Hachiro-gata record, is shown in Figure 9. This behaviour was typical of all of the specimens tested on the shaking table. The loop followed the shape of the backbone curve of the specimens tested by applied lateral loading. Yielding occurred almost entirely in one direction resulting in the energy absorbed being similar to that in a monotonic test. The maximum displacements observed were larger than those estimated by the equal energy assumption and there were large residual displacements at the top of these specimens at the end of the tests.

EFFECT OF LOADING TYPE:
The curve shape and ductility capacity of Specimens S1, S8 and S9, which were obtained using regimes with 10, 3 and 5 cycles of loading to each displacement ductility respectively, had similar results as shown in Figure 10. The deformation capacity of Specimen S6, which was subjected to only 1 cycle of loading to each displacement ductility, had a greater ductility capacity. Dependence of ductility on the number of load cycles was smaller in these steel pier tests than in reinforced concrete piers [4]. The strength of the specimens on the shaking table dropped off more slowly than those tested by applied lateral loading because they were subjected to only a small amount of yield reversal. Specimen S7, which was subjected to decreasing displacement ductilities, did not fail but had a backbone curve similar to that of monotonically loaded specimens because the first cycle of loading determined this curve.

It would normally be expected that the number of cycles of loading would strongly influence the deformation capacity of members subjected to both axial load and cyclic loading because axial shortening occurs and increases the damage [5]. This axial shortening is proportional to the cumulative inelastic rotation within the region of yielding before buckling becomes severe [6]. The fact that there was little difference in the behaviour of the pier specimens which were subjected to between 3 and 10 load cycles to each ductility is thought to be because low levels of axial load were applied in these tests.

The behaviour of Specimens S1 and S2 were almost identical. The 3.0mm welds of Specimen S2 were strong enough to develop the full section strength but were insufficient to form a truly composite section. However, the welds remained together long enough to achieve the same ductility as that attained by Specimen S1 which had a 4.5mm weld.

There was a large difference between the monotonic type of hysteresis loop observed in the shaking table testing and the hysteresis loop from the applied loading tests. A research program is presently underway at the Public Works Research Institute to understand why very little reversal of yielding occurred in the shaking table tests by running dynamic analyses of piers with different bilinear stiffness factors.

MODE OF FAILURE:
1) Wall Buckling
Specimens with a gamma* ratio up to about 2.0 had a failure mechanism of overall wall buckling after several load reversals. While the specimens with gamma* ratios less than 1.0 failed by only wall buckling, the specimens with gamma* ratios between 1.0 and 2.0

sustained buckling of the panels between the longitudinal stiffeners before the longitudinal stiffeners carried the load and overall wall buckling caused strength loss. The maximum amplitude of buckling generally occurred mid-distance between the base of the specimen and the first lateral stiffener and the wavelength of the buckle was spread over the whole base panel. The web of the section also started to buckle as the longitudinal stiffeners twisted. Strength was rapidly lost during the later stages of buckling and finally the weld connecting the flange and web together fractured. This mode of "overall wall buckling" is shown for Specimen S1 in Figure 11 where Face 1 and Face 3 are the flanges. In the shaking table tests, in which yielding occurred predominantly in one direction, it was found that buckling generally became severe on only one side of the specimen.

While buckling was generally concentrated in the base section of most of the specimens there were cases where some buckling was also observed in the adjoining section. In Specimen S13 it was found that buckling was concentrated in the second section up from the base on one flange and on the opposite flange deformation in the two bottom sections caused twisting of the first lateral stiffener from the base. Buckling was observed in the adjoining section as well as the base section of Specimen S14 and also slightly in Specimens S1 and S19. Specimens with deformation in more than one section would generally be expected to have a ductility capacity which is greater than that of specimens with deformation in only one section.

2) Panel Buckling and Fracture

Limited panel buckling occurred in specimens with large gamma* ratios and fracture of the steel near the base of the specimens caused final failure. When the gamma* ratio is large the gamma ratio is also required to be high in order that the panel buckling limits are not violated. Therefore, local panel buckling will not generally occur until a large amount of inelastic strain has been sustained. The buckle wavelength was much smaller than when wall buckling occurred. Fracture occurred in Specimen S11 at the centre of the buckle where the strain was concentrated and fracture near or in the weld at the base of both Specimens S11 and S12 was also observed. These types of fracture are very dependent on the strength of the weld, on the amount of welding residual stresses in the plate, the fracture strengths of the steel and the weld, and on any material discontinuities which may initiate fracture.

The concrete-filled specimens suffered little buckling and failed by fracture of the weld or of the steel beside the weld at the base. It seems as though the concrete cracked at the base of the specimen causing concentrated localised deformation in the steel plate beside the concrete crack which eventually resulted in fracture. This mode of behaviour is especially likely to occur if the uncracked section strength is considerably greater than the overstrength of the cracked section because only one crack will occur giving the behaviour shown in Figure 12. The use of the "T"-shaped longitudinal stiffener in Specimen S17 was of no benefit as the mode of failure of concrete-filled specimens was fracture near the base rather than buckling. It seems as though filling the specimens with concrete to 1/3 of their height was satisfactory to ensure that the major amount of the deformation occurred at the base rather than above the level of concrete infill.

STRENGTH:

The specimen overstrength, ϕ_s, which was calculated as the ultimate specimen strength, P_{max}, divided by the initially calculated strength, P_y, ranged from 1.27 to 2.14 as shown in Table 2. The increase in the strength of the hollow specimens above the yield strength was thought to occur for the following reasons; the section stresses may be more like that assumed by plastic behaviour in which all the fibres in the section are at yield, strain hardening increases the strength, and the axial load on the section will allow even larger overstrength values to be obtained [6]. The strength of concrete-filled specimens were

1.26 and 1.34 times greater than that of the identical hollow specimens because the concrete also resisted load. The average overstrength values were 43% and 84% for hollow and concrete-filled specimens respectively.

Lay [7] has proposed an empirical method, based on the results of experiments on steel beams, to estimate the maximum strength of a steel member, P_{max}, as a function of the material overstrength, $\phi_{om} = \sigma_{max}/\sigma_y$, and plastic load, P_p, as $P_{max} = (\phi_m + 1)/2.P_p$ where $P_p = S/Z.P_y$ and S and Z are the plastic and elastic section modulii respectively. When this method was used on Specimen S13 it was found that the ratio of the plastic strength to the yield strength, P_p/P_y, considering the effect of axial load was 1.155 and the maximum stress, σ_{max}, divided by the yield stress, σ_y, of the steel material used in this specimen was 1.43. The predicted strength was therefore $(1.43 + 1)/2 \times 1.155P_y = 1.40P_y$ which was close to the actual strength of $1.38P_y$. It may be seen in Figure 13 that this method estimated the strengths of the specimens to ±10%. The strengths of Specimens S1 to S5 were not included in this figure because it was considered that there were some gross errors in the material tests for these specimens. The maximum strengths of Specimens S1 to S5 were even greater than $\phi_{om}P_p$. The slenderness of the sections did not seem to effect the maximum strengths because these members were compact.

DEFORMATION CAPACITY:
The ductility capacity was generally greater in the more compact sections, with a high gamma ratio, than in those with more slender characteristics as may be seen from the results of Specimens S14, S18, S15 and S13, in which the ductilities were 3.05, 3.13, 3.99 and 4.21, as well as Specimens S10, S11 and S12, in which the ductilities were 3.34, 4.11 and 4.31. However, the ductility of Specimen S1, which was 4.33, was higher than for Specimens S10, S11, and S12. This is possibly because some buckling occurred in the section above the base as well as in the base section in this specimen.

The specimens tested on the shaking table had large maximum displacement and ductility capacities because they were subjected to little reversal of loading and their behaviour was almost monotonic. Similarly, the ductility capacity of Specimen S6 of 5.04 was larger than that of Specimens S1 of 4.33, S2 of 4.02, S8 of 3.67 and S9 of 3.81 as a result of it only being subjected to one cycle of loading at each ductility step.

Placing concrete inside these specimens did not increase the ductility capacity because the mode of failure was different. The ductility capacity of the Specimen S16, which was filled with concrete was 10% less that of Specimen S15 which was identical but hollow. Similarly the ductility capacity of Specimen S20, which was filled with concrete was 23% less than that of Specimen S19.

The backbone curves of specimens tested with 10 cycles of applied loading to each ductility are given in Figure 14. It may be seen that the ductility capacities of these specimens, calculated from the point when the backbone curve became less than the yield strength, ranged between 3 and 5. A method for predicting the deformation capacity of steel specimens has also been produced from the testing described herein which considers the maximum strain in an equivalent plastic hinge length and the resistance against buckling [3].

SUMMARY

The results of 22 tests on hollow and concrete-filled steel specimens with different configurations of internal steel using applied lateral loading and shaking table testing were described in this paper. The major findings are given below:

1) The ductilities of the specimens tested with between 3 and 10 cycles of loading to each displacement step ranged from 3.67 to 4.33. The specimen subjected to one

cycle of loading to each displacement step and the specimen tested on the shaking table had increased ductilities of 5.09 and 12.9 respectively.

2) The specimens tested on a shaking table sustained little reversal of yielding. Their load history was therefore different from the assumed lateral loading regime in the applied lateral load tests.
3) The final mode of buckling of specimens with a gamma* ratio less than about 2.0 was overall wall buckling. The major buckling deformation in these specimens generally occurred midway between the base and the first lateral stiffener.
4) Severe local panel buckling and fracture were observed in specimens with a gamma* ratio greater than 2.0.
5) Concrete infill increased the strength and decreased the deformation capacity of specimens in these tests.
6) The maximum strengths of the compact hollow sections could be estimated satisfactorily without considering the effects of section slenderness.
7) The ductility capacities of specimens tested by applied lateral loading ranged from about 3 to 5.
8) The displacement ductility capacity generally decreased for members with greater section slendernesses.

REFERENCES

1. Japan Road Association, "Specifications for Highway Bridges", Part II : Steel Bridges, English Edition, 1987.
2. Subcommittee on Stability Design, "Guidelines for the Stability of Steel Structures", edited by Fukumoto Y, Committee on Steel Structures, Japan Society of Civil Engineers, 1987.
3. MacRae G. A. and Kawashima K., "Estimation of the Deformation Capacity of Steel Bridge Piers", US-Japan Workshop on Cyclic Buckling of Steel Structures and Structural Elements under Dynamic Loading Conditions, Osaka, 1-3 July 1991. (Accompanying paper)
4. Kawashima K. and Koyama T., "Effect of Number of Cycles of Loading Cycles on Dynamic Characteristics of Reinforced Concrete Bridge Piers", Proc. JSCE, Structural Eng., Earthquake Eng., Vol. 15, No. 1, 1988.
5. Popov E. P., Bertero V. V. and Chandramoulli S., "Hysteretic Behaviour of Steel Columns", UCB/EERC 75-11, September 1975.
6. MacRae G. A., Carr A. J., and Walpole W. R., "The Seismic Response of Steel Frames", Research Report 90-06, Department of Civil Engineering, University of Canterbury, 1990.
7. Lay M. G., "Flange Local Buckling in Wide-Flange Shapes", *Journal of the Structural Division*, ASCE, ST6, December 1965, p95-116.

Table 1. Pier Characteristics

Pier	Height to Load (m)	Height of Concrete (m)	Steel Strength Grade	Youngs Modulus ($\times 10^5$ kgf/cm^2)	Yield Stress (kgf/cm^2)	Material Over-strength ϕ_{om}	Axial Load (tf)	Axial Load Ratio	Load Cycles	Calculated Period (sec)	Actual Period (secs)	Section Size (mm) b + 2t	Section Size (mm) b	Plate Thick. t (mm)	Longitudinal Stiffeners Size (mm^2)	Longitudinal Stiffeners No. n-1	Lateral Stiffener Spacing (mm)	Lateral Stiffener Size (mm^2)	Gamma Ratio >1.0	b/E_y / tn <1047	Gamma' Ratio
S1	2.40	-	SS41	1.321	2133	1.045	20	0.110	10	-	-	409 x 400		4.5	35x3.2	3	350	55x3.2	1.559	831	0.950
S2	2.40	-	SS41	1.321	2133	1.045	20	0.110	10	-	-	409 x 400		4.5	35x3.2	3	350	55x3.2	1.559	831	0.950
S3	2.40	-	SS41	1.321	2133	1.045	20	0.110	x2H	.422	.490	409 x 400		4.5	35x3.2	3	350	55x3.2	1.559	831	0.950
S4	2.40	-	SS41	1.321	2133	1.045	20	0.110	x3H	.422	.481	409 x 400		4.5	35x3.2	3	350	55x3.2	1.559	831	0.950
S5	2.40	-	SS41	1.321	2133	1.045	20	0.110	x4H	.422	.476	409 x 400		4.5	35x3.2	3	350	55x3.2	1.559	831	0.950
S6	2.40	-	SS41	1.736	2089	1.349	20	0.083	1	-	-	409 x 400		4.5	35x3.2	3	350	55x3.2	1.559	831	0.950
S7	2.40	-	SS41	1.736	2089	1.349	20	0.083	1 (decr)	-	-	409 x 400		4.5	35x3.2	3	350	55x3.2	1.559	831	0.950
S8	2.40	-	SS41	1.848	2977	1.318	20	0.079	3	-	-	409 x 400		4.5	35x3.2	3	350	55x3.2	1.559	831	0.950
S9	2.40	-	SS41	1.848	2977	1.318	20	0.079	5	-	-	409 x 400		4.5	35x3.2	3	350	55x3.2	1.559	831	0.950
S10	2.40	-	SS41	1.736	2089	1.349	20	0.082	10	-	-	409 x 400		4.5	40x3.2	3	350	55x3.2	2.259	831	1.38
S11	2.40	-	SS41	1.736	2089	1.349	20	0.078	10	-	-	409 x 400		4.5	50x3.2	3	350	55x3.2	4.158	831	2.54
S12	2.40	-	SS41	1.736	2089	1.349	20	0.054	10	-	-	409 x 400		4.5	50x10.	3	350	55x3.2	8.110	831	5.01
S13	6.00	-	SM50	1.729	3845	1.432	105	0.092	10	-	-	800 x 820		10.	64x6.0	5	300	112x4.5	6.409	580	1.746
S14	6.00	-	SM50	1.729	3845	1.432	105	0.092	10	-	-	800 x 820		10.	64x6.0	5	680	112x4.5	1.127	580	0.294
S15	6.00	-	SM50	1.729	3845	1.432	105	0.092	10	-	-	800 x 820		10.	64x6.0	5	390	112x4.5	3.583	580	1.017
S16	6.00	2.00	SM50	1.729	3845	1.432	105	0.092	10	-	-	800 x 820		10.	64x6.0	5	390	112x4.5	>3.583	580	1.017
S17	6.00	2.00	SM50	1.729	3845	1.432	105	0.092	10	-	-	800 x 820		10.	64x6.0	5T	390	112x4.5	>3.583	580	1.017
S18	6.00	-	SM50	1.729	3845	1.432	105	0.092	10	-	-	800 x 820		10.	64x6.0	4	390	112x4.5	3.117	599	1.290
S19	2.40	-	SS41	1.591	2418	1.54	20	0.078	10	-	-	329 x 320		4.5	30x3.2	3	260	50x32	2.299	666	0.854
S20	2.40	0.78	SS41	1.591	2418	1.54	20	0.078	10	-	-	329 x 320		4.5	30x3.2	3	260	50x32	>2.299	666	
S21	2.40	-	SS41	1.591	2418	1.54	20	0.078	3&3.5H	0.46	0.500	329 x 320		4.5	30x3.2	3	260	50x32	2.299	666	0.854
S22	2.40	0.78	SS41	1.591	2418	1.54	20	0.078	3&3.5H	0.46	0.454	329 x 320		4.5	30x3.2	3	260	50x32	>2.299	666	

Table 2. Calculated and Experimental Loads and Displacements

Pier	Calculated Yield Load P_y (tf)	Maximum Load P_{max} (tf)	Specimen Overstrength ϕ_s	Calculated Yield Displ. d_y (mm)	Maximum Displ. d_u (mm)	Ductility $\frac{d_u}{d_y}$ μ	Mode of Failure
S1	8.6	13.8	1.60	13.5	58.5	4.33	Buckling
S2	8.6	14.2	1.65	13.5	54.3	4.02	Buckling
S3	8.6	-	-	13.5	-	-	No failure
S4	8.6	-	-	13.5	-	-	No failure
S5	8.6	15.9	1.85	13.5	173.5	12.9	Buckling
S6	11.7	16.5	1.41	13.9	70.0	5.04	Buckling
S7	11.7	16.9	1.44	13.9	-	-	Buckling
S8	12.4	17.3	1.40	13.9	51.0	3.67	Buckling
S9	12.4	17.1	1.38	13.9	53.0	3.81	Buckling
S10	12.4	15.0	1.27	13.9	46.7	3.34	Buckling
S11	12.4	17.2	1.41	13.9	57.5	4.11	Buckling-Base Weld Failure
S12	12.4	23.7	1.43	13.9	62.1	4.31	Base Weld Failure
S13	59.4	81.7	1.38	62.1	261.3	4.21	Buckling
S14	59.4	79.1	1.33	62.1	189.2	3.05	Buckling
S15	59.4	80.0	1.35	62.1	247.7	3.99	Buckling
S16	59.4	100.0	1.69	62.1	221.9	3.57	Base Weld Failure
S17	59.4	101.0	1.70	62.1	222.1	3.57	Base Weld Failure
S18	59.4	76.1	1.33	62.0	194.2	3.13	Buckling
S19	6.5	10.4	1.60	16.3	85.1	5.19	Buckling
S20	6.5	13.9	2.14	16.3	65.3	3.98	Base Weld Failure
S21	6.5	12.4	-	16.3	116.	-	Buckling
S22	6.5	14.5	-	16.3	88.	-	Base and Side Weld Failure

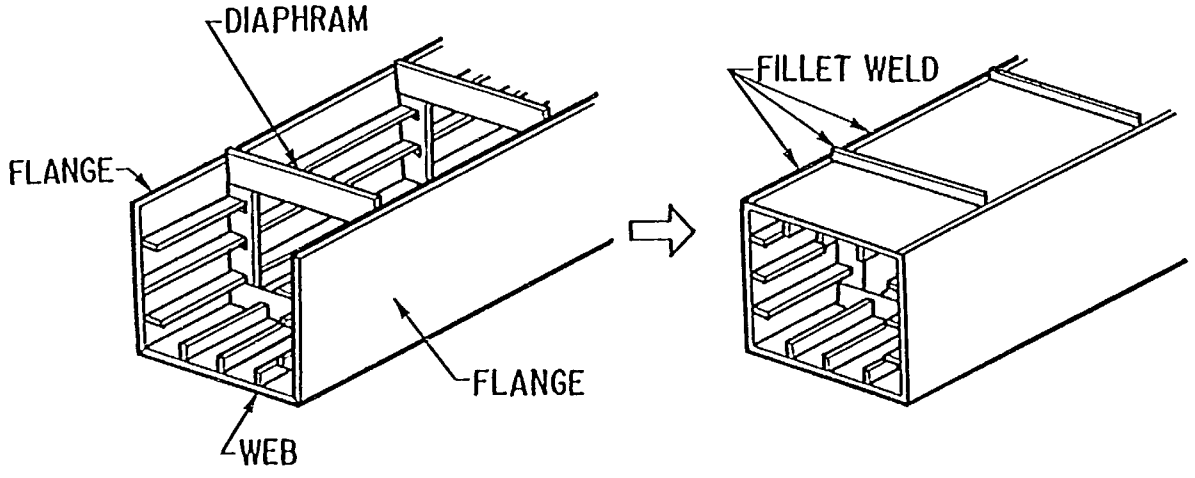


Figure 1 - Pier Construction

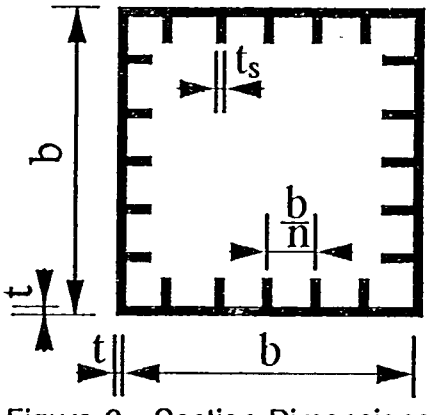
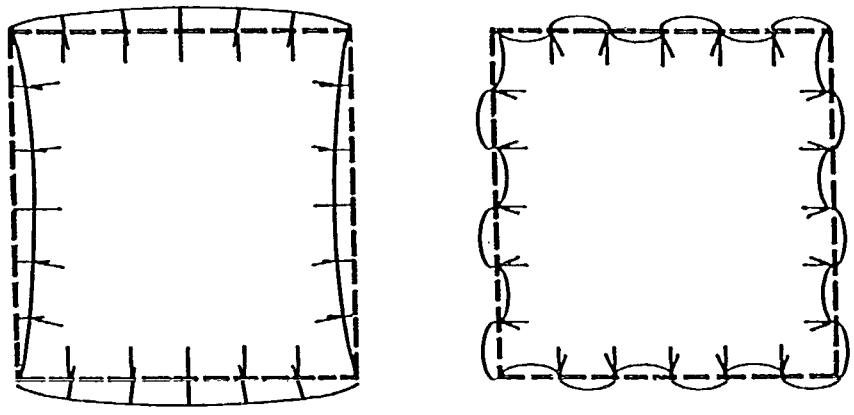


Figure 2 - Section Dimensions



(a) Overall Wall Buckling (b) Local Panel Buckling

Figure 3 - Modes of Deformation

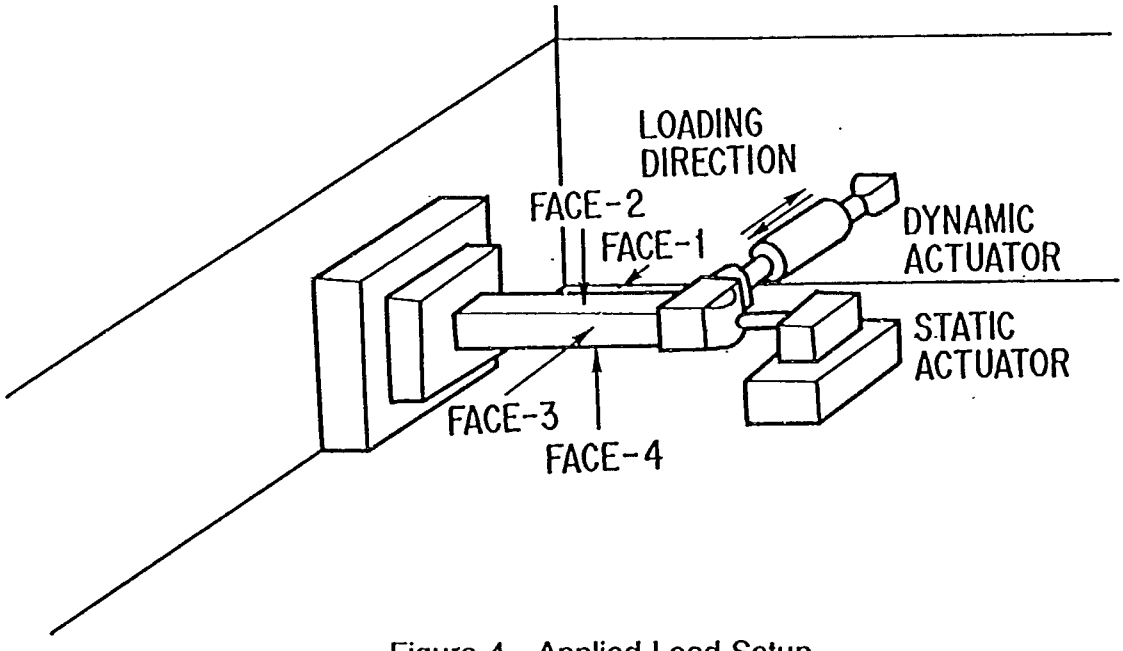


Figure 4 - Applied Load Setup

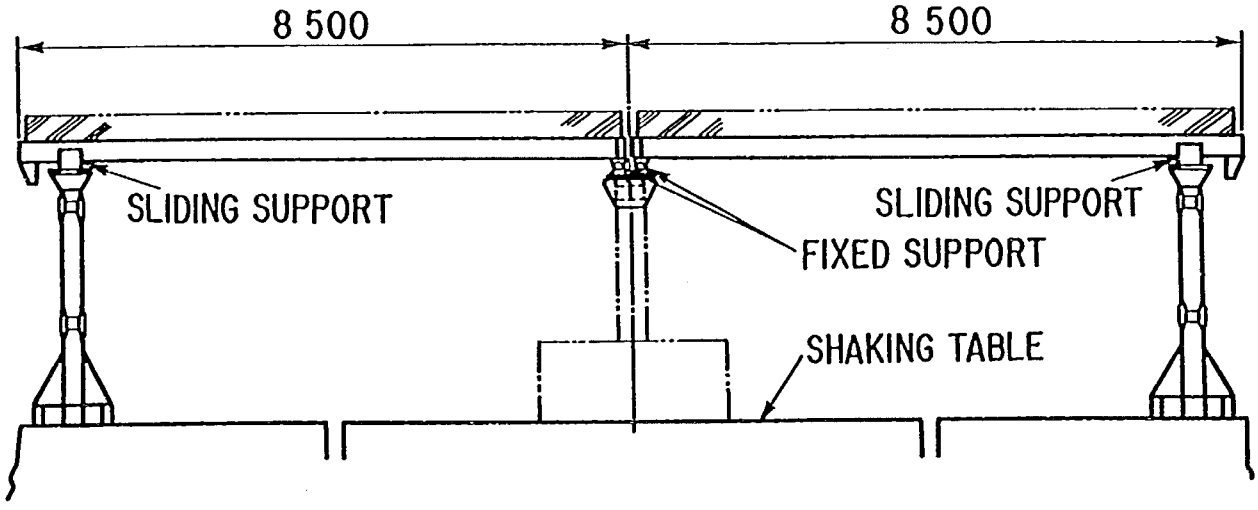


Figure 5 - Shaking Table Setup

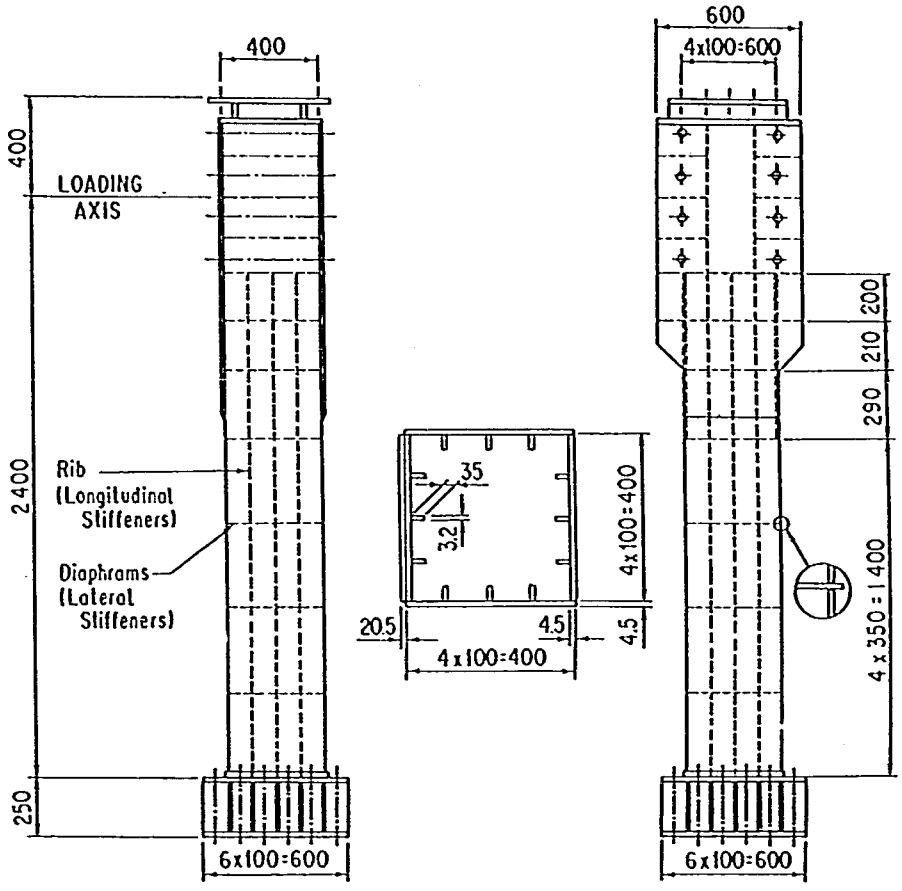


Figure 6 - Specimen S1

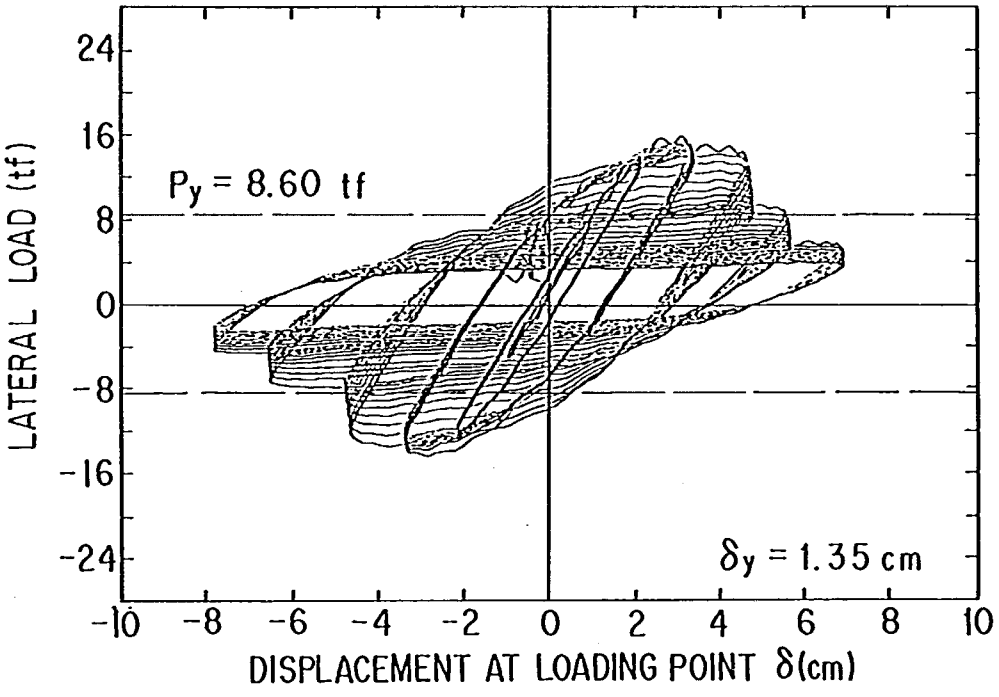


Figure 7 - Hollow Specimen Hysteresis Curve - Specimen S1

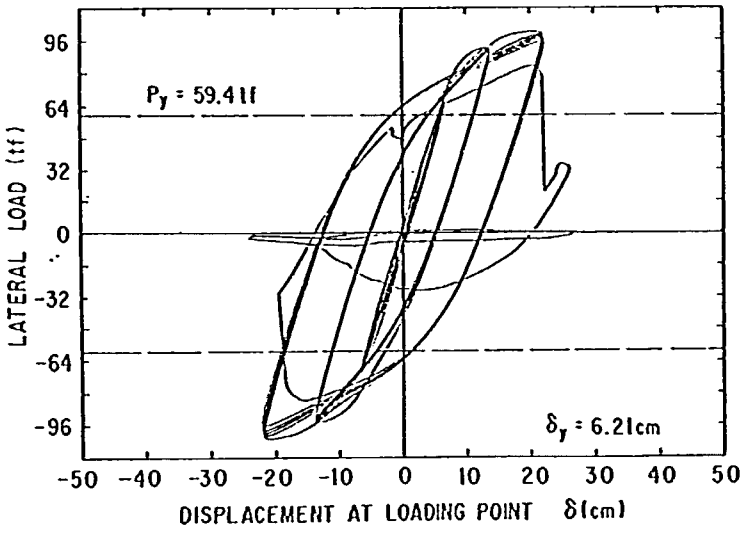


Figure 8 - Concrete-Filled Specimen Hysteresis Curve - Specimen S16

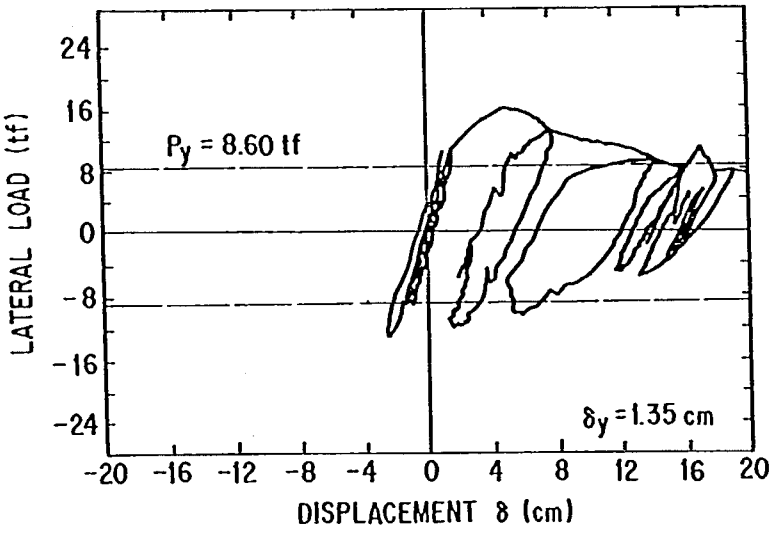


Figure 9 - Hysteresis Loop of Specimen on the Shaking Table - Specimen S5

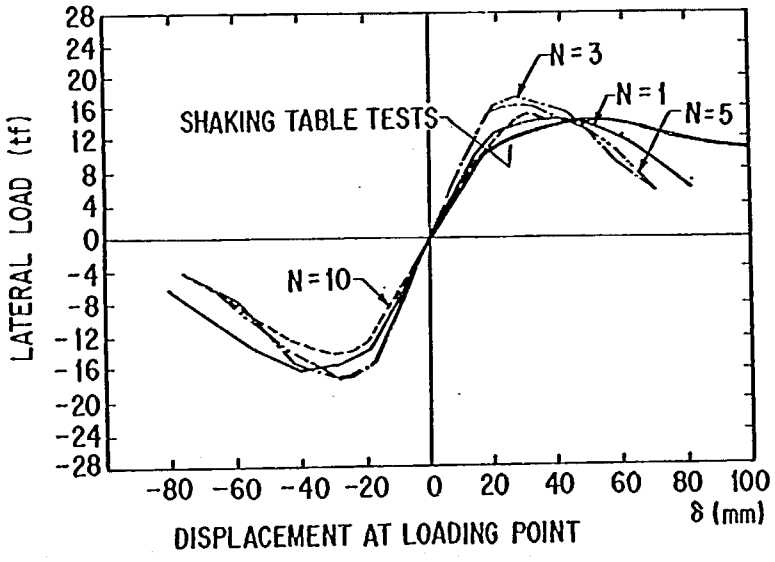


Figure 10 - Backbone Curve of Specimens S1, S6, S8, S9 and Shaking Table Tests

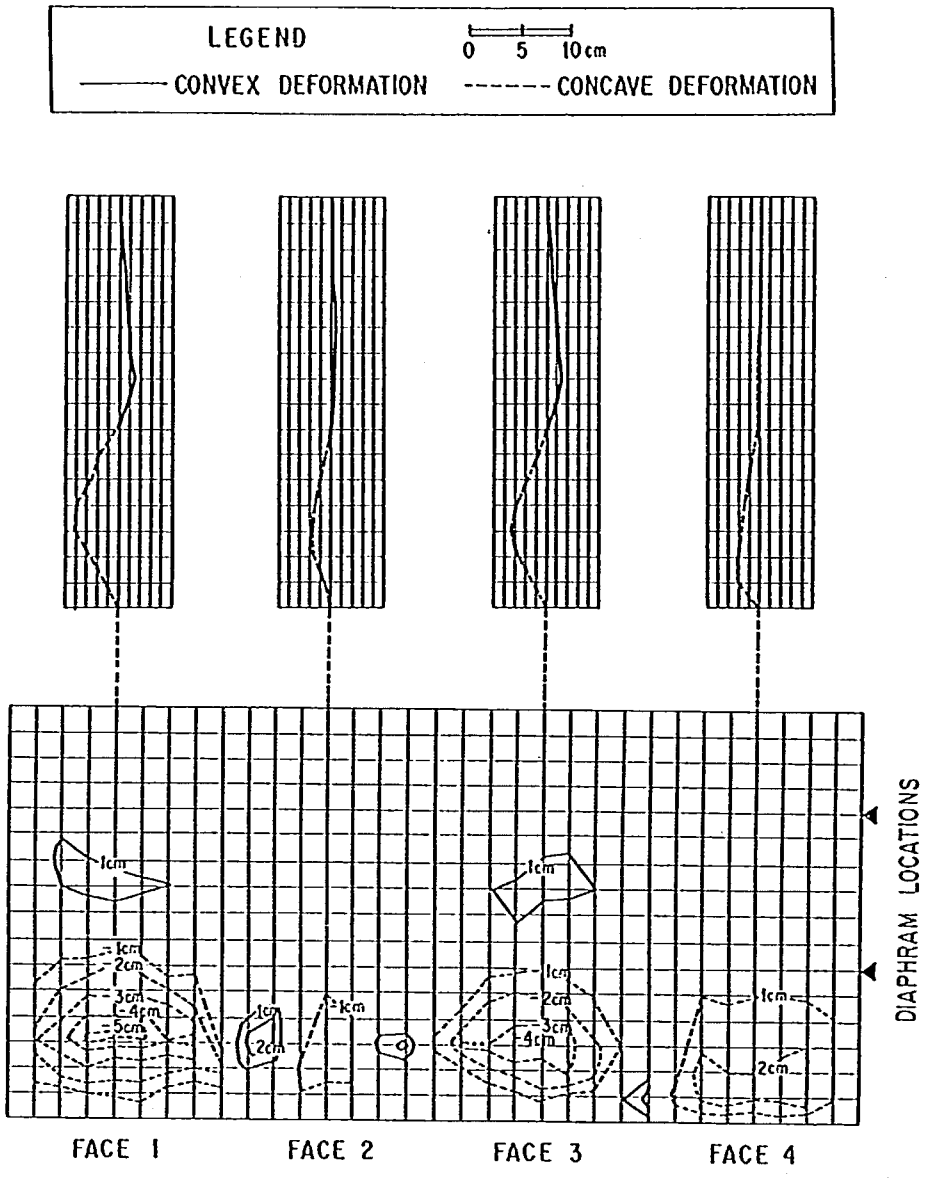


Figure 11 - Buckling of Specimen S1 at the End of the Test

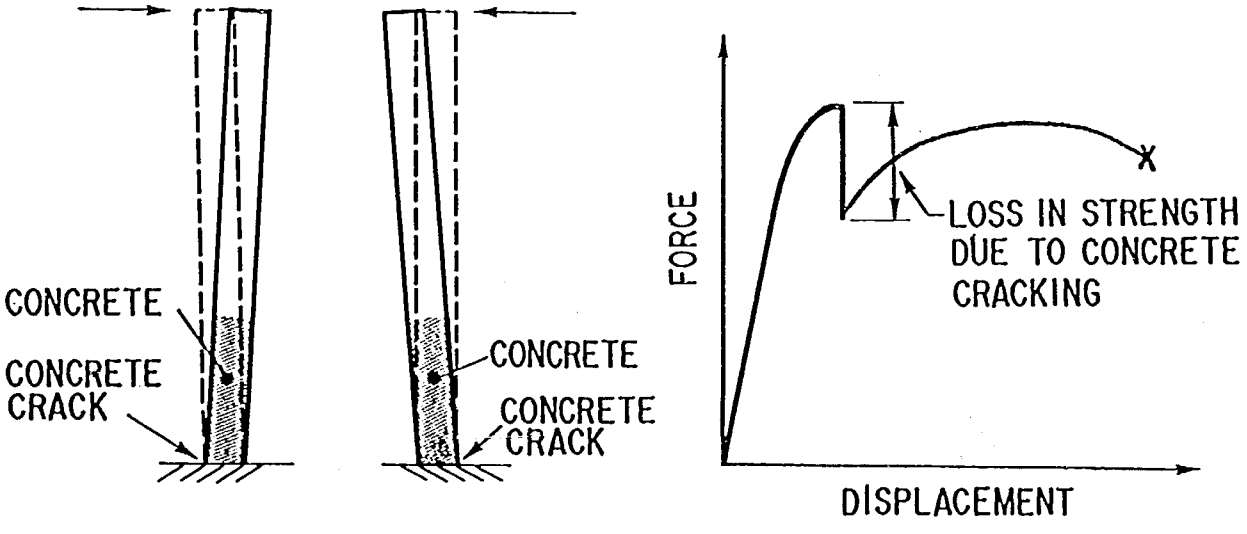


Figure 12 - Deformation of Concrete-Filled Piers

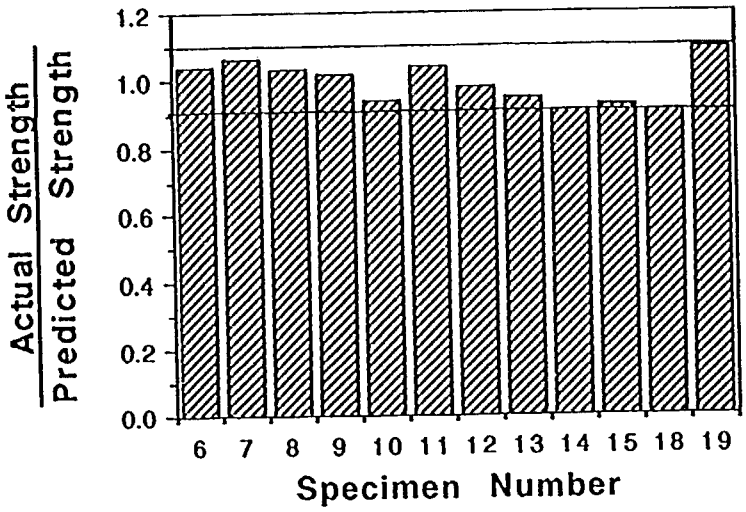


Figure 13 - Comparison of Overstrengths

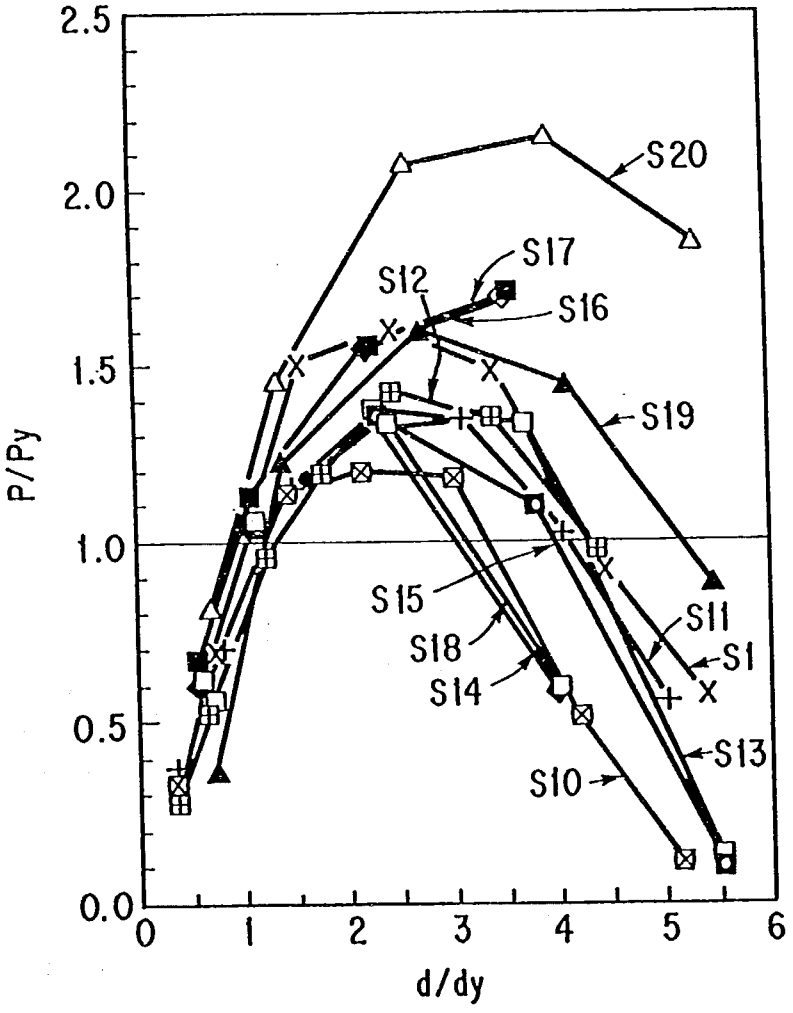


Figure 14 - Comparison of Specimen Backbone Curves

ESTIMATION OF THE DEFORMATION CAPACITY OF STEEL BRIDGE PIERS

by
Gregory A. MACRAE
and
Kazuhiko KAWASHIMA

U.S. — JAPAN SEMINAR ON CYCLIC BUCKLING
OF STEEL STRUCTURES AND STRUCTURAL
ELEMENTS UNDER DYNAMIC LOADING CONDITIONS
Osaka, Japan
July 1991

Estimation of The Deformation Capacity of Steel Bridge Piers

by

Gregory A. MacRae
Researcher, Earthquake Engineering Division, PWRI, Tsukuba, Japan

Kazuhiko Kawashima
Head, Earthquake Engineering Division, Public Works Research Institute, Tsukuba

ABSTRACT

A semi-rational method to assess the deformation capacity of steel members subjected to repeated cyclic displacements in the inelastic range is described. The method assumes that the maximum deformation capacity of a member will be related to the inelastic strain over an equivalent plastic hinge length and to the resistance of the section against buckling. It is shown that the method worked satisfactorily on recently tested steel bridge pier specimens and that the number of cycles of loading is an important parameter in the testing of members with large axial loads.

INTRODUCTION

Simple methods for assessing the deformation capacity of reinforced concrete bridge piers in the event of an earthquake are incorporated in both the Japan and New Zealand bridge design codes [1,2]. Methods for routine design are also needed to evaluate the deformation capacity and earthquake resistance of steel members in structures which are not strong enough to resist a major earthquake elastically.

In this paper a semirational method is outlined to assess the deformation capacity of steel members. Firstly, the effect of different axial load ratios on the deformation capacity of identical H-shaped column sections which were subjected to a fixed number of load cycles to each displacement ductility is described and a method for assessing the deformation capacity of this type of member is discussed. Then, using the results of steel piers tested at PWRI, Tsukuba, Japan, a preliminary method is proposed to assess the deformation capacity of pier specimens with different section slenderness ratios. This method considers the damage in the section and the resistance of the section against buckling.

COLUMN TESTS AND RESULTS

Eight identical 250 UC 73 H-shaped steel beam-columns were tested at the University of Canterbury, New Zealand [3,4,5], in order to assess the effect of axial load on the cyclic behaviour of steel beam columns. The axial load ratios, P/P_y, used for seven specimens were 0.0, 0.3, 0.4, 0.5, 0.6, 0.7, 0.8 and a further specimen was tested which had an axial load ratio which varied with the displacement. Two cycles of loading were applied to displacement ductilities of 2, 4, 6, 8 etc. until the strength of the specimen dropped to less than 70% of the calculated plastic moment capacity, M_p. It was found that all of the specimens had fat hysteresis loops which absorbed a large amount of energy as shown for the specimen in Figure 1 with an axial load ratio, P/P_y, equal to 0.50. A large amount of axial shortening was also observed to occur in this specimen and the other axially

loaded specimens as shown in Figure 2 but very little change in length occurred in the specimen with no applied axial load. The buckle length was generally equal to the breadth of the flange as shown in the yield line mechanism in Figure 3. From the strain measured at the base of these specimens with potentiometers an equivalent plastic hinge length approximately equal to the flange breadth was found to be reasonable for these specimens. The equivalent plastic hinge length concept is described below.

Plastic Hinge Concept

The actual strain over the base of a member depends on the distance from the point of contraflexure as shown in Figure 4. In order to approximate the damage in a real member it is convenient to consider that this strain is distributed uniformly over a fixed length, L_p. This length, L_p, is known as the "plastic hinge length". The inelastic rotation, Θ_H, of a member over the plastic hinge length may then be approximated as

$$\Theta_H = (d_u - d_y)/L = (\phi_u - \phi_y)\, L_p \qquad (1)$$

where d_u and d_y are the ultimate and yield displacements and ϕ_u and ϕ_y are the ultimate and yield curvatures over the plastic hinge length respectively and L is the length of the member. A slightly more accurate version of this formula is available [6] which considers that the centre of rotation is at the centre of the plastic hinge length, however, this is more difficult to apply.

Maximum Section Strain

It was found in these tests that the maximum section strain was a major factor in the assessment of deformation capacity. The maximum strain at the centre of a beam or column flange may be calculated as:

$$\varepsilon_f = \varepsilon_{av} + \phi\,(D - T)/2 \qquad (2)$$

where D is the depth of the member, T is the flange thickness, and the curvature, ϕ, is able to be calculated from the elastic curvature plus the inelastic curvature, as $\phi = M_p/(EI) + \Theta_H/L_p$. Based on the tests of H-shaped columns with various levels of axial load it was found that the rate of accumulation of average axial strain, ε_{av}, over the hinge length in the members increased linearly with cumulative inelastic rotation, $\Sigma\Theta_H$, before buckling became severe as shown in Figure 5. When buckling became significant at the larger strains the curves became non-linear. The amount of axial shortening for members with a low axial load depended on the level of applied axial load. However, the amount of axial shortening did not seem to be sensitive to the amount of applied axial load for members with very high levels of axial load because the neutral axis was in the flange allowing very little yielding in tension. It may be seen in Figure 6 that when the neutral axis is in the compression flange a change in the axial load level leads to only a very small change in the position of the neutral axis and in the value of flange tension strain for a particular hinge rotation. The neutral axis will be in the web in specimens with low axial loads and the section is likely to yield in tension as well as in compression. A specimen with no applied axial load would not be expected to shorten axially before buckling occurs.

The expected column axial strain, ε_{av}, over the plastic hinge length, L_p, for the H-shaped columns was able to be calculated as:

$$\varepsilon_{av} = \delta_{av}/L_p = \alpha.\,\Sigma\Theta_H \qquad P/P_y > \beta A_w/A \qquad (3)$$

$$= [(P/P_y) / (\beta A_w/A)].\alpha.\,\Sigma\Theta_H \qquad P/P_y < \beta A_w/A$$

where α and β are parameters predicted by experiment, A_w is the area of the web in the section, A is the total area of the section, and $\Sigma\Theta_H$ is the cumulated inelastic curvature which is given as $\Sigma\Theta_H = d_y/L.\Sigma\mu_i$. The cumulative inelastic ductility, $\Sigma\mu_i$, is found from the inelastic part of the loading regime as shown in Figure 7. When $P/P_y < \beta A_w/A$ it is

assumed that the neutral axis is between the flange and the web. Values of α and β of 0.446 and 2.54 respectively fitted the experimental results.

In the column specimens tested, the effect of the average axial strain was much larger than the effect of the curvature. The calculated and actual axial strains at failure given in Table 1 are significantly different because of the effect of buckling. Apart from Specimen C6 the amount of axial shortening was approximately constant ranging from 48mm to 62mm for the specimens failing by buckling. The maximum axial displacement of Specimen C6 is recorded as being much larger than that of Specimen C7 because it sustained one more cycle of loading. This is because the load dropped off very slowly in all of the specimens making it difficult to assess when the failure criterion was reached. All values given in this table should therefore be regarded as being approximate. As Specimens C0 and CA did not fail by buckling they unable to be considered in the equations.

It was considered that the maximum flange strain, which is almost equal to the average strain for the specimens tested, was the most important parameter to determine the deformation capacity of those members which failed by buckling. The pure axial strain in these members, which does not consider the effect of the deformation due to buckling, may be estimated using the formulae given and the actual axial strain was in all cases less than 1.6 times the predicted pure strain for these specimens at failure. The resistance against buckling was the same for these specimens because they were identical.

DESIGN METHOD AND ESTIMATION OF THE DEFORMATION CAPACITY OF HOLLOW STEEL BRIDGE PIERS

Pier Design Method

A method is presently being developed to predict the behaviour of steel members with different section slendernesses based on the results of the 22 hollow stiffened steel bridge pier specimens which were discussed in the accompanying paper [7]. Design of these pier specimens was carried out according to the Japanese bridge design code [1] which is based on elastic design considerations. The background to the buckling design criteria for these piers is published in design guidelines [2]. There are two important section slenderness ratios which are required to be greater than certain values in order that premature buckling does not reduce their strength. They are:

1) The **panel slenderness ratio, b/(nft)**, which must be less than 28 or 24 for Grades SS41 or SM50 steel respectively. This check ensures that local panel buckling will not occur before the yield strength of the section is reached. Local panel buckling refers to buckling of the panels between the vertical stiffeners. In this ratio b is the width of the section (cm), t is the plate thickness (cm), n is the number of panels divided by vertical stiffeners and f is given as $f = 0.65(\phi/n)^2 + 0.13(\phi/n) + 1.0$, ϕ is the stress gradient given as $\phi = (\sigma_2 - \sigma_1)/\sigma_1$, and σ_2 and σ_1 are the stresses at each edge of the plate, where $\sigma_1 > \sigma_2$, and compressive stress is defined as positive. It was conservatively assumed that $f = 1.0$ in the panels which yielded.

2) The **gamma ratio, $\gamma_l/\gamma_{l,req}$**, which must be greater than unity. This check ensures that overall wall buckling of the pier will not occur before the yield strength of the section is reached. The stiffness of each panel and longitudinal stiffener was used to obtain an equivalent stiffness for the side as a whole and the effect of the lateral stiffeners was also considered. The value of γ_l, which is the relative stiffness of the longitudinal stiffeners, was able to be calculated as $\gamma_l = I_l/(bt^3/11)$ where the value of I_l is given below. The value of $\gamma_{l,req}$ was able to be calculated using the appropriate value from Equations 4 or 6 as described below.

i) Equation 1 should be used to calculate $\gamma_{l,req}$ when α is not greater than α_o and the moment of inertia I_l (cm^4) of a transverse stiffener satisfies Equation 5.

$$\gamma_{l,req} = 4\alpha^2 n \left(\frac{t_o}{t}\right)^2 (1 + n\,d_l) - \frac{(\alpha^2+1)^2}{n} \qquad (t \geq t_o)$$

$$\gamma_{l,req} = 4\alpha^2 n (1 + n\,d_l) - \frac{(\alpha^2+1)^2}{n} \qquad (t < t_o) \tag{4}$$

$$I_l \geq \frac{bt^3}{11} \cdot \frac{1 + n\,\gamma_{l,req}}{4\alpha^3} \tag{5}$$

ii) Equation 6 should be used in all other cases such as when the effect of the transverse stiffeners in the computation of $\gamma_{l,req}$ is insignificant and their effect is ignored.

$$\gamma_{l,req} = \frac{1}{n}\left[\left\{2n^2\left(\frac{t_o}{t}\right)^2(1 + n\,d_l) - 1\right\}^2 - 1\right] \quad (t \geq t_o)$$

$$= \frac{1}{n}\left[\left\{2n^2(1 + n\,d_l) - 1\right\}^2 - 1\right] \qquad (t < t_o) \tag{6}$$

where

α is the aspect ratio of stiffened plate, $\alpha = a/b$,

α_o is the critical aspect ratio, $\alpha_o = \sqrt[4]{1 + n\,\gamma_l}$

a is the spacing of transverse stiffeners (cm)

b is the width of stiffened plate (cm)

d_l is the ratio of the longitudinal stiffener cross sectional area to that of the main plate, $d_l = A_l/(bt)$

A_l is the area of each longitudinal stiffener, $A_l = b_s t_s$

I_l is the second moment of area of each longitudinal stiffener. The code requires that the moment of inertia of stiffeners such as those used in steel piers be calculated about the surface of the stiffened plate on the stiffener side. The value of I_l is therefore given as $I_l = b_s{}^3 t_s/3$.

t_o is the minimum thickness of plate which is given as b/(28fn) for SS41 and b/(24fn) for SM50 plate. A more general expression for the allowable buckling ratio of compact sections using the allowable yield stress is given in Equation 7.

$$\frac{b}{t_o.n.f} \cdot \frac{\sqrt{F_y}}{1047.7} = 1.0 \tag{7}$$

t_s is the thickness of each longitudinal stiffener

A further ratio, the **gamma* ratio** [2], γ_l/γ_l^*, is able to be used to <u>predict whether local panel buckling or overall wall buckling will occur first</u> as shown in Figure 8. If $\gamma_l/\gamma_l^* > 1$ then local buckling of the panels between the longitudinal stiffeners is the expected initial buckling mode but if $\gamma_l/\gamma_l^* < 1$ then overall wall buckling is expected. The value of γ_l^* is given in Equation 8.

$$\gamma_l^* = 4\,\alpha^2\,n\,(1+n\,d_l) - \frac{(\alpha^2+1)^2}{n} \quad (\alpha \leq \alpha_o)$$

$$= \frac{1}{n}\left[\left\{2\,n^2(1 + n\,d_l) - 1\right\}^2 - 1\right] \quad (\alpha > \alpha_o) \tag{8}$$

It should be noted that the first part of Equation 4, which was applicable for all of the piers designed, and Equation 8 are very similar when $t > t_o$ and $\alpha < \alpha_o$. The value of $\gamma_{l,req}/\gamma_l^*$ is almost equal to $(t_o/t)^2$ as the term subtracted at the end of these equations is usually

small. Therefore $\gamma_{l,req}$ must be greater than γ_l^* in sections which are designed to be fully effective to resist load (compact sections) because t_o/t must be greater than or equal to 1.0 in order to satisfy the local panel buckling requirements. The ratio $\gamma_l/\gamma_{l,req}$ is also required to be greater than 1.0 giving the allowable area for the design of piers shown graphically in Figure 9.

Deformation Capacity

Specimens Failing By Overall Wall Buckling

A definition of deformation capacity which is related to the actual physical damage is required in order to understand the seismic behaviour of the pier specimens tested [7]. Displacement ductility is not a good measure of damage because the definition is affected by the elastic behaviour of the piers. In the methods used below it was assumed that the maximum inelastic section strain was the main parameter which determined member behaviour and that the effects of axial load were insignificant on these pier specimens. This was considered to be reasonable because the axial load ratio was always less than 11% and there was little difference in the behaviour of the members with different numbers of cycles of loading to each displacement ductility [7].

The plastic hinge length of the specimens was assumed to be equal to the distance between the lateral stiffeners "a" at the base of the specimens [7]. This is because almost all of the buckling deformation tended to concentrate in the section below the first lateral stiffener at the base of the specimens. The inelastic curvature over this region may be calculated as $\phi_i = \theta_i/a$, where θ_i is the plastic rotation capacity, $\theta_i = (d_u - d_y)/L$, L is the height of the pier, and d_u and d_y are the ultimate and yield displacements respectively. The inelastic strain, ε_i, may be calculated approximately as $\varepsilon_i = \phi_i\, D/2$, where D is the depth of the steel section and the inelastic strain is given as $\varepsilon_i = \theta_i\, D/(2a)$.

The inelastic strain calculated by this method, as shown in Figure 10, was considered to be a measure of the damage suffered by the specimens. The effect of the damage sustained in the form of strain will be dependent on the damage resistance factor for each of the specimens. It would be expected that the strain able to be sustained would be greater in more compact sections than in those with more slender characteristics.

The gamma ratio, $\gamma_l/\gamma_{l,req}$, which is used for the design against buckling of one side of elastic structures was selected as the damage resistance factor for inelastically behaving specimens which failed by overall wall buckling. Further background to the selection of this ratio for damage resistance is given in the Appendix. If the gamma ratio and the inelastic strain defined above are good measures of member deformation capacity, then this strain divided by the gamma ratio should be approximately constant for the members tested. This is called the "deformation factor for wall buckling", ξ_o, where $\xi_o = \varepsilon_i/(\gamma_l/\gamma_{l,req})$. For example, in Specimen S1, θ_i = (5.85 - 1.35)/240cm = 0.0188 rad, ε_i = 0.0188 x 40cm/(2 x 35cm) = 0.0107 and ξ_o = 0.0107/1.559 = 0.00689.

The values of ξ_o is given for the specimens in Figure 11. It may be seen that the piers which failed in the mode of "overall wall buckling" had a ξ_o factor between about 0.006 and 0.0075. The piers which did not have results within this range were Specimen S10 which failed by overall wall buckling after sustain reasonable panel buckling, Specimens S11 and S12 which failed by local panel buckling and finally fracture at the base, Specimens S16, S17 and S20 which were filled with concrete and Specimens S14 and S15. Specimen S14, like Specimens S1, S19 and S13, sustained some distortion of the section above the base section as well as in the base section which would be expected

to give it more deformation capacity. It is considered that this type of damage should not be relied upon to provide greater deformation capacities as it is not yet able to be predicted. It was also considered that the deformation capacity of Specimen S6 was slightly larger than that of Specimens S1, S2, S8, and S9 as a result of it only being subjected to one cycle of loading at each ductility step.

The method described above seems to be satisfactory for members which fail by buckling of one side and a value of ξ_o of 0.006 is thought to be reasonable for the design of these specimens. However, a modification should be made for those specimens which did not fail in this manner.

Specimens Failing By Local Panel Buckling

Using the same principles as those used to determine the deformation capacity of members deforming by overall wall buckling a deformation factor for local panel buckling, ξ_p, is defined as $\xi_p = \varepsilon_i/(tnf/b)^2$. This value is shown for the different specimens in Figure 12. A reasonable value for the members which were strongly influenced by local panel buckling, that is Specimens S11, S12, S13 and S19 is about 5. Other specimens, which failed by buckling of one side, would not generally be expected to have deformation greater than those which failed by local panel buckling when calculated by this method. However, the value of ξ_p for Specimen 13 was significantly greater than the level for the other piers because buckling occurred in the two bottom sections on one side of the specimen causing deformation of the lateral stiffener and the value of ξ_p of Specimen S6 was greater because it was only subjected to one cycle to each displacement ductility.The fact that many of the specimens which failed by local panel buckling have a ξ_p value around this level reflects that many of these specimens had gamma' factors near to unity and were probably affected to some extent by both local panel buckling and overall wall buckling.

Specimens Failing By Both Wall and Panel Buckling

In order to obtain a combined resistance, ψ, for the specimens under the two types of buckling the greater of the values of $\xi_o/0.006$ and $\xi_p/5$ were plotted together on the same graph in Figure 13. Local panel buckling affected the strengths of Specimens S10 to S13. Higher values of this combined ratio, ψ, indicate lower resistances against damage. The mode of buckling with the lowest resistance is likely to control failure. Specimen S10 was still significantly less than one indicating that perhaps interaction of buckling reduced the resistance of this specimen. Using the approach outlined above a method for the design of these sort of piers is given below.

Design Steps For Determining the Ductility Capacity of Bridge Piers

1. Determine the plastic hinge length of the member. This distance over which a full buckle wavelength occurs should be taken as the plastic hinge length, L_p. This is generally equal to the breadth of the flange in H-shaped members but in members where there are closely-spaced lateral stiffeners the plastic hinge length may be equal to the distance between these stiffeners.

2. Calculate the maximum inelastic strain which may be resisted as

$$\varepsilon_i < \xi_o (\gamma/\gamma_{i,req}) = 0.006 (\gamma/\gamma_{i,req})$$
$$< \xi_p (tnf/b)^2 = 5 (tnf/b)^2$$

3. Using the plastic hinge length the ductility capacity, μ, may be calculated as

$$\mu = 1 + \frac{2\varepsilon_i L L_p}{D d_y}$$

In this method described it is assumed that all members are compact and are able to attain their full moment capacity, the members all sustain the same effects from cyclic loading, the effect of axial load was negligible and that interaction between the different types of buckling may be ignored.

SUMMARY, AND SUGGESTIONS FOR FURTHER RESEARCH

In this paper it was shown that

i) The axial deformation of H-shape columns before buckling became severe could be estimated by using the concept of an equivalent plastic hinge length.
ii) The maximum flange strain was considered to be a good measure of the damage suffered and of the deformation capacity of the H-shape columns.
iii) A method of estimating the damage resistance of members based on using the elastic section buckling design requirements was proposed.
iv) By considering the damage suffered and the damage resistance of the specimens a simple, semi-rational method for estimating the deformation capacity of steel members was proposed.
v) It was found that the method worked satisfactorily for certain types of steel bridge piers which were subjected to two modes of buckling when empirical factors were used to calibrate the design method to the results of tests. A step-by-step method for the design of these piers was given.

Many assumptions were required in order to obtain the method described. Further work is required to verify these assumptions and to adapt the method to different types of member.

REFERENCES

1. Japan Road Association, "Specifications for Highway Bridges", 1990 (in Japanese).
2. Transit New Zealand, "Bridge Manual : Design and Evaluation", (Draft for Comment), Wellington, 1991.
3. MacRae G. A., Carr A. J., and Walpole W. R., "The Seismic Response of Steel Frames", Research Report 90-06, Department of Civil Engineering, University of Canterbury, 1990.
4. MacRae G. A., Carr A. J. and Walpole W. R., "Cyclic Behaviour of Steel I-Shaped Beam-Columns", Pacific Structural Steel Conference, Brisbane, 1989.
5. MacRae G. A., Walpole W. R. and Carr A. J., "Inelastic I-Shaped Beam-Columns in Earthquake-Resistant Structures", Pacific Structural Steel Conference, Brisbane, 1989.
6. Priestley M. N. J. and Park R., "Strength and Ductility of Bridge Substructures", Road Research Unit Bulletin 71, National Roads Board, Wellington, New Zealand.
7. Kawashima K., Hasegawa K., MacRae G. A., Ikeuchi T., and Oshima K. "Ductility of Steel Bridge Piers from Dynamic Loading Tests", US-Japan Seminar, July 1-8, 1991 (Accompanying Paper).
8. Japan Road Association, "Specifications for Highway Bridges", Part II : Steel Bridges, English Edition, 1987.
9. Subcommittee on Stability Design, "Guidelines for the Stability of Steel Structures", edited by Fukumoto Y., Committee on Steel Structures, Japan Society of Civil Engineers, 1987.

APPENDIX. VERIFICATION OF METHOD TO OBTAIN COMPARATIVE STIFFNESS

In order to assess the resistance of a pier against overall wall buckling an equation of the form given below was used:

$$(\gamma_l/\gamma_{l,req})^n > 1 \qquad \text{A1}$$

Most buckling design ratios are presented in codes in a pass/fail form which is easy to use but it does not relate to comparative safety of different specimens. It is therefore necessary to find an appropriate value of "n" in order to be able to estimate the relative likelihood of damage. The "n" value chosen must result in a $\gamma_{l,req}$ value which is linearly related to the Youngs modulus, E, because the elastic buckling load is proportional to the material tangent stiffness. Most design formulae however do not use the Youngs modulus directly because it is a constant. The Youngs modulus is often divided by the yield stress, F_y, and the results of the buckling equations are dependent on the units used for the yield stress. Therefore, formulae which are proportional to the yield stress will be inversely proportional to the Youngs modulus. The value of $\gamma_{l,req}$ given for the design of piers is proportional to t_o^2 where t_o is given as:

$$t_o = \frac{b}{fn} \cdot \frac{\sqrt{F_y}}{1047.7} \qquad \text{A2}$$

Therefore $\gamma_{l,req}$ is proportional to F_y and inversely proportional to the Youngs modulus. The $\gamma_l/\gamma_{l,req}$ ratio is dependent directly on the Youngs modulus giving a value of "n" in Equation A1 of 1.0. The $\gamma_l/\gamma_{l,req}$ ratio is therefore used to assess the resistance of a pier against buckling. In the case of local panel buckling the resistance against buckling is given as $(fnt/b)^2$.

It should be noted that in these assumptions the effect of the strain hardening stiffness is considered to be the same for all grades of steel independently of the initial yield stress. Verification of this assumption is required.

Table 1.
Results of H-Shaped Steel Beam-Columns

Unit	Axial Load Ratio	Cycles	Maximum Disp. (mm)	Cumulative Disp. (mm)	Cumulative Ductility	Axial Disp. Predicted (mm)	Axial Disp. Observed (mm)
C0*	0.0	10x8	44.2	1719	389	0	≈5
C3*	0.3	10x2	39.2	678	173	47	62
C4	0.4	-8x2	25.9	392	121	36	51
C5	0.5	10x1	27.0	370	137	42	60
C6	0.6	10x3	22.4	468	209	62	78
C7	0.7	10x2	16.2	280	173	38	60
C8	0.8	14x1	14.6	313	301	42	48
CA*	Varying	10x2	31.3	-	173	-	43

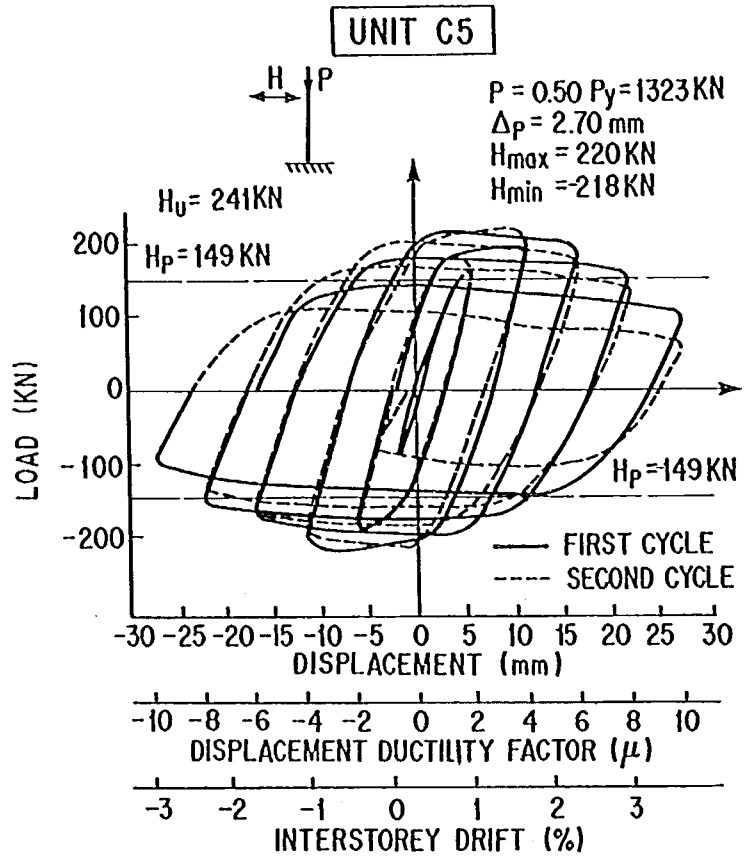


Figure 1. Column C5 - Hysteresis Loop

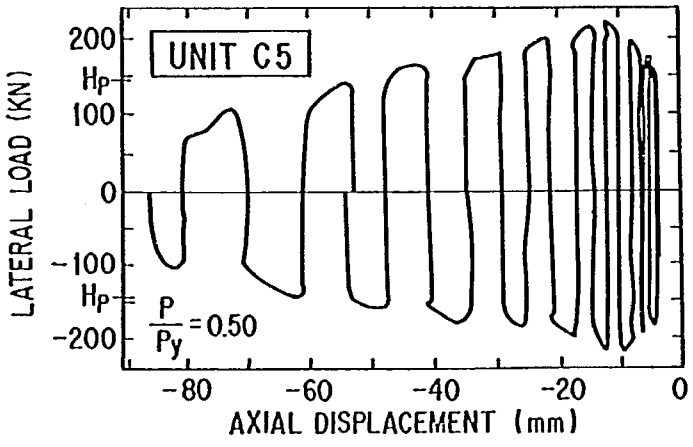


Figure 2. Column C5 - Axial Deformation

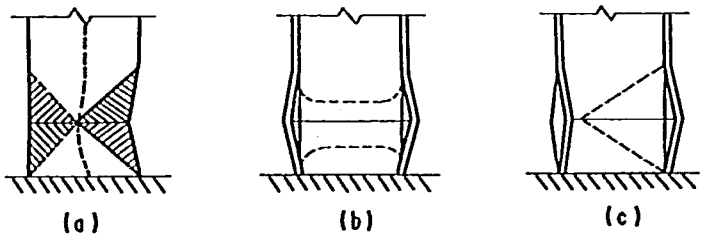


Figure 3. H - Shaped Column Yield Line Mechanisms

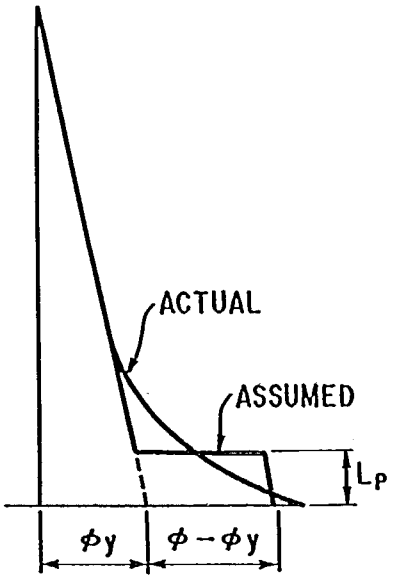


Figure 4. Plastic Hinge Length, L_p

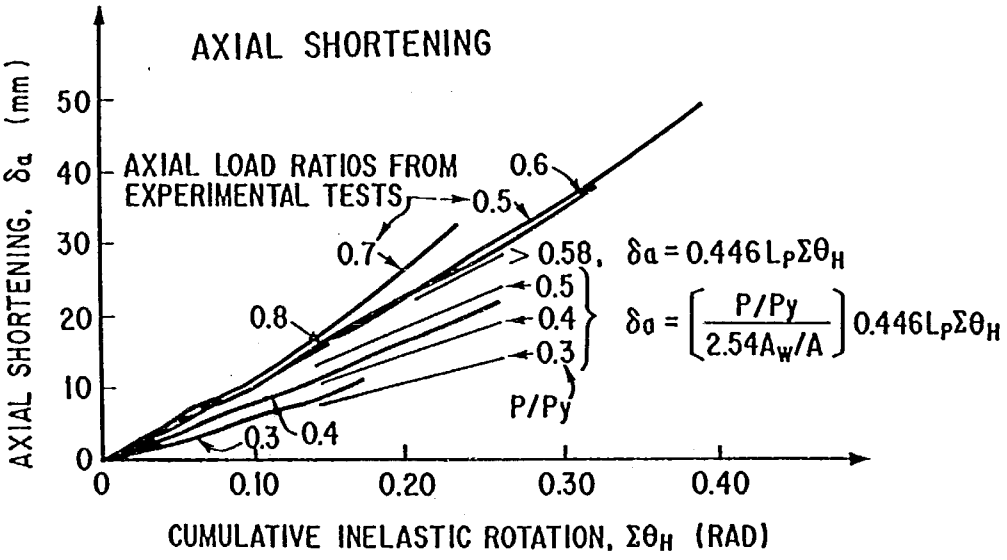


Figure 5. Accumulation of Axial Displacement with Inelastic Rotation

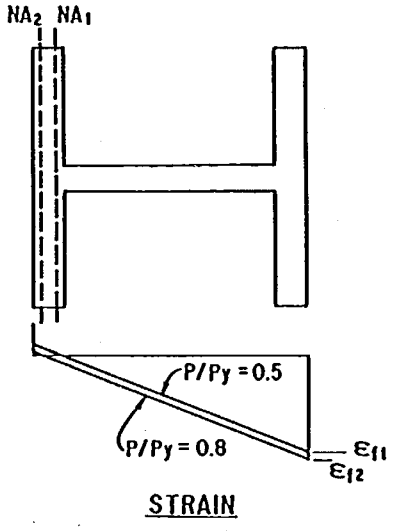


Figure 6. Strain Distribution on Members with NA in the Flange

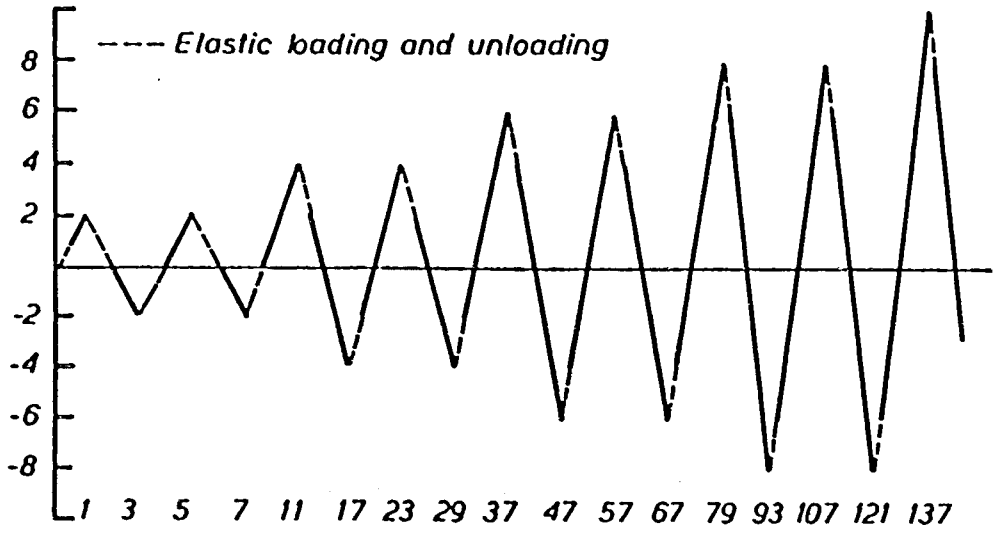
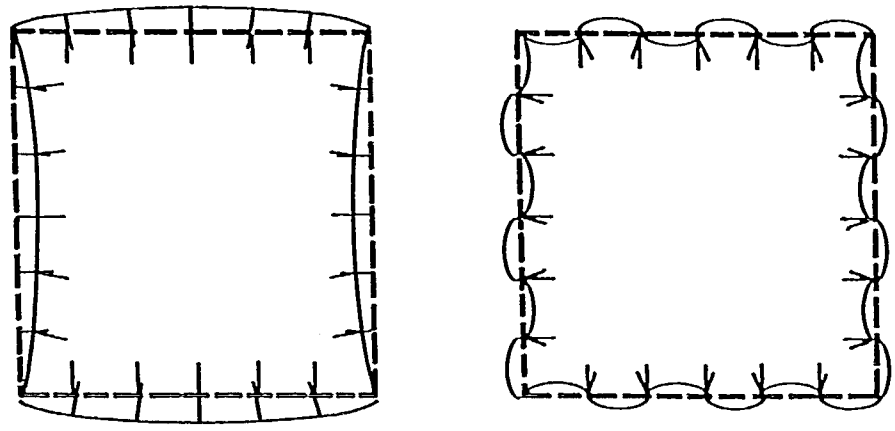


Figure 7. Cumulative Inelastic Ductility



(a) Overall Wall Buckling (b) Local Panel Buckling

Figure 8. Buckling Modes of Steel Piers

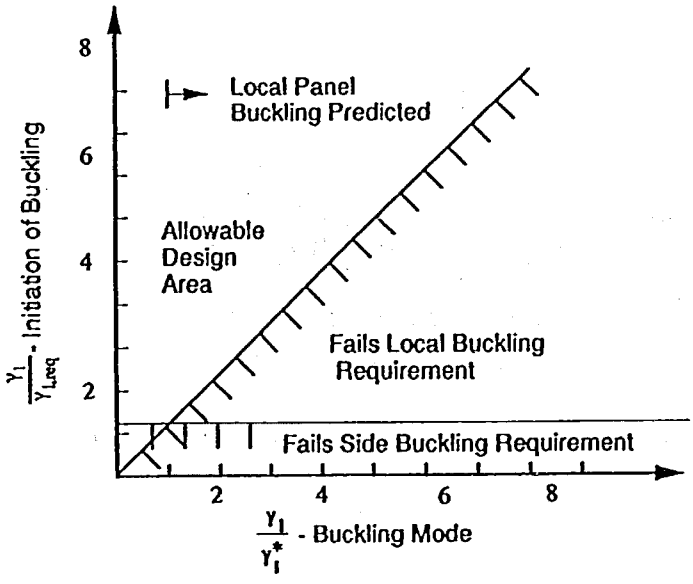


Figure 9. Allowable Design Ratios for Steel Piers

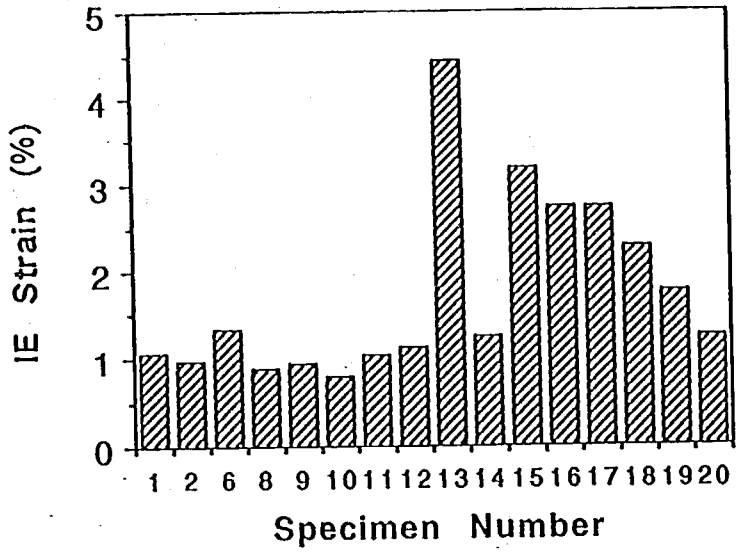


Figure 10. Inelastic Strain in Steel Piers

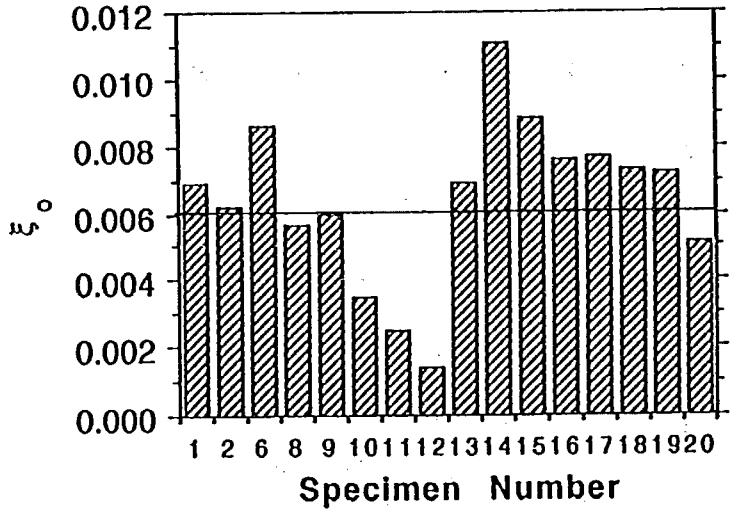


Figure 11. Deformation Factor, ξ_o, for Buckling of One Side

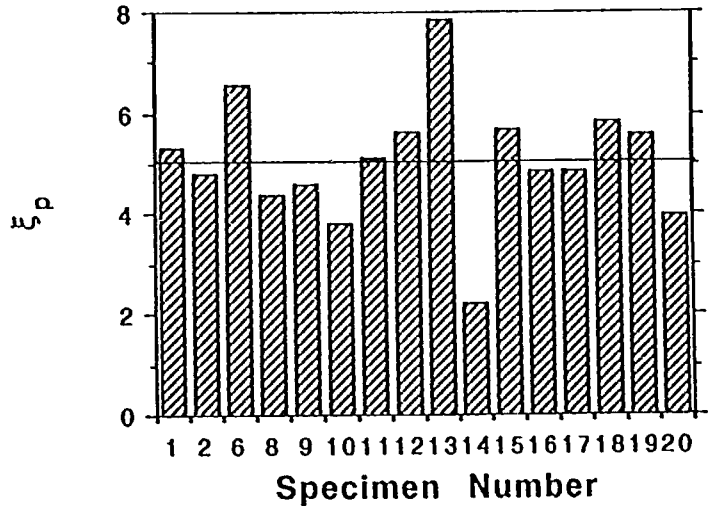


Figure 12. Deformation Factor, ξ_p, for Local Panel Buckling

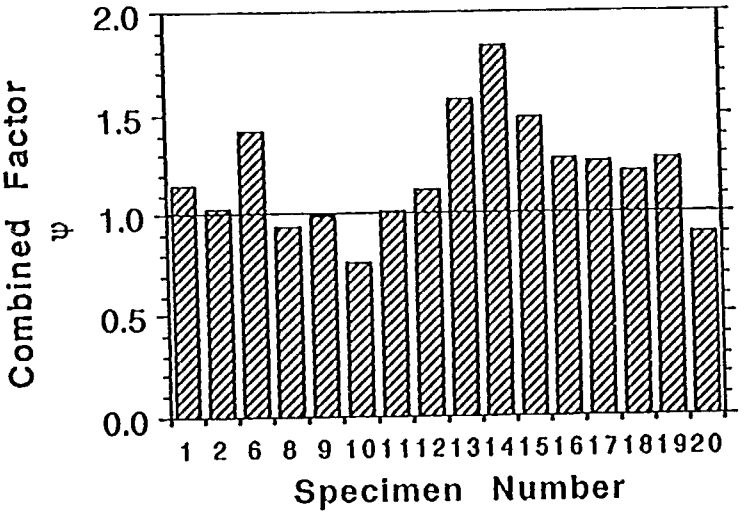


Figure 13. Combined Deformation Factor, ψ

DAMAGE INSPECTION SYSTEMS IMMEDIATELY AFTER A MAJOR EARTHQUAKE

by
Kazuhiko KAWASHIMA
Hideki SUGITA
and
Takashi KANOH

4TH U.S. — JAPAN WORKSHOP ON
EARTHQUAKE DISASTER PREVENTION FOR LIFELINE SYSTEMS
Los Angeles, CA, U.S.A.
August 1991

DAMAGE INSPECTION SYSTEMS IMMEDIATELY AFTER A MAJOR EARTHQUAKE

By Kazuhiko KAWASHIMA, Hideki SUGITA, and Takashi KANOH

Earthquake Engineering Division, Earthquake Disaster Prevention Department,
Public Works Research Institute, Ministry of Construction

ABSTRACT

This paper introduces a part of a comprehensive 5 year research program entitled "Development of Information Collecting and Processing Systems for Disaster Mitigation" of the Ministry of Construction. Description is given to the current problems for correcting damage information immediately after a destructive earthquake in urban area and basic requirements for developing a new system. Emphasis is placed for a proposed seismic damage information systems. Damage inspection way with use of video camera from a helicopter is also presented.

INTRODUCTION

When a destructive earthquake occurs, it is of significant importance to immediately collect accurate information on the extent of damage in the area affected by the earthquake. Road transportation is likely to be interrupted in urban area such as Tokyo as a direct result of damage of not only transportation facilities but buildings and lifeline facilities along the road. Confusion caused by people in evacuation and automobiles left on road are anticipated, and they would also cause considerable disruption of transportation. It is required therefore to develop a new information collecting and processing systems which will enable the extent of damage to be recognized immediately after an earthquake for formulating the repair and restoration strategy promptly.

A comprehensive 5 year research program entitled "Development of Information Collecting and Processing Systems for Disaster Mitigation" was initiated in 1987 by the Ministry of Construction. Public Works Research Institute, Building Research Institute and Geographical Survey Research Institute are involved in the research. The objectives of this research project were to develop new information collecting and processing systems, using advanced new technologies, for various disasters such as earthquake, floods and debris flows. As shown in Fig. 1, key items of the research development are :

a) Bird's eye information collecting systems from helicopter,
b) On-line information processing systems, and
c) Real-time digital mapping systems.

For this purpose, measuring and assessing technology of the damage degree of

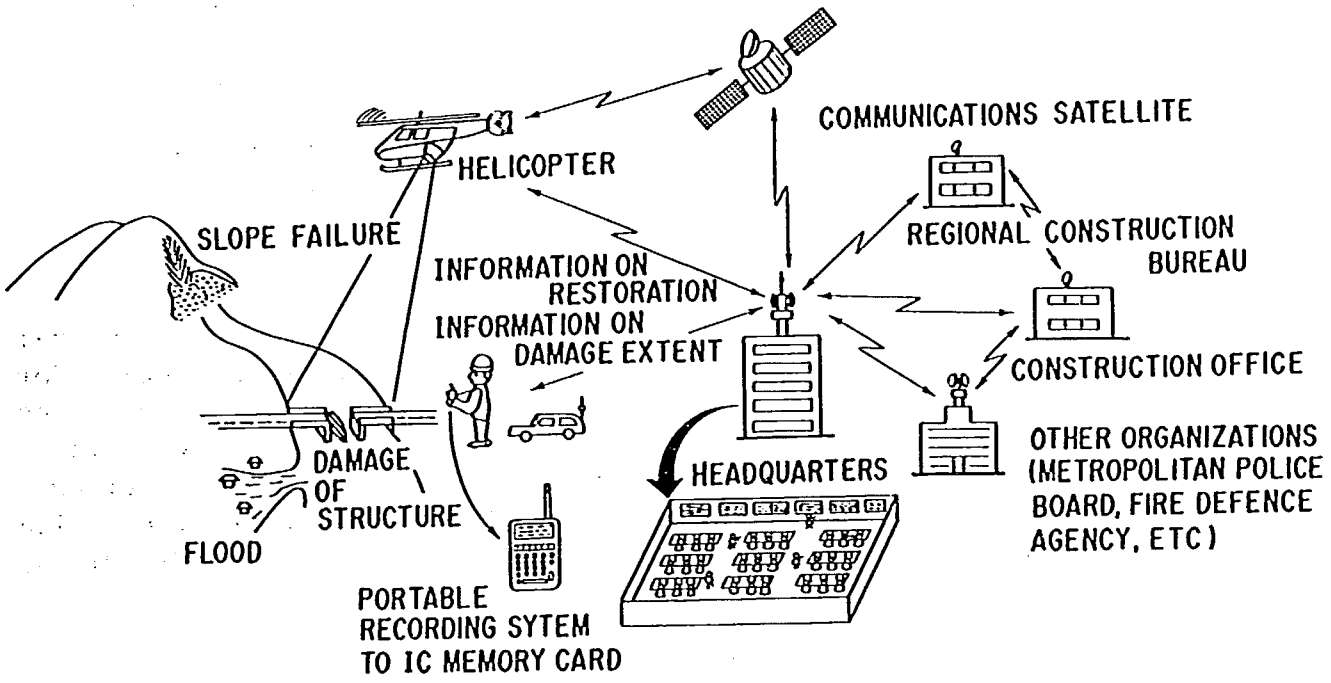


Fig. 1 Information Collection and Processing Systems

structures using moving picture information detected from helicopter and new media oriented high-grade disaster prediction methods as well as planning systems for repair and restoration in the damaged area is now under development. To avoid distortion of information during transferring from regional office to headquarters, it is aimed to adopt visual motion picture systems.

This paper briefly describes a part of the comprehensive research program with emphasis on damage information collecting and processing systems for road and river facilities[1].

PROBLEMS OF CURRENT DAMAGE INFORMATION COLLECTING SYSTEMS AND BASIC REQUIREMENTS FOR DEVELOPING NEW SYSTEMS

Although there were not destructive earthquakes which seriously hitted urban area in the last 40 years in Japan, it has been repeatedly pointed out from the experience of local seismic damage that information collection and dissemination are the most important but difficult issues for central and regional governments in charge of control of public facilities[2,3]. This was also pointed out at the Loma Prieta, U.S.A., Earthquake in October 1989[4,5]. From the past experiences, various obstacles for collecting damage information are anticipated[2,3]. The most important one is unexpectedly long time required for collecting damage information due to interruption of road and damage of information transferring media such as telephone. Even if the telephone could survive an earthquake,

disruption of communication repeatedly happened due to concentration of call to a specific region.

Inadequate accuracy of the collected information is the second problem. Unconfirmed and sometimes uncorrect information are sent. Only a part of total information arrives. It is difficult to know the accuracy and correctness. Sometimes the same information arrives through different routes, and they are misunderstood as different information. Confirmation of source of information is very important. When a series of events occurred, information on subsequent event sometimes arrives earlier than the information of the preceding event. There were examples that this caused significant misunderstanding on what were going on the events and the repair.

Because most of information is transferred by a voice and letters, correct evaluation on the information is difficult. Distortion of information always occurs. Therefore it is required to send information in a form of visible information. Still picture and moving picture information are quite effective.

Basic requirements for solving the problems of the current damage information collecting systems are:

(1)Prompt Information Collection
Collection of damage information in wide area has to be made at not only day time but night. Because accuracy of the damage information required changes in accordance with time following an earthquake, it is important to be able to collect damage information with reasonable accuracy depending on the time after an earthquake. Visible information through video camera is quite important.

(2)Delivery of Updated and Same Information for All Bodies Involved in Repair and Restoration
Although quality of the information required depends on the task of individuals involved in repair and restoration, it is essentially important that the same and updated damage information is able to be delivered for all individuals from site engineers to decision makers. The real-time damage information has to be displayed in the form of not only letters but moving picture. Because it is important for site engineers involved in inspection and emergency treatment to know real-time progress of damage and repair in other area for which they are not in charge of, the systems should have capability to display the damage information of not only inside but outside of the controlled area.

(3)Data Processing Systems for Repair and Restoration
The data processing systems has to be capable to control all the damage information in a system, and can be used from the first stage (immediately after an earthquake) to third stage (stage of permanent repair and restoration)[2)3)]. It should also have a capability to execute various simulation for studying restoration strategy.

PROPOSED SEISMIC DAMAGE INFORMATION SYSTEMS

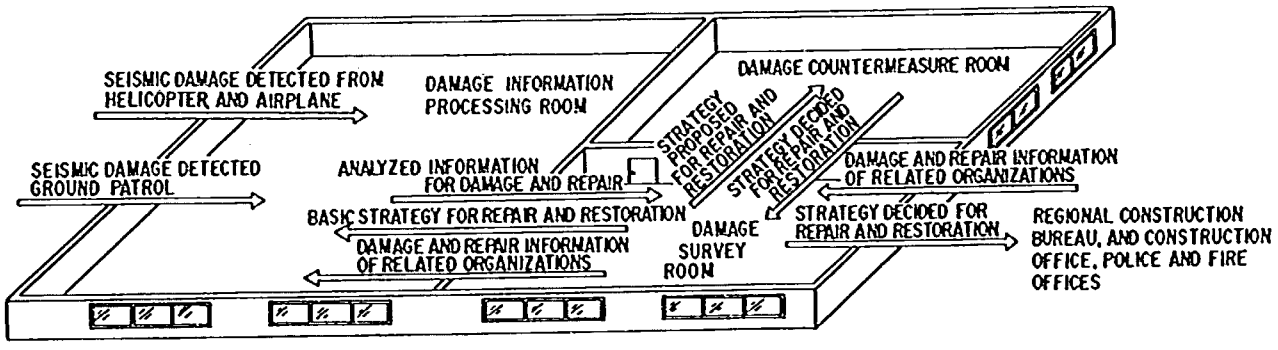
For enabling the requirements presented in the preceding chapter, Seismic Damage Information Systems is proposed for collecting and processing seismic damage information for repair and restoration of road and river facilities. The Seismic Damage Information Systems is to be operated at the Main Headquarters for Disaster Countermeasures (Headquarters Office of the Ministry of Construction), the Headquarters for Disaster Countermeasures (Headquarters Office of Regional Construction Bureaus) and the Branch for Disaster Countermeasures (Construction Offices).

Fig. 2 shows layout and role of three sub-sections of the Seismic Damage Information Systems. At Damage Information Processing Room, all damage information are collected from various sources such as ground patrol teams, helicopter patrol teams, other organizations and public. From such every types of information, important information required for repair and restoration of road and river facilities are identified. Preliminary statistical analysis of the damage are made. At Damage Survey Room, repair and restoration plan based on the damage information compiled at the Damage Information Processing Room are formulated. Communication and adjustment for restoration with related organizations such as police, fire department and local governments have to be made at this stage. At Damage Countermeasure Room, basic policy and strategy for repair and restoration based on the information compiled at the Damage Survey Room is decide.

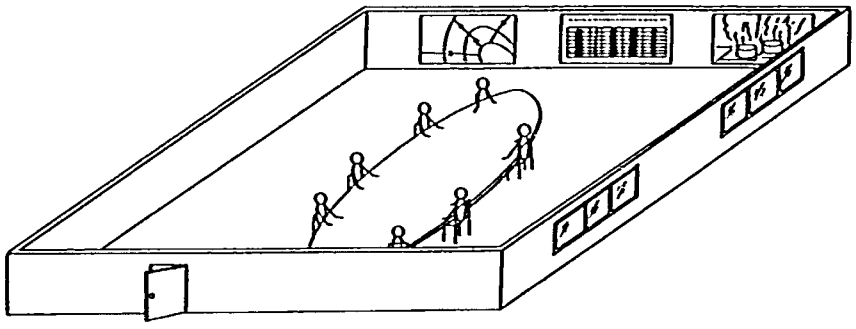
Fig. 3 shows an image of the Damage Survey Room and the Damage Information Processing Room which should be placed at the Headquarters Office of Regional Construction Bureaus.

The Seismic Damage Information Systems is of four sub-systems for collecting, transferring, processing and maintenance of the damage information. The outline of the sub-systems are as follows.

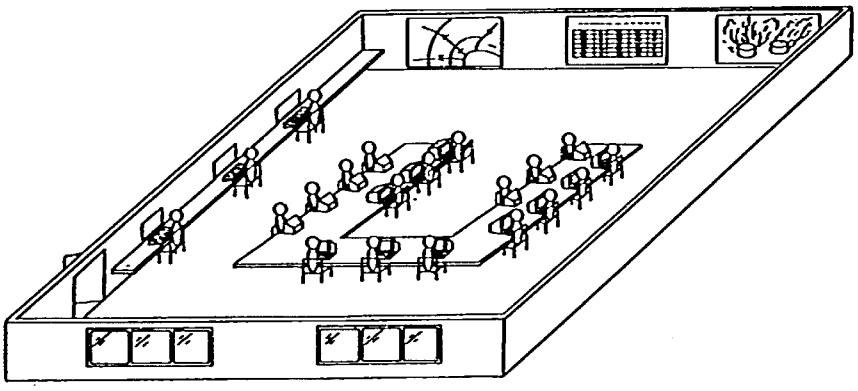
(1) Seismic Damage Information Collecting Systems
Information on seismic damage detected by helicopter patrol teams and ground patrol teams is collected and processed in this systems. The damage information is of moving picture, still picture and letters. They have to be detected by video camera, electric still camera and electric hand notes. The electric hand notes are specially designed man-machine handy type personal computers for exclusive use for recording seismic damage. When the electric notes are operated by field engineers, they automatically display and ask important items for identifying the damage situation such as location, size, type and degree of damage. The data are stored on floppy disk, and they can be sent to host computer at headquarters by cables or radio communication systems.



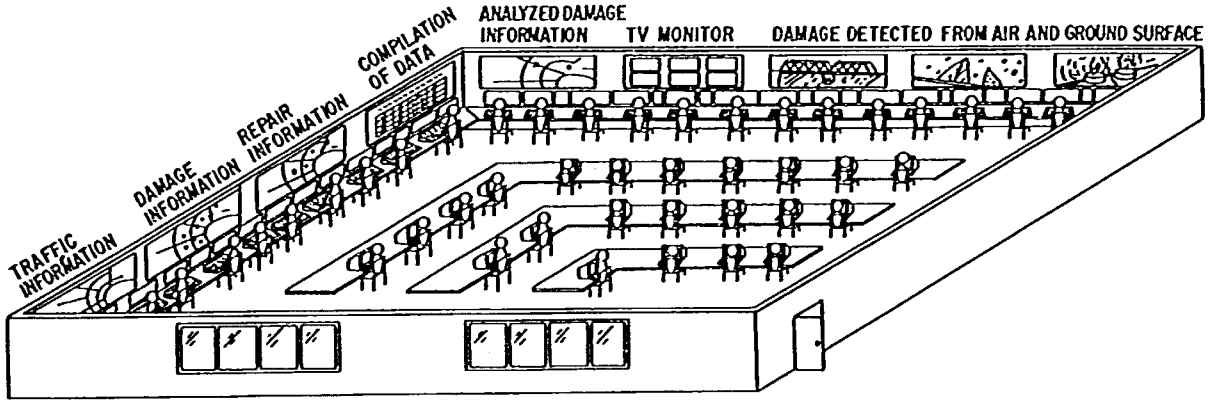
(a) FLOW OF INFORMATION



(b) DAMAGE COUNTERMEASURE ROOM

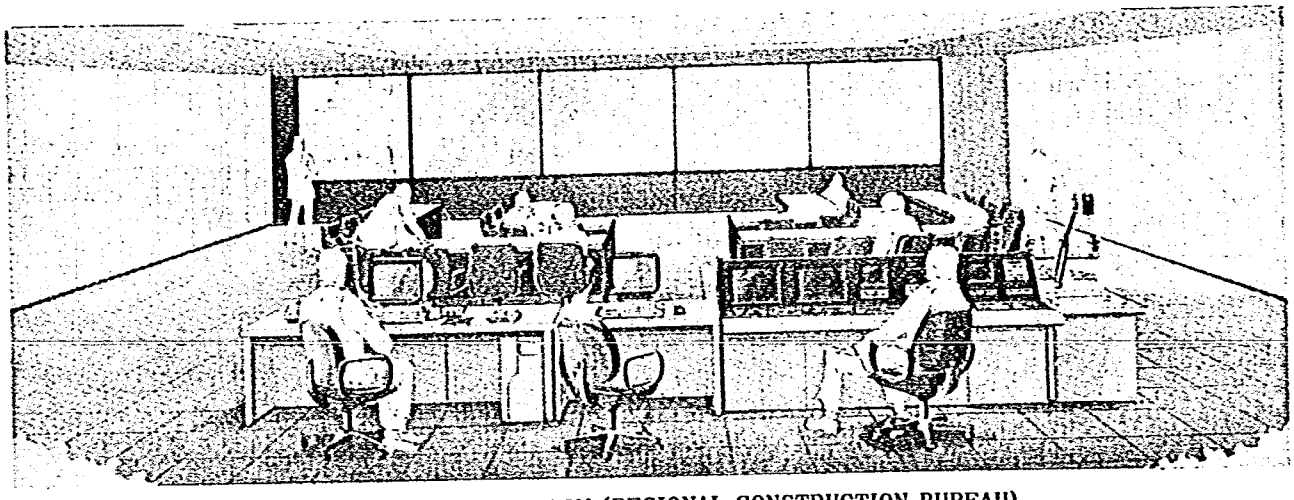


(c) DAMAGE SURVEY ROOM

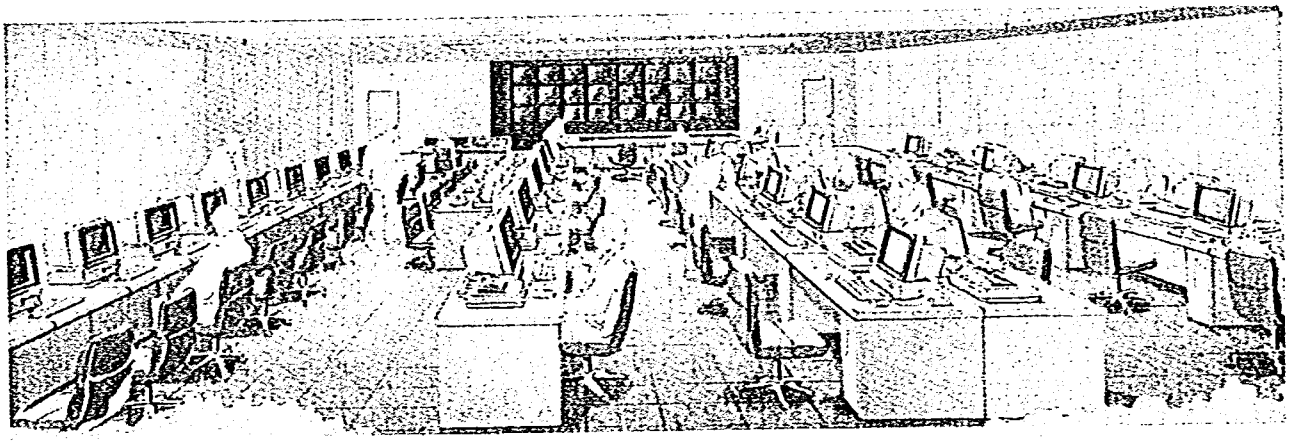


(d) DAMAGE INFORMATION PROCESSING ROOM

Fig. 2 Damage Information Processing Room, Damage Survey Room and Damage Countermeasure Room of Seismic Damage Information Systems



(a) DAMAGE SURVEY ROOM (REGIONAL CONSTRUCTION BUREAU)



(b) DAMAGE INFORMATION PROCESSING ROOM (REGIONAL CONSTRUCTION BUREAU)

Fig. 3 Image of Damage Information Processing Room and Damage Survey Room

(2) Data Transferring Systems

Fig. 4 shows an image of the Data Transferring Systems for transferring the damage information between Head-quarters, Regional Construction Bureaus, Regional Construction Offices, patrol helicopters and ground patrol teams. The information to be covered by the systems includes;

a) moving picture motion detected by video camera on helicopter
b) moving picture motion by video camera of ground patrol team
c) still picture motion by still camera of ground patrol team
d) character and mapping data used in the Seismic Damage Information Processing Systems
e) Data on earthquake and meteorology which are telemetered
g) Information through telephone and faximile

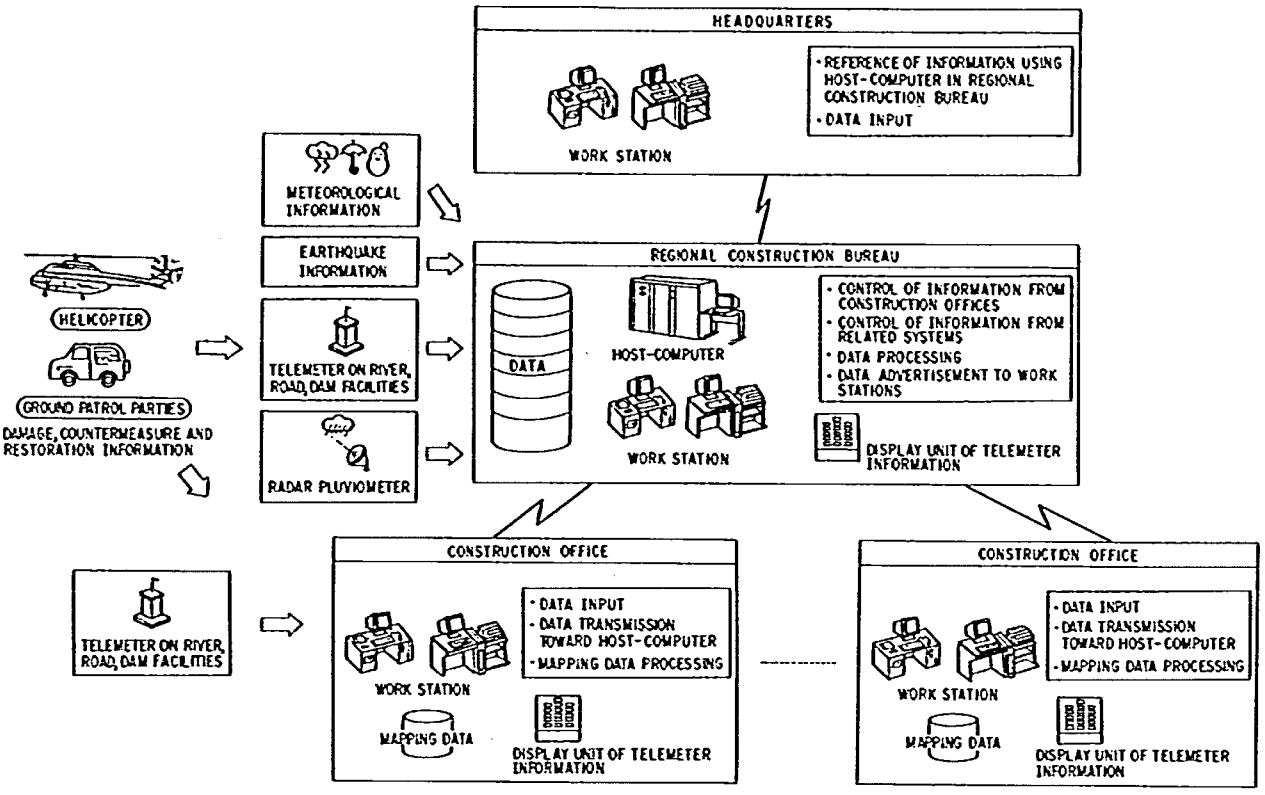


Fig. 4 Image of Data Transferring Systems

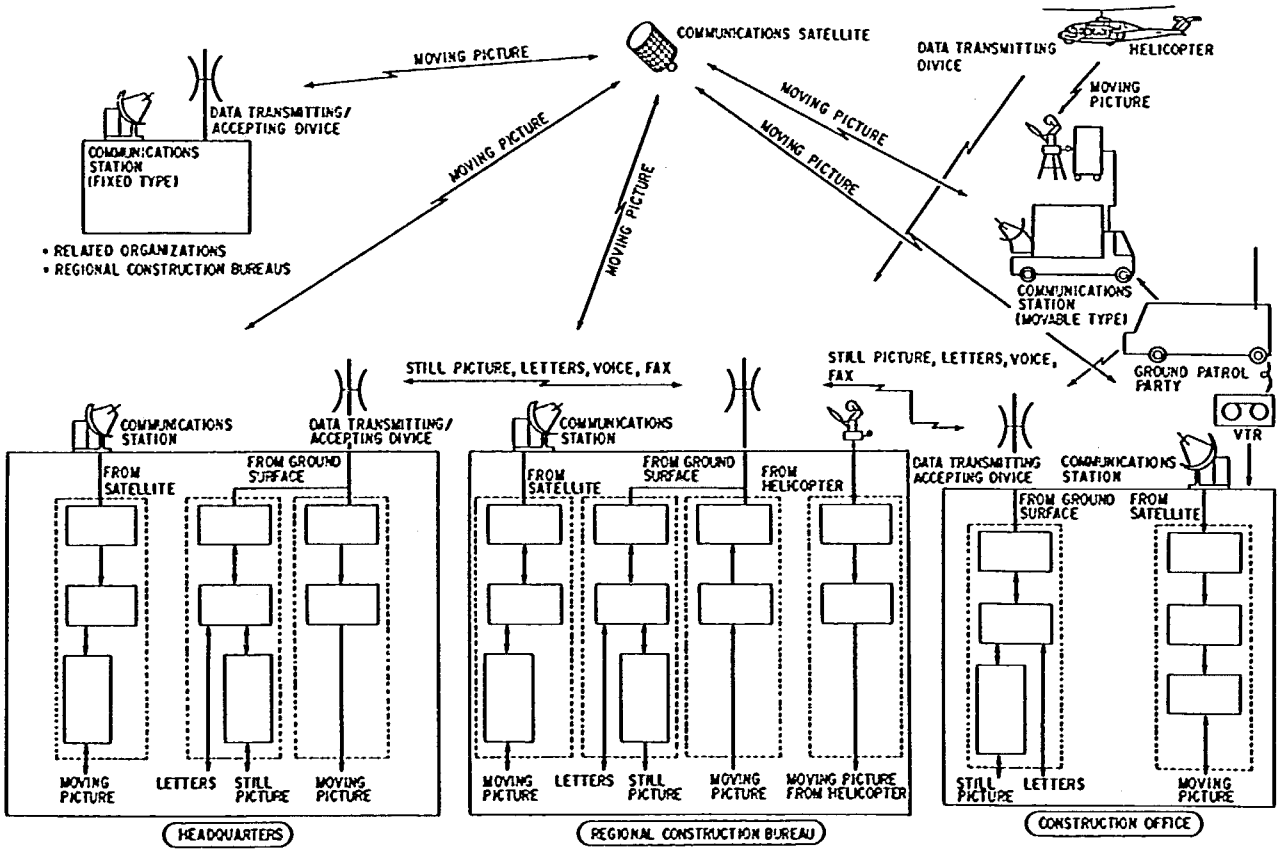


Fig. 5 Main Facilities for Data Transferring Systems

Main facilities required for the Data Transferring Systems are presented in Fig. 5. Main facilities included in the systems are of satellite communication systems and ground communication systems. The satellite communication systems includes satellite, fixed receivers, portable receivers and moving picture transmitting systems. The fixed receiver and portable receivers were already installed at two and five of eight Regional Construction Bureaus, respectively. The ground communication systems are of radio network for exclusive use of the Ministry of Construction and picture motion communication systems. The radio network of the Ministry of Construction covers about 800 locations including Regional Construction Offices and local governments throughout the country.

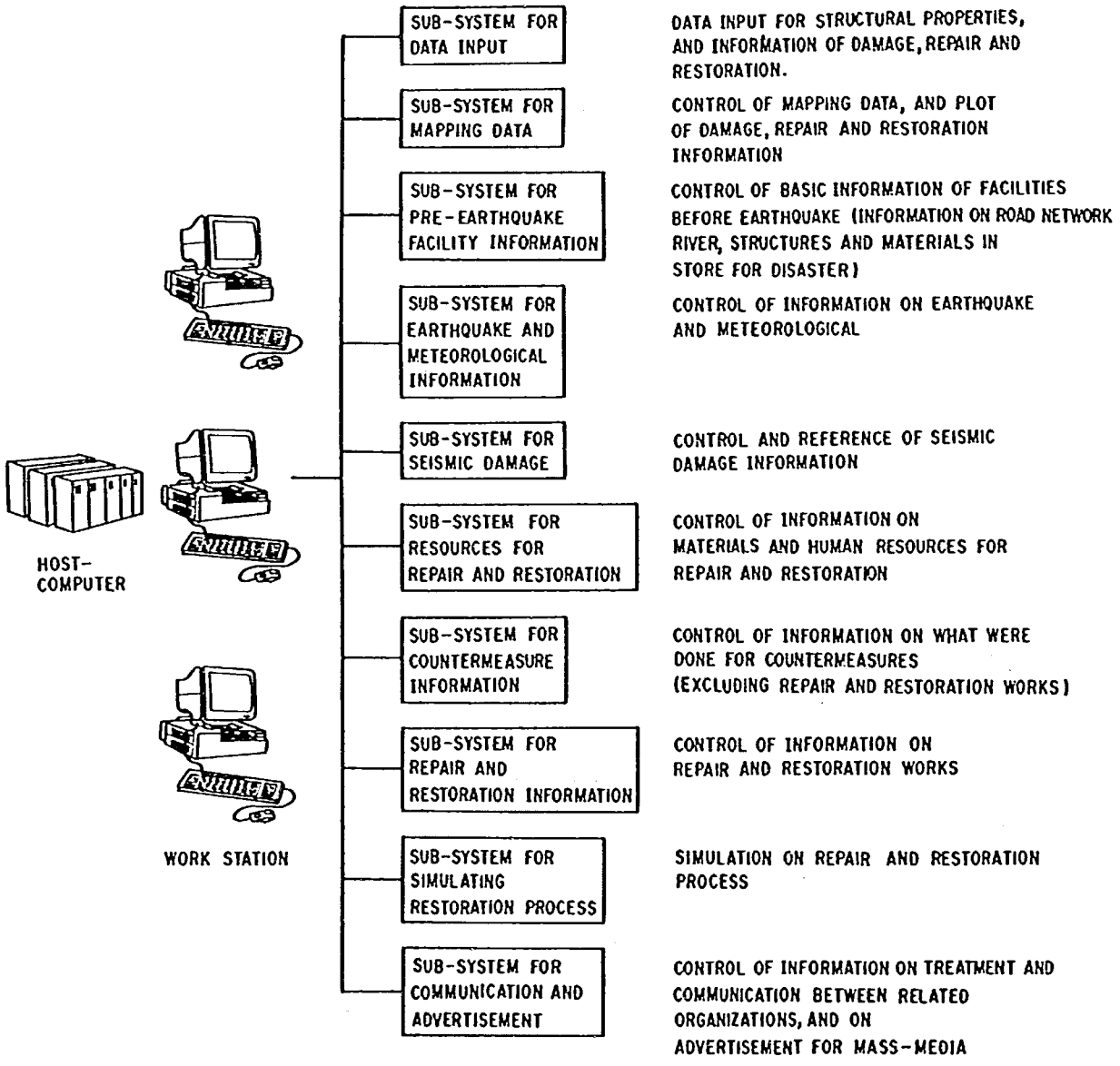


Fig. 6 Sub-systems of Seismic Damage Information Processing Systems

(3) Seismic Damage Information Processing Systems

Fig. 6 shows ten sub-systems for operating the Seismic Damage Information Processing Systems. Whole seismic damage data, repair and restoration data, mapping information, and facilities information prior to an earthquake are compiled and controlled in this systems. Simulation of restoration strategy can be made for clarifying the most appropriate way of restoration. Control of information on adjustment with other organizations are made. Notice and advertisement of damage situation and repair to mass-media is also controlled by this systems. It is of host computer for data processing and work-stations for data input and output. Analyzed data should be displayed on monitor in a well organized form for deciding repair and restoration strategy.

(4) Audio Visible Systems

Fig. 7 shows an image of the Audio Visible systems. It includes screens with 200 inches and 70 inches, monitor of telemeters, projectors and electric black boards. The Audio Visible Systems should have the capability to monitor the damaged area through large screen, to understand the damage feature by comparing the still and moving pictures taken prior to the earthquake, and to conduct TV conference.

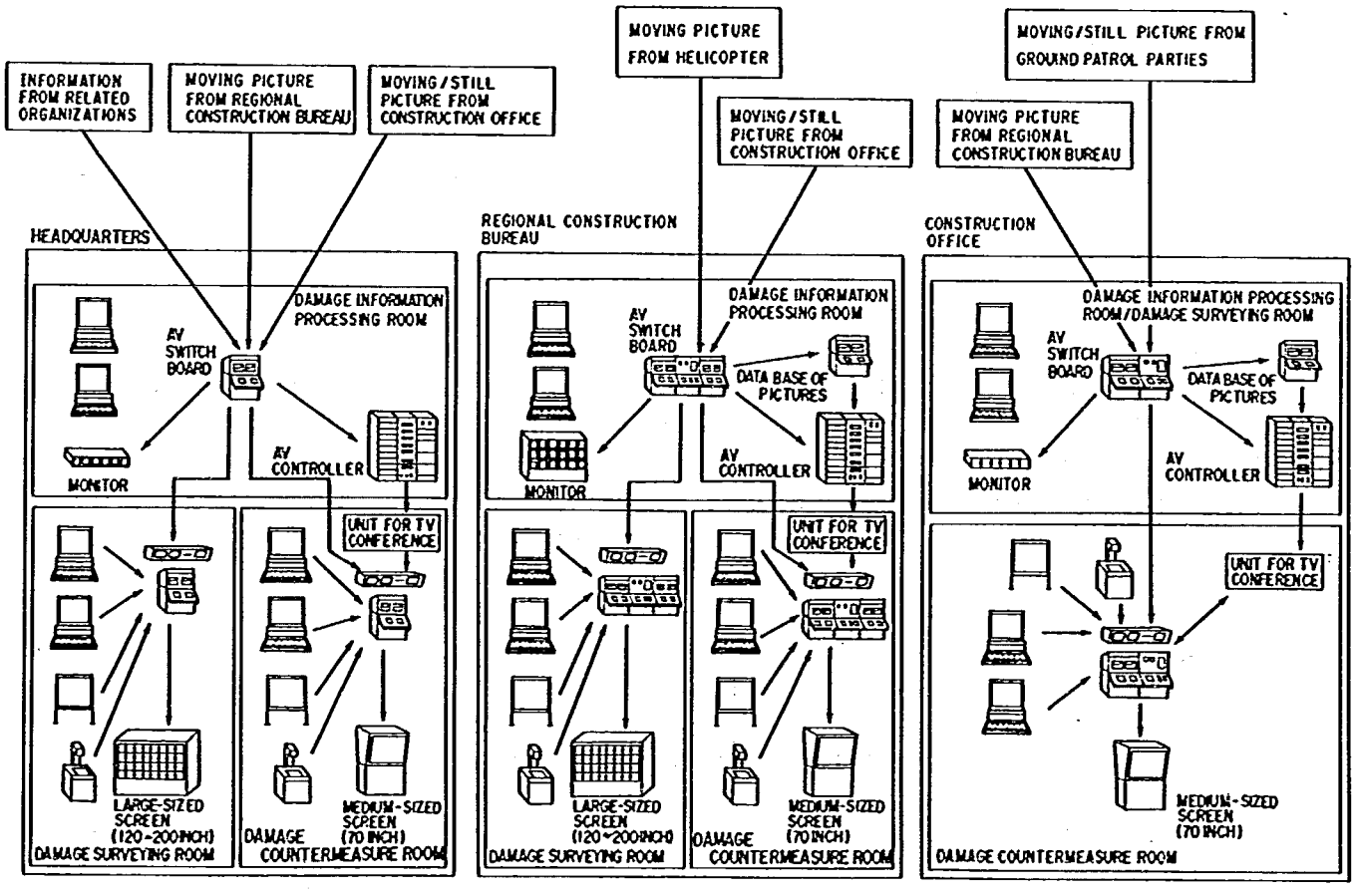


Fig. 7 Image of Audio Visible Systems

DAMAGE INSPECTION FROM HELICOPTER

Damage inspection from helicopter seems attractive to collect damage information promptly because it is not interrupted by traffic congestion and road suspension. To investigate the effectiveness of the damage survey from helicopter, model damages were intentionally placed on various road and river facilities. A helicopter owned by the Ministry of Construction was used for this test. It is for exclusive use for disaster prevention as shown in Photo 1.



Photo 1 Helicopter for Disaster Prevention Owned by Ministry of Construction

A video camera which is set in a specially designed camera case for isolating the camera from vibration of the helicopter was used to detect artificial damage. The focal distance of the video camera is from 12.5 mm to 550 mm. By using the focal distance of 550 mm, a flame of 4.8 m by 3.6 m can be recorded when the height of the helicopter is 300 m which is regulated minimum height at city area. Real time transferring of the picture from the helicopter to the ground receiver can be made. A thermal image sensor is also provided on the helicopter. It can detect the difference of temperature with the resolution of 0.25 degree in Centigrade. Because zoom as large as 4 times is provided in the thermal image sensor, a flame with 37 m by 21 m can be recorded.

Various seismic damage was intentionally developed on bridges, pavement, road embankment and river structures. Photo 2 shows cracks which were made by placing white vinyl tape with width of 5 cm for aiming to represent a damage developed at mid-height of reinforced concrete pier and a damage of prestressed concrete deck. The former damage is likely to be developed when reinforcing bars are terminated at mid-height with inadequate anchoring length[5], and the

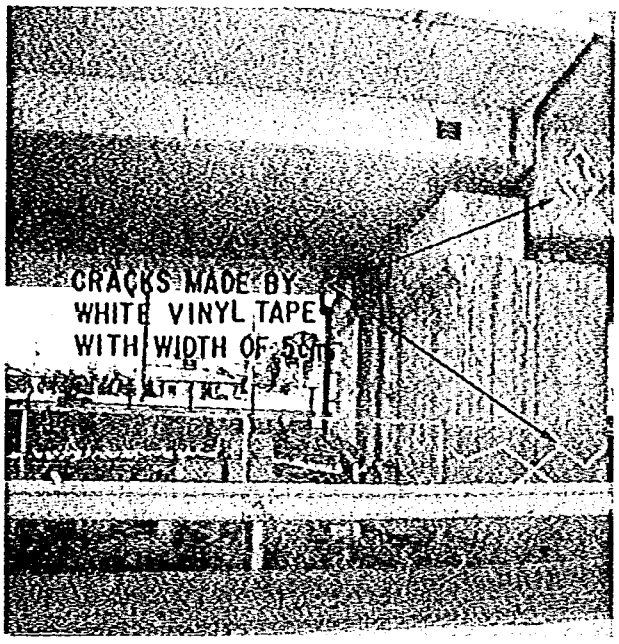


Photo 2 Cracks Placed on Mid-height of Pier and Girder

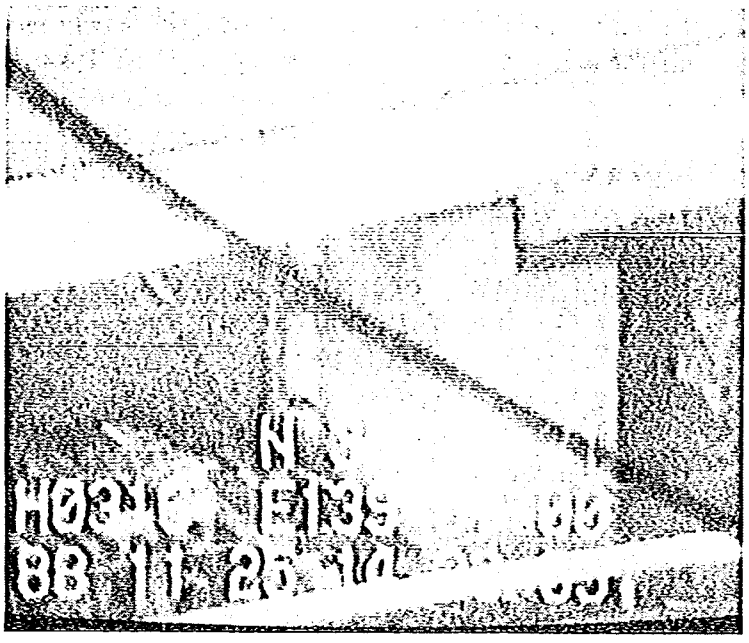


Photo 3 Damage Detected by Video Camera Placed on Helicopter (Height is 321 m, Focal Distance is 550 mm)

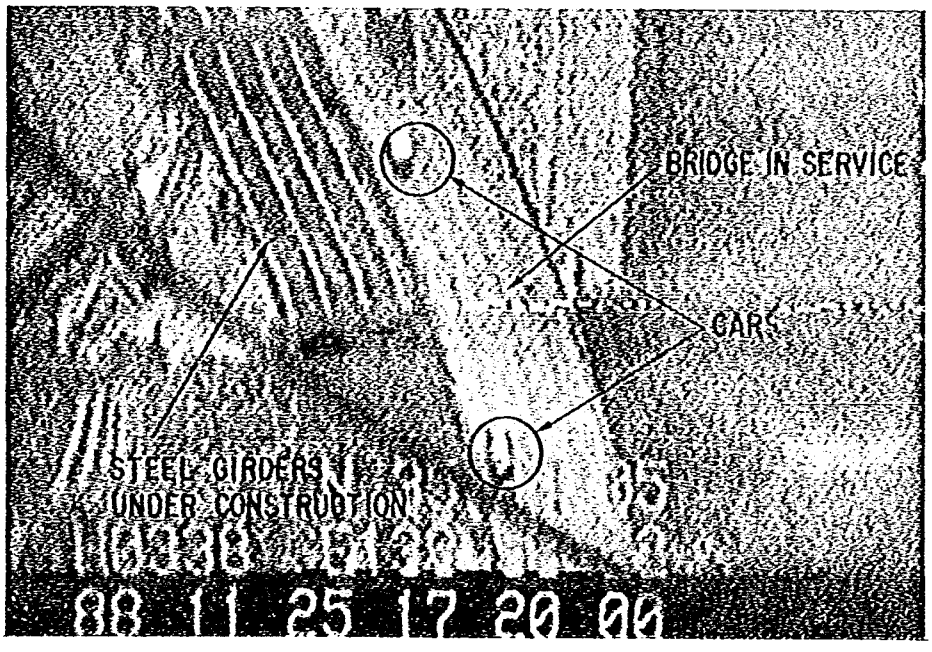


Photo 4 Bridges Detected by Thermal Image Sensor at Night (Height is 338 m)

latter damage tends to be developed on the concrete near the bearing supports[7] when the deck is pulled laterally. Photo 3 shows how such damages are detected from helicopter flying 321 m above the ground surface with velocity of 60 km/h[8]. The focal distance was 550 mm. It is apparent that the cracks at pier and deck can be clearly detected. The test was made by varying the velocity and height of flight.

Photo 4 shows picture representing a new bridge construction along an existing bridge in use for traffic. This was detected by the thermal image sensor at night. Flight height was 338 m from the ground surface. Automobiles driving on the existing bridge and four girders under construction can be apparently seen[8]. The thermal image sensor is effective to detect large damage of steel and concrete structures.

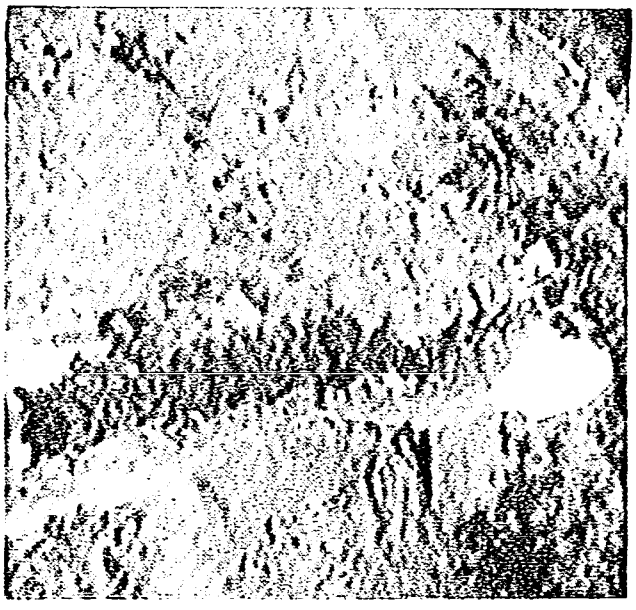


Photo 5 Slope Failure at Nashimoto District of Izu Peninsula Detected by Video Camera from Helicopter

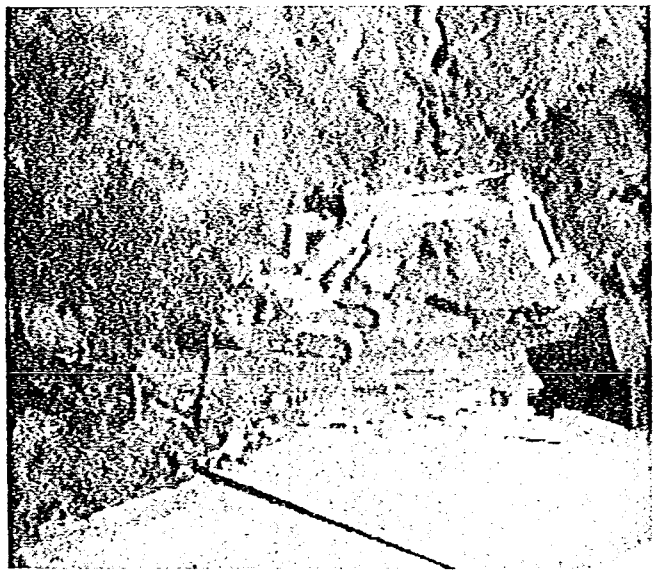


Photo 6 Repair Work Detected by Video Camera from Helicopter

Photos 5 and 6 show the seismic damage of road along natural slope , which was caused by the Izu Ohshima-kinkai Earthquake[9] with the Richter magnitude of 7.0 in January 1978. Extensive slope failure was developed along the road with total distance of about 125 m and height of 30 to 50 m , and this embedded a public bus with three being killed. Photo 6 shows the repairing job by a crane. Because this is a part of video taken by a TV company for broadcasting, the flight information such as height and velocity is unknown. By carefully examining the video record, length, depth and soil volume were surveyed by three geologists with different professional careers[8]. The geologist with 17, 10 and 5 years professional career is designated herein as A, B and C geologist, respectively.

Table 1 Accuracy of Estimation by Three Geologists with Different Professional Career

DAMAGE	GEOLOGISTS			MEASURED AT SITE
	A	B	C	
AVERAGE WIDTH	70(CRANE(10m)x7)	60~80	10~30	100m
AVERAGE DEPTH	10(AVERAGE WIDTHx 1/7~1/10)	5~10	*	5m
FAILURE AREA	*	320~480	*	-
SOIL VOLUME	20,000(30mx70mx10m)	20,000	*	26,500
LENGTH OF ROAD INTERRUPTED BY SLOPE FAILURE	100(AVERAGE WIDTH +α)	80	*	125

1. * MEANS THAT IT WAS UNABLE TO ESTIMATE FROM VIDEO TAPE
2. ( ) REPRESENTS HOW GEOLOGISTS EVALUATED LENGTH, DEPTH AND DISTANCE

Table 1 compares the accuracy of the estimation by three geologists based on the video film. It is interesting to note that the geologist A gives the most appropriate estimation, and that the geologists with shorter professional career tends to give 30 to 50 % smaller estimation. Because estimation was made through video picture which is, of course, much smaller in size than the actual damage, the surveyors tend to give smaller estimation in size.

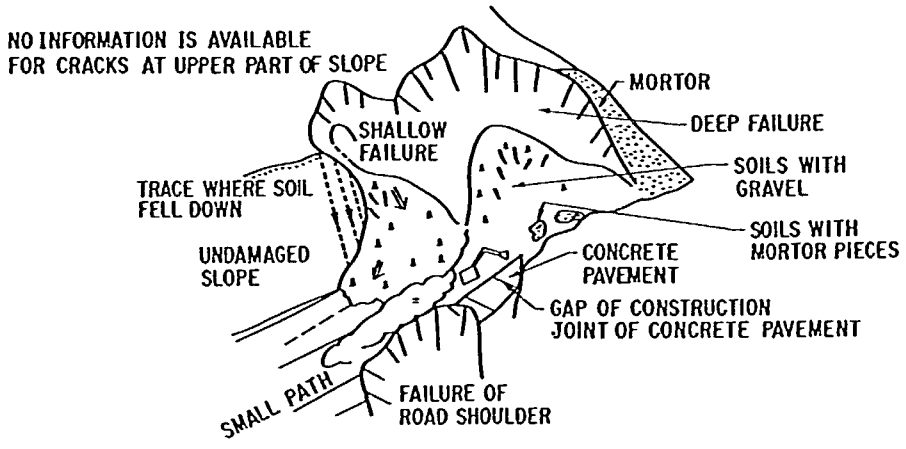


Fig. 8 Geological Feature Detected by Geologist A based on Video Film

Fig. 8 shows the geological feature detected by the geologist A based on the video film. Various information which is useful to judge the cause of failure and probability to cause further progress of the failure can be obtained if the video picture is carefully evaluated by a person with enough professional knowledge.

It was found from the study that estimation of the volume and length of failure is easier when artificial goods and facilities such as car, gird rails, house are found in the moving picture because they can be used as a reference to measure the distance[10]. On the other hand, it was found difficult to estimate the distance and length when the failure is enormously large as compared with the size of such artificial goods and facilities.

The study presented here is now being extended for studying the maximum flight velocity to detect a certain size of damage[11], effect of temperature and wind velocity for detecting damage by thermal image sensor[12], and the most appropriate way of flight[13].

CONCLUDING REMARKS

When the Kanto Earthquake which resulted in about 120 thousands of death occurred in September 1923, there were only about 4,500 vehicles in Tokyo City. People evacuated by either walking or bicycle. This clearly indicates the great difference of anticipated damage situation, between in 1923 and current time, in urban area hitted by a destructive earthquake. It is important to note that there have not be destructive earthquakes which hitted badly urban areas in the last 40 years, and during this time the size, structures of living, lifelines and techniques completely changed. It is therefore anticipated to face a new situation when a large event happens near urban area. It is quite important to develop and introduce a new systems for collecting and processing seismic damage information.

FUTURE DIRECTIONS

Because the proposed systems would become a large systems consisting of a number of hardwares and softwares, further study has to be made for an integrated architecture so that they are capable to be used even after a destructive earthquake. Special training for operating the systems is inevitably important. Because sudden operation immediately after an earthquake can not be made, it has to be used as a part of the comprehensive systems for daily use. Appropriate form of the emergency operation systems in normal time has to be well examined.

Although the thermal image sensors are effective to detect large damage at night, they can be used for surveying more detailed damage if the camera with longer focus distance was developed. The use of new technology such as the high vision camera is promising.

ACKNOWLEDGEMENTS

In executing the project, the Technical Research Center for National Land

Development established the Committee for the Development of Disaster Information Systems, which is chaired by Dr. H. Umemura, Professor Emeritus of the University of Tokyo, with the commitment of the Ministry of Construction. The reports presented in this paper are being executed with the supervision by the Subcommittee for the Development of Supporting Systems for Disaster Restoration Plan (Chairman : Professor Emeritus K. Kubo) and the Working Group for the Development of Supporting Systems for Seismic Disaster Restoration Plan (Chairman : Professor E. Kuribayashi) . The authors express their sincere thanks to all committees members for their invaluable suggestions and guidance. Special thanks go to Prof. T. Katayama, University of Tokyo and Prof. H. Kameda University of Kyoto, for their invaluable suggestions. Final accomplishments of the project are to be complied in March 1992 in the form of guidelines.

REFERENCES

1) Committee for Development of Disaster Information Systems : Report on Development of Disaster Information Systems, March 1987, March 1989, March 1990, March 1991, Technical Research Center for National Land Development.
2) Public Works Research Institute : Manuals for Repair Methods for Civil Engineering Structures Damaged by Earthquakes, Technical Note of the Public Works Research Institute, Vol. 45, December 1986 (in Japanese). Translated version is published from the National Center for Earthquake Engineering Research, University of New York, Buffalo, U.S.A.
3) Japan Road Association : Guide Specifications for Earthquake Hazard Mitigation for Transportation Facilities - Repair and Restoration - , February 1987
4) Katayama, T. and Eisner, R. : What were the Lessons of the 1989 Loma Prieta ?, Bulletin of Earthquake Research Institute, University of Tokyo, No. 24, 1991
5) Kameda, H., Asaoka, K., Scawthorn, C. and Khater, M. : Effects of the 1989 Loma Prieta Earthquake on the Bat Area Transportation Systems, Proc. 8th Japan Earthquake Engineering Symposium, Vol. 2, Tokyo, Japan, December 1990
6) Kawashima, K., Unjoh, S. and Iida, H. : U.S.-Japan Workshop on Seismic Retrofit of Bridges, Public Works Research Institute, Tsukuba, Japan, December 1990
7) For example, Kawashima, K. and Nishikawa, K. : Earthquake Damage to Bearing Supports of Highway Bridges Caused by the Miyagi-ken-oki Earthquake, Civil Engineering Journal, Vol. 22-10, October 1980
8) Kawashima, K., Unjoh, S., Sugita, H., Kanoh, T. and Iida, H. : Survey on Seismic Damage from Helicopter, Civil Engineering Journal, Vol. 32-1, January 1990
9) Public Works Research Institute: Report on the Disaster Caused by the Izu-ohshima-kinkai Earthquake, Report of the Public Works Research Institute, Vol.158, March 1982
10) Kawashima, K., Sugita, H. and Kanoh, T. : Survey of Seismic Damage by Video Tapes Taken from Helicopter, Civil Engineering Journal, Vol. 33-1, January 1991
11) Kawashima, K., Sugita, H. and Kanoh, T. : Maximum Flight Velocity of Helicopter for Surveying Seismic Damage With Use of Audio Visual Picture, Civil

Engineering Journal, Vol.33-9, 1991
12) Kawashima, K., Sugita, H., Kanoh, T. and Iida, H. : Application of Thermal Image Sensor for Survey of Seismic Damage, Civil Engineering Journal, Vol. 33-1, January 1991
13) Kawashima, K., Sugita, H. and Kanoh, T. : Flight Method of Helicopter for Surveying Damage Information Immediately After An Earthquake, Civil Engineering Journal, Vol.33-9, 1991

SEISMIC INSPECTION AND SEISMIC STRENGTHENING OF HIGHWAY BRIDGES IN JAPAN

by
Kazuhiko KAWASHIMA
Shigeki UNJOH
and
Hiroyuki IIDA

4TH U.S. — JAPAN WORKSHOP ON
EARTHQUAKE DISASTER PREVENTION FOR LIFELINE SYSTEMS
Los Angeles, CA, U.S.A.

SEISMIC INSPECTION AND SEISMIC STRENGTHENING OF HIGHWAY BRIDGES IN JAPAN

BY

Kazuhiko KAWASHIMA[1]
Shigeki UNJOH[2]
and
Hiroyuki IIDA[3]

1) Head, Earthquake Engineering Division, Public Works Research Institute, Ministry of Construction, Tsukuba Science City, Ibaraki-ken, Japan
2) Research Engineer, ditto
3) Assistant Research Engineer, ditto

ABSTRACT

This paper presents a state of practice of seismic inspection and seismic strengthening of highway bridges in Japan. Description is firstly given to the history of seismic inspection and seismic strengthening of highway bridges in Japan. An inspection method of existing highway bridges based on a statistical analysis of past seismic damage is presented. Practical seismic strengthening methods for vulnerable highway bridges are described. Finally, current research efforts for developing seismic inspection and seismic strengthening methods of reinforced concrete bridge piers with termination of main reinforcement at mid-height are presented.

INTRODUCTION

Highways in Japan consist of Expressways (3,721 km), National Highways (46,661 km), Prefectural Roads (128,202 km), and Municipal Roads (925,138 km). Along the highways and roads, excluding the Municipal Roads, there are about 60,000 bridges with span lengths (deck length between two adjacent substructures) of 15 m or longer.

Although the number of bridges constructed per year depends on the year and span length, it is about 6,000 for concrete bridges and 2,000 for steel bridges with a length of 15 m or longer.

Located along the Pacific Seismic Belt, Japan is one of the most seismically disastrous countries in the world and has often suffered significant damage from large earthquakes. Fig. 1 shows the largest magnitude of the earthquakes which occurred in the past[1]. It is recognized that the earthquakes with magnitude over 8 have occurred with rather short recurrent period in and around Japan in the past. It should be noted that seismicity is especially high along the Pacific coast. Cities large in population and industrial products such as Tokyo, Osaka and Nagoya are located in this region.

Table 1 shows the highway bridges which suffered damage in the past earthquakes since the Kanto Earthquake of 1923. It should be noted that although there were many bridges which suffered damage due to earthquakes, the number of bridges which fell down was only 15.

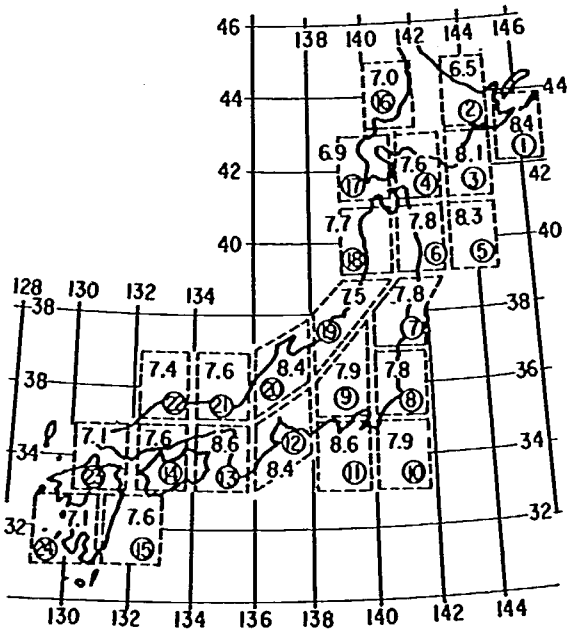


Fig. 1 Largest Magnitude of Earthquakes in the Past

Based on surveys of the damaged bridges, it is pointed out that the three major factors which contributed to the damage of bridges are[2] :

a) weakness of substructures
b) weakness of bearing supports, and
c) weakness of surrounding subsoils.

From such factors, the following types of damages were most often developed in the past:

a) substructure : tilting, settlement, sliding, cracks, and overturning
b) superstructure : movement, buckling and cracks near the supports, and falling of girder
c) bearing supports : failure of supports, and pull-out or rupture of anchor bolts

Although these kinds of damage are the ones commonly observed in the past earthquakes, the damage types have been changing as shown in Table 2 in accordance with the progress of seismic design methods and improvements in construction practice[3].

Table 1 Damage of Highway Bridges in the Past since Kanto Earthquake of 1923

DATE	EARTHQUAKE	MAGNITUDE	NUMBER OF BRIDGES DAMAGED	NUMBER OF BRIDGES WHICH FELL DOWN
1923. 9. 1	KANTO	7.9	1,785	6
1946.12.21	NANKAI	8.1	346	1
1948. 6.28	FUKUI	7.3	243	4
1949.12.26	IMAICHI	6.4	1	0
1952. 3. 4	TOKACHI-OKI	8.1	128	0
1962. 4.30	MIYAGI-KEN-HOKUBU	6.5	187	0
1964. 6.16	NIIGATA	7.5	98	3
1968. 2.21	EBINO	6.1	10	0
1968. 5.16	TOKACHI-OKI	7.9	101	0
1978. 1.14	IZU-OHSHIMA	7.0	7	0
1978. 6.12	MIYAGI-KEN-OKI	7.4	95	1
1982. 3.21	URAKAWA-OKI	7.1	5	0
1983. 5.26	NIHON-KAI-CHUBU	7.7	176	0
1984. 9.14	NAGANO-KEN-SEIBU	6.8	14	0
TOTAL			3,191	15

Table 2 Change of Damage Types

Year	Major Earthquakes	Change of Major Seismic Damage	Seismic Design Method	Seismic Inspection and Strengthening
1920	1923 Kanto Earthquake (M7.9)	Failure of Superstructure due to Tilting/Movement of Foundation	1926 Initiation of Seismic Design (Details of Road Structures)	
1930				
1940	1946 Nankai Earthquake (M8.1) 1948 Fukui Earthquake (M7.3)	Failure of Concrete around Fixed Bearing Damage due to Liquefaction	1939 Introduction of Standard Seismic Coefficient (Design Specifications of Steel Highway Bridges)	
1950	1952 Tokachi-oki Earthquake (M8.1)	Failure of RC Piers, and Bearing	1956 Seismic Coefficient depending on Zone and Ground Condition (Design Specifications of Steel Highway Bridges)	
1960	1964 Niigata Earthquake (M7.5)			
1970	1978 Miyagi-ken-oki Earthquake (M7.4)		1971 • Seismic Coefficient depending on Zone, Ground Conditions, Importance and Structural Response • Introduction of Evaluation Method for Liquefaction (Specifications for Seismic Design)	1971 Seismic Inspection 1976 Seismic Inspection
1980	1982 Urakawa-oki Earthquake (M7.1) 1983 Nihon-kai-chubu Earthquake (M7.7)		1980 • Part V Seismic Design, Specifications for Design of Highway Bridges • Introduction of New Evaluation Method for Liquefactions	1979 Seismic Inspection 1986 Seismic Inspection
1990			1990 Part V Seismic Design, Specifications for Design of Highway Bridges	

This paper presents pre-earthquake measures for mitigating earthquake hazards of highway bridges in Japan. Development of seismic inspection and seismic strengthening methods for existing highway bridges are presented.

HISTORY OF SEISMIC INSPECTION AND SEISMIC STRENGTHENING OF HIGHWAY BRIDGES IN JAPAN

The nationwide seismic inspection of highway bridges with span length longer than 15 m was made in 1971, 1976, 1979 and 1986 by the Ministry of Construction. Overcrossings in city area are also included in "bridges". Table 3 shows the inspected items of the past seismic inspections of highway bridges. The first inspection in 1971 and second inspection in 1976 were to detect deteriorated highway bridges susceptible to falling-off of superstructures during earthquakes. The third and fourth seismic inspection in 1979 and 1986 was to clarify structural resistance of highway bridges against falling-off of superstructures during destructive earthquakes.

Table 3 Inspection Items Considered in the Past Seismic Inspection of Highway Bridges in Japan

Year	Inspection Items
1971	· Deterioration · Bearing Seat Length S for Bridges supported by Bent Piles
1976	· Deterioration of Substructures, Bearing Supports and Girders/Slabs · Bearing Seat Length S and Devices for Preventing Falling-off of Superstructure
1979	· Deterioration of Substructures and Bearing Supports · Devices for Preventing Falling-off of Superstructure · Effect of Soil Liquefaction · Bearing Capacity of Soils and Piles, and Strength of RC Piers · Vulnerable Foundations (Bent Piles and RC Frame on Two Independent Caisson Foundation)
1986	· Deterioration of Substructures, Bearing Supports and Concrete Girders · Devices for Preventing Falling-off of Superstructure · Effect of Soil Liquefaction · Strength of RC Piers (Bottom of Piers and Termination Zone of Main Reinforcement) · Bearing Capacity of Piles · Vulnerable Foundations (Bent Piles and RC Frame on Two Independent Caisson Foundation)

Note) Deterioration includes cracks of concrete members, excessive inclination, slip and subsidence of foundations, and scouring of surrounding soils of foundation.

For those bridges which were judged vulnerable to destructive damages during earthquakes, seismic strengthening works have been made. Table 4 shows the number of highway bridges inspected and the budget spent for the seismic strengthening works. For those bridges consisting of several spans for crossing rivers and valleys, a whole group of bridges is counted as "a bridge" in Table 4. Therefore actual number of bridges is much larger than the number presented in Table 4. Because bridges inspected in the past also require the latest inspection, the number of bridges inspected and strengthened includes duplication. In the latest 1986 inspection, about 40,000 bridges were inspected and about 11,700 bridges were found to require seismic strengthening. Most of the bridges require installation of the device for preventing superstructure from falling-off from the substructures as shown in Fig. 2[5]. In the past four seismic strengthening programs by 1989 fiscal year, 23,466 bridges were strengthened. As of 1989, about 300 billion Yen was spent for the seismic strengthening works including bridges.

Table 4 Number of Highway Bridges Inspected by the Past Seismic Inspection in Japan[4),5)]

Year	Inspected	Require Strengthening	Strengthened
1971	17,970	3,200	1,441
1976	24,504	7,110	2,742
1979	34,712	16,011	13,580
1986	40,370	11,764	5,703

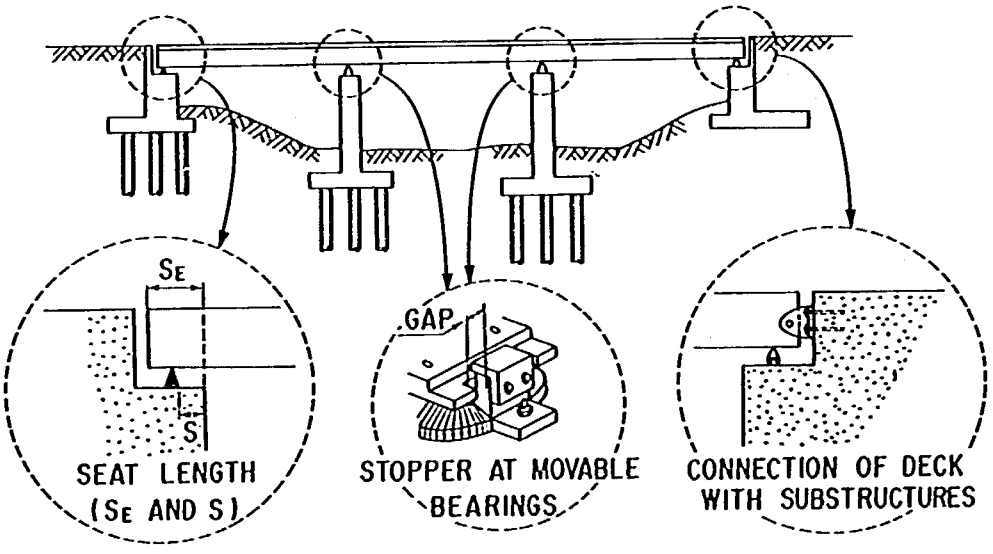


Fig. 2 Devices for Preventing Superstructure from Falling

VULNERABILITY INSPECTION OF HIGHWAY BRIDGES

Seismic inspection method s to detect highway bridges vulnerable to earthquakes have been developed and amended several times to reflect progress of bridge earthquake engineering and lessons learned from the past seismic damage. The most important requirement for the inspection method was to be able to assess the vulnerability of a number of highway bridges at site without complex calculations. The latest seismic inspection method[7] which was referenced in the 1986 seismic inspection was formulated on the statistical analyses of 124 bridges damaged in the past earthquakes[8].

In the statistical analyses, factors which are likely to affect the seismic vulnerability of highway bridges were firstly studied with use of the Type II quantification analysis. The rank of damage degree was classified into high vulnerability (Rank A), moderate vulnerability (Rank B) and low vulnerability (Rank C) as shown in Table 5. From the analysis of the past seismic damage, 15 items, as shown in Table 6, were selected as the factors likely to affect seismic vulnerability. The 15 items consists of four principal factors, i.e., intensity of earthquake ground motions, properties of superstructure and substructures, devices for preventing falling-off of superstructure from substructures, and ground condition. Each item was further divided into several categories.

Table 5 Definition of Seismic Vulnerability

Rank	Vulnerability of Seismic Damage	Rank of Damage Degree
Rank A — High Vulnerability	Possibility for suffering damage or damage degree is high	5 Falling-off of Superstructure or 4 Extensive Damage
Rank B — Moderate Vulnerability	Possibility for suffering damage or damage degree is moderate	3 Moderate Damage
Rank C — Low Vulnerability	Possibility for suffering damage or damage degree is low	2 Slight Damage or 1 Minor Damage or 0 No Damage

Predicted damage rank y_i was assumed to have a form of

$$y_i = \sum_j \sum_k \delta_{ijk} \cdot x_{jk} \qquad (1)$$

in which x_{jk} represents a weighting factor for the k-th category of the j-th item, and δ_{ijk} represents a variable corresponding to the category k in the item j of the i-th bridge. The variable δ_{ijk} was so defined that it takes a value of 1 if the characteristics of the i-th bridge correspond to the category k in the item j, and is 0 otherwise. The weighting factor x_{jk} was determined so as to minimize the sum of square of the difference between the predicted damage rank and the actual damage rank.

Table 6 Items and Categories which Affect Seismic Vulnerability of Highway Bridges

Item	Category	Seismic Damage Rank						Results of Statistical Analysis		
		0 No Damage	1 Minor Damage	2 Slight Damage	3 Moderate Damage	4 Extensive Damage	5 Falling-off of Superstructure	Normalized Score	Range	Partial Correlation Coefficient
①Intensity of Peak Ground Acceleration a_{max} [cm/sec^2]	$a_{max} < 200$	1 (5%)			1 (5%)			0.169	1.219	0.343
	$200 \leq a_{max} < 300$	13 (68%)	5 (42%)	36 (65%)	8 (40%)	1 (13%)		−0.283		
	$300 \leq a_{max} < 400$	5 (26%)	5 (42%)	18 (33%)	10 (50%)	6 (75%)	4 (40%)	0.176		
	$400 \leq a_{max} < 500$		2 (17%)	1 (2%)	1 (5%)	1 (13%)	2 (20%)	0.936		
	$500 \leq a_{max}$						4 (40%)	0.616		
②Design Specifications	1926 or 1939	1 (5%)		6 (11%)	6 (30%)	5 (63%)	7 (70%)	0.517	0.740	0.319
	1956 or 1964	17 (89%)	6 (50%)	41 (75%)	11 (55%)	3 (38%)	3 (30%)	−0.223		
	1971 or 1980	1 (5%)	6 (50%)	8 (15%)	3 (15%)			0.284		
③Type of Superstructure	Gerber or Simply Supported Girder (2 or More Spans)	12 (63%)	7 (68%)	40 (73%)	17 (85%)	8 (100%)	10 (100%)	0.081	0.390	0.161
	One-span Simply Supported Girder, or Countinuous Girder with 2-spans or More	5 (26%)	3 (23%)	11 (20%)	2 (10%)			−0.232		
	Arch, Frame, One-span Continuous Girder, Cable-stayed Bridge, Suspension Bridge	2 (11%)	2 (17%)	4 (7%)	1 (5%)			−0.308		
④Shape of Superstructure	Skewed or Curved	3 (16%)	1 (8%)	4 (7%)				−0.396	0.424	0.122
	Straight	16 (84%)	11 (92%)	51 (93%)	20 (100%)	8 (100%)	10 (100%)	0.027		
⑤Materials of Superstructure	RC or PC	7 (37%)	5 (42%)	22 (40%)	7 (35%)	1 (13%)	6 (60%)	−0.141	0.233	0.131
	Steel	12 (63%)	7 (58%)	33 (60%)	13 (65%)	7 (88%)	4 (40%)	0.092		
⑥Slope in Bridge Axis	6% or Steeper			1 (2%)		1 (13%)	1 (10%)	0.919	0.941	0.161
	Less than 6%	19 (100%)	12 (100%)	54 (98%)	20 (100%)	7 (88%)	9 (90%)	−0.023		
⑦Device to Prevent Falling-off of Superstructure	None	1 (5%)	1 (8%)	20 (36%)	8 (40%)	6 (75%)	10 (100%)	0.459	1.106	0.358
	One Device	16 (83%)	6 (50%)	28 (51%)	11 (55%)	2 (25%)		−0.181		
	Two Devices or More	2 (11%)	5 (42%)	7 (13%)	1 (5%)			−0.647		
⑧Type of Substructure	Single-line Bent Pile	1 (5%)		5 (9%)	2 (10%)		3 (30%)	0.292	0.411	0.178
	Reinforced Concrete Frame	1 (5%)	1 (8%)	9 (16%)	8 (40%)	4 (50%)	4 (40%)	0.259		
	Others	17 (89%)	11 (92%)	41 (75%)	10 (50%)	4 (50%)	3 (30%)	−0.119		
⑨Height of Pier H	10m ≦ H	4 (21%)	5 (42%)	12 (22%)	8 (40%)	2 (25%)	3 (30%)	0.172	0.284	0.125
	5m ≦ H < 10m	7 (37%)	3 (25%)	29 (53%)	7 (35%)	6 (75%)	5 (50%)	−0.038		
	H < 5m	8 (42%)	4 (33%)	14 (25%)	5 (25%)		2 (20%)	−0.112		
⑫Ground Condition	Extremely Soft in Group 4	1 (5%)			1 (5%)	2 (25%)		0.523	0.983	0.273
	Group 4	5 (26%)		2 (4%)	11 (35%)	4 (50%)	7 (70%)	0.224		
	Group 3	3 (16%)	8 (67%)	33 (60%)	6 (30%)	1 (13%)	3 (30%)	0.040		
	Group 2	1 (5%)	1 (8%)	8 (15%)	1 (5%)			0.112		
	Group 1	9 (47%)	3 (23%)	12 (22%)	1 (5%)	1 (13%)		−0.461		
⑪Irregularity of Supporting Ground	Irregular		1 (8%)	1 (2%)	4 (20%)	1 (13%)		0.307	0.420	0.104
	Almost Uniform	19 (100%)	11 (92%)	54 (98%)	16 (80%)	7 (88%)	10 (100%)	−0.024		
⑫Effect of Soil Liquefaction	Liquefiable			4 (7%)	2 (10%)	2 (25%)	6 (60%)	0.724	0.816	0.255
	Non-liquefiable	19 (100%)	12 (100%)	51 (93%)	18 (90%)	6 (75%)	4 (40%)	−0.092		
⑬Effect of Scouring	Recognized				1 (5%)			0.312	0.315	0.033
	None	19 (100%)	12 (100%)	55 (100%)	19 (95%)	8 (100%)	10 (100%)	−0.003		
⑭Materials of Substructure	Plane Concrete in Accordance with 1926 Specs. or 1939 specs.				1 (5%)		2 (20%)	0.995	1.020	0.167
	RC, PC, Steel or Unreinforced Concrete in Accordance with Specs. in 1956 or Later	19 (100%)	12 (100%)	55 (100%)	19 (95%)	8 (100%)	8 (80%)	−0.025		
⑮Type of Substructure	Timber, Brick, Masonry, Other Old Unknown Materials		1 (8%)	1 (2%)	1 (5%)	1 (13%)	4 (40%)	0.383	0.697	0.171
	RC Piles, Pedestal Piles or Pier Supported by Two Independent Caissons	2 (11%)	1 (8%)	9 (16%)	4 (20%)	2 (25%)	2 (20%)	−0.314		
	Foundations Designed by Specs. in 1971 or Later	17 (89%)	10 (83%)	45 (82%)	15 (75%)	5 (63%)	4 (40%)	0.034		

From the weighting factors presented in Table 6, the effects of each item were found as shown in Table 7. The following considerations were subsequently included in the statistical analysis to formulate an inspection method.

a) Because the objectives of the inspection method are to assess the seismic vulnerability of highway bridges subjected to ground shaking of JMA Intensity V or larger (peak ground acceleration larger than 0.25 g), the Intensity of Peak Ground Acceleration a_{max} is dropped from the evaluation item assuming that a_{max} is larger than 0.25 g.

b) Evaluation of the strength of reinforced concrete piers at the mid-height where main reinforcement is terminated was introduced.

c) Because collapse, such as falling-off of superstructure, generally occurred because of excessive relative movements between the superstructure and the substructures, and failure of substructures due to inadequate strength, the evaluation of the seismic vulnerability for both the relative movement and for the strength of substructures should be made.

d) Even if there are some unsatisfactory conditions in the evaluation, final evaluation may not consider them to be critical if the remaining factors are in good evaluation. Consequently, it was decided that those bridges with at least one "critical" or "safe" condition are to be considered to have either high or low seismic vulnerability. Below are some examples of evaluation of such specific types of structure :

- Those designed in accordance with the 1980 Specifications shall be classified into Rank C (safe) unless appreciable deterioration is detected.
- Those constructed by timber, brick, masonry, or old unknown materials shall be classified into Rank A (vulnerable).
- Those supported by single-line bent piles foundation which are constructed on loose alluvial sandy layer vulnerable to liquefaction or very loose clayey deposits shall be classified into Rank A (vulnerable).
- Single-span simply supported girder bridges with the span length less than 15 m shall be classified into Rank C (safe).

The procedure of seismic inspection and an inspection sheet are shown in Fig. 3 and Table 8, respectively[7,8]. The evaluation of the seismic vulnerability is made in accordance with the points which reflect the vulnerability to excessive relative movement between superstructure and substructures (point X), and the strength of substructures (point Y) as shown in Table 9.

Table 7 Factors which Affect Seismic Vulnerability of Highway Bridges

Items	Seismic Vulnerability
① Design Specifications	Those designed in accordance with 1926 or 1939 Specifications have higher vulnerability
② Type of Superstructure	• Gerber or simply supported girders with 2 or more spans have higher vulnerability • Arch, frame, continuous girders, cable-slayed bridges or suspension bridges have lower vulnerability
③ Shape of Superstructure	Skewed or curved bridges do not necessarily have higher vulnerability than straight bridges
④ Materisls of Superstructure	Reinforced concrete bridges or prestressed concrete bridges have lower vulnerability than steel bridges although the difference is small
⑤ Slope in Bridge Axis	Bridges with slope in bridge axis have higher vulnerability
⑥ Device for Preventing Falling-off of Superstructure	Bridges with devices for preventing falling-off of superstructure have lower vulnerability
⑦ Type of Substructure	Bridges supported by single-line bent piles or by reinforced concrete frame placed on two separate caisson foundations have higher vulnerability
⑧ Height of Piers	Bridges supported by higher piers have higher vulnerability
⑨ Ground Condition	Bridges constructed on soft soil have higher vulnerability
⑩ Effect of Soil Liquefaction	Bridges constructed on sandy soil layers susceptible to liquefaction have higher vulnerability
⑪ Irregularity of Supporting Soil Condition	Bridges constructed on soils with irregularity of supporting conditions have higher vulnerability
⑫ Effect of Scouring	Bridges where the surface soils are scoured have higher vulnerability
⑬ Materials of Substructures	Bridges supported by plane-concrete substructures designed in accordance with 1926 or 1939 specifications have higher vulnerability
⑭ Type of Foundation	Bridges supported by timber, brick, masonry or other old unknown type substructures have higher vulnerability
⑮ Intensity of Ground Motion	Bridges subjected to higher intensity of ground acceleration have higher vulnerability. In particular, vulnerability becomes quite high when the bridges are subjected to peak ground acceleration larger than 400 gal (0.4g)

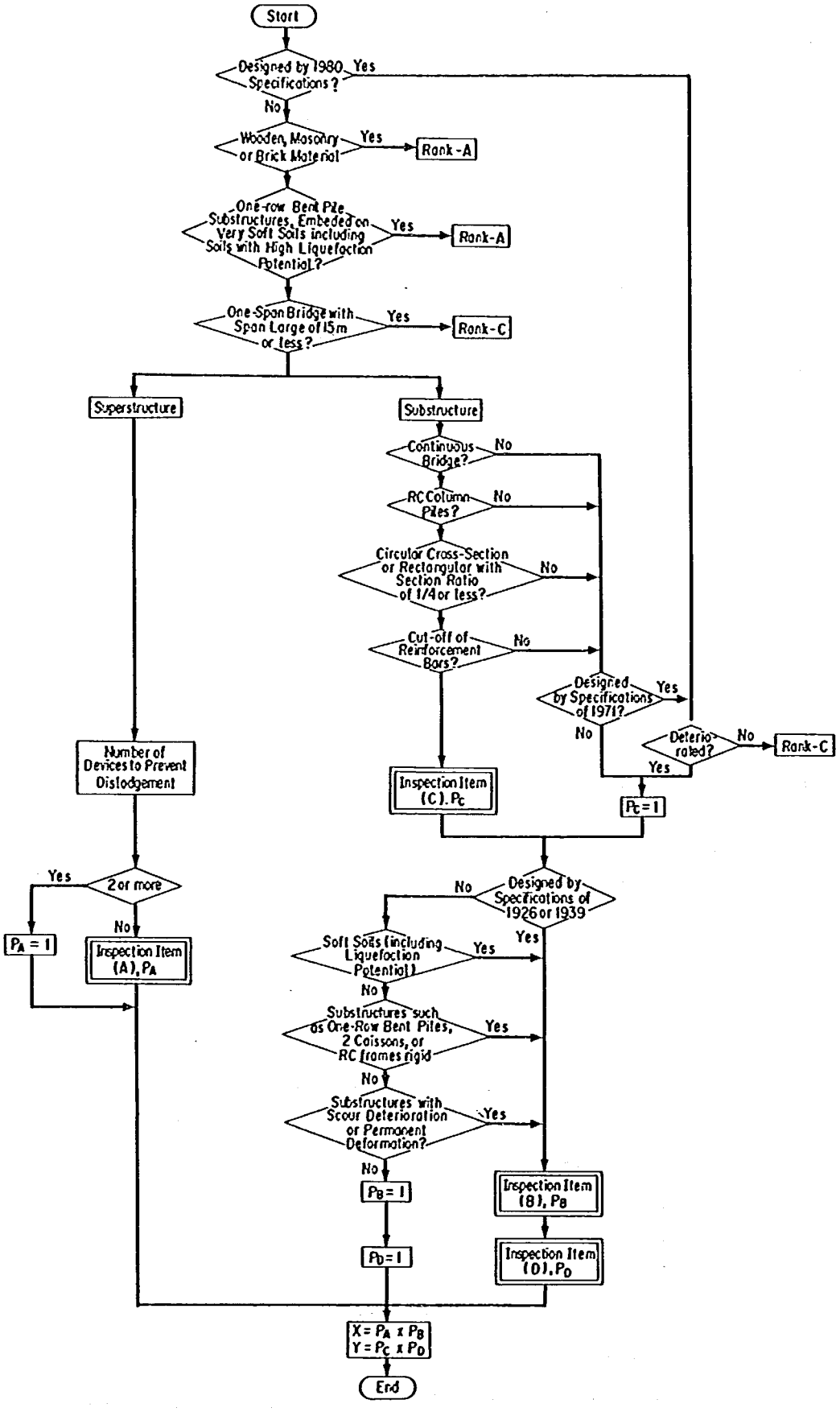


Fig. 3 Procedure of Seismic Inspection for Highway Bridges

Table 8 Inspection Sheet for Seismic Vulnerability of Highway Bridges

Point of Inspection		Factors of Inspection	Evaluation
Inspection for Vulnerability to Develop Excessive Deformation	Inspection Format (A) Inspection for Deformation of Superstructure	① Design Specifications	4.0: 1926 Specs. or 1939 Specs. / 2.0: 1956 Specs. or 1964 Specs. / 1.0: 1971 Specs. or 1980 Specs.
		② Superstructure Type	3.0: Gerber Girder or Simply-supported Girders with Two Spans or More / 1.5: Simply-supported Girder or Continuous Girders Consisting of Two Spans or More / 1.0: Arch, Flame, Continuous Girder (One Span), Cable-stayed Bridge, Suspension Bridge
		③ Shape of Superstructure	1.2: Skewed or Curved Bridge / 1.0: Straight Bridge
		④ Materials of Superstructure	1.2: Rc or PC / 1.0: Steel
		⑤ Gradient	1.2: 6% or Steeper / 1.0: Less Than 6%
		⑥ Falling-off Prevention Device	2.0: None / 1.0: One Device
		$P_A = ① \times ② \times ③ \times ④ \times ⑤ \times ⑥$	$P_A =$
	Inspection Format (B) Inspection for Deformation of Substructure	⑦ Type of Substructure	2.0: Single-line Bent Pile Foundation / 1.0: Others
		⑧ Height of Pier H	2.0: $H \geqq 10m$ / 1.5: $5 \leqq H < 10m$ / 1.0: $H < 5m$
		⑨ Ground Condition	5.0: Extremely Soft in Group 4 / 2.5: Group 4 / 2.0: Group 3 / 1.2: Group 2 / 1.0: Group 1
		⑩ Effects of Liquefaction	2.0: Liquefiable / 1.0: Non-liquefiable
		⑪ Supporting Ground Condition	1.2: Irregular / 1.0: Almost Uniform
		⑫ Scouring	1.5: Recognized / 1.0: None
		$P_B = ⑦ \times ⑧ \times ⑨ \times ⑩ \times ⑪ \times ⑫$	$P_B =$
Inspection for Vulnerability to Develop Failure Due to Inadequate Strength of Substructure	Inspection Format (C) Inspection for Strength of RC Pier at Termination of Reinforcement	⑬ Shear Span Ratio (h/D)	2.0: $1 < h/D < 4$ / 1.0: $h/D \geqq 4$ / 0.5: $h/D \leqq 1$
		⑭ Tension Cracks in Flexure at Terminated Point of Main Reinforcement	2.0: Cracks Will Occur / 1.0: Cracks Will Possibly Occur / 0.3: Cracks will Not Occur
		⑮ Safety Factor for Yield Strength at Terminated Section of Main Reinforcement: (15-1) S_{ta}	3.0: $S_{ta} \leqq 1.1$ / 2.0: $1.1 < S_{ta} < 1.5$ / 0.5: $S_{ta} \geqq 1.5$
		(15-2) S_{cm}	3.0: $S_{cm} \leqq 1.1$ / 2.0: $1.1 < S_{cm} \leqq 1.3$ / 1.0: $1.3 < S_{cm} < 1.5$ / 0.5: $S_c \geqq 1.5$
		⑯ Shear Stress σ (tf/m²)	3.0: $\sigma \geqq 45$ / 2.0: $30 \leqq \sigma < 45$ / 1.0: $15 \leqq \sigma < 30$ / 0.5: $\sigma < 15$
		$P_C = ⑬ \times ⑭ \times (15\text{-}1) \times (15\text{-}2) \times ⑯$	$P_C =$
	Inspection Format (D) Inspection for Strength of Substructure	⑰ Failure of Fixed Supports and Proximity	5.0: Extensive Failure / 2.0: Small Failure / 1.0: None
		⑱ Extraordinary Damage of Pier	5.0: Extensive Damage / 2.0: Small Damage / 1.0: None
		⑲ Materials of Substructure	2.0: Plane Concrete Older Than 1926 Excluding Gravity-type Abutment / 1.0: Others
		㉒ Construction method of Foundation	2.0: Timer Pile, Masonry, Brick, Other Old Construction Methods / 1.5: RC Piles, Pedestal Piles, Pier Supported by Two Independent Caissons / 1.0: Foundation Designed by 1971 Specs. and Other Later Specs.
		㉑ Foundation Type	1.5: RC Flame Supported by Two Independent Caisson Foundations / 1.0: Others
		⑫ Extraordinary Failure of Foundation	2.0: Recognized / 1.0: None
		$P_D = ⑰ \times ⑱ \times ⑲ \times ㉒ \times ㉑ \times ㉒$	$P_D =$
Evaluation of Deformation and Strength			$X = P_A \times P_B =$ and $Y = P_C \times P_D =$

Table 9 Evaluation of Seismic Vulnerability

Rank of Seismic Vulnerability	Evaluation Points		
	X	Y	
		$Pc = 1.0$	$Pc \neq 1.0$
A—Vulnerable	$X \geqq 60$	$Y \geqq 10$	$Y \geqq 100$
B—Moderate	$20 \leqq X < 60$	$5 \leqq Y < 10$	$50 \leqq Y < 100$
C—Safe	$X < 20$	$Y < 5$	$Y < 50$

Note) Out of two ranks obtaind from X-point and Y-point, higher rank (A is the highest) should be taken as the final ranking of the bridge inspected. For obtaining evaluation points X and Y, refer to Table 8.

Table 10 shows the feasibility of seismic strengthening against the 16 factors which would affect the seismic vulnerability of highway bridges (refer to Table 7). Among the 16 factors, ⑥ Devices for Preventing Falling-off of the Superstructure, ⑦ Type of Substructure, ⑩ Effect of Soil Liquefaction, ⑫ Effect of Scouring, ⑬ Materials of Substructures, ⑭ Types of Foundation, and ⑯ Effect of Termination of Main Reinforcement at Mid-height are the factors for which countermeasures for strengthening the bridge are feasible. Countermeasures against for the remaining 9 factors can not be made unless the whole bridge be replaced.

Table 10 Feasibility of Seismic Strengthening for 16 Factors which Affect Seismic Vulnerability of Highway Bridges

Items	Feasibility of Seismic Strengthening	Principles of Countermeasures
① Design Specifications	×	———
② Type of Superstructure	×	———
③ Shape of Superstructure	×	———
④ Materials of Superstructure	×	———
⑤ Slope in Bridge Axis	×	———
⑥ Device for Preventing Falling-off of Superstructure	O	Installation of Devices
⑦ Type of Substructure	O	Strengthening of Substructures
⑧ Height of Piers	×	———
⑨ Ground Condition	×	———
⑩ Effect of Soil Liquefaction	O	Strengthening of Fundations or Strengthening of Surrounding Soils
⑪ Irregularity of Supporting Soil Condition	×	———
⑫ Effect of Scouring	O	Treatment for Prevention of Scouring, or Strengthening of Foundations
⑬ Materials of Substructures	O	Strengthening of Substructures
⑭ Type of Foundation	O	Strengthening of Foundations
⑮ Intensity of Ground Motion	×	———
⑯ Effect of Termination of Main Reinforcement at Mid-height	O	Strengthening of Substructures

Note O Items for which seismic strengthening is feasible
× Items for which seismic strengthening is not feasible

Fig. 4 shows how the countermeasures can be made for the above described 7 factors. Installation of devices for preventing falling-off of superstructure, strengthening of foundations, and strengthening of piers and abutments are the main measures of seismic strengthening.

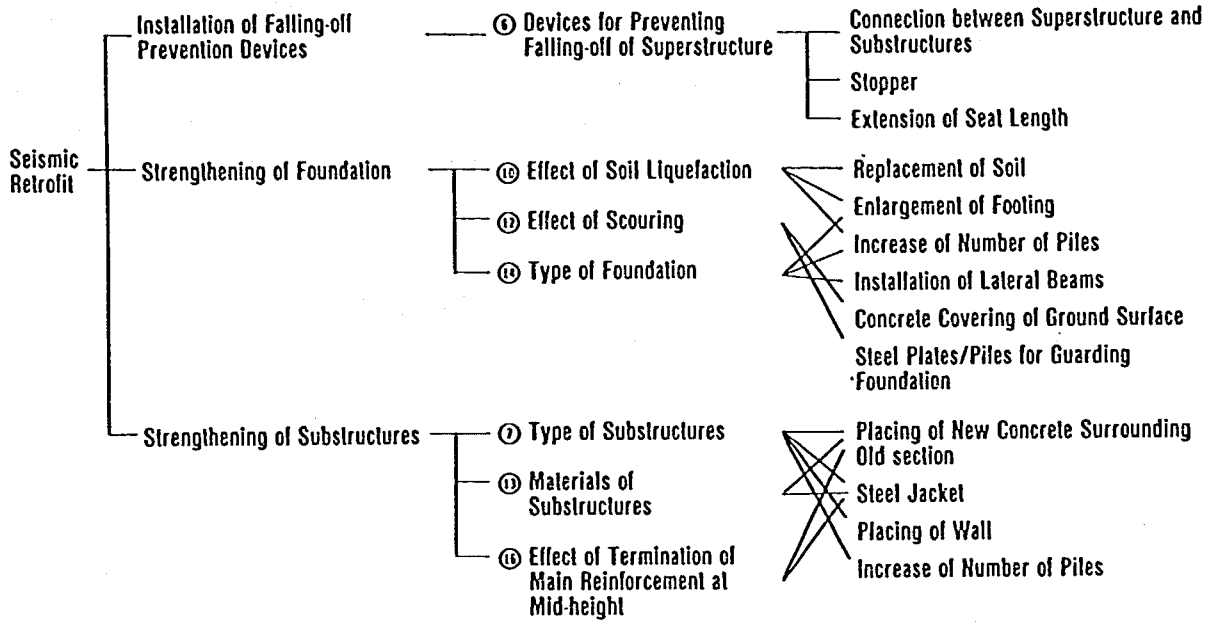


Fig. 4 Selection of Seismic Strengthening Measures for Highway Bridges

Figs. 5, 6 and 7 show the methods for selecting the installation of the stoppers at movable supports, falling-off prevention devices, and elongation of seat length S_E and bearing seat length S as measures of seismic strengthening for existing bridges. The methods are based on a number of practices in the past[9].

Figs. 8 and 9 show measures for strengthening foundations and strengthening substructures for existing bridges, respectively.

The seismic inspection and strengthening methods of transportation facilities including highway bridges were compiled and published from the Japan Road Association in the form of the "Guide Specifications for Earthquake Hazard Mitigation for Transportation Facilities – Pre-Earthquake Countermeasures –" in 1987[9].

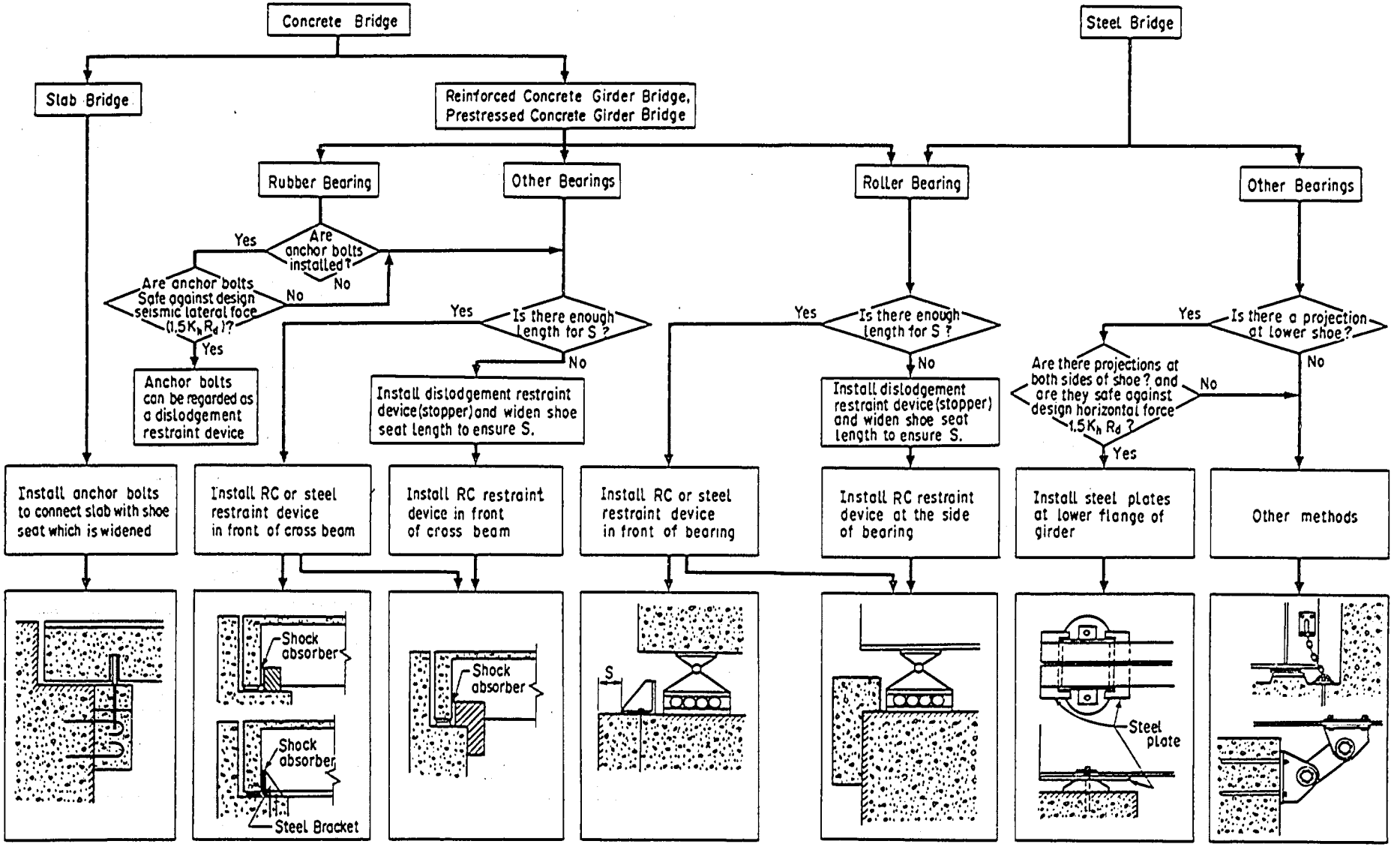


Fig. 5 Installation of Stopper at Movable Bearings for Existing Bridges

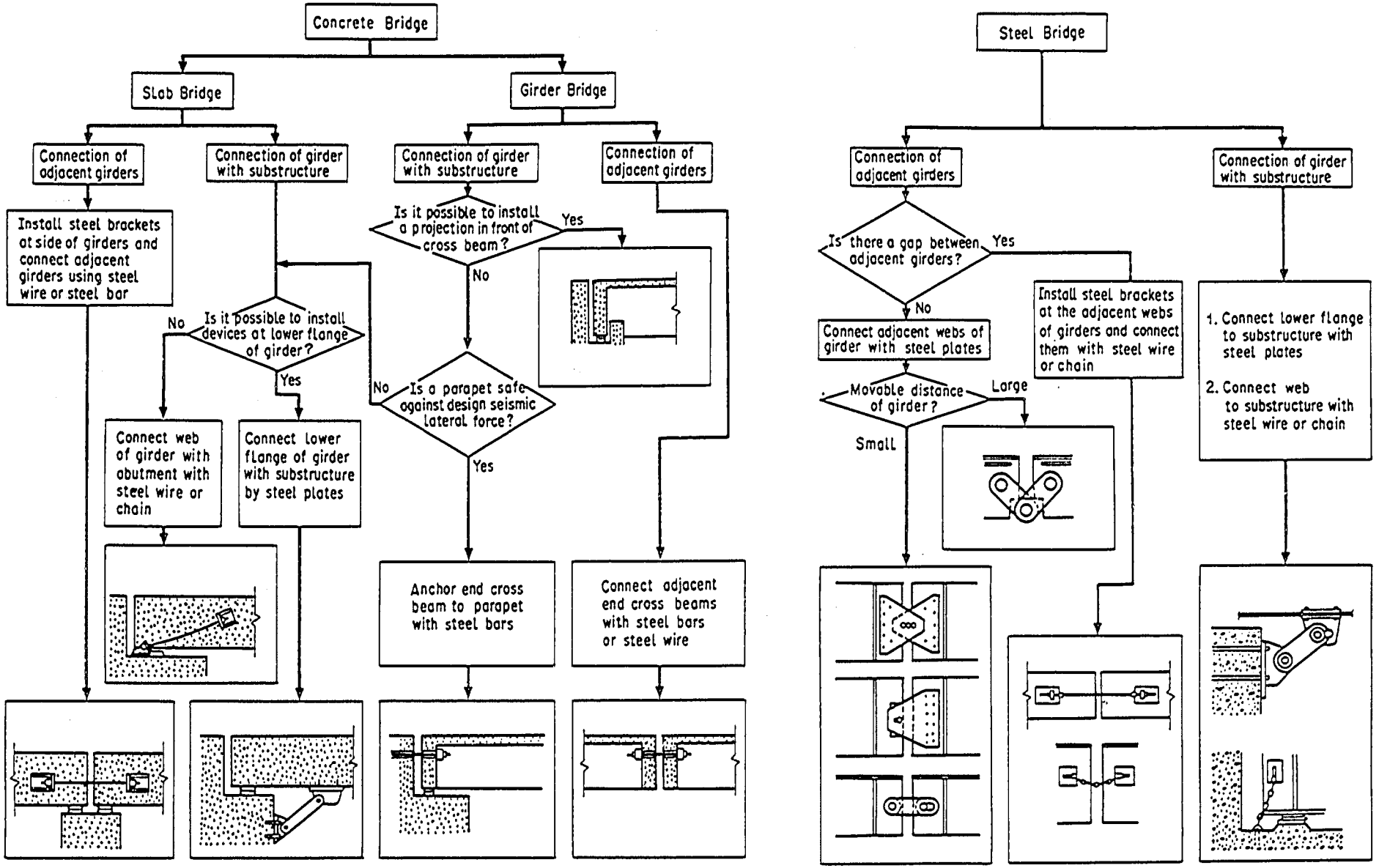


Fig. 6 Installation of Devices Connecting Deck and Substructure, and Device Connecting Two Adjacent Decks for Existing Highway Bridges

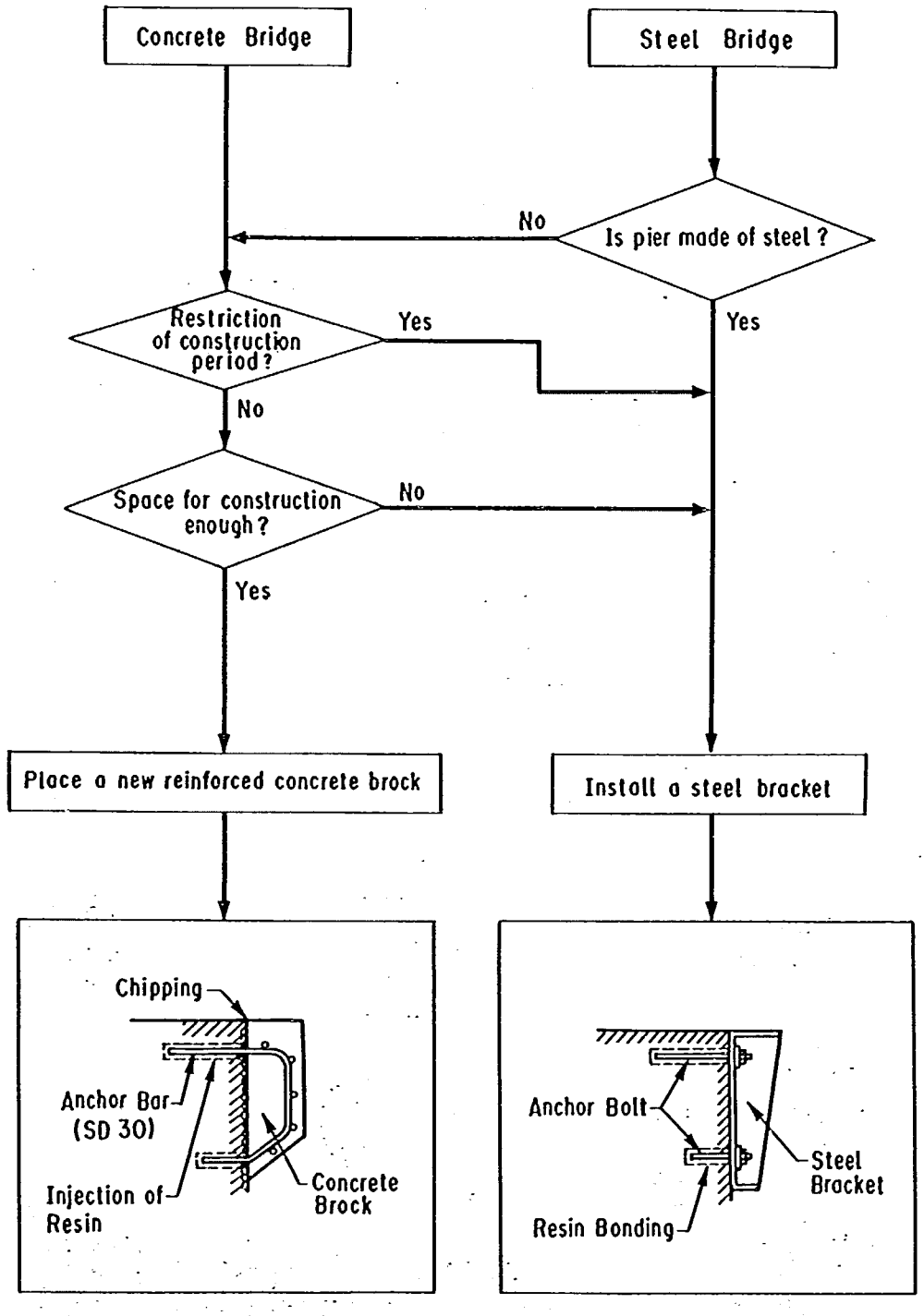
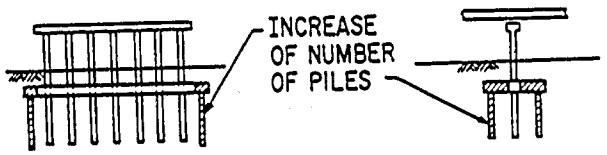
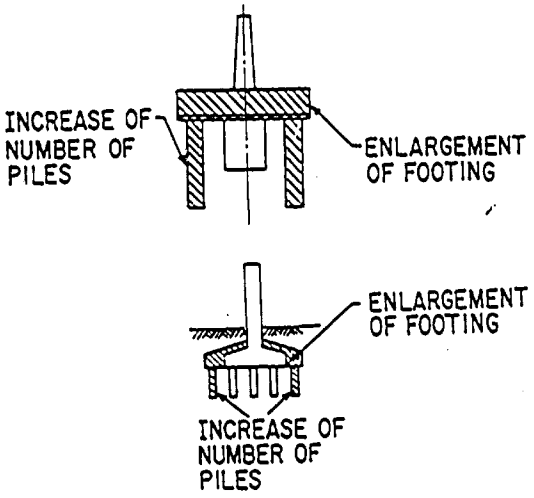


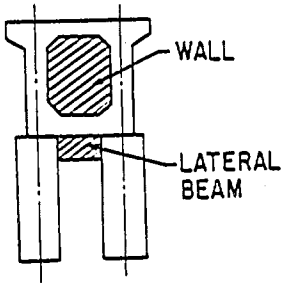
Fig. 7 Elongation of Seat Length S_E and Bearing Seat Length S for Existing Highway Bridges



(1) STRENGTHENING OF
BENT PILE

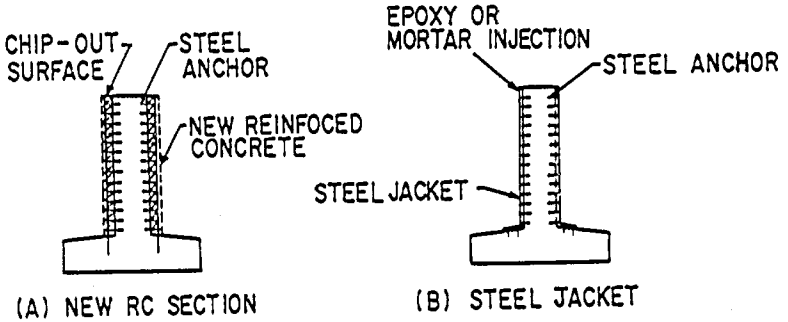


(2) STRENGTHENING
OF FOUNDATION
WITH INADEQUATE
BEARING CAPACITY



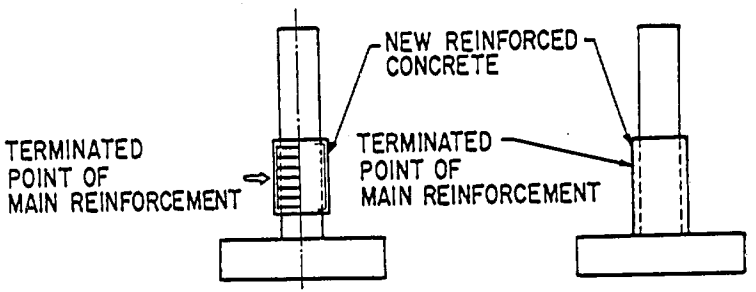
(3) STRENGTHENING
OF RC FRAME
ON TWO INDEPENDENT
CAISSON FOUNDATIONS

Fig. 8 Strengthening of Foundations

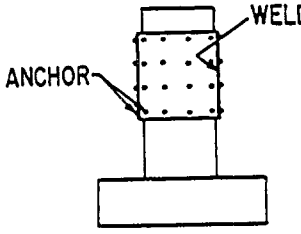


(A) NEW RC SECTION (B) STEEL JACKET

(1) STRENGTHENING OF WEAK PIERS



(A) NEW RC SECTION



(B) STEEL JACKET

(2) STRENGTHENING OF RC PIERS WITH TERMINATION
OF MAIN REINFORCEMENT AT MID-HEIGHT

Fig. 9 Strengthening of Piers

EXAMPLE OF SEISMIC STRENGTHENING

Fig. 10 shows an example of seismic strengthening of reinforced concrete frame supporting a bridge, constructed in 1968, on the Tomei Expressway of Japan Highway Public Corporation[10)11)]. The frame was strengthened so that the seismic safety be ensured against the Tokai Earthquake which is anticipated to occur with the magnitude over 8 in the Tokai area. The piers were strengthened by placing new reinforced concrete with thickness of 17 cm. Reinforcing bars were anchored into the footing. They were bent at the base of piers with anchorage length of 112 cm (35 times the diameter of reinforcing bars) being provided to prevent pulling-out from the footing. Photo 1 shows the completion of the strengthening work.

Photo 1 Seismic Strengthening of RC Frame by Placing New Reinforced Concrete

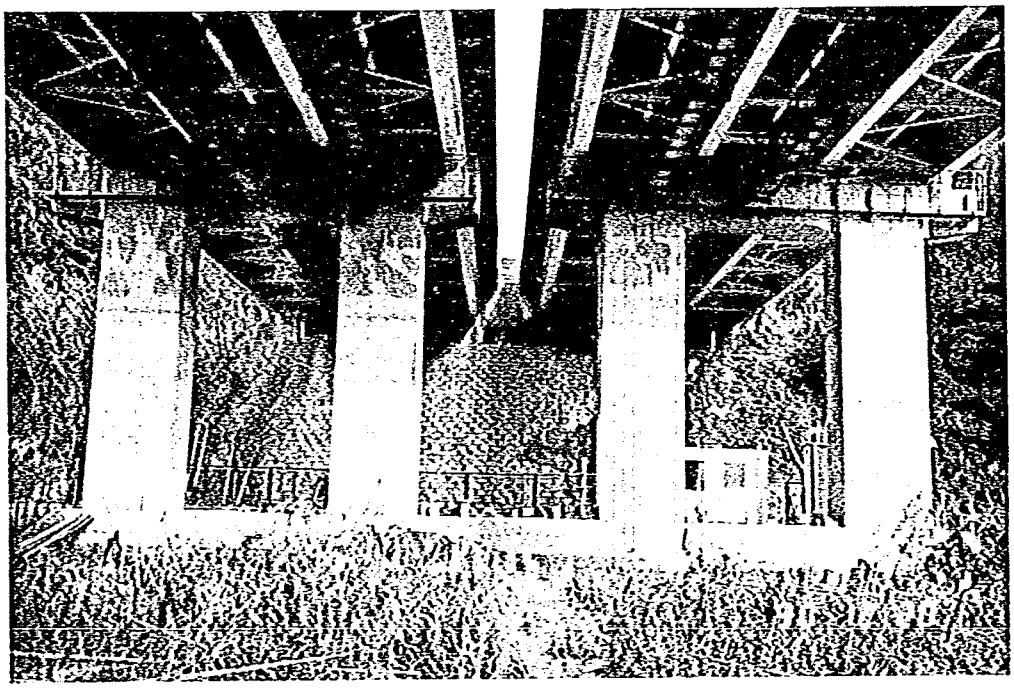
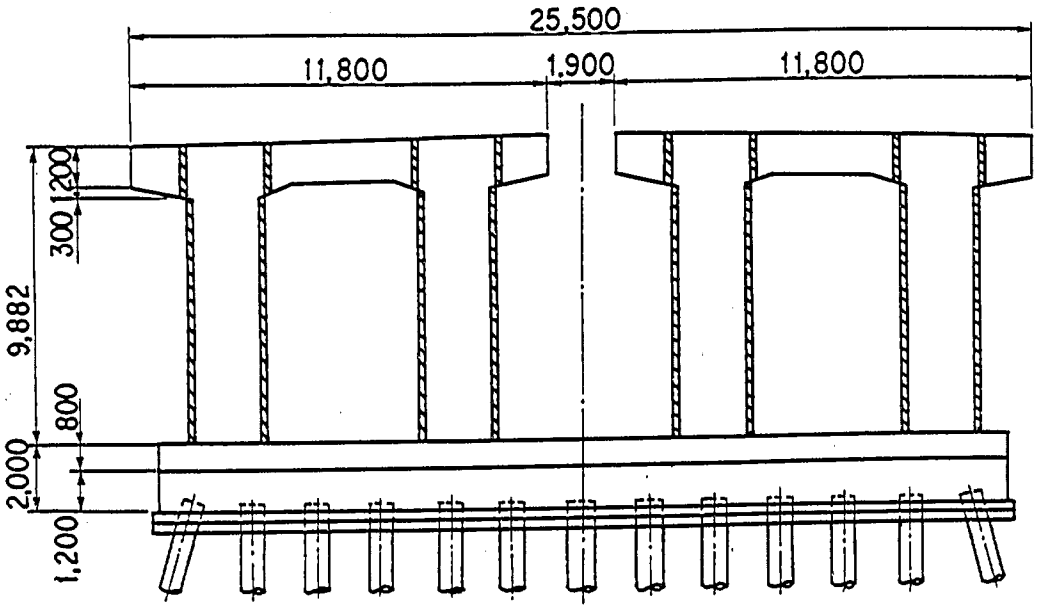
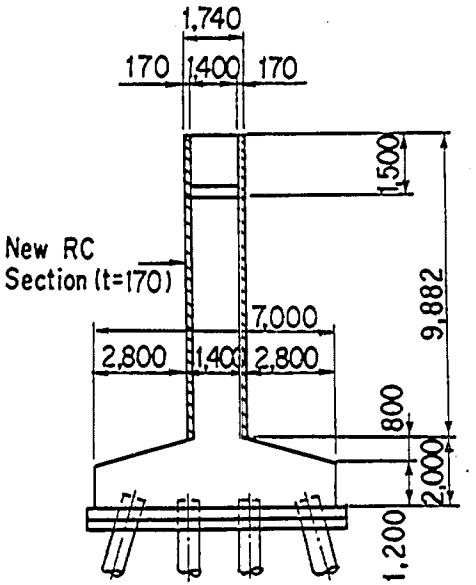


Fig. 11 shows an example of seismic strengthening of foundation constructed in 1952. To increase bearing capacity of the foundation, number of piles was increased by enlarging the foundation[12)].

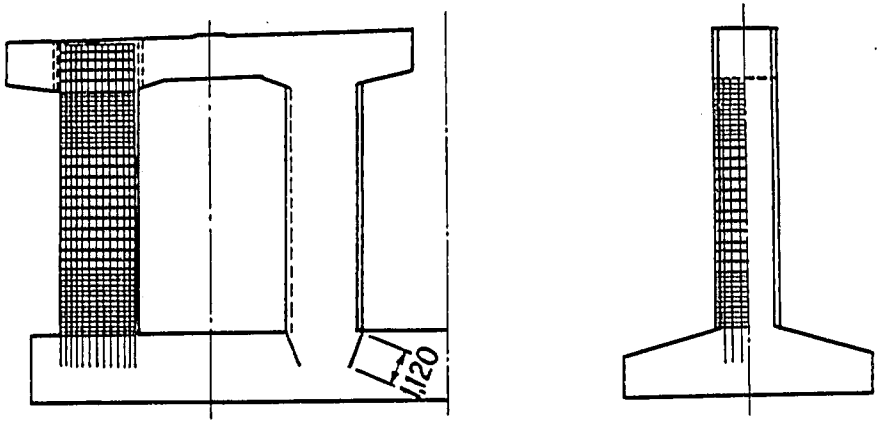
Fig. 12 shows an example of seismic strengthening of bent piles which was constructed in 1959. Because bent pile has small stiffness to inertia force in longitudinal direction, it was judged vulnerable. A unique strengthening method was adopted in this bridge[12)]. Instead of strengthening each bent pile, only two abutments at both ends of the deck were strengthened by constructing new cast-in-place concrete piles, and the top of the bent piles was tied to a steel beam which was newly placed on both sides of the deck.



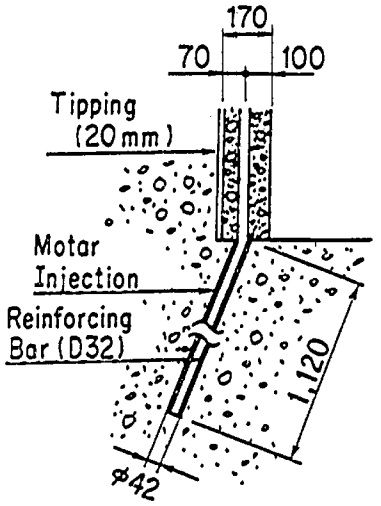
(a) Elevation



(b) Side View



(c) Arrangement of Reinforcement



(d) Anchorage of Reinforcing Bars

Fig. 10 Seismic Strengthening of RC Frame by Placing New Reinforced Concrete

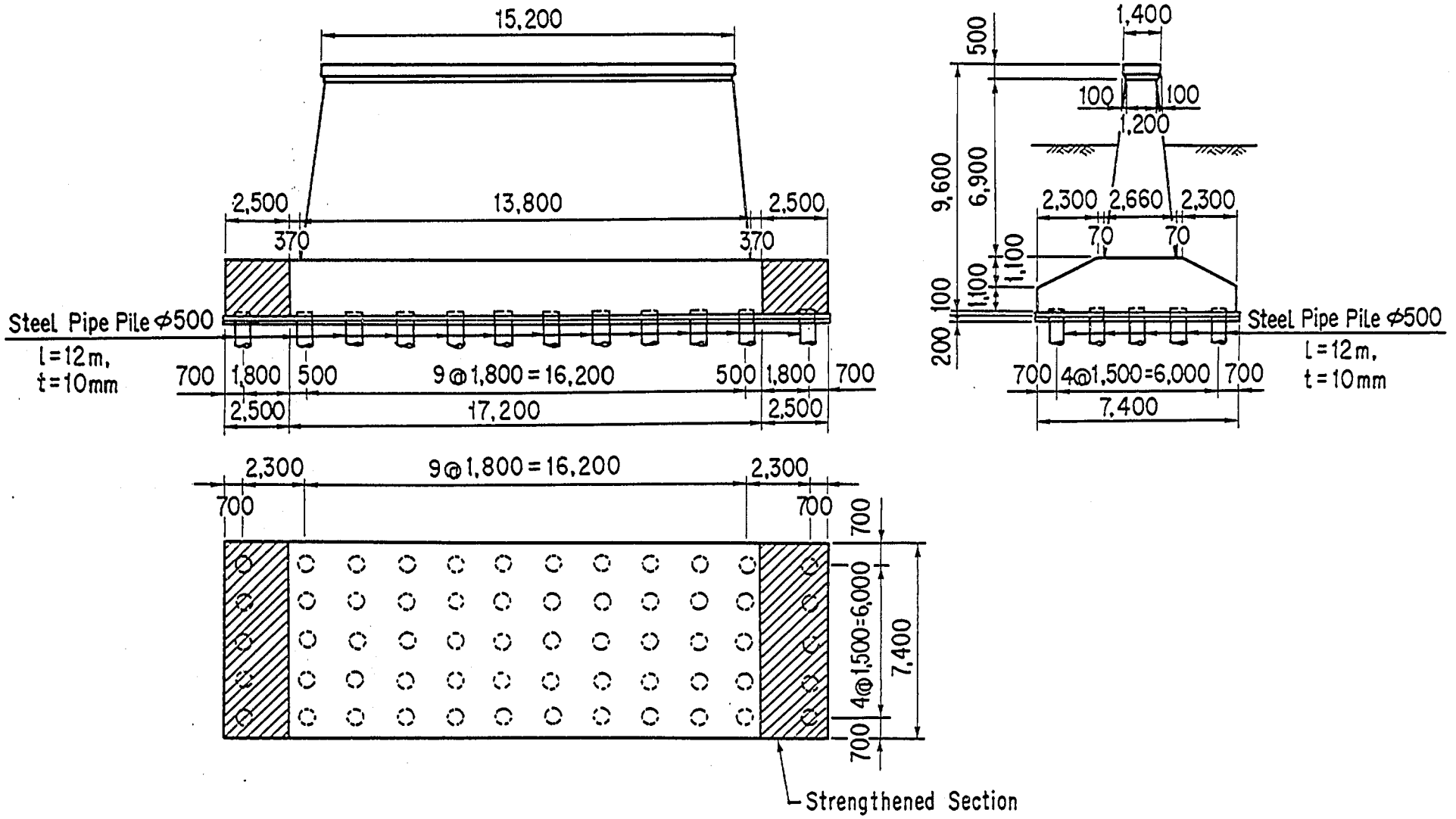


Fig. 11 Seismic Strengthening of Foundation by Increasing Number of Piles

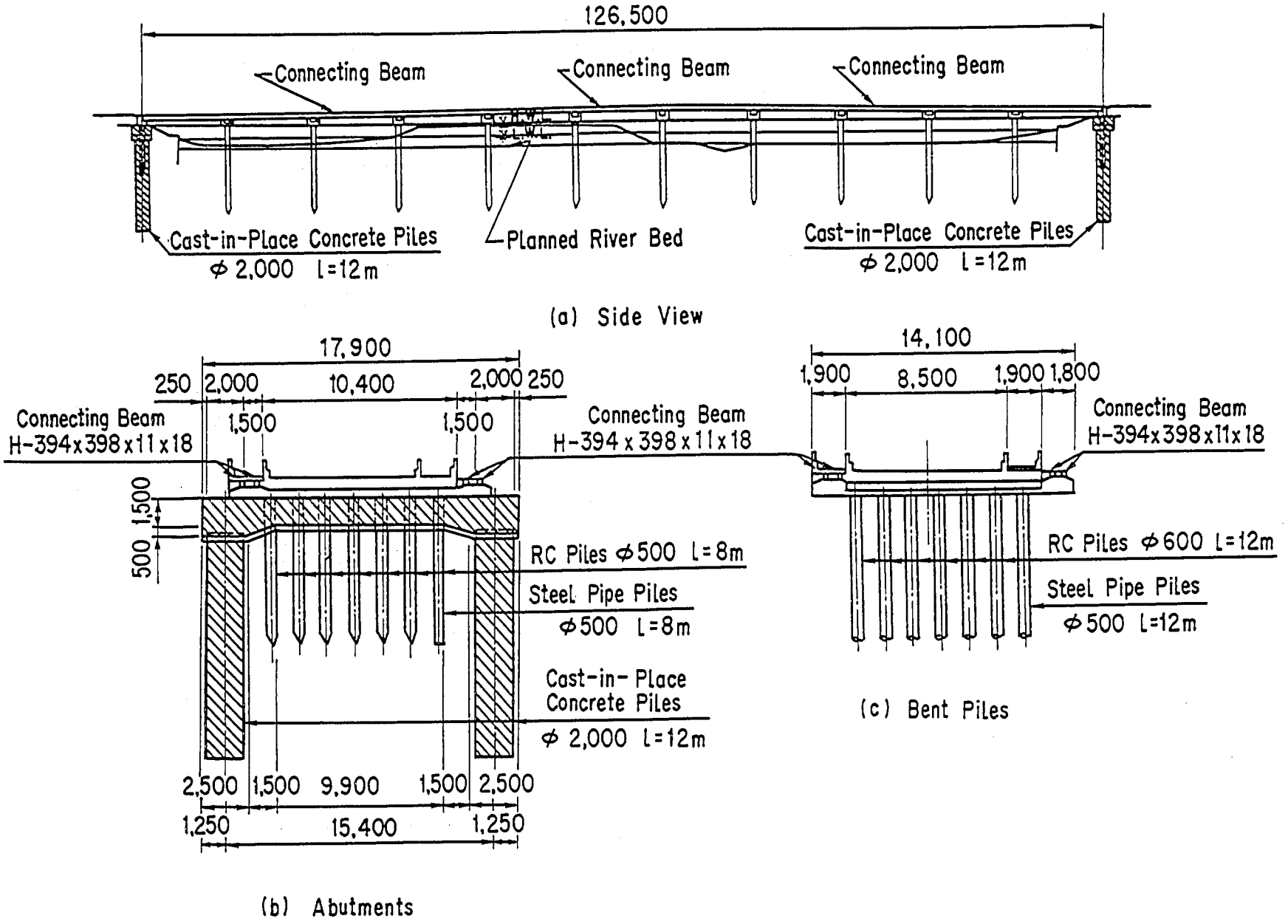


Fig. 12 Seismic Strengthening of Bent Piles on Liquefiable Soils by Connecting Beams

RESEARCH FOR DEVELOPING SEISMIC STRENGTHENING METHODS

Various research efforts have been paid to develop rational seismic inspection and strengthening method. Because current efforts are being concentrated to develop an inspection and strengthening method of reinforced concrete piers with termination of main reinforcement at mid-height, research progress for the termination zone is introduced.

The importance for this type of damage became apparent when a bridge was critically damaged during the Urakawa-oki Earthquake in 1982[13]. The Shizunai bridge which is of five-span continuous girders and reinforced concrete piers suffered destructive damage at the piers as shown in Photo 2.

Significant shear failure was found at mid-height of reinforced concrete piers, where some of main reinforcement were terminated. Photo 3 shows the similar damage during the 1978 Miyagi-ken-oki Earthquake[14]. Although the damage was not so serious as the Shizunai Bridge, it was found that this type of failure occurred widely in the past earthquakes. Because wall type piers were commonly constructed in the past, shear failure developed by the inadequate anchorage length of main reinforcement did not become so pronounced in the past. Single columns with smaller concrete sectional area are likely to be adopted in recent years, and it is considered important to investigate failure mechanism of this type of damage for developing seismic inspection and strengthening method.

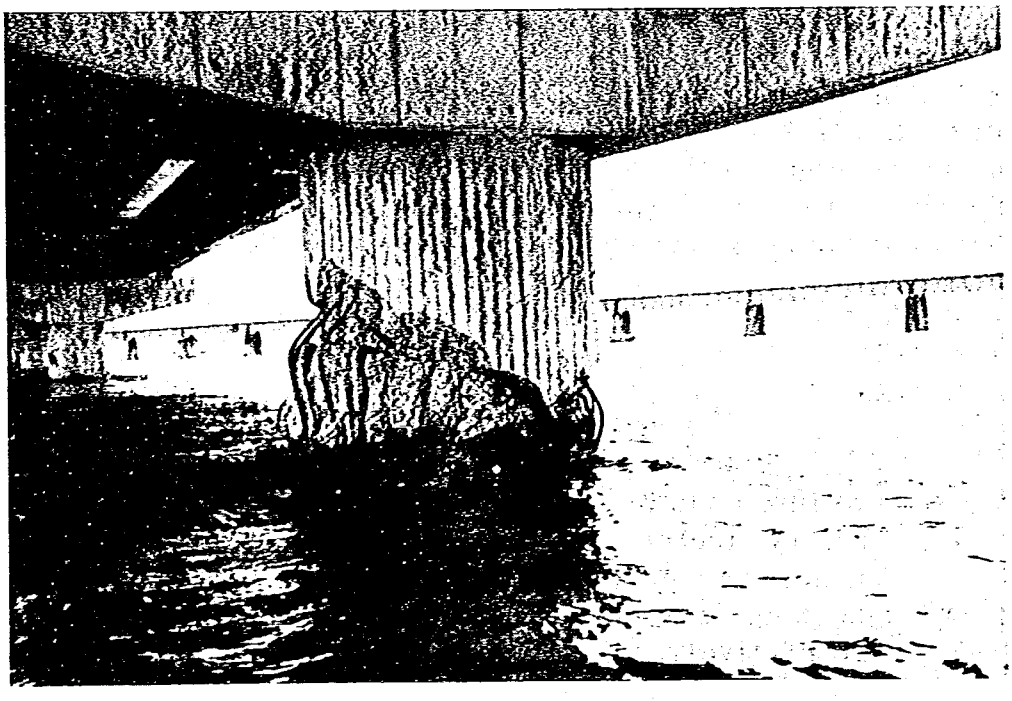


Photo 2 Damage of Shizunai Bridge during Urakawa-oki Earthquake in 1982

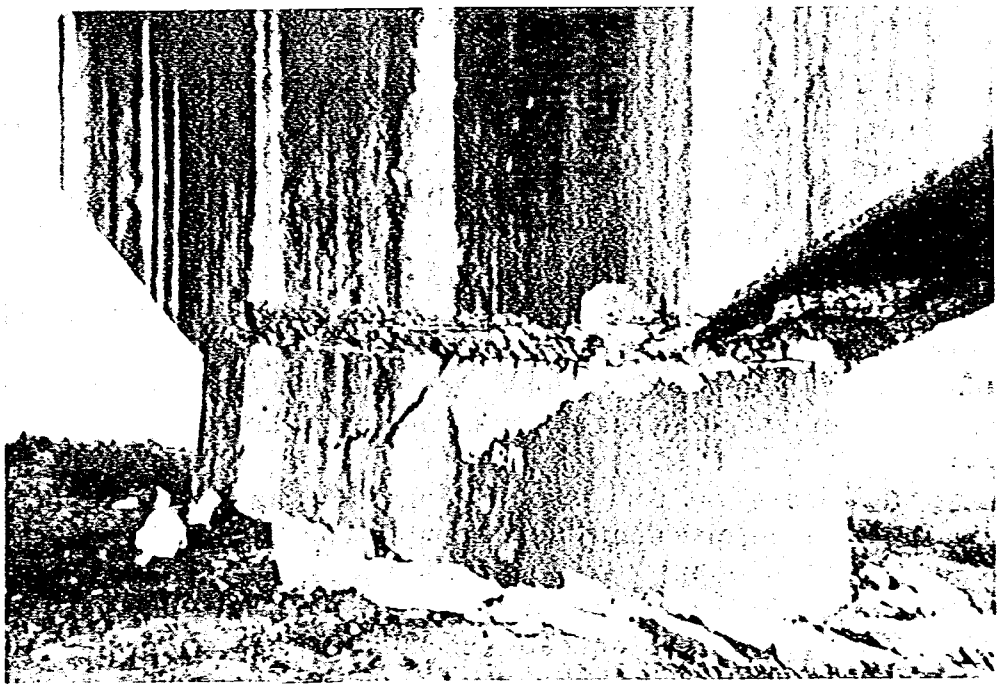


Photo 3 Damage of Sendai Bridge during Miyagi-ken-oki Earthquake in 1978

Before the Design Specifications of Highway Bridges was revised in 1980, anchorage length of main reinforcement terminated at tension zone was only 20 - 30 times a diameter of reinforcing bars. It was increased in 1980 to effective width of the piers plus 20 times the diameter or the termination has to be made upper than the point where the stress of the reinforcing bar becomes half of the allowable stress.

For investigating failure mechanism, a series of loading test were made at the Public Works Research Institute as shown in Photos 4 and 5[15]. Fig. 13 shows a method proposed based on the tests at PWRI for identifying the vulnerability at the termination zone. The inspection is made by two parameters, i.e., failure mode factor S_y and safety factor at termination zone F_y^T, which are defined as

$$S_y = F_y^T / F_y^B \quad (2)$$

$$F_y^T = M_y^T / M^T \quad (3)$$

$$F_y^B = M_y^B / M^B \quad (4)$$

where

S_y : failure mode factor

F_y^T, F_y^B : safety factor representing strength of pier in terms of bending moment at termination point and base, respectively

M^T, M^B : bending moment developed at termination point and base, respectively, when pier is subjected to a lateral inertia force during earthquakes (tf·m)

M_y^T, M_y^B : yielding bending moment at termination point and base, respectively (tf·m)

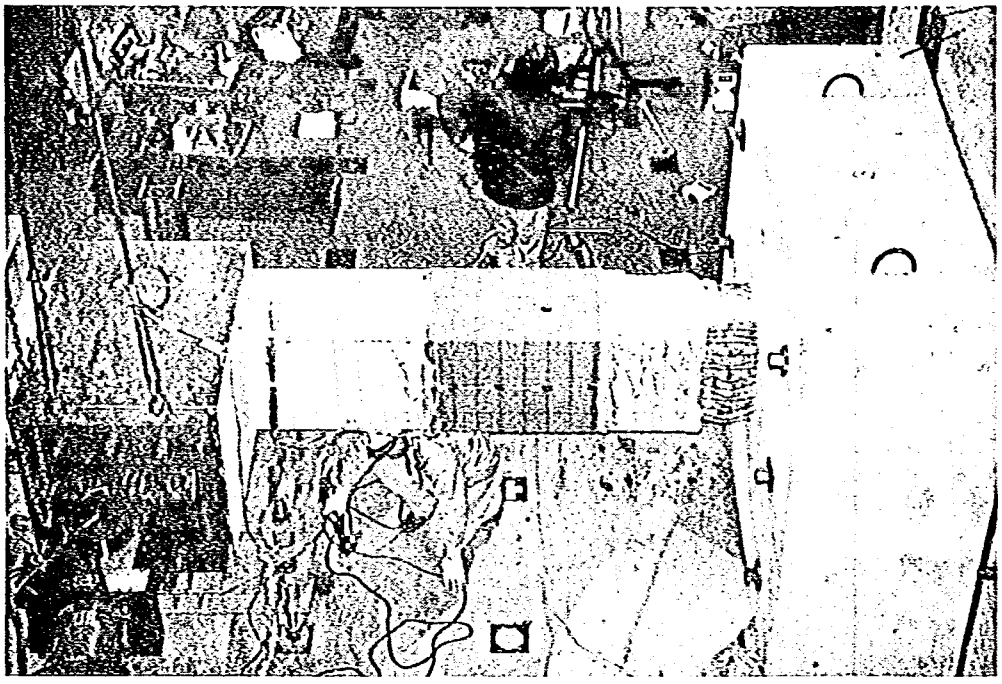


Photo 4 Loading Tests of RC Pier with Termination of Main Reinforcement at Mid-Height (Square Section)

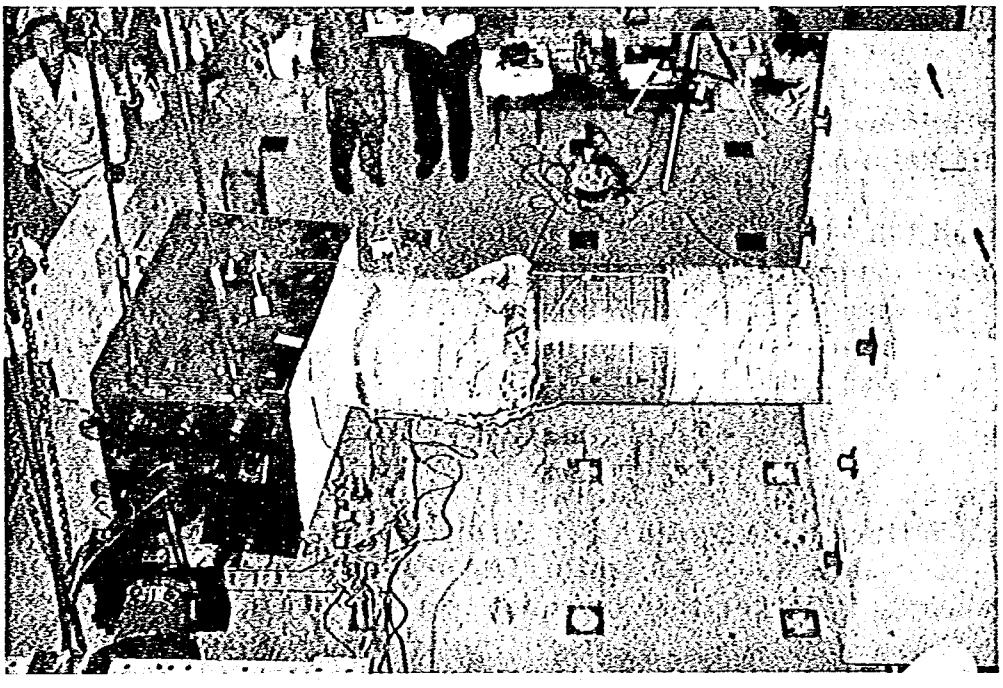


Photo 5 Loading Tests of RC Pier with Termination of Main Reinforcement at Mid-Height (Circular Hollow Section)

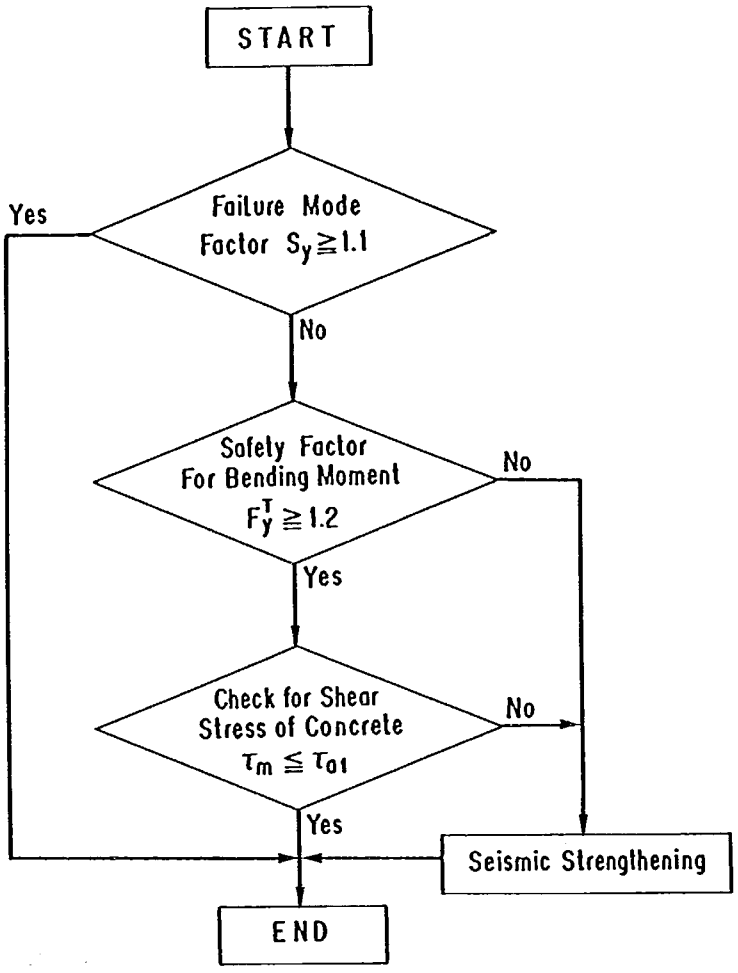


Fig. 13 Seismic Inspection for Reinforced Concrete Piers with Termination of Main Reinforcement at Mid-Height

In Eqs. (2) and (3), the failure mode factor S_y is used to identify where failure is likely developed firstly at either termination zone or base, and safety factor F_y^T represents redundancy to failure at the termination zone. With use of S_y and F_y^T, the decision is made in accordance with Table 11 by following a flow chart as shown in Fig. 13. Check of shear stress is also made as shown in Fig. 13.

Fig. 14 shows the effectiveness to identify where the failure was developed by means of the failure mode factors S_y. Failure is likely to be developed at the termination zone when $S_y \leqq 0.9$, while, flexural failure at the base tends to be developed when S_y is larger than or equal to 1.1 as shown in Table 11.

Fig. 15 shows how the safety factor F_y^T is effective to assess the damage degree. The damage degree is defined as the failure which is possibly developed at the loading stage of 5 times the yielding displacement ($5\delta_y$). From Fig. 15, it is clear that significant failure including rupture of main reinforcements tends to be developed when $F_y^T < 1.2$.

Table 11 Estimation of Seismic Vulnerability on the Strength of Termination Zone by Failure Mode Factor S_y and Safety Factor F_y^T

(a) Estimation of Failure Mode

Failure Mode Factor Sy	Failure Mode
$Sy \geqq 1.1$	Flexural Failure at Base
$Sy < 1.1$	Vulnerable to Failure at Termination Zone

(b) Estimation of Damage Degree (In Case of $Sy < 1.1$)

Safety Factor F_y^T	Damage Degree at Termination Zone at the Loading Displacement of $5\delta y$
$F_y^T < 1.2$	Rupture and Serious Buckling of Main Reinforcement
$F_y^T \geqq 1.2$	Diagonal Cracks, Spalling-off of Cover Concrete, Slight Buckling of Main Reinforcement

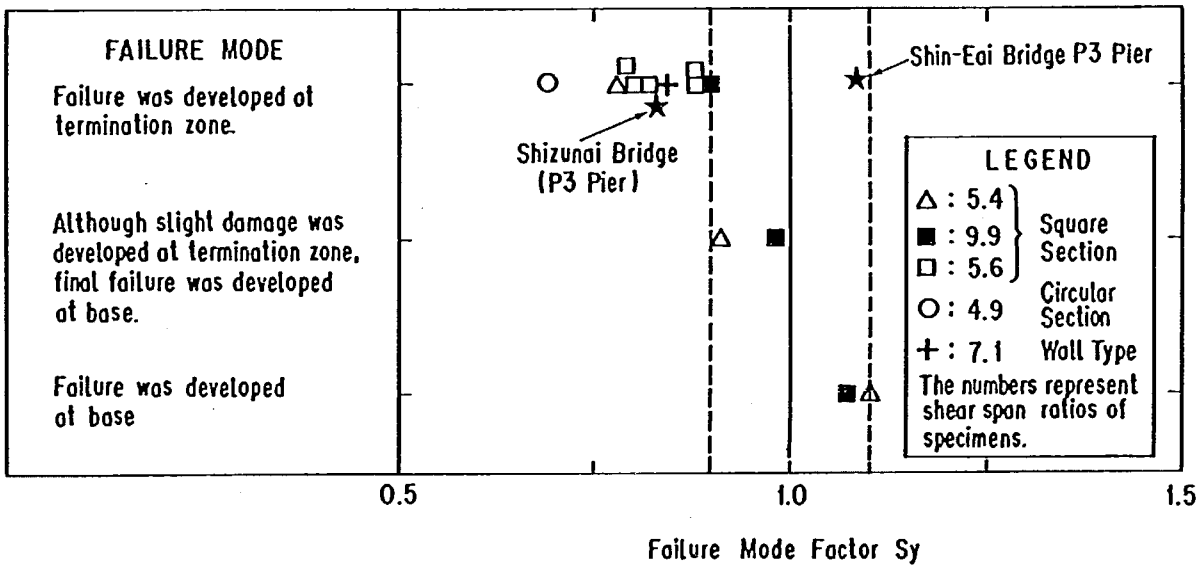


Fig. 14 Estimation of Failure Mode by S_y

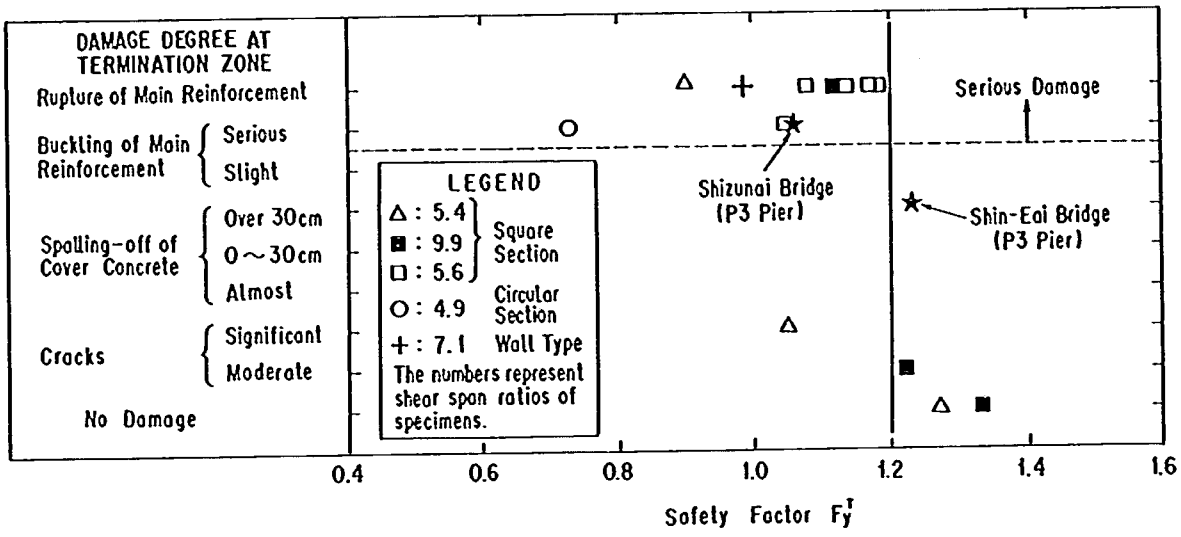


Fig. 15 Relation between Safety Factor F_y^T and Damage Degree at the Loading Displacement of $5\delta_0$

Seismic strengthening methods for the termination zone are being developed at various organizations[15)-21)]. There are several possible ways for strengthening the termination zone. One is to place new reinforced concrete section around the existing section. However, in this method, increase of the mass of the pier for requires additional increase of the foundation, and noise and air pollution during tipping of cover concrete make it difficult to be adopted in urban area. To avoid such difficulties strengthening by means of a steel jacket wrapped around the existing pier seems promising. Another wrapping by means of carbon fiber is also being studied[18)].

A series of dynamic loading tests of specimens strengthened by a steel jacket are being made at the Public Works Research Institute jointly with the Metropolitan Expressway Public Corporation and Hanshin Expressway Public Corporation[15)-17)]. Parameters considered in the tests are length and thickness of steel jacket, and injection material between steel jacket and concrete. Tests are being made for circular, square and wall type piers.

According to the past tests, steel jackets were effective to strengthen piers vulnerable to shear failure at the termination zone. The minimum length of the steel jacket may be 1.5 to 2.0 times the pier width D. Epoxy resin seems better than concrete mortar as an injection material, because separation of steel jacket from concrete surface is more restricted.

Based on the test results, about 20 piers each were strengthened at the Metropolitan Expressway Public Corporation[16)] and Hanshin Expressway Public Corporation[17)]. Figs. 16 and 17, and Photos 6 and 7 show seismic strengthening of reinforced concrete piers. The piers were covered fully from the top to the bottom by steel jackets with thickness of 6 mm and epoxy resin was used injected.

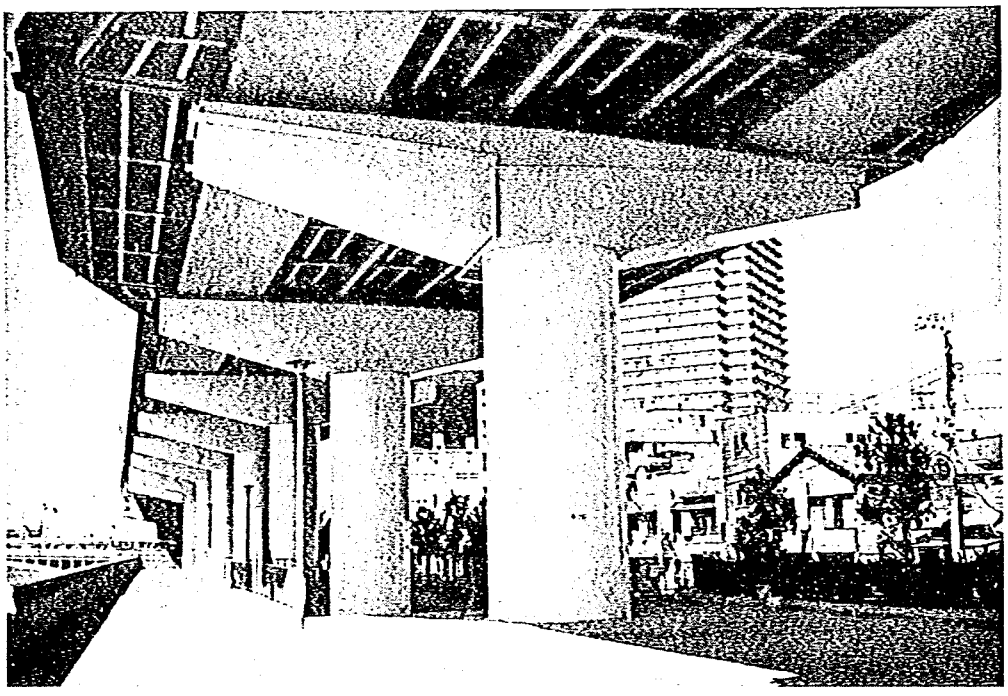


Photo 6 Seismic Strengthening of RC Piers on Metropolitan Expressway by Steel Jackets

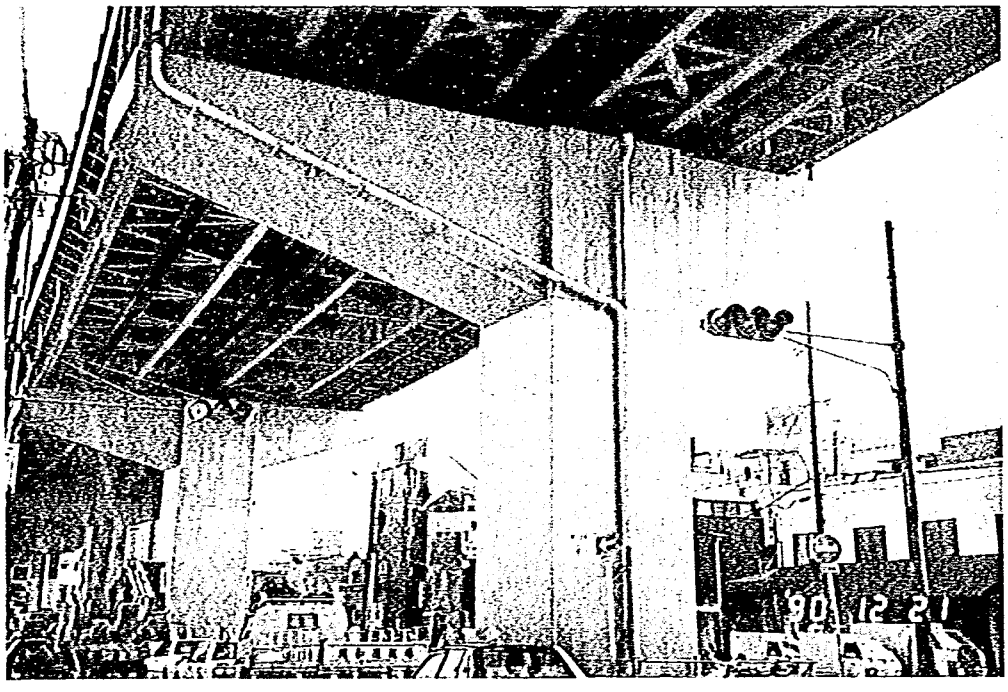


Photo 7 Seismic Strengthening of RC Piers on Hanshin Expressway by Steel Jackets

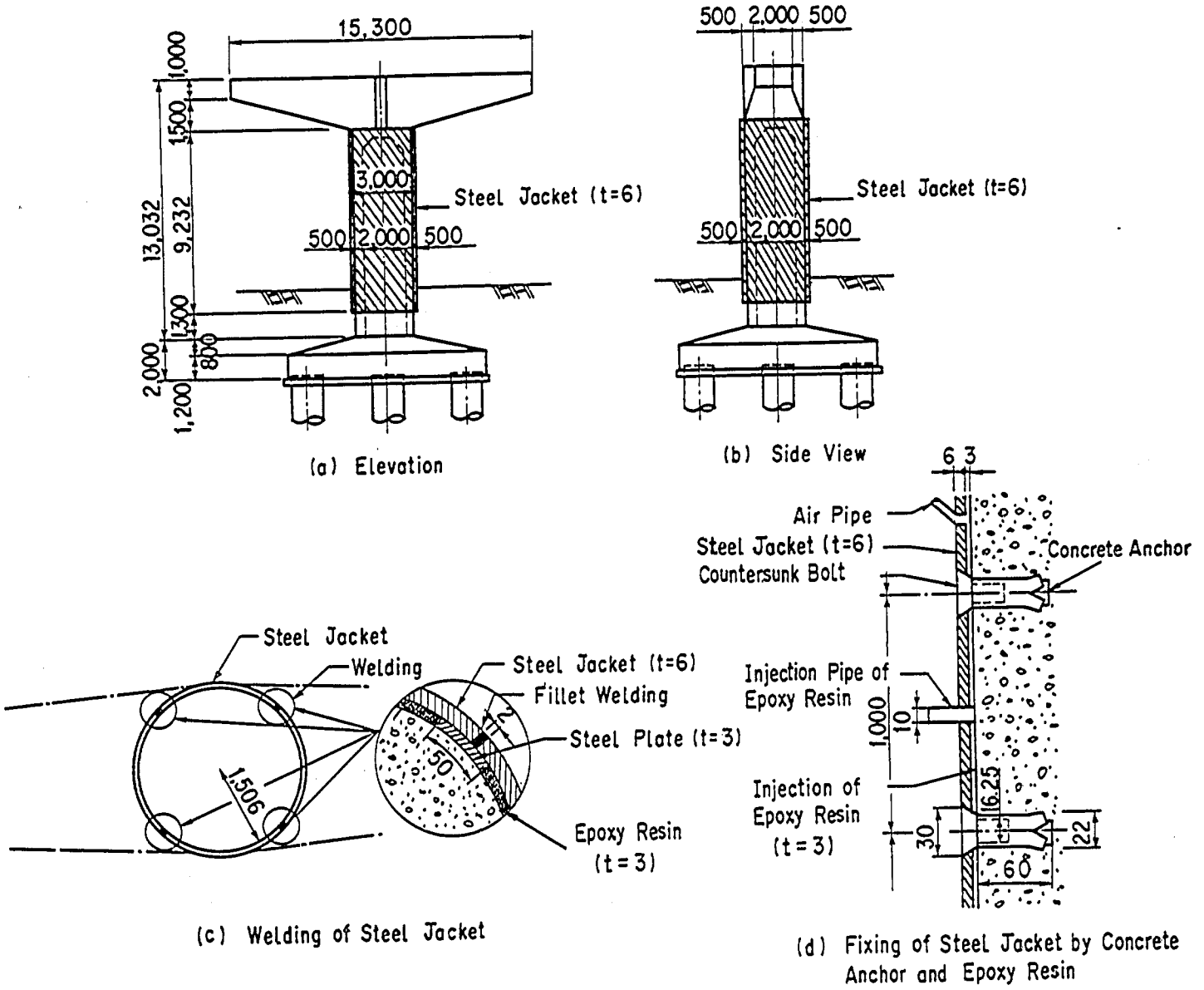


Fig. 16 Seismic Strengthening of RC Piers on Metropolitan Expressway by Steel Jackets

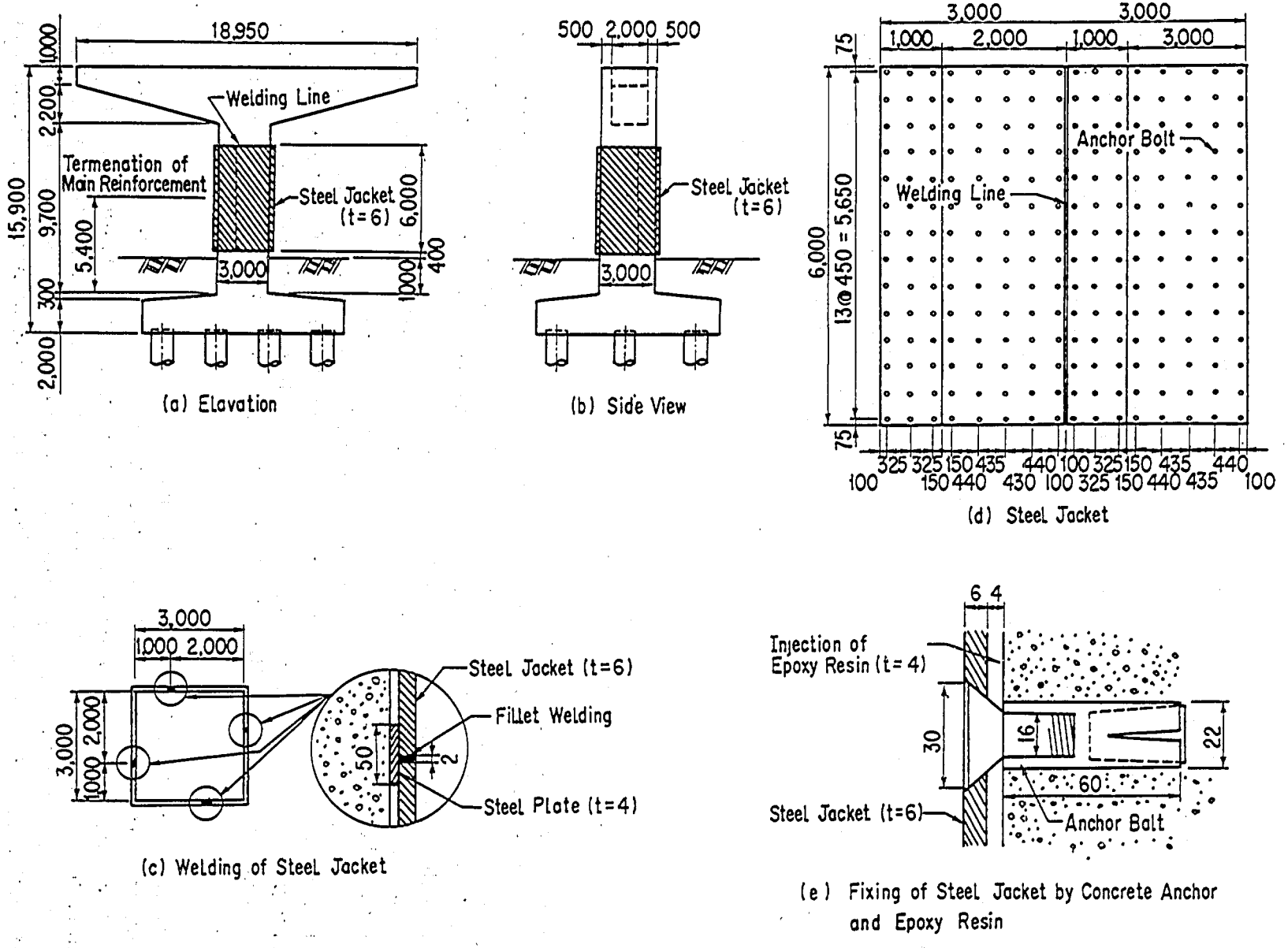


Fig. 17 Seismic Strengthening of RC Piers on Hanshin Expressway by Steel Jackets

CONCLUDING REMARKS

Because seismic design for highway bridges was initiated in 1926, and because revision and amending of seismic design codes have been made based on bitter experiences learned from a number of seismic damage in the past, seismic performance of highway bridges designed by the current seismic design code is considered adequate. However, there are a number of existing bridges vulnerable to seismic effects, which were designed by the past design practices.

By the great efforts in the past seismic strengthening works, installation of falling-off prevention device is now almost being completed for important bridges, but seismic strengthening of foundations and piers have been made for few bridges. Therefore it is now facing to a time to initiate seismic strengthening of foundations and piers. For this purpose, it is absolutely important to develop a reliable seismic inspection method of existing highway bridges. Further research efforts for improving reliability and accuracy of seismic inspection method is required as well as development for seismic strengthening method.

FUTURE DIRECTION

It is required to develop various subjects for seismic inspection and seismic strengthening including the following issues :

a) Level of Seismic Strengthening
There is no wonder to require strengthening for those bridges vulnerable to developing critical failures such as falling-down during an earthquake. However, from the view of importance of highway bridges as a vital component of transportation facilities, a certain type of bridges requires to keep their function without causing damage even after a destructive earthquake. On the other hand, there may be bridges which were constructed in old time and are now in use for a few amount of traffic. Depending on importance, impact causing indirect damage, difficulty for repair and service time left before replacement, an appropriate evaluation method for deciding priority of seismic strengthening and for deciding the target level required for strengthening is important.

b) Improvement of Reliability of Seismic Inspection
It is required to have more reliable evaluation on the seismic performance of bridges for spending a big amount of budget such as for seismic strengthening of foundations. The point required in the seismic inspection is not to know whether the design of a highway bridges is appropriate in accordance with the current design specifications, but to know whether the bridge could perform in a way expected in accordance with the target of seismic strengthening during an anticipated earthquake. Much more improvement on the structural

performance is required.

c) Development of Seismic Strengthening Method for Vulnerable Highway Bridges
Because there are several possible modes which lead to critical failure of highway bridges, development of seismic strengthening method is required for them. These includes the strengthening method for bent pile foundation, reinforced concrete frame on two independent caisson foundations and plain concrete piers. Strengthening method of reinforced concrete piers with termination of main reinforcement with inadequate anchorage length is also important. Strengthening methods by applying new materials such as carbon fiber and fiber reinforced plastic, and new technology such as connection of adjacent girders or slabs, non-destructive inspection method and devices for preventing falling-off of superstructure with energy absorbing capability are also to be developed.

REFERENCES

1) Arakawa, T. and Kawashima, K. : Seismicity and Maximum Possible Earthquakes around Japan for Application to Seismic Risk Analysis, Technical Note of PWRI, Vol. 2098, Public Works Research Institute, Ministry of Construction, 1984
2) Iwasaki, T., Penzien, J. and Clough, R., W. : Literature Survey – Seismic Effects on Highway Bridges, Report No. EERC 71-11, Earthquake Engineering Research Center, University of California, Berkeley, 1972
3) Kawashima, K. : Seismic Design, Seismic Strengthening and Repair of Highway Bridges in Japan, U.S.-Japan Workshop on Seismic Retrofit of Bridges, Public Works Research Institute, Tsukuba, Japan, December 1990
4) Ministry of Construction : Economic Surveys of Road Traffic, 1971- 1990
5) Ministry of Construction : The Construction White Papers, 1971-1990
6) Japan Road Association : Part V Seismic Design, Design Specifications of Highway Bridges, February 1990
7) Japan Road Association : Countermeasures for Roads against Earthquakes, March 1986
8) Kawashima, K. and Unjoh, S. : An Inspection Method of Seismically Vulnerable Existing Highway Bridges, Structural Eng./Earthquake Eng., Vol.7, No.1, Proc. Japan Society of Civil Engineers, April 1990
9) Japan Road Association : Guide Specifications for Earthquake Hazard Mitigation for Transportation Facilities – Pre-Earthquake Countermeasures –, February 1987
10) Okawa, S., Maeda, Y., Kawashima, K. and Saeki, M. : Large Earthquake Countermeasures for Tomei Expressway Bridges, 4th Joint U.S.-Japan Workshop on Bridge Engineering Performance, Strengthening, and Innovation, San Diego, California, USA, May 1988
11) Tsubouchi, T., Ohashi, K. and Arakawa, K. : Large Earthquake Countermeasures for Bridge Substructures on the Tomei Expressway, U.S.-Japan Workshop on Seismic Retrofit of Bridges, Public Works Research Institute, Tsukuba, Japan,

December 1990
12) Kawashima, K., Unjoh, S. and Azuta, Y. : Examples of Seismic Strengthening of Highway Bridges, Technical Note of PWRI, Vol.2674, Public Works Research Institute, Ministry of Construction, October 1988
13) Narita, N., Murakami, M. and Asanuma, H. : Report of the Investigation on Earthquake Damage to Shizunai Bridge, 15th Joint Meeting, U.S.-Japan Panel on Wind and Seismic Effects, UJNR, Tsukuba, Japan, May 1983
14) Public Works Research Institute : Disaster Caused by the Miyagi-ken-oki Earthquake of 1978, Report of PWRI, Vol.159, March 1983 (in Japanese) .
15) Kawashima, K., Unjoh, S. and Iida, H. : Seismic Inspection and Seismic Strengthening of Reinforced Concrete Bridge Piers with Termination of Main Reinforcement at Mid-Height, U.S.-Japan Workshop on Seismic Retrofit of Bridges, Public Works Research Institute, Tsukuba, Japan, December 1990
16) Akimoto, T., Nakajima, H. and Kogure, F. : Seismic Strengthening of Reinforced Concrete Bridge Piers on Metropolitan Expressway, U.S.-Japan Workshop on Seismic Retrofit of Bridges, Public Works Research Institute,Tsukuba, Japan, December 1990
17) Matsuura, Y., Nakamura, I. and Sekimoto, H. : Seismic Strengthening of Reinforced Concrete Bridge Piers on Hanshin Expressway, U.S.-Japan Workshop on Seismic Retrofit of Bridges, Public Works REsearch Institute, Tsukuba, Japan, December 1990
18) Matsuda, T., Sato, T., Fujiwara, H. and Higashida, N. : Effect of Carbon Fiber Reinforcement as a Seismic Strengthening Measure for Reinforced Concrete Bridge Piers, U.S.-Japan Workshop on Seismic Retrofit of Bridges, Public Works Research Institute, Tsukuba, Japan, December 1990
19) Yamamoto, T., Ishibashi, T., Otsubo, M. and Kobayashi, S. : Experimental Studies on Seismic Resistant of a Pier with Reinforcement Terminated in a Tension Zone, Proc. Japan Society of Civil Engineers, Vol.348/V-1, August 1984
20) Miyamoto, M., Ishibashi, T. and Saito, T. : Experimental Studies on Seismic Strengthening Method of Existing Bridge Piers by Steel Jackets, Technical Note of Japan Railway Corporation, Vol.89, Institution of Japan Railway Facilities, March 1987
21) Kawashima, K., Ichimasu, H. and Kodera, J. : Basic Principle/ Ichimasu, H., Kodera, J. and Kawashima, K. : Design Details/ Kawashima, K., Ichimasu, H. and Kodera, J and Tanaka, Y. : Example of Applications/ Kawashima, K., Ichimasu, H. and Ohuchi, H. : Seismic Strengthening, International Workshop on Seismic Design and Retrofitting of Highway Bridge, Bormio, Italy, April 1991
22) Roberts, J., E. : Bridge Seismic Retrofit Program for California Highway Systems, Proc. 3rd U.S.-Japan Workshop on Earthquake Disaster Prevention for Lifeline Systems, Public Works Research Institute, Tsukuba, Japan, May 1989
23) Priestley, M., J., N. : Seismic Retrofitting of Bridge Columns for Enhanced Shear Strength and Flexible Ductility, Proc. 3rd U.S.-Japan Workshop on Earthquake Disaster Prevention for Lifeline Systems, Public Works Research Institute, Tsukuba, Japan, May 1989

A PERSPECTIVE OF MENSHIN DESIGN FOR HIGHWAY BRIDGES IN JAPAN

by
Kazuhiko KAWASHIMA
Kinji HASEGAWA
and
Hiroyuki NAGASHIMA

U.S. — JAPAN WORKSHOP ON EARTHQUAKE
PROTECTIVE SYSTEMS FOR BRIDGES
BUFFALO, NY, U.S.A.
September 1991

A PERSPECTIVE OF MENSHIN DESIGN FOR HIGHWAY BRIDGES IN JAPAN

Kazuhiko KAWASHIMA, Kinji HASEGAWA and Hiroyuki NAGASHIMA

Earthquake Engineering Division, Public Works Research Institute

SUMMARY

Presented are current technical developments for the base isolation to ordinary size of highway bridges with span length from 10 m to 50 m in Japan. Seismic environment, history of seismic damage and formulation of seismic design codes are firstly described with emphasis on motivation for introducing the base isolation. Because elongation of natural period of bridges is quite difficult to be adopted due to various restrictions associated with deck displacement, a "Menshin Design" which aims even distribution of lateral force to each substructure as well as increase of energy dissipating capability is becoming to be incorporated. Existing and current efforts for developing the Menshin Design including pilot construction and a joint arch program of the Menshin Design is presented.

INTRODUCTION

Highways in Japan consist of Expressways (3,721 km), National Highways (46,661 km), Prefectural Roads (128,202 km) and Municipal Roads (925,138 km). Along the highways and roads, excluding the Municipal Roads, there are about 60,000 bridges with span length of 15 m or longer. Although the number of bridges constructed per year depends on the year and span length, it is about 6,000 for concrete bridges and 2,000 for steel bridges with the length of 15 m or longer.

Base isolation has been highlighted in Japan as a new technology to reduce seismic response of structures, and more than 30 base-isolated buildings have been constructed. The principles of base isolation is to elongation the natural period of a structure and enhance the energy dissipating capability with a base isolation device, which consist of an isolator and an energy dissipator. Although the base isolation has been applied to highway bridges in New Zealand and U.S.A.(Refs. 1 - 4), seismicity is higher and ground condition is softer in Japan, so that a specific research and development be inevitable for applying the base isolation to highway bridges in Japan.

This paper describes the current efforts for incorporating the base isolation to seismic design of highway bridges. Because design consideration is different with large bridges such as cable-stayed bridges, description is concentrated here to ordinary size of highway bridges with span length of 10 to 50 m. Overcrossing and viaduct in city area is also included here as "bridge". Seismic design philosophy of those highway bridges including the the history of bridge damage in the past and past revision of seismic design codes is presented with emphasis on the motivation for incorporating the base isolation. Because elongation of natural period is difficult to be adopted and

distribution of lateral force to substructures is now becoming considerably important, a slightly different concept with the base isolation is being introduced by taking advantages of energy dissipation and distribution of lateral force. It is referred as "Menshin Design". Outline of the existing and on-going researches including a joint program between the Public Works Research Institute and 28 private firms entitled "Development of Menshin Design of Highway Bridges" (Ref. 5) are also presented.

CURRENT SEISMIC DESIGN AND PHILOSOPHY OF HIGHWAY BRIDGES

History of Earthquake Damages Located along the Pacific Seismic Belt, Japan is one of the most seismically disastrous countries in the world and has often suffered significant damage from large earthquakes. Fig. 1 shows the largest magnitude of the earthquakes which occurred in the past (Ref. 6). It is recognized that the earthquakes with magnitude over 8 occurred with rather short recurrent period in and around Japan in the past. It should be noted that seismicity is especially high along the Pacific coast where large cities in population and industrial products such as Tokyo, Osaka and Nagoya are located.

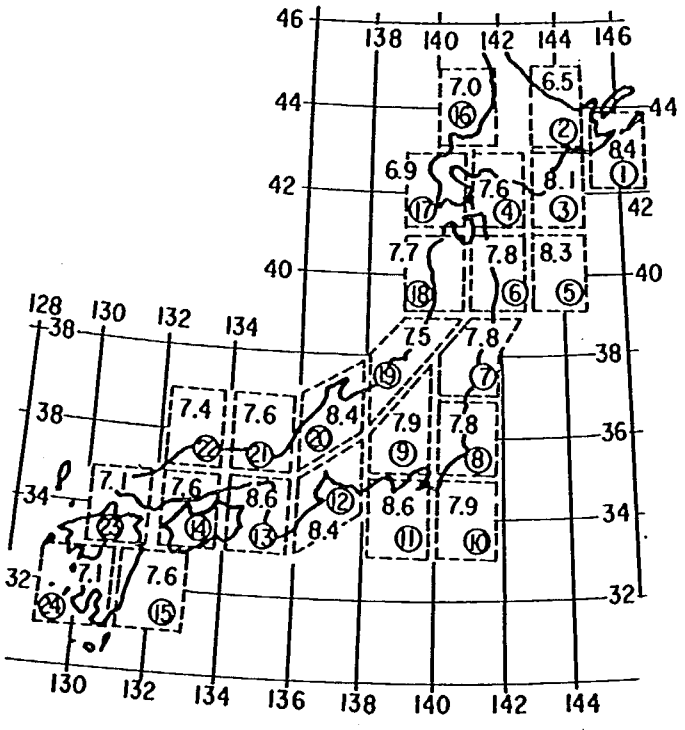


Fig. 1 Largest Earthquake Magnitude Which Occurred in the Past

Table 1 shows the highway bridges which suffered damages in the past earthquakes since the Kanto Earthquake of 1923 (Ref. 7). It should be noted that although there were many bridges which suffered damages due to earthquakes, number of bridges which fell down was only 15. It is important to note that damage types have been varying as shown in Table 2 in accordance with the progress of the seismic design method and improvement of construction practice. Seismic damage since the 1923 Kanto Earthquake may be classified into three stages from their significance (Refs. 8, 9).

Table 1 Number of Highway Bridges Which Suffered Damage in the Past Earthquakes after 1923 Kanto Earthquake

DATE	EARTHQUAKE	MAGNITUDE	NUMBER OF BRIDGES DAMAGED	NUMBER OF BRIDGES WHICH FELL DOWN
1923. 9. 1	KANTO	7.9	1,785	6
1946.12.21	NANKAI	8.1	346	1
1948. 6.28	FUKUI	7.3	243	4
1949.12.26	IMAICHI	6.4	1	0
1952. 3. 4	TOKACHI-OKI	8.1	128	0
1962. 4.30	MIYAGI-KEN-HOKUBU	6.5	187	0
1964. 6.16	NIIGATA	7.5	98	3
1968. 2.21	EBINO	6.1	10	0
1968. 5.16	TOKACHI-OKI	7.9	101	0
1978. 1.14	IZU-OHSHIMA	7.0	7	0
1978. 6.12	MIYAGI-KEN-OKI	7.4	95	1
1982. 3.21	URAKAWA-OKI	7.1	5	0
1983. 5.26	NIHON-KAI-CHUBU	7.7	176	0
1984. 9.14	NAGANO-KEN-SEIBU	6.8	14	0
TOTAL			3,191	15

Table 2 Change of Seismic Damage Mode

Year	Major Earthquakes	Change of Major Seismic Damage	Seismic Design Method	Seismic Inspection and Strengthening
1920	1923 Kanto Earthquake (M7.9)	Failure of Superstructure due to Tilting/Movement of Foundation	1926 Initiation of Seismic Design (Details of Road Structures)	
1930				
1940		Failure of Concrete around Fixed Bearing	1939 Introduction of Standard Seismic Coefficient (Design Specifications of Steel Highway Bridges)	
	1946 Nankai Earthquake (M8.1)	Damage due to Liquefaction		
	1948 Fukui Earthquake (M7.3)			
1950	1952 Tokachi-oki Earthquake (M8.1)			
		Failure of RC Piers, and Bearing	1956 Seismic Coefficient depending on Zone and Ground Condition (Design Specifications of Steel Highway Bridges)	
1960	1964 Niigata Earthquake (M7.5)			
1970			1971 • Seismic Coefficient depending on Zone, Ground Conditions, Importance and Structural Response • Introduction of Evaluation Method for Liquefaction (Specifications for Seismic Design)	1971 Seismic Inspection
	1978 Miyagi-ken-oki Earthquake (M7.4)			1976 Seismic Inspection
1980	1982 Urakawa-oki Earthquake (M7.1) 1983 Nihon-kai-chubu Earthquake (M7.7)		1980 • Part V Seismic Design, Specifications for Design of Highway Bridges • Introduction of New Evaluation Method for Liquefactions	1979 Seismic Inspection
				1986 Seismic Inspection
1990			1990 Part V Seismic Design, Specifications for Design of Highway Bridges	

1) Stage 1 - Damage due to Inadequate Strength of Foundations

After experiencing the destructive damage of the 1923 Kanto Earthquake, the first requirements for seismic design of highway bridges were included in the "Details of Road Structures (Draft)" issued in 1926. No seismic effects were considered for design of highway bridges prior to the Kanto Earthquake. Even after the first stipulations, seismic design was not adequate because the stipulations only described design force levels without providing detailed design method and design details. Therefore, seismic safety of bridges was short until the 1950's when seismic design for foundations and substructures came to be widely improved.

In those days when seismic effects were either disregarded or poorly considered, seismic damage was characterized by failure of foundations and substructures as shown in Photo 1. In most cases, foundations were tilted, moved or even overturned due to insufficient strength of the foundations and the surrounding subsoils, which led to falling-off of the superstructures (Ref. 10).

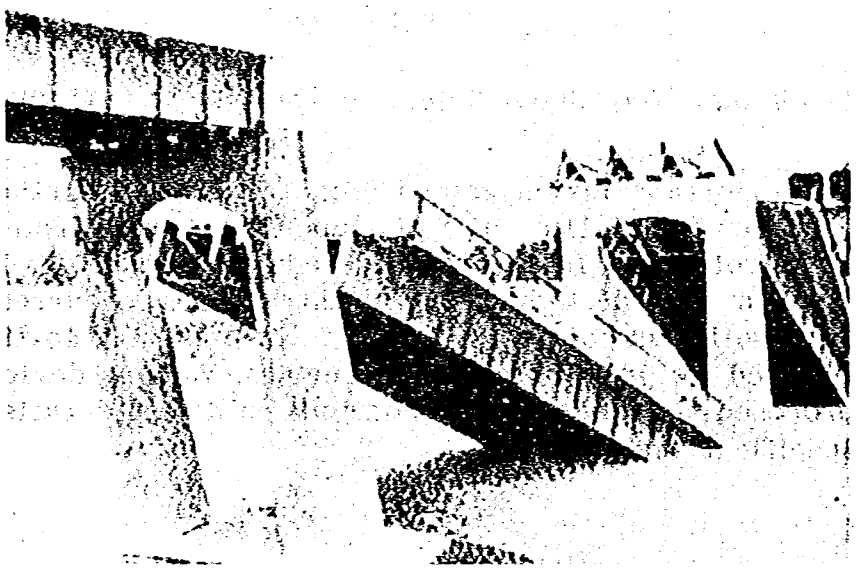


Photo 1 Damage of Nakazuno Bridge by the Fukui Earthquake of 1948

2) Stage 2 - Damage due to Soil Liquefaction

Although the damage due to inadequate strength of foundations became less frequent by the improvement of seismic design and construction methods for substructures, the next stage of earthquake damage encountered was soil failure in conjunction with liquefaction prominently observed during the 1964 Niigata earthquake. Photo 2. shows the falling-off of the decks of the Showa bridge in the earthquake. Extensive soil movement associated with liquefaction produced large lateral movements of the bent pile foundations, which caused the dropping-off of the deck (Ref. 11). Responding to the damage, the first stipulations for assessing vulnerability of liquefaction were introduced in the "Design Specifications for Seismic Design of Highway Bridges" in 1971 through extensive studies initiated after the earthquake.

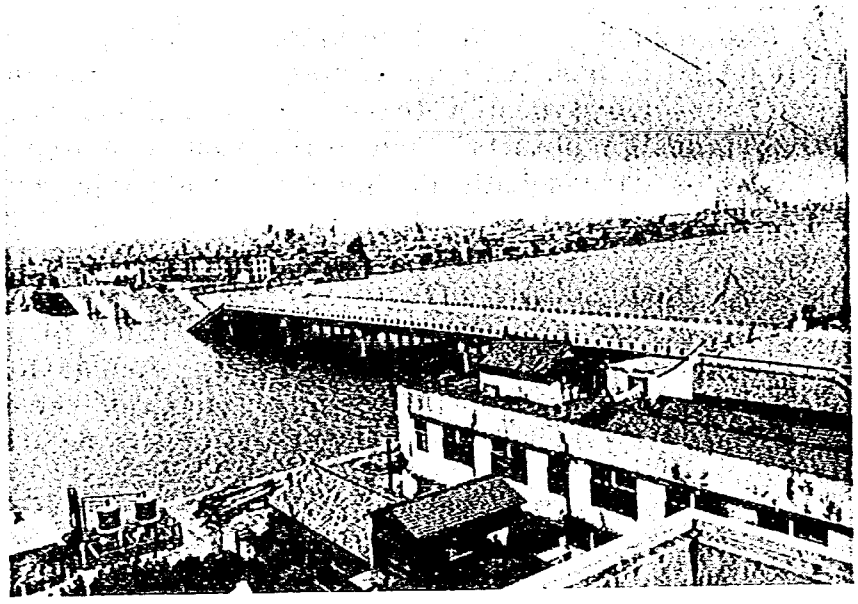


Photo 2 Damage of Showa Bridge by the Niigata Earthquake of 1964

The other important lesson gained from the Niigata earthquake was that devices for preventing falling-off of superstructures from the crest of columns are unavoidable. It was considered that even if large relative movements between the deck and the substructures occurred due to soil failures such as soil liquefaction, critical failure causing falling-off of deck could be prevented by providing special devices. Various devices as shown in Fig. 2 were proposed then, and recommendations on design details were included in the 1971 Specifications.

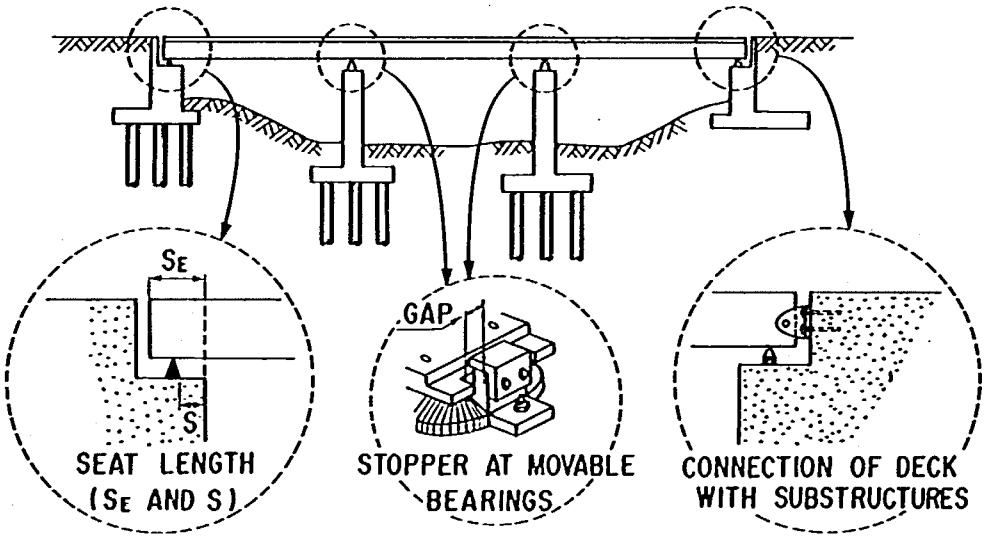


Fig.2 Devices for Preventing Superstructure from Falling

3) Stage 3 - Damage to Columns and Bearing Supports

In recent earthquakes including the 1978 Miyagi-ken-oki earthquake and the 1983 Nihon-kai-chubu earthquake, substantial damage due to shortage of foundation strength and effect of soil liquefaction was not developed in those bridges designed and constructed in accordance with the recent design specifications after 1971. However, damages to reinforced concrete columns and bearing supports, which were rarely suffered in the earlier earthquakes, were developed extensively as shown in Photo 3. This is due to the fact that old failure modes such as tilting or movement of the foundations, soil liquefaction and falling-off of superstructures were prevented by the new design recommendations.

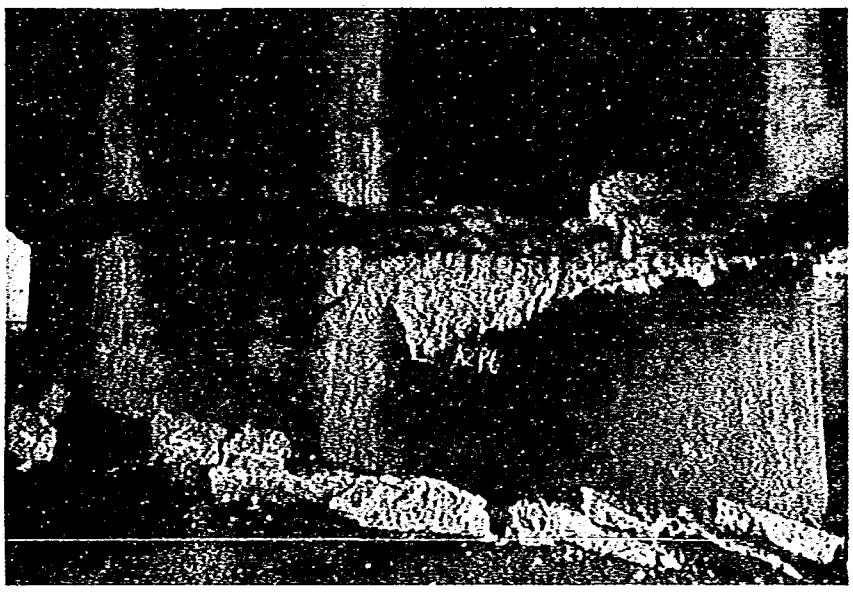


Photo 3 Damage to Reinforced Concrete Piers of Sendai Bridge by the Miyagi-ken-oki Earthquake in 1978

Through these evidences of seismic damage and effect of countermeasures, it is becoming apparent that certain types of failure developed in recent years at bearing supports and columns may not be prevented by only increasing the lateral force, although large lateral force has been adopted for seismic design of highway bridges. It may be effective to allow some relative displacement between deck and substructures for preventing the damage of bearings. Because lateral force developed during a destructive earthquake with the magnitude over 8 would be at least 3 times larger that the force level considered in the current seismic design based on the allowable stress design approach, occurrence of some damage may be unavoidable. Incorporation of structural members which develop stable energy dissipation under destructive seismic loading may be required. This is one of the motivations for incorporating the base isolation to highway bridges in Japan.

<u>Seismic Design Philosophy of Highway Bridges</u> The latest specifications were issued by the Ministry of Construction in February 1990 (Ref. 12). Major revisions introduced in the 1990 Specifications were unification of static lateral force method and the modified static lateral force method including the revision of the modification factors for design seismic force, a new method for computing inertia force for multi-span continuous bridges, a new ductility check for reinforced concrete columns, and detailed stipulations for dynamic response analysis. These revisions were incorporated based on the recent

studies for predicting earthquake ground motions and strength of reinforced concrete columns (Ref. 13).

The current specifications, with which highway bridges constructed in Japan with less than or equal to 200 m span length shall be designed in complete accordance, stipulates the principles of the seismic design of highway bridges as :

1) A highway bridge shall be designed to have sufficient stability against earthquakes not only as an individual superstructure and substructure but also as a whole structure by considering the structural characteristic of the bridge, topographical and geological conditions at the site, damage experiences in past earthquakes, importance and circumstances of the bridge.

2) The earthquake resistant design shall be based on the static lateral force method. The seismic safety of a bridge shall be evaluated by comparing the resultant values due to the static lateral force method with the allowable values such as allowable stresses, allowable bearing capacities, allowable displacements and safety factors.

3) A reinforced concrete column which is designed by the static lateral force method should be checked on the bearing capacity for lateral force to prevent the brittle failure from taking place.

4) A bridge which is designed by the static lateral force method and has complicated seismic response should be checked by the dynamic analysis.

The lateral force coefficient in the static lateral force method, which is equivalent to the fraction of design lateral response acceleration to the gravity acceleration, is stipulated as shown in Fig. 3, in which the zoning modification coefficient and the modification coefficient for importance are assumed as 1.0. The design lateral acceleration from 0.1 g to 0.3 g is taken into the seismic design. This represents the seismic force for moderate earthquakes which are supposed to take place with higher possibility.

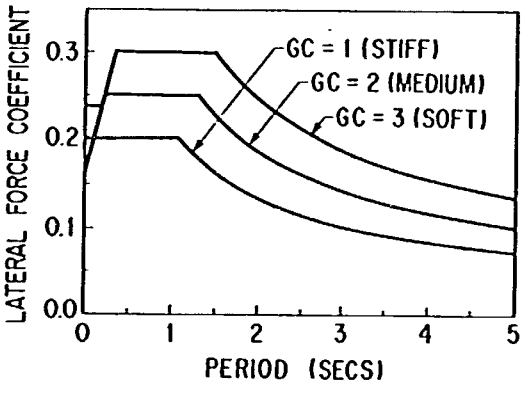


Fig. 3 Lateral Force Coefficient k_h for Static Lateral Force Method ($c_Z = c_I = 1.0$)

The specifications adopt the allowable stress method, or working stress method. Although the ductility check of reinforced concrete columns for lateral force as shown in Fig. 4 objects larger earthquakes such as the 1923

Kanto earthquake which are supposed to take place rarely, basic philosophy of seismic design for highway bridges in Japan is to review the dynamic performance within elastic range. With the philosophy, it is difficult to come to use a energy dissipator aiming to reduce the seismic response. This is one of the reasons why base isolation was not so interested in bridges, compared with buildings, in Japan.

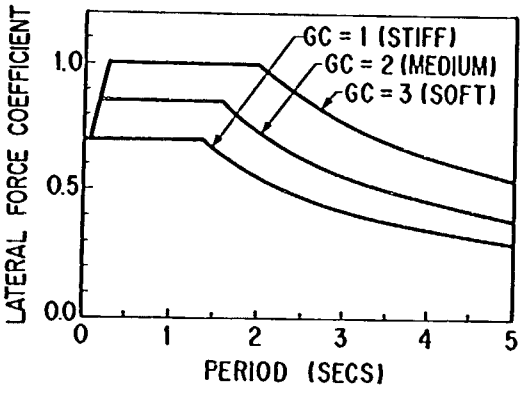


Fig. 4 Lateral Force Coefficient $k_{h\theta}$ for Check of Bearing Capacity of Reinforced Concrete Piers for Lateral Force ($c_Z = c_I = 1.0$)

EXISTING EFFORTS TO MITIGATE SEISMIC RESPONSE OF HIGHWAY BRIDGES

Reduction of Lateral Force Efforts to reduce lateral force for design of substructures have been made in Japan (Ref. 14). The first attempt was to reduce lateral force by increasing energy dissipation capability. Viscous dampers such as cylinder type viscous dampers were tried to be adopted in early stage. Fig. 5 shows the result of an analytical study for a simple highway bridge. One of the two ends of the deck is supported by a fixed bearing with the other end being supported by roller . This is the usual way for supporting the deck. Viscous dampers were assumed to be provided between the deck and the column on the side where the deck is supported by the roller. The viscous dampers were assumed to have viscous coefficient of C.

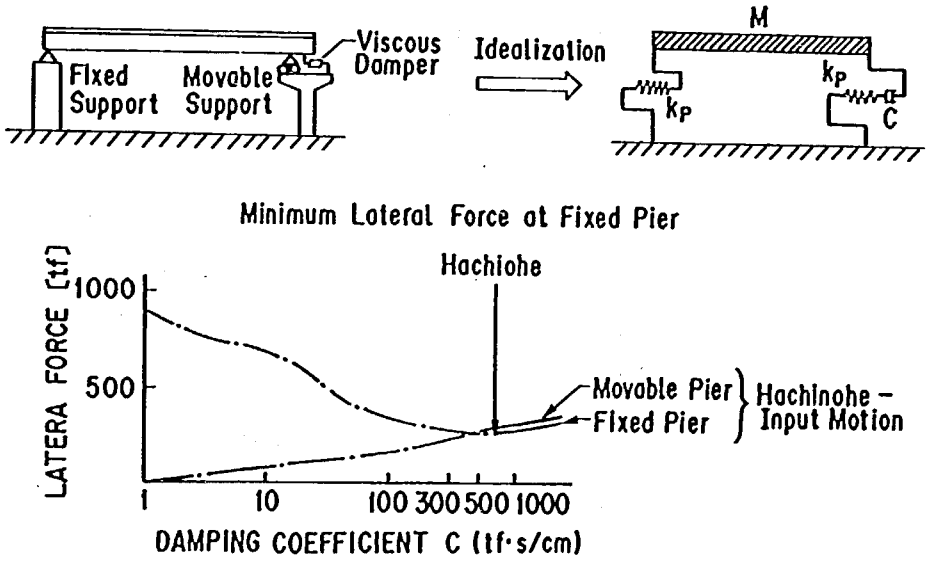


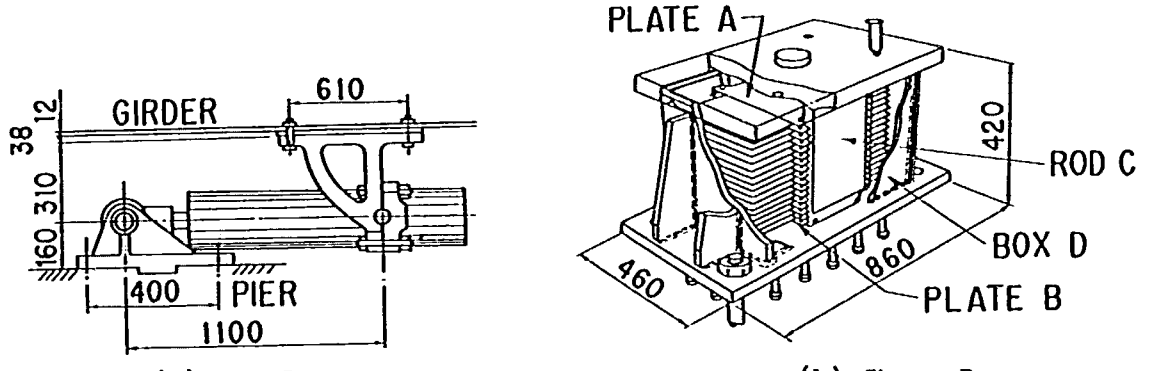
Fig. 5 Effect of Viscous Coefficient on Distribution and Reduction of Lateral Force

The maximum shear forces developed at the columns were computed for the Hachinohe record observed during the 1968 Tokachi-oki Earthquake (M=7.9). It can be seen in Fig. 5 that the lateral force developed at the column which supports the deck with roller and the viscous damper increases as the viscous damping coefficient C increases. It tends to support the half lateral force of the deck when the viscous damping coefficient C becomes infinitively large. There is however a best viscous coefficient C which makes the total lateral force minimum. In the case presented in Fig. 5, 600 tf s/cm may be the best viscous coefficient.

However this type of finding was not incorporated into practice because of two reasons (Ref. 15). The first reason was that the optimum value of viscous coefficient significantly depends on ground motion. Adjustment of the viscous coefficient depending on ground motion was impossible. The other reason was temperature dependence of the viscous coefficient. The viscous coefficient significantly varied with temperature for materials available at those days.

Therefore, instead of aiming to reduce the lateral force, viscous damper has been adopted to distribute the lateral force. The viscous damper gives a resistive force when subjected to high-velocity motion such as the one encountered during an earthquake, and does not offer resistance to low-velocity motion such as the deck movement caused by temperature change. Hence, by providing the viscous damper the seismic lateral force may be more evenly carried by many columns without giving harmful effects due to temperature change. It should be noted that the temperature dependence of the viscous coefficient was no more significant for such high viscous coefficient range. In this mean, the viscous damper adopted in the past has been regarded as "damper stopper", because the dampers were used to work as a stopper instead of energy dissipator during an earthquake.

Various damper stoppers have been developed and adopted in the past (Refs. 16, 17). Some typical damper stoppers are presented in Fig. 6. Fig. 7 show an example of this type of damper installed in a five-span continuous bridge of the Tokyo Metropolitan Expressway. The bridge was designed for lateral force coefficient of 0.3 and its superstructure weighs of 3,000 tf. The total lateral force of 1,200 tf is expected to be almost evenly distributed to the ten columns through twenty dampers.



(a) Oil Damper (b) Shear Damper

Fig. 6 Various Damper Stoppers Adopted to Highway Bridges

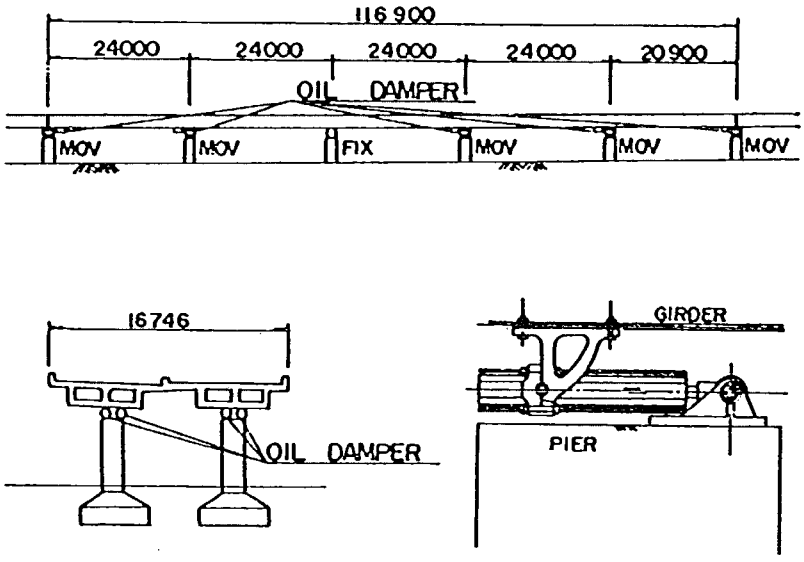


Fig. 7 5-Span Continuous Highway Bridge with Viscous Damper Stoppers

A unique device similar with the base isolation is the "SU Damper" as shown in Fig. 8 (Ref. 18). Original concept of the SU-Damper was to avoid the transmission of excessive lateral force larger than that considered in seismic design. Therefore the deck was supported by columns with friction bearings. For preventing excessive movement of the deck, prestressed strands which connect the deck and columns were provided. As well as the function of restrainer, the strands were considered as device to control the natural period of the bridge. The stiffness can be arbitrarily controlled by adjusting the length and size of the strands. The energy is dissipated by the friction developed at the bearings. Fig. 9 shows an analytical model to consider the effect of the SU Damper. Because of elongation of natural period and energy dissipation, the SU Damper may be considered as one of the base isolation devices. The SU Damper was firstly adopted in 1963 at an overcrossing on Route 1 of the Metropolitan Expressway. Photo 4. shows the SU Damper installed on the 9 span continuous prestressed concrete bridge of the Metropolitan Expressway.

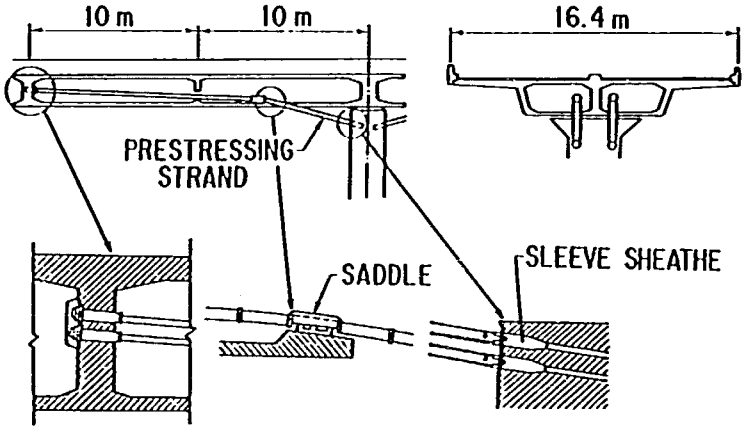
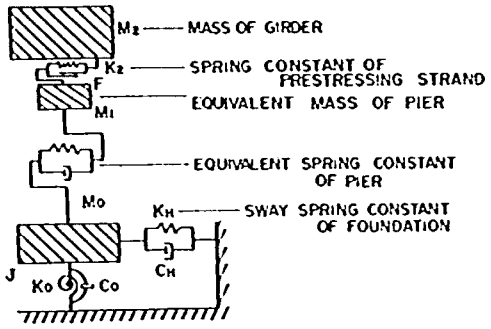
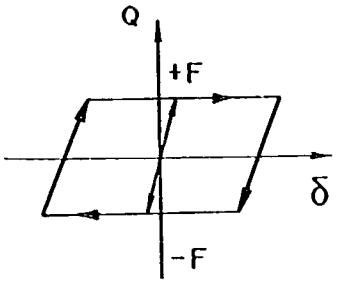


Fig. 8 SU-Damper



(a) Structural Model



(b) Nonlinear Hysteretic Model Representing Friction at Saddle and Stiffness of Prestressed Strands

Fig. 9 Analytical Idealization of SU Damper

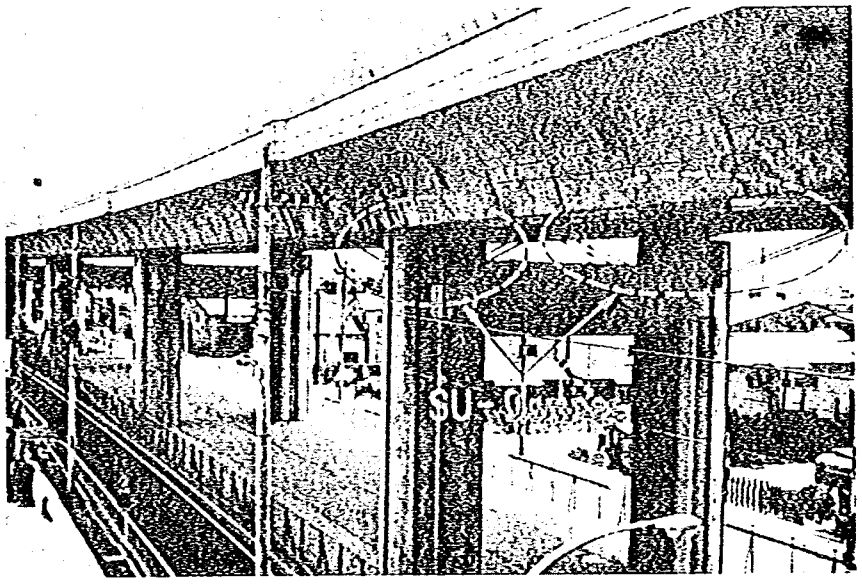
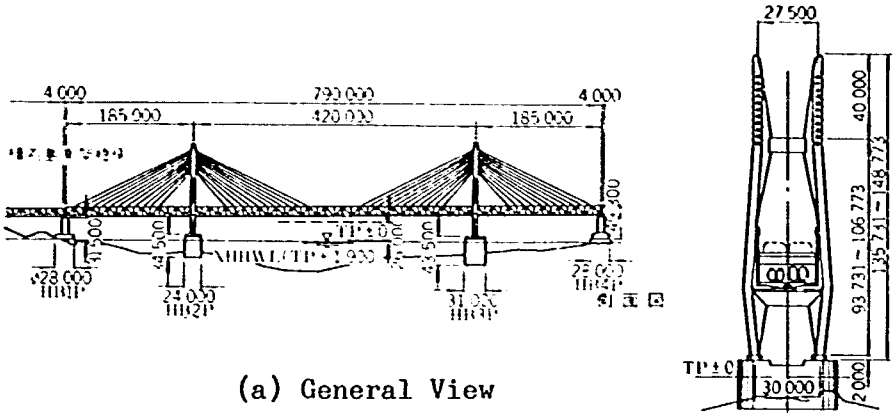
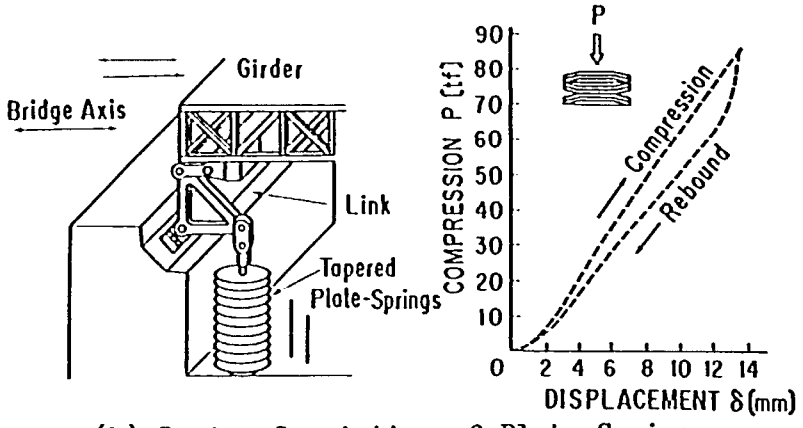


Photo 4 Bridge with SU Damper, Ukizuka Viaduct

Elongation of natural period has been adopted as a measure to reduce seismic lateral force, in particular for cable stayed bridges. Various devices have been developed to elongate natural period of cable stayed bridges. Deck was either isolated from tower (Ref. 19) or supported by links (Ref. 20) for making the deck being free to move in longitudinal direction. For either adjusting the natural period or preventing excessive deck movement, special devices h as springs (Ref. 21) and prestressed strands (Ref. 22) were used. Fig. 10 shows an example of such attempt in which the deck was supported by plate springs at the end.



(a) General View



(b) Device Consisting of Plate Springs

Fig. 10 Adoption of Elastic Spring to Prevent Excessive Deck Movement Associated with Elongation of Natural Period (Hitsuishi-Iwaguro Bridge)

Distribution of Lateral Force Multi-span continuous highway bridges are likely to be constructed recently with demand of decreasing the number of expansion joints, which make annoying vibration and are vulnerable to traffic load, in order to secure comfortable driving with flat road surface and be released from bothersome maintenance work of the joints. Furthermore, multi-span continuous bridges are known to be more earthquake-resistive from past seismic experiences since they have larger degrees of redundancy than simple supported girder bridges.

However, the seismic lateral force in longitudinal direction for multi-span continuous bridges becomes extremely large as the number of the spans and/or the length of each individual span is extended. Traditionally, the lateral force was concentrated to a single substructure with a fixed bearing and the other substructures support only the vertical dead weight of the girder with movable bearings. However, the size of the single fixed substructure often becomes excessively large from the practical design point of view. To avoid such concentration of lateral force to a single substructure, various devices including rubber bearings have been developed and put into practice.

Distribution of lateral force to substructures can be performed by several methods (Ref. 14). The simplest method is to support the girder by fixed bearings at every piers. Although indeterminate lateral force will be

developed due to the elongation and shrinkage of the girder by thermal change, this method may be adopted unless the effect of the force is critical to design substructures. A highway bridge having as many as twelve continuous spans with a total deck length of 507 m has already been constructed (Ref. 23).

The second way is use of rubber bearing. Lateral stiffness of the rubber bearing can be easily adjusted by changing the rubber thickness or rubber material to intentionally modify the distribution ratio to each substructure. Many multi-span continuous bridges have been successfully constructed with use of rubber bearings for distribution of lateral force (Ref. 24). The third way is to adopt a viscous damper as described above.

PERSPECTIVE OF "MENSHIN DESIGN" IN JAPAN

Although elongation of the natural period and increase of energy dissipation capability of a structure are key factors in base-isolation, the elongation of the fundamental natural period for highway bridges leads to large relative displacement between the girder and the substructures, and requires the special expansion joints with large displacement capacity. Because the elongation of natural period has been attempted for cable stayed bridges, further technical development would be made. However for ordinary highway bridges in multi-span continuous type with span length of 10 m to 50 m, it is not appropriate to elongate the natural period so forcibly as in buildings, deeply related with various reasons constrained to highway bridges in Japan.

First reason is softer soil condition. Because most of populated areas are located on alluvial fan deposits, soils are very weak. Second reason is the high seismicity accompanying large earthquakes with magnitude over 8. These large earthquakes caused considerable damage in the past. Reflecting the occurrence of destructive earthquake as well as the worse soil condition, lateral force coefficient as shown in Figs. 3 and 4 are very high up to long natural period.

Third reason is difficulty to widen the clearance between decks. From the demand of driving comfort, maintenance problems and release from annoying noise and vibration, various efforts have been paid to develop expansion joint with small clearance. Even the regular expansion joints currently used cause considerable problems, increase of gap clearance can not be incorporated.

Fourth reason is the evaluation on collision developed either between abutment and deck or between adjacent decks. When enough clearance is not provided collision would be taken place. Actually collision frequently took place during the past earthquakes (Ref. 25). It should be noted from these past experiences that collision did not cause critical structural problems although expansion joints were often badly damaged. Although collision caused failure at contact face (Ref. 25) and/or bearings and stoppers, they were not serious. Although bearings have not been intentionally designed taking account of the fact that they would be damaged during a destructive earthquake, they did behave as a "fuse" to prevent the transmission of larger lateral force than that considered in seismic design. Therefore it may be said that the failure of bearing have been behaved as "isolator" (Ref. 26).

Now turning to the fourth reason, did collision cause serious problem to highway bridges ? The answer is "no" ! As long as enough seat length was provided, it caused no serious structural damage such as falling-off of superstructure. Attention has to be paid only when two adjacent decks with considerable different mass collides. In such case, the heavier deck tends to push the lighter deck, and damage is likely to be developed at the bearings and piers supporting the light deck (Ref. 25). Although the energy dissipating effect is not included in the current seismic design method, it constrains the deck response. It is effective to constrain deck response at early smaller stage of deck movement (Refs. 27, 28, 29). Therefore the superiority for causing collision would become clear if the energy dissipation and constrain of deck movement at small response stage were considered.

Based on these considerations, it seems preferable not to intentionally increase natural period and not to widen the gap clearance at joints in highway bridges in Japan. Therefore instead of intentionally increasing natural period, combination of increase of energy dissipating capability and distribution of seismic lateral force is considered to be preferred to highway bridges in Japan. It may be important to adjust natural period to avoid resonance with ground. This is an extension of the existing seismic design concept of highway bridge in Japan. The design concept in which bridges are designed taking advantage of the increase of energy dissipating capability and the distribution of seismic lateral force is proposed to be referred as "menshin design" (Ref. 5). Although the original meaning of "menshin" in Japanese is "base isolation", it is a little bit different with "base isolation" in design concept.

The followings are the basic principles considered required to activate menshin design in ordinary size of highway bridges in Japan :

1) Distribution of lateral seismic force should be attempted by adjusting the lateral stiffness of menshin bearings, while the lateral seismic force would be reduced by improving the energy dissipating capability with use of menshin bearings.
2) The fundamental natural period of menshin bridge should be adjusted to avoid the resonance with the ground, being balanced with the distribution effect. Attempt for elongating natural period so forcibly as buildings should not be made.
3) The menshin effect should be used not to make dimension and size of substructures small, but to improve the seismic performance of bridges.
4) Gap at an expansion joint should not be widened in menshin bridges, although a little larger relative displacement is expected to be developed between a girder and substructures during a destructive earthquake.
5) The menshin design should be adopted only at the site with stable soil behavior. The site vulnerable to soil liquefaction and other type of failure should be avoided.
6) The menshin design should be encouraged to construct super-multi-span continuous bridges with the effect of lateral force distribution.

EXISTING AND CURRENT EFFORTS FOR MENSHIN DESIGN

Guidelines for Base Isolation Design of Highway Bridges For studying the application of base isolation to highway bridges, a committee chaired by

Professor Tsuneo Katayama, University of Tokyo, was formed through 1986 to 1989 at the Technology Research Center for National Land Development, which is the first public activity for the base isolation of highway bridges in Japan. Three programs were studied in the committee, i.e., 1) survey of base isolation devices which can be used for highway bridges, 2) study on the key points of the base isolation design of highway bridges, and 3) trial designs of base isolated highway bridges. As the final accomplishments of the three year study, "Guidelines for Base Isolation Design of Highway Bridges (Draft)" was published in 1989 (Ref. 30).

Pilot Construction Program of Menshin Bridges Five pilot menshin highway bridges as shown in Table 3 are under construction or completed under the supervision of the Ministry of Construction in order to verify the performance of the menshin highway bridges (Refs. 31,32,33). A working group is formulated in the Ministry of Construction for supervising the design and construction. One of them, Miyagawa Bridge in Shizuoka-ken, was completed and opened for the public traffic in March 15, 1991 as the first menshin highway bridge under the program (Ref. 32). Some other bridges following the first five are in design stage.

Table 3 Construction Program of Menshin Bridge

Owner	Name of Bridge	Type of Superstructure	Total Length
Hokkaido developing Bureau	On-netoh Bridge	Steel Girder	456 m
Tohoku Regional Construction Bureau, MOC	Nagakigawa Bridge	Steel Girder	97 m
Iwate-ken	Maruki Bridge	Prestressed Concrete	92 m
Tochigi-ken	Daiichi Karasuyama Bridge	Prestressed Concrete	250 m
Shizuoka-ken	Miyagawa Bridge	Steel Girder	110 m

Joint Research Program on Menshin Bridges The three-year joint research program on the menshin highway bridges is now under way between Public Works Research Institute and twenty eight private firms since July 1989 (Refs. 5, 34). The goal of the program is to develop the menshin design method and the new menshin devices for highway bridges in order to improve the seismic performance of new and existing bridges with less cost. Table 4 shows the research items and the contribution of each organization. The program will be accomplished in March 1992. "Design Manual of Menshin Design of Highway Bridges" is to be composed as fruits of the research program. There are four research topics in this joint program:

Table 4 Research Items and Organization of Joint Research between Public Works Research Institute and 28 Private Firms for Developing Menshin Systems for Highway Bridges

Research Theme	P	Ka	Si	Ob	Ku	Tn	H	Ni	Su	M	G	Or	Ti	I	Nk	Ko	Ns	Ot	Y	To	Bs	Bb	Sh	Pc	J	N	Chief	Sub-Chief
1. Development of Device for Isolation																												
1.1 High Energy Absorbing Rubber Bearing								○					○						○	○	○		○				Ol	Bs
1.2 Friction Damper															○							○						
1.3 Steel Damper								○									○											
1.4 Link Bearing Develop of																		○										
1.5 Viscous Damper																												
1.6 Test Method	○							○							○		○	◎	○	○	○	○	○					
2. Development of Expansion Joint and Falling-off Prevention Device for Isolated Bridge																											Tc	—
2.1 Expansion Joint				○									○															
2.2 Falling-off Prevention Device	○												○					○										
3. Development of Design Method for Isolated Bridge																												
3.1 Design Philosophy	○	○	○	○		○						○	◎					○						○	○	○	Ka	Pc
3.2 Dynamic Responce Analysis Method	○		○		○	◎		○			○			○														
3.3 Design Method of Device for Isolation	○						○	○				◎	○		○		○	○	○	○	○	○	○					
3.4 Simplified Design Method	○	○	◎		○	○					○	○												◎				
3.5 Design Method of Expansion Joint and Falling-off Prevention Device	○			○			○								○			○										
4. Application of Base Isolation to Bridge																												
4.1 Application to Prestressed Concrete Bridge	○	◎							○	○			○													○		
4.2 Application to Steel Bridge	○													○	○	○										◎	Ob	J
4.3 Application to Multiple Super-long Bridge	○			◎					○							○								○	○	○		
4.4 Application to Seismic Retrofit	○									○				○				○							◎			

P: Public Works Research Institute, Ka: Kajima, Si: Shimizu, Ob: Ohbayashi, Ku: Kumagai, Tn: Takenaka Doboku + Takenaka, H: Hazama, Ni: Nishimatsu, Su: Sumitomo, M: Mitsui, G: Goyoh, Ok: Okumura, Ti: Taisei + Tokyo Fablic + Nippon Chuzo, I: Ishikawajima Harima, Nk: NKK + Nippon Chuzo, Ko: Kobe Steel, Ns: Nippon Seiko, Oe: Oiles, Y: Yokohama Rubber, To: Toyo Rubber, Bs: Bridgestone, Bb: BBM, Sh: Showa Densen, Pc: Pacific Consultants, J: Japan Engineering Consultant, N: New Structural Engineering Consultants.

1)Development of new menshin devices

The menshin devices for highway bridges have to be more compact and more weather-proof than the base-isolation devices for buildings since the menshin devices would be installed at narrow and exposed crests of bridge columns. The new menshin devices should be developed exclusively for menshin highway bridges to be effectively constructed. The following ten new devices in the six types are now being developed under the research program.

1) high damping rubber bearing ---------- 4 devices
2) sliding friction damper ---------- 2 devices
3) steel damper ---------- 1 device
4) roller menshin bearing ---------- 1 device
5) link bearing ---------- 1 device
6) viscous damper ---------- 1 device

All developed menshin devices but the link bearing were tested with use of the dynamic loading systems of PWRI under the same loading conditions to verify their performance as shown in Photos 5 and 6.

2)Development of expansion joints and restrainers for menshin bridges

The knock-off mechanism at an abutment to ease the impact force induced by the collision between the superstructure and the abutment, and the finger expansion joints which is distinguished from the regular finger joints by the transverse movement, are being developed. The restrainer which consists of the steel bar installed in the crest of the substructure and the steel casing with rubber inside is also being developed.

3)Development of menshin design method

Taking into account the high seismic activity and the philosophy of seismic design in Japan, the flow chart of the menshin design method illustrated in Fig. 11 are proposed, in which two levels of design force are considered as limits states. The first level, called as Level 1, is equivalent to the design seismic force considered in the current static lateral force method (refer to Fig. 3). This represents the force level developed by moderate earthquakes. The second level, called as Level 2, is equivalent to the design seismic force for the check of the bearing capacity of the reinforced concrete columns for the lateral force (refer to Fig. 4), and this corresponds to larger earthquakes such as the 1923 Kanto Earthquake.

4)Application of menshin design

The menshin multi-span continuous bridge with the deck length over 1 km, which is called in the research program as a super multi-span continuous bridge, is examined as a crucial research item. Connecting of existing simple supported girders to lessen the number of troublesome expansion joints, and retrofitting of existing bridges to increase the seismic bearing capacity by using menshin bearings are also studied in the research program.

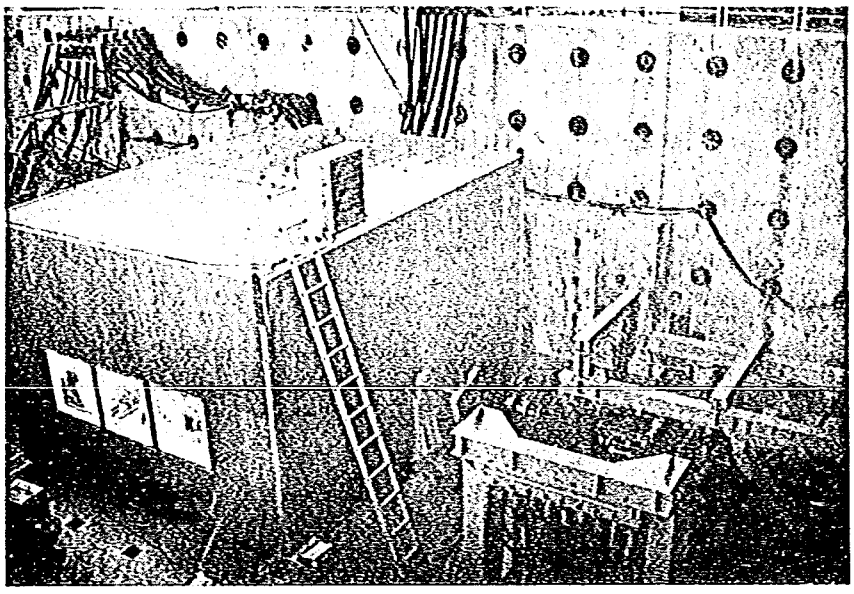


Photo 5 Dynamic Loading Test of Menshin Devices at Public Works Research Institute

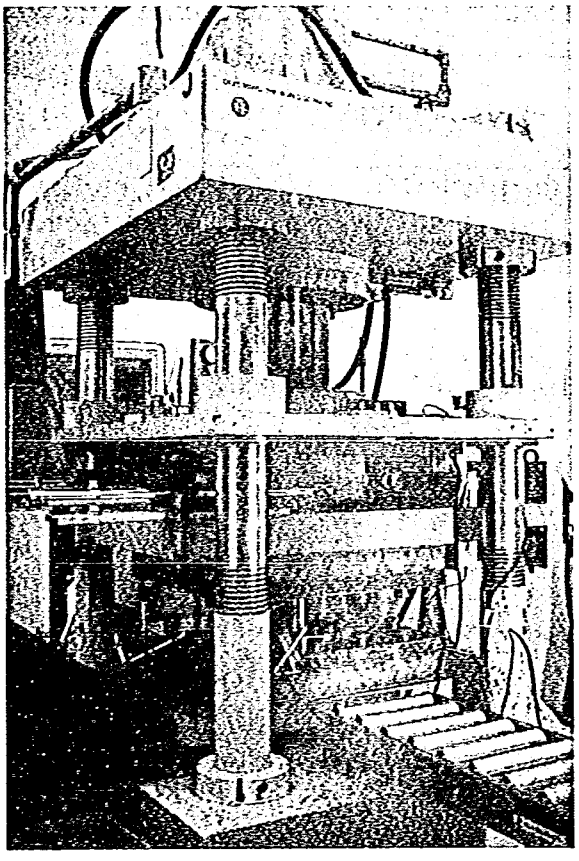


Photo 6 Cyclic Shear Test of Menshin Devices

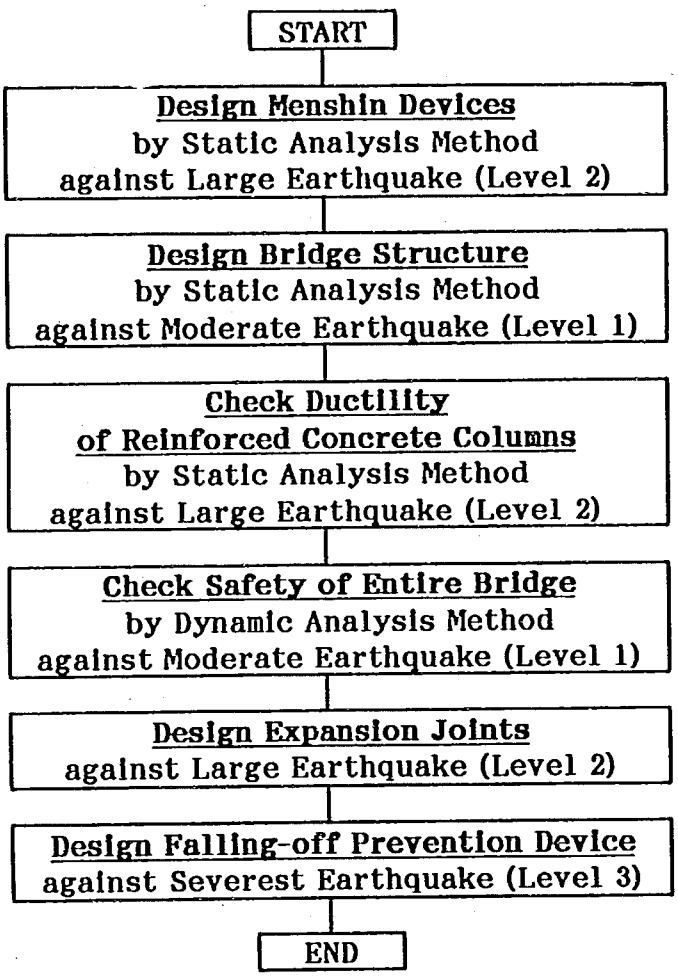


Fig. 11 Flow of Menshin Design of Highway Bridges

CONCLUDING REMARKS

Application of the base isolation to highway bridges in Japan was described in the preceding pages. Seismic damage has been decreased by improving seismic design method as well as construction practices by adopting large lateral force based on the allowable design approach. For further decreasing seismic damage at bearings and reinforced concrete piers, it is appropriate to provide a member where seismic damage would be intentionally concentrated. On the other hand, construction of multi-span continuous bridges is being pursued from the view point of driving comfort, maintenance and release from annoying noise and vibration.

Taking advantage of increasing energy dissipating capability and distribution of lateral force to many piers, the menshin design which is slightly different in concept is being introduced in Japan. The menshin design will be spotlighted in Japan as a new technology for making possible to easily construct multi-span continuous bridges as well as for reducing seismic lateral force.

ACKNOWLEDGEMENTS

For executing investigations presented here, various supports and suggestions have been obtained from many organizations and persons. Special thanks go to Professor I. Buckle, National Center for Earthquake Engineering Research, University of Buffalo, U.S.A., and Mr. Donald K. Kirkcaldie, Works and Development, New Zealand (former Visiting Researcher at PWRI), for their guidance and invaluable discussions on the base isolation. Special appreciation also goes to Professor T. Katayama, Institute of Industrial Science, University of Tokyo, for chairing the Committee formulated at the Technical Research Center for National Land Development for preparing the Guidelines for Base Isolation Design of Highway Bridges (Draft) in 1989. The authors express sincere thanks to all organizations and participants involved in the Joint Research with the Public Works Research Institute for studying the Menshin Design of Highway Bridges , with special appreciation to Mr. Y. Goto, Research Institute of Obayashi Corporation, for his endeavour to organize the research group.

REFERENCES

1)Buckle, I. G. and Mayes, R. L. : Seismic Isolation:History, Application and Performance -A World View, Earthquake Spectra, Vol. 6, No. 2, May 1990

2)McKay, G. R., Chapman, H.E. and Kirkcaldie, D. K. : Seismic Isolation : New Zealand Application, Earthquake Spectra, Vol. 6, No. 2, May 1990

3)Skinner, R.I., Tyler, R. G., Heine, A. J. and Robinson, W. H. : Hysteresis Dampers for the Protection of Structures from Earthquakes, Proc. New Zealand - Japan Workshop on Base Isolation of Highway Bridges, Wellington, New Zealand, December 1987

4)Billings, I. J. and Kirkcaldie, D. K. : Base Isolation of Bridges in New Zealand, Proc. New Zealand - Japan Workshop on Base Isolation of Highway Bridges, Wellington, New Zealand, December 1987

5)Public Works Research Institute : Report of Joint Research between PWRI and 28 Private Firms on Development of Menshin Systems for Highway Bridges, Technical Report of Cooperative Research, No. 44 and No. 60, March 1990 and

March 1991 (in Japanese)
6)Arakawa, T. and Kawashima, K. : Seismicity and Maximum Possible Earthquake around Japan for Application to Seismic Risk Analysis, Technical Note No. 2098, Public Works Research Institute, March 1984 (in Japanese)
7)Japan Road Association : Guide Specifications for Earthquake Hazard Mitigation for Transportation Facilities - Post-Earthquake Countermeasures-, February 1987 (in Japanese)
8)Kawashima, K. : Seismic Design, Seismic Strengthening and Repair of Highway Bridges in Japan, Proc. U.S.-Japan Workshop on Seismic Retrofit of Bridges, Public Works Research Institute, Tsukuba, Japan, 1990
9)Japan Road Association : Guide Specifications for Earthquake Hazard Mitigation for Transportation Facilities - Pre-Earthquake Countermeasures-, February 1987 (in Japanese)
10)Iwasaki, T., Penzien, J. and Clough, R.W. : Literature Survey - Seismic Effects on Highway Bridges, Report No. EERC 71-11, Earthquake Engineering Research Center, University of California, Berkeley, 1972
11)Public Works Research Institute : Report on Niigata Earthquake, Vol.125, June 1965 (in Japanese)
12)Japan Road Associations : Design Specifications for Highway Bridges - Part V Seismic Design -, February 1990 (in Japanese)
13)Iwasaki, T., Kawashima, K. and Hasegawa, K. : New Seismic Design Specifications of Highway Bridges in Japan, 22nd Joint Meeting, U.S.-Japan Panel on Wind and Seismic Effects, UJNR, Gaithersburg, U.S.A., May 1990
14)For example, Katayama, T., Kawashima, K., and Murakami, Y. : Current Design Considerations for Reducing Seismic Lateral Force of Highway Bridges in Japan, New Zealand - Japan Workshop on Base Isolation of Highway Bridges, Wellington, New Zealand, December, 1987 (Procs. are available from Technical Research Center for National Land Development, Tokyo, Japan)
15)Yahagi, K. and Mizumoto, Y. : Past and Present of Seismic Design, Bridge and Foundation Engineering, Vol. 13, No. 10, 1979(in Japanese)
16)Matsumura, S., Fukuoka, S., Mizumoto, Y. and Nakata, T. : Seismic Design of Multi-span Continuous Bridge with Damper, Bridge and Foundaiton Engineering, Vol. 16, No. 5, 1982 (in Japanese)
17)Iseki, J. : Viscous Damper, Society of PC Technology, Vol. 21, No. 4, August 1979 (in Japanese)
18)Okamoto, S. and Uemae, Y. : Aseismic Bridge Structure by Elastic Supports Using Tie Members (SU Damper Method), Proc. Symposium on New Ideas in Structural Design, Japan Society of Civil Engineers and Architectural Institute of Japan, 1963 (in Japanese)
19)Kitazawa, M., Ishizaki, H., Emi, S. and Nishimori, K. : Characteristics of Earthquake Responses and Design of Aseismic Design on the Long-period Cable-stayed Bridge (Higashi-Kobe Bridge) with All Movable Shoes in Longitudinal Direction, Procs. Japan Society of Civil Engineers, No. 422/I-14, October 1990 (in Japanese)
20)Maeda, K. and Eya, S. : Adoption and Dynamic Characteristic of Short Link Bearing in Yokohama Bay Bridge, Bridge and Foundation Engineering, Vol.24, No.9, September 1990 (in Japanese)
21)Kanemitsu, H. and Higuchi, K. : Displacement Control of Bridges with Suspended Girder, Technical Report of the Honshu-Shikoku Bridge Authority, 1981 (in Japanese)
22)Kato, N., Hoka, Y. and Kawahito, T. : Design of Meiko-nishi Bridge, Bridge and Foundation Engineering, 1983 (in Japanese)
23)Fukuoka, S. : Design of Multi-span Continuous Highway Bridges with Use of

Shear Viscous Damper, Bridge Engineering, 1980 (in Japanese)
24)Sakairi, Tominaga, Kiyota and Sasaki : Vibration Characteristics of 5-span Continuous Steel Box Girder Bridge Supported by Rubber Bearings, 44th Annual Meeting, Japan Society of Civil Engineering, September 1989 (in Japanese)
25)Public Works Research Institute : Report on the Disaster Caused by the Miyagi-ken-oki Earthquake of 1978, Vol. 159, March 1983 (in Japanese)
26)Personal Discussion with Mr. James Gate, California Department of Transportation, and Mr. Shoichi Saeki, Honshu Shikoku Bridge Authority
27)Williams, D. and Godden, W. G. : Experimental Model Studies on the Seismic Response of High Curved Overcrossings, Report No. EERC 76-18, Earthquake Engineering Research Center University of California, Berkeley, 197
28)Kawashima, K. and Penzien, J. : Correlative Investigation on Theoretical and Experimental Dynamic Behavior of A Model Bridge Structure, Report No. EERC 76-26, Earthquake Engineering Research Center, University of California, Berkeley, 1976
29)Kawashima, K. : An Analytical Model of Contact and Impact in Dynamic Response Analysis, Proc. Japan Society of Civil Engineers, Vol. 308, April 1981
30)Technology Research Center for National Land Development : Guidelines for Design of Base-isolated Highway Bridges, Final Report of Base Isolation to Seismic Design of Highway Bridges (Chairperson : Professor T. Katayama), March, 1989 (in Japanese)
31)Kakizaki, H. and Ito, T. : Menshin Design of Nagaki-gawa Bridge, Bridge and Foundation Engineering, Vol. 90-9, September 1990 (in Japanese)
32)Matsuo, Y., Ooishi, A., Hara, K. and Yamashita, M. : Design and Construction of Miyagawa Bridge, Bridge and Foundation Engineering, Vol. 91-2, February 1991 (in Japanese)
33)Ikeda, T., Oozeki, K., Kumakura K. and Abe, N. : Design of Karasuyama No. 1 Bridge (Base Isolated Bridge), Bridge and Foundation Engineering, Vol. 25, No. 6, June 1991(in Japanese)
34)Kawashima, K., Hasegawa, K., Unjoh, S., Nagashima, H., and Shimizu, H. : Current Research Efforts in Japan for Passive and Active Control of Highway Bridges against Earthquake, 23rd Joint Meeting, U.S.-Japan Panel on Wind and Seismic Effects, U.J.N.R., Public Works Research Institute, Tsukuba, Japan, May 1991

EXPERIMENT AND ANALYSIS ON SEISMIC RESPONSE OF MENSHIN BRIDGES

by
Kazuhiko KAWASHIMA
Kinji HASEGAWA
and
Hiroyuki NAGASHIMA

U.S. — JAPAN WORKSHOP ON EARTHQUAKE
PROTECTIVE SYSTEMS FOR BRIDGES
BUFFALO, NY, U.S.A.
September 1991

EXPERIMENT AND ANALYSIS ON SEISMIC RESPONSE OF MENSHIN BRIDGES

Kazuhiko KAWASHIMA, Kinji HASEGAWA and Hiroyuki NAGASHIMA

Earthquake Engineering Division, Public Works Research Institute

SUMMARY

To provide with realistic seismic response data of Menshin bridges, a series of shaking table tests were conducted at the Public Works Research Institute. Structural response characteristics were presented with emphasis on the effect of stopper and vertical excitation. Hysteretic behavior of Menshin bearings was studied by means of cyclic shear tests and a comparison with the seismic behavior during the excitation tests is presented. Analytical simulations are also presented for the excitation tests. Depending on the idealization of the nonlinear hysteretic behavior of the Menshin bearings, the equivalent linear analysis and the bilinear analysis were made. Analytical simulation for the effect of collision between the deck and the columns due to the stoppers was also presented.

INTRODUCTION

Seismic response of Menshin bridges subjected to significant earthquakes is of great interest for designing Menshin bridges in Japan. Because there have been so far no Menshin bridges which experienced significant earthquakes with the magnitude over 8, it is required to study their critical behavior carefully.

The most important issue in the structural response of Menshin bridges is the analytical idealization of the nonlinear hysteretic behavior of the Menshin bearings. Effect of stoppers which are provided to prevent excessive deck response is of another interest. When collision of deck with columns occurs, this would cause large impact force. Because bridges are subjected to large vertical excitation during destructive earthquakes, it is also important to study the response of Menshin bridges subjected to lateral and vertical excitations simultaneously.

For aiming to study the response of Menshin bridges, a series of excitation tests was made at the Public Works Research Institute. Two types of large scale model were used for the excitation tests. Analytical simulations by means of the equivalent linear analysis and bilinear analysis were made.

This paper shows structural response characteristic of Menshin bridges through shaking table tests and analytical simulation (Ref. 1,2,3).

STRUCTURAL RESPONSE OF MENSHIN BRIDGES THROUGH SHAKING TABLE TESTS

Model and Test Procedure To provide a realistic seismic response data of a Menshin bridge, a series of shaking table tests were made at the Public Works Research Institute. A Menshin bridge model tested which is referred as "model 1" is a simple girder bridge supported by two columns placed on a shaking table as shown in Photo 1. The span length is 6 m and the deck weight is 39.8 tf. Two

types of Menshin bearing, i.e., lead rubber bearing (LRB) shown in Photo 2 and high damping rubber bearing (HDR) shown in Photo 3 were used. Two bearings were installed on each column, and totally four bearings supported the girder.

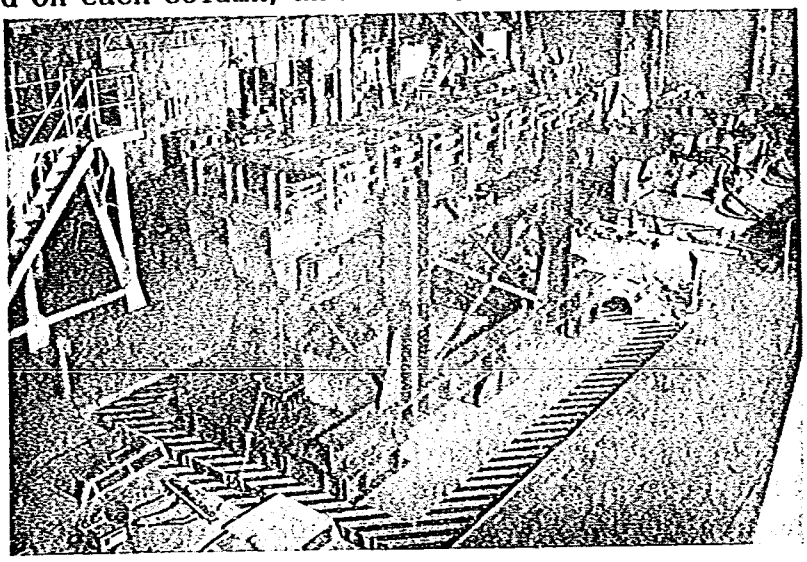


Photo 1 Setup of Shaking Table Test (Model 1)

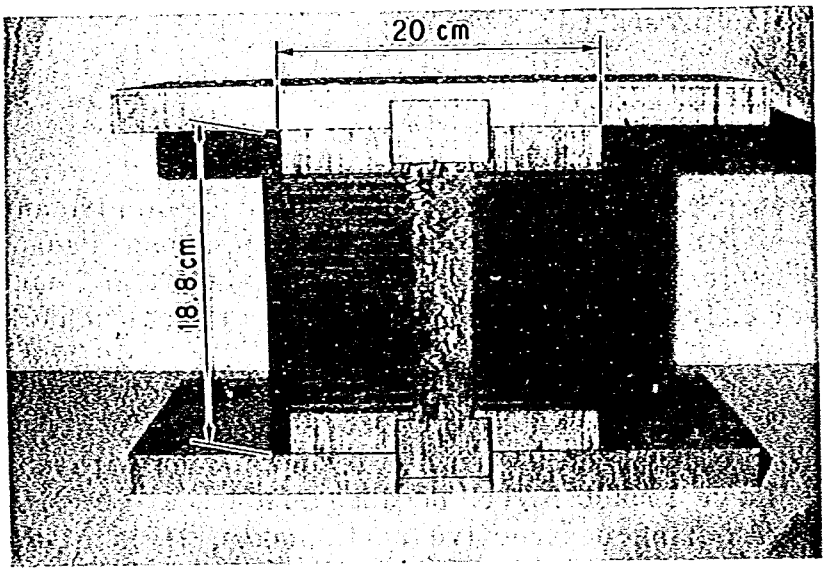


Photo 2 Lead Rubber Bearing

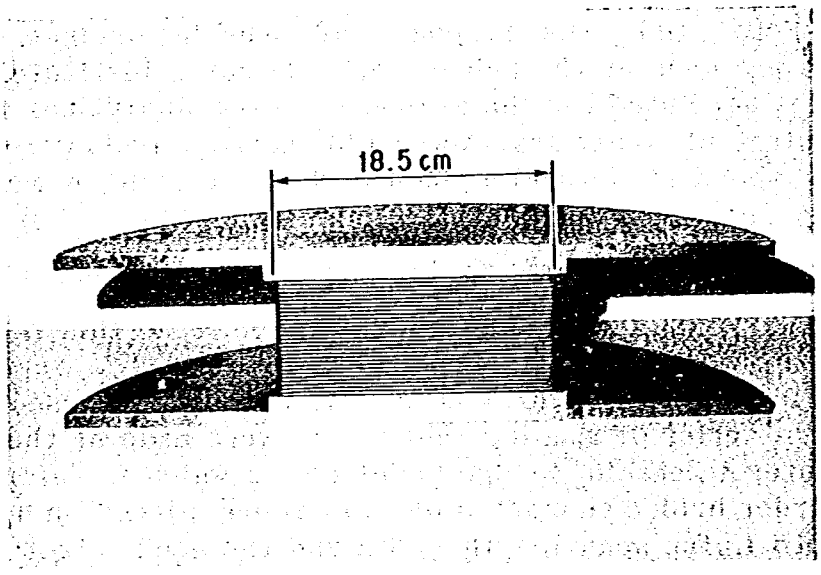


Photo 3 High Damping Rubber Bearing

The LRB (Ref. 4,5,6,7) was formed by laminating 20 layers of rubber with thickness of 5 mm and 19 steel plates with thickness of 2 mm, and the lead plug with diameter of 35 mm was pressed into at the center hole of the bearing. The HDR (Ref. 8) is composed of special rubber which is distinguished by damping characteristic from regular linear rubber. Therefore, the rubber itself would work as an energy dissipator as well as an isolator without any unique mechanism such as the lead plug, when it is subjected to shear deformation. The HDR was formed by vulcanizing 31 layers of the rubber with thickness of 2 mm, each layer of which was laminated between two steel plates with thickness of 0.6 mm. Both bearings are simple and compact as Menshin bearings for bridges so that they are very likely to be used in Menshin bridges.

Specific scale rule was not taken into consideration when the dimension of the model was decided, and the model was assumed as a small prototype. When the deck is supported by a fixed bearing at one end with the other end being supported by roller bearing, the fundamental natural period is about 1 sec. The stiffness of the Menshin bearings was designed to make the fundamental natural period about 2 sec, two times of regular one, so that the Menshin system performs effectively.

Excitation by sinusoidal motions and earthquake ground motions was made. Frequency as well as intensity was varied in the sinusoidal excitation to study the natural period of the model. Two ground motions which were recorded on the ground near the Kaihoku bridge during the Miyagi-ken-oki earthquake (M7.4) of 1978 and on the Hachiro-gata bank during the Nihon-kai-chubu earthquake (M7.7) of 1983 were used for the excitation. They are hereafter designated as a Kaihoku record and a Hachiro-gata record, respectively. The time of the Hachiro-gata record was reduced one half of the original. The intensity of the records was varied. Fig. 1 shows the response acceleration spectrum ratio (acceleration response/peak input acceleration) of the two records.

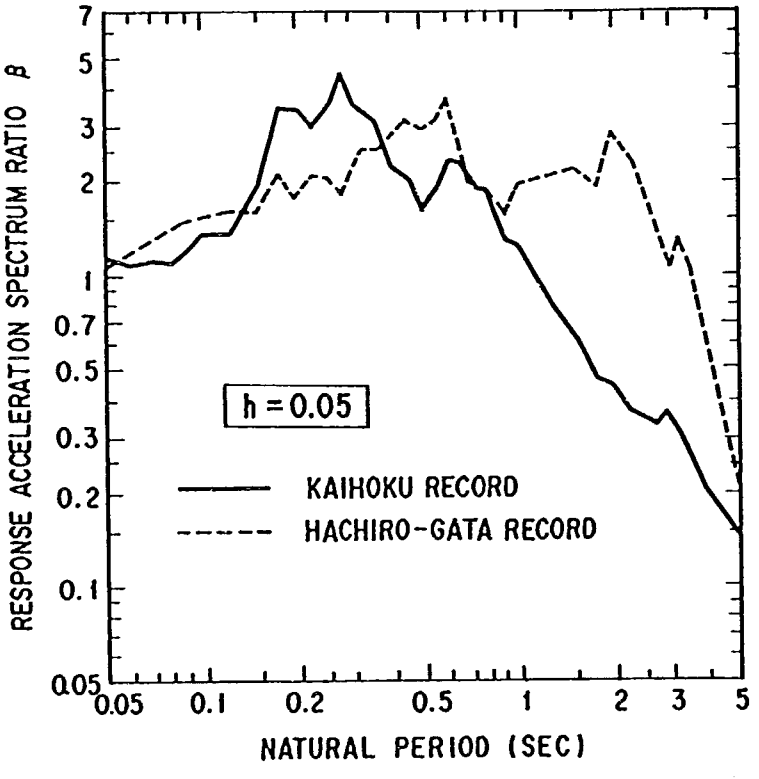


Fig.1 Response Acceleration Spectrum Ratio

Sinusoidal Excitation Figs. 2 and 3 show the resonance curve of acceleration and displacement. The fundamental natural frequency varied from 1.62 Hz to 0.67 Hz for the LRB model and from 1.95 Hz to 0.95 Hz for the HDR model by increasing the input acceleration from 0.01 g to 0.04 g. This clearly shows the shear-strain dependence of the stiffness of LRB and HDR. The fundamental natural frequency of the model supported by regular fix and roller bearings does not depend on the input acceleration.

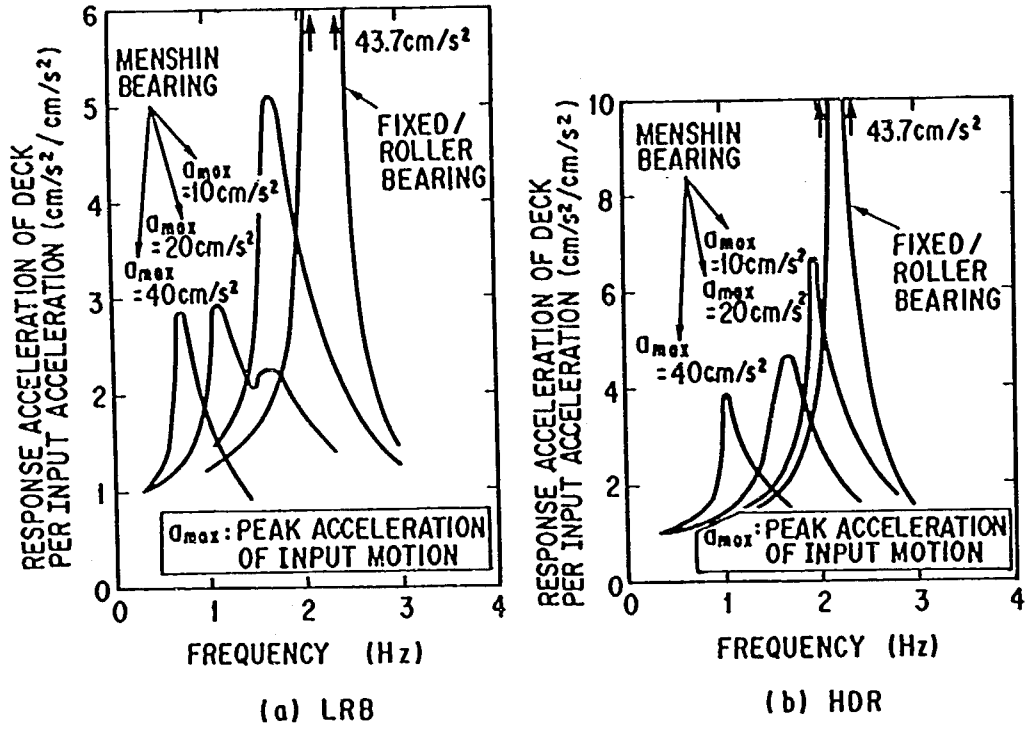


Fig.2 Amplification of Resonance Acceleration Curve

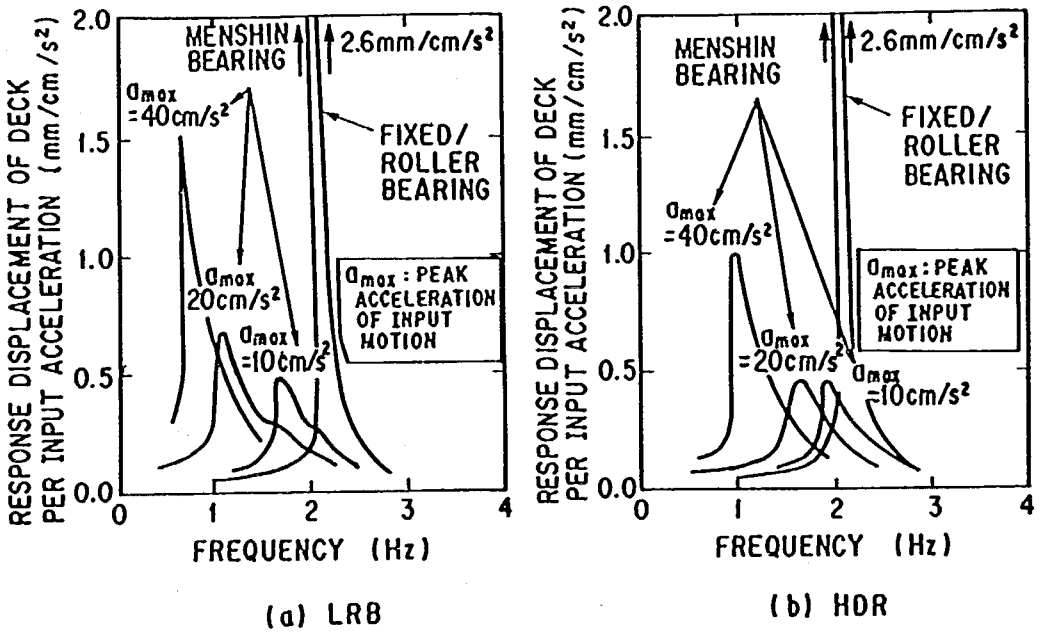


Fig.3 Amplification of Resonance Displacement Curve

Table 1 shows damping ratio by the half-power method with use of the resonance curves. The damping ratio is about 2 % for the model supported by the regular fix and roller bearings, and about 11 % and 9 % for the model supported by the LRB and the HDR, respectively, when subjected to the sinusoidal excitation with peak input acceleration of 0.04 g. It means that an increase of the damping ratio of 9 % and 5 % was made by adopting the LRB and the HDR, respectively.

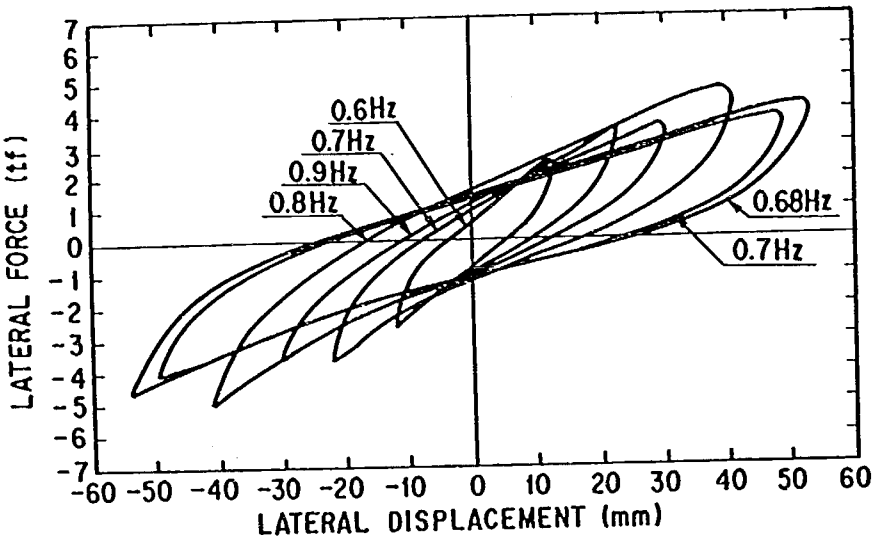
Table 1 Equivalent Viscous Damping Ratio by Half-Power Method

INPUT INTENSITY / BEARING	10 (cm/s^2)	20 (cm/s^2)	30 (cm/s^2)
L R B	0.08	0.092	0.113
H D R	0.064	0.087	0.092
FIXED/MOVABLE BEARING	0.02		

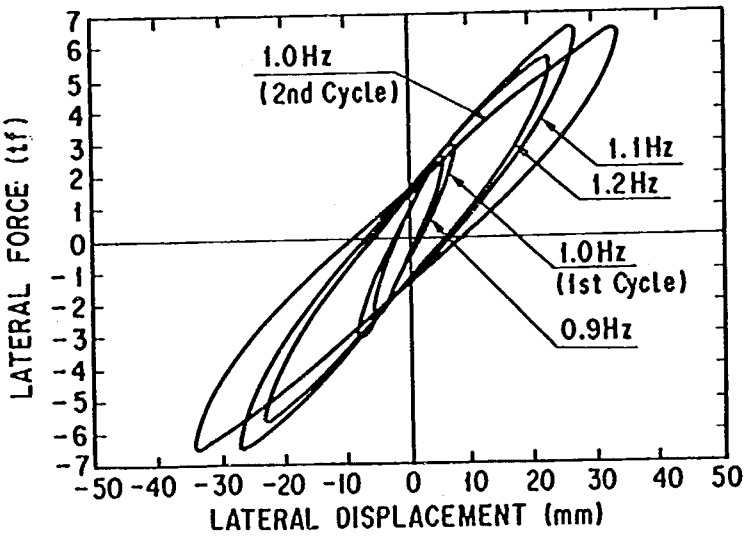
The hysteresis loops of shear force vs. shear deformation of the bearings are shown in Fig. 4. The hysteresis loops of the LRB look bilinear shape, especially in small amplitude, while the HDR is featured by the spindle-like shape. The lead plug of the LRB, which gives high initial stiffness, produces the bilinear shape. On the other hand, the HDR does not create high stiffness in small deformation and does not form the bilinear shape.

Figs. 5 and 6 show the dependency of the equivalent stiffness and the equivalent damping ratio on the deformation acquired from the sinusoidal excitation tests. The equivalent stiffness is defined as gradient of a line connecting the two points at the maximum and minimum displacement of a hysteresis loop, and the equivalent damping ratio is defined as a value proportional to the ratio of damping energy loss per cycle to strain energy stored at maximum displacement as shown in Fig. 7. An empirical equation for the equivalent stiffness k_e was obtained as shown in Fig. 5. Though the equivalent damping ratio is scattered, compared with the equivalent stiffness k_e, the damping ratio h_e may be considered 0.16 for the LRB and 0.13 for HDR in the range of the shear deformation from 1 to 50 mm.

The equivalent stiffness and the equivalent damping ratio from the cyclic shear loading tests of the bearing alone, which were conducted prior to the shaking table tests, are also shown in Figs. 5 and 6 for comparison. In the cyclic shear loading tests, alternating shear deformation was repeatedly applied to the bearings under constant vertical force corresponding to the dead weight of the deck. The equivalent stiffness and equivalent damping ratio estimated from the sinusoidal excitation tests are in good agreement with the result of the cyclic shear loading tests of the bearing alone so that it can be deduced that the test method, a shaking table test or a cyclic shear loading test, does not affect the equivalent stiffness and the equivalent damping ratio of a Menshin bearing.



(a) LRB



(b) HDR

Fig.4 Hysteresis of Lateral Force vs. Lateral Displacement

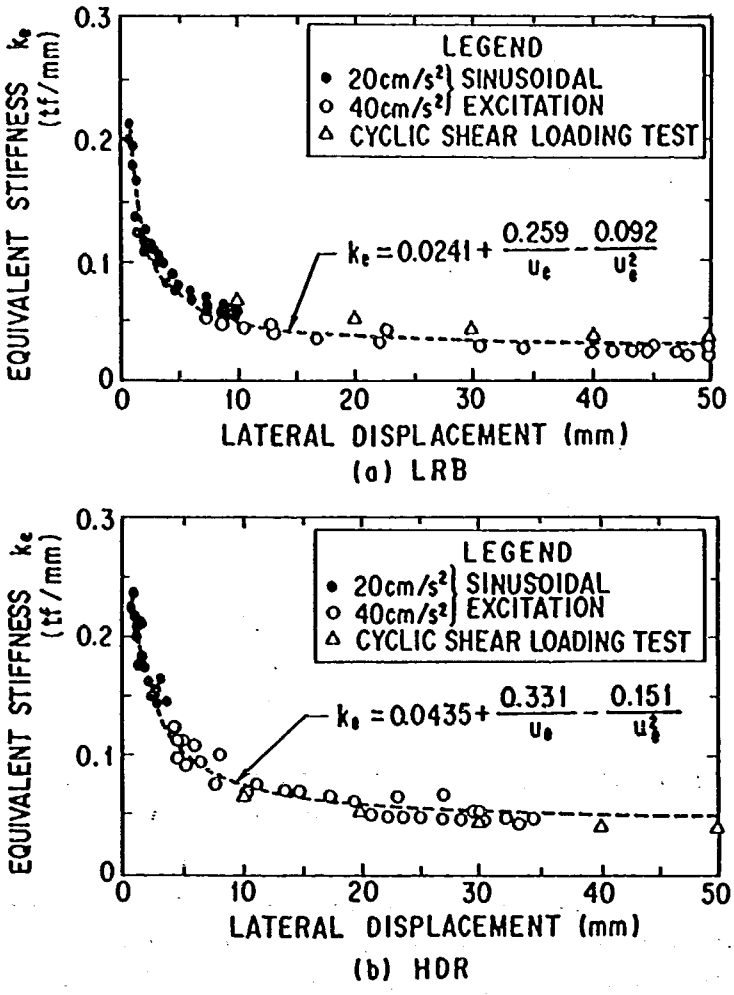


Fig.5 Equivalent Stiffness

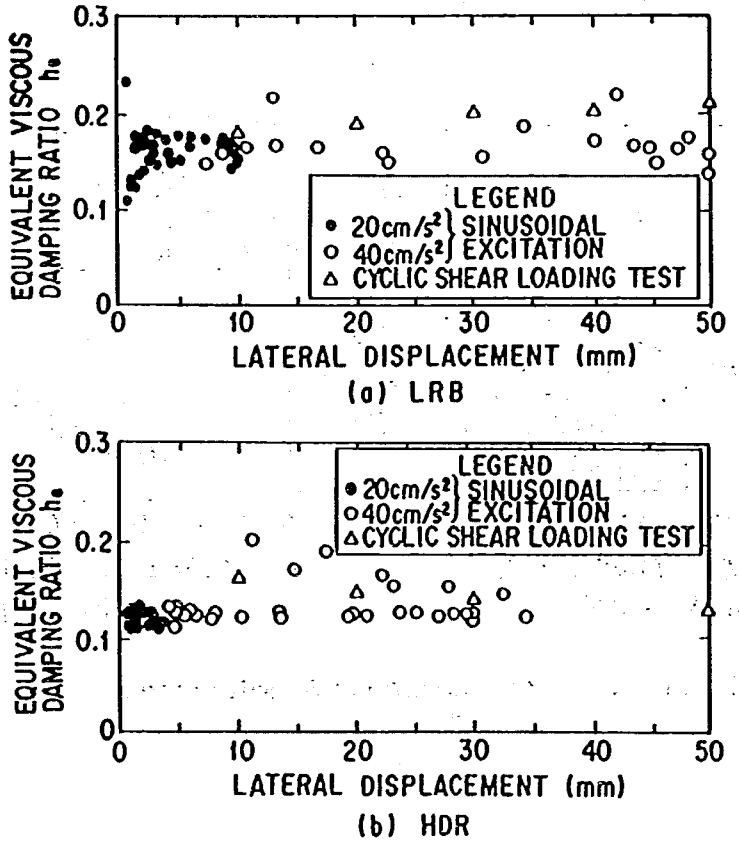


Fig.6 Equivalent Viscous Damping Ratio

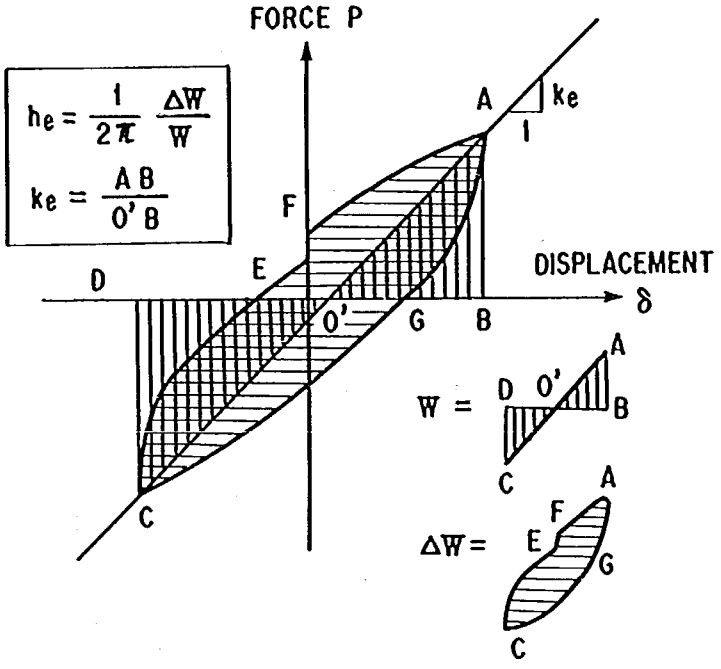


Fig.7 Definition of Equivalent Stiffness k_e and Equivalent Viscous Damping Ratio h_e

Ground Motion Excitation Figs. 8 and 9 show how the peak deck response acceleration and displacement increase with the peak input acceleration. The effect of Menshin system can be apparently observed in Fig. 8, where the acceleration of the regular bridge amounts to more than two times acceleration of the Menshin bridge under the same input motion.

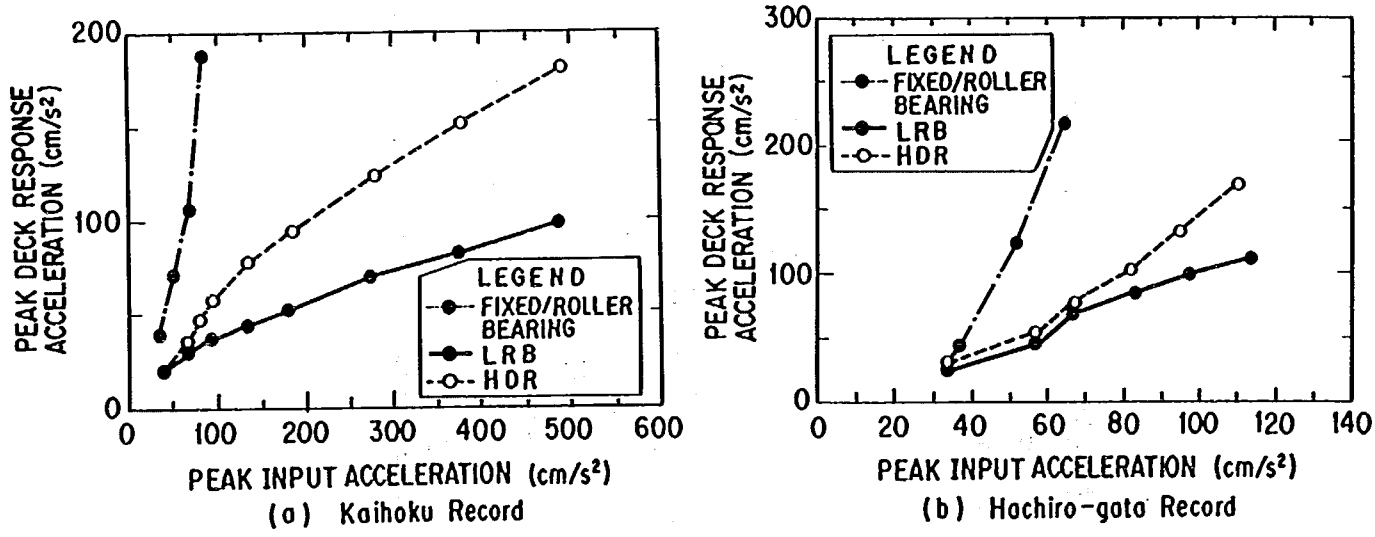


Fig.8 Peak Deck Response Acceleration

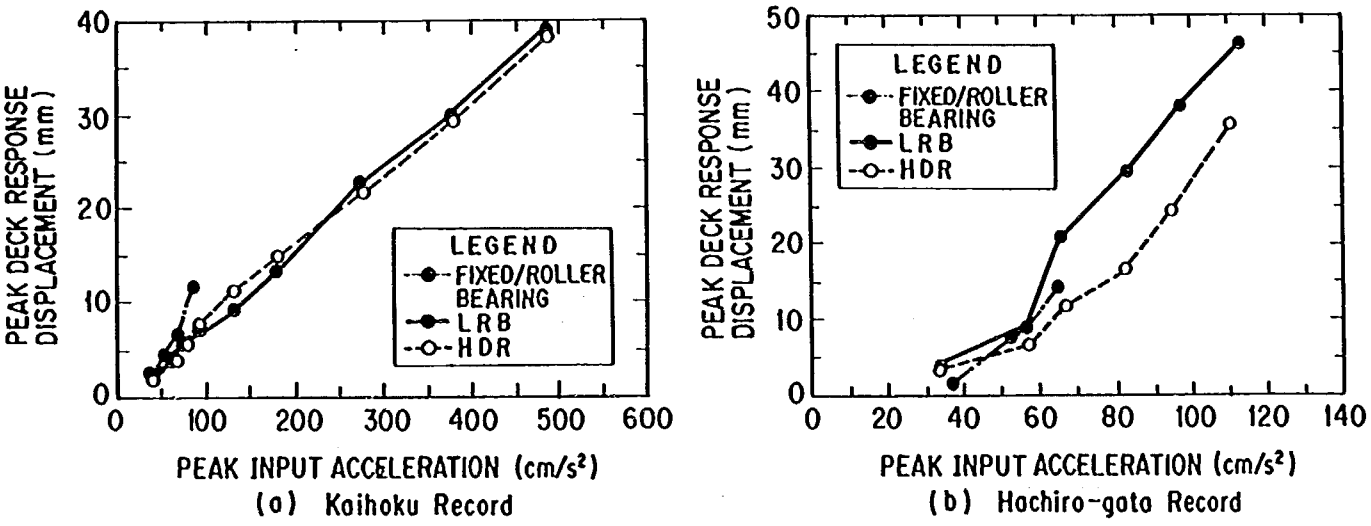


Fig.9 Peak Deck Response Displacement

EFFECT OF STOPPER AND VERTICAL EXCITATION

Tested Model For aiming to study effect of stopper and vertical excitation, another series of excitation tests were made. The columns and the Menshin bearings were replaced with new ones. The column was designed to have higher stiffness than an actual column since a flexible column could soften impact force due to collision developed at a stopper. The Menshin bearings, the lead rubber bearing and the high damping rubber bearing, were designed to make the fundamental natural period of the model about 0.6 sec. Photo 4 shows the Menshin bridge studied for the effect of stopper and vertical excitation. To distinguish the model with the one presented in Photo 1, it is referred as "model 2".

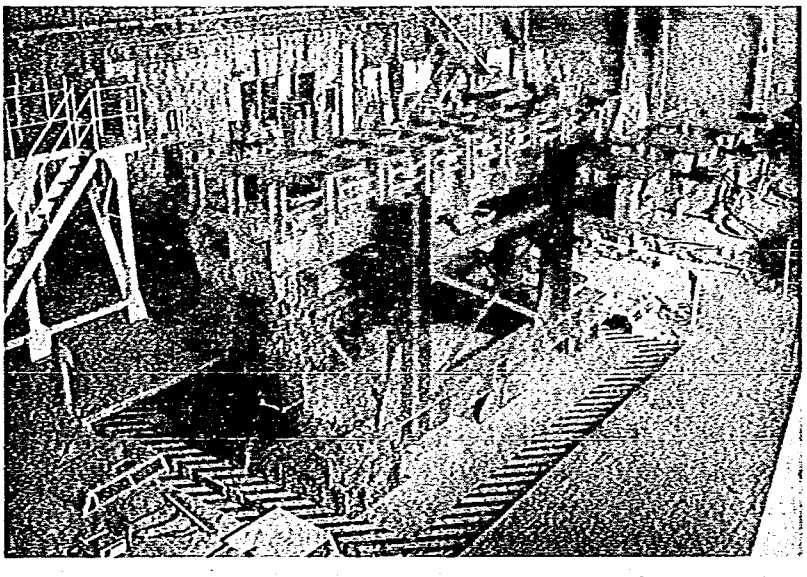


Photo 4 Setup of Shaking Table Test (Model 2)

The LRB was fabricated by vulcanizing 12 layers of rubber with thickness and diameter of 5 mm and 320 mm, respectively. They were laminated with 13 steel plates with thickness of 2 mm. The total thickness of rubber is 60 mm, and the total thickness of the entire bearing after fabrication is 110mm. The diameter of the lead plug is 40 mm. The HDR was fabricated by vulcanizing 16 layers of high damping rubber with thickness of 1.3 mm, and by laminating with steel plates with thickness of 3 mm.

Two stoppers which prevent excessive relative displacement between the deck and the columns were provided with the top of the each column as shown in Photo 5. A rubber was placed on the stopper to lessen the impact force of collision. Although the gap space of the stopper at both columns was adjusted to equalize each other as much as possible, it is noted that collision did not always take place simultaneously at each stopper.

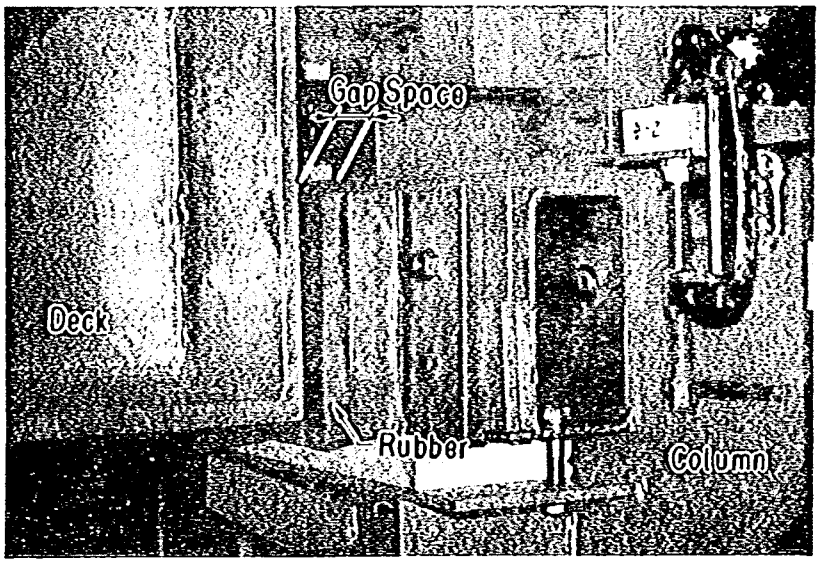


Photo 5 Stopper

Excitation was made either in longitudinal direction or in longitudinal and vertical direction. The horizontal and vertical components of the Kaihoku record and the Hachiro-gata record were used for the excitation. Ratio of acceleration intensity between horizontal and vertical components was assumed the same with the original records.

Effect of Collision and Vertical Excitation Fig. 10 shows the response of the model when the stoppers are not provided, and Fig. 11 shows the response when the stoppers with the gap space of 2 cm each were provided. Collisions, which took place when the stoppers of 2 cm gap was provided, developed greater acceleration at the deck and the columns.

Fig. 12 shows the hysteresis loops of the LRB for the tests shown in Figs. 10 and 11. Since the shear force computed by multiplying the acceleration developed at the deck by the mass of the deck is presented in Fig. 12, it should be noted that the shear force represents the total force transmitted to the columns through only the bearings when not colliding, and through both bearings and stoppers when colliding. The shear force jumped up significantly due to the collision.

Figs. 13 and 14 show the peak input acceleration vs. the peak deck response. It is seen in Figs. 13 and 14 that when the collision did not take place at the stoppers, the response displacement and acceleration of the deck are almost proportioned to the input acceleration. However, when the collision took place at the stoppers, the displacement of the deck is controlled by the stoppers within a little bit more than the gap space as shown in Fig. 13 (b). The acceleration of the deck is raised by the collision as shown in Fig. 14 (b). For example, the acceleration amounts to 0.69 g and 0.83 g for the gap of 3 cm and 2 cm, respectively, contrasted to 0.59 g without stoppers, under the excitation

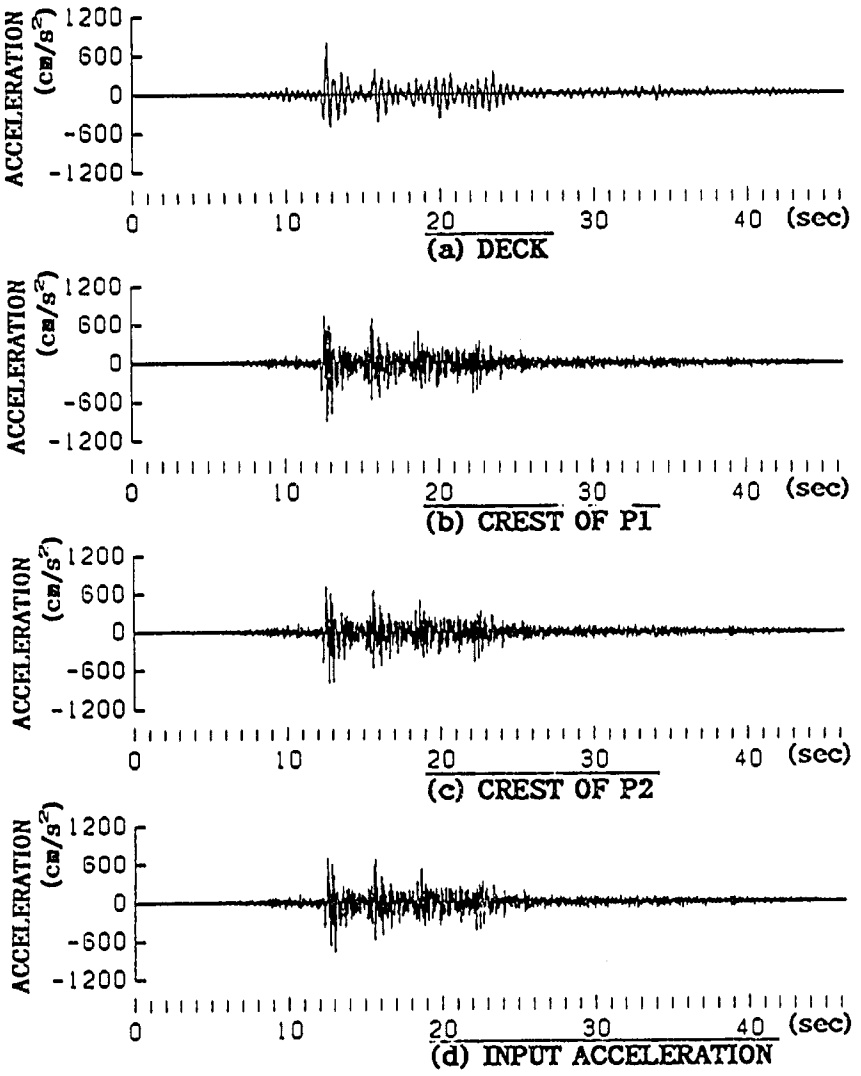


Fig.10 Response When Stopper Is Not Provided

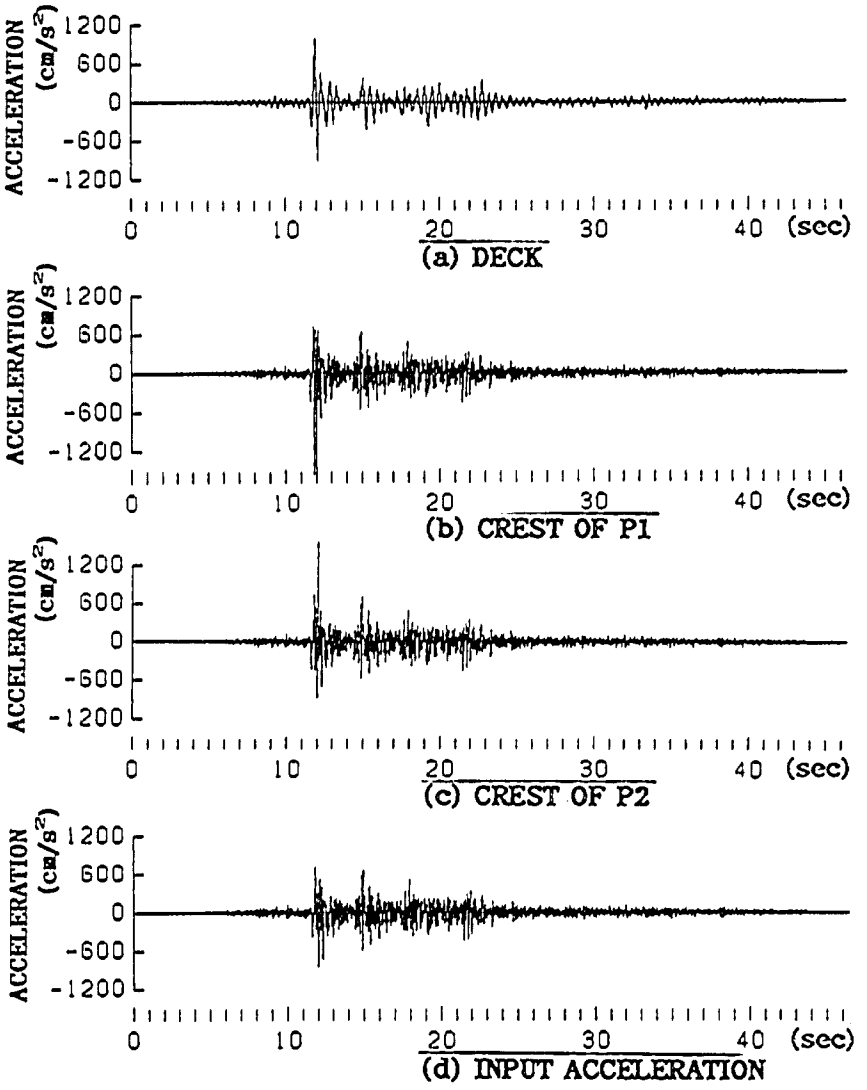


Fig.11 Response When Stopper with 2cm Gap Is Provided

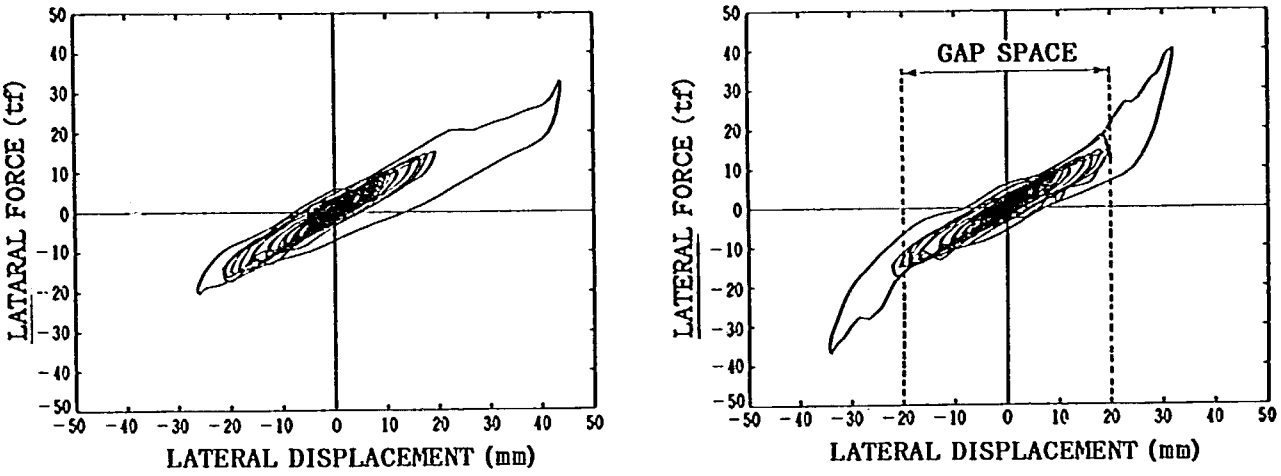
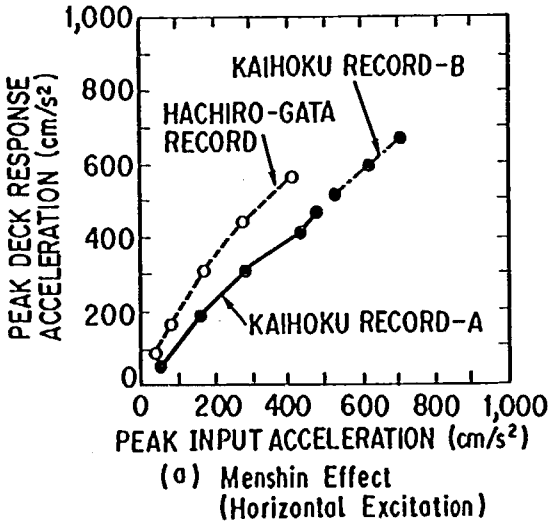
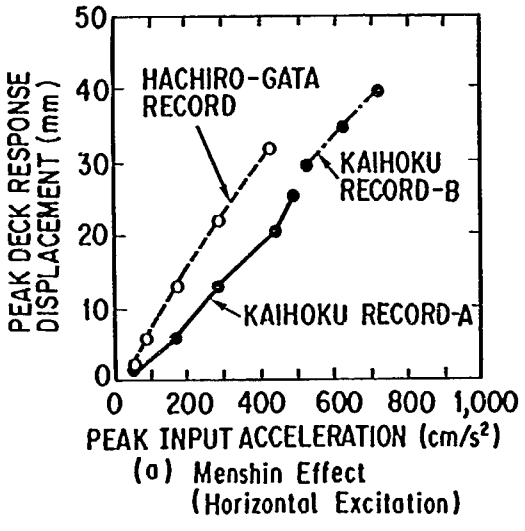
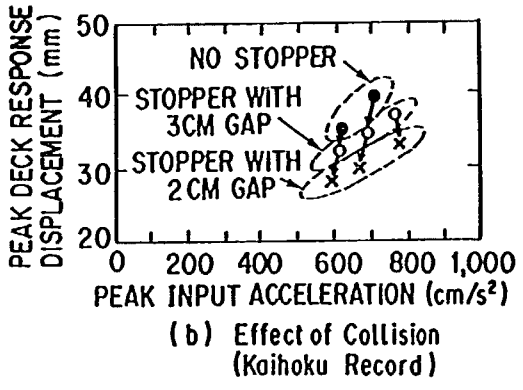


Fig.12 Hysteresis of Lateral Force vs. Lateral Displacement







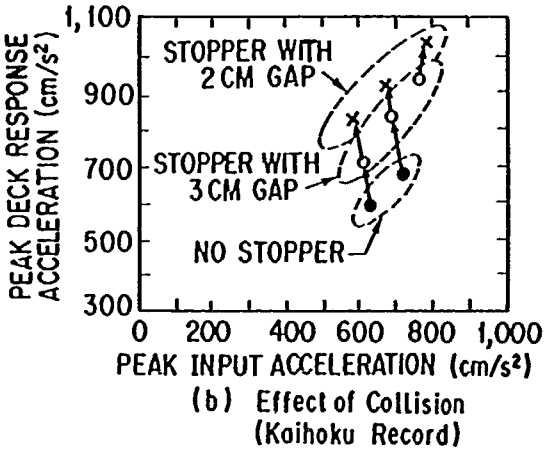


FIg.13 Effect of Stopper for Deck Response Displacement

FIg.14 Effect of Stopper for Deck Response Acceleration

of 0.6 g acceleration. This means that the seismic lateral force transmitted to the columns is increased by 1.2 times and 1.4 times for the gap of 3 and 2 cm, respectively, due to the collision.

Fig. 15 shows the effect of vertical excitation in terms of peak deck response. Although some effects of simultaneous excitation which was presumably caused by changes of the equivalent stiffness of the LRB due to variation of vertical force are seen, they are practically small.

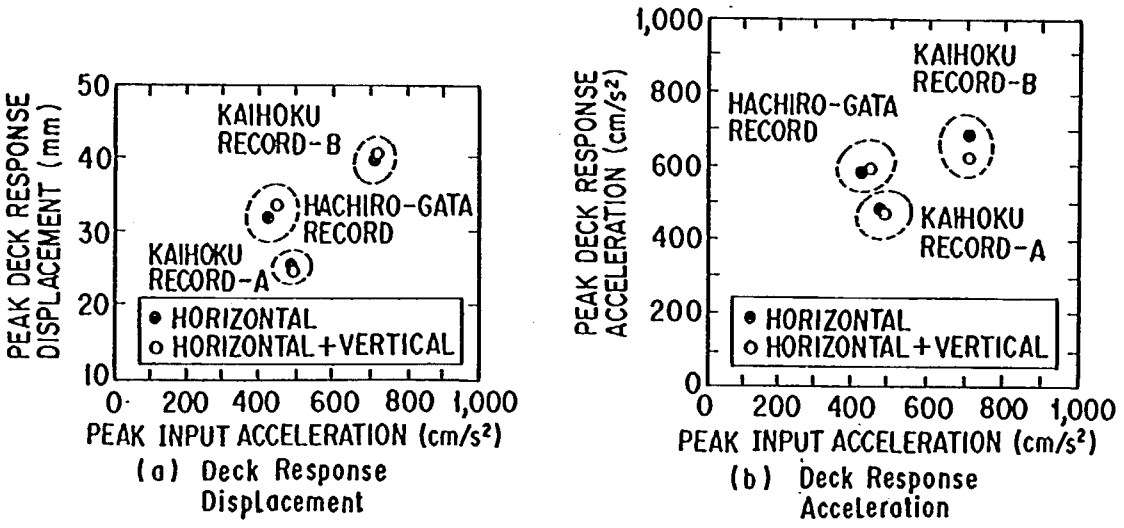


Fig.15 Effect of Vertical Excitation

Deck response when the HDR was adopted is basically analogous to that for the LRB, and so they are not presented here.

ANALYTICAL SIMULATION BY EQUIVALENT LINEAR ANALYSIS

Because the equivalent stiffness and the equivalent damping ratio of Menshin bearing depend on the displacement developed in it as shown in Figs. 5 and 6, they have to be evaluated for a specific response displacement ue in the equivalent linear analysis. Therefore the response displacement u_e was assumed to be specified in the form of

$$u_e = c \cdot u_{max} \qquad (1)$$

where u_{max} is the peak displacement of the Menshin bearing, and c is a coefficient ($0 \leqq c \leqq 1.0$) representing the intensity of the specific response displacement. The coefficient c was assigned as 0.7 and 1.0. Because the purpose of this study is to clarify the coefficient c, a simplification was introduced in the calculation, i.e., since the peak displacement u_{max} is unknown before the analysis, the iteration of analysis is inevitable in the equivalent linear analysis. However, since the peak displacement obtained from the tests should be the right peak displacement, it was used in Eq. (1) instead of the iteration.

Mode damping ratio of the entire bridge model with Menshin bearings was computed by the proportional-to-strain-energy damping computing method (Ref. 9). The method is to estimate the damping ratio for each mode shape of an entire structure as the weighted average of damping ratio of each element with

proportion to its strain energy as

$$h_i = \frac{\sum_{j=1}^{n} \phi_{ij}^T \cdot h_j \cdot k_j \cdot \phi_{ij}}{\phi_i^T \cdot K \cdot \phi_i} \qquad (2)$$

where h_i is the damping ratio of i-th mode, ϕ_j is an i-th mode vector for j-th structural element, h_j is the damping ratio of j-th element, K_j is the stiffness matrix of j-th element, ϕ_i is i-th mode vector, K is stiffness matrix of the entire structure and n is the number of elements.

The model 1 supported by the LRB was analyzed. Table 2 shows the fundamental natural period and the mode damping ratio for the fundamental natural mode. Damping ratio of the columns was assumed as 0.2 %, which was estimated from the shaking table test results of the bridge model supported by the regular fix and roller bearings. It is seen in Table 2 that difference of the fundamental natural period and the mode damping ratio between for c = 0.7 and c = 1.0 is up to only 7 % and 2 % at most, respectively. This means that the fundamental natural period and the mode damping ratio are less sensitive on the coefficient c.

Table 2 Natural Period and Damping Ratio

(a) Natural Period

INPUT MOTION		L R B		H D R	
		c=0.7	c=1.0	c=0.7	c=1.0
KAIHOKU RECORD	A	1.04	1.11	0.84	0.88
	B	1.13	1.18	0.90	0.93
HACHIRO-GATA RECORD	A	1.08	1.14	0.80	0.85
	B	1.15	1.20	0.89	0.92

(b) Viscous Damping Ratio

BEARING	INPUT MOTION		c=0.7	c=1.0
L R B	KAIHOKU RECORD	A	0.149	0.150
		B	0.151	0.152
	HACHIRO-GATA RECORD	A	0.150	0.151
		B	0.152	0.152
H D R	KAIHOKU RECORD	A	0.111	0.112
		B	0.113	0.114
	HACHIRO-GATA RECORD	A	0.109	0.111
		B	0.113	0.114

Fig. 16 compares the predicted and measured deck response acceleration for the Kaihoku record. The predicted response assuming c = 0.7 and c = 1.0 sufficiently assesses the experimental response, and these two values of c do not give meaningful difference on the response. Table 3 compares the peak response between the predicted and the measured. Although the analysis assuming c = 1.0 gives a little better outcome compared with the analysis assuming c = 0.7, it may be said that the accuracy of both cases are satisfactory enough in practical sense.

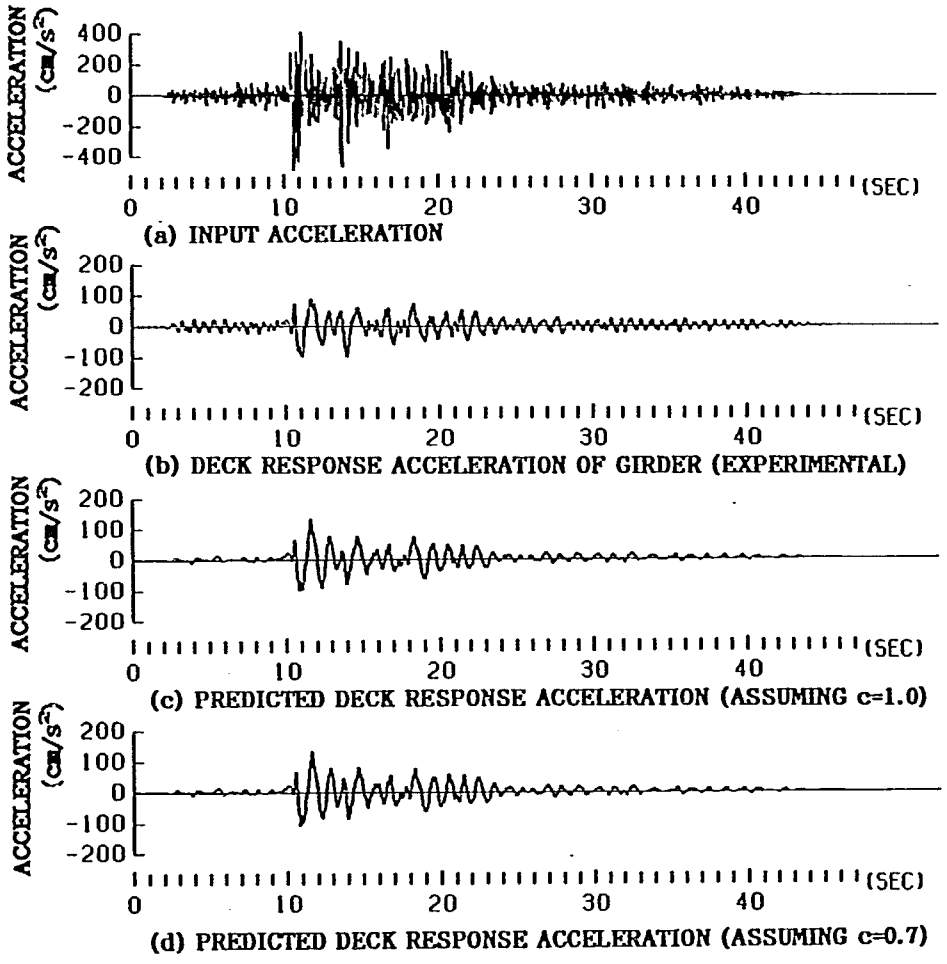


Fig.16 Deck Response Acceleration for Kaihoku Record B

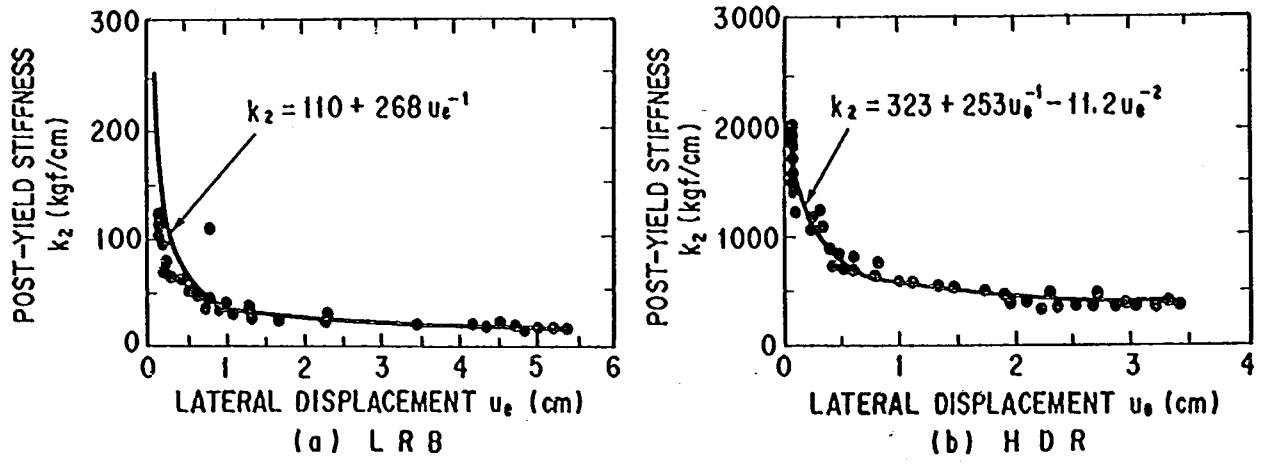


Fig.18 Post-yield Stiffness

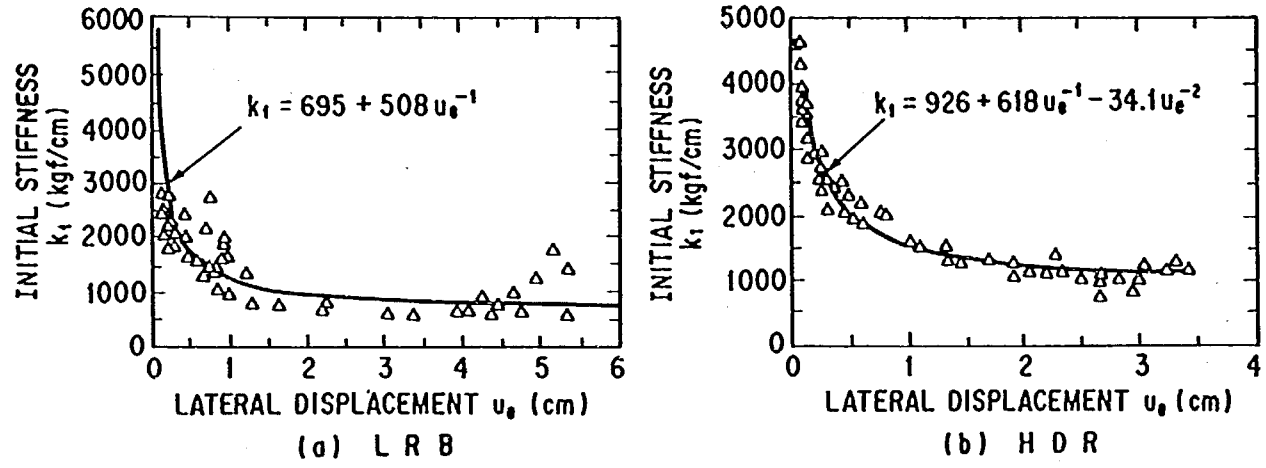


Fig.19 Initial Stiffness

Fig. 20 compares the hysteresis loop thus idealized with the bilinear model and the experimental result. The model remarkably agrees with the experimental loop.

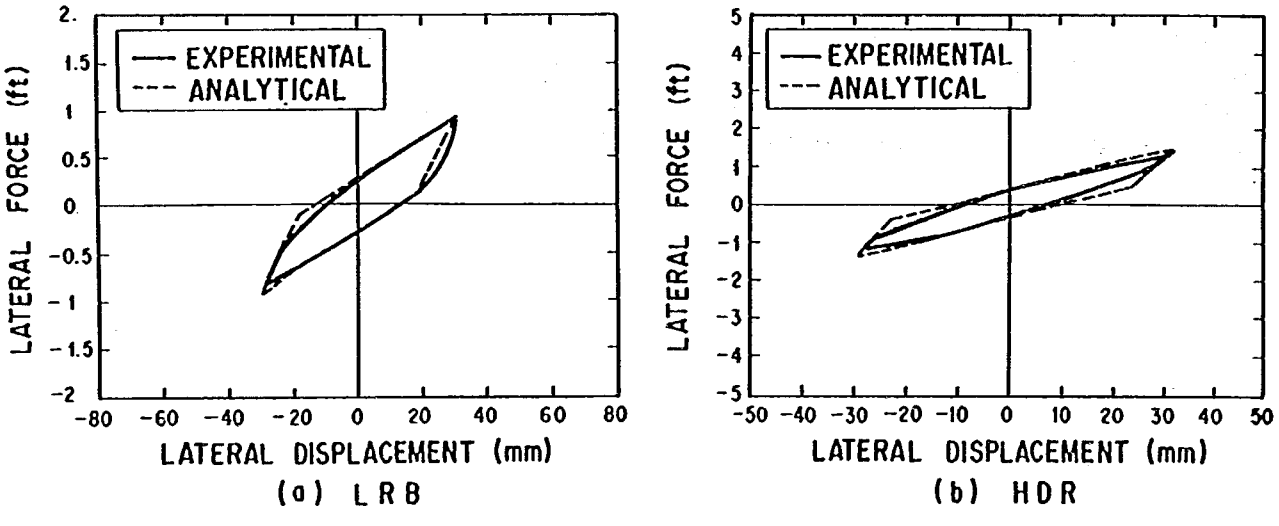


Fig.20 Analytical Idealization by Bilinear Spring Model

It should be however noted here that because the parameters k_1, k_2 and Q depend on the shear deformation of the Menshin bearings, the idealization with the bilinear model has to be made depending on the shear deformation developed in the Menshin bearings. Because a computer program in which the displacement-independent bilinear model is assumed was used, iteration similar with the equivalent linear analysis was required to determine the most appropriate shear deformation of the Menshin bearings. Therefore, the response displacement of the Menshin bearings ue was assumed as

$$u_e = c_{NL} \cdot u_{max} \qquad (3)$$

where c_{NL} is a coefficient ($0 \leqq c_{NL} \leqq 1.0$) and u_{max} is the peak displacement of a Menshin bearing developed during excitation. Although it was anticipated from the preceding analysis by the equivalent linear analysis that the coefficient c_{NL} of 0.7 and 1.0 gives practically small difference, analytical simulation was made assuming these two values for the coefficient c_{NL}. Similar with the equivalent linear analysis, the peak response displacement actually developed in the Menshin bearings during the excitation tests was assigned for u_{max} in Eq. (3), and the iteration was avoided in the analytical simulation.

The same cases studied as in the equivalent linear method were analyzed. To represent energy dissipation at the columns, Rayleigh damping was included. Coefficients of Rayleigh damping were determined so that it gives the mode damping ratio computed by the proportional-to-strain-energy damping computing method for the first and second vibration modes, i.e., $h_1 = 0.0$ and $h_2 = 0.02$.

Fig. 21 compares the deck response between the analysis and the experiment. The analysis gives good agreement with the experiment, and no significant difference can been observed between $c_{NL} = 0.7$ and $c_{NL} = 1.0$. Only slight discrepancy is the decay of the deck response after the main vibration. The tests show faster attenuation than the analysis. This is because the bilinear hysteresis loop of the Menshin bearing was so adjusted to be applicable for the larger shear deformation during the main vibration, and is not fitting for the smaller deformation after that.

Table 4 compares the peak deck response. Defining a ratio of the predicted and experimental peak deck response, the ratio ranges from 0.9 to 1.1 for $c_{NL} = 1.0$, while it scatters widely for $c_{NL} = 0.7$. Based on such evaluation, c_{NL} is proposed to be assigned 1.0.

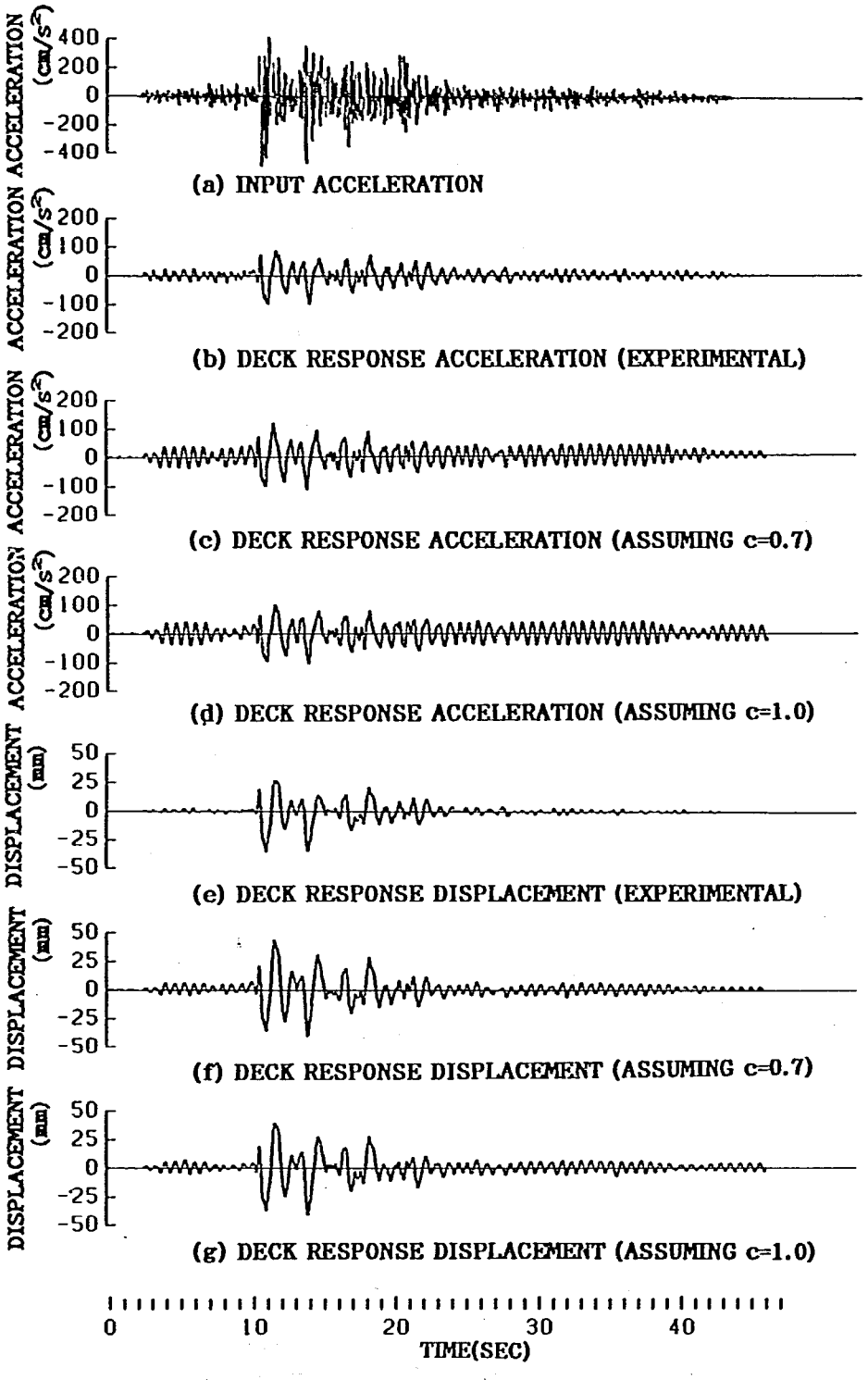


Fig.21 Deck Response for Kalhoku Record B

Table 4 Comparison between Experimental and Analytical by Nonlinear Analysis

MENSHIN BEARING	INPUT MOTION		PEAK INPUT ACCELERATION (cm/s²)	EXPERIMENT		SIMULATION			
						c = 0.7		c = 1.0	
				PEAK DECK RESPONSE ACCELERATION (cm/s²)	PEAK DECK RESPONSE DISPLACEMENT (mm)	PEAK DECK RESPONSE ACCELERATION (cm/s²)	PEAK DECK RESPONSE DISPLACEMENT (mm)	PEAK DECK RESPONSE ACCELERATION (cm/s²)	PEAK DECK RESPONSE DISPLACEMENT (mm)
LRB	KAIHOKU	A	273.2	72.5	21.0	92.2 (1.27)	25.3 (1.20)	83.6 (1.15)	25.7 (1.22)
	RECORD	B	481.3	101.0	35.8	118.3 (1.17)	43.4 (1.21)	102.7 (1.02)	40.4 (1.13)
	HACHIRO-GATA	A	85.1	81.7	26.1	123.7 (1.51)	40.3 (1.54)	97.3 (1.19)	34.1 (1.31)
	RECORD	B	115.6	110.2	41.6	148.4 (1.35)	60.7 (1.46)	123.0 (1.12)	53.8 (1.29)
HDR	KAIHOKU	A	276.4	124.6	18.6	128.6 (1.03)	22.1 (1.19)	116.5 (0.93)	20.7 (1.11)
	RECORD	B	484.7	181.9	33.1	172.3 (0.95)	34.4 (1.04)	156.9 (0.86)	31.7 (0.96)
	HACHIRO-GATA	A	83.1	102.7	14.0	95.0 (0.93)	15.6 (1.11)	93.6 (0.91)	15.4 (1.10)
	RECORD	B	111.5	170.4	30.4	189.9 (1.11)	39.3 (1.29)	185.3 (1.09)	39.8 (1.31)
AVERAGE OF RATIO						(1.17)	(1.26)	(1.03)	(1.18)

( ) Represents Ratio of Experimental to Analytical

ANALYTICAL SIMULATION FOR COLLISION

The stopper of Menshin bridges has to be properly modeled in Menshin design since it would cause great impact force to the columns due to collision. As shown in Fig. 22, the stopper was idealized as a linear spring functioning only when collision takes place. In the range over the gap space Δ_G of the stopper, a spring with the compression stiffness of the rubber installed on the stopper resists for further compression. Energy dissipation due to collision was disregarded in this idealization (Ref. 10).

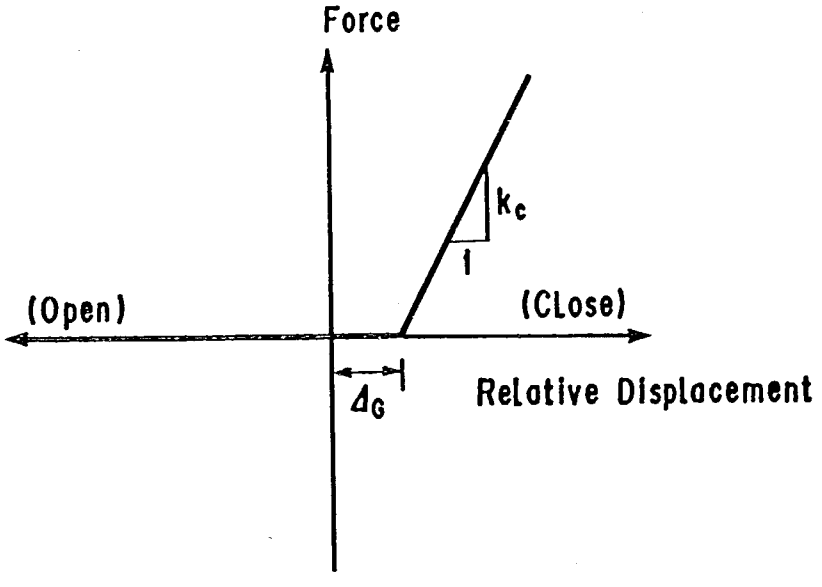


Fig.22 Idealization of Stopper

The width w, height h, thickness t, and young modulus E of the rubber are 40 cm, 20 cm, 7.1 cm and 40.0 kgf/cm^2, respectively, so that the compression stiffness k_o is obtained as

$$\begin{aligned} k_o &= E \times w \times h / t \\ &= 40.0 \times 40 \times 20 / 7.1 \\ &= 4{,}507 \text{ kgf/cm} \end{aligned} \qquad (4)$$

The deck response of the model 2 supported by the LRB was simulated with nonlinear dynamic analysis. The Menshin bearing was modeled as a bilinear model. The initial stiffness, post-yield stiffness and characteristic load of the Menshin bearing were determined by the method proposed in the preceding chapter. The damping of other structural elements than the Menshin bearings is taken into account by Rayleigh damping with the same method as described also in the preceding chapter.

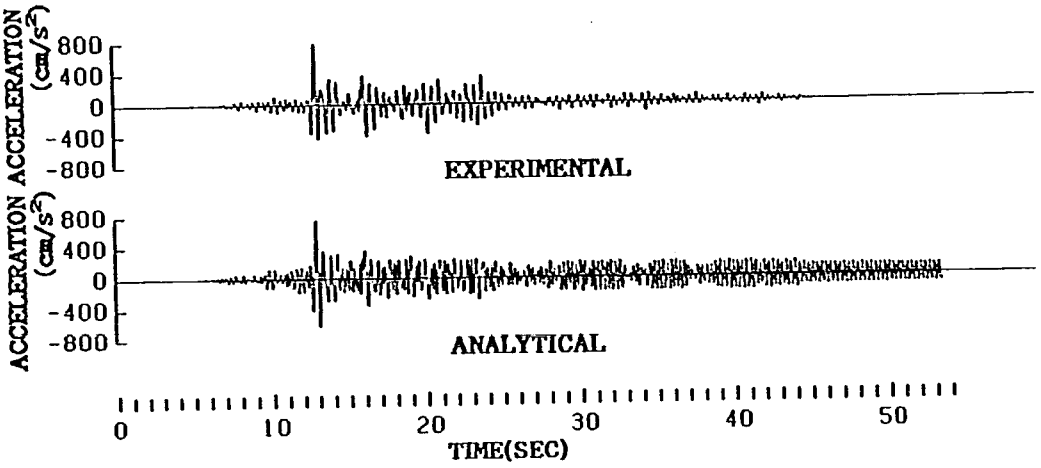
Figs. 23 and 24 compare the deck response acceleration and the response displacement of the bearing between the analysis and the experiments. The analysis can successfully simulate the effect of collision. Figs. 25, 26 and 27 show the hysteresis loops between the force transmitted to the columns and the relative displacement of the bearing. Sudden increase of the force when collision occurred can be realistically predicted by the analysis, although the effect of strain hardening of rubber can not be simulated in the analysis.

Table 5 compares the peak response of the analysis and the experiment. The accuracy of the analytical prediction expressed in terms of a ratio of the peak predicted response to the peak measured response ranges from 0.92 to 0.95 for the acceleration and from 1.03 to 1.16 for the displacement. They are quite sufficient.

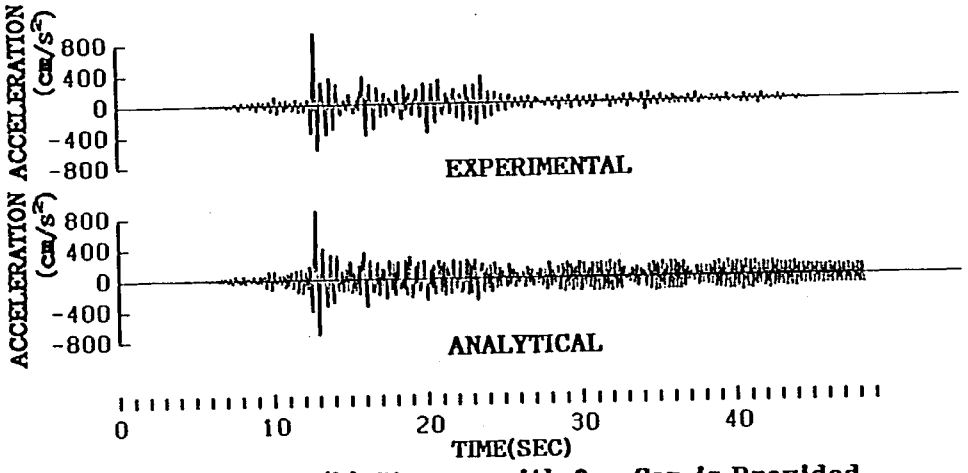
Table 5 Comparison between Experimental Analytical Deck Response

GAP SPACE	PEAK INPUT ACCELERATION (cm/s^2)	EXPERIMENT		SIMULATION	
		PEAK DECK RESPONSE ACCELERATION (cm/s^2)	PEAK DECK RESPONSE DISPLACEMENT (mm)	PEAK DECK RESPONSE ACCELERATION (cm/s^2)	PEAK DECK RESPONSE DISPLACEMENT (mm)
No Stopper	751.6	785.8	43.1	744.7 (0.95)	44.5 (1.03)
3 cm	768.6	937.4	39.1	891.9 (0.95)	44.0 (1.13)
2 cm	787.2	1023.1	35.7	936.8 (0.92)	41.4 (1.16)

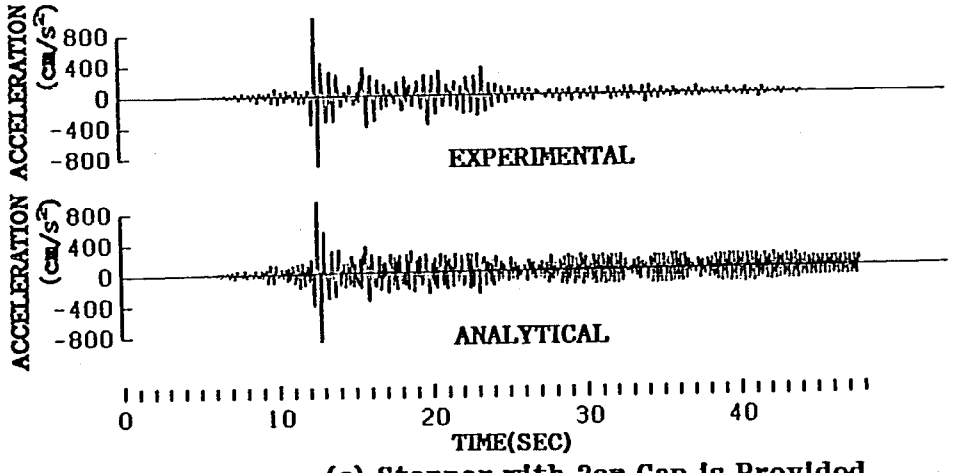
( ) Represents Ratio of Experimental to Analytical



(a) No Stopper is Provided

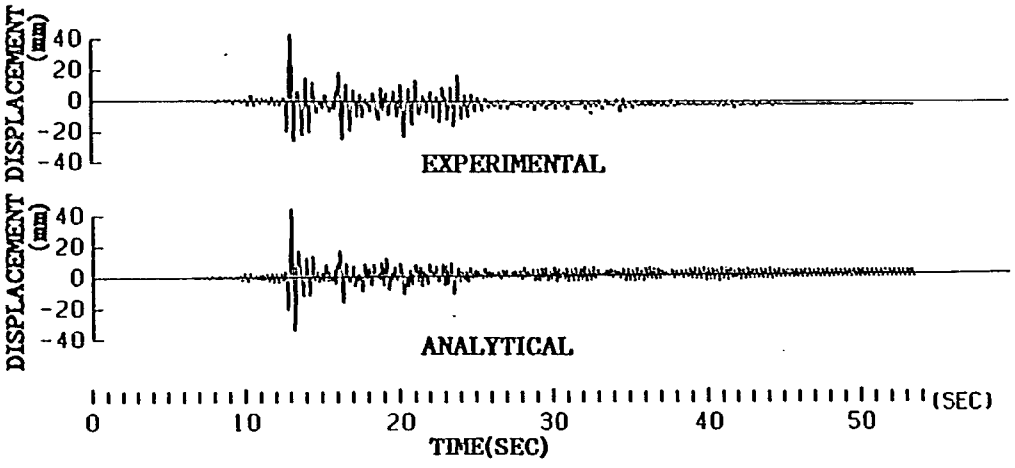


(b) Stopper with 3cm Gap is Provided

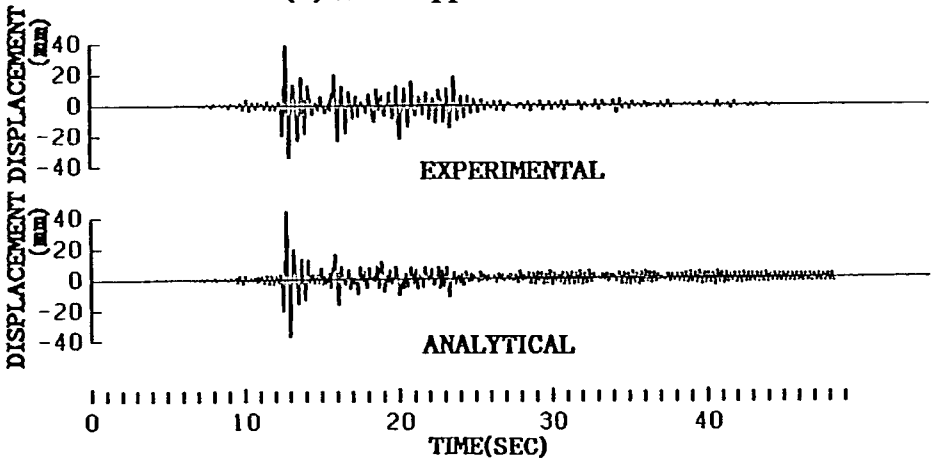


(c) Stopper with 2cm Gap is Provided

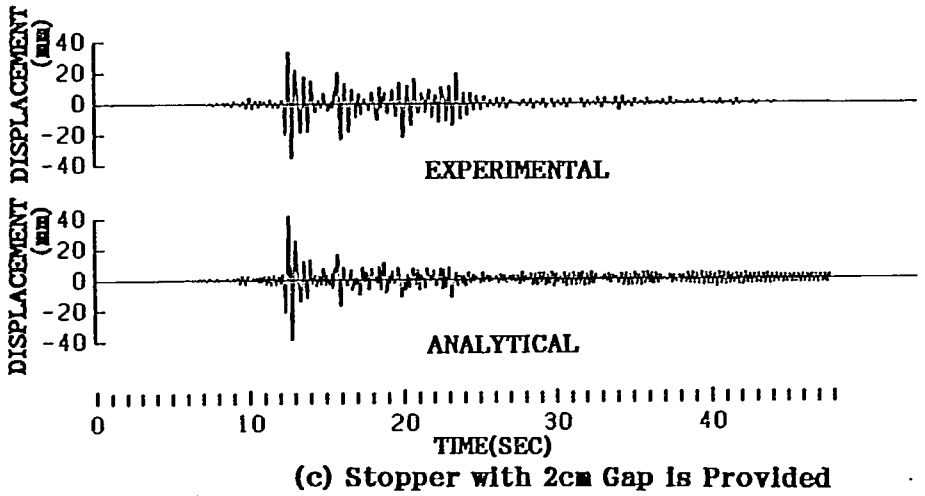
Fig.23 Comparison between Experimental and Analytical Deck Response Acceleration



(a) No Stopper is Provided



(b) Stopper with 3cm Gap is Provided



(c) Stopper with 2cm Gap is Provided

Fig.24 Comparison between Experimental and Analytical Deck Response Displacement

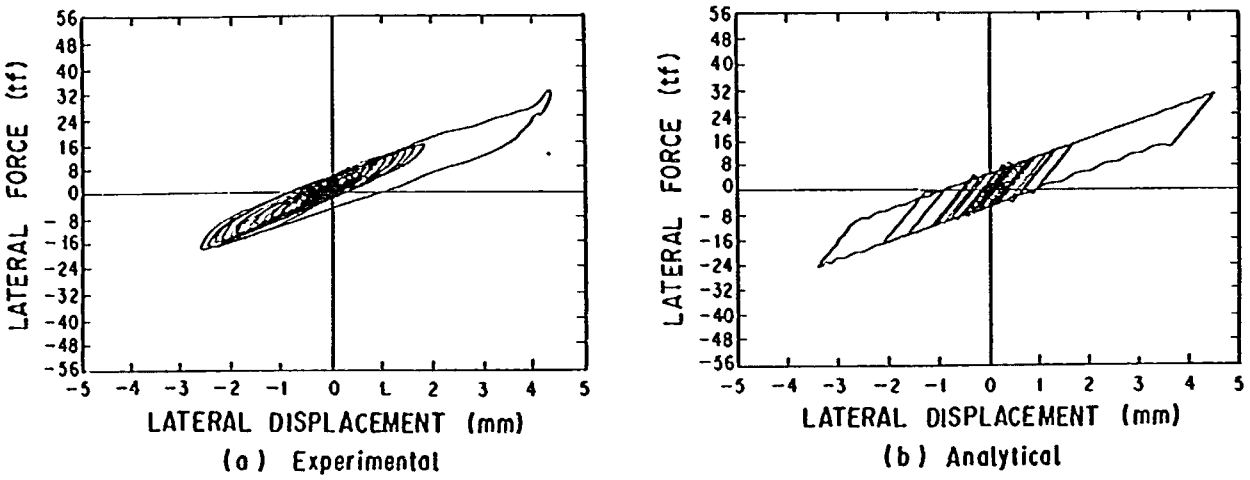


Fig.25 Hysteresis When No Stopper is Provided

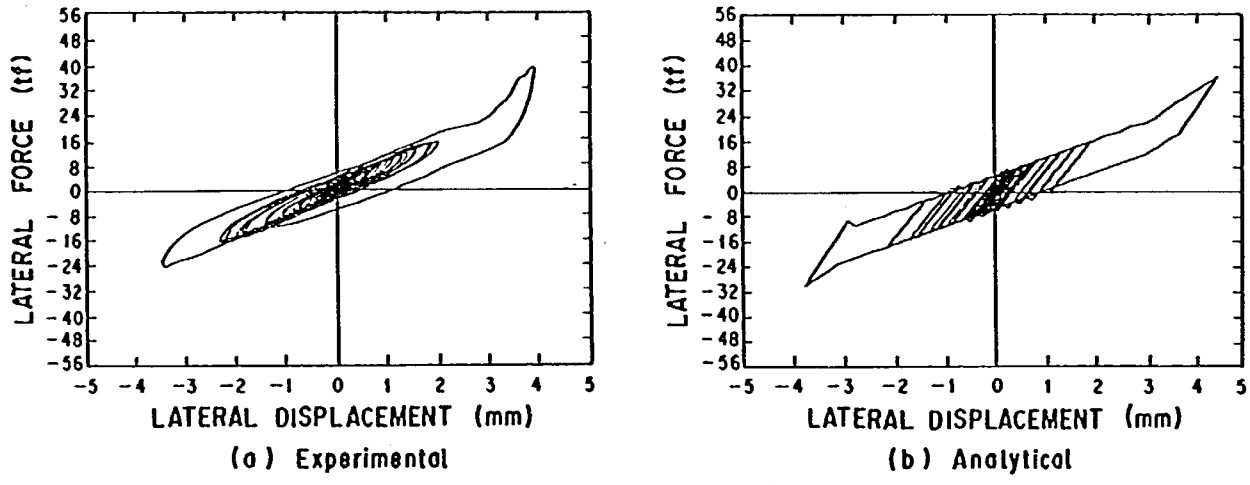


Fig.26 Hysteresis When Stopper with 3cm Gap is Provided

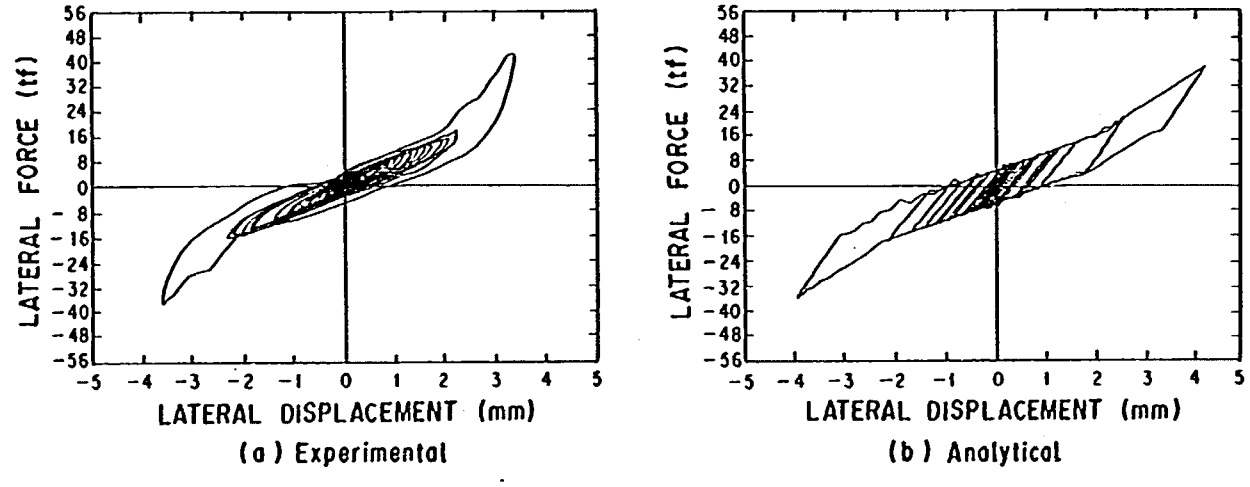


Fig.27 Hysteresis When Stopper with 2cm Gap is Provided

CONCLUSIONS

Response characteristics of two Menshin bridges were investigated through a series of shaking table tests. The response data of the model bridges were analyzed by the equivalent linear and bilinear analysis. The following conclusions may be deduced from the result presented herein.

1) The stoppers, which can effectively control the excessive relative displacement between the deck and the column, could develop great impact forces at the columns. Effect of such impact force needs to be considered in the Menshin design. The force and the displacement can be assessed by nonlinear dynamic analysis with the model of stoppers functioning as a linear spring only when the collision occurs.

2) Effect of vertical excitation is less significant to lateral response of the deck.

3) The response of the Menshin bridge can be successfully simulated by the equivalent linear analysis if the equivalent stiffness and the equivalent damping ratio are appropriately assumed in the analysis. The coefficient c in Eq. (1) is proposed to be assigned as 1.0 although the difference of the response by assuming c = 0.7 is small.

4) The response of the Menshin bridge can be successfully assessed by idealizing the nonlinear hysteretic behavior of the Menshin bearings with the bilinear model. The coefficient c_{NL} of 1.0 gives better result than c_{NL} of 0.7 to determine the initial stiffness, the post-yield stiffness and the characteristic load of the Menshin bearing.

ACKNOWLEDGEMENT

This study was achieved as a part of joint research program entitled "Development of Menshin System for Highway Bridges" between the Public Works Research Institute and 28 private firms. The shaking table tests shown in this paper were performed under the joint research program between the Public Works Research Institute and the Metropolitan Expressway Public Corporation. The authors express their sincere appreciation for their cooperation to proceed the research.

REFERENCES

1)Public Works Research Institute : Report of Joint Research between PWRI and 28 Private Firms on Development of Menshin Systems for Highway Bridges, Technical Report of Cooperative Research, No. 44 and No. 60, Public Works Research Institute, March 1990 and March 1991 (in Japanese)

2)Kawashima, K., Hasegawa, K., Yoshida, T., Yamauchi, H. and Kosaka, H. : Shaking Table Test on Dynamic Response of Base-isolated Bridges, Civil Engineering Journal, Vol. 30-10, pp. 521 - 526, October 1988 (in Japanese)

3)Kawashima, K., Hasegawa K. and Nagashima, H. : Seismic Response Analysis of a Base-isolated Bridge with an Equivalent Linear Analysis, Civil Engineering Journal, to be presented (in Japanese)

4)Buckle, I. G. and Mayes, R. L. : Seismic Isolation : History, Application, and Performance - A World View, Earthquake Spectra, Vol. 6, No. 2, pp. 161 - 202, May 1990
5)McKay, G. R., Chapman, H. E. and Kirkcaldie, D. K. : Seismic Isolation : New Zealand Applications, Earthquake Spectra, Vol. 6, No. 2, pp. 203 - 222, May 1990
6)Robinson, W. H. : Lead-rubber Hysteretic Bearings Suitable for Protecting Structures during Earthquakes, Earthquake Engineering and Structural Dynamics, Vol. 10, pp. 593 - 604, 1982
7)Tyler, R. G. and Robinson, W. H. : High-strain Test on Lead Rubber Bearings for Earthquake Loadings, Bull. New Zealand National Society for Earthquake Engineering, Vol. 17, No. 2, pp. 90 - 105, June 1984
8)Kojima, H. and Fukahori, Y., : Performance, Durability of High Damping Rubber Bearings for Earthquake Protection, Rubber World, Vol. 202, No. 1, April 1990
9)Japan Road Association : Design Specifications for Highway Bridges - Part V Seismic Design -, February 1990 (in Japanese)
10)Kawashima, K. : An Analytical Model of Contact and Impact in Dynamic Response Analysis, Proc. Japan Society of Civil Engineers, Vol. 308, pp. 123 - 126, April 1981

LOADING TEST OF SHIELD TUNNEL SPECIMENS SUBJECTED TO ALTERNATIVE AXIAL LOADING

by
Kazuhiko KAWASHIMA
Hideki SUGITA
and
Takashi KANOH

Public Works Research Institute
Ministry of Construction

FOURTH U.S. NATIONAL CONFERENCE
ON EARTHQUAKE ENGINEERING
Palm Springs
May 20 — 24, 1990

LOADING TEST OF SHIELD TUNNEL SPECIMENS SUBJECTED TO ALTERNATIVE AXIAL LOADING

K. Kawashima[I], H. Sugita[II] and T. Kanoh[III]

ABSTRACT

This paper presents a series of loading test results of shield tunnel specimens subjected to alternative tension and compression for studying deformation characteristics. Because shield tunnel is fablicated by assembling a number of segments and joints, it's stiffness is significantly nonlinear and the failure mode is sophisticated. Therefore, nonlinear deformation capability of shield tunnel is experimentally studied.

General failure patterns, effect of second lining for increasing the ductility and minimum longitudinal reinforcement required to avoid the concentration of failure are presented.

INTRODUCTION

In recent years, major parts of tunnel in city area for lifelines have been constructed by shield tunneling method. Development and improvement of tunnel boring method has made it possible to construct shield tunnel with a diameter as large as 14 m. Linings of the shield tunnel are constructed by assembling a number of segments and joints as shown in Fig. 1.

Shield tunnel has been adopted in city area where construction of open-cut tunnel can not be made due to various restriction derived from land use and existing structures on ground. It has been constructed in soft soil deposit. It is therefore one of the major technical importance in Japan to take account of seismic effects in design. Empirical knowledges on the seismic effects are insufficient, because shield tunnel has not yet experienced major earthquake.

Seismic design for pipe-like underground structures have been made by the seismic deformation method[1], in which the structure is idealized by an elastically supported beam, and is subjected to a assumed ground deformation. It is necessary to study the response of shield tunnnel from a different point of view from other pipe-like underground structures, due to the fact that stiffness of shield tunnel has significant nonlinearlity and that failure mode is complicated.

A comprehensive research for aiming to develop seismic design of shield tunnels was initiated at the Public Works Research Institute[2][3][4].

I Head, Earthquake Engineering Division, PWRI, Ministry of Construction
II Research Engineer, Earthquake Engineering Division, ditto
III Assistant Research Engineer, Earthquake Engineering Division, ditto

Because evaluation of discontinuous behavior in longitudinal stiffness and failure mode requires model test, a series of loading tests of shield tunnel specimens subjected to alternative tension/compression, bending, torsion have been made.

This paper presents a loading test result of shield tunnel specimens subjected to alternative tension and compression for studying deformation characteristics[5].

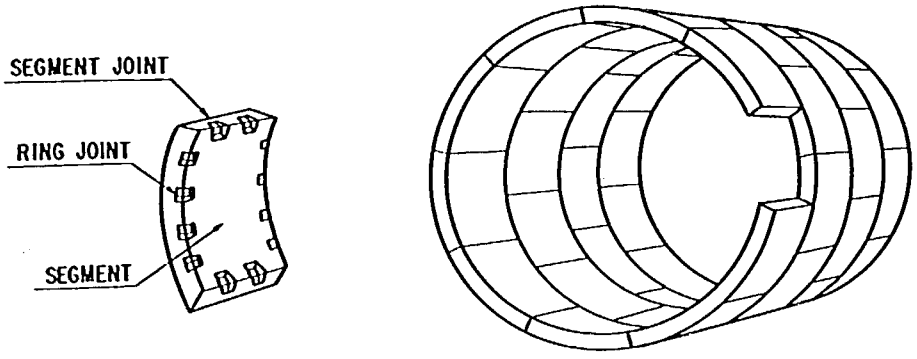


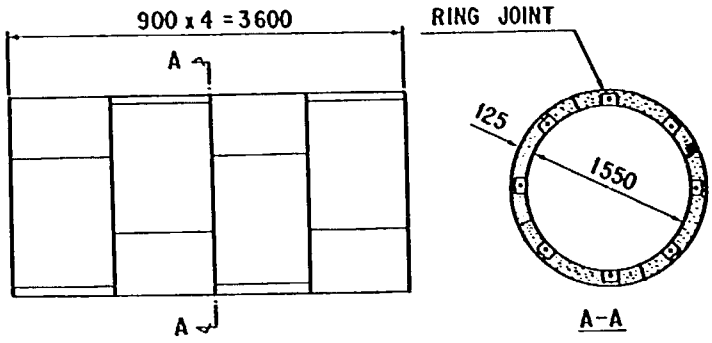
Fig. 1 Segment and Joint of Shield Tunnel Lining

SPECIMENS AND LOADING METHOD

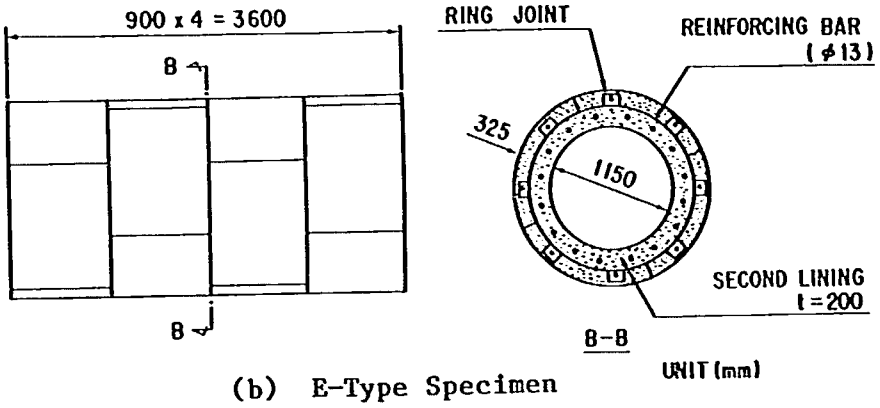
Two types of specimen were fablicated in accordance with the standard sewerage segments[6] as shown in Fig. 2. First-type specimen which is designated hereinafter as D-Type was made by assembling four reinforced concrete segments with 900 mm long and 125 mm thick in ring shape and by coupling the four rings in the tunnel axis. Second-type specimen which is designated as E-Type was made by placing reinforced concrete lining (second lining) with 200 mm thick inside the D-Type specimen. Reinforcement ratio of the second lining is 0.22% and 0.32% in peripheral and longitudinal direction, respectively.

Joint adopted for the test to connect segments is shown in Fig. 3. The joint connecting the segment in tunnel axis and in peripheral direction is referred here as a ring joint and segment joint, respectively (refer to Fig. 1). The joint is anchored to the segment by two anchor bars with a diameter of 10 mm (ring joint) and 13 mm (segment joint), and length of 300 mm. Adjacent joints are connected with joint bolt with 20 mm diameter. Prestressed force of 4.7 tf which is approximately 80% of yield strength is introduced in the joint bolts. Strength of segment concrete was 47.7 kgf/cm^2 and 573 kgf/cm^2 for tension and compression, respectively, and rupture stress of anchor bars for ring joint and segment joint was 4,920 kgf/cm^2 and 5,300 kgf/cm^2, respectively.

Fig. 4 shows the experimental set-up of specimen. One of the two end of specimen was fixed to the reaction wall, and the other end to the loading girder. Specimen was subjected to alternative tension and compression with two digital control dynamic actuators. It was assumed that the tunnel specimen was subjected to an axial deformation due to ground strain induced during an earthquake. Although there is confining pressure in peripheral direction due to water and soil pressure, it was disregarded in this test for simplicity. Loading hysteresis for D-Type specimen is presented in Fig. 5.

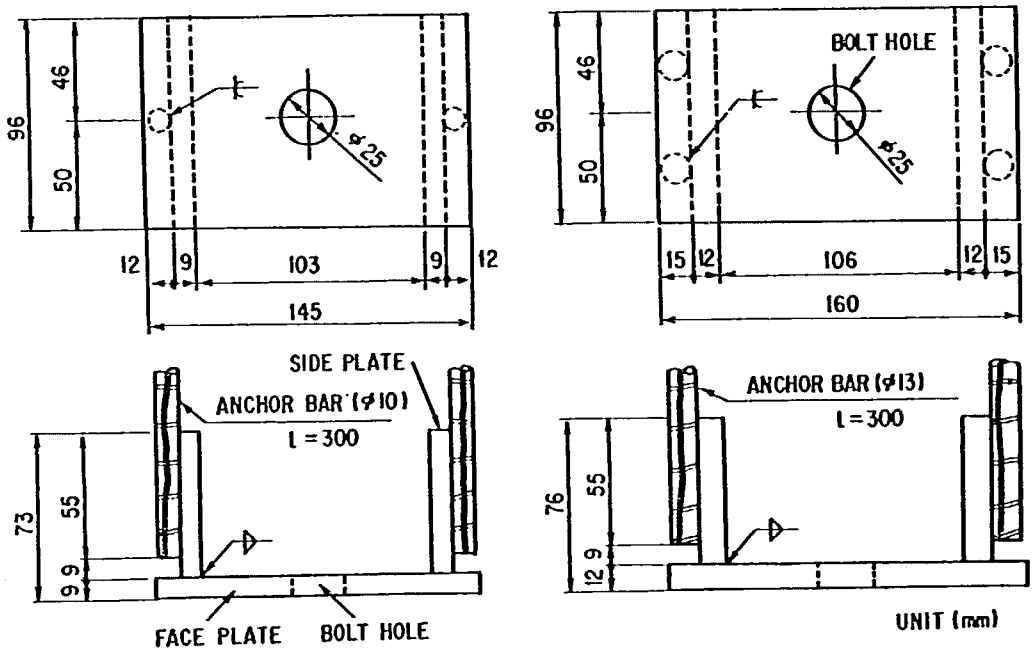


(a) D-Type Specimen



(b) E-Type Specimen

Fig. 2 Test Specimens



(a) Ring Joint

(b) Segment Joint

Fig. 3 Ring Joint and Segment Joint

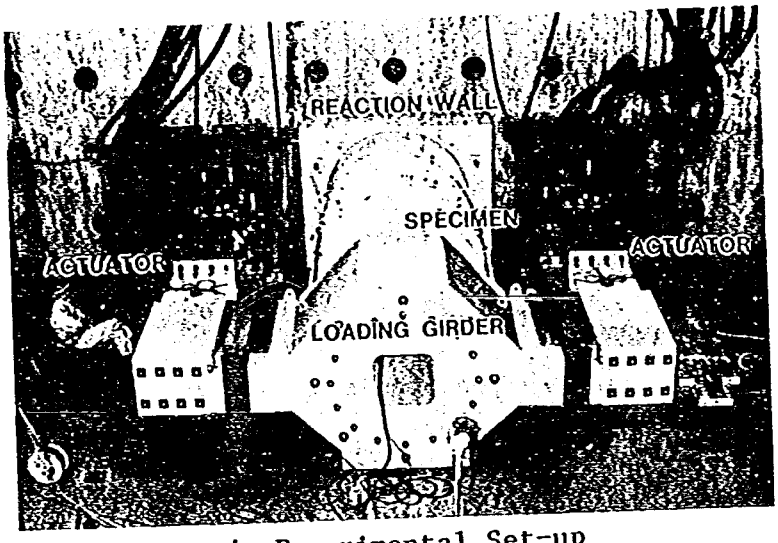


Fig. 4 Experimental Set-up

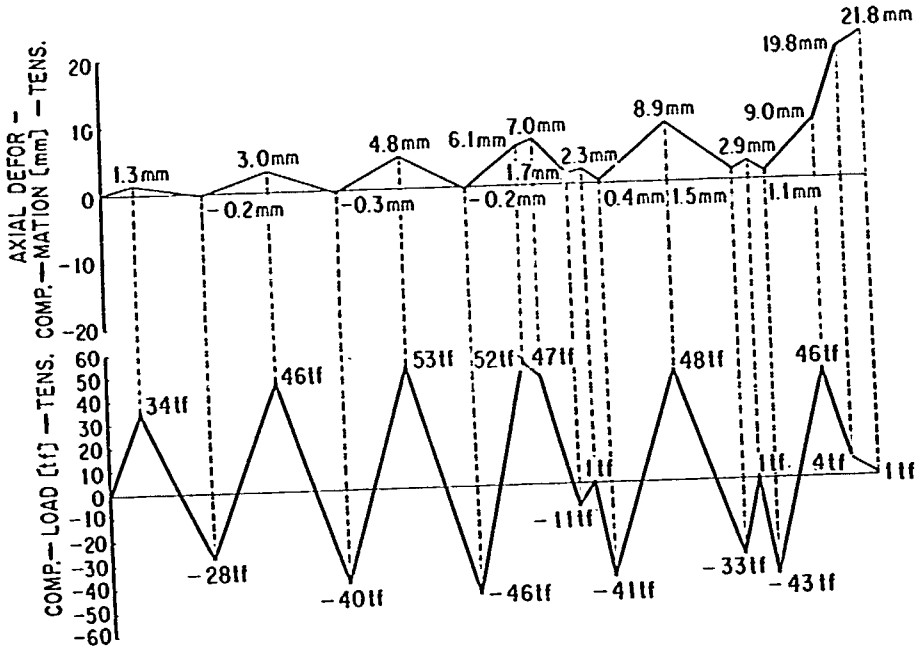


Fig. 5 Loading Hysteresis for D-Type Specimen

DEFORMATION CHARACTERISTICS OF D-TYPE SPECIMEN

Progress of failure

Fig. 6 shows a failure mode of the D-Type specimen after the loading. Damage concentrated only at the ring joint and surrounding concrete segment, and no damage was developed on the other parts in the specimen.

Hysteresis loop between loading force and axial deformation is shown in Fig. 7. Progress of failure was developed in the following order;

1) crack occurred around the ring joints,
2) face plate of ring joint started to yield,

3) loading force reached to the maximum,
4) yielding of anchor bars of ring joint started,
5) cracks started to occur outside the segment, and
6) rupture of anchor bars of ring joint occurred.

It should be noted in the progress of the failure that the deformation occurred almost uniformly among the three ring sections between steps 1) and 4). However, once cracks occurred at the concrete at the ring section (JT3, refer to Fig. 6), damage concentrated to this section to result the final rupture of anchor bars of the ring joints. This is considered very important for seismic design of shield tunnel where second lining is not provided.

Fig. 8 shows the failure mode of ring joint. Two anchor bars which connect side plate with the segment concrete ruptured at the end of the side plate. Because of U-shaped deformation of the face plate developed by tension at its center, anchor bars were subjected to bending moment as well as tension/compression. From such failure mode, it seems that restriction of the deformation of face plate seems effective to prevent the rupture of anchor bars, and thus to increase the strength and ductility of the shield tunnel.

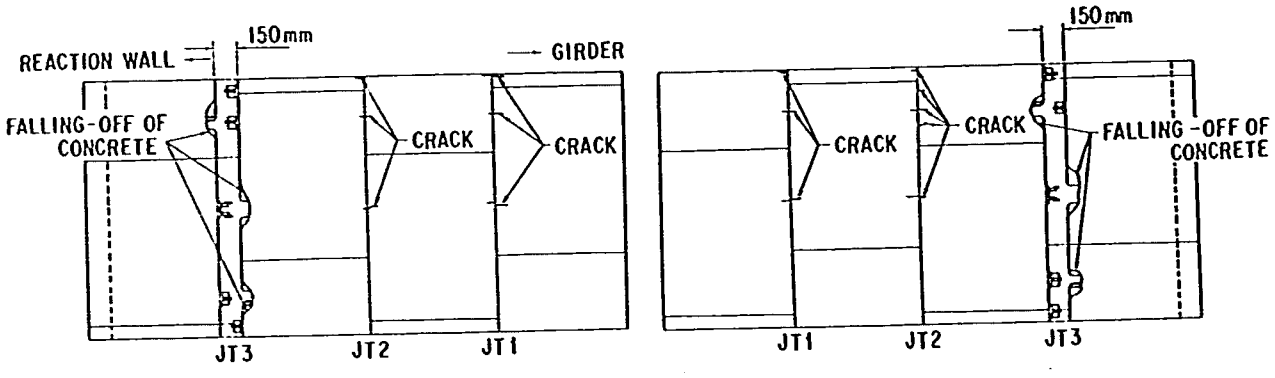


Fig. 6 Failure Mode of D-Type Specimen

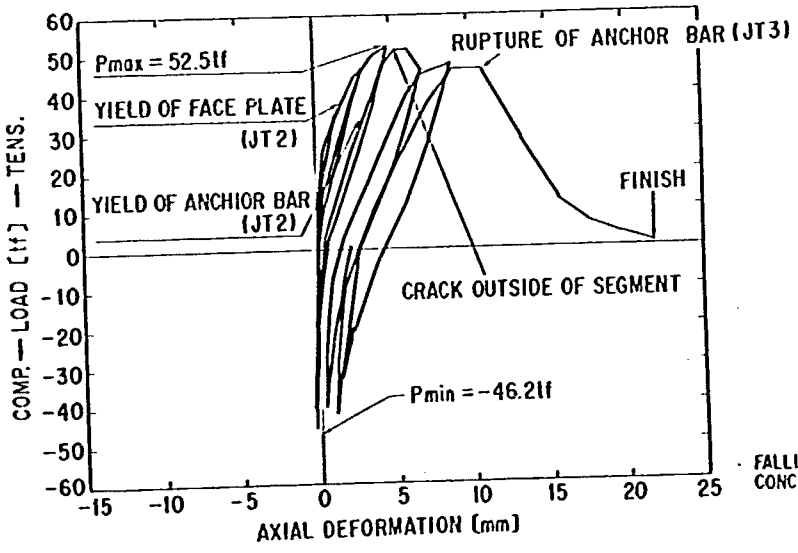


Fig. 7 Loading Hysteresis Loop of D-Type Specimen

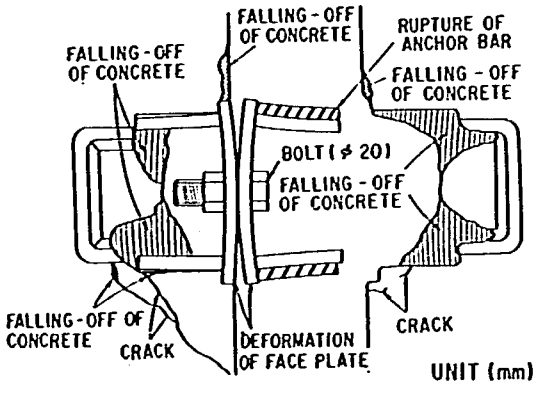


Fig. 8 Failure Mode of Ring Joint

Prestressed Bolt Force

Fig. 9 shows the hysteresis loop between loading force and force developed in one of the bolts of ring joints located at the right section (JT3, refer to Fig. 6). It should be reminded here that the prestressed force prior to loading is 4.7 tf. Because of the prestressed force, hysteresis of bolt force exhibits significant nonlinearity, i.e., when axial force is loaded to the ring joints tightened together with the ring bolt, the deformation of face plate developed by the prestresses force is released., so that the increment of axial force developed at the ring bolt is smaller than the increment of loading force. When the loading force increases to separate two adjacent face plates, the load charged to the recovery from deformation of face plates disappears. Therefore, the loading force directly acts to the bolt, so that the increment of axial force developed at bolt becomes equal to the increment of loading force.

It is interesting to note that axial force developed at the ring bolt gradually decreases in accordance with the progress of failure. The axial force of the bolt before the rupture of the anchor bars is 2.3 tf which is only 49% of the initial value of 4.7 tf.

Fig. 10 shows the hysteresis loop of axial force developed in one of the bolts of segment joints. The initial bolt force developed by the prestress prior to the loading did not decrease throughout the loading process. It means that the deformation of the segment in the peripheral direction was less significant. Because relative stiffness for inplane deformation at the shield tunnel constructed at site is much less than that of the specimen, inplane deformation capability subjected to seismic ground deformation has to be separately studied in the future.

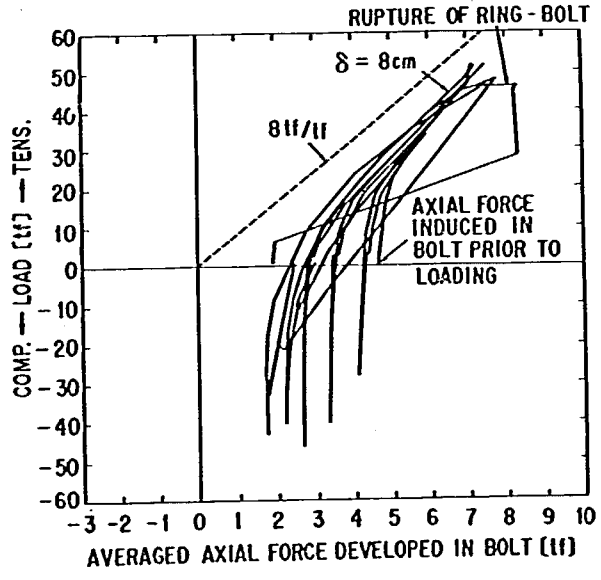


Fig. 9 Hysteresis Loop of Axial Force Developed in Ring-Bolt

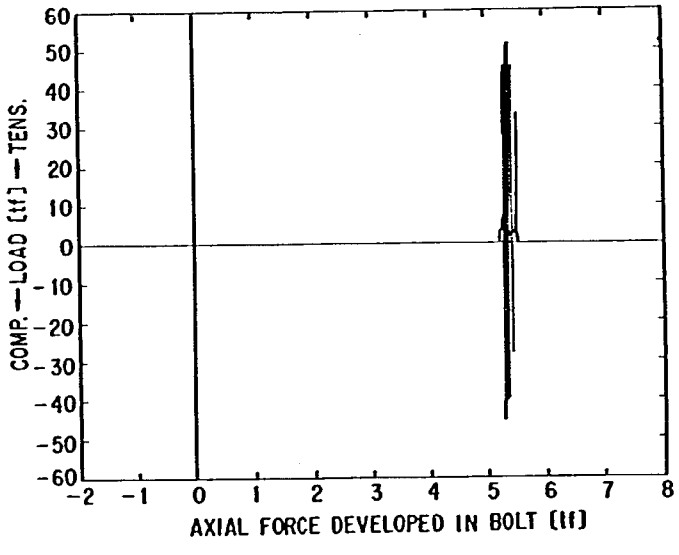


Fig. 10 Hysteresis Loop of Axial Force Developed in Segment-Bolt

DEFORMATION CHARACTERISTICS OF E-TYPE SPECIMEN

Fig. 11 and 12 show the failure mode of segments and second lining, respectively, of E-Type specimen. Although the specimen was loaded to develop the deformation as large as 100 mm, final rupture of the model was not developed.

It is apparent from Fig. 11 that even in the E-Type specimen, damage occurred only at the ring joints and surrounding segment/second lining, and no damage occurred on the other parts. It should be noted in Fig. 12 that initial cracks due to dry shrinkage and the deformation during set-up process of the specimen were observed on the second lining prior to the loading. However, although the cracks at the ring section progressed as load increased, cracks located at the other parts showed no change in their width.

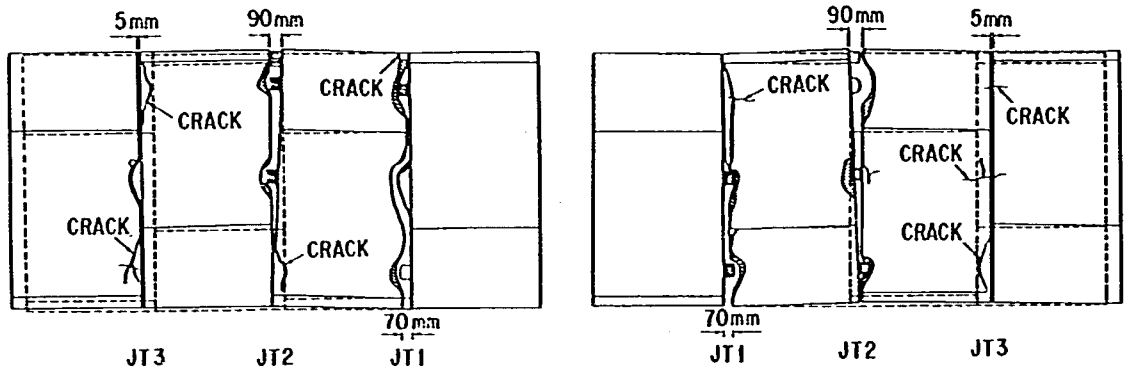


Fig. 11 Failure Mode of E-Type Specimen

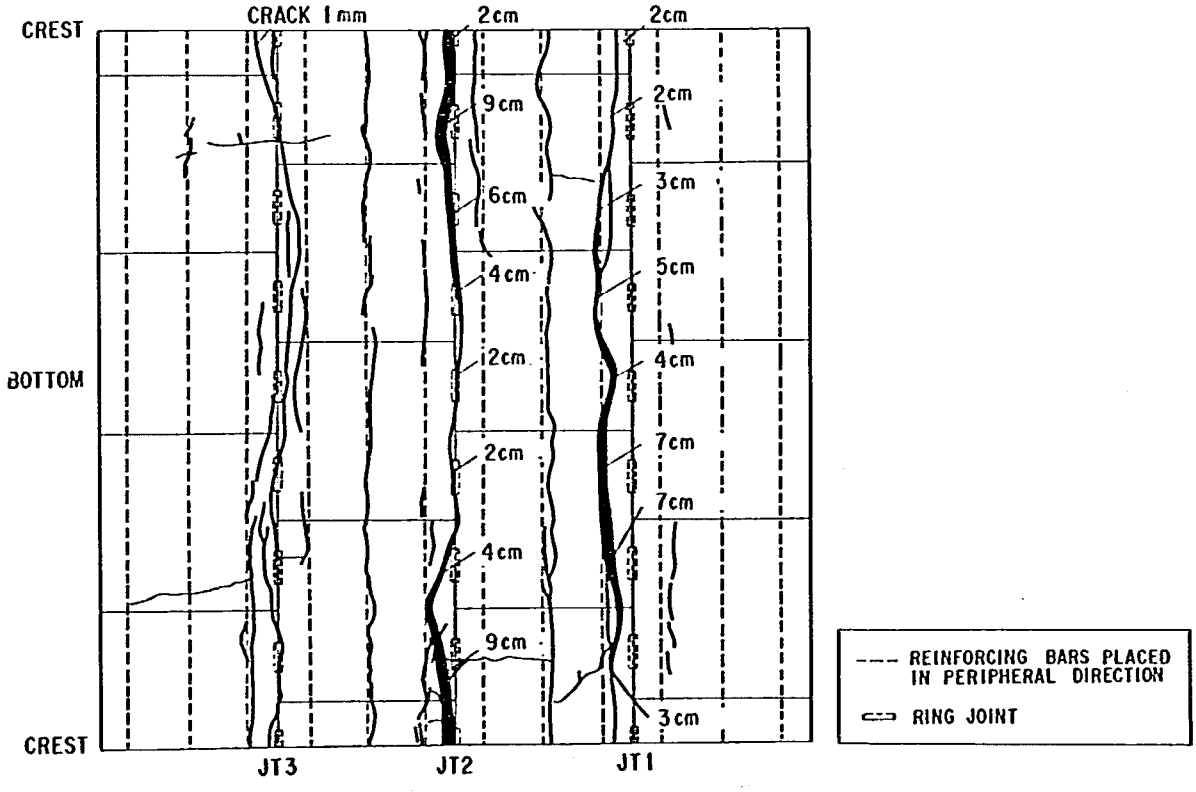


Fig. 12 Failure Mode of Second (Inner) Lining

Fig. 13 shows a hysteresis loop between loading force and axial deformation of the specimen. The failure process was in the following order;

1) cracks started to occur and increase on the second lining concrete only at the ring section,
2) reinforcing bars started to yield at the ring section where cracks of second lining were developed,
3) face plate of ring joint started to yield,
4) cracks occurred outside of the specimen at the ring section,
5) anchor bars of the ring joint started to yield,
6) loading force reached to the maximum,
7) rupture of the anchor bars of the ring joint initiated, and
8) rupture of the reinforcing bar of the second lining initiated.

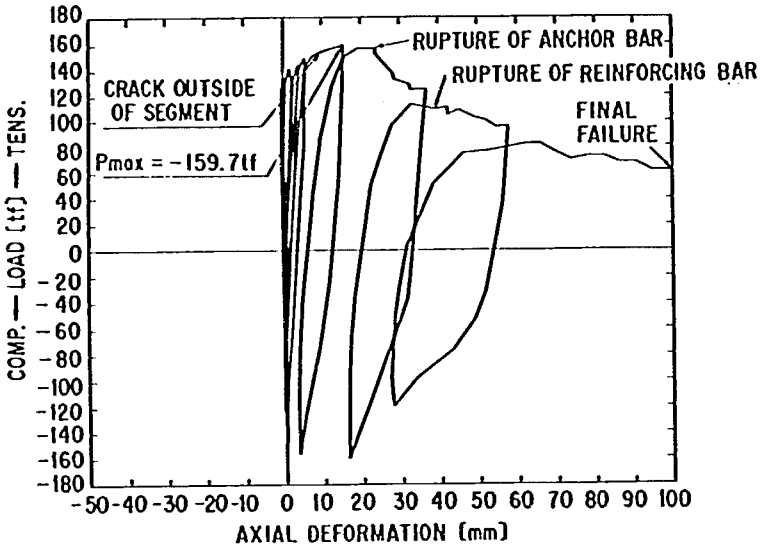


Fig. 13 Loading Hysteresis Loop of E-Type Specimen

In such progress of the failure, it should be noted that deformation at the ring section occurred almost uniformly among the three ring sections between steps 1) and 7). This is quite different from the D-Type specimen in which damage concentrated to one of the ring sections immediately after anchor bars of the ring joint started to yield followed by the cracks outside of the segment. Although cracks at outside of the segment (step 4) and yielding of anchor bars (step 5) occurred at one of the ring sections, the second lining prevents to concentrate failure at this ring section. The second lining is extremely effective to distribute the failure to all ring sections, provided that the reinforcing bars are arranged in the second lining as

$$A_{smin} > A_c \times \sigma_c / \sigma_s \qquad (1)$$

where

A_{smin}: minimum amount of reinforcing bars arranged into second lining in tunnel axis (cm^2)

σ_s : allowable stress of reinforcing bars taking account of stress increase for load combination of static load and seismic effect (kgf/cm^2)

A_c : sectional area of concrete of the second lining (cm^2)

σ_c : tensile strength of concrete of the second lining (kgf/cm^2)

Owning to the effect of the second lining, the specimen did not cause final rupture even for 100 mm loading displacement which is 4.5 times as large as the rupture displacement of the D-Type specimen.

Fig. 14 shows a hysteresis loop of the axial force developed at one of the ring bolts at left ring section (JT1 refer to Fig. 11). Although the prestressed tension of 4.7 tf was introduced in the ring bolt before the second lining was placed, it decreased to 2.7 tf at the initiation of the loading. It is interesting that the ring bolt force did not vary from the initial value until the cracks occurred at the ring section of the second lining. This means that all the loading force is charged to the second lining until the cracks occur in the second lining.

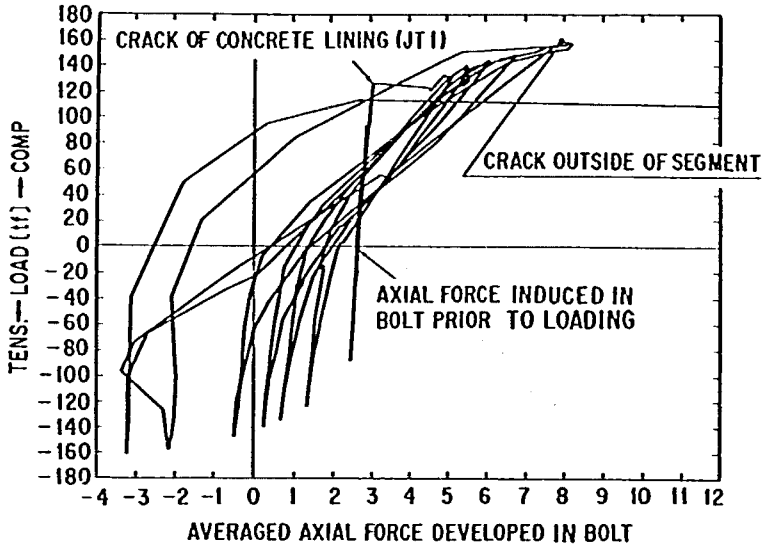


Fig. 14 Hysteresis Loop of Axial Force developed in Ring-Bolt

CONCLUSIONS

An alternative loading test was made on two shield tunnel models with and without second lining to study deformation capability and failure mode. From the results presented, the following conclusions may be deduced;

1) Major failure occurred only at ring section in both D-Type and E-Type specimens. Study on the behavior of ring section consisted of anchor bolt, ring plate, ring joint and segments is essentially importance for seismic design.

2) In the D-Type specimen, the final failure occurred as a direct result of rupture of anchor bars of ring joints. Such a final failure is

likely to be developed exclusively at one of the ring sections where a certain degree of damage such as cracks of segment lining firstly occurs.

3) In the E-Type specimen, the final failure occurred after rupture of both reinforcing bars in the second lining and anchor bars of the ring joint was developed. The failures are distributed to all ring sections, and no concentration of failure to a specific ring section, which was observed in the D-Type specimen, was developed. Tunnel deformation developed up to the final failure is at least 4 times as large as that of D-type specimen. For preventing the concentration of the damage to a certain ring section, it is extremely effective to place the reinforcing bars in the second lining so that tension force charged to second lining concrete be alternatively supported by the reinforcing bars.

REFERENCES

1) Kuribayashi, E., Iwasaki, T. and Kawashima, K.: Dynamic Behavior of A Subsurface Tubular Structures, Bull. New Zealand National Society of Earthquake Engineering, Vol.7, No.4, pp. 200-209, 1974.12

2) Kawashima, K., Obinata, N., Kanoh, T. and Shiba, Y.: Experimental Study on Seismic Resistance of Reinforced Concrete Lining of Shield Tunnel, 9th WCEE, Tokyo/Kyoto, Japan, 1988.8

3) Shiba, Y., Kawashima, K., Obinata, N. and Kanoh, T.: An Evaluation Method of Longitudinal Stiffness of Shield Tunnel Lining for Application to Seismic Response Analysis, Structural Eng./Earthquake Eng., Proc. JSCE, No.398/I-10, 1988.10

4) Shiba, Y., Kawashima, K., Obinata, N. and Kanoh, T.: Evaluation Procedure for Seismic Stress Developed in Shield Tunnels Based on Seismic Deformation Method, Structural Eng./Earthquake Eng., Proc JSCE, Vol.404/I-11, 1989.4

5) Kawashima, K., Sugita, H. and Kanoh, T.: Development of Seismic Resistant Design Procedure of Shield Tunnels (Part 5), Technical Note of Public Works Research Institute, No.2649, 1988.7

6) Japan Society of Civil Engineering and Japan Sewage Works Association, Standard Segment for Shield Tunnels, 1973.

EVALUATION OF INDIRECT ECONOMIC EFFECTS CAUSED BY THE 1983 NIHONKAI-CHUBU, JAPAN, EARTHQUAKE

by
Kazuhiko KAWASHIMA
and
Takashi KANOH

Earthquake Spectral
Vol. 6, No. 4, 1990

6.

Evaluation of Indirect Economic Effects Caused by the 1983 Nihonkai-chubu, Japan, Earthquake

Kazuhiko Kawashima, M.EERI, and Takashi Kanoh

Effects of an earthquake are not necessarily restricted to damage of structures, but extend much further. This paper presents a method for estimating indirect economical effects caused by an earthquake. Loss of production may be caused by a decrease of products due to damage of production, damage of transportation facilities, and damage of materials and goods. Effect of investment for restoration is also considered. Based on direct loss associated with production loss, a secondary "ripple" effect was estimated through an inter-industry relation analysis (input-output analysis). The procedure was applied to the Nihonkai-chubu, Japan, Earthquake of 1983. Estimated gross products at the damaged region agreed fairly well with those actually observed after the earthquake.

INTRODUCTION

Damage due to earthquakes has been evaluated mostly in terms of damages associated with failure of facilities and structures. However, effects of an earthquake are not necessarily restricted to such physical damages but may include much wider aspects, such as loss of production due to suspension of production, decrease of consumption due to decreased social activities, etc. Losses associated with such effects would be much greater and more widespread than those counted only from physical failures. However, mechanism of economic losses induced by an earthquake is so complicated that little is known about the effects.

This paper presents an evaluation of indirect economical effects caused by the Nihonkai-chubu, Japan, Earthquake of 1983, based on an inter-industry relation analysis (input-output analysis).

EFFECTS OF AN EARTHQUAKE ON ECONOMIC LOSSES

(KK) Head, Earthquake Engineering Division, Earthquake Disaster Prevention Department, Public Works Research Institute, Tsukuba Science City, Japan
(TK) Assistant Research Engineer, Earthquake Engineering Division, ditto

©Earthquake Spectra, Vol. 6, No. 4, 1990

Economic losses associated with an earthquake may be evaluated based on a decrease of products within a region. An amount of products $G_0(t)$ within a region after an earthquake may be defined, and evaluated as

$$G_0(t) = G_N(t) - G_D(t) + G_R(t) \quad (1)$$

in which $G_N(t)$: products which were supposedly achieved at t fiscal year in a region if an earthquake had not taken place, $G_D(t)$: a decrease of products in a region due to the earthquake damages, $G_R(t)$: an increase of products in a region due to investments for restoration.

Consequently, it may be possible to evaluate $G_0(t)$ if $G_N(t)$, $G_D(t)$ and $G_R(t)$ are appropriately evaluated. If one prefecture is regarded as a region for evaluating the economic losses, the products $G_0(t)$ can be obtained in a form of gross prefectural products. Because Japan consists of 47 prefectures, prefecture may be an appropriate unit to express local activities. However, because the gross prefectural products describe only final products achieved in a prefecture, detailed economic effects caused by an earthquake can not be traced. Therefore, it is required to develop an analytical method for clarifying economic effects of an earthquake.

There are a number of aspects which may be regarded as economical effects induced by an earthquake. They may be classified as shown in Table-1, in which losses of facilities, properties, goods and materials are generally evaluated through damage surveys conducted by industries and regional governments following an earthquake. As an effect of earthquake damage, following decreases of products are considered.

- decrease of products due to damage of facilities for production
- decrease of products due to damage of transportation facilities
- decrease of products due to damage of materials and goods

Considering the three types of damage, economic effects of an earthquake may be evaluated in accordance with a flow chart shown in Fig.1. A reduction factor α_i which represents a degree of reduction of products of i-th industry due to an earthquake is defined here as

$$\alpha_i = \Delta X_i / X_{iN} \quad (2)$$

in which ΔX_i and X_{iN} represent a decrease of yearly products of i-th industry due to an earthquake and yearly products supposedly developed in i-th industry if the earthquake had not taken place, respectively.

EVALUATION OF ECONOMICAL LOSSES CAUSED BY AN EARTHQUAKE

Although the reduction factor of products can be estimated independently for the three types of damage, inter-relation between the three types of damage has to be taken into account. Because the products for i-th industry are likely to be affected by the most critical damage among the three types of damages, the decrease of products for i-th industry ΔX_i is assumed here to be evaluated as

Table-1 Classification of Earthquake Effects

Classification	Objective and/or Form of Damage	Effects of Loss and/or Damage
Human Life	Death, Injury	Loss of man power, Mental effects
Facilities for Living	House, Educational Facilities, Hospitals, etc.	Functional loss for Daily Human Activities
Facilities for Production	Cultivate Field, Non-Residential House (Factory, Shops), etc.	Decrease of Production, Loss of Products
Lifeline Facilities	Electricity, Telecommunication, Gas, Water and Sewage, Trash	Decrease and/or Loss of Capability for Production
Transportation Facilities	Road, Bridge, Port, Rail-way	Decrease of Production due to Decrease of Transportation Capability for Material and Products Decrease of Production due to Decrease of Transportation Capability for Passengers
Public Works Excluding Transportation Facilities	River, Sabo-works, Slope Failure	Damage associated with Failure
Transportation Media	Trucks, Buses, Trains, Ships	Decrease of Production due to Decrease of Transportation Capability
Manufactured Goods, Partially Manufactured Goods	Loss of Manufactured and/or Partially Manufactured Goods	Decrease and/or Loss of Value of Goods, Decrease of Products due to Loss of Manufactured and/or Partially Manufacture Goods

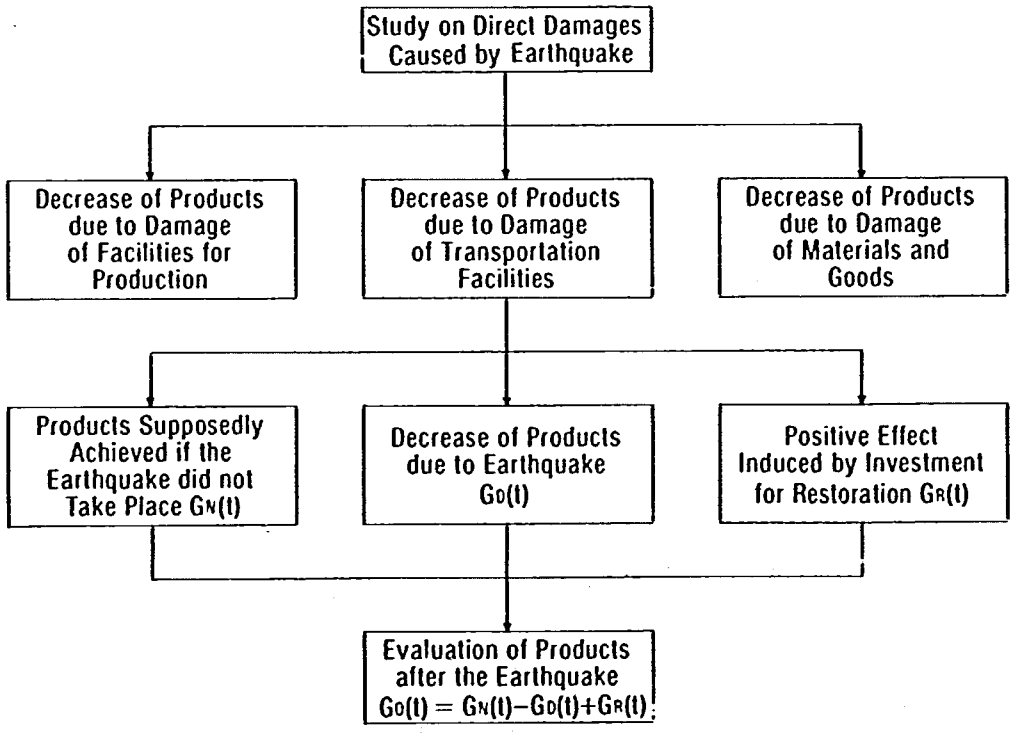


Fig.1 Evaluation of Economic Effects of Earthquake

$$\Delta X_i = X_{iN} \cdot \alpha_{max} \tag{3}$$

in which α_{max} represents the maximum reduction factor among the three reduction factors which are evaluated independently for the damage of facilities for production, for the damage of transportation facilities, and for the damage of materials and goods. X_{iN} represents the products supposedly developed in i-th industry if an earthquake had not occurred.

Besides such decrease of products in i-th industry, productions of other industries which depend on the products of i-th industry would also decrease, even if their facilities suffered no direct damages by the earthquake. This effect is designated in this study as a first effect, and is analyzed through an inter-industry relation analysis.

An inter-industry relation table has a form of Table-2 in which I_i represents i-th industry. The relation may be written as[1]

$$\underline{A} \cdot \underline{X} + \underline{F} = \underline{X} \tag{4}$$

where

$\underline{A}$: input coefficient matrix

$\underline{X}$: products vector, and

$\underline{X} = \{ X_1, X_2, \ldots\ldots, X_n \}^T$

$\underline{F}$: final demand vector, and

$\underline{F} = \{ f_1, f_2, \ldots\ldots, f_n \}^T$

Table-2 Inter-industry Relation Table (Input-output Table)

Purchase / Sell		Intermediate Demand			Final Demand	Products
		I_1 I_2	I_i	I_j		
Intermediate Sales	I_1 I_2 ⋮					
	I_i	.....	X_{ij}		f_i	X_i
	I_j	.....	X_{ji}		f_j	X_j
Gross Value Added		.....	V_i	V_j		
Products		.....	X_i	X_j		

Coefficient X_{ij} of a matrix $\underline{A} \cdot \underline{X}$ of Eq.(4) represents products used from I_i to I_j, or an amount paid from I_i to I_j, and X_i and f_i represent the products and final demand of I_i, respectively.

When an amount of $\alpha_i (0 \leq \alpha_i \leq 1)$ of the products X_{iN} of i-th industry becomes unusable due to an earthquake, such an effect may be considered in the analysis by substituting X_{ij} and f_i on i-th line of the inter-industry relation table with $(1-\alpha_i)X_{ij}$ and $(1-\alpha_i)f_i$, respectively. It should be noted here that even if j-th industry did not suffer damages from the earthquake, the products of j-th industry decreases from X_{jN} to $(1-\alpha_i)X_{jN}$. Similarly, when an amount of $\alpha_k (0 \leq \alpha_k \leq 1)$ of the products in k-th industry suffered damage, it also makes the products of j-th industry decrease

from X_{jN} to $(1-\alpha_k)X_{jN}$.

Therefore, when products decrease in industries i and k simultaneously, both would influence the production of j-th industry. Although interactions of the decrease of products between various industries are quite complex, it is assumed here that the decrease of products in j-th industry is affected by either I_i or I_k which gives a larger reduction factor. Decrease of products ΔX_j in j-th industry is, then, assumed as

$$\Delta X_j = X_{jN} \cdot \max(\alpha_i, \alpha_k \mid X_{ij} \neq 0, X_{kj} \neq 0) \quad (5)$$

Decrease of product $\Delta \underline{X} = \{\Delta X_1, \Delta X_2, \ldots\ldots, \Delta X_n\}^T$ is called here as a first effect.

To represent a decrease of income and consumption, a decrease of products on gross value added basis is often used. Decrease of products on gross value added basis $\Delta \underline{V}$ is generally obtained from $\Delta \underline{X}$ by

$$\Delta \underline{V} = \Delta \underline{X}^T \cdot \underline{v} \quad (6)$$

in which $\underline{v}$ represents a gross value added ratio matrix, which is generally assumed as a diagonal matrix consisting of gross value added ratios. The gross value added ratios are generally evaluated for each industry by prefectures. To distinguish $\Delta \underline{X}$ from $\Delta \underline{V}$, $\Delta \underline{X}$ is referred hereinafter as a decrease of products on product basis.

Decrease of income and operating profit in the gross value added $\Delta \underline{V}$ given by Eq.(6) would cause further decrease of products, because they were to be used to produce products in a form of consumption and formation of fixed assets. Such an effect is defined here as a second ripple effect. To evaluate the second ripple effect, the decrease of final demand vector $\Delta \underline{F}_S$ associated with the decrease of income and operating profit has to be obtained. Empirical formulae based on relations between consumption vs. income and operating profit are assumed for computing the final demand. The second ripple effects may then be evaluated from Eq.(4) as

$$\Delta \underline{X}_S = (\underline{I} - \underline{A})^{-1} \cdot \Delta \underline{F}_S \quad (7)$$

$$\Delta \underline{V}_S = \Delta \underline{X}_S^T \cdot \underline{v} \quad (8)$$

in which, $\Delta \underline{X}_S$: second ripple decrease of products on product basis, $\Delta \underline{V}_S$: second ripple decrease of product on the gross value added basis, and $\underline{v}$: the gross value added ratio matrix.

One point to be noted in the application of the inter-industry relation analysis for evaluating the economic effect of an earthquake is that the inter-industry relation defined by Eq.(4) is assumed constant during the year considered in the analysis. Although the confusion of economic activities would be gradually recovered with time after an earthquake, the process of recovery can not be considered in this analysis.

Repair and restoration after an earthquake may consist of expenditures for purchasing materials and goods for restoration. Such expenditures give

a positive impact on various industries, which, in turn, develops a ripple effect. The ripple effects caused by such a positive impact may be analyzed by the standard inter-industry table analysis by introducing the investment for restoration to the final demand vector. Analytical procedure is the same as described above.

APPLICATION TO THE NIHONKAI-CHUBU EARTHQUAKE OF 1983

Brief Description of The Nihonkai-chubu Earthquake

The Nihonkai-chubu earthquake occurred approximately 90 Km offshore of the Akita prefecture at 12:00 noon on May 26, 1983. It had an earthquake magnitude of 7.7 and a focal depth of 5 Km. Fig.2 shows a distribution of JMA (Japan Meteorological Agency) seismic intensity scale as well as the approximate aftershock area, 60 Km by 120 Km in east-west and north-south

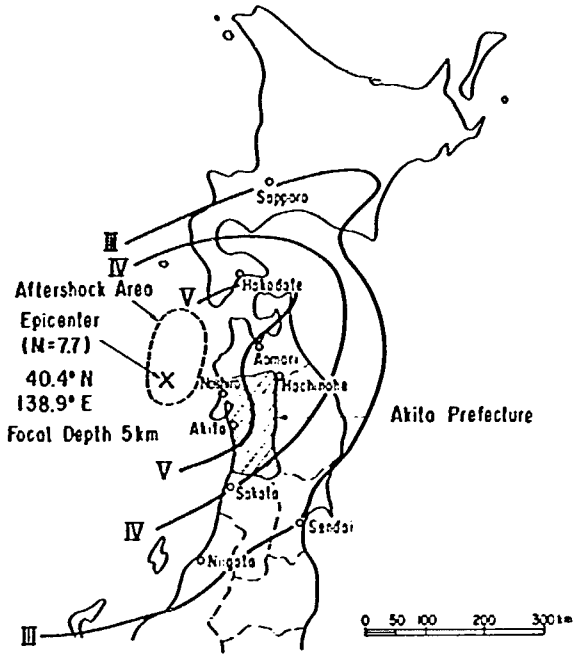


Fig.2 Distribution of Seismic Intensity
(Japan Meteorological Agency's Scale)

directions, respectively. The JMA intensity of III, IV and V is generally referred as the peak ground acceleration of 0.008g~0.025g, 0.025g~0.08g, and 0.08g~0.25g, respectively. Fig.3 shows peak accelerations (cm/sec^2) measured with strong motion accelerographs installed on ground surface and on structures[2),3)]. The largest peak ground acceleration was about 0.4g recorded at a site near the Nanamine Bridge at the Hokkaido.

Extensive damage resulted from the earthquake. Table-3 summarizes the damage statistics in the Hokkaido, Aomori, Akita and other prefectures[4)].

The most extensive damage occurred in the Akita prefecture, where 83 persons were killed and 265 were injured.

Table-4 shows the direct damage in the Akita prefecture. Total amount of the damage is 145.7 billion yen in the 1983 price (1 U.S. dollar = 235 yen in 1983 exchange rate). This corresponds to 6.5% of the gross prefectural products of the Akita prefecture (2,272.8 billion yen). Because of

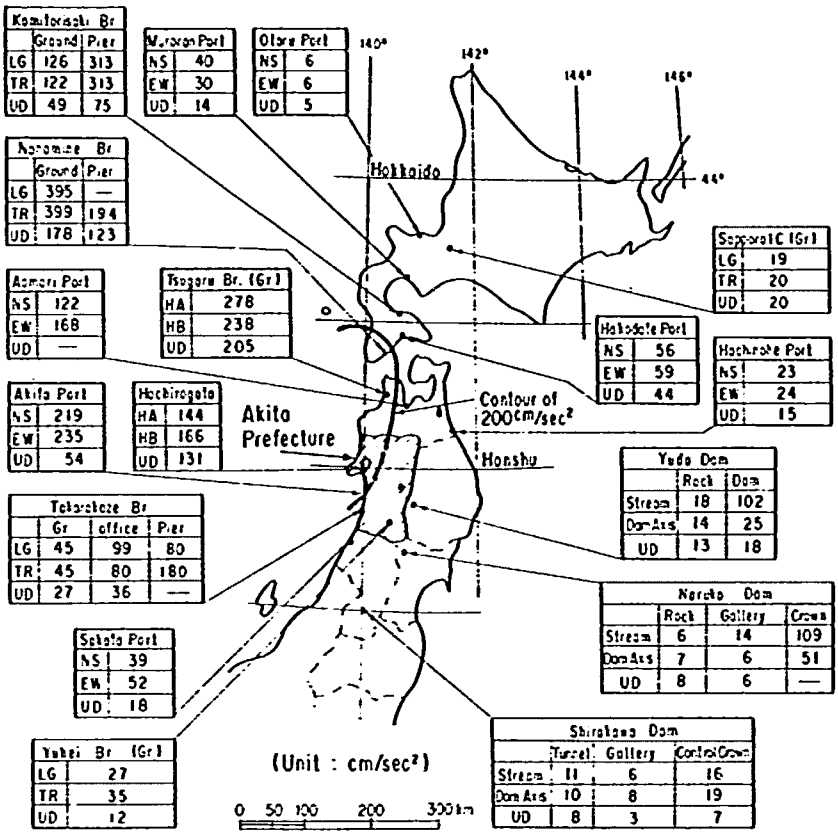


Fig.3 Peak Accelerations Measured with Strong Motion Accelerographs

Table-3 Damage Statistics by the Nihonkai-chubu Earthquake

	Category	Unit	Hokkaido	Aomori	Akita	Others	Total
Human Damage	Fatality	Person	4	17	83		104
	Injury	Person	24	25	265	10	324
Damage of facilities	Highway	Site	3	702	670	4	1.379
	Bridge	Bridge		48	84	1	133
	River	Site	3	243	196	3	445
	School	School	70	370	272	44	756
	Ship	Ship	637	853	681	480	2.651
	Water Supply	Household	770	17.399	22.187	46	40.402
	Electricity	Household	2.200	19.840	17.563	563	40.166
Damage of residential houses	Complete Failure	House	5	447	1.132		1.584
	Partial Failure	House	85	3.883	5.489	2	9.457

Table-4 Direct Damage in Akita Prefecture (Billion Yen)

Type	Classification	Damage	Type	Classification	Damage
Damage of Facilities	Agricultural Facilities	24.48	Damage of Materials and Goods	Agriculture	2.41
	Fishery Port Facilities	1.49		Livestock	0.01
	Marine Facilities	4.20		Forestry	0.40
	Forestry Facilities	5.56		Commerce	1.34
	Commercial Facilities	2.93		Industry	3.44
	Industrial Facilities	4.92		Other Commerce and Industry	0.71
	Other Commercial and Industrial Facilities	2.267	Total		145.74
	Public Works	59.25			
	Other Public Works	3.96			
	House	26.67			
	Educational Facilities	1.73			

the significance of the damage, the economic losses in the Akita prefecture due to the Nihonkai-chubu Earthquake is analyzed in the following.

Decrease of Products due to Damage of Facilities for Production

Direct damage of facilities and properties for production was surveyed by private and regional government bodies in the Akita prefecture, and the data for agriculture, forestry, fisheries, manufacturing industries, wholesale and retail are available[4]. Among these damages, only decrease of products associated with damages of forestry is disregarded in this analysis because of difficulty to evaluate products vs. properties relation.

A reduction factor for agricultural products was estimated through an unit product model. Agricultural products per unit cultivated area were estimated by regressing the data between 1970 and 1981 as

$$U = 14.1 - 0.217 \times (t - 1925) \qquad (R = 0.95) \qquad (9)$$

in which U : agricultural products per unit cultivated area(million yen / ha), t : year($1970 \leq t \leq 1981$), and R : a regression coefficient. The agricultural products per unit cultivated area U in 1983 are estimated by an extrapolation of Eq.(9) as 1.56 million yen/ha.

On the other hand, total cultivated area in 1983 in the Akita prefecture is estimated as 162,329 ha, and a cultivated area of 3,139 ha is reported damaged by the earthquake. Therefore assuming that the damaged area could not be used for agricultural products in 1983, agricultural products at this year X_{AE} may be estimated as

$$X_{AE} = U \times (162,329 - 3,139) = 248,687 \text{ (million yen)} \qquad (10)$$

Similarly, the agricultural products X_{AN}, which would be possibly developed in 1983 if the Nihonkai-chubu Earthquake had not occurred, are estimated as 1.56 x 162,329 = 253,591 million yen.

Therefore substituting X_{AE} and X_{AN} into Eq.(2), one obtains the reduction factor α_A for agriculture as

$$\alpha_A = (X_{AN} - X_{AE}) / X_{AN} = 1.9\ \% \quad (11)$$

Fisheries facilities suffered severe damage by tsunami, in the amount of 4,195 million yen. Based on fisheries products per unit fisheries capital stock, the reduction factor α_F for fisheries facilities is estimated as 26.5 %.

For manufacturing industries, total products of goods are estimated by a production function model which is formulated by regressing the data of 1982 as

$$Y = 8.03K^{0.519}L^{0.481} \quad (R = 0.87) \quad (12)$$

in which Y : products of goods in million yen, K : fixed assets for production in million yen, and L : number of employees. Because a separate regression analysis predicts K as 179,939 million yen and L as 87,700 persons in 1983, the product of manufacturing industries X_{MN}, which would be supposedly developed in 1983 if the earthquake had not taken place, may be estimated as

$$X_{MN} = 8.03 \times 179{,}939^{0.519} \times 87{,}700^{0.481} = 1{,}022{,}741 \text{(million yen)} \quad (13)$$

On the other hand, damage of facilities in manufacturing industries is reported as 2,925 million yen. Therefore, the products of manufacturing industries X_{ME} in 1983 may be estimated as

$$X_{ME} = 8.03 \times (179{,}939 - 2{,}925)^{0.519} \times 87{,}700^{0.481} = 1{,}014{,}081 \text{ (million yen)} \quad (14)$$

It should be noted in Eq.(14) that the loss of number of employees due to death and/or injuries is disregarded due to the limited effect. The reduction factor α_M for the manufacturing industries is, then, estimated from Eq.(2) as

$$\alpha_M = (X_{MN} - X_{ME}) / X_{MN} = 0.85\ \% \quad (15)$$

Reduction factor for wholesale and retail is similarly estimated by formulating a production function model between the products and capital for wholesale and retail.

The reduction factors of products for the damages of facilities and properties for production were thus estimated as shown in Table-5. Reduction factors of products for damage of transportation facilities, and for materials and goods, which will be described later, are also presented in Table-5.

Decrease of Products due to Damage of Transportation Facilities

Because damage of roads was limited and restoration was made promptly after the earthquake, the effect of road damage is disregarded in this analysis. Reduction of products is considered here only for railways and ship transportation.

In the railways, service was suspended at the Oh-u Main-Line, Oga Line

Table-5 Reduction Factor of Products (%)

Classification		① Due to Damage of Facilities for Production	② Due to Damage of Transportation Facilities	③ Due to Damage of Materials and Goods	④ Maximum Reduction Factor α_{max}
Agriculture		1.93	0	0.79	1.93
Forestries		0	0	0.48	0.48
Fisheries		26.27	0	0	26.27
Mining		0	0	0	0
Manufacturing		0.85	0	0.12	0.85
Construction		0	0	0	0
Electricity. Gas. Water		0	0	0	0
Commercial		0.01	0	0.75	0.75
Finance and Insurance		0	0	0	0
Landed Estate		0	0	0	0
Transportation and Communication	Road	0	0	0	0
	Rail Way	0	1.7[1]	0	1.7[1]
	Ship	0	45.0[2]	0	45.0[2]
	Communication	0	0	0	0
Service		0	0	0	0
Official Business		0	0	0	0
Unclassificable		0	0	0	0

Note: 1) Reduction factor only for products for third industry
2) Reduction factor only for products for electricity

and Gonoh Line for 10 to 20 days. Number of passengers affected by the suspension is reported as approximately 1.7 % of the annual number of passengers. However because freight transportation was made alternatively by truck, the effect of suspension of the railways for the freight transportation was limited. Therefore the effect of railway damage is taken into account only for the third industry by disregarding their effects for first and second industries. The reduction factor for railway is assumed from the number of passengers as 1.7 %.

Port and harbor facilities suffered severe damage. It took one year and five months for their full restoration. Handling volume of the materials which depend on ship transportation such as crude oil, cement, heavy oil and petroleum goods substantially decreased in the Akita prefecture. However, the decrease of landing volume did not directly bring a decrease of products. Most cement was landed at ports located in adjacent prefectures and transported to the Akita prefecture by trucks. Heavy oil and petroleum goods were landed with use of exclusive wharves which survived the earthquake. Crude oil for use at the Tohoku Electrical Power Station was the only case where alternative transportation could not be made. Fig.4 shows the landing volume of the crude oil in the Akita port. The landing volume was only 450,000 tf in 1983. It corresponds to approximately 45 % decrease of the volume of 820,000 tf which would be supposedly made if the earthquake did not take place. Therefore, it is assumed here that damage of

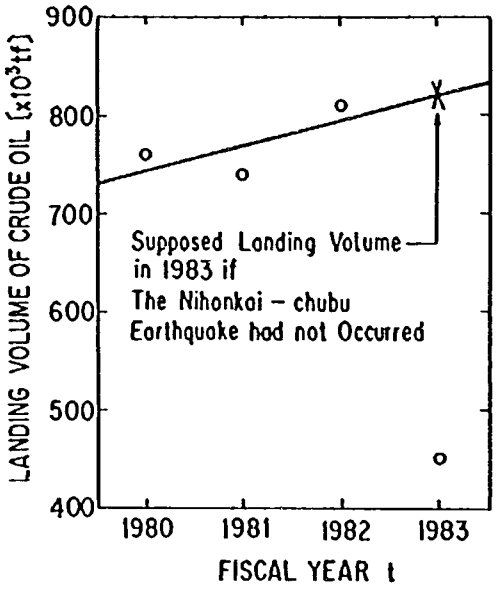


Fig.4 Variation of Landing Volume of Crude Oil at Akita Port

ports developed a decrease of electricity by an amount of 45 %. It should be, however, noted that because shortage of electricity in the Akita prefecture was supplied from surrounding prefectures, it is assumed that the decrease of products due to the shortage of electricity was not developed. This means that the reduction factor of 45 % is considered only for production of the electricity. The reduction factor of products due to damage of transportation facilities thus estimated is shown in Table-5.

Decrease of Products due to Damage of Materials and Goods

Decrease of products due to damage of materials and goods is evaluated for agriculture, livestock, forestry, commerce and industry (refer to Table-4). Dividing the decreases of products by the products(output) of the inter-industry relation table, the reduction factors of the products are evaluated for each industry as shown in Table-5. The reduction factors associated with the damage of materials and goods are generally small.

Decrease of Products due to Seismic Damages

Based on the reduction factors which have been estimated in the preceding sections for the damage of facilities for production, for the damage of transportation facilities, and for the damage of materials and goods, the maximum reduction factors α_{max} given by Eq.(3) were evaluated as shown in Table-5. It is noted that the maximum reduction factor α_{max} is significantly high for the ship transportation and the fisheries.

With use of the maximum reduction factors α_{max}, the reduction of products, which was designated in this paper as the first effect, was calculated by Eq.(5) as shown in Table-6. The inter-industry relation table of 1980 version was used for the analysis. Large classifications with 14 categories and small classifications with 164 categories were used for the

Table-6 Decrease of Products Predicted (Billion Yen)

Classification	Product Basis	
	Original Products X_{iN}	Reduction of Products ΔX_i
Cultivated Agriculture	253.6	4.9
Livestock	52.9	1.02
Forestry	82.8	1.04
Fisheries	11.5	3.02
Mining	91.6	0.78
Food	181.7	18.55
Texture and Clothes	100.5	1.81
Wood and Woden Goods	236.8	2.36
Pulp and Paper	48.4	0.7
Printing and Publishing	20.2	0.17
Leather and Rubber Goods	1.3	0.02
Chemical Products	35.1	0.3
Petroleum and Coal Goods	43.5	0.42
Ceramics	47.6	0.4
Iron and Steel	13.9	0.12
Iron and Non-iron Goods	146.5	1.24
General Machinery	44.3	0.38
Electric Machinery	149.6	1.27
Transportation Machinery	62.9	0.53
Precision Machinery	14.8	0.13
Other Manufactures	12.6	3.31
Construction of Buildings	356.3	5.28
Construction of Public Works	246.9	4.77
Electricity, Gas, Water	193.0	73.02
Commerce	460.2	7.82
Finance and Insurance	114.5	1.95
Landed Estate	264.1	4.22
Transportation and Communication	307.5	5.23
Service	641.4	95.4
Official Business	145.2	7.32
Unclassificable	34.4	0.66
Total	4,415.6	248.14

input and output, respectively, of the analysis.

Total amount of the first effect is predicted as 248.1 billion yen on the products basis, which is approximately 1.7 times as large as the direct damage of 145.7 billion yen developed in the Akita prefecture (refer to Table-4). The most significant decrease of the products occurred in the service industry (95.4 billion yen) followed by the electricity, gas and water industry (73.0 billion yen).

The second ripple effect was calculated by Eqs.(7) and (8) as shown in Table-7(a). It is predicted as 114.6 billion yen on the products basis, which is 46% of the first effect of 248.1 billion yen. It should be noted in Table-7(a) that the damage of materials and goods presented in Table-4 are also included in a part of the decrease of products by the earthquake. Although the reduction of products due to the fact that the productions which depend on the damaged materials and goods would reduce was taken into account in the analysis as shown in Table-5, the materials and goods which were damaged by the earthquake could be sold if the earthquake had not

taken place. This could develop incomes in industries and shops. However because the damaged materials and goods could not be sold after the earthquake, it would be considered as a part of the decrease of products by the earthquake.

The total decrease of products by the earthquake, which consists of the first effect, second ripple effect and the damage of materials and goods, is predicted as 371.0 billion yen on the products basis and 166.6 billion yen on the gross value added basis. This is 2.5 times and 2.3 times larger than the direct damage on the products basis and gross value added basis, respectively.

Increase of Products due to Investment for Restoration

After the earthquake, 44.3 billion yen and 11.9 billion yen were invested for restoration of public works and housing, respectively. An increase of products due to the investments for restoration is evaluated separately. It is assumed in the inter-industry relation analysis that 22 billion yen of the total restoration of 44.3 billion yen for public works was paid to the industries, and that the rest (22.3 billion yen) was spent for the gross value added. Due to the original investments, products of 66.9 billion yen were developed including the original investments, which,

Table-7 Effect of Nihonkai-chubu Earthquake of 1983 on Economy of Akita Prefecture (Billion Yen)

(a) Direct Damage and Decrease of Products (First Effect and Second Ripple Effect)

Damage and Decrease of Products		Products Basis	Gross Value Added Basis
Direct Damage		145.7	72.1
Decrease of Products by the Earthquake	Damage of Materials and Goods	8.3	4.1
	Direct Decrease associated with Decrease of Products (First Effect)	248.1	121.8
	Decrease of Consumption (Second Ripple Effect)	114.6	40.7
	Total	371.0	166.6

(b) Increase of Products due to Investment for Restoration

Increase of Products		Products Basis	Gross Value Added Basis
Restoration of Public Works	First Effect	66.9	29.2
	Second Ripple Effect	33.1	11.7
	Sub-total	100.0	40.9
Restoration of Housing	First Effect	18.4	6.7
	Second Ripple Effect	6.4	2.3
	Sub-total	24.9	9.0
Increase of Products due to Restoration		124.9	49.9

in turn, developed the second ripple effects of 33.1 billion yen on the products basis shown in Table-7(b). Including all these effects, it is found that the investment for restoration of public works developed the products of 100.0 billion yen on the products basis and 40.9 billion yen on the gross value added basis.

The same analysis was made for the investment for the housing restoration as shown in Table-7(b), and it is found that the investments developed products of 24.9 billion yen and 9.0 billion yen based on the product basis and the gross value added basis, respectively. Therefore by adding the increase of products due to investment for restoration of public works, the increase of products due to investment for restoration is predicted as 124.9 billion yen on the products basis and 49.9 billion yen on the gross value added basis.

EFFECT OF THE NIHONKAI-CHUBU EARTHQUAKE ON ECONOMY IN AKITA PREFECTURE

Table-8 summarizes the direct damage, the decrease of products by the earthquake and the increase of products due to the restoration works. The direct damage of 145.7 billion yen plus the decrease of products of 371 billion yen is 516.7 billion yen, which represents the damage predicted on the products basis. Therefore if the restoration works had not been made, this amount of the damage would be developed in the Akita prefecture.

Because the restoration works are predicted to develop the increase of products of 124.9 billion yen, an actual decrease of the products is predicted by substituting it from the decrease of products by the earthquake as 246.1 billion yen on the products basis and 116.7 billion yen on the gross value added basis.

Table-8 Summary of Decrease of Products Predicted (Billion Yen)

Damage and Products	Products Basis	Gross Value Added Basis
Direct Damage	145.7	72.1
Decrease of Products by the Earthquake	371.0	166.6
Increase of Products due to Restoration	− 124.9	− 49.9
Total	391.8	188.8

To estimate the products by Eq.(1), the gross prefectural products of the Akita prefecture which would be supposedly developed in 1983 if the earthquake did not occur has to be evaluated. Fig.5 shows a variation of gross prefectural products of the Akita prefecture on the gross value added basis between 1975 and 1982. The gross prefectural products in 1983 may be estimated by extrapolating the relation of Fig.5 as 2348.0 billion yen. Because the decrease of products by the earthquake and the increase of products due to the restoration are 166.6 billion yen and 49.9 billion yen, respectively, on the gross value added basis, it is predicted that the gross prefectural products of the Akita prefecture in 1983 would be about 2231.3 billion yen (2348.0-166.6+49.9) on the gross value added basis. It

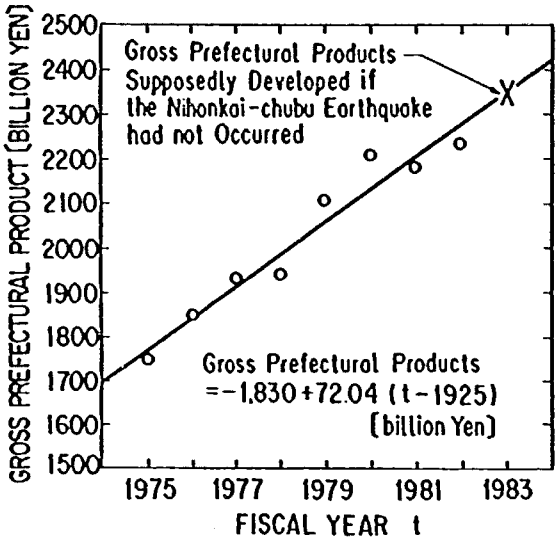


Fig.5 Variation of Gross Prefectural Products of Akita Prefecture between 1975 and 1982

is noted here that the decrease of products by the earthquake of 166.6 billion yen corresponds to 7.1% of the predicted gross prefectural products of 2348.0 billion yen.

On the other hand, actual gross prefectural products of the Akita prefecture in 1983 was reported in 1985 as 2,272.8 billion yen, which is 41.5

Table-9 Comparison of Predicted and Actual Products Developed in Akita Prefecture in 1983 on Gross Value Added Basis

(Billion yen)

Classification	Prediction on Products of Akita Prefecture in 1983 Fiscal Year						⑦Actual Products Developed in 1983	Ratio ⑥/⑦
	Reduction of Products				⑤ Products Supposedly Developed if the Earthquake had not Occurred	⑥Predicted Products ⑥=⑤-④		
	① Decrease of Products	② Increase of Products due to Investment for Restoration of Public Works	③ Increase of Products due to Investment for Restoration of Housings	④Sub-total ①-②-③				
Agriculture	5.4	0.2	0.03	5.2	205.0	199.8	201.6	0.99
Forestries	1.8	0.4	0.3	1.1	34.7	33.7	30.9	1.09
Fisheries	1.9	0.03	0.01	1.9	6.8	4.9	5.2	0.95
Minings	1.4	1.5	0.2	-0.2	36.1	36.4	41.0	0.89
Manufacturing	10.5	2.9	0.7	6.9	331.4	324.5	322.2	1.01
Construction	7.9	23.4	5.1	-20.6	268.5	289.1	244.5	1.18
Electricity. Gas. Water	26.2	0.5	0.1	25.6	77.9	52.3	78.3	0.67
Commercial	14.6	2.7	0.6	11.3	351.3	340.0	334.1	1.02
Finance and Insurance	4.5	1.5	0.3	2.7	96.8	94.1	91.7	1.03
Landed Estate	4.5	0.6	0.1	3.7	231.5	227.8	226.2	1.01
Transportation and Communication	5.1	1.7	0.4	3.0	112.1	109.1	105.0	1.04
Service	82.8	5.6	1.2	76.0	595.8	519.7	592.2	0.88
Total	166.6	40.9	9.0	116.7	2,348.0	2,231.3	2,272.8	0.98

billion yen larger than the prediction. Table-9 compares the predicted products with the actual ones for each industry. When a ratio is defined for each industry as the actual gross products divided by the predicted gross products, the ratio takes a value between 0.67 and 1.18. The predicted results seem to give good approximations, except for the electricity, gas and water industry. The actual products for this industry are approximately 1.5 times larger than those predicted. This may be possibly attributed to the difference of the assumption made in this analysis. Although the products of the electricity was assumed to decrease in proportion to the decrease of the landing volume of crude oil at the port, actual products seem not to be decreased so significantly.

CONCLUDING REMARKS

For analyzing economic losses caused by an earthquake, an analytical procedure with use of the inter-industry relation analysis, which has been widely used to evaluate an indirect impact by constructing new facilities, was applied to the Nihonkai-chubu Earthquake of 1983. The following conclusions may be deduced from the study presented herein:

1) Total direct damage in the Akita prefecture caused by the Nihonkai-chubu Earthquake was 145.7 billion yen on the products basis. Decrease of products associated with the direct damage is predicted as 371.0 billion yen, which is 2.5 times larger than the total direct damage.

2) The decrease of product of 371.0 billion yen on the product basis is predicted to be caused by a decrease of production (first effect) of 248.1 billion yen, a decrease of consumption (second ripple effect) of 114.6 billion yen, and a damage of materials and goods of 8.3 billion yen. The second ripple effect corresponds to 46% of the first effect.

3) Decrease of products by the earthquake and increase of products due to restoration are predicted as 166.6 billion yen and 49.9 billion yen, respectively, on the gross value added basis. This means that the actual decrease of products would be 166.6-49.9 = 116.7 billion yen. The decrease of products of 166.6 billion yen and 116.7 billion correspond to 7.1% and 5.0%, respectively, of the gross prefectural products of 2348.0 billion yen which would be supposedly developed in 1983 if the earthquake had not taken place.

4) Because the gross prefectural products of the Akita prefecture which were supposedly developed in 1983 if the earthquake had not taken place is estimated as 2348.0 billion yen, the gross prefectural products which would be developed in the Akita prefecture in 1983 is predicted as 2348.0 - 116.7 = 2231.3 billion yen. In comparison, the actual gross prefectural products in 1983 were reported by the Akita prefecture in 1985 as 2272.8 billion yen, which is 41.5 billion yen larger than the prediction.

5) Indirect damage is very important for assessing an extent of the impact caused by an earthquake. Further study to clarify the dependence of indirect damage on the damage extent and characteristics of the damaged area need to be made.

ACKNOWLEDGEMENTS

The authors express their sincere appreciations to Dr. C. Scawthorn, EQE Incorporated, for his review and collection of the manuscript.

REFERENCE

1) Miyazawa, K. : Introduction to Inter-industry Relation Analysis, Nippon Keizai Shinbun, 1983(in Japanese).
2) Report on the Disaster Caused by the Nihonkai-chubu Earthquake of 1983, Report of PWRI, Vol.165, Public Works Research Institute, Ministry of Construction, 1985(in Japanese).
3) Kawashima, K., Aizawa, K., and Takahashi, K. : Attenuation of Peak Ground Acceleration, Velocity and Displacement Based on Multiple Regression Analysis of Japanese Strong Motion Records, Earthquake Engineering and Structural Dynamics, Vol.14, 1986.
4) Akita Prefecture : Record of the Nihonkai-chubu Earthquake of 1983, 1983(in Japanese)
5) Kawashima, K., Obinata, N. and Kanoh, T. : Estimation of Economic Damage Induced by An Earthquake, —Part 1 Case Study for the 1983 Nihonkai-chubu Earthquake——, Technical Note of PWRI, No.2267, Public Works Research Institute, Ministry of Construction, 1985(in Japanese).

NOTATIONS

$\underline{A}$: input coefficient matrix
α_i : reduction factor of i-th industry, and
$\alpha_i = \Delta X_i / X_{iN}$
$\underline{F}$: final demand vector, and
$\underline{F} = \{ f_1, f_2, \ldots\ldots, f_n \}^T$
$\Delta\underline{F}$: final demand vector associated with decrease of income and operating profit
$G_D(t)$: decrease of productions at t fiscal year due to an earthquake (product basis / gross value added basis)
$G_O(t)$: products which were achieved after an earthquake at t fiscal year (product basis / gross value added basis)
$G_N(t)$: products which were supposedly developed at t fiscal year if an earthquake had not occurred (product basis / gross value added basis)
$G_R(t)$: increase of products due to restoration (product basis / gross value added basis)
I_i : i-th industry
$\underline{V}$: products based on gross value added basis, and
$\underline{V} = \{ V_1, V_2, \ldots\ldots, V_n \}^T$
$\Delta\underline{V}$: decrease of products (first effect) based on gross value added basis, and
$\Delta\underline{V} = \{ \Delta V_1, \Delta V_2, \ldots\ldots, \Delta V_n \}^T$
$\underline{v}$: gross value added ratio matrix
$\Delta\underline{V}_S$: decrease of products (second ripple effect) on gross value added basis, and

$\Delta \underline{V}_S = \{\Delta V_{1S}, \Delta V_{2S}, \ldots\ldots, \Delta V_{nS}\}^T$

$\underline{X}$: products based on product basis, and
$\underline{X} = \{X_1, X_2, \ldots\ldots, X_n\}^T$

$\underline{X}_E$: products based on product basis which were developed after an earthquake, and
$\underline{X}_E = \{X_{1E}, X_{2E}, \ldots\ldots, X_{nE}\}^T$

$\underline{X}_N$: products based on product basis which were supposedly developed when an earthquake had not occurred, and
$\underline{X}_N = \{X_{1N}, X_{2N}, \ldots\ldots, X_{nN}\}^T$

$\Delta \underline{X}$: decrease of products (first effect) based on product basis, and
$\Delta \underline{X} = \{\Delta X_1, \Delta X_2, \ldots\ldots, \Delta X_n\}^T$

X_{ij} : products used from I_i to I_j

$\Delta \underline{X}_S$: decrease of products (second ripple effect) on product basis
$\Delta \underline{X}_S = \{\Delta X_{1S}, \Delta X_{2S}, \ldots\ldots, \Delta X_{nS}\}^T$

SEISMIC BEHAVIOR OF CABLE STAYED BRIDGES

by
Kazuhiko KAWASHIMA
and
Shigeki UNJOH

Earthquake Engineering Division
Public Works Research Institute
Ministry of Construction

INTERNATIONAL SEMINAR ON
CABLE-SUPPORTED BRIDGES
WITH EMPHASIS ON STEEL CABLE-STAYED BRIDGES
Yokohama, Japan
December 10 and 11, 1991

SEISMIC BEHAVIOR OF CABLE STAYED BRIDGES

Kazuhiko Kawashima[a] and Shigeki Unjoh[b]

[a] Head, Earthquake Engineering Division, Earthquake Disaster Prevention Department, Public Works Research Institute, Ministry of Construction, Tsukuba Science City, Japan

[b] Research Engineer, ditto

ABSTRACT

Seismic behavior of cable stayed bridges is presented with emphasis on damping characteristics. Damping ratio contributed from various sources including energy dissipation due to hysteretic behavior and radiation from foundation is presented. A method to evaluate damping ratio of a total bridge system is proposed.

1. INTRODUCTION

Cable stayed bridges have not yet experienced significant earthquakes in the past. According to the previous field forced vibration tests on cable stayed bridges, it is well recognized that the natural frequencies and the natural mode shapes measured from the experiments can be predicted with satisfactory accuracy by appropriate analytical simulations[1]. However, in many cases damping ratios determined from the field forced excitation tests conducted in the past are likely to show considerably smaller value compared to the values assumed in seismic design. Because the structural response of cable stayed bridges significantly depends on the damping ratio, correct estimation of the damping ratio is of critical importance in seismic design.

It is the objectives of this paper to discuss damping characteristics of cable stayed bridges. Analysis of strong motion records measured at a cable stayed bridge, analytical simulations for energy dissipation due to friction at movable bearings and radiation of energy from foundation to subground, cable configuration dependence of damping ratio through model oscillation tests are presented. A method to predict damping ratio of cable stayed bridges is finally proposed. Engineering significance of the damping ratio is studied placing emphasis on how the damping ratio depends on mode shapes and amplitude.

2. DEPENDENCE OF DAMPING RATIO ON STRUCTURAL COMPONENTS THROUGH ANALYSIS OF MEASURED EARTHQUAKE RECORDS[2]

2.1. Suigo Bridge

Suigo Bridge is a two-span continuous cable stayed bridge as shown in Figure 1. The deck is of steel box girder with the length of 290.45 m, and it is rigidly connected to a single steel tower with the height of 47.2 m. The superstructure is supported by three substructures, i.e., two caisson foundations and a pile foundation. Fixed bearings are provided on the mid-substructure to connect and prevent the deck movement in both longitudinal and transverse directions.

A series of forced excitation tests for vertical and torsional modes were conducted soon after the completion to study frequency and damping characteristics for aerodynamic stability analysis[3]. Natural frequencies and mode shapes could be predicted with reasonable accuracy.

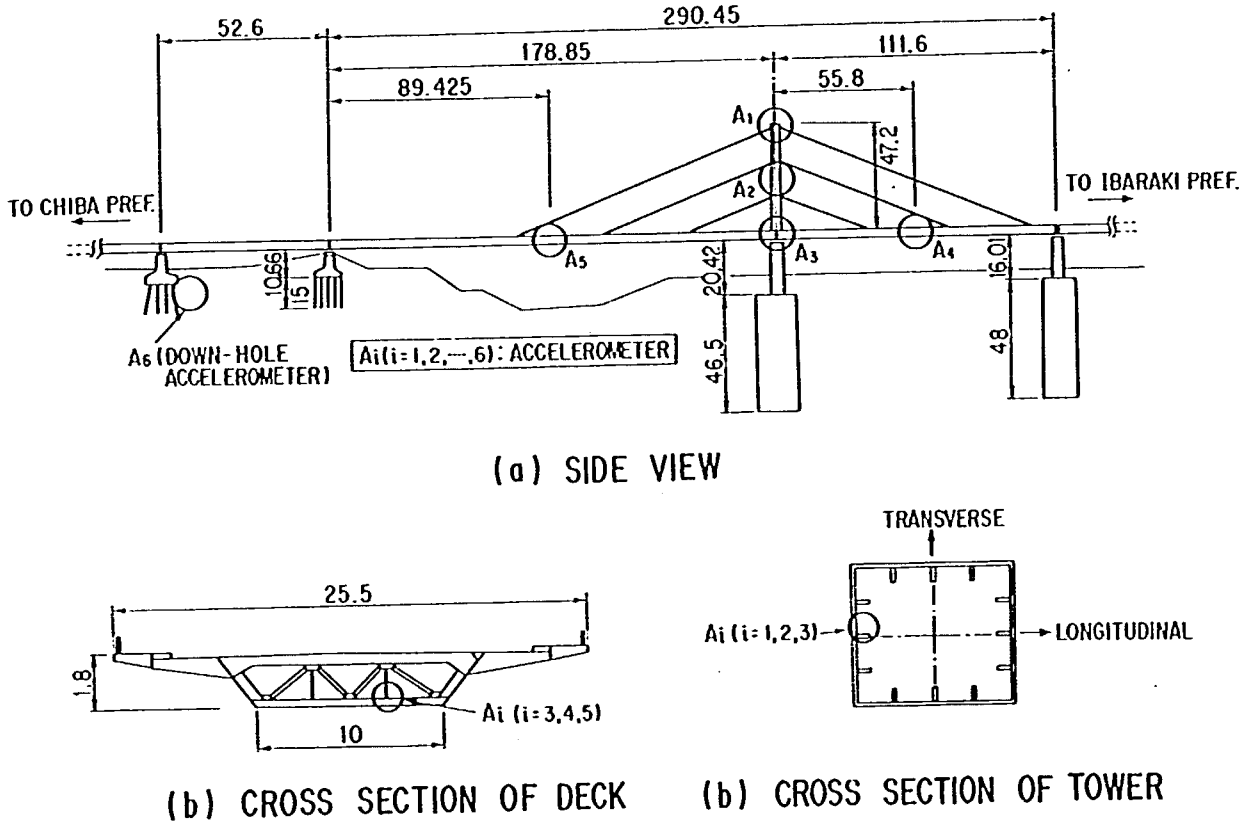


Figure 1. Suigo Bridge and Observation Points

2.2. Strong Motion Observation and Dynamic Characteristics

Strong motion observation has been made at the bridge since March 1986. Two horizontal components force-balanced accelerometers were placed at six points as shown in Figure 1. Three records with sufficiently large accelerations were obtained by the earthquakes as shown in Table 1. Table 2

represents the peak acceleration thus measured.

As an example of the records, Figure 2 shows the accelerations by the East Chiba-ken Earthquake (EQ-33). Of particular importance is the large response at the tower top (A1 point) in transverse direction. Peak acceleration at A1 point reached to 999.8 gal (cm/sec^2). Because the peak acceleration at the mid-height (A2 point) and the bottom (A3 point) of the tower is 471 gal and 173 gal, respectively, it is obvious that the tower vibrated in accordance with a cantilevered mode shape.

Natural frequencies and mode shapes were evaluated from spectral analysis of the data, and they could be predicted with satisfactory accuracy by a linear analysis[2].

Table 1
Magnitude and Location of Major Earthquakes

EQ.NO.	DATE	EPICENTER			EPICENTRAL DISNTANCE(Km)	MAGNITUDE	DEPTH (Km)
		LOCATION	LONGITUDE	LATITUDE			
EQ-6	1986. 6.24	OFF CHIBA	140° 43'	34° 49'	123	6.5	73
EQ-16	1987. 2. 6	OFF FUKUSHIMA	141° 54'	36° 59'	173	6.7	31
EQ-33	1987.12.17	OFF CHIBAKEN	140° 29'	35° 21'	62	6.7	58

Table 2
Peak Accelerations Measured at Suigo Bridge

EQ.NO.	A1 POINT		A2 POINT		A3 POINT		A4 POINT		A5 POINT		A6 POINT	
	LG	TR	LG	TR	LG	TR	LG	TR	LG	TR	LG	TR
EQ-6	189	217	75	111	55	34	61	—	62	77	13	13
EQ-16	238	322	109	218	87	54	91	—	100	104	23	22
EQ-33	446	999.8	297	471	216	173	257	—	247	363	99	114

1) LG and TR represent peak acceleration in longitudinal and transverse direction, respectively.

2) Records in transverse direction at A4 point were not obtained due to malfunction of the accelerometer.

2.3. Damping Ratio of Suigo Bridge Based on Measured Data

Damping characteristics of Suigo Bridge were analyzed through analytical simulations. Because the response acceleration at the bottom of the tower (A3 point) was measured, it was prescribed to the A3 point of the analytical model as an input motion, and the response of the superstructure was computed.

Analytical idealization presented in Figure 3 was used for the simulation. Damping ratio assumed in the analysis was varied as 0%, 1%, 2% and 5 % of critical as a parameter to be studied.

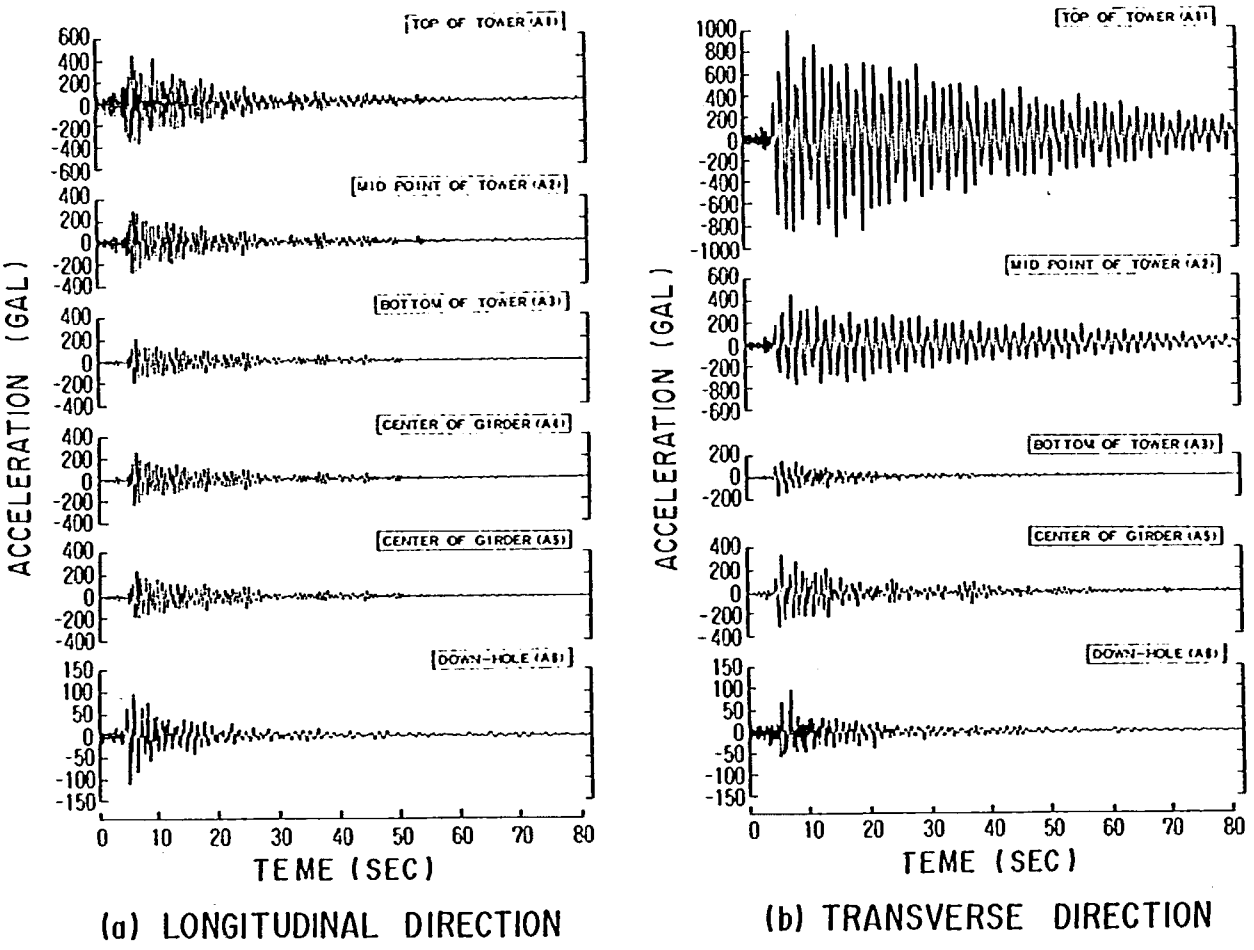


Figure 2. Acceleration Records during East Chiba-ken Earthquake (EQ-33)

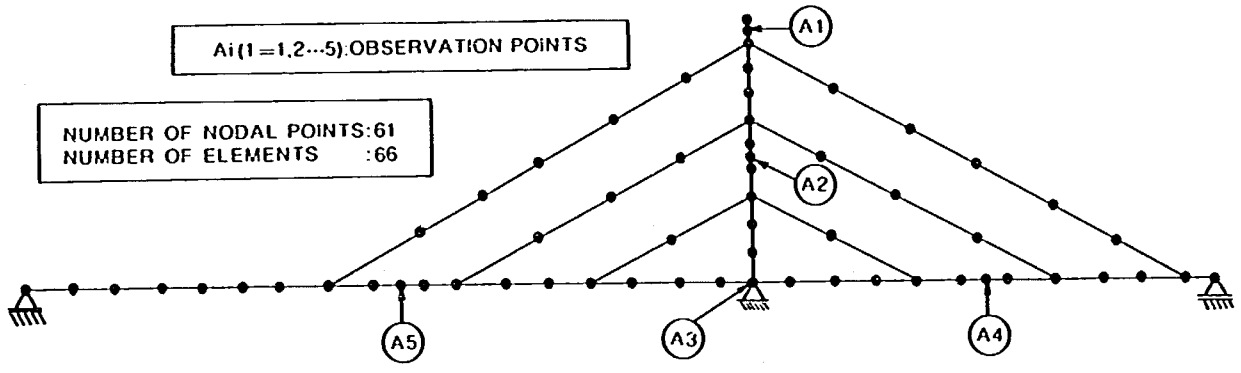


Figure 3. Analytical Model of Suigo Bridge

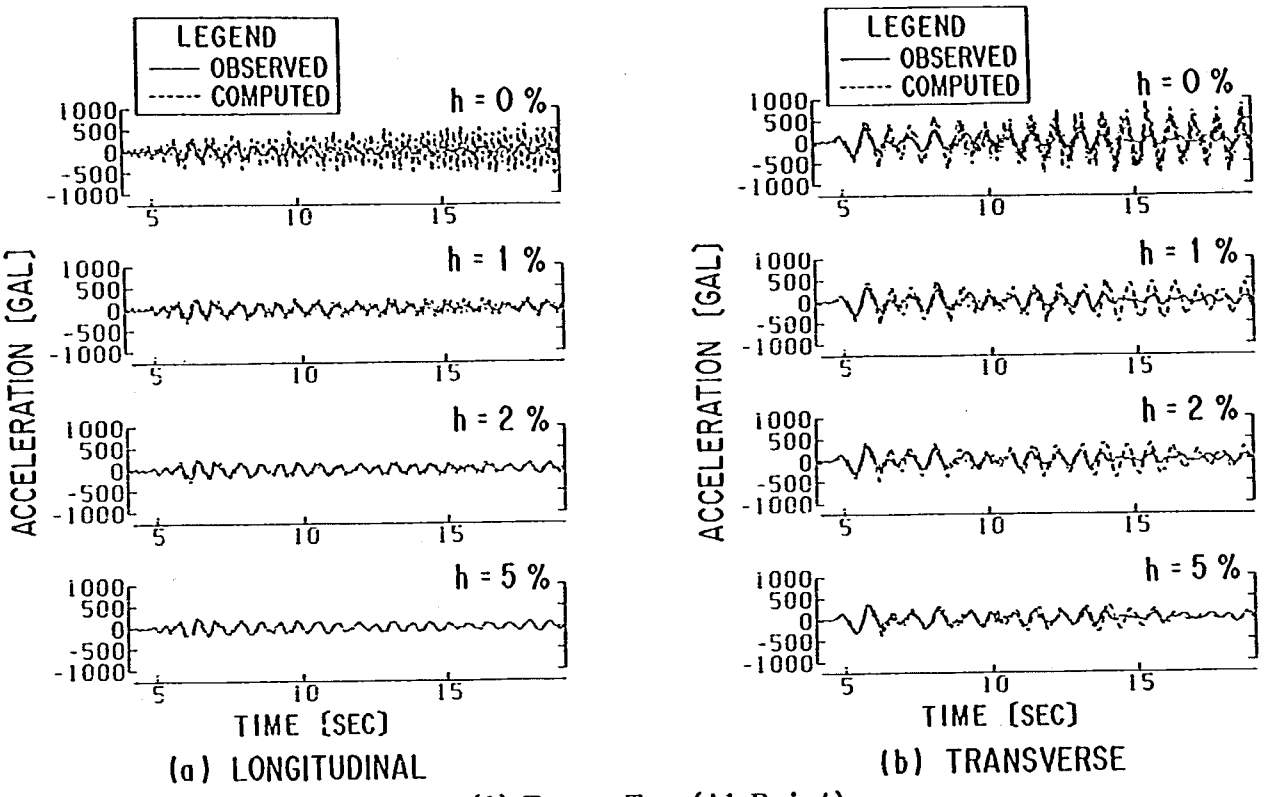
Analysis was made for the three records presented in Table 1. As an example, Figure 4 shows comparative plots of acceleration time history between the measured and the predicted at the tower top (A1 point) and the center of the girder (A5 point) for the Chiba-ken Earthquake (EQ-33). It is obvious that the damping ratio of 0% gives larger response of the tower than the measured acceleration in longitudinal direction and that 5% damping ratio would be appropriate to develop a close correlation between the predicted and the measured accelerations. Overall predicted response accelerations assuming the 5% damping ratio agree well with the measured accelerations. However, for the response at the tower top (A1 point) in transverse direction, the damping ratio of 5% is an overestimation, and 0% damping ratio would be appropriate. On the other hand, 5 % damping ratio gives a nice agreement for the deck response in both longitudinal and transverse directions.

Table 3 shows the damping ratio which gives the best correlation for the peak acceleration. It is approximately 2 % and 0 - 1 % for the tower response in longitudinal and transverse directions, respectively, and is approximately 5 % for deck response in both directions.

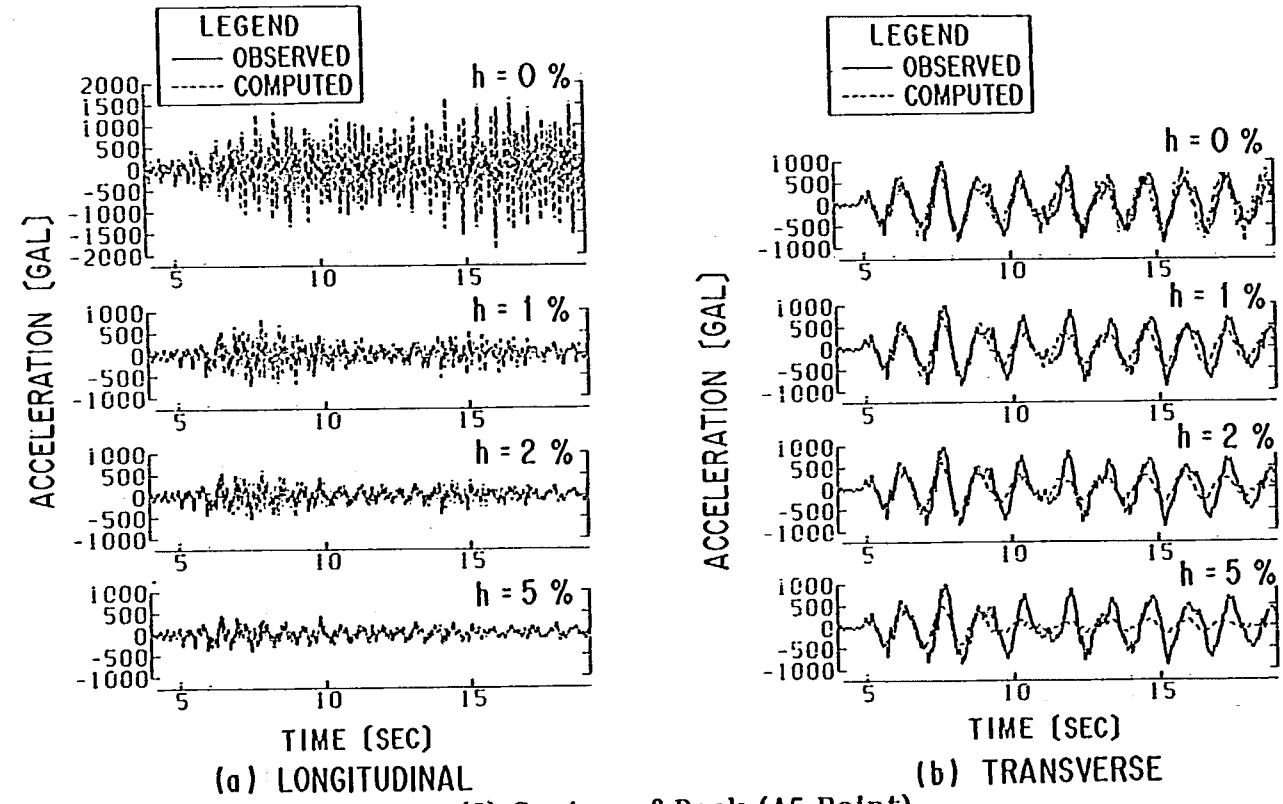
It is important to note that the damping ratio depends on structural components. It is also interesting to note the difference of the damping ratio of the tower depending on direction. This may be due to the effect of cables. Because flexural rigidity of the cables is negligibly small, the tower is almost free to move from cables in transverse direction. Therefore the tower may be considered as a free standing column. Damping ratio of free standing column which is of steel box section is, generally, substantially small, and it seems reasonable to take a damping ratio of 0 - 1 %. On the other hand, in longitudinal direction, the tower is no more free standing column but is coupled with the deck by means of the cables. Therefore it seems reasonable that the tower takes larger damping ratio in longitudinal direction than in transverse direction.

Table 3
Damping Ratio which gives Best Correlation

EQ. NO.	LONGITUDINAL				TRANSVERSE		
	A1	A2	A4	A5	A1	A2	A5
EQ - 6	2	5	5	5	0 ~ 1	1	5
EQ - 16	2	5	5	5	0 ~ 1	1	5
EQ - 33	5	5	5	5	0 ~ 1	1	5



(1) Tower Top (A1 Point)



(2) Center of Deck (A5 Point)

Figure 4. Comparison of Response Accelerations between Measured and Predicted

3. DAMPING RATIO DUE TO ENERGY DISSIPATION AT MOVABLE SUPPORTS[4]

3.1. Energy Dissipation at Movable Supports and Analytical Idealization

When relative movement between deck and substructure occurs at movable bearing, energy dissipation due to friction would be developed. Amount of energy dissipation depends on type of bearing supports. To study the contribution of friction to damping ratio of a total bridge system, a cable stayed bridge was idealized as a discrete analytical model as shown in Figure 5. The friction force developed at movable supports due to relative displacement between deck and abutments was idealized by Coulomb friction.

The idealized cable stayed bridge was laterally displaced 30 cm in accordance with a mode shape, and then released smoothly to result in a free oscillation. Damping ratio was evaluated from decay of free oscillation as

$$\delta = \frac{2\pi h}{\sqrt{1-h^2}} = \log_e \frac{a_m}{a_{m+1}} \qquad (1)$$

in which δ and h represent logarithmic damping ratio and damping ratio of critical, respectively, and a_m and a_{m+1} represent amplitude of free oscillation at m-th and (m+1)th oscillation, respectively.

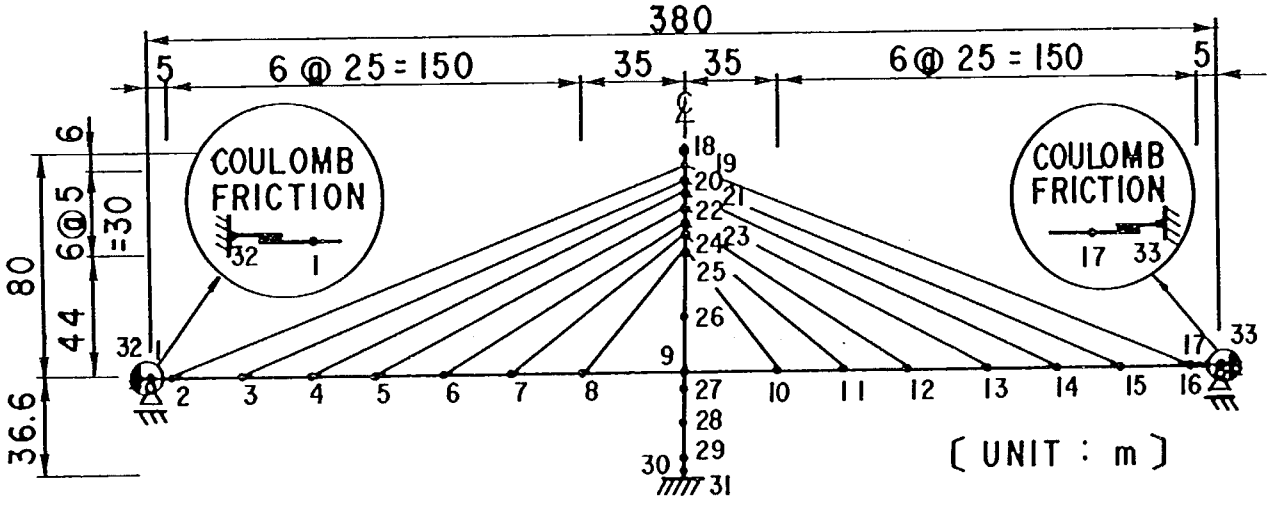


Figure 5. Cable Stayed Bridge Studied for Effect of Friction at Movable Supports

3.2. Effect of Energy Dissipation at Movable Supports

Figure 6 represents 5th and 6th mode shapes of the bridge disregarding the friction at the movable supports. They are the most and secondarily predominant mode shapes in longitudinal direction with natural period of 0.52 sec and 0.48 sec.

Figure 7 shows decay of free oscillation of the deck as well as damping ratio computed from Eq.(1). It is important in Figure 7 that the damping ratio depends on the mode shapes. Figure 8 shows damping ratio vs. free oscillation amplitude of the deck relation. It has to be reminded here that the damping

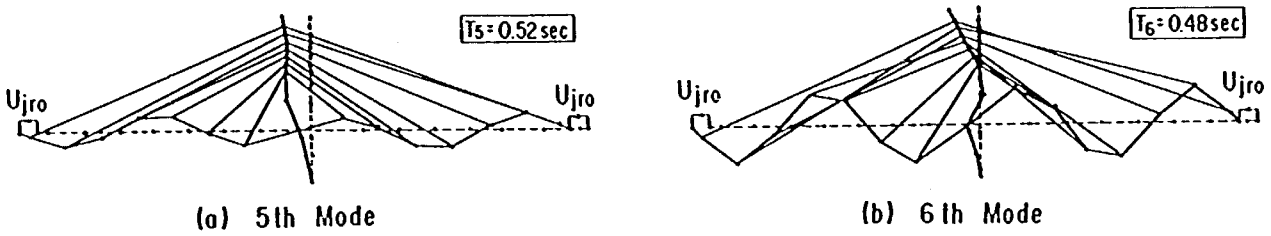


Figure 6. Predominant Modes

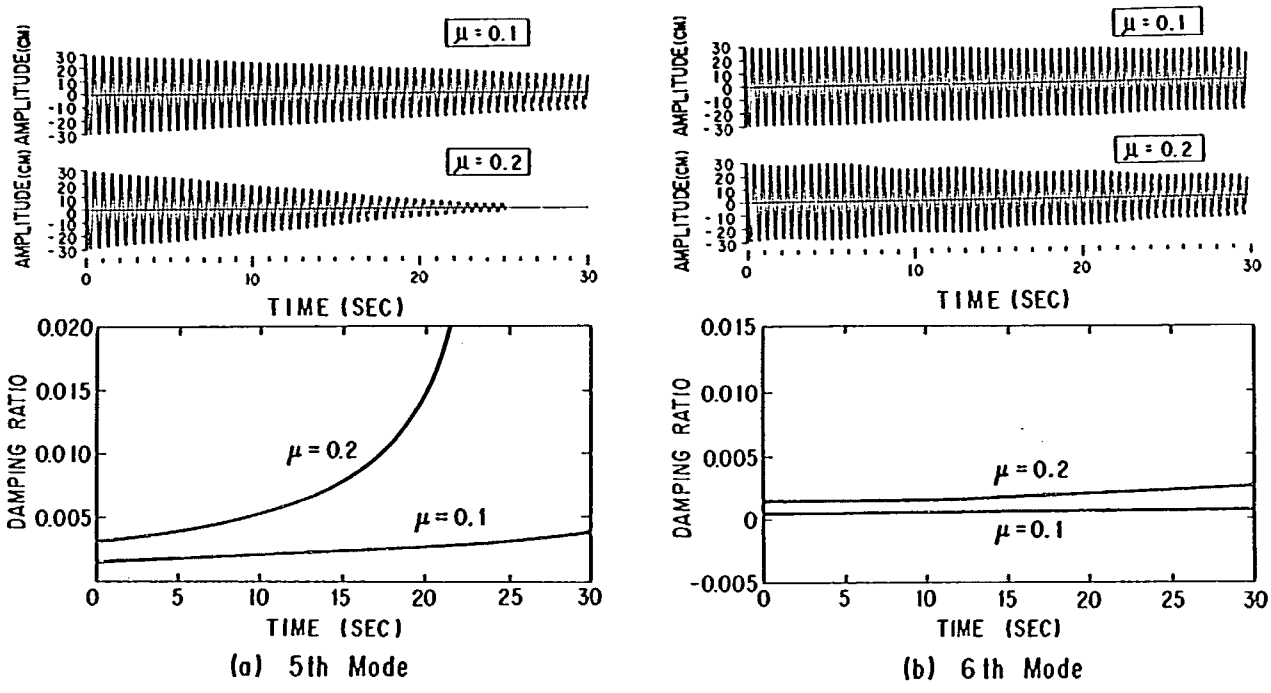


Figure 7. Decay of Free Oscillation and Damping Ratio Computed from Decay

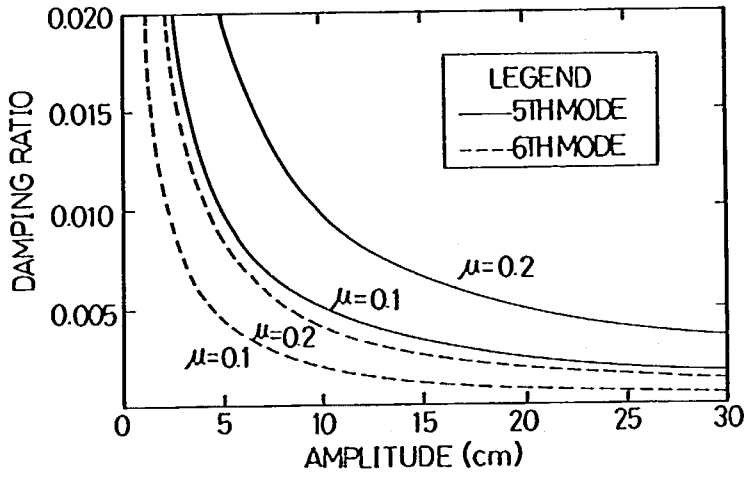


Figure 8. Damping Ratio vs. Amplitude of Free Oscillation Relation

ratio which results from the same amount of energy dissipation with Coulomb friction force increases as the oscillation amplitude decreases. This is the opposite tendency which was frequently observed in the past forced excitation tests. Damping ratio is larger in 5th mode than in 6th mode. Damping ratio increases linearly with increasing the friction coefficient.

Table 4 summarizes the damping ratio thus estimated. Assuming the friction coefficient as 0.1, damping ratio of the bridge takes a value ranging from 0.0007 (6th mode) to 0.0016 (5th mode).

Table 4
Damping Ratio due to Friction Force at Movable Supports

Natural Mode Specified	Friction Coefficient	Relative Displacement at Movable Support		
		30 cm	20 cm	10 cm
5 th	0.1	0.0016	0.0024	0.0049
	0.2	0.0032	0.0049	0.0099
6 th	0.1	0.0007	0.0010	0.0020
	0.2	0.0013	0.0020	0.0039

4. DAMPING RATIO DUE TO RADIATION OF ENERGY FROM FOUNDATION[5]

4.1. Radiational Damping and Analytical Idealization

When foundations of cable stayed bridges vibrate in ground, energy dissipation due to radiation of energy from foundations to surrounding subsoils occurs. To study the effects of radiation of energy from foundations, a cable stayed bridge was idealized as shown in Figure 9. The foundation was idealized by a rigid mass-less circular plate. Subsoils supporting the foundation was assumed as an elastic half space with shear modulus of G_s and Poisson's ratio of ν. Dynamic complex stiffness of the rigid circular plate can be available for such an idealization. Radius of the rigid circular plate was simply assumed so that it gives the same surface area with the foundation, and was varied as a parameter to be studied. The bridge and the subsoils were assumed elastic with no energy dissipation.

Dynamic complex stiffness of the foundation was assumed in a frequency independent form as[6]

$$
\begin{aligned}
K_x &= 8\, G_s a / (2-\nu) \\
K_r &= 8 G_s a^3 / 3(1-\nu) \\
C_x &= \pi\, G_s a^2 / V_s \\
C_r &= 0.25\pi \sqrt{2(1-\nu)/(1-2\nu)}\, G_s a^4 / V_s
\end{aligned}
\qquad (2)
$$

in which K_x and C_x represent spring and damping coefficient for sway motion, and K_r and C_r represent those for rocking motion. V_s and a represent shear wave velocity of subsoils and radius of foundation, respectively.

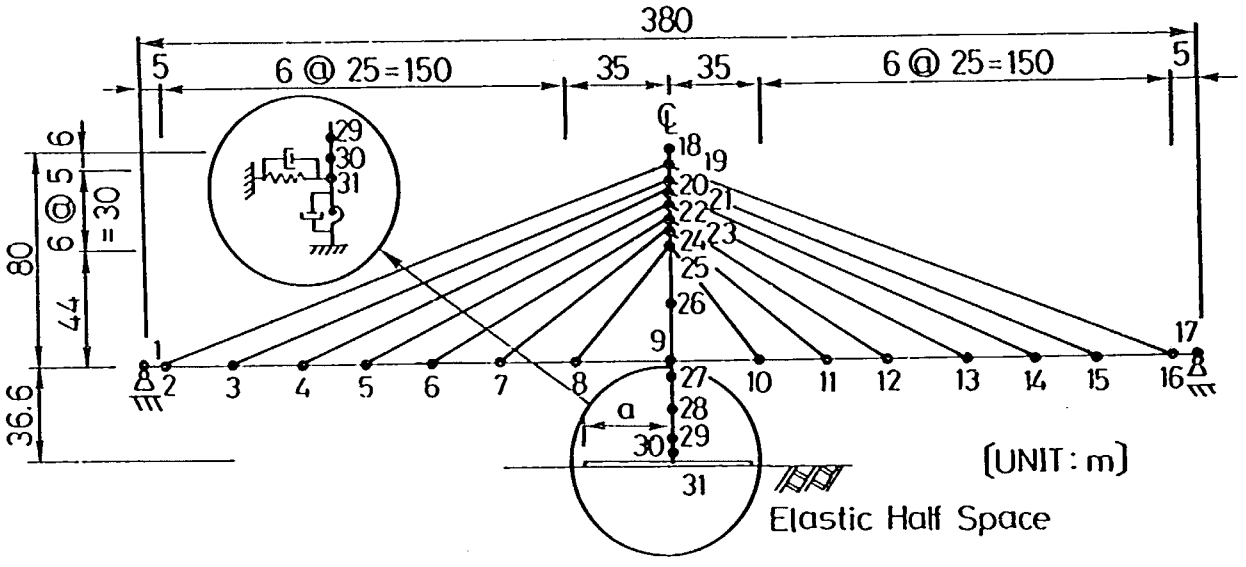


Figure 9. Cable Stayed Bridge Studied for Effect of Radiational Damping

4.2. Effects of Energy Dissipation at Foundation

Table 5 shows natural period and damping ratio computed by the complex eigenvalue analysis for the cable stayed bridge constructed on subsoils with shear wave velocity of 150 m/sec and 300 m/sec. Radius of the foundation and Poisson's ratio was assumed as 30 m and 0.4, respectively. Figure 10 shows two predominant mode shapes; one is a sway motion of tower and deck, and the other is a flexure motion of the tower with rocking of foundation. Damping ratio for the sway mode is 0.175 (V_s = 150 m/sec) and 0.034 (V_s = 300 m/sec), which are considerably higher than those experienced through field forced excitation tests. Of particular interest is much higher damping ratio for the

Table 5
Damping Ratio due to Radiation of Energy From Foundation

Shear Wave Velocity Vs (m/sec)		1	2	3	4	5	6	7	8	9	10	11	12
150	Natural Period T(sec)	2.83	1.26	0.89	0.71	0.57	0.49	0.44	0.41	0.30	0.28	0.25	0.23
	Damping Ratio h	0.0	0.0	0.0	0.0	0.175	0.0	0.0	0.744	0.0	0.0	0.004	0.0
300	Natural Period T(sec)	2.83	1.26	0.89	0.71	0.54	0.49	0.44	0.30	0.28	0.25	0.23	0.21
	Damping Ratio h	0.0	0.0	0.0	0.0	0.034	0.0	0.0	0.0	0.0	0.002	0.0	0.830

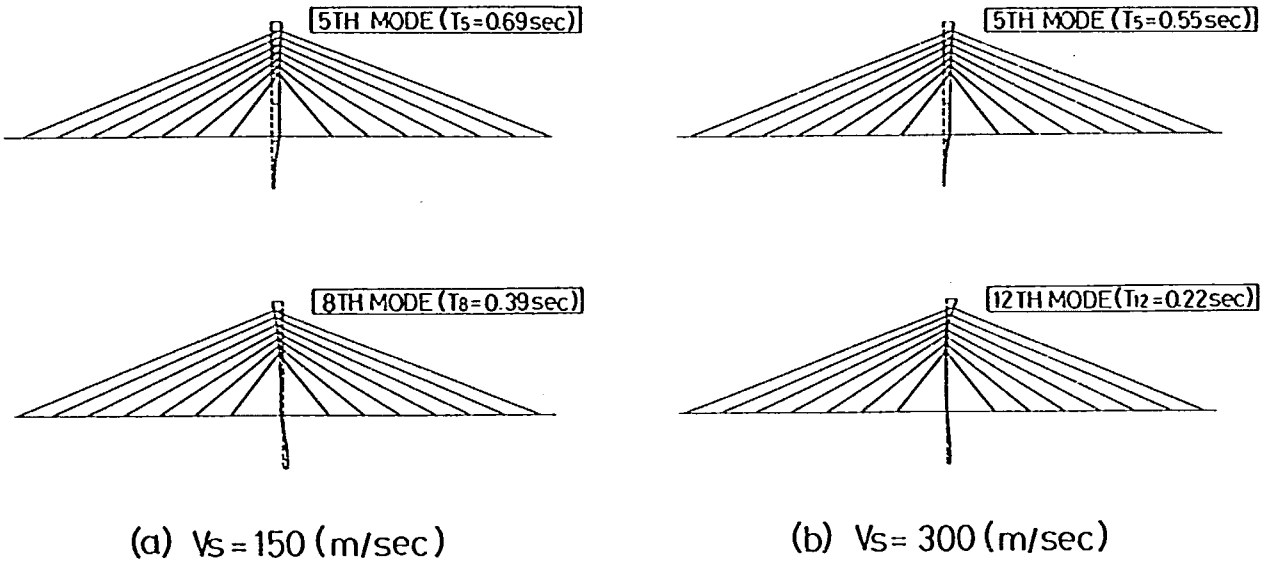


Figure 10. Predominant Mode Shapes

flexural mode of the tower associated with rocking of foundation. It is 0.744 for V_s = 150 m/sec and 0.830 for V_s = 300 m/sec. This clearly shows a significance of the radiational damping associated with rocking motion of the foundation.

Figure 11 shows an effect of shear wave velocity of the subsoils and the radius of the foundation for two selected predominant modes. The selected

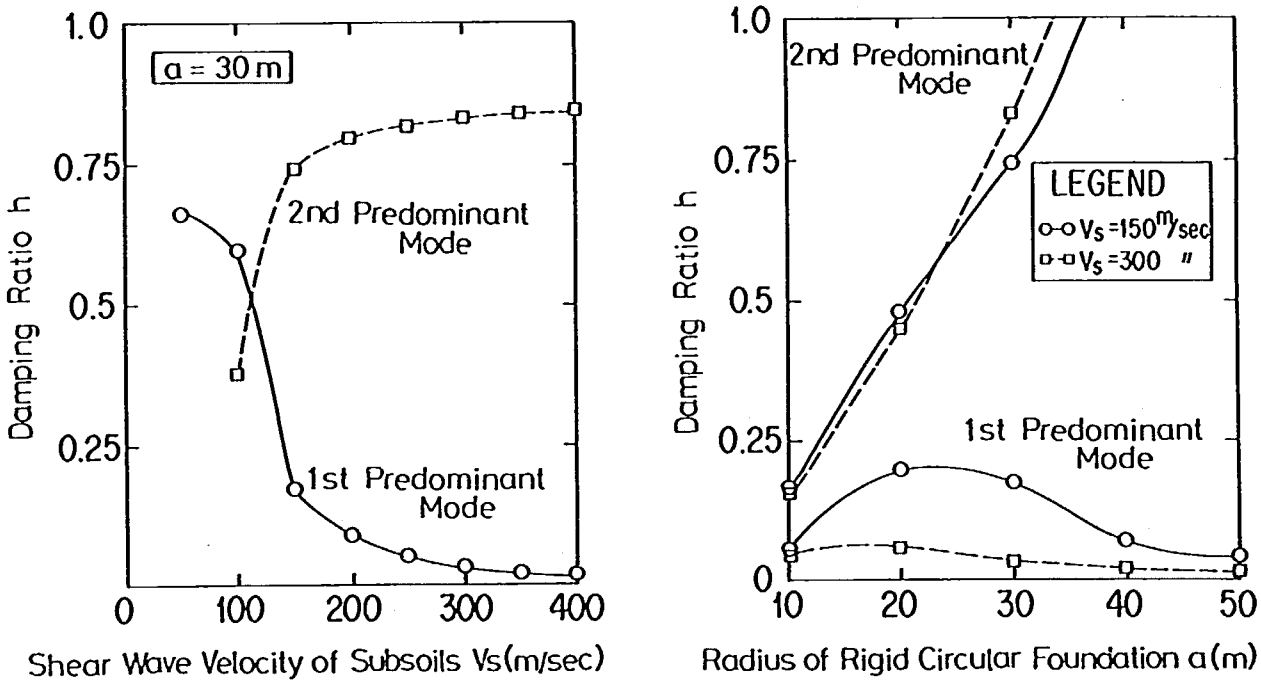


Figure 11. Effect of Shear Wave Velocity and Radius of Foundation

modes depends on the assumed values for V_s and a. It should be noted however that the most predominant modes represents a sway mode of the tower and deck, and the secondarily predominant mode represents a flexural mode of the deck associated with rocking of foundation. It is seen in Figure 11 that the shear wave velocity of subsoils is a significant parameter for the damping ratio of the bridge. Damping ratio for the most predominant mode decreases as Vs increases. Damping ratio becomes 2 - 5 %, which is generally assumed in seismic design, at about Vs = 300 m/sec. On the other hand, damping ratio for the secondarily predominant mode increases as V_s increases. The damping ratio for this mode is extremely high.

It is also seen in Figure 11 that the radius of the foundation is the other important parameter for the damping ratio. The effect of the radius is especially high for the secondarily predominant mode.

5. DEPENDENCE OF DAMPING RATIO ON MODE SHAPES THROUGH FREE OSCILLATION TESTS OF A CABLE STAYED BRIDGE MODEL[7]

5.1. Experimental Model and Free Oscillation Tests

To study damping characteristics of cable stayed bridges, a series of model oscillation tests were made. Figure 12 shows an experimental model which was accurately fabricated for simulating the Meiko-nishi Bridge[8] as prototype. The rigidity and mass of the model was determined assuming the scale of length, density and time of 1/150, 1/1 and $1/\sqrt{150}$, respectively.

The deck was supported by only cables so that friction between the deck and the tower due to relative movement of the deck in longitudinal direction can be disregarded. The elastic cable restrainers[8] were disregarded in the model for simplicity. Cable arrangement and number of cables were varied as 3 cases as shown in Figure 13. Figure 14 shows the fundamental natural frequencies and natural mode shapes of the model predicted by a linear discrete frame model.

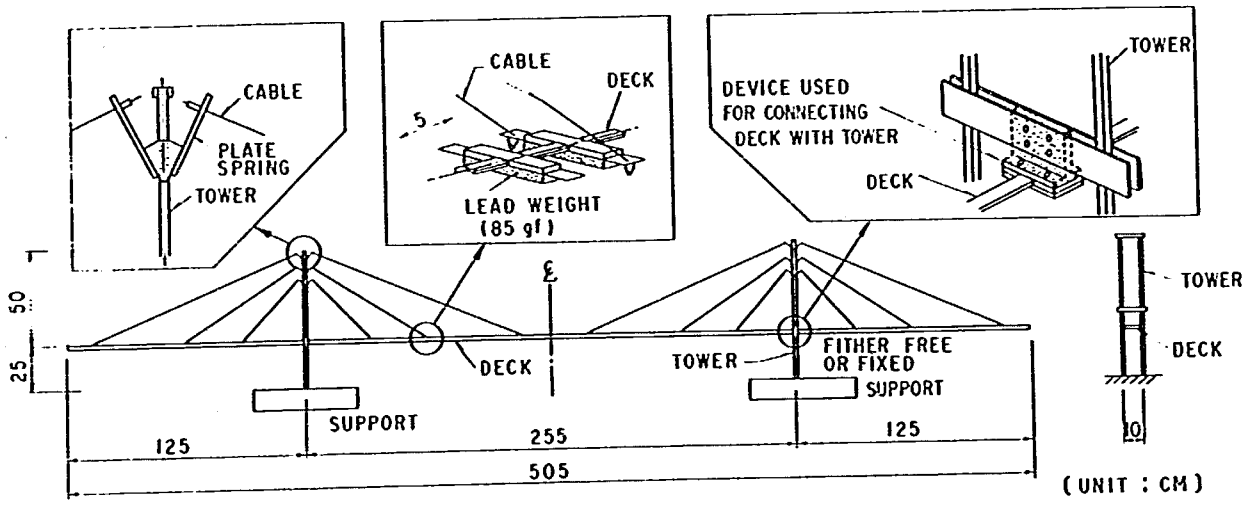


Figure 12. Experimental Bridge Model

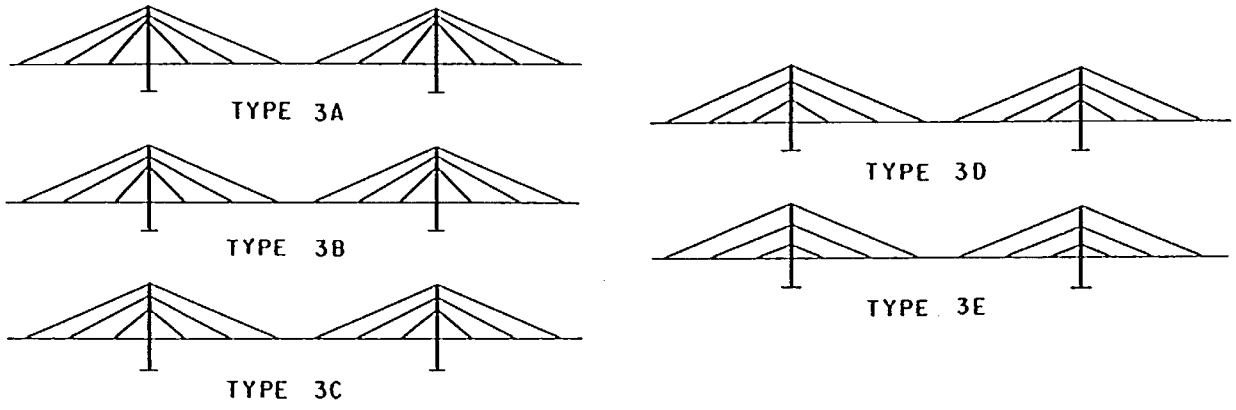


Figure 13. Cable Arrangement of Bridge Model

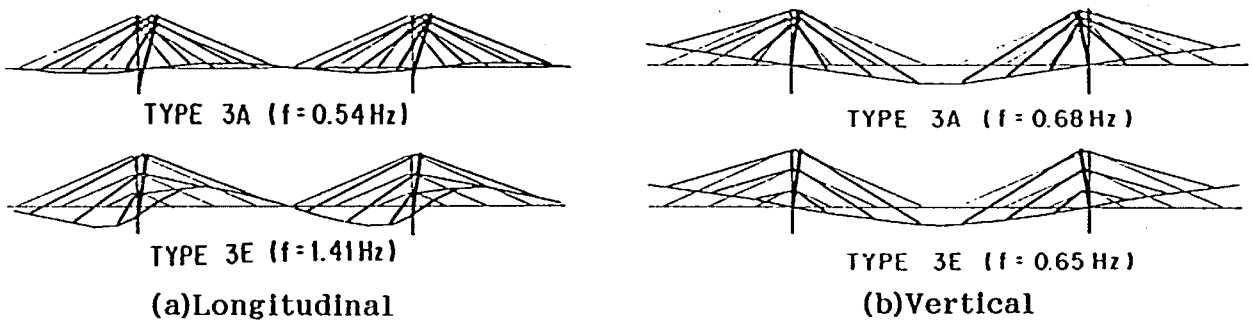


Figure 14. Predicted Mode Shapes

The deck was statically displaced so as to create an initial deformation close to the target mode shape. It was smoothly released to result in a free oscillation. Damping ratio was computed from decay of free oscillation by Eq.(1).

5.2. Effect of Cable Type in Longitudinal Oscillation

Cable type dependence of the damping ratio is considerable as shown in Figure 15(a). The damping ratio at the same amplitude increases as the cable type changes from the fan type (Type 3A) to the harp type (Type 3E). Such a significant cable type dependence of the damping ratio may be clearly related with the flexural deformation of the deck in vertical direction per unit deck displacement in longitudinal direction (as shown in Figure 14). Larger flexural deformation of the deck in vertical direction dissipates larger energy, which would result in larger damping ratio.

The damping ratio also depends on the amplitude, and its amplitude dependence increases as the cable type changes from the fan type (Type 3A) to the harp type (Type 3E). The amplitude dependence of the damping ratio tends to increase as the amplitude becomes smaller.

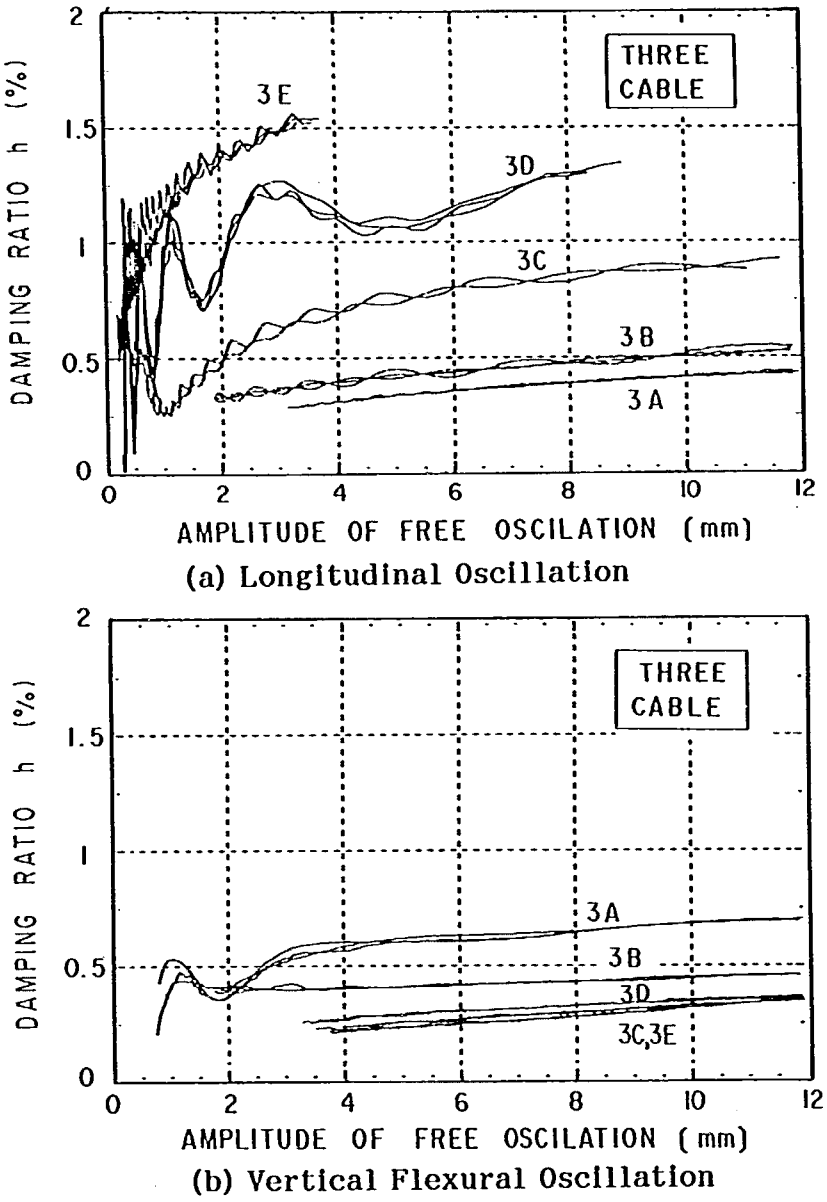


Figure 15. Damping Ratio vs. Oscillation Amplitude

5.3. Effect of Cable Type in Vertical Oscillation

Damping ratio decreases as the cable type changes from the fan type (Type 3A) to the harp type (Type 3E) as shown in Figure 15(b). Damping ratio for the flexural oscillation in vertical direction is generally smaller than that for the longitudinal oscillation. However it is quite interesting to note that such cable type dependence of the damping ratio is opposite in order to that developed in the longitudinal oscillation.

6. EVALUATION METHOD OF DAMPING RATIO OF CABLE STAYED BRIDGES[1,7]

6.1. Evaluation Method

There are various factors causing energy dissipation in cable stayed bridges. Energy dissipation are generally developed by material

nonlinearity, structural damping such as friction at movable bearings, radiation of energy from foundations to subground, and friction with air. Predominant factors contributing to damping ratio of cable stayed bridges varies with structural types. However important point to estimate damping ratio of cable stayed bridges is to evaluate total energy dissipation.

Because the energy dissipation capability may not be the same in the whole bridge, it is required to evaluate the energy dissipation in each structural segment depending on the type of the energy dissipation. Once the energy dissipation in individual structural segments can be determined, the total energy dissipation in the whole structural system may be evaluated by summing up the energy dissipation developed in each structural segment.

Based on such considerations, it is proposed to evaluate energy dissipation of a cable stayed bridge as;

1) Divide a cable stayed bridge into several structural segments in which energy dissipation capability can be considered practically the same. Such a structural segment is referred hereinafter as "sub-structure".

2) When the i-th sub-structure is idealized by a n-degree of freedom discrete system, the strain energy E_j^i of the i-th sub-structure for j-th mode may be represented as

$$E_j^i = \frac{1}{2} \sum_k (u_j^{ik})^T \, k^i \, u_j^{ik} \tag{3}$$

in which u_j^{ik} = amplitude at node k of i-th sub-structure for j-th mode and k^i = stiffness matrix of the i-th sub-structure.

Strain energy of the whole structural system for j-th mode can, then, be evaluated as

$$E_j = \sum_i E_j^i \tag{4}$$

3) For the i-th sub-structure where energy dissipation due to material nonlinearity is predominant, the energy dissipation associated with j-th mode may be written as

$$\delta E_j^i = f_j^i(E_j^i) \tag{5}$$

in which δE_j^i = energy dissipation in i-th sub-structure for j-th mode, E_j^i = strain energy in i-th sub-structure for j-th mode, and f_j^i = function relating δE_j^i with E_j^i.

The function f_j^i represents how the energy dissipation in i-th sub-structure δE_j^i be developed associated with the strain energy in i-th sub-structure E_j^i. This is referred hereinafter as "energy dissipation function"[1]. Because it is quite difficult in most cases to directly evaluate the energy dissipation function f_j^i from analytical studies, it has to be determined based on appropriate experiments.

4) For i-th sub-structure where the energy dissipation function f_j^i is such a form that it can be represented in terms of a displacement at a specific

point u_j^{ik} within the i-th sub-structure, the energy dissipation function may be represented as

$$\delta E_j^i = f_j^i(u_j^{ik}) \tag{6}$$

in which δE_j^i = energy dissipation in i-th sub-structure for j-th mode, u_j^{ik} = displacement at point k in i-th sub-structure for j-th mode, and f_j^i = energy dissipation function relating δE_j^i with u_j^{ik}.

5) Energy dissipation in the whole structural system can be obtained by summing up the energy dissipation developed in individual sub-structures determined by Eqs.(5) and/or (6) as

$$\delta E_j = \sum_i \delta E_j^i \tag{7}$$

in which δE_j = total energy dissipation in whole structure for j-th mode, and δE_j^i = energy dissipation in i-th sub-structure for j-th mode.

6) Damping ratio of the whole structure for j-th mode may then be obtained from Eqs.(4) and (7) as

$$h_j = \frac{\delta E_j}{4\pi E_j} \tag{8}$$

6.2. Evaluation of Energy Dissipation Functions

To show an evaluation of the energy dissipation functions, it is appropriate to refer a specific bridge for which actual damping characteristics was accurately estimated. Therefore, the energy dissipation functions are evaluated for the cable stayed bridge model presented in Chapter 5.

Because the model bridge was supported by only cables, friction between the deck and the tower can be neglected. Effect of radiation of energy from the foundation to subsoils can be neglected in the model because bottom of the tower was rigidly fixed by a steel base plate. Therefore it was assumed that the energy dissipation of the model bridge occurs due to material nonlinearity of the deck and the tower, and friction at the anchoring portion of the cables to the deck and the tower. The tower, the deck and the cable anchoring portion were therefore considered as "sub-structure" in the analysis.

For estimating the energy dissipation function of the tower, a simple free oscillation test of the tower was made as shown in Figure 16. Only the tower was taken out from the whole model, and it was supported as a cantilevered beam with one of the ends being fixed and the other being free. By smoothly releasing the tower top from a displaced position, a free oscillation simulating the first mode was developed.

Figure 17 shows how the damping ratio of the tower varies with the oscillation amplitude and the mass of the weight placed on the free end. Predicted damping ratio which will be described later is also presented for comparison. Damping ratio of the tower increases as the oscillation amplitude increases.

Because the damping ratio h_1 of the tower for the first mode shape can be determined through the decay of the free oscillation and the strain energy E_1 can be computed from Eq.(3), one can determine the energy dissipation δE_1 by substituting h_1 and E_1 into Eq.(8).

Figure 18 shows the relation between δE_1 and E_1 for the first mode. The relation seems almost independent of the weight of the mass placed on the tower top. It was approximated by a least square fit as

$$\delta E_1 = 0.016 E_1 + 0.0021 E_1^{3/2} \quad (9)$$

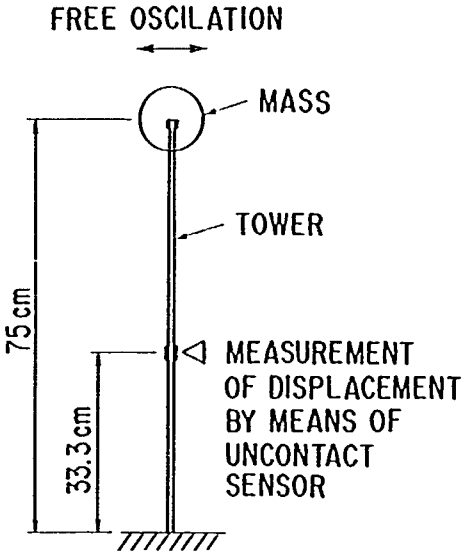


Figure 16. Free Oscillation Test for Tower

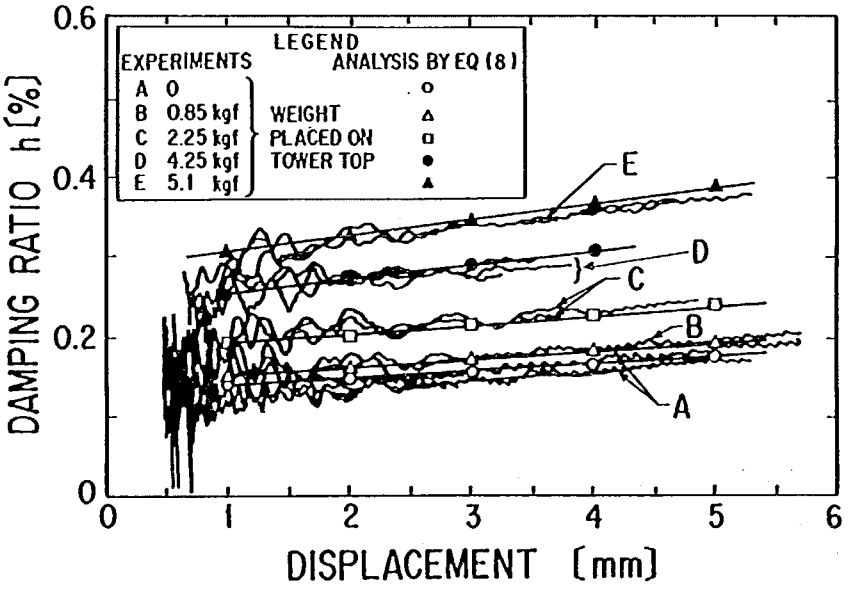


Figure 17. Damping Ratio vs. Oscillation Amplitude for Tower

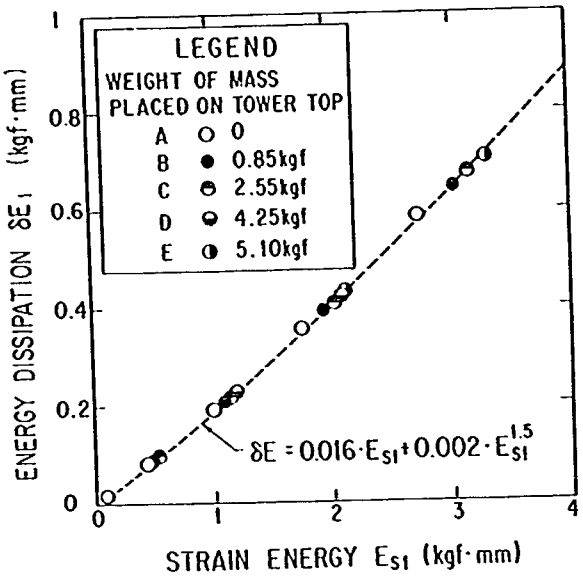


Figure 18. Energy Dissipation δE_1 vs. Strain Energy E_1 for Tower (1 kgf = 9.81 N)

Based on Eq.(9), the damping ratio vs. the oscillation amplitude of the tower was evaluated as shown in Figure 17. It is seen that the predicted damping ratio for the tower agrees reasonably well with the experimental result.

Similarly, the energy dissipation functions for the deck and cable anchoring portion were evaluated as [1]

$$\delta E_1 = 0.016\, E_1 + 0.083\, E_1^{1.37} \quad \text{(deck)} \tag{10}$$

$$\delta E_1 = 0.018\, \omega^{2.15} \cdot \theta^2 \quad \text{(cable anchoring portion)} \tag{11}$$

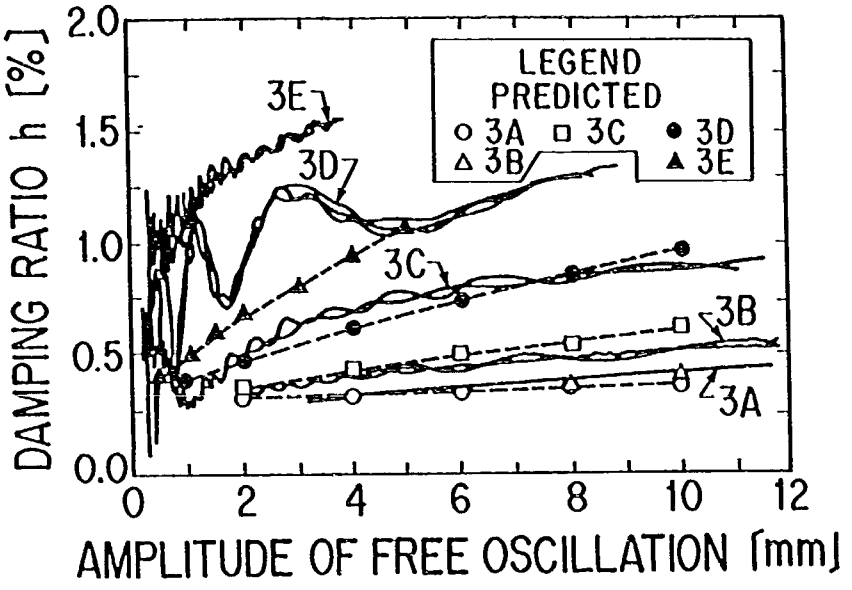
in which θ and ω represent an angle between the tower and the cable, and angular frequency of the free oscillation, respectively.

6.3. Evaluation of Damping Ratio Based on Energy Dissipation Functions

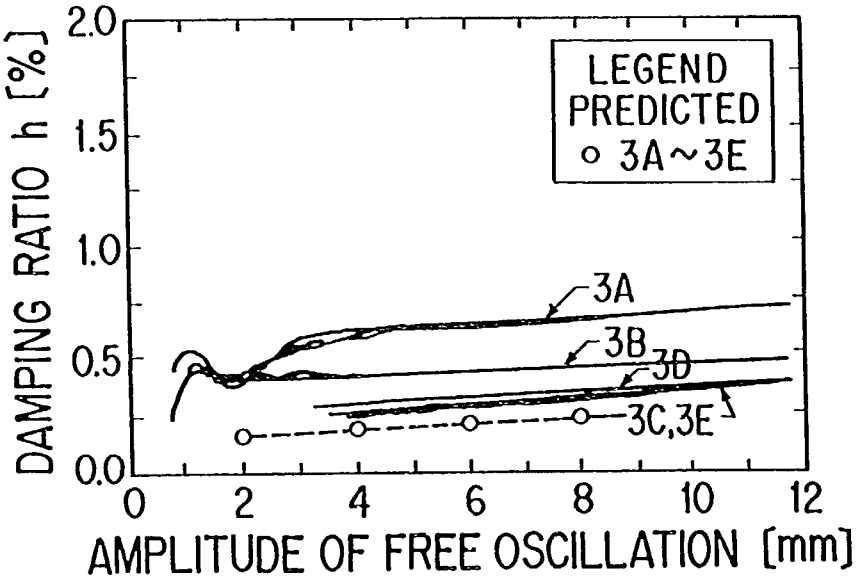
Predicted damping ratio by Eq.(8) assuming the energy dissipation functions of the sub-structures by Eqs.(9), (10) and (11) is presented in Figure 19 in comparison with the experimental results.

The predicted damping ratio of the model in the longitudinal oscillation increases as the cable type changes from the fan type (type 3A) to the harp type (type 3E) in the same manner with the test. The dependence of the predicted damping ratio on the oscillation amplitude increases in the same order with the experiments. Such characteristics agree reasonably well with the experiments, although the predicted damping ratio is underestimated as the cable type approaches to the harp type.

The predicted damping ratio of the model for the vertical flexural oscillation is almost independent of the cable type. Although the damping ratio estimated from the experiments slightly decreases as the cable type changes from the fan type to the harp type, the overall characteristics of the predicted damping ratio seem reasonably close with the experimental results.



(a) Longitudinal Oscillation



(b) Flexural Vertical Oscillation

Figure 19. Prediction of Damping Ratio vs. Oscillation Amplitude Relation

The damping ratio predicted is somewhat smaller than the experimental results probably because the energy dissipation which are not considered in this analysis would contribute to the total energy dissipation. If the energy dissipation at each portion is evaluated in detail, it is expected to further improve the accuracy of the above estimation.

7. CONCLUDING REMARKS

Cable stayed bridges have complex dynamic behavior, and it is of great importance to correctly evaluate their dynamic characteristics for developing a rational seismic design method. The characteristics of damping which were presented in the preceding pages may be summarized as :

1) Damping ratio depends on the mechanism of energy dissipation and the mode shapes. It is therefore important to consider what type of and how much energy dissipation are made in each sub-structure. Even in the same bridge, different damping ratio may be measured if the direction or the point of excitation is different because of the difference of the mode shapes considered. Unless taking considerations on such characteristics into account, attempts to formulate empirical relations for assessing the damping ratio would only cause large scatters around the prediction.

2) Dependence of the damping ratio on the mode shape seems to be one of the reasons which cause considerable scatters observed in the past forced excitation tests results.

3) Cable configuration such as number of cables and type of cable arrangement is a controlling factor for damping ratio. The harp type cable arrangement tends to develop larger damping ratio than the fan type cable arrangement for the oscillation mode in longitudinal direction, because it causes larger deck deformation in vertical direction.

4) Application of the proposed method for assessing the damping ratio of cable stayed bridges needs to be made. It is required to conduct careful and elaborate forced excitation tests so that the energy dissipation mechanism in sub-structures can be clarified.

8.REFERENCES

1 K. Kawashima and S. Unjoh : Damping Characteristics of Cable Stayed Bridges for Seismic Design, Technical Report, Vol.187, Public Works Research Institute, January 1992

2 K. Kawashima, S. Unjoh. and Y. Azuta : Analysis of Damping Characteristics of A Cable Stayed Bridge Based on Strong Motion Records, Proc. Japan Society of Civil Engineers, Structural Eng./Earthquake Eng., Vol.7, No.1, April 1990, pp.181-190

3 N. Narita : Forced Vibration Test of Suigo Bridge, Technical Note, Vol. 1349, Public Works research Institute, March 1978

4 K. Kawashima and S. Unjoh : Damping Characteristics of Cable Stayed Bridges Associated with Energy Dissipation at Movable Supports, Proc. Japan Society of Civil Engineers, Structural Eng./Earthquake Eng., Vol.6, No. 1, April 1989, pp.145-152

5 K. Kawashima, S. Unjoh and Y. Azuta : Damping Characteristics of Cable Stayed Bridges, Proc. 9th World Conference on Earthquake Engineering, Tokyo/Kyoto, Japan, August 1988

6 H. Yamahara : Investigation on Vibrational Properties of Foundations and Structures on Elastic Medium, Proc. Architectural Institute of Japan, Vol.115, pp.6-14, 1965.

7 K. Kawashima and S. Unjoh : Estimation of Damping Characteristics of Cable Stayed Bridges for Seimsic Design, 7th U.S.-Japan Bridge Workshop, May, 1991, Tsukuba, Japan

8 Japan Road Association : Design and Construction of Meiko-nishi Bridge, March 1986 (in Japanese)

RECENT SELECTED PUBLICATIONS AT EARTHQUAKE ENGINEERING DIVISION, PUBLIC WORKS RESEARCH INSTITUTE

ISSN 0386-5878
Technical Memorandum of PWRI No. 3035
October, 1991

Kazuhiko Kawashima, Head
Earthquake Engineering Division

This reports presents some of the selected publications on the research on seismic design, seismic inspection and strengthening of highway bridges, dynamic strength and ductility of structural components such as steel bridge piers and shield tunnel segments, structural response of menshin bridges (base isolated bridges), seismic response of embedded pipes, soil amplification, damping characteristics of cable stayed bridges, seismic damage information systems, and evaluation of indirect economical loss caused by an earthquake.

郵 便 は が き

Postage stamp

3 0 5 - □ □

建設省土木研究所地震防災部耐震研究室
〒305 茨城県つくば市大字旭1番地

Earthquake Engineering Division,
Public Works Research Institute
Tsukuba Science City
Japan 305

No. 03

No. 03

配布先氏名

配布先住所

Receipt of

Technical Memorandum of PWRI No. 3035

Name _____

Address _____

_____

_____